THE RIGIDITY AND PERFORMANCE OF ROLLING BEARINGS IN HOUSINGS

by

Malik Mohammad Abu Taha

Thesis submitted for the Degree of Doctor of Philosophy
in the Faculty of Engineering of the University of London

Department of Mechanical Engineering,
Imperial College of Science and Technology,
University of London

November, 1970

TO MY PARENTS

ABSTRACT

Spindle-assembly design for machine tools, and other applications in which stiffness is of paramount importance, requires accurate knowledge of the stiffness of the associated bearings. Calculations of the stiffness of rolling bearings are normally made assuming zero clearance and 'infinitely rigid' races. The resulting discrepancy between a calculated value of stiffness and that which is likely to obtain for the assembled bearing in practice is normally resolved by a correction factor, whose value can cover a wide range, and about which comparatively little is known. In this investigation the effect of clearance or interference, and the use of a range of compliant shafts and housings has been examined.

The work is in two sections, the first being concerned with calculations and results for rigid races, in which the effect of clearance and interference is of primary interest. Nomograms for radial roller and ball bearings are presented, to enable the bearing deflection to be found quickly and easily.

The second section concerns the investigation of various types of fully-flexible bearing assembly, using a finite-element computer program which has been developed to evaluate the deflections, rolling element load distributions, stresses, and deflected shapes of races. Computed results show good correlation with experimental results on an Araldite model using a modified frozen-stress technique. Using the finite-element analysis, the effects on bearing performance of boss, wall thickness of shaft, local stiffening members, and the existence of other bores or openings in the supporting wall of the housing, were evaluated for a range of values of radial clearance or interference, radial load and rotational speed. A further point of investigation concerned the feasibility of artificially modifying the roller load distribution, by using slightly non-circular outer races, to obtain both improved life and rigidity for a given bearing configuration.

The work shows that the 'rigid race' assumption can lead to unrepresentative values of calculated bearing stiffness. The results of computation indicate and provide means of achieving improved design of an overall bearing assembly.

ACKNOWLEDGEMENTS

I take pleasure in expressing my most sincere thanks to my supervisor Dr. J. R. Crookall for his valued advice, encouragement and guidance at every stage of the work.

Thanks are due to the staff of the Computing Centre and of the Mechanical Engineering Department. I also acknowledge with thanks the help of Mr. A. Christie during experimental work in the Machine Tool Laboratory.

Thanks are also due to Mr. S. P. Poole of National Physical Laboratory for the use of the Talyrond roundness measuring machine and to my colleagues Mr. U. R. K. Rao, Mr. P. B. Macpherson and others for their help.

Finally, I wish to thank the authorities of Imperial College for the award of the W. E. Dalby scholarship for the last two years of the work.

M. M. A. Taha.

CONTENTS

Chapter			Page
1	Introduction, review of literature, and outline plan of work		
	1.1	Introduction	11
	1.2	Review of literature	12
	1.2.1	Components of spindle deflection	12
	1.2.2	Preloading a rolling bearing	14
	1.2.3	Effect of flexibility of the bearig support	15
	1.2.4	Influence of bearings in components other than the spindle assembly	16
	1.2.5	General techniques	16
	1.3	Outline plan of present work	17
2	Theoretical background for bearings with rigid races		
	2.1	General	18
	2.2	Selection of bearing type and size	18
	2.3	Contact stresses	20
	2.4	Contact deformation	22
	2.5	Comparison of the contact deformation formulae	24
	2.6	Deflection for hollow rollers	25
	2.7	Load distribution in a statically loaded bearing	26
	2.7.1	Stribeck's solution	26
	2.7.2	Bearing with play or interference but otherwise ideal geometry	28
	2.7.3	An iterative method for bearing with play or interference, but otherwise ideal geometry	30
	2.7.4	General case for imperfect geometrical shape, and dynamic loading due to rotation, of a radial rolling bearing	32
	2.8	Centrifugal force of the rolling elements	34
	2.9	Capacity of bearings	35
	2.9.1	Basic static capacity of bearings	35
	2.9.2	Basic dynamic capacity and life of bearings	36
	2.10	Experimental representation of rigid radial rolling bearings	37
3	Calculated performance for bearings with rigid races		
	3.1	General	38
	3.2	Load zone factor, ϵ	38
	3.3	Explanation and analogy for stiffness of preloaded-bearings	39
	3.4	Deflection of radial roller bearings	40
	3.5	Load distribution in radial roller bearings	42
	3.6	Stiffness of radial roller bearings	44
	3.7	Life of radial roller bearings	46
	3.8	Graphical solution for radial rolling bearings with rigid races	47
	3.8.1	Solution for radial roller bearings with rigid races	48
	3.8.2	Solution for radial ball bearings with rigid races	49

Contents continued

Chapter			Page
4	Bearings with fully-flexible races - experiments with Araldite models		
	4.1	General	50
	4.2	Model technique	50
	4.3	Production of models	50
	4.4	Stress freezing	51
	4.5	Calibration of model material	52
	4.6	Calibration of rollers	53
	4.6.1	Measurement of models	53
	4.6.2	Experimental results	54
	4.6.3	Discussion of results	55
	4.7	Experiment on the complete model bearing	56
	4.7.1	Dimensions of models	57
	4.7.2	Method of obtaining preload	57
	4.7.3	Measurement of deflections	58
	4.7.4	Experimental results	60
	4.7.5	Discussion of results	61
5	Development of finite-element program for bearings with fully-elastic supports		
	5.1	General	63
	5.2	Finite-element analysis of two-dimensional problems	63
	5.3	Procedure used for solving the system of simultaneous linear equations	64
	5.4	Notes on the program FINELM	66
	5.4.1	Descriptive flowchart	67
	5.5	Smaller version of the program	72
	5.6	Types of rolling bearing that can be considered with the program	72
	5.7	Equivalent radial load for any given roller load distribution	73
6	Computed results for bearings with fully-elastic supports, with the elastic properties of Araldite		
	6.1	General	75
	6.2	Calibration of an 'Araldite' roller loaded between two 'Araldite' platens	75
	6.2.1	Finite-element mesh for calibration of roller and platen	76
	6.2.2	Calibration results	76
	6.3	Finite-element mesh for 'Araldite' radial roller bearing with housing and shaft	77
	6.3.1	Coding of the Araldite radial roller bearings	78
	6.4	Comparison of finite-element results for complete bearing with the results obtained by experiment and theory	79
	6.5	Equivalent thickness of the inner race core (i.e. the shaft)	80

Contents continued

Chapter			Page
6	6.6	Convergence of roller load distribution	81
	6.7	Results and discussion for Araldite radial roller bearings	81
	6.7.1	The effect of radial clearances and radial load on bearing with fully-elastic races	82
	6.7.2	The effect of rotational speed on bearing with fully-elastic races	86
	6.7.3	The effect of relieved outer race on bearings with fully-elastic races	87
	6.7.4	The effect of parabolic shear stress distribution in the inner race	92
7	Computed results for bearings with fully-elastic supports, with the elastic properties of steel.		
	7.1	General	93
	7.2	Calibration of rollers on platens	93
	7.3	Finite element mesh of steel radial roller bearing with housing and shaft	94
	7.3.1	Some design considerations of the finite element model mesh	95
	7.3.2	Coding of the steel radial roller bearings in housings	97
	7.4	Convergence of roller load distribution for steel radial roller bearings	99
	7.5	Results and discussion of the effects of different types of housing and shaft on the performance of steel radial roller bearings	100
	7.5.1	Bearings with hollow shafts	100
	7.5.2	Bearings in housings with other holes	104
	7.5.3	Bearings in bossed housings	106
	7.5.4	Bearings in housings with bosses and ribs	107
	7.5.5	Circular (bossed) housings on rib supports only	110
8	Conclusions and suggestions for further work		
	8.1	Conclusions	118
	8.2	Suggestions for further work	120
	References		122
	Figures		126
	Tables		357
	Appendix 2.1		395
	Appendix 5.1		398
	Appendix 5.2		401
	Appendix 5.3		404
	Appendix 6.1		409
	Appendix 7.1		411
	Listing of Computer programs		417

LIST OF SYMBOLS

Symbol	Description
A	Constant of deflection equation of the form, $\delta = AP^N$, for a single rolling element loaded between two platens, considering δ in in. and P in lbs. A_1 is for one contact area and, A_2 for two contact areas.
C	Basic dyanmic capacity.
C_s	Basic static capacity.
c	Radial clearance (positive for play and negative for interference).
D	Pitch diameter of rolling elements.
D_o	Outer race track diameter.
D_i	Inner race track diameter.
d	Diameter of rolling element.
E	Young's modulus in $lb./in^2$.
E'	$E/(1-1/m^2)$.
F_c	Centrifugal force of a rolling element.
F_r	External radial load on bearing.
f	Material factor, 49,500 for roller bearings when pound and inch units are used.
f_c	Factor for dynamic capacity.
G	Modulus of rigidity, $G = E/(2(1+1/m))$.
G_j	Gap between the races at roller position j.
K	Constant for load deflection relation of the form $P = K\delta^t$ for a single rolling element loaded between two platens, considering δ in in. and P in lbs. K_1 is for one contact area and, K_2 is for two contact areas.
K_t	Ratio of total radial bearing deflection considering fully-elastic races to the bearing radial deflection considering rigid races.
K_b	Ratio of the body deflectin of bearing outer race considering fully-elastic races to the bearing radial deflection considering rigid races.
k	Incremental stiffness of bearing (inverse of slope of δ vs. F_r curve).
k_{av}	Average stiffness = F_r/δ
L	Fatigue life of bearing in millions of revolutions (mr).
ℓ	Length of roller.

Symbol	Description
$1/m$	Poisson's ratio.
N	Exponent in deflection equation of the form, $\delta = AP^N$, for a single rolling element loaded between two platens.
n	Angular speed in revolutions per minute (R.P.M.).
P_l	Load on the peak rolling element which is in direction of radial load.
P_{lr}	Radial load component on the peak rolling element.
P_r	Equivalent radial load.
P_j	Load on any roller at position j.
P_{oj}	Load on rolling element j at outer race contact.
P_{ij}	Load on a rolling element j at inner race contact.
p	Exponent for bearing life-load relationship.
r	Radius of a contacting body.
t	Exponent in load deflection relation of the form $P = K\delta^t$ for a single roller loaded between two platens, $t = 1/N$.
S_f	Load sharing factor, $(P_{lr} \times Z/F_r)$.
v	Surface velocity.
Z	Number of rolling elements in a bearing.
ε	Normal strain.
γ	Shear strain.
δ_r	Radial deflection of bearing.
δ_{or}	Outer race deflection.
δ_{ir}	Inner race deflection.
δ_b	Body deflection of outer race.
δ_l	Deflection of peak rolling element which is in the direction of radial load.
δ_j	Deflection at rolling element position j.
δ_{oj}	Deflection at outer race contact for rolling element position j.
δ_{ij}	Deflection at inner race contact for rolling element position j.
ϵ	Projection of loaded zone on bearing diameter, $\epsilon = \frac{1}{2}(1-\frac{c}{\delta_r})$
λ	Capacity reduction factor for stress concentration.
ρ	Mass density.
σ	Normal stress.
τ	Shear stress.

Symbol	Description
ϕ	Angular pitch between two consecutive rolling elements.
ψ_j	Angular position of rolling element j from direction of radial load.
ψ_ℓ	Angular extent of loaded zone from direction of radial load.
ω	Angular speed in radians per sec.

SUBSCRIPTS

o	Outer race.
i	Inner Race.
c	Cage.
j	Roller position.
r	Radial.

CHAPTER 1 INTRODUCTION, REVIEW OF LITERATURE, AND OUTLINE PLAN OF WORK

1.1 INTRODUCTION

The primary consideration in machine tool bearing applications is high rigidity, and this is therefore of predominant interest in this work. All structural elements in the load path must deflect under cutting loads, and the work of Opitz (1)* has shown that a significant part of the overall deflection occurs at the spindle assembly.

The spindle deflection at the cutting zone is due partly to the bending of the spindle itself, and partly to the deflection of the bearings and housings. The bearing deflection contributes about 30 to 50 percent of the total spindle deflection. The optimum bearing spacing to spindle overhang ratio of a spindle assembly for minimum deflection at the cutting zone depends partly on the rigidity of the associated bearings, which if inaccurately estimated will influence the calculated 'optimum' bearing layout.

It is thus important to have procedures for determining accurately the deflection of an assembled bearing, and information concerning the achievement of maximum rigidity.

The methods most widely available in literature for calculating rolling bearing deflection are based on the assumptions of zero clearance, and that the races are rigid and remain circular on loading. However, the deflection of a given rolling bearing naturally depends upon the condition of play or preload, and the shape of the races under load, and hence the design of its supporting housing and shaft.

In some experiments reported in the literature, the deflection of a radial rolling bearing is taken to be the deflection at the 'peak' roller, which is in the direction of the radial load. This is very nearly true in cases where the housing and shafts provide sufficient 'backing up' rigidity for the races, so that they virtually retain their circular shape on loading. However, the actual deflection of the bearing is the sum of the deflection of the peak roller and the associated contact deflections of the races, the deflection due to change in shape of the races, and the deflection due to the change in position of the outer race. Hence overall deflection is dependent on the

---

* Numbers in brackets designate references.

bearing assembly (bearing, shaft, and housing) as a complete structure.

Information is needed on the deflection behaviour of bearings under realistic support conditions. The designer needs to know what scope exists for obtaining more rigidity from a given bearing by the judicious use of preload, and also the effects of different designs of housing and shaft on the overall performance of the spindle assembly.

Although applications to machine tool spindles have been a guiding consideration, the results are, of course, relevant to other applications in which rigidity is an important criterion.

1.2 REIVEW OF LITERATURE

Research on the rigidity of individual elements of machine tool structures, such as flanged joints, columns, spindles, etc., has been carried out by a number of workers, and these, and other aspects of importance in machine-tool engineering have been comprehensively reported by Koenigsberger in reference 2.

In tests on a grinding machine, Opitz (1) found that the total deflection at the cutting zone comprised

element	deflection as percentage of total
flange at base of column	13%
slide between beam and column	27%
grinding spindle assembly	42%
feed spindle	18%

This specific example illustrates the importance of reducing spindle deflection, which can be taken as applying equally to machine tools in general. The stiffness of the spindle assembly is generally greater in the axial direction, than in a direction perpendicular to the axis. However, in most cutting operations, adequate stiffness in the perpendicular direction is of first importance, although axial stiffness is of importance in lathe facing operations, and end milling and drilling.

1.2.1 COMPONENTS OF SPINDLE DEFLECTION

The deflection measured at the cutting zone due to a force at right angles to the spindle axis, references 1, 3, comprises:

(1) the deflection of the support, (i.e. bearings and their housings).

(2) the deflection of the spindle itself.

The spindle deflection is derived from the case of an elastic beam

on rigid supports, and the bearing component from the case of a rigid beam on elastic supports. Superimposition gives the total deflection as shown in fig. 1.1a.

Investigations by Opitz (1) on different lathes have shown that the share of the total deflection due to the spindle amounts to 50-70 percent and that of the bearing between 50 and 30 percent.

From these deflections the optimum bearing span to overhang ratio for minimum deflection at the point of application of load of a spindle can be found, as shown in fig. 1.1b.

Stansfield and Bell (4) give procedures for determining the optimum spacing of bearings for a two-bearing spindle taking into account bearing stiffness and spindle deflection due to bending and shear. The design of machine tool spindles supported at three positions is treated in reference 5.

Opitz et al. in reference 3 have shown that the compliance of the spindle-bearing system can be considerably influenced by the compliance of the bearings if the spindle is very stiff. As shown in fig. 1.2a, at low values of bearing stiffness the increase of total compliance, consisting of the spindle compliance and the bearing compliance is mainly due to the bearings. Conversely, at high values of bearing stiffness, the compliance of the system is almost unaffected by the bearings.

The importance of finding the stiffness of the bearing is also stressed in the above reference, by illustrating the effect of the front bearing stiffness on the optimum bearing spacing at which the deflection at the point of load application is a minimum for a given overhang, moment of inertia of spindle cross-section, and stiffness of the rear bearing, as shown in fig. 1.2b. This figure shows that the optimum bearing spacing, in particular at low values of bearing stiffness, has to be adjusted to suit the bearing that is to be used in order to maintain high static stiffness. The stiffness of the bearing must therefore be known precisely in order to optimise the design of a spindle-bearing assembly.

The deflection of the bearing can be reduced in a number of ways, for example by increasing the number of rolling elements, by reducing the clearance and, if it is a roller bearing, by increasing the length of the rollers.

1.2.2 PRELOADING A ROLLING BEARING

Preloading a rolling bearing means the introduction of some 'negative play'. Preloading bearings by even a small amount increases the stiffness considerably. This fact was reported early in the 1930's, for example in references 6 and 7. A number of recent papers (1, 3, 8 - 10) have appeared, some of which give detailed analysis of calculating deflections of bearings with play or preload.

An appropriate degree of preloading also increases bearing life. This is reported in references 9, 11 , which also give the method of estimating the life of bearings with play or preload, assuming rigid races.

A recent book by Harris (12) gives a comprehensive account of these aspects.

However, the effect of play or preload on bearing has not so far been considered fully; a few examples covering a narrow range in the case of rigid races only having been presented. The need was therefore for a full investigation into the effects of play and preload for rigid races, over a wide range of conditions. To investigate further the effect of flexibility of the races necessitated the development of a new procedure for calculation (as well as experiment), and this was to form the main part of the work.

Opitz (1) investigated the effects of preloading on the stiffness of the spindle-bearing system. Fig. 1.3a, taken from this reference, shows that, the total deflection due to the 1000 kg. load is reduced from 30 μm to 16 μm by reducing the 15 μm radial play of the front bearing to an interference of -15μm. The main effect is on the bearing deflection, which is reduced from 16μm to 5μm. The spindle deflection is also reduced from 14μm to 11μm due to the clamping action of the bearing which resists moments. The radial play of the rear bearing was kept constant at 2μm.

Errors of roundness in the spindle and the housing readily deform the relatively flexible races, and the resulting slightly non-round races produce rotationally non-uniform stiffness of the bearing. Stiffness variation with direction of applied load is much wider for positive play than for negative play. Opitz et al.(3) found 18 percent variation in deflection for a bearing with positive play of 5μm, which decreased to 5 percent when it was preloaded with an interference of -15μm.

Fig. 1.3b (from Opitz (1)) shows the static and dynamic deflections of the chuck and tool-holder of a lathe, taking the relative deflections (i.e. type 1) as 100 percent. The tool-holder deflection decreases from 70 percent

under a static load to only 10 percent under dynamic load, due to the effective damping in the slide-ways of the cross slide. However, chuck deflection increases from 30 percent to 90 percent due to the lower damping of the spindle assembly. Fig. 1.3c shows that the resonance amplitude decreases, and damping increases, with decrease in radial clearance. This illustrates the beneficial effect of increasing static stiffness by preloading, on the dynamic performance of a bearing.

1.2.3 EFFECT OF FLEXIBILITY OF THE BEARING SUPPORT

For calculation of bearing deflection, the assumption is normally made that the races are rigid, and retain their circular shape on loading. However, races are in fact elastic and deflect under load; in turn, this modifies the load distribution among the rolling elements, and hence the deflection of the bearing. The deflected shape of the races depends upon the design of the supporting structure (i.e. housing and shaft). The effect of flexibility of races and supports has been considered by some research workers and reported in references 3, 13 - 16. Opitz et al.(3) report an increase in deflection of approximately 6 percent using hollow spindles with a ratio of bore to outer diameter of up to 0.5, and reduction in the external diameter of the bearing housing from 320 mm. (12.6 in.) to 240 mm. (9.4 in.) leads to an increase in deflection of approximately 32 percent with zero clearance bearing, and 29 percent with 5 μm negative clearance. Münnich et al.(13) have found the effect of different types of elastic races on the load distribution among the rollers in zero clearance radial roller bearings by photoelasticity.

Crookall (15) investigated the rigidity of bosses on flat plates subjected to a transverse moment, using a modified frozen-stress technique. The bearing configuration simulated was that of a pair of ball or roller bearings, one situated at each end of the bore; this gives good support to a moment on the spindle. The use of this modified frozen-stress technique has the advantage that it permits direct measurement of the deformation of the race tracks. Datta (16) used the same technique to find the effect of fully elastic races on rolling element load distribution and the shape of the races under load. He also used Araldite rollers in aluminium races to simulate bearing having infinitely rigid races.

Jones (17) gives a general theory for a system of ball and radial roller bearings under arbitrary condition of load and speed. He considers the deflection of the shaft and supporting structure and sets up a system of simul-

taneous non-linear equations in terms of 'influence coefficients'. If the influence coefficients are known, the system of equations can be solved for deflections of the system and load distribution among the rolling elements. However, in this theory he assumes that the bearing races retain their circular shape on loading.

Stansfield and Bell (4) give values (table 1.1) for a correction factor K, which when multiplied by the calculated bearing deflection assuming zero clearance and rigid races, gives the deflection for the 'actual' bearing application. This table was prepared from the measurements reported by other research workers. One of the objectives in the present work was to re-evaluate this correction factor, and values for different types of housings and shaft used in the present investigation are given in chapters 6 and 7.

1.2.4 INFLUENCE OF BEARINGS IN COMPONENTS OTHER THAN THE SPINDLE ASSEMBLY

The rigidity of bearings used in other parts of the machine tool (besides the spindle assembly) also affects the accuracy of the work-piece. For example, the radial deflection of bearings in gear boxes also has quite an important effect on the torsional rigidity of transmission as shown by the calculation of E. Tamimi (18). He showed that the total torsional stiffness of the gear box increases considerably with increase in the bearing stiffness. His calculation of the percentage of element contribution for different arrangement gear boxes shown in table 1.2, indicates that the contribution of the bearings to the torsional rigidity of transmission may be as high as 57 percent, and this may be reduced to around 13 percent by increasing the bearing rigidity.

1.2.5 GENERAL TECHNIQUES

The analysis of machine tool structures and elements can be made either,

(1) by analytical methods,

(2) by experimentation with actual machine tools, as is described in, for example, references 1, 3.

(3) experimentally using models as is described in, for example, references 13, 15, 16, 19, 20, and

(4) by using a computer as is described in, for example, references 21 - 25.

Methods 1, 3 and 4 have been used in this investigation.

1.3 OUTLINE PLAN OF PRESENT WORK

The work has been divided into two main parts, one considering rigid bearing races (chapters 2 and 3), and the other considering fully elastic races (chapters 4 to 6).

In the first part, bearing deflection, rigidity, rolling element load distribution, etc., have been calculated on the assumption of rigid races, varying the radial clearance and number of rollers.

The background theory is given in chapter 2. The load-deflection relationships for individual rolling elements have been investigated, and different load-deflection formulae are also compared in this chapter. The results of calculation for rigid race bearings are given in chapter 3. A method of finding the deflection of these bearings using nomograms, is also given in this chapter.

A complete model radial roller bearing has been tested, and the results obtained are compared with those for rigid races, in chapter 4.

A finite element program has been developed to give the deflected shapes of the races, deflection of the various bearing components, rolling element load distribution and stress distribution in the races, for a bearing with fully elastic races. Some short notes on this program are given in chapter 5. In this chapter a method of comparing lives of different rolling bearings, by calculating the equivalent load on the bearing from the rolling element load distribution, is also given.

Load-deflection characteristics for individual Araldite rolling elements have been found using the finite element method, and compared with the experimental results. They have then been used as data in the computer program developed in chapter 5 to solve the complete Araldite rolling bearing problem with fully elastic races. The results obtained are compared with the experimental ones, in chapter 6. This chapter also gives other results obtained by the computer program for Araldite bearings having different radial clearances, radial loads, speeds and shapes and amounts of outer race relief. Outer race relief has been used, in an attempt to modify artificially the rolling element load distribution to increase both life and rigidity for a given bearing configuration.

Various types of housing and hollowness of shafts have been considered for steel bearings with the finite element program, to find their effect on the total and component bearing deflections, the rolling element load distribution, equivalent load, etc. The results are given in chapter 7.

CHAPTER 2 THEORETICAL BACKGROUND FOR BEARINGS WITH RIGID RACES

2.1 GENERAL

The load applied on a rolling bearing is transmitted through the rolling elements from one race to the other. The magnitude of load transmitted by any individual rolling element depends on the internal geometry of the bearing and the type of load impressed on it. The object of this chapter is to present the theoretical methods used to determine the rolling element load distribution, bearing deflection and bearing performance taking into account the radial play or interference that may be present in the bearing by considering the bearing races to be rigid.

2.2 SELECTION OF BEARING TYPE AND SIZE

Type of bearing:

There are mainly two types of load component which have to be carried by the bearings of a machine tool spindle. They are radial load and axial load. These loads may be carried by a combination of:

(a) radial and thrust bearings

(b) angular contact bearings

(c) both (a) and (b).

The peak rolling element load in a radial rolling bearing, which theoretically (assuming rigid races) defines the deflection of the bearing, is given by the relation

$$P_{lr} = \frac{S_f \times F_r}{Z} \qquad (2.1)$$

where S_f is the load sharing factor

F_r is the radial load

Z is the number of rolling elements.

For a thrust bearing with axial load any rolling element load, which defines bearing deflection, is given by

$$P_j = \frac{F_r}{Z} \qquad (2.2)$$

Equations (2.1) and (2.2) show that the peak rolling element load (and hence bearing deflection) is greater for radial bearing by the load-sharing factor S_f. For radial roller bearings $S_f = 4.08$, and for radial ball bearings, $S_f = 4.37$, with zero play. In practice, bearing races are not of course rigid, and the rolling element load distribution in a radial bearing

may change significantly due to deflections of the races under load, with resulting effects on the load-sharing factor, and overall bearing performance. This represents a major area for investigation.

In the case of thrust bearings with axi-symmetric races and housings, the change in rolling element load distribution due to true axial load is small to negligible as the change in geometry of the tracks perpendicular to the direction of rolling (which is responsible for the load distribution), is insignificant, though the races are compressed uniformly in this direction. Similar considerations apply to some extent for the effects of radial and axial components of load on an angular contact bearing.

The most rigid form of rolling bearing is the 'line contact' or roller type, and thus for this and the reasons mentioned earlier, the present investigation is mainly concerned with radial cylindrical roller bearings. However, similar considerations and principles would apply to the other types of radial bearings.

Size of bearing:

The circular pitch of roller spacing in a radial roller bearing is given by

$$\text{circular pitch} = \frac{\pi}{Z} \quad (D_o - d) \qquad (2.3)$$

where D_o is the outer race diameter

d is the roller diameter.

As one of the main interests is to find the effect of race deformation on roller load distribution, at least 5 rolling elements in one quarter of the bearing has been deemed desirable, giving the total number of rollers in the bearing, $Z = 20$. The only exception to this bearing configuration concerned a study of the effect of the number of rollers on rigidity of bearings when considering rigid races.

The dimensions of the various bearing components chosen are as follows:

Outer race diameter = D_o = 3.0 in. (76.2mm)

Inner race diameter = D_i = 2.4 in. (60.96mm)

Roller diameter = d = 0.3 in. (7.62mm)

Length of roller = ℓ = 0.45 in. (11.43mm)

The above roller and race diameters give circular pitch of roller spacing to roller diameter ratio of 1.414, which leaves reasonable space between the rollers for the cage. The length of rollers was chosen taking the length to diameter ratio of roller (ℓ/d) to be 1.5. The

clearance, or interference, in the bearing can be obtained by varying the diameter of either the races or the rollers.

2.3 CONTACT STRESSES

For inelastic bodies in contact under load, contact stresses would be infinite due to zero contact areas. All materials are of course elastic; however, as the resulting contact areas are normally small, large contact stresses are usual, even for moderate loads. The surface compressive stresses in a rolling bearing may well be of the order of 200,000 lb/in^2 (13.79×10^2 MN/m^2) or even larger. The magnitude of compressive stress decreases rapidly with depth below contact area. Stress distribution inside the material affects the fatigue life of the bearing and is considered in detail in refs. 26, 27. Some of the final results are used in deriving the equivalent radial load in section 5.7. However, for the purpose of distributing the roller load in the contact area (in subroutine NPF of the finite element program of chapter 5) it is only necessary to consider the stress distribution at the surface. This will be considered here.

Fig. 2.1 shows the surface stress distribution between two cylindrical bodies in contact. The contact area is shown in an exaggerated scale for clarity. According to Hertz the surface stress distribution in the contact area is semi-elliptical. This may be expressed as:

$$\sigma = \sigma_{max} \left[1 - \left(\frac{x}{b}\right)^2\right]^{\frac{1}{2}} \qquad (2.4)$$

Now, the total load acting on the contact is

$$P = \ell \int_{-b}^{b} \sigma \, dx = \ell \sigma_{max} \int_{-b}^{b} \left(1 - \frac{x^2}{b^2}\right)^{\frac{1}{2}} dx$$

$$= \frac{\pi b \ell}{2} \sigma_{max}$$

therefore $$\sigma_{max} = \frac{2P}{\pi b \ell} = \frac{4}{\pi} \cdot \frac{P}{2b\ell} = \frac{4}{\pi} \sigma_m \qquad (2.5)$$

where σ_m = mean surface stress.

The surface stress distribution from equation (2.4) is given by

$$\sigma = \frac{2P}{\pi b \ell} \left[1 - \left(\frac{x}{b}\right)^2\right]^{\frac{1}{2}} \qquad (2.6)$$

According to Hertz the half-width, b, of contact area for line contact is given by

$$b = \sqrt{\frac{4P}{\pi \ell \Sigma(\frac{1}{r})} \left(\frac{1}{E'_1} + \frac{1}{E'_2}\right)} \qquad (2.7)$$

Where the material constants E'_1 and E'_2 for the contacting bodies are given by

$$E'_1 = \frac{E_1}{1 - \frac{1}{m_1^2}} \quad , \qquad E'_2 = \frac{E_2}{1 - \frac{1}{m_2^2}} \qquad (2.8)$$

where E_1 and E_2 are the Young's moduli and $\frac{1}{m_1}$ and $\frac{1}{m_2}$ are the Poisson's ratios of the contacting bodies.

The sum of the principal curvatures of the two bodies in contact $\Sigma(\frac{1}{r})$ in equation (2.7) is given by

$$\Sigma(\frac{1}{r}) = \frac{1}{r_{11}} + \frac{1}{r_{12}} + \frac{1}{r_{21}} + \frac{1}{r_{22}} \qquad (2.9)$$

where r_{11} = radius of body 1 in a plane in direction of rolling

r_{12} = radius of body 1 in a plane at 90° to the direction of rolling

r_{21} = radius of body 2 in a plane in the direction of rolling

r_{22} = radius of body 2 in a plane at 90° to the direction of rolling.

Curvature of the surface of a body may be positive or negative, according to whether it is convex or concave, respectively. For a cylindrical roller on flat platens denoting the roller by '1' and the platen by '2', $^1/r_{12} = {}^1/r_{21} = {}^1/r_{22} = 0$ and $^1/r_{11} = {}^2/d$ and hence the sum of principal curvatures

$$\Sigma(\frac{1}{r}) = \frac{2}{d} \qquad (2.10)$$

For a cylindrical roller in contact with an outer ring $^1/r_{12} = {}^1/r_{22} = 0$, $^1/r_{11} = {}^2/d$ and $^1/r_{21} = -({}^2/D_o)$. Thus the sum of principal curvatures at contact is

$$\Sigma(\frac{1}{r}) = \frac{2}{d} - \frac{2}{D_o} \qquad (2.11)$$

Similarly, for a cylindrical roller in contact with an inner ring, the sum of principal curvatures is given by

$$\Sigma(\frac{1}{r}) = \frac{2}{d} + \frac{2}{D_i} \qquad (2.12)$$

Tables 2.1(a) and (b) give the width of contact area 2b for steel and Araldite respectively and are represented graphically in figs. 2.2 and 2.3.

2.4 CONTACT DEFORMATION

Contact deformations are caused by contact stresses. Hertz originally (about 1880 - 81) derived the deformation of elastic bodies of any curvature while in contact under pressure. His investigations were not specifically related to bearings, but his deductions have generally been accepted as the basis for subsequent work. Later, the knowledge of contact stresses and deformation has been advanced by theoretical analyses, and with experimental confirmation by Stribeck (reported in ref. 28), Goodman(29 - 31), Palmgreen(32) and others. Thus several such formulae exist some being theoretically, and others empirically based. Some only of the formulae for line contact deformation will be involved here.

Bochmann established empirically an approximate formula for the mutual approach of two steel bodies with line contact

$$\delta = \frac{1.105 \times 10^{-7} P}{\sqrt[3]{d} \times \ell} \quad \text{ins.} \tag{2.13}$$

where P is the load acting on the contacting bodies in lbs. and d and ℓ are the diameter and length respectively of the roller in ins.

If the bodies are made of materials other than steel, the deflection can be found from the above equation by multiplying the deflection obtained by a combination constant α. If the elasticity constants for steel are denoted by 'st' and those of the other two materials by '1' and '2', the combination constant is

$$\alpha = \tfrac{1}{2} \cdot E'_{st} \left[\frac{1}{E'_1} + \frac{1}{E'_2} \right] \tag{2.14}$$

where material constant for steel E'_{st} is given by

$$E'_{st} = \frac{E_{st}}{1 - \frac{1}{m_{st}^2}} \tag{2.15}$$

and material constants E'_1, and E'_2 for the contacting bodies are given by equation (2.8).

Föppl deduced analytically the 'mutual approach' for two bodies with line contact, given by

$$\delta = \frac{2}{\pi E} \left(1 - \frac{1}{m^2}\right) \frac{P}{\ell} \left[1.207 + \log_e \frac{\ell E}{P \Sigma(\frac{1}{r})} \right] \tag{2.16}$$

where the sum of the principal curvatures of the two contacting bodies is given by equation (2.9) for the general case, and by equations (2.10), (2.11), (2.12) for the particular cases of cylindrical rollers in contact with a flat platen, and with outer and inner races respectively. Equation (2.16) for steel becomes

$$\delta = 45 \times 10^{-9} \times \frac{P}{\ell} \left[7.4 - \log_{10} \frac{P\Sigma(\frac{1}{r})}{4\ell} \right] \qquad (2.17)$$

According to Allan[28] this expression gives values that are too low, presumably due in part to the effect of edge pressure (discussed in chapter 4) and he suggested the following modification

$$\delta = 45 \times 10^{-9} \times \frac{P}{\ell} \left[8.4 - \log_{10} \frac{P\Sigma(\frac{1}{r})}{4\ell} \right] \qquad (2.18)$$

This change has no theoretical basis. However, for comparing the different formulae of deflection, the original Föppl formula given by equation (2.16) is used.

Palmgren (32) gives an expression for the approach between the axis of a cylindrical body of finite length pressed between two plane-surfaced bodies of infinite extension and a distant point in either of the support bodies

$$\delta = 4.36 \times 10^{-7} \theta_1^{2.7} \frac{P^{0.9}}{\ell^{0.8}} \qquad (2.19)$$

where P is in lbs. and ℓ is in inches. This expression was originally given in metric form in ref. 32 and has been converted for the units used here. The above formula is valid, if all the three bodies are of the same material, and is also applicable to the conditions which exist in normal roller bearings. From equation (2.19) it is apparent that the diameter of the roller does not affect the deflection. Material constant θ_1 in the above equation is given by

$$\theta_1 = \sqrt[3]{\frac{1.643 \times 10^{+7} \, (E_1' + E_2')}{E_1' \, E_2'}} \qquad (2.20)$$

where E_1' and E_2' are as defined in equation (2.8) and are in lb/in^2 units. A similar formula is also given by Lundberg.

Dowson and Higginson (10) derived the expression for the deflection of a cylindrical roller and its race. This is given by

$$\delta = \frac{P\theta_2}{\ell}\left[\log_e \frac{\ell d}{2P\theta_2} - 0.22 + \log_e \frac{2h}{d}\right] \qquad (2.21)$$

where

$$\theta_2 = \frac{2}{\pi E'} \qquad (2.22)$$

E' is as in equation (2.8).

The deflection given by the above expression is the approach between the axis of the roller and a point at depth h below the surface of the platen. In conventional bearings h is approximately equal to d/2. The term $\log_e (\frac{2h}{d})$ is small in comparison with the others, and hence is not very significant.

From experimental results, Hoffmann Manufacturing Co., Ltd., (33) obtained the relationship for the approach of the axis of a roller loaded between two platens, towards either platen. This is given by

$$\delta = \frac{0.42\ P^{0.9}}{10^6\ \ell^{0.7}} \qquad (2.23)$$

It should be noted that all the above formulae for deflection give the deflection at one of the contact areas. To obtain the total deflection for a roller loaded between two platens, or the mutual approach of the two platens, the calculated deflection must be doubled.

All the deflection formulae given above are either in the form, or can be expressed with sufficient accuracy, in the form

$$\delta = A_1 P^N \qquad (2.24)$$

where A_1 and N are constants. The constant A_1 depends on the material properties, dimensions (especially length of roller) and to some extent (as found in some of the previous equations) upon the geometry of the contacting bodies. The constant N represents the non-linearity of the deflection vs. load curve. For the Bochmann formula N = 1 (i.e. a linear relationship). For all other formulae given above N is close to 0.9.

2.5 COMPARISON OF THE CONTACT DEFORMATION FORMULAE

The total deflections (i.e. due to both contact areas) of a steel roller loaded between steel platens as calculated by computer from the different formulae given in the previous section (equations (2.13), (2.16), (2.19), (2.21) (2.23)), are given in table 2.2 and shown graphically in fig. 2.4. The first four formulae were also used to calculate the deflections for Araldite, and the results are given in table 2.3 and shown graphically in fig. 2.5. For steel the differences in deflections given the different formulae (fig. 2.4) are less than those for Araldite (fig. 2.

For Araldite the highest value for deflection is given by the formula due to Bochmann and the lowest by that due to Dowson and Higginson. The deflection given by the former formula at the far end of the load scale is more than double the value given by the latter formula. For steel the highest value for deflection is given by the Palmgren formula and the lowest by the Dowson and Higginson formula. Here the deflection given by the former formula at the far end of the load scale is about 1.25 times more than the value given by the latter formula. It should be noted that for Araldite the value of Young's modulus taken was 2730 lb/in^2. (18.82 MN/m^2) and Poisson's ratio was 0.5.

These formulae were compared subsequently with experimental and finite-element results and will be discussed in the relevant chapters. It may be stated here that the Palmgren formula gives results which agree quite well with the experimental and the finite-element results (both being for Araldite rollers and platens, the platen width being equal to the length of the rollers).

2.6 DEFLECTION FOR HOLLOW ROLLERS

When a hollow roller is loaded between two platens as shown in fig. 2.6(b), the total deflection is given by the deflection at the contact areas plus the deflection of the hollow roller as a cylinder. When a cylinder is loaded in diametral compression as shown in fig. 2.6(a), the decrease in diameter in the direction of load is given (see for example refs. 34, 35) by

$$\Delta d = \frac{2Pr_m^3}{EI} \left(\frac{1}{\pi} - \frac{1}{4}\right) \qquad (2.25)$$

and more exactly the decrease is

$$\Delta d = \frac{2Pr_m^3}{EI} \left(\frac{A}{A'} \cdot \frac{1}{\pi} - \frac{1}{4}\right) \qquad (2.26)$$

where

r_m is the mean diameter of the ring

I is the moment of inertia of cross sectional area of the ring about the neutral axis

A is the cross-sectional area of the ring

A' is the modified area according to ref. 34.

For a rectangular cross section

$$\frac{A'}{A} = 1 + \frac{1}{12}\left(\frac{h}{r_m}\right)^2 + \frac{1}{80}\left(\frac{h}{r_m}\right)^4 + \cdots$$

where h is the cylinder radial thickness

As A/A' is nearly equal to 1, equation (2.25) gives the decrease in diameter of the cylinder to a good approximation.

When this diametral deflection is added to the deflections at the two contact areas given by any of the previous formulae, e.g. the Föppl formula (equation 2.16), the total deflection given by the approach of the two platens when a hollow roller is loaded between them is obtained. The total deflection thus obtained for Araldite is given in table 2.4 and shown graphically in fig. 2.7.

2.7 LOAD DISTRIBUTION IN A STATICALLY LOADED BEARING

The calculation of load distribution among the rolling elements of a rolling bearing presents four main problems, (1) the support of the inner ring by a number of rolling elements represents a statically indeterminate structure, (2) the load deflection relationship of the rolling elements and races is non-linear, (3) play or interference (pre-load) may be present in the bearing and (4) the races do not retain their circular shape on loading. For the moment, point (4) will not be considered, and it will be assumed for all the cases considered in the present chapter 2, and chapter 3, that the races are rigid and retain the circular shape on loading.

Definition of radial clearance

Radial clearance of a radial rolling bearing is defined as the amount by which the inner race is smaller in radius than the radius required for size-to-size metal contact of the rolling elements and the races as shown in fig. 2.8(a).

If the radial clearance is negative the bearing is said to have some interference or preload. In this case the rolling elements are compressed and exert a force on the races without an application of external load as shown in fig. 2.8(b).

2.7.1 STRIBECK'S SOLUTION

The method of calculation originally developed by Stribeck (see for instance ref. 28) and in widespread current use is based on the assumptions of zero clearance, and rigid races.

The unloaded position of the bearing is shown dotted in fig. 2.9. If the inner race is displaced radially downwards by δ_r when a radial load F_r acts on the bearing all the rolling elements in the lower half of the bearing are loaded as shown in fig. 2.9. The deflection at the rolling element position directly under the radial load, δ_1 is greatest

and is equal to the bearing deflection δ_r. The deflections at the other rolling element positions are

$$\delta_2 = \delta_r \cos \phi = \delta_1 \cos \phi \qquad (2.27)$$

$$\delta_3 = \delta_r \cos 2\phi = \delta_1 \cos 2\phi$$

and so on, where $\phi = 2\pi/Z$ is the angular pitch between two consecutive rolling elements, and Z is the number of rolling elements.

The load-deflection relationship of equation (2.24) for a rolling element loaded between the races can be expressed as

$$P = K_2 \delta^t \qquad (2.28)$$

where K_2 (for two contact areas) is a constant depending on the material and geometry of the contacting bodies and t represents the non-linearity of the load vs. deflection curve. For point contact t = 1.5 and for line contact t = 1.11 (or other values depending on the formula used as described earlier). K_2 and t can be expressed in terms of A_1 and N used in equation (2.24) as

$$t = {}^1/_N, \quad K_2 = \left(\frac{1}{A_2}\right)^{1/N} = \left(\frac{1}{2A_1}\right)^{1/N} \qquad (2.29)$$

From equation (2.28),

$$\frac{P_1}{\delta_1^t} = \frac{P_2}{\delta_2^t} = \frac{P_3}{\delta_3^t} = \text{etc.} = K_2 \qquad (2.30)$$

The deflections and load distribution at the different rolling element positions are as shown in fig. 2.9.

From equations (2.27) and (2.30)

$$P_2 = P_1 \left(\frac{\delta_2}{\delta_1}\right)^t = P_1 \cos^t \phi$$

$$P_3 = P_1 \left(\frac{\delta_3}{\delta_1}\right)^t = P_1 \cos^t 2\phi \qquad (2.31)$$

and so on.

The equilibrium equation for the complete bearing can be written as

$$F_r = P_1 + 2P_2 \cos\phi + 2P_3 \cos 2\phi + \ldots + 2P_n \cos(n-1)\phi \qquad (2.32)$$

where P_n is the rolling element load at or near the 90° position to the radial load, and n is the nearest integer from (Z+3)/4.

From equation (2.31) and (2.32)

$$F_r = P_1 + 2P_1 \cos^{t+1}\phi + 2P_1 \cos^{t+1} 2\phi + \ldots + 2P_1 \cos^{t+1}(n-1)\phi$$

or

$$\frac{F_r}{P_1} = \left[1 + 2(\cos^{t+1}\phi + \cos^{t+1} 2\phi + \ldots + \cos^{t+1}(n-1)\phi)\right] = M \qquad (2.33)$$

Stribeck found that, for ball bearings M increased with increase in Z, but the ratio Z/M remained approximately constant at 4.37. For roller bearings (taking t = 1.11) Z/M is constant at 4.08 (as found from the computer results). The factor Z/M is called the load-sharing factor and is represented by

$$S_f = \frac{Z}{M} = \frac{ZP_1}{F_r} \qquad (2.34)$$

As this calculation is based on the assumption of perfect geometry, Stribeck found it necessary to increase the factor S_f to 5 to allow for the geometrical errors in the bearing (which may be due to play or small departures from accuracy in the bearing).

After finding the peak rolling-element load from equation (2.33) or equation (2.34) the deflection of the bearing, (theoretically equal to that at the peak rolling element position), may be found using equation (2.28). The load distribution in the bearing can be found from the equations (2.31).

2.7.2 BEARING WITH PLAY OR INTERFERENCE BUT OTHERWISE IDEAL GEOMETRY

Stribeck's solution is valid when the geometry of the bearing is ideal. In this section the case where there is geometrical imperfection, in particular the cases of radial play and interference in the bearing will be examined. It is assumed that apart from play or interference, the geometry of the bearing is ideal, i.e. the rolling elements are identical in size, true in geometry, and the races remain circular.

The radial clearance in the bearing, which is given by

$$c = \frac{D_o - D_i}{2} - d \qquad (2.35)$$

is treated algebraically, thus a negative value of c indicates an appropriate 'negative play' or preload. This convention is followed throughout the thesis.

If the inner ring is given a deflection δ_r from centred position in the outer race (fig.2.10), the deflection at any rolling element position

j, noting that a rolling element can carry compression but not, of course, tension, represented by the notation

$$\begin{aligned} \{\delta_j\} &= \delta_r \cos\psi_j - c \quad \text{when } \delta_r \cos\psi_j - c \geqslant 0 \\ \{\delta_j\} &= 0 \qquad\qquad\quad \text{when } \delta_r \cos\psi_j - c < 0 \end{aligned} \tag{2.36}$$

The brackets $\{\}$ represent an unilateral quantity.

For a bearing with positive clearance, some of the rolling elements in the lower half (external load is downwards) will be loaded. For a zero-play bearing all the rolling elements in the bottom half will be loaded. For negative clearance bearing either all or more than half of the rolling elements will be loaded depending on the radial load. At zero external radial load each rolling element will transmit load due to preload. When a radial load is applied on the bearing the load on the bottom half of rolling elements will increase while that of the top half will decrease. With increase in radial load the radial deflection of the bearing will increase and at some point the top rolling element will be released. With further increase in radial load more and more of the rolling elements at the top will be un-loaded.

The load transmitted by the j th rolling element can be found from equation (2.28), i.e.

$$P_j = K_2 \{\delta_j\}^t \tag{2.37}$$

For equilibrium

$$F_r = P_1 + 2P_2 \cos\phi + 2P_3 \cos 2\phi + \ldots + \tau P_n \cos(n-1)\phi \tag{2.38}$$

where

$$n = \frac{Z+2}{2}, \quad \tau = 1 \text{ when Z is even}$$

$$n = \frac{Z+1}{2}, \quad \tau = 2 \text{ when Z is odd}$$

using equation (2.37)

$$\frac{F_r}{P_1} = 1 + \frac{2}{(\delta_r - c)^t} \left[\{\delta_r \cos\phi - c\}^t \cos\phi + \{\delta_r \cos 2\phi - c\}^t \cos 2\phi + \ldots + \tau/2 \{\delta_r \cos(n-1)\phi - c\}^t \cos(n-1)\phi \right] \tag{2.39}$$

Equation (2.39) can be solved to find δ_r, expressing P_1 in terms of deflection. The solution is difficult due to the non-linearity of the equation. However, numerical methods (e.g. Newton-Raphson method) can be used, and this is of course most conveniently carried out by a digital computer.

Alternatively, the inner race can be given a series of deflections δ_r and the corresponding radial loads F_r can be calculated. The deflection at any intermediate radial load can be found by interpolation. The load distribution can then be found using equations (2.36) and (2.37). This method is quite simple, takes little computer time and is particularly suitable when the deflection is given, or when a large number of results are required (e.g. when the characteristics of bearings have to be compared.

COMPUTER PROGRAM 'RRBC':

A computer program 'RRBC' was developed to find the bearing deflection, load distribution etc., using this method. The version of the program for steel roller bearings is given in the computer program section. In the program distinction is made between δ and δ_r as

δ_r = deflection of the bearing given by radial deflection of inner race from centered position in outer race.

δ = deflection of the bearing after the peak roller is loaded.

Thus $\delta = \delta_r - c$ for positive clearance bearing

$\delta = \delta_r$ for zero or negative clearance bearing.

2.7.3 AN ITERATIVE METHOD FOR BEARING WITH PLAY OR INTERFERENCE, BUT OTHERWISE IDEAL GEOMETRY

It will be assumed, as in the previous section, that the geometrical shapes of the rolling elements and races are perfect. The radial 'clearance' (positive or negative) is given by equation (2.35).

When a rolling bearing is loaded by a radial load F_r the inner ring will deflect from centered position in the outer ring by δ_r and deform the rolling elements in the loaded zone $\pm \psi_\ell$ as shown in fig. 2.10. The deflection at the peak rolling element position (for which $\psi = 0$), is given by

$$\delta_1 = \delta_r - c \qquad (2.40)$$

The deflection at any rolling element position j is given by

$$\delta_j = \delta_r \cos\psi_j - c \qquad (2.41)$$

$$= \frac{\delta_1}{\delta_r - c} \left[\delta_r \cos\psi_j - c\right]$$

$$= \frac{\delta_1}{\delta_r - c} \left[\delta_r - c - \delta_r (1 - \cos\psi_j)\right]$$

$$= \delta_1 \left[1 - \frac{1}{(1-\frac{c}{\delta_r})} \ (1 - \cos \Psi_j)\right]$$

or

$$\delta_j = \delta_1 \left[1 - \frac{1}{2\epsilon} (1 - \cos \Psi_j)\right] \qquad (2.42)$$

where

$$\epsilon = \tfrac{1}{2} \left(1 - \frac{c}{\delta_r}\right) \qquad (2.43)$$

ϵ depends on the extent of loaded zone as shown in fig. 2.10, and is the ratio of the projected load zone on the inner race diameter to the inner race diameter. For positive clearance bearing $\epsilon < 0.5$ and for negative clearance bearing $\epsilon > 0.5$.

If, $\epsilon < 1$, then the loaded zone covers only part of the circumference,

if, $\epsilon \geqslant 1$, then the whole circumference is loaded,

if, $\epsilon = 0.5$, then half the circumference is loaded (as for zero-clearance bearing).

The angular extent of loaded zone can be found from equation (2.41) by putting $\delta_j = 0$.

$$\Psi_\ell = \cos^{-1} \left(\frac{c}{\delta_r}\right) \qquad (2.44)$$

From equation (2.28)

$$\frac{P_j}{P_1} = \left(\frac{\delta_j}{\delta_1}\right)^t \qquad (2.45)$$

Substituting equation (2.45) in equation (2.42)

$$P_j = P_1 \left[1 - \frac{1}{2\epsilon} \ (1 - \cos \Psi_j)\right]^t \qquad (2.46)$$

For equilibrium, summation of the vertical components of the rolling element load must be balanced by the radial load

$$F_r = \sum_{\Psi=-\Psi_\ell}^{\Psi=+\Psi_\ell} P_j \cos \Psi_j \qquad (2.47)$$

Equation (2.47) can also be written in integral form,

$$F_r = \int_{-\Psi_\ell}^{+\Psi_\ell} \frac{P_j}{\frac{\pi D_i}{Z}} \ \frac{D_i}{2} \cos \Psi \, d\psi$$

$$= Z \, P_1 \times \frac{1}{2\pi} \int_{-\Psi_\ell}^{+\Psi_\ell} \left[1 - \frac{1}{2\epsilon} \ (1-\cos\psi)\right]^t \cos\psi d\Psi$$

or

$$F_r = Z\, P_1\, J_r\,(\epsilon) \tag{2.48}$$

where

$$J_r\,(\epsilon) = \frac{1}{2\pi} \int_{-\psi_\ell}^{+\psi_\ell} \left[1 - \frac{1}{2\epsilon} \times (1-\cos\psi)\right]^t \cos\psi d\psi \tag{2.49}$$

The values of the load distribution integral are given in table (2.5) for line contact (t = 1.11) and point contact (t = 1.5).

From equations (2.28), (2.40) and (2.48)

$$F_r = Z\, K_2\, (\delta_r - c)^t\, J_r\,(\epsilon) \tag{2.50}$$

When F_r and c for a radial rolling bearing are known, δ_r can be found by trial as follows:

(a) assume a value of δ_r

(b) ϵ is calculated from equation (2.43),

(c) $J_r\,(\epsilon)$ is then found from table (2.5), if necessary, by interpolation,

(d) these values are then substituted in equation (2.50),

(e) if equation (2.50) does not balance, the process is repeated with a new value of δ_r.

Obviously, this method needs a number of iterations for convergence. To save time, the deflection of a radial rolling bearing can be found when F_r, c, Z and rolling element dimension are given, from the nomograms given in chapter 3. Two sets of nomograms (one for line contact and the other for point contact) were constructed using the above procedure. Considerable time can be saved by using these nomograms. If greater accuracy is required, the values of deflection found from them can be used as the first estimate to calculate the deflection using the above procedure. This will reduce the number of successive approximations.

After finding δ_r the load distribution in the bearing is then evaluated from equations (2.41) and (2.28).

2.7.4 GENERAL CASE FOR IMPERFECT GEOMETRICAL SHAPE, AND DYNAMIC LOADING DUE TO ROTATION, OF A RADIAL ROLLING BEARING

The following is a general method for radial rolling bearings having imperfect geometrical shape (due possibly to out-of-roundness of the races and non-uniform diameters of the rolling elements) and subjected to

high rotational speeds. The cases dealt with previously now represent a particular case of the present solution. Fig. 2.11 shows a radial bearing with (exaggerated) imperfect geometrical shape.

The radial clearance here is a variable quantity, and at any rolling element position j it is given by

$$c_j = G_j - d_j \tag{2.51}$$

where G_j is the radial distance (or gap) between the outer and inner race at rolling element position j,

d_j is the diameter of the rolling element j.

The forces acting on any rolling element j of the bearing is shown in the lower right hand corner of fig. 2.11. From equilibrium considerations, for this single rolling element

$$P_{oj} - P_{ij} - F_c = 0 \tag{2.52}$$

where F_c is the centrifugal force on the rolling element and subscripts 'i' and 'o' refer to inner and outer races respectively.

Substituting expressions of the form of equation (2.28), for a single contact area

$$K_1 \delta_{oj}^t - K_1 \delta_{ij}^t - F_c = 0 \tag{2.53}$$

where δ_{oj} is the deflection at the outer race contact at rolling element position j,

δ_{ij} is the deflection at the inner race contact at rolling element position j,

K_1 is the constant as described in equation (2.28) for a single contact area.

It should be noted that K_1 may differ for the inner and outer races due to the different curvatures, in which case this should be taken into account in the above equation. However, in many cases the effect may be negligible especially for cylindrical roller bearings, which are of primary interest in this study. K_1 may be written in terms of A_1 (or A_2) and N, as used in equation (2.24), thus

$$K_1 = \left(\frac{1}{A_1}\right)^{1/N} = \left(\frac{2}{A_2}\right)^{1/N} \tag{2.54}$$

The total deflection at the rolling element position j is

$$\begin{aligned} \delta_j &= \delta_{ij} + \delta_{oj} \\ &= \delta_r \cos\psi_j - c_j \geqslant 0 \end{aligned} \tag{2.55}$$

$\delta_j \geqslant 0$ indicates that rollers cannot be loaded in tension, thus negative values of δ_j are taken as zero.

From equations (2.53) and (2.55)

$$(\delta_j - \delta_{ij})^t - \delta_{ij}^t - \frac{F_c}{K_1} = 0 \qquad (2.56)$$

or

$$(\delta_r \cos\psi_j - c_j - \delta_{ij})^t - \delta_{ij}^t - \frac{F_c}{K_1} = 0 \qquad (2.57)$$

From the equilibrium conditions of the complete bearing,

$$F_r = \sum_{j=1}^{Z} P_{ij} \cos\psi_j \qquad (2.58)$$

or

$$\frac{F_r}{K_1} - \sum_{j=1}^{Z} \delta_{ij}^t \cos\psi_j = 0 \qquad (2.59)$$

Equations (2.57) and (2.59) represent a system of (Z+1) simultaneous non-linear equations with unknowns δ_r and δ_{ij}. They can be solved by using the Newton-Raphson method (see for example ref. 36). The method is given in appendix 2.1.

After finding the deflections at the different roller positions, the load distributions at inner and outer races can be found from

$$P_{ij} = K_1 \delta_{ij}^t \qquad (2.60)$$

$$P_{oj} = K_1 \delta_{ij}^t + F_c \qquad (2.61)$$

A computer subroutine 'DTBN' was developed to solve the equations, using the method described in appendix 2.1, and to find the load distribution in a radial roller bearing. This subroutine is used in the main finite-element program.

2.8 CENTRIFUGAL FORCE OF THE ROLLING ELEMENTS

If the inner and outer races of a radial rolling bearing are rotating with speeds n_i and n_o r.p.m. respectively, the angular speeds in rad./sec. are given by

$$\omega_i = \frac{2\pi n_i}{60} \quad , \qquad \omega_o = \frac{2\pi n_o}{60} \qquad (2.62)$$

The surface velocity of the inner and outer races are

$$v_i = \tfrac{1}{2}\omega_i D_i = \frac{\pi n_i}{60} D_i \qquad (2.63)$$

$$v_o = \tfrac{1}{2}\omega_o D_o = \frac{\pi n_o}{60} D_o \qquad (2.63)$$

The linear speed of the cage and the axis of the rolling elements, assuming that no slip occurs at the contact areas, is the mean of the inner and outer race surface velocities

$$v_c = \tfrac{1}{2}(v_i + v_o)$$

$$= \frac{\pi}{120}(n_i D_i + n_o D_o) \qquad (2.64)$$

The linear speed of cage is also

$$v_c = \omega_c \frac{D}{2} = \frac{\pi n_c D}{60} \qquad (2.65)$$

where D is the pitch diameter of rolling elements ($= D_i + d$).

From equations (2.64) and (2.65) the angular speed of cage is

$$n_c = \tfrac{1}{2}\left(n_i \frac{D_i}{D} + n_o \frac{D_o}{D}\right) \qquad (2.66)$$

The centrifugal force in the case of a cylindrical roller is given by

$$F_c = \rho\, \pi\left(\frac{d}{2}\right)^2 \ell \cdot \frac{D}{2}\left(\frac{2\pi n_c}{60}\right)^2 \text{ lbs.} \qquad (2.67)$$

where ρ is the mass density of roller material in $\text{lb.sec}^2/\text{in}^4$.

2.9 CAPACITY OF BEARINGS

2.9.1 BASIC STATIC CAPACITY OF BEARINGS

With the high peak stresses in rolling bearings, permanent deformations appear, even under very low loads, and increase with increasing load. The question is how much permanent deformation can be tolerated for satisfactory functioning of the bearing. According to Palmgren (32) permanent deformations have negligible influence on the functioning of the bearing if their magnitude at any one contact point is less than 0.0001 times the diameter of the rolling element. If the deformations are much larger, the cavities formed on the raceway cause the bearing to vibrate and thus become noisier when running, even though the bearing friction does not noticeably increase.

From the above observations the basic static capacity C_s of a bearing is defined as that load which, acting on the bearing, causes a permanent deformation of 0.0001d at the position of maximum load, and on the inner (weaker) race.

According to Palmgren (32) the permanent deformation for line

contact between steel roller and track is given by the following relation

$$\delta_s = \frac{1.98 \times 10^{-17}}{d^2} \left[\frac{P}{\ell} \left(\frac{1}{1 \mp \frac{d}{D}} \right)^{\frac{1}{2}} \right]^3 \qquad (2.68)$$

where the upper sign is for inner and lower sign is for outer raceway.

D is the pitch diameter of the rolling elements.

Using the above definition of basic static capacity and equation (2.68), the maximum rolling element load P_{max} at the basic static capacity for the roller bearing dimensions chosen in section 2.2, i.e d = 0.3 in. (7.62mm.), D = 2.7 in. (68.58mm.), is 2185 lbs.(9.73 KN) considering the inner race.

2.9.2 BASIC DYNAMIC CAPACITY AND LIFE OF BEARINGS

The basic dynamic capacity C of a radial rolling bearing is defined as that constant stationary radial load which 90 per cent (L_{10}) of a group of apparently identical bearings with stationary outer ring can endure for one million revolutions of the inner ring before the first evidence of fatigue develops. Lundberg and Palmgren performed extensive tests to determine the basic dynamic capacities of different types of rolling bearings (see papers refs. 26, 27, and book ref. 12).

The fatigue life of a rolling bearing is the number of revolutions (or hours at a given constant speed) ~~for~~ which 90 per cent of a group of apparently identical bearings will run or exceed, before the first evidence of fatigue develops. The life of a bearing in millions of revolutions (mr) of the inner race when a radial load F_r acts upon it, is given by

$$L_{10} = \left(\frac{C}{F_r} \right)^p \qquad (2.69)$$

For line contact with both rings the exponent p = 4, and for point contact with both rings p = 3. If the outer race is rotating with respect to load, the radial load, F_r should be multiplied by a rotation factor 'V', in this case 1.2.

Another definition of life is the median life L_{50}, i.e. the life which 50 per cent of a group of apparently identical bearings will endure. The relation between these two definitions of life is approximately given by $L_{50} = 5L_{10}$, and is based on fatigue stress/cycle data of different research workers.

Generally, the basic dynamic capacity is calculated for zero clearance of the bearing as in refs. 26, 27. If either play or interference

is present the equivalent load P_r should be used instead of F_r and equation (2.69) becomes

$$L_{10} = \left(\frac{C}{P_r}\right)^p \qquad (2.70)$$

The determination of equivalent load of a bearing, when the rolling element load distribution is known, is given in chapter 5.

Alternatively, when play or interference is present the corresponding capacity of the bearing may be found by the method of Rumbarger (11). This value of capacity may then be used in equation (2.69) to find the life of the bearing.

2.10 EXPERIMENTAL REPRESENTATION OF RIGID RADIAL ROLLING BEARINGS

The load distributions in radial rolling bearings presented in this chapter are all based on the assumption that the races are rigid and retain their circular shape under load. This can be represented experimentally by making the races 'infinitely' rigid in comparison to the rigidity of the rollers, by using materials having widely differing values of Young's modulus. This method was used by Datta (16), who used aluminium as the race material and Araldite epoxy resin for the rollers. Young's modulus of aluminium is approximately four thousand times that of Araldite at the stress freezing temperature, making the race deformations negligible compared with the rollers. Of course, by using Araldite races the normal case where these are also subject to deformations can be simulated.

CHAPTER 3 CALCULATED PERFORMANCE FOR BEARINGS WITH RIGID RACES

3.1 GENERAL

Using the method given in section 2.7.2 of the previous chapter a computer program RRBC (rigid race bearing calculations) was developed to calculate mainly roller load distribution, load sharing factor, radial deflection and stiffness (both average and incremental) of rolling bearings when the size of the different components of the bearing (from which the radial clearance can be found), number of rolling elements, radial load and the material properties are given. The life of the bearing was also calculated in the program using subroutine BLIFE. Both the programs RRBC and BLIFE were developed for roller and ball bearings, but only the versions for roller bearings are given in the computer program section.

Nomograms and graphs were prepared to solve radial rolling (both roller and ball) bearing problems, and are given in the later part of this chapter. Considerable time and labour can be saved by using these nomograms and graphs.

The assumption throughout this chapter, as in section 2.7.2 of the previous chapter, is that the bearing races are rigid, and retain their circular shape on loading.

The sizes of the bearing components used for the present calculations are as given in section 2.2 of the last chapter. The number of rolling elements was varied (Z= 10, 15, 20, 25). The clearance was varied by making small changes in the diameter of the inner race. Calculations were made for both Araldite (for comparison with experiments) and steel, but the results for steel only will be presented here.

3.2 THE LOAD ZONE FACTOR, ϵ

This factor, defined by equation (2.43) of the previous chapter, represents the projection of loading arc onto the bearing diameter, and is a measure of the extent of loaded zone.

As the load carried by any rolling element is proportional to δ_j^t, the rolling element load distribution depends upon the factor ϵ, as is evident from equation (2.42). The load distribution in turn influences stiffness, load sharing factor, fatigue life, etc., of the bearing, thus

it is evident that the load zone factor ϵ influences the bearing performance considerably. It will therefore be frequently used as a parameter throughout this thesis.

The variation of ϵ with dimensionless radial load for different values of radial clearance in a particular bearing (Z = 20), is shown in fig. 3.1. For the bearing with interference, ϵ decreases with increasing radial load, because the load on the top rollers decreases and they are progressively released from load. The curves ultimately become asymptotic to the curve for the zero play bearing, for which ϵ is constant at 0.5. For positive clearance bearings, the number of rollers supporting the load increases with radial load, and hence ϵ increases. Thus the maximum arc of load-bearing contact for positive clearance tends to subtend an angle 180° (as $\epsilon \rightarrow 0.5$) and at this point approximately half of the rollers are loaded.

The variation of ϵ with radial clearance is shown clearly in fig. 3.2, indicating a much greater effect for negative clearance than for positive clearance. The increase in ϵ with increase in interference becomes linear after $\epsilon = 0.7$.

3.3 EXPLANATION AND ANALOGY FOR STIFFNESS OF PRELOADED-BEARINGS

Swanson in ref. 8 cites the analogy of a 'bolt and spacer' to show why the axial stiffness for a pair of preloaded duplex angular contact bearings under axial load increases. The analogy can also be used to explain the deflection vs. load characteristics of a preloaded radial rolling bearing under radial load.

Fig. 3.3 shows how the deflection vs. load curve for a bolt and spacer system is obtained from the characteristics of its elements, which in this example are both linear. The relieving element (spacer) curve is the mirror image of its actual deflection vs. load curve, and its location is determined by the initial preload. The intersection of the two curves indicates the amount of preload. The composite deflection curve can be constructed by assuming different magnitude of external load and obtaining their corresponding deflections, as shown in fig. 3.3.

At external load F_2, the spacer is completely relieved, and has no further effect on the composite curve, the composite curve thereafter being parallel to that for the bolt. Increasing the preload on the system increases F_2. It is shown in fig. 3.3 that the stiffness of the composite curve before F_2 is equal to the sum of the stiffness for each element.

Beyond F_2, though the stiffness of the system is equal to the stiffness of the bolt k_b, its deflection is lower than the deflection of this bolt alone.

In the case of preloaded radial bearings the lower half of rolling elements can be assumed to be equivalent to the bolt (because load on these elements increases with external radial load) and the upper half of rolling elements can be assumed to be equivalent to the relieving element or 'spacer' (these elements are relieved with increase in external load).

The composite curve of fig. 3.4, for the preloaded bearing is obtained in the same way as for the bolt and spacer assembly. This figure also shows that up to a certain external load (i.e. for $\epsilon > 1.0$) the stiffness of the complete bearing is nearly twice that for the upper or lower half rollers alone, i.e. nearly twice the stiffness of a zero-clearance bearing, as may be seen in fig. 3.4. With increase in the external load (i.e. for $\epsilon < 1.0$) the stiffness of the complete bearing decreases, to approach the stiffness of the lower half rollers (or zero-clearance bearing). However, when all the top half rollers are relieved, although the incremental stiffness is the same as for zero clearance, the deflection of the bearing is much lower, and hence the average stiffness is increased.

It may be seen in fig. 3.3 or 3.4 that the deflection vs. load curve for the lower half rollers (equivalent to the bolt) below preload has no effect on the total deflection vs. load curve for the complete bearing. The deflection vs. load curve for (zero-clearance) ball bearings has greater non-linearity than for roller bearings, i.e. the rigidity of ball bearings (and to a lesser extent of roller bearings) is lower at low loads. For the reason mentioned, this low rigidity portion is eliminated by preloading. Thus preloading increases rigidity due to two effects:

(a) realisation of a parallel spring system, and

(b) elimination of lower stiffness portion of the deflection vs. load curve.

From the point of view of (b) the preloading of ball bearings is more significant than for roller bearings.

3.4 DEFLECTION OF RADIAL ROLLER BEARINGS

Fig. 3.5 shows deflection against load* for a radial roller bearing with various radial clearances. As would be expected from a consideration of the load distribution, the deflection is always higher for positive clearance, and increases rapidly with increasing radial load.

* load is plotted as (F_r / Ed^v), but this is not a basic dimensionless parameter

The initial slope also rises with increase in positive clearance, as the number of rollers carrying load is small under this condition, and decreases at any load with increasing positive clearance. By comparison, for interference the initial slope is much lower.

The deflection of a bearing can be found from equation (2.50) of the previous chapter, namely

$$F_r = Z K_2 (\delta_r - c)^t J_r(\epsilon) \qquad (3.1)$$

where $J_r(\epsilon)$ is the load distribution integral given by equation (2.49). K_2 is proportional to $\ell^{8/9}$. So, from equation (3.1), it is obvious that the bearing deflection decreases with an increase in the number or length of the rollers.

Fig. 3.5 shows that the deflection characteristics for negative clearance become parallel with the zero clearance case, after $\epsilon = 1.0$. Also the deflection curves for positive clearance tend to become parallel to the zero clearance case, once the rollers in the lower half are in load-bearing contact, i.e. $\epsilon \rightarrow 0.5$.

For a bearing with interference the peak roller load can be found from equation (2.28)

$$P_1 = K_2 (\delta_r - c)^t$$
$$= K_2 \delta_r^t (2\epsilon)^t \qquad (3.2)$$

Now, from fig. 3.26 it will be seen that for constant Z and F_r, P_1 is the same for a bearing with interference, having $\epsilon = 1.04$ and for a zero-clearance bearing ($\epsilon = 0.5$).

Denoting the deflections of interference and zero clearance bearings at constant peak roller load by δ_{rp} and δ_{ro} respectively,

$$P_1 = K_2 \delta_{rp}^t (2 \times 1.04)^t = K_2 \delta_{ro}^t (2 \times 0.5)^t$$

from which, $\delta_{rp} \simeq \frac{\delta_{ro}}{2}$. In other words, for $\epsilon = 1.04$ ($\simeq 1.0$) in a rigid race bearing with interference, the deflection is about 50% lower than for a bearing with zero-clearance, for the same radial load. When $\epsilon > 1.0$ the reduction in deflection is more than 50%, but as will be shown later, the attendant decrease in fatigue life is considerable.

Fig. 3.6 shows the variation of deflection with radial clearance and radial load for a bearing with rigid races. It may be seen from this figure that the surface of deflection for small interference is very steep

in comparison to the other portions of the surface and joins the surface for positive clearance at a sharp corner at the line of zero clearance. Thus the deflection decreases sharply on the introduction of interference.

The region between $\epsilon = 0.5$ and $\epsilon = 1.0$ (see also fig. 3.7) is of importance because it signifies rapidly decreasing deflection with interference, and also as will be shown later, that the maximum life attainable (due to the effect of load distribution) in a bearing lies within a range of ϵ of about $\epsilon = 0.70$ to 0.76. When $\epsilon \geqslant 1.0$, increasing interference decreases deflection slightly, but life decreases rapidly (as may be seen in fig. 3.21). The desirable interference at which the bearing is to be operated depends upon the radial load applied.

Fig. 3.7 shows the variation of deflection with radial clearance for different numbers of rollers in the bearing. It is apparent that as the number of rollers is decreased the steep sector between $\epsilon = 0.5$ and 1.0 increases and hence the range of interference through which maximum decrease in deflection is possible increases.

It should be noted that as the curves between $\epsilon = 0.5$ and 1.0 are almost parallel for any number of rollers and radial load, a given increase in interference will result in almost the same decrease in deflection within the linear portion of the curves.

Fig. 3.8 shows, for a zero-clearance bearing, the relationship between deflection and number of rollers for different radial loads. The curves are approximately rectangular hyperbolas and their equations may be derived from equation (3.1) by putting $c = 0$.

$$Z\delta_r^t = \frac{F_r}{K_2 \times J_r\ (0.5)} \qquad (3.3)$$

$$= \text{constant (when } F_r \text{ is constant).}$$

The constant depends on the radial load and the dimensions of the bearing elements, in particular the length of the rollers.

3.5 LOAD DISTRIBUTION IN RADIAL ROLLER BEARINGS

The load distributions for rigid-race bearings with different radial clearances are shown in fig. 3.9. With increase in positive clearance the 'peakiness' of the load distribution curve increases, because the number of rollers carrying load is decreasing. Conversely, peakiness decreases and the curve becomes flatter with interference. For a particular radial load, as interference increases, peakiness reaches a minimum at

ϵ = 0.76, approximately. Up to ϵ = 1.0, the roller diametrically opposite to the peak roller carried no load. As the interference is increased still further, the curves are flatter than for zero or positive clearance bearings, but they are shifted upwards and so every roller carries more load than in a zero-clearance bearing.

Fig. 3.10 shows the variation of peak roller load with radial load for values of different radial play in the bearing. Peak roller load for a bearing with interference is greater than that for zero clearance up to a certain radial load (for which ϵ = 1.04), after which the peak roller load is always less than that for the zero clearance bearing. The peak roller load for positive clearance is always greater than for zero-clearance.

Fig. 3.11 shows the variation of peak roller load with radial clearance. Peak roller load increases with increase in positive clearance, due to the reduction in the number of rollers carrying load. However, the peak roller load to radial load ratio for a particular positive clearance decreases with increasing radial load, due to the rising number of rollers carrying load.

The curves in fig. 3.11 cross at zero play. With increase in interference, peak roller load first decreases, attains a minimum at about ϵ = 0.76, and then begins to rise at a rate which increases with decrease in radial load. The curves for the component of radial load due only to the external load (shown dotted) is similar in shape to that of deflection vs. radial clearance curves (fig. 3.7). The difference between curves for P_l/F_r and P_{lr}/F_r is of course due to the preload.

Fig. 3.12 shows the effect of the number of rollers in the bearing on the variation of peak roller load with clearance, for a radial load F_r = 4000 lbs. (17.8 kN). It will be seen that the preload required to attain minimum peak roller load increases with decrease in the number of rollers.

The load sharing factor S_f, defined by equation (2.1) is plotted in figs. 3.13, 3.14 and 3.26. It should be noted that, in the equation for load sharing factor, the radial load component of the total peak roller load which is responsible for bearing deflection is used.

From figs. 3.13, 3.14 and 3.26 it may be seen that the limiting minimum value of S_f for a bearing with interference is half that for zero clearance (for which S_f = 4.08, for roller bearings). This is because the limiting minimum value of radial component of peak roller load for a preloaded bearing is half that for zero clearance (fig. 3.12).

Fig. 3.13 shows the variation of load sharing factor with radial load for different radial clearances. S_f for bearings with interference

is always lower than that for zero clearance, and increases with radial load. For positive clearance bearings S_f is always higher than that for zero clearance, and decreases with radial load.

The load sharing factor falls quite rapidly with small interference, until $\epsilon \simeq 1.0$ (see fig. 3.14), thereafter attaining a limiting value for any further increase in interference. The number of rollers influences the rate of decrease of S_f with increase in interference (for $\epsilon < 1.0$), and also the rate of increase with positive clearance.

From equation (2.48) it may be seen that

$$\frac{ZP_l}{F_r} = \frac{1}{J_r(\epsilon)} \qquad (3.4)$$

thus factor (ZP_l/F_r) depends only on ϵ, and is the load sharing factor for positive and zero clearance bearings. For interference bearings, from equations (3.4) and (2.50),

$$S_f = \frac{Z.\ P_{lr}}{F_r} = \frac{Z(P_l - \text{Preload})}{F_r}$$

$$= \frac{1}{J_r(\epsilon)} \left[1 - \frac{1}{\left(\frac{2\epsilon}{2\epsilon-1}\right)^t}\right] \qquad (3.5)$$

Thus for bearings with interference also the load sharing factor depends on ϵ. The variation of load sharing factor S_f with ϵ for radial roller bearings is shown in fig. 3.26. In this figure the variation of $(P_l Z/F_r)$ is also shown (dotted curve).

The curve for $(P_l Z/F_r)$ for interference bearings ($\epsilon > 0.5$) is the continuation of the S_f curve for positive clearance ($\epsilon < 0.5$) bearings. The value of $(P_l Z/F_r)$ attains a minimum at about $\epsilon = 0.75$ to 0.80. The value of peak roller load can be determined once ϵ is known (which can be found by trial and error, as stated in the previous chapter, or more easily from the nomograms given later in this chapter).

3.6 STIFFNESS OF RADIAL ROLLER BEARINGS

Two measures of stiffness are used, firstly incremental stiffness, i.e. the inverse of the local slope of deflection vs. load curve (fig. 3.5) and termed simply 'stiffness'. The variation of this incremental stiffness with different variables is shown in figs. 3.15 to 3.18. The second measure is termed the average stiffness, defined as the ratio of radial load

to radial deflection (F_r/δ) of the bearing. The variation of average stiffness with radial load is shown in fig. 3.19.

Fig. 3.15 shows the variation of incremental stiffness with radial load for different radial clearances. The limiting maximum incremental stiffness for an interference bearing is about twice the incremental stiffness of zero clearance bearing. With increase in load the incremental stiffness in an interference bearing decreases. A point of inflection exists when $\epsilon = 1.0$ (i.e. when the top roller is just released). With further increase in radial load the incremental stiffness curve for interference bearings joins the curve for zero clearance (as the top half of rollers are successively released, i.e. $\epsilon \rightarrow 0.5$).

Fig. 3.15 shows that incremental stiffness is minimum at about $\epsilon = 0.75$. Nevertheless, the overall bearing deflection, and hence average stiffness, depends on the total 'history' of the incremental stiffness curve before $\epsilon = 0.75$ (which represents the high stiffness portion) is reached. Thus average stiffness is not minimum at $\epsilon = 0.75$ as may be seen in fig. 3.19. For example, when the load is increased from 1000 lbs. (4.4 kN) to 6000 lbs (26.7 kN) for a 20 roller bearing with -0.0003 in. (-0.0076 mm.) interference, incremental stiffness is reduced by 42% (from fig. 3.15), but average stiffness falls by 21% (from fig. 3.19). It follows that average stiffness is less sensitive to effects such as have been described, than is incremental stiffness.

For positive clearance the incremental stiffness increases with radial load, thus when all the lower half rollers carry load (i.e. $\epsilon \rightarrow 0.5$) the curve joins that for zero clearance. In this case the low stiffness portion of the curve dictates the bearing deflection at any load, and hence average stiffness is low.

Fig. 3.16 shows the variation of incremental stiffness with radial clearance for different radial loads. The incremental stiffness increases rapidly at first with interference, passes through a point of inflection at $\epsilon = 1.0$, and then starts to flatten out. Average stiffness has a similar, though expectedly less pronounced behaviour.

The effect of the number of rollers, with radial load and clearance (figs. 3.17 and 3.18 respectively) show that the increase in incremental stiffness possible in a bearing increases with the number of rollers.

3.7 LIFE OF RADIAL ROLLER BEARINGS

The life of radial roller bearings with rigid races was calculated using the subroutine BLIFE, the development of which was based on the method given by Rumbarger (11).

According to reference 11 the basic dynamic capacity of a roller bearing is given by

$$C = \lambda f_c (\ell)^{7/9} Z^{3/4} D^{29/27} \qquad (3.6)$$

The factor for dynamic capacity f_c is a function of d/D and of ϵ. Values of (f_c/f) are given in subroutine BLIFE. The material factor is $f = 49,500$ for steel roller bearings when pound and inch units are used. The reduction factor λ takes into account the stress concentration due to edge loading (explained in chapter 4) and also due to eccentric loading. In the present calculations the value $\lambda = 1.0$ is taken (this value represents accurately guided rollers with modified line contact for both races).

Following evaluation of basic dynamic capacity, the life of the bearing in millions of revolutions (mr) is calculated from equation (2.69), which assumes that the inner race is rotating with respect to load (for outer race rotation, a value $1.2F_r$ is taken as the external load). Rumbarger (11) has taken the value $p = 10/3$ for roller bearings.

Roller bearing life is plotted in figs. 3.20 to 3.22. Fig. 3.20 shows that the life for bearings with interference is lower than for zero-clearance, up to a radial load, for which $\epsilon \simeq 0.9$, whence ϵ decreases, and life becomes slightly greater than for zero clearance.

Fig. 3.21 shows the decrease in life with increase in positive clearance. Maximum life occurs for a bearing with interference, in the region $\epsilon = 0.70$ to 0.76. For example, if the clearance of a bearing with a radial load of 6000 lbs. (26.7 kN) is changed from zero to -0.0003 in. (-0.0076 mm.) the life increases from 6.62 mr. to 7.4 mr, an increase of 11.8%. Deflection decreases from 0.00103 in. (0.0262 mm.) to 0.00066 in. (0.0168 mm.), or about 36%.

As the interference is increased further from the point at which life is maximum ($\epsilon = 0.70$ to 0.76), ϵ increases and the life decreases rapidly. It is also clear from the above curves that the interference required in a particular bearing, for maximum life increases with increase in the radial load. For a 20 roller bearing the interference required for maximum life at 6000 lbs. (26.7 kN) radial load is -0.0003 in. (-0.0076 mm.),

whereas, the interference required for maximum life at a radial load of 10000 lbs. (44.5 kN) is -0.0005 in. (-0.0127 mm.).

Fig. 3.22 shows the effect of different numbers of rollers in the bearing on life, for a radial load of 6000 lbs. (26.7 kN). The interference required for maximum life for a particular radial load increases with decrease in the number of rollers.

3.8 GRAPHICAL SOLUTION FOR RADIAL ROLLING BEARINGS WITH RIGID RACES

The deflection of radial rolling bearings, even with the assumption of rigid races, depends on factors such as bearing geometry, number of rollers, material, external radial load and clearance. The deflection of a rolling bearing can be found by solving equations (2.43) and (2.50) simultaneously by trial and error, as explained in chapter 2. This is a time-consuming process. Thus to save time and also a considerable amount of labour, nomograms were constructed for both radial roller and ball bearings. If very high accuracy is required, the value of ϵ obtained from these nomograms may be used as the first assumption in the trial and error method, for rapid convergence.

Using equation (2.43), equation (2.50) can be written for positive clearance as,

$$\frac{F_r}{B} = c^t \left[\left(\frac{2\epsilon}{1-2\epsilon} \right)^t J_r (\epsilon) \right] \qquad (3.7)$$

and for negative clearance as,

$$\frac{F_r}{B} = (-c)^t \left[\left(\frac{2\epsilon}{2\epsilon-1} \right)^t J_r (\epsilon) \right] \qquad (3.8)$$

where $B = Z \times K_2$. (3.9)

Equations (3.7) and (3.8) can be written as,

$$F^* = f_1 (c) \times f_2 (\epsilon) \qquad (3.10)$$

where $F^* = \frac{F_r}{B}$ (3.11)

and f_1 and f_2 are functions of c and ϵ respectively.

Alignment charts of the form 'Z' were constructed (see for example ref. 37) to solve equations (3.9), (3.10) and (3.11) for ϵ. After finding ϵ, the radial deflection δ_r of the bearing can be found easily from equation (2.43), except for the value of $\epsilon = 0.5$ i.e. when $c = 0$. A nomo-

gram could be constructed for this purpose, but obviously this would not give deflection at $\epsilon = 0.5$. To avoid this difficulty another nomogram was constructed to find the radial deflection from F^* and ϵ. This nomogram was again constructed from equation (2.50), which for this purpose can be expressed in the form,

$$F^* = \delta_r^t \left[(2\epsilon)^t J_r (\epsilon) \right]$$

$$= f_3 (\delta_r) \times f_4 (\epsilon) \qquad (3.12)$$

where f_3 and f_4 are functions of δ_r and ϵ respectively.

3.8.1 SOLUTION FOR RADIAL ROLLER BEARINGS WITH RIGID RACES

The deflection of radial roller bearings with rigid races may be found from the nomograms given in figs. 3.23, 3.24 and 3.25, which were constructed taking,

$$K_2 = 5.21 \times 10^6 (\ell)^{8/9} \text{ and } t = 1.11 \qquad (3.13)$$

where, ℓ is the length of the rolers, or the effective length for crowned or end-relieved rollers. Fig. 3.26 gives the variation of load sharing factor and the factor $(P_1 Z/F_r)$ with loaded zone factor ϵ for radial roller bearings.

Sample solution: It is required to find the radial deflection of a bearing having Z = 25 rollers, each $\ell = 0.45$ in. long, a radial interference of c = -0.0006 in., under a radial load, $F_r = 4000$ lbs.

1. Enter the nomogram in fig. 3.23 with the values of Z, ℓ, and F_r, joining these points with straight lines to meet at a common point on line B, as shown. Obtain $F^* = 3.2$, in this case.
2. Enter the nomogram in fig. 3.24 with values F^* and c, obtaining $\epsilon = 1.67$.
3. Enter the nomogram in fig. 3.25 at previously determined values of F^* and ϵ, to obtain the radial deflection $\delta_r = 0.00026$ in.

N.B. This deflection is that of the inner race from the centred position within the outer race.

The peak roller load and the radial load component on the peak roller can now be found. Read the values of $(P_1 Z/F_r)$ and S_f corresponding to the value of ϵ from fig. 3.26. In this case they are 6.25 and 2.05 respectively.

Thus, total peak roller load = $P_1 = \frac{6.25 \times 4000}{25} = 1005$ lbs.

Radial load component on the peak roller = $\frac{2.05 \times 4000}{25} = 328$ lbs.

3.8.2 SOLUTION FOR RADIAL BALL BEARINGS WITH RIGID RACES

The value of K_2 taken in the construction of nomograms for this case is for bearings with standard groove radii (i.e. inner race groove radius at 52% of the ball diameter, and outer race groove radius not greater than 53% of ball diameter) and is approximated by (11),

$$K_2 = 14.2 \times 10^6 \, d^{\frac{1}{2}} \text{ and } t = 1.5 \qquad (3.14)$$

where d is the diameter of the ball.

The graphical solution is presented by nomograms in figs. 3.27 to 3.31 and the curves of fig. 3.32.

Sample solution: The radial deflection of a ball bearing having Z = 15 balls, each d = 0.3 in. diameter, a positive radial clearance of c = 0.0003 in., under a radial load, F_r = 1000 lbs., is to be found.

1. Enter the nomogram in fig. 3.27 with the values of Z, d and F_r, joining these points with straight lines to meet at a common point on line B, as shown. Obtain F* = 1.8.
2. Enter the nomogram in fig. 3.28 with the values of F* and c, obtaining $\epsilon = 0.4$. In case where $\epsilon > 1.0$ the nomogram in fig. 3.29 is to be used.
3. Enter the nomogram in fig. 3.30 at previously determined values of F* and ϵ, to obtain the radial deflection $\delta_r = 0.00148$ in. If the deflection is greater than 0.002 in., fig. 3.31 is to be used.

N.B. This deflection is that of the inner race from the centered position within the outer race. Thus, the deflection after the peak ball is loaded is (0.00148 - c) or 0.00118 in.

Using the value of ϵ (found from fig. 3.28 or 3.29), the peak ball load can be found from fig. 3.32. In this case, $\epsilon = 0.40$ and hence, the load sharing factor $S_f = 4.73$ from the above figure.

Therefore, Peak ball load $= \frac{S_f \times F_r}{Z} = \frac{4.73 \times 1000}{15}$

$= 316$ lbs.

CHAPTER 4 BEARINGS WITH FULLY-FLEXIBLE RACES – EXPERIMENTS WITH ARALDITE MODELS

4.1 GENERAL

The results given in the previous chapter applied to 'rigid races' (which also implies rigid housings and shafts), thus races remained circular on loading. Only the contact deflections at the roller and race contact areas due to Hertzian stresses were considered. However, the load distribution within a bearing will obviously depend partly upon the compliance (flexibility) of the races and their supporting members. In this chapter, the practical situation in which all elements in the bearing assembly are subject to deflection will be investigated experimentally.

4.2 MODEL TECHNIQUE

The effect of housing and supporting structure on the bearing can be studied by experiment either with actual (steel) bearing or by use of a model. Model method using 'frozen-stress technique' (see Crookall (15)) was chosen, which offers the following advantages in the present study:

(a) the lower Young's modulus of about 2.5×10^3 lb./in.^{2} (17 MN/m^2.) at stress freezing temperature (compared to 5×10^5 lb./in^2. (34×10^2 MN/m^2.) at room temperature) allows convenient deformations to be obtained with quite small load, with consequent increase in the accuracy of measurement.

(b) model 'frozen' under load can be dismantled and the deformations in the individual parts measured. Thus detailed information such as deformations near contact areas, distortion from roudness, and the deflections of individual rollers can be obtained, which would be impossible otherwise, and which are relevant to this study.

4.3 PRODUCTION OF MODELS

Model material - CIBA (A.R.L.) Ltd., epoxy resin (100 parts by weight of Araldite CT200 and 30 parts by weight of hardener HT901).

Moulds used were of mild steel, and allowed for subsequent machining of models and also for a tensile test specimen to be made from the same casting as the model. Also, rollers and platens were made from the same casting. The Araldite plates (for the outer race) were cast to size, in moulds consisting

essentially of two 12 in. x 12 in. x $\frac{1}{4}$ in. steel plates with their surfaces ground and polished for smoothness and flatness. The steel plates were separated by a 0.45 in. steel spacer, thus setting the thickness of the cast plate.

All casting surfaces were thinly coated with Silicone oil release agent and baked at 200°C for easy removal of the casting. Casting and annealing procedure followed were according to the instruction sheet issued by the manufacturer (details can also be seen in refs. 15, 16). Machining of the castings was initially done to within 1/8 or 1/16 in. of the finished size. This was followed by annealing and the finish machining to required size. A diamond slitting machine was used for machining rectangular calibration test strips. The machining tolerances were $\pm$0.0002 in. (0.0025 mm.) for all important dimensions.

Stabilisation of the models requiring repeated heating cycles was shown to be necessary by Crookall (15). This is to avoid the rise in Young's modulus with the number of heating cycles due to secondary curing. This was done in the present experiments by preheating the finished models at 140°C for 48 hours.

When a number of parts of a model were derived from the same casting they were all kept together during all heating cycles (irrespective of whether they were actually being used)so that there was no relative change of properties due to secondary curing.

4.4 STRESS FREEZING

With the model assembled in the loading rig, the following heating cycle was used:

	time - hours
Heating to 130°C	8
Stress freezing at 130°C	3
Slow cooling (from 130°C - 70°C)	30
Rapid cooling (from 70°C - 25°C)	6
total cycle time	47

As the Young's modulus at the loading temperature (130°C) is low, the body force i.e. the self weight, of the model might have produced exaggerated deflection. This could be avoided by stress freezing the model in a fluid (e.g. glycerine) having specific gravity similar to that of Araldite. However, this would have been rather inconvenient experimentally, and

was not done. For the calibration of rollers the effect of self weight was taken into account by adding the (comparatively small) weight of the upper platen to the external load, in evaluating the results. For the complete bearing, it was found, by the finite-element method, that the total deflection of the bearing with self weight was about 5% higher than without self weight, but that the effect on the load distribution among the rollers was negligible.

4.5 CALIBRATION OF MODEL MATERIAL

Two types of calibration specimens were used as shown in figs. 4.1a and b. The first type (used in calibration of rollers) was of circular cross section 0.375 in. in diameter and 5.5 in. long (fig. 4.1a). Six fine gauge lines were scribed, each on the circumference of the specimen with a scriber on a Société Genevoise Type MU-214B Universal measuring machine. The specimen was held lightly between centres during scribing and measuring.

The second type of specimen was of rectangular section, 0.25 in. by 0.1 in., and about 6 in. long (fig. 4.1b). The strip was cut with a diamond wheel. Six gauge lines were scribed, as shown,with the specimen lightly clamped on the table of the measuring machine.

Eighteen gauge lengths were obtained from each specimen, and the effect of bending due to non-axial pull was avoided by taking readings on two opposite sides of the specimens. The loads applied to the circular and rectangular specimens were about 3 lbs. and 1 lb., respectively.

The tensile specimens were measured before and after each loading, on the Universal measuring machine. The elongations were plotted against their corresponding gauge lengths, a typical result being shown in fig. 4.2. A mean line was drawn, and the slope of which indicated the mean strain.

Later, a computer program 'ELSTCT' was developed to calculate Young's modulus from the individual readings, using least squares regression to find the mean strain. A listing of this program is given in the computer program section.

Variation of Young's modulus for roller material with the number of stress-freezing cycle (which is half the total number of heating cycles) is shown in fig. 4.3. The value of Young's modulus was reasonably constant at 2730 lb./in^2. (18.82 MN/m^2.). For bearing races this was found to be 2765 lb./in^2. Hence, for all theoretical calculations a constant value of E = 2730 lb./in^2. (18.82 MN/m^2.) was used.

4.6 CALIBRATION OF ROLLERS

The load distribution in a bearing depends upon the deflection distribution, and the load-deflection characteristics of the rollers and races. Hence, it was necessary to determine the latter for different types of rollers and platens.

Details of the rig for loading a roller between two platens may be seen in fig. 4.4a. As the stress freezing and annealing cycles take considerable time, ten rollers were loaded between platens simultaneously, as shown in fig. 4.4b. Thus the entire load-deflection characteristics were determined in a single heating cycle. The calibration of solid and hollow rollers were made between

(a) Araldite platens having width 0.616 in., (15.65 mm.)

(b) Araldite platens having width 0.45 in., (11.43 mm., i.e. equal to the length of roller)

(c) Aluminium platens.

4.6.1 MEASUREMENT OF MODELS

Rollers were measured with a Matrix Diameter measuring machine (reading to 0.00001 in.) before and after loading. The measurements were made at three equidistant positions (one at the middle and two at the two ends) along the length of the roller and the average of them (according to a modification of Simpson's rule given later) was taken. This is to overcome the effect of any taper in the rollers (less than 0.0001 in.), and any eccentric loading.

Platen deformations were measured by dial gauge (reading to 0.0001 in.) held in a magnetic stand, the platen being mounted on a co-ordinate table. The deformation was measured with respect to two points 0.15 in. (3.81 mm.), i.e. equal to the roller radius on either side of the centre of the contact area. The results were thus directly applicable to tests on the complete bearing. The race deformation at any roller position is the result of the combined effects of all roller loads, and hence the effect of a particular roller cannot be found by direct measurement. However, the local deformation at any roller position (with respect to the two equidistant points on either side of the contact area) is practically independent of the other roller loads.

To avoid the effect of eccentric loading the platen deformations were also measured at three equidistant positions (one at the middle and the

other two at the two ends) along the length of contact area and the average was calculated according to a modification of Simpson's rule as follows:

$$\delta_{av} = \frac{1}{6} [\delta_1 + 4\delta_2 + \delta_3] \qquad (4.1)$$

where δ_2 is the deflection at the centre of contact area, and δ_1, δ_3 are deflections 0.15 in. (3.81 mm.) on either side of the centre along the length of contact area.

Width of contact area was measured by travelling microscope. However, the surface outside the contact area was very carefully 'shaded' by rubbing the platen against a paper coated with chalk. Without this treatment the edge of the contact area could not be seen under the microscope at all.

4.6.2 EXPERIMENTAL RESULTS

The results of the roller and platen calibration experiments are given in tables 4.1 to 4.6 and represented graphically in figs. 4.5 to 4.14. The results for solid and hollow Araldite rollers in Araldite platens wider than the length of rollers are given in tables 4.1 and 4.2 respectively. Fig. 4.5 shows the load-deflection characteristics of a solid Araldite roller between Araldite platens wider than the length of the roller, and fig. 4.6 shows the variation of width of contact area for the same case. Figs. 4.7 and 4.8 are the similar graphs for a hollow Araldite roller between Araldite platens wider than the length of the roller.

Tables 4.3 and 4.4 represent the experimental results for solid and hollow Araldite rollers, respectively, between Araldite platens of widths equal to the length of roller. Fig. 4.9 illustrates the variation of deflection with load for a solid Araldite roller between Araldite platens of widths equal to the length of the roller, and fig. 4.10 shows the relation between width of contact area and load for the same assembly. Similar relations for a hollow Araldite roller loaded between Araldite platens of widths equal to the length of the roller are shown in figs. 4.11 and 4.12.

Experimental results for solid and hollow Araldite rollers between aluminium platens are illustrated in figs. 4.13 and 4.14 respectively and the corresponding results are given in tables 4.5 and 4.6.

Smooth curves were drawn through the experimental points using the method of least squares (see for example ref. 36). A computer program 'POWER' was developed for this purpose, the listing of which is given in the computer program section. The equation of the curves considered were of the

form given by equation (2.24), namely

$$\delta = AP^N \qquad (4.2)$$

The load and deflection values for the computer-fitted curves, and the corresponding values of A and N, are given in the second part of each of the tables 4.1 to 4.6. As in chapter 2, A_1 represents the constant for one contact area, and A_2 represents the constant for two contact areas (i.e. at the two platen contacts of a roller).

4.6.3 DISUCSSION OF RESULTS

Note that the deflection of platens and total assembly given in the experimental results are not the 'overall' deflections, but those with respect to the two points 0.15 in. (3.81 mm.) on each side of the centre of contact area. Thus deflections of the two datum points are excluded. The reason for doing this is given before while mentioning the measuring procedure of platen deflection.

Platen, roller, and hence total deflections for a solid Araldite roller and Araldite platens wider than the length of the roller, fig. 4.5 (and table 4.1) is less than the corresponding deflections for the case of Araldite platens of same width as the roller, fig. 4.9 (table 4.3). This is due to the edge effect of the wider platen. When the platens are wider than the length of the roller, the ends of the contact area are more highly stressed than the rest of the area as shown in fig. 4.15. Ideal contact does not exist in this case, and some work is expended in compressing the material laterally, i.e. perpendicular to the direction of rolling. The smaller compressive stress at the middle portion of contact area gives rise to smaller deflection. The edge loading reduces the life of a bearing, and it is important to consider it during bearing design. More information about edge loading can be obtained from ref. 12, page 138, and ref. 28, page 146.

The edge loading can be reduced or eliminated completely by 'crowning' the rollers or raceways, or less effectively by chamfering the ends of rollers. It is also possible to reduce the edge loading by using hollow rollers, or by making the ends of the roller hollow. This is noticeable from the results of hollow Araldite rollers between Araldite platens wider than the roller length, fig. 4.7 (table 4.2) and between Araldite platens of widths equal to the length of the roller, fig. 4.11 (table 4.4). The differences in deflections of roller, platen, and total, between the two cases are much smaller than the corresponding differences for solid rollers.

Total deflection for a solid Araldite roller in wider Araldite platens, fig. 4.5 (which excludes the deflection of the datum points) shows quite good agreement with the Föppl formula. Also, for Araldite platens of widths equal to the length of the roller, the deflection curve lies between the curves of the Föppl and Palmgren formulae. It will be shown later in the section for roller calibration by finite element method, that for the latter case the results agree very closely with the Palmgren formula if the deflection of the datum points is included.

The total deflection for a hollow Araldite roller between wider platens, fig. 4.7, is also nearer to the theoretical curve obtained by adding the compression of the hollow roller (see section 2.6) to that given by the Föppl formula.

The difference in Araldite platen deflection for the same width of platen is small for solid and hollow Araldite rollers. There is little difference in the widths of contact areas for the different Araldite platen and roller combinations, figs. 4.6, 4.8, 4.10, and 4.12. Curves for the width of contact area using Hertz's formula are also shown dotted in the above figures. They are somewhat lower than the experimental results. This is attributed to the fact that it is difficult to locate precisely the edges of the contact area, as no sharp transition exists. The method of measurement employed tended to overestimate slightly the width of contact area.

The deflection component of a solid Araldite roller between Araldite platens equal to the length of the roller, fig. 4.9 (table 4.3) and between aluminium platens, fig. 4.13 (table 4.5) is very nearly the same. The virtual absence of edge-loading effect makes these cases equivalent (With aluminium platens the edge loading effect is negligible due to the relatively high Young's modulus). The same result can be seen for a hollow Araldite roller between Araldite platens equal to the length of the roller, fig. 4.11 (table 4.4) and between aluminium platens, fig. 4.14 (table4.6).

4.7 EXPERIMENT ON THE COMPLETE MODEL BEARING

The deflections of the inner and the outer races comprise:

(a) local deflections due to loading by individual rollers, and

(b) overall distortion of the races due to the combined action of the roller loads.

It is this second component of total deflection which causes the roller load distribution in practice to be different from that obtained theoretically with the assumption of rigid races. The aim is thus to inves-

tigate the effect of this deflection component on bearing performance.

The experimental arrangement for loading an Araldite model bearing inside the stress-freezing oven, is illustrated diagrammatically in fig. 4.16. The integral outer race and housing is in the form of a plate, which rested on one edge upon the ground surface of a flat, rigid steel beam. The plate could be set vertically using a spirit level and was thereafter located lightly by four screws. Loading was applied to the bearing through the shaft and integral inner race. A calibration strip was also loaded in tension at the same time as the model, as shown.

4.7.1 DIMENSIONS OF MODELS

Bearing 'races' were made integral with their respective shaft and housing, therefore implying a 'perfect fit' in practice.

Photographs of the housing and the shaft are shown in fig. 4.17. The essential dimensions are given in fig. 4.18. Shaft length projecting on either side of the collar (inner race track) is sufficient to sensibly remove from the stress distribution at the race position, any effect due to the concentrated loading of the ends of the shaft.

The interference in the bearing is 0.01006 in. (0.2555 mm.), i.e. $\simeq$0.010 in.

The cage (see fig. 4.17b) comprises twenty, 1/8 in. square Araldite spacers of $\frac{1}{2}$ in. in length bonded between two Araldite rings. One ring (A) is just larger than the shaft, and the other ring (B) will pass over the collar on the shaft (fig. 4.18). After assembly a third ring is push-fitted into the ring (B) so that, the cage is centered on the shaft. A photograph of the cage and rollers, both solid and hollow (the latter were not used in this experiment) is shown in fig. 4.17b. The assembly of cage and rollers on the inner race is shown in the photograph of fig. 4.17c.

4.7.2 METHOD OF OBTAINING PRELOAD

The inner race, cage and rollers were assembled on a wooden fixture as shown in fig. 4.18, using an elastic band to retain the rollers. The integral outer race and housing was heated to 140^{o}C, together with the calibration strip, by placing it in a preheated oven. The coefficient of linear expansion of Araldite is 5 x 10^{-5} per ^{o}C below 94^{o}C, and 15 x 10^{-5} per ^{o}C above this temperature. The outer race was then quickly fitted over the assembled rollers and inner race, no force being required. On cooling, the model was ready for assembly into the loading rig.

4.7.3 MEASUREMENT OF DEFLECTIONS

Bearing deflection was measured in two ways:-

Method 1

Two lines were scribed (fig. 4.19a) diametrically opposite and perpendicular to the direction of radial load, on both sides of the collar. Their height from the top surface of the loading beam was measured before and after loading. The mean difference of the heights of the four lines before and after loading gave the bearing deflection. This procedure avoids any slight angular tilt in the shaft. Slip gauges and a 'knife edge' (used for measuring root diameter of screw threads) were stacked on the top surface of the beam beside each line and the height difference between the lines and the top of the knife edge was measured using a travelling microscope. Placing and adjusting the microscope in the oven presented certain difficulties.

Method 2

This consists of measuring and summing the deflections of all the individual components in the line of load, i.e. the inner race, the peak roller and the outer race. The measurement of deflection of the individual components is as follows:

The outer race deflection was measured on the Universal measuring machine MU-214B. For this purpose, two pairs of diametrically opposite lines (A,B,C, and D in fig. 4.19a) were marked on the circumference of the outer race track using a Société Genevoise Rotoptic-2 optical circular table. A fifth line was marked on the supported edge at E, in line with C and A. Overall deflection of the housing comprises local (contact) deflection, the deflection due to the race distortion, and the body deflection of the outer race with respect to its supported lower edge. This δ_{A}^{body} deflection is shown in fig. 4.19b as the distance between an imaginary line BD, and its deflected position B'D'. This can also be visualised as the deflection of the 'centre' of the bore.

The total deflection of the outer race is the compression of the distance AE, and is given by,

$$\delta_A = \delta_D + \delta_{A/D} \qquad (4.3)$$

where, δ_D is the body deflection of outer race and $\delta_{A/D}$ is the combination of the local deflection at peak roller and the deflection due to the distortion of the outer race.

The total deflection of the housing was determined by measuring AE before and after stress freezing, first by the measuring microscope on the

MU-214B, and then as a check by the diameter-measuring feeler attachment. It was found after stress freezing that line A was slightly displaced from the centre of the peak roller contact area. Correction for this was made by measuring the height of A from the centre of the peak roller contact area. A check was made to confirm that the line of the centre of contact area was square with the plate surface, and that it was not curved, using the feeler on the MU-214B.

The radial distortion at A, $\delta_{A/D}$ (i.e. the change in perpendicular distance between A and the line joining B and D measured before and after loading) was measured using the microscope attachment on the MU-214B. The correction for A not being on the centre of the contact area was also made as before. The diameters AC and BD and the radius at B before and after loading were also measured to find quantitatively the deformed shape from the Talyrond chart.

The inner race deflection was measured by scribing two pairs of diametrically opposed lines with a MATRIX optical projection dividing head, as shown in fig. 4.19a. One pair (F and I) was in the direction of the load and the other (H and G) perpendicular to it. The radius at F (which is in the direction of the load, and lies at the centre of peak roller contact area) was measured before and after loading. The difference between the two readings gave the deflection of the inner race.

The radius at F (which is defined as the perpendicular distance between F and a line joining HG) was measured by holding the inner race with the line F upwards on a specially prepared V-block (fig. 4.20a). This V-block holds the inner race on the two sides of the collar and does not touch the inner race track. This arrangement was more stable than a conventional V-block for locating the bent shaft. The V-block was clamped on the circular table of the Universal measuring machine (MU-214B). A special holder was made to locate a travelling microscope on the MU-214B horizontally, as shown in fig. 4.20b. With the microscope in the horizontal position, the lines H and G on the inner race were alternatively viewed in the microscope by rotating the circular table. The inner race and the height of the microscope were adjusted until both of the lines passed the cross wires in the microscope, ensuring that the line joining HG was horizontal, and that joining IF was vertical. The height of the microscope was recorded. A pile of slip gauges bearing a knife edge of known height (fig. 4.20b) was sighted in the microscope, and the reading was taken. From these measurements the height of the line HG above the top surface of the circular table

was established.

The holder and microscope were then removed without disturbing the inner race. A depth-measuring attachment was used, as shown in fig. 4.20c, to establish the height of line F above the top surface of the circular table, again using the slip gauges as a reference. The radius at point F was thus found by subtracting the height of line HG measured previously from that height of F above the table. A check on this measurement was made by also measuring the radius at I, and comparing their sum with the diameter FI (measured directly by the diameter-measuring feeler attachment). The diameter HG before and after loading was also measured.

The roller deflections were measured as in the previous experiments, using the MATRIX diameter measuring machine.

From these measurements, the total deflection of the radial roller bearing is given by

$$\delta_{bearing} = \Delta R_A + \Delta R_F + \delta_{peak\ roller} + \Delta DE + \text{radial clearance}$$

$$= \delta_{A/D} + \delta_F + \delta_{peak\ roller} + \delta_D + c \qquad (4.4)$$

For simplicity, $\delta_{bearing}$, δ_D, $\delta_{A/D}$ and δ_F will be represented in the next chapters as δ_r, δ_b, δ_{or} and δ_{ir} respectively.

The shape of the races after deformation was measured with a Talyrond machine at the National Physical Laboratory.

In order to obtain a true circumferential trace of the inner race (thus avoiding location by the bent shaft) a fixture was made (see fig. 4.21) to hold the shaft by the collar on the Talyrond table.

From the Talyrond charts the local deflections were determined using a plastic template marked with concentric circles. The local deflections were measured with respect to two points 0.15 in. (3.81mm., equal to the radius of rollers) on either side of the centre of the contact area; this procedure is the same as that adopted in section 4.6.1 for measuring platen deflection.

4.7.4 EXPERIMENTAL RESULTS

The component and the total bearing deflections (both experimental and theoretical) are given in table 4.7 for the applied load of 9.5 lbs. (42.3 N) and radial interference of approximately 0.010 in. (0.254 mm.).

The roller load distribution in this bearing*, and also the load distribution calculated using the 'rigid race' assumption are given in table 4.8, and are presented graphically in fig. 4.22. Roller position is plotted with respect to the peak roller ($\psi_j = 0^o$), which is directly in line with the radial load. The Talyrond traces of deflected outer and inner races are shown in figs. 4.23a and 4.24a, respectively.

4.7.5 DISCUSSION OF RESULTS

Table 4.7 shows that the deflections of the outer race, the inner race, and the complete bearing, for the fully flexible model are significantly different from those calculated on the assumption of 'rigid races'. This difference will naturally depend upon the flexibility of the races, radial clearance, radial load and other factors. The body deflection of the outer race is finite (although it is not considered in the case of 'rigid races'), and it may represent a substantial part of the total bearing deflection, depending upon its design.

From experimental measurements of the outer and inner races, and the Talyrond charts given in figs. 4.23a and 4.24a, the following conclusions can be drawn:-

(a) The outer race expands, and the inner race contracts if preload is present in the bearing. The amounts will depend upon the degree of preload and the relative radial stiffness of the races.

(b) The combined effect of the roller loads due to an external load causes distortion of the bearing tracks, the outer race becoming elliptical, with the major axis perpendicular to the direction of load. This is partly due to the action of the components of roller loads perpendicular to the direction of radial load and, in this case, partly due to the particular restriction on the deflection of the plate due to its edge-mounting on a rigid support. It will be shown later that if the outer race is sufficiently flexible in the direction of the radial load (due possibly to lack of support, or the presence of other openings in the plate) the major axis can lie in the

---

* This was calculated from the experimental values of local deflections of races, deflections of rollers and total deflections, using an equation of the form $P=K\delta^t$, where K and t are calculated from the previous calibration results (table 4.3). In another method used, K was found from the equilibrium equation of the complete bearing in the direction of radial load, taking the value of t from the calibration result.

direction of the radial load, notwithstanding the action of roller load components perpendicular to it.

The shape of the inner race also depends upon its radial rigidity and the roller load distribution. For the present case of a solid shaft and preloaded bearing, the distortion of the inner race is comparatively small.

(c) The load distribution differs from that calculated from the rigid race assumption due to the change in size and shape of the races (conclusions (a) and (b) respectively). The change in size of the races resulted in a decrease in the general level of load, in this case. Also, as the shape of the outer race in this case was elliptical with its major axis perpendicular to the direction of the radial load, the load distribution was in fact somewhat 'peakier' than for the theoretical 'rigid race' situation. Obviously the shape adopted by the outer race exerts an important influence on load distribution, and this is investigated further in chapters 6 and 7.

CHAPTER 5 DEVELOPMENT OF FINITE-ELEMENT PROGRAM FOR BEARINGS WITH FULLY-ELASTIC SUPPORTS

5.1 GENERAL

A computer program involving the finite-element method has been developed to evaluate the performance of radial rolling bearings under realistic support conditions. In this chapter a short discussion on the finite-element method and some short notes on the computer program developed is given. In the later part of the chapter a method of finding the equivalent radial load, which is used to calculate the life of radial rolling bearings having any arbitrary rolling element load distribution, is given. This equivalent radial load is used in the next two chapters to compare the rolling element load distributions for different cases.

5.2 FINITE-ELEMENT ANALYSIS OF TWO DIMENSIONAL PROBLEMS

The finite-element method involves the sub-division of a structure into a finite number of 'elements' interconnected at a finite number of 'nodal points'. The analysis of this elemental structure can be used to determine the displacements and stresses developed in two-dimensional structures of any desired geometry and material property, from the force-displacement relations of the individual elements. Triangular or quadrilateral element shapes may be used for two-dimensional problems, and in the present investigation, triangular elements have been used.

The two basic approaches are the displacement method, and the force method, although a combination of these two methods is sometimes used. In the present work the displacement method has been used. The strain energy of the system resulting from the displacement and force methods represents a lower and upper bound, respectively, to the true strain energy of the continuum. The finite-element solution will converge on the true solution as the mesh size is reduced.

For the force-displacement relations (stiffness matrix) of an individual element the following assumptions are made;

(a) displacement within each element is assumed to vary linearly, i.e. 'lines initially straight remain straight in their displaced position'. This maintains the continuity between elements of the system, and also makes the strains and hence the stresses within each element, constant.

(b) stresses acting on the edges of each element are replaced by stress resultants which act at the corners of the element.

After finding the stiffness matrix of each element based on the above assumptions (procedure given in appendix 5.1), the overall stiffness matrix for the complete structure is formed by the systematic addition of these individual element stiffness matrices. Forces acting on the actual structure are then replaced by statically equivalent concentrated forces acting at the nodal points of the finite element system, and the force matrix for the complete structure is formed.

The equilibrium of the complete system of elements which express the nodal point loads, F, in terms of nodal point displacements, δ, can be expressed by the following matrix equation;

$$[K][\delta] = [F] \qquad (5.1)$$

where $[K]$ is the overall stiffness matrix for the complete structure. This matrix equation represents a system of simultaneous linear equations which can be solved, to find the unknown nodal point displacements. From these nodal point displacements the element stresses can be calculated.

As has been stated, the 'true' solution for a structure is obtained only with an infinite number of elements. However, mesh size is unimportant in regions of constant stress as virtually any mesh size will give the true stress distributions in such regions. In regions of high stress gradients, however, mesh size is critical, and by a careful grading of the mesh size so that the smallest elements occur in the regions of highest stress gradients, it is possible to obtain results that lie well within the limits of normal experimental error. The finite-element mesh used for radial roller bearing with housing and shaft made of Araldite and steel are shown in figs. 6.4 and 7.3 respectively.

Only a brief account of finite-element analysis for two-dimensional structures is given here, as details of the method in general are given in references 38 - 40.

5.3 PROCEDURE USED FOR SOLVING THE SYSTEM OF SIMULTANEOUS LINEAR EQUATIONS

In the system of simultaneous linear equations represented by equation (5.1), the actual number of equations in the system is twice the number of nodal points in the structure. They can be solved by various iterative or matrix inversion methods given in references 38, 39, 41 - 43. The iterative method given in reference 39 is quite fast, but the number of

elements and nodal points that can be used in a structure is limited to about 400 and 250 respectively, for 32K computers such as the IBM7094.

In the present investigation the solution technique of references 38, 42, 43 is used. The matrices in equation (5.1) are sub-divided into convenient parts, taking into account the symmetry and sparseness of the overall stiffness matrix, and the fact that the non-zero elements usually lie close to the diagonal. Descriptions of this technique can be found in the above references and a brief procedure is given in appendix 5.2. This method offers the following main advantages:

(a) The number of elements and nodes that can be used in a structure is unlimited, provided the number of nodal points in each partition (described later) is limited to a figure which depends upon the storage capacity of the computer used.

(b) The stiffness matrix is sub-divided in a tridiagonalised manner, and the zero elements outside the tridiagonal band are not stored in the computer.

(c) After generating and storing the intermediate matrices given in appendix 5.2, the time required for solving the problem is comparatively very short. For any additional load matrix only little additional time is spent in obtaining the solution. This was found extremely useful in the present investigation. The intermediate matrices are stored on magnetic tape for a bearing with a particular housing and shaft. They are used subsequently for any radial load, radial clearance and amplitude (and type) of outer race relief of the bearing.

(d) Symmetry of the overall stiffness matrix is utilised by storing only one of two symmetrical sub-matrices.

The matrix partitioning corresponds to a physical division of the actual structure. In the finite element mesh used for radial roller bearing (see figs. 6.4 and 7.3), only one half of the housing and shaft is considered, due to symmetry. The outer and the inner race rings are considered to be an integral part of the housing and the shaft respectively. Radial lines passing through the centre of contact areas and between two contact areas shown in the mesh of the housings, are the division links of the mesh. These lines of division are known as the 'partition lines' and the divisions as the 'partitions'. Similar partitions are also present in the meshes for the shafts; there are 20 partitions in the housing and the shaft. Elements and nodal points are numbered serially, starting from the first partition, the numbering

of elements within each partition being arbitrary. However, nodal points on a partition line are common to the adjacent partitions. Thus the nodal points on the partition line are numbered serially, the numbers being the last nodal point numbers of the preceding partition and the first nodal point numbers of the succeding partition.

5.4 NOTES ON THE PROGRAM FINELM

A flow chart of the program FINELM is given in fig. 5.1, and the listing of the latest version of the program is in the computer program section. The basic finite element part of the program is similar to that given by Zienkiewicz in reference 38, with some reorganisation and changes for the present investigation. The major reorganisation is in subdividing the solution part of the program in the above reference into subroutines, MSM, MFM and FORCE. This was found necessary as the inner and outer races of the bearing are treated as separate problems, but they are solved simultaneously and are combined together in the iterative part of the subroutine SOLN. Some intermediate matrices are also stored for subsequent use. The tapes 1 to 4 have been re-allocated to store intermediate results of the two problems in such a way that minimum amount of tape manipulation is required. Another tape (No. 8) has been added to store all the information and intermediate matrices necessary to solve other cases of the same bearing having the same outer and inner races, by using a smaller program. The maximum time required by the program is in the subroutine MSM (especially in inverting the 40 sub-matrices) and is about 220 secs. of the central processor time on the CDC 6600 computer (about 25 mins on the IBM7094). Solution for one iteration (described later) of the outer and inner races to find the nodal point displacements after forming the modified stiffness matrices (in MSM) takes only about 10 secs. of the central processor time of the CDC 6600. Thus storing the intermediate matrices for subsequent cases saves a considerable amount of computer time.

Subroutine LOAD has been changed to distribute the shear stress acting on the surface either uniformly or parabolically, as desired. From simple beam theory the shear stress distribution in any cross section of a beam having rectangular or circular (solid or hollow) section is parabolic, due to the change in bending moment along the length of the beam. The formulae used in LOAD subroutine were checked by considering some typical rectangular and circular cross sections which were solid or hollow (to different

extents). The nodal point load distributions found were quite close to those obtained by conventional beam theory. Some new subroutines LMAT, DTBN and NPF were added which, together with subroutine LOAD, forms automatically the load matrices for the outer and inner races from the external radial load acting on the bearing. Thus reading of the load matrices from the data cards is not necessary; only the radial load acting on the bearing need be read.

Subroutines DRAW and POLE were added to draw the deflected and the undeflected shapes of bearing races.

The program was first run on the IBM 7094 computer. The flowchart given in fig. 5.1 is for this version of the program. Because of core storage limitations in the IBM 7094 computer the program was loaded in the computer as an overlay program. During the last year of the investigation the program was run on the CDC 6600, a very much larger and faster computer. Minor alterations in the program were necessary for this change to the CDC 6600. The overlay feature of the program was retained to save some computer core storage. The first deck of the main link of this computer program is called FINELM.

5.4.1 DESCRIPTIVE FLOWCHART

An outline of the program in the form of a descriptive flowchart is given as follows:

(1) Call subroutine RWST of link (1,0) and execute operations up to step no. 14 by this subroutine.

(2) Read and print the characteristic data such as bearing component dimensions, elastic properties, densities, thicknesses, constants for roller and race way contact deformations etc.

(3) Steps up to 13 are repeated for outer and inner races (DO LOOP'20').

(4) Read and print data such as number of partitions, nodal points, elements, nodal points with prescribed displacements etc., of the race under consideration. Also, read and print, variables used to select the type of shear stress distribution of the race, nodal point numbers on the race, prescribed displacements, first and last nodal point and element numbers of each partition, etc.

(5) Repeat steps up to no. 13 for each partition of the race under consideration (DO LOOP '70').

(6) Read and print co-ordinates of the nodal points, and find the

co-ordinates of the nodal points on the race for the partition.

(7) Repeat up to step no. 11 for the elements of the partition under consideration (DO LOOP '80').

(8) Read and print the nodal point numbers (given in anti-clockwise order) and elastic property number of the element. To reduce the number of data cards, the nodal point numbers and elastic property numbers of four elements are read from one card.

(9) Call subroutine FEM which forms the element stiffness and stress matrices. The stress matrices are stored on tape nos. 1 and 8.

(10) Call subroutine LOAD to form body-force matrix. Force due to shear stress on the element is distributed to the nodal points considering uniform or parabolic shear stress distribution. The term body force is retained because as far as this program is concerned, the shear stresses and body forces are treated in a similar way. In case of only body force being present, the proper densities should be read for the proper areas of the mesh in step 2, and the value of the variable NSR read in step 4 should be anything but 1. If shear stress is acting in any area of a race the value of the density for that area to be read in step 2 should be 1.0 with the proper sign indicating the sign of shear stress and the value of NSR read in step 4 should also be 1 (integer).

(11) Add the element stiffness matrix to the stiffness matrix of the partition in accordance with the nodal point numbers of the element under consideration.

(12) Introduce the prescribed displacements. To do this, for a point with one or both components of displacements prescribed, the corresponding diagonal term is multiplied by a large number (0.1×10^{12}) and the corresponding force on the right-hand side (equation 5.1) is at the same time replaced by this newly-formed diagonal term multiplied by the prescribed displacement value δ_p. Expanding the appropriate row (i th row) of the equation 5.1 gives

$$k_{i1}\,\delta_1 + k_{i2}\,\delta_2 + \ldots + 0.1 \times 10^{12} \times k_{ii}\,\delta_i + \ldots + k_{iN}\,\delta_N = 0.1 \times 10^{12} \times k_{ii}\,\delta_p \qquad (5.2)$$

As all the other coefficients are nearly zero,

$$\delta_i = \delta_p \qquad (5.3)$$

to a good degree of approximation.

(13) Partition the stiffness matrix of the partition to form the sub-matrices of the tri-diagonalised overall stiffness matrix as described in appendix 5.2, and store them in tape 4. Partition the load matrix of the partition in a similar way and store in tape 2.

(14) Transfer the load matrices for outer and inner races from tape 2 to tapes 3 and 8, and return to the main program.

(15) Call subroutine MSM of link (2,0) and form the modified stiffness matrices and the intermediate matrices and store them on tapes for later use, as stated in appendix 5.2. This subroutine uses the matrix inversion subroutine SPNIST, which was obtained from the Imperial College 7094 Fortran IV Library (IBLIB).

(16) Read the number of problems to be solved, and repeat up to step no. 28 for the number of problems.

(17) Read the radial load, amplitude of relief in the outer race, diameter of roller (which gives the bearing radial clearance for the given race diameters), density of roller material, shaft speed in RPM and the value of the variable NSF for the bearing. If NSF = 1, stresses and nodal point forces will be calculated and printed, and deflections of all nodal points will be printed. Any other value of NSF will omit these (i.e. omit step nos. 26 and 27).

(18) In LOAD subroutine the nodal point force matrices were formed by calculating the nodal point forces of the regions where shear stresses act, taking the value of density to be unity. In this step form the actual nodal point force matrices, from the previous matrices, taking into account the radial load acting on the bearing and the area of the race subjected to the shear stress. As the areas subjected to shear stress in any race have constant thickness in the cases considered, the volume, rather than the area, subjected to shear stress was calculated in the subroutine LOAD.

(19) Call subroutine SOLN of Link (3,0), and execute operations up to step no. 27 by this subroutine.

(20) Calculate the radial clearances at each roller position, considering rigid races from the diameters of the races and rollers, and amplitude and type of relief in the outer race. Call subroutine LMAT, which calls subroutine DTEN, to find the roller load distribution from the radial load, shaft speed and contact deflection constants. The process is described in chapter 2, section 2.7.4. Subroutine LMAT then calls subroutine NPF for each roller position in outer and inner races. NPF distributes the roller load

among the nodal points in the region of the contact area, assuming Hertzian stress distribution (given in section 2.3). Subroutine LMAT puts all these nodal point forces in the correct position to form the force matrix of the race tracks.

(21) Call subroutine MFM. This subroutine adds the force matrix of the race tracks to the body force matrices developed in step no. 18 for successive partitions for the outer and inner races to form the total force matrices. Changes are made as stated in step no. 12 to introduce prescribed displacements. The modified force matrices are then formed for the partitions of the outer and inner races from the intermediate matrices formed and stored in subroutine MSM (step no. 15) and as described in appendix 5.2.

(22) Call subroutine SOLVE. This subroutine solves for the nodal point displacements from the matrices developed in subroutines MSM and MFM by back-substitution as described in appendix 5.2.

(23) Calculate the radial clearances at the different roller positions by considering the displacements of the nodal points on the race tracks calculated in the previous step, and removing the local contact deformations of the races. Removing the local contact deformations is found to be essential because, otherwise, the roller load distribution does not converge with the successive iterations, which start from step no. 21 and end in step no. 25. So, this step in fact calculates the radial clearances from the overall deflected shapes of the races.

(24) Call subroutine LMAT. This subroutine in turn calls subroutines DTBN and NPF to form the force matrix of the race tracks as in step no. 20. The only difference here is that, LMAT in this step takes some mean roller load distribution of that calculated in this step by DTBN from the radial clearances of the previous step and that taken in the previous iteration, to form the force matrix of the race tracks. The mean roller load of either race, taken at any roller position 'j' is according to the following equation,

$$P_j = \frac{(P_{(i-1),j} - \Delta P) + FCTR \times P_{i,j}}{1 + FCTR} \qquad (5.4)$$

where $P_{(i-1),j}$ is the roller load at position j taken in the previous iteration and $P_{i,j}$ is the roller load at position j found by DTBN in the present iteration. ΔP is the constant load subtracted from all the roller loads (if all of them are loaded) and is given by

$$\Delta P = FCTR1 \times (P_{(i-1),\,11} - P_{i,\,11}) \qquad (5.5)$$

The factor inside the bracket is the difference in top roller load at the outer race, between the previous iteration and that found by DTBN in the present iteration. If ΔP for any roller position 'j' is greater than $P_{(i-1),j}$, so that $(P_{(i-1),j} - \Delta P)$ is negative, then, ΔP is taken as the minimum value of the roller load. It may be noted that the resultant load of all these mean roller loads is still equal to the radial load.

FCTR1 was found to have little influence on convergence and, hence, taken as zero for most cases. However, the value of FCTR is most important for convergence, and depends upon the rigidity of the races, being greater for more rigid races and vice-versa; the best value is found by trial runs. The value of FCTR (and also FCTR1) used for the different cases is given in the next two chapters; from these an estimate of the value for other cases can be made.

(25) Calculate the RMS (root mean square) difference in roller load distribution between those taken in the previous iteration and those found by DTBN in the present iteration. If it is less than a certain given small quality (e.g. 1 lb. for steel bearings) then proceed to the next step, otherwise return to step no. 21 and repeat the complete procedure.

(26) Print the final results of radial clearances at the different roller positions, roller load distribution, bearing radial and component deflections, and the bearing rigidity for all successive iterations. A sample of this main portion of the computer output is given in the computer program section.

(26) Call subroutine FORCE to calculate and print the nodal point forces from the nodal point displacements calculated in subroutine SOLVE and the stiffness matrices.

(27) Call subroutine STRESS to calculate and print the element stresses from the nodal point displacements calculated in subroutine SOLVE and the stress matrices calculated in subroutine FEM. Return to the main program.

(28) Call subroutine DRAW to draw the deflected and undeflected shapes of the races using the CALCOMP plotter. Subroutine DRAW calls subroutine POLE to draw the polar scales.

(29) STOP

5.5 SMALLER VERSION OF THE PROGRAM

As stated previously, the main consumption of computer time required in the program FINELM is in forming the modified stiffness matrices and the intermediate matrices in subroutine MSM. All these matrices are stored in tape 8, and hence for other investigations of a bearing having identical races, these matrices may be used directly from tape 8. Also, if for any reason the computer stops executing the program FINELM after calling the subroutine MSM, a substantial amount of computer time will be saved, as the necessary information is stored in tape 8. To use this information from tape 8, a smaller version of the program was developed, called CHOTTO. A listing of this program and a subroutine RWTN of it is given in the computer program section. Subroutine RWTN reads the data from tape 8 and transfers them to the other tapes. After reading these data, the steps 16 to 29 of the previous section are followed. All the other subroutines of program CHOTTO are the same as in the program FINELM. Subroutine SOLN of the program CHOTTO is in link (2,0).

5.6 TYPES OF ROLLING BEARING THAT CAN BE CONSIDERED WITH THE PROGRAM

Radial roller bearings having race track width equal to the length of the rollers have been considered in this study. However, bearings with tracks wider than the roller length could be tackled with the program, and also spherical roller bearings, ball bearings etc., can be considered. All subroutines will be identical, excepting subroutine DRAW. It is necessary only to supply the deformation constants for a single roller and platens in the equation $\delta = A \times P^N$, so that in step no. 23 the local deformation for the races (which should be always considered as line contact throughout the entire width) are removed. In the subroutine DTBN the correct values of the constants for the type of rolling elements under consideration are to be used. This means that the values of CON1 and AAN1 read in step no. 2 should be for the type of the rolling element and race track used, and the values of CON2 and AAN2 should be for local deflection (for line contact) for the mesh used in the race tracks near the contact areas. If this method is used it may be possible to reduce the number of nodal points near the contact areas, thus reducing computer time considerably. The values of CON1 and AAN1 should be determined accurately by experiment, finite-element analysis or other method, and the values of CON2 and AAN2 by finite-element analysis, using

the mesh near the contact area.

The subroutine DRAW must be changed as the local deformations calculated are not the true local deformations of the bearing under consideration. Two ways of solving the problem are:

(a) remove the local deformations and draw the overall deflected shapes of the races, which are of greater interest.

(b) find the shape of the local deformations of the race tracks for the actual rolling element used at different rolling element loads. Read them as data cards and superimpose these local deformations on the overall deflected shapes as found in (a), considering the rolling element load distribution. Interpolation will be necessary to find the local deformations at intermediate rolling element loads from the data supplied to the computer.

5.7 EQUIVALENT RADIAL LOAD FOR ANY GIVEN ROLLER LOAD DISTRIBUTION

From equation (2.69) the dynamic life of a radial bearing is given by

$$L = \left(\frac{C}{F_r}\right)^p \qquad (5.6)$$

where C is the basic dynamic capacity of the bearing and F_r is the radial load. For point contact p = 3 and for line contact p = 4 (ref. 27, 12). The above equation is valid for an ideal distribution of the load on the rolling elements; this is the case for bearings having zero radial clearance, rigid races, and low speed of rotation. The bearing life for arbitrary conditions of load distribution and rotation can be determined from the equation

$$L = \left(\frac{C}{P}\right)^p \qquad (5.7)$$

where P is the so-called equivalent load of the bearing. For radial bearings the equivalent radial load is denoted by P_r. Equivalent radial load P_r is that radial load which, under the running conditions used (zero radial clearance, rigid races, and low speed of rotation) in determining the basic dynamic capacity, gives a fatigue life equivalent to that of the actual radial load F_r, under the actual operating conditions.

Originally the functional relation for equivalent load was given by Lundberg and Palmgren (26, 27). It is also covered in some detail in ref. 12. Ref. 44 contains a general method of finding the equivalent load

for any arbitrary rolling element load distribution, and also considers some particular cases of commonly occurring rolling element load distribution.

Appendix 5.3 gives the method of finding the value of non-dimensional equivalent radial load (P_r/F_r) of a radial rolling bearing, for an arbitrary rolling element load distribution as in fig. 5.2a. An estimation of the effect of the rolling element load distribution arising with different types of housings and shafts on the dynamic life of the bearing can be made from the factor (P_r/F_r). This factor may thus be used to relate the life of a given bearing in housings, with a given state of radial adjustment, etc., to that of the 'standard' bearing with rigid races, zero clearance, etc. Thus values of (P_r/F_r) greater than, equal to, or less than 1.0, means that the life of the bearing is respectively less than, equal to, or greater than, the life of a zero-clearance, rigid-race bearing at low speed, and having the same radial load F_r.

In the next two chapters (P_r/F_r) is plotted for comparison of the roller load distributions given by the different types of housings. The values of (P_r/F_r) for the roller load distributions of these chapters were calculated by the computer using the program EQLOD which was developed using the theory given in appendix 5.3. Program EQLOD is employed as a subroutine of program TABLE which is used to analyse and present the bearing results in a tabular form. A listing of these programs is given in the computer program section.

The increase in life for any radial rolling bearing having equivalent radial load to radial load ratio of (P_r/F_r), compared to a zero-clearance, rigid race radial bearing at low speed of rotation and having the same radial load F_r is given by the relation

$$\text{Percentage increase in life} = \left[\frac{1}{(P_r/F_r)^p} - 1\right] \times 100 \qquad (5.8)$$

For roller bearings (p=4), the precentage increase in life with (P_r/F_r) is shown in fig. 5.2b. This figure may be used to indicate the increase in life corresponding to the (P_r/F_r) values established and given in the next two chapters.

CHAPTER 6 COMPUTED RESULTS FOR BEARINGS WITH FULLY-ELASTIC SUPPORTS, WITH THE ELASTIC PROPERTIES OF ARALDITE

6.1 GENERAL

The finite-element program developed in the previous chapter for radial roller bearings was used here to calculate the deformation of the Araldite bearing, housing and shaft case used in the experimental work. The values of Young's modulus and Poisson's ratio taken for all the calculations in this chapter are 2730 lbs/in^2. (18.82 MN/m^2.) and 0.5 respectively. The deflection constants for an 'Araldite roller loaded between platens' were found by the finite-element method, these constants being subsequently used in the program for solution of the complete roller bearing.

The results presented in this chapter may be applied with a good degree of approximation to similar actual steel bearings having similar boundary conditions. The corresponding amount of radial load and radial clearance can be found taking the value of loaded zone factor ϵ (calculated on the basis of rigid races) to be the same as for the Araldite case.

The roller load distribution results can be made generally applicable by dividing all the roller loads by the heaviest roller load (peak roller) for rigid races.

6.2 CALIBRATION OF AN 'ARALDITE' ROLLER LOADED BETWEEN TWO 'ARALDITE' PLATENS

A program was used which was somewhat similar to the finite element program for a complete bearing, but in a basic form, simply to calibrate the load-deflection behaviour of a single roller loaded between two flat platens. Listing of this program is not given. However, by eliminating some of the subroutines of the program FINELM and some other small changes, the program can be made suitable for this purpose. The load acting on the roller was distributed at the nodal points at the contact area, assuming a semi-elliptical contact stress distribution, using a program which was the same as subroutine NPF of FINELM. The platen and roller were treated as separate problems.

6.2.1 FINITE-ELEMENT MESH FOR CALIBRATION OF ROLLER AND PLATEN

Fig. 6.1 shows the finite-element mesh for calibration of an Araldite roller loaded between two Araldite platens. Because of symmetry only a quarter of the physical model is used. The deflection of points on the line of symmetry perpendicular to it is taken as zero. The platens are assumed to rest on rigid supports and, hence, deflection of points adjacent to the support perpendicular to it is also taken as zero.

The mesh near the contact area was designed for roller loads below 10 lbs. (44.5 N). The semi-width of contact area for 10 lbs. according to Hertz's formula is 0.049 in. (1.245 mm.). However, the mesh can also be used for semi width of contact area up to about 0.070 in. (1.78 mm.). The dimensions of this mesh near the contact area was also adopted for the complete bearing, and are given in figs. 6.5 and 6.6. Though roller loads up to 10 lbs. were used for calibration purposes, in the complete bearing analysis load was always below 3.0 lbs. (13N).

6.2.2 CALIBRATION RESULTS

Table 6.1 gives the calibration results for an Araldite roller and platens, and fig. 6.2 shows these results graphically. Experimental results for a similar case (for the data given in table 4.3), and the total deflection given by Palmgren's formula, are also plotted.

In chapter 4 the deflection of the platens and the total assembly were taken with respect to two points 0.15 in. (3.81 mm.) on each side of the centre of the contact area. Thus in those results the deflections of the two points were not included, and hence were slightly smaller than the true total deflections. The reasons for doing this were given in section 4.6.1.

The effect of neglecting the deflections of the datum points (points A in the figure given below table 6.1) was found in the calibration of roller and platen by finite element method. The platen deflection $(\delta_C - \delta_A)$ with respect to the datum point A obtained by finite element method, and the total deflection based on this platen deflection, are also given in table 6.1, C being the point at the centre of contact area. Fig. 6.2 shows that platen deflections $(\delta_C - \delta_A)$ and roller deflections, obtained by experiment and finite-element method, agree quite well. Also the total deflection by finite-element method, given by the approach of the two platens, agrees closely with the deflection given by Palmgren's formula. These indicate that

the experimental results for total deflection given in fig. 4.9 (for width of platen = 0.45 in.) would agree more closely with the values given by Palmgren's formula, if the deflection of the datum points A were included.

The values of the constants A and N for a curve of the form,

$$\delta = A \times P^N$$

fitted by the method of least squares to the values of roller, platen and total deflections, are also given in table 6.1. The subscripts 1 and 2 of A indicate the value of the constant for one and two contact areas respectively. The values of A and N for total and platen deflection are used in the computer program FINELM (as the values of CON1, AAN1 and CON2, AAN2 respectively) for solving complete Araldite roller bearing problems.

The effect of platen curvature on its deflection under roller load was also studied by using the finite-element method. The results of platen deflections for a flat platen, a platen with concave surface having radius 1.5 in. (38.1 mm., equal to the outer race radius), and a platen with convex surface having radius 1.2 in. (30.48 mm., equal to the inner race radius) are given in table 6.2. With a concave surface deflection is slightly smaller than for the flat platen, due to a slightly greater width of contact area, and for a convex surface it is slightly larger. Thus the total deflection given by the approach of two platens, one concave and the other convex will be very nearly the same as the total deflection for flat platens.

The deflected shape of Araldite roller and platen assembly, as obtained by finite element method for a load of 5 lbs. (22.2 N), is shown in fig. 6.3.

6.3 FINITE-ELEMENT MESH FOR 'ARALDITE' RADIAL ROLLER BEARING WITH HOUSING AND SHAFT

Fig. 6.4 shows the mesh for the Araldite radial roller bearing in housings. Figs. 6.5 and 6.6 show the detail of the mesh near the contact areas in the outer and the inner races, respectively.

The number of elements and nodal points in the 'integral' shaft and inner race ring, and the 'integral' housing and outer race ring are given in the following table,

	No. of nodal points	No. of elements
Inner race ring and shaft	385	582
Outer race ring and housing	421	642

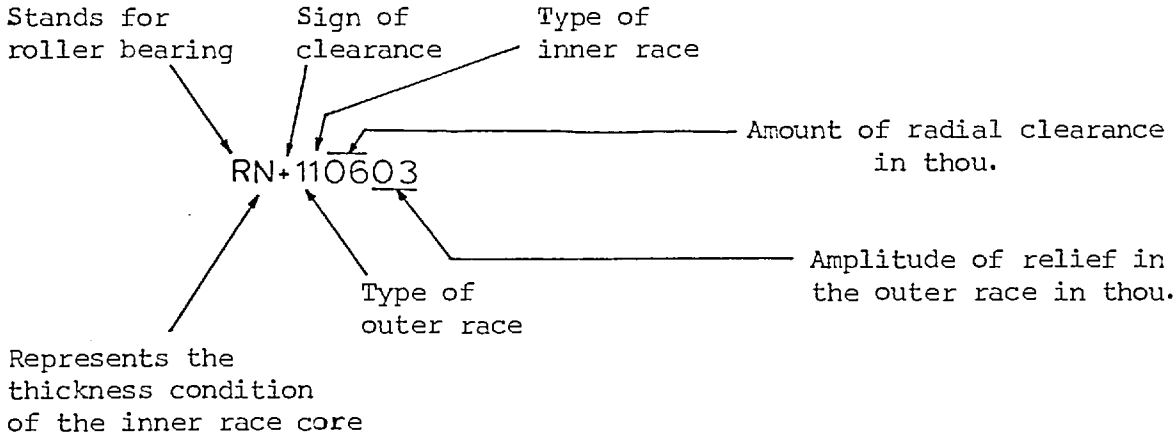
The co-ordinates of nodal points near the contact areas were calculated using a program developed for this purpose (listing of which is not given here). Nodal points at the other relatively coarse regions were found manually by plotting these regions on large scale graph paper. The computer data cards for element nodal point numbers and nodal point co-ordinates were checked by plotting the complete mesh with the computer calcomp package, using a program (MESH) developed for this purpose. A listing of this program is given in the computer program section.

The amount of play or interference in the bearing was varied by changing the diameter of the rollers, thus keeping the mesh of the bearing outer and inner race the same for all these variations.

The thickness of housing and race rings are 0.45 in. (11.43 mm., i.e. equal to the length of rollers). The thickness of shaft (i.e. core of the inner race) for most of the cases is 0.9 in.

6.3.1 CODING OF THE ARALDITE RADIAL ROLLER BEARINGS

To represent in compact form the configuration of the bearing housing and shaft and the amount of clearance and relief in the bearing, a coding system is followed, a typical example being:



If any quantity is a variable, the corresponding characters are replaced by 'x'. The second letter represents the thickness condition of the inner race core (i.e. shaft). If it is 'E', it represents that the core thickness of inner race is equal to the length of the rollers (i.e. 0.45 in.). If it is 'N', it represents that the core thickness of inner race is not equal to the length of the rollers, and the core thickness is

actually specified for the different cases. If the second character is 'N' and no core thickness is specified then the core thickness is 0.9 in., (22.86 mm.). 'N' and 'E' are used as the second character only for Araldite bearings, so their presence also indicates that the bearing material is Araldite.

For Araldite bearings only one type of outer race and one type of inner race have been used. They are:

Outer race no. 1 is in the form of a plate and resting on a rigid support. Outer race ring radial thickness is 0.062 in. (1.58 mm.).

Inner race no. 1 is composed of a solid shaft and race ring (radial thickness is 0.062 in. (1.58 mm.)).

6.4 COMPARISON OF FINITE ELEMENT - RESULTS FOR COMPLETE BEARING WITH THE RESULTS OBTAINED BY EXPERIMENT AND THEORY

Table 4.8 gives the experimental results obtained compared with calculated load distribution, based on assumptions of fully elastic races (finite-element analysis), and also the 'rigid race' condition. These results are also shown plotted in fig. 6.7. The bearing under consideration has radial clearance of c = -0.010 in. (0.254 mm.) and a radial load of 9.5 lbs. (42.26N). The theoretical load distribution assuming rigid races is considerably higher than the actual experimental load distribution. The results of experiment and of finite-element analysis are in good agreement.

Figs. 4.23(a) and 4.24(a) show Talyrond charts of the outer and inner races respectively of the Araldite experimental model of the above bearing. Figs. 4.23(b) and 4.24(b) show the Calcomp (graph plotter) traces of computed deflected shape, of outer and inner races respectively, for the same bearing obtained by finite-element analysis. The inner circle in fig. 4.23(b) and outer circle in fig. 4.24(b) represent the undeformed shape of the outer and inner races respectively. Note that the difference in effective 'size' of the Talyrond and computed plots are not significant, due to the indefinite 'zero' setting of the Talyrond, hence the important aspect of comparison is the shape. Good agreement is evident between the deflected shapes obtained by experiment and by finite-element analysis.

Table 4.7 shows the comparison of total and component deflection of the bearing under consideration obtained by theory assuming rigid races, by experiment, and by finite-element analysis. The deflections of inner and outer races by experiment and finite-element analysis agree quite closely.

The body deflection of outer race obtained by finite-element analysis is larger than that obtained by experiment. The difference may be due to the friction between the housing and the rigid support present in the actual case, but which is not considered in the finite-element analysis. Fig. 6.8 shows the deflected shape of the housing outer boundary for the same bearing as obtained by finite element analysis. The deflection at base will be restricted to some extent, if there is friction between the housing and the support. Thus, if friction is considered in the finite-element analysis (which can be done if the co-efficient of friction is known), the body deflection of outer race would be smaller than the value given in table 4.7.

6.5 EQUIVALENT THICKNESS OF THE INNER RACE CORE (i.e. THE SHAFT)

The significance of equivalent core thickness arises from the fact that all the parts, including the shaft, are considered to be in plane stress condition (provision for considering plane strain condition is present in the program FINELM). In fact, the inner race core will be subjected to a three-dimensional stress distribution. The inner race core (i.e. the shaft) is considered as a disc of a certain thickness, this 'equivalent core thickness' being defined as that value which, when subjected to plane stress condition, gives minimum RMS (root mean square) error in the roller load distribution as compared to actual case (i.e. when the core is subjected to three dimensional stress distribution). The effect of varying the core thickness on the bearing is shown in table 6.3, case nos. 2 to 6.

The experimental roller load distribution obtained is considered here as the actual roller load distribution. If the inner race core thickness is taken to be equal to the length of the rollers, the level of roller load distribution is lower than that obtained by experiment or, in other words, all the rollers carry comparatively lower load in finite-element analysis. The level of load distribution rises slowly (and the RMS error decreases), as the inner race core thickness is increased. Fig. 6.9 shows the variation of RMS error and also the average error with respect to experimental results, with the inner race core thickness for an Araldite radial roller bearing with the same radial clearance and load as in the experiment. If average error in roller load distribution were the criterion, the equivalent core thickness would have been 1.94 times the length of the rollers (where the average error is zero). After an initial increase in the core thickness, the change in RMS error is very small. The lowest RMS error in roller load distribution is

0.062 lbs. at nearly the same core thickness at which the average error is zero. The range of inner race core thickness is 1.6 to 2.4 times the length of rollers if the RMS error is increased to 0.065 lbs.(i.e. a 5% increase from the minimum RMS error). From the above discussions the equivalent core thickness of the inner race was taken as twice the length of rollers, i.e. 0.9 in. (22.05 mm.).

6.6 CONVERGENCE OF ROLLER LOAD DISTRIBUTION

For all the Araldite radial bearing cases studied, the value of FCTR and FCTR1 was taken as 1.0 and 0.0 respectively. A typical example of the rate of convergence for an Araldite bearing is given in fig. 6.10. Two convergence curves are shown, one for the RMS error in roller load distribution with respect to the final iteration result, and the other to the RMS error in roller load distribution between successive iteration results (the latter is used as the criterion for convergence in the program FINELM). The RMS error first decreases rapidly with increase in the number of iterations, thereafter convergence is much slower.

Iteration is stopped in program FINELM for Araldite bearings when the RMS error in roller load distribution between successive iterations is lower than about 0.05 to 0.01 lbs., depending on the radial load (the higher value being used for higher radial loads). The number of iterations required for the majority of cases was 3.

6.7 RESULTS AND DISCUSSION FOR ARALDITE RADIAL ROLLER BEARINGS

The summary of results obtained by finite element analysis for Araldite radial roller bearing cases studied are given in table 6.3.

Factors K_t and K_b are defined as,

$$K_t = \frac{\text{total radial bearing deflection considering fully-elastic races}}{\text{total radial bearing deflection assuming rigid races}}$$

$$K_b = \frac{\text{body deflection of outer race considering fully-elastic races}}{\text{total radial bearing deflection assuming rigid races}}$$

The values of K_t and K_b were calculated from the finite-element results and plotted for different cases of housing and shaft in this and the next chapters. From the bearing deflection of a radial roller bearing with rigid races, calculated by any of the methods given in chapter 2, or determined from the nomograms in chapter 3, an estimate of the actual bearing

deflection for fully elastic races can be made, for the type of housing and shaft used, from these values of K_t and K_b.

It should be noted that K_t includes K_b, and thus if only the bearing deflection (i.e. without the body deflection of the outer race) is required then K_b should be subtracted from K_t. The body deflection of the outer race depends mostly upon the radial load and size of the housing and adjoining parts. For sizes other than those investigated, K_b (and hence K_t) should be re-considered.

6.7.1 THE EFFECT OF RADIAL CLEARANCE AND RADIAL LOAD ON BEARING WITH FULLY-ELASTIC RACES

Figs. 6.11 and 6.12 show the deflection for an Araldite radial roller bearing. The values of K_t and K_b are given in figs. 6.11 and 6.13. Non-dimensional equivalent radial load (P_r/F_r) is given in figs. 6.14, 6.15 and 6.17. The effect of fully-elastic races on the peak roller load is given in fig. 6.16. Figs. 6.18 and 6.19 show the roller load distribution in the bearing for different radial loads and radial clearances.

The effect of varying radial clearance (c) on the deflected shapes of races at a particular radial load is shown in figs. 4.23b, 4.24b, 6.31, 6.32 and 6.34. The effect of varying radial load on deflected shapes of races at c = -0.006 in. is shown in figs. 6.30 and 6.31, and at c = +0.003 in. in figs. 6.33 and 6.34. The circle within the deflected shape of outer race, and that outside the deflected shape of the inner race in each of the above figures, represents the undeflected shapes of the respective races.

Fig. 6.18a shows the roller load distribution in the bearing for a constant radial load, at different radial clearances. Three distinct effects of fully elastic races are shown in this figure:

(A) . For highly preloaded bearings, when all the rollers are loaded, e.g. for radial clearances, c = -0.010 in. (0.254 mm.) the actual roller load distribution is lower than the theoretical distribution obtained by assuming rigid races. This is due to the expansion of the outer race and the shrinkage of the inner race by the roller loads, as may be seen in figs. 4.23b and 4.24b (and also in fig. 6.30 which is for c = -0.006 in. and F_r = 4 lbs.).

(B) Due to the rigid support of the housing and component of roller loads perpendicular to the radial load, the deflected shape of outer race tends to be elliptical with the major axis perpendicular to the radial load as may be seen in figs. 4.23 and 6.31. The roller load distribution curve

is thus 'peakier' for fully elastic races than for rigid races, as may be seen from the curve for c = -0.006 in. (0.152 mm.) of fig. 6.18a. The peak roller load for c = -0.003 in. (and F_r = 9.5 lbs.) is actually higher than the peak roller load considering rigid races. This effect is greater for preloaded bearings, as the rollers at 90° to radial load carry larger load.

(C) For positive clearance bearings with large radial load only a few rollers near the peak roller carry load. So the effect given in (B) is small and the outer race deforms more in the direction of radial load, as may be seen from fig. 6.34. The load distribution for elastic-races is therefore less 'peaky' than for rigid races, as may be seen from the curve for c = +0.006 in. (0.152 mm.) of fig. 6.18a.

The above effects can also be observed to some extent when the radial clearance is kept constant and the radial load is varied as in figs. 6.18b, 6.19a and 6.19b. The first two figures show the effects discussed in (A) and (B), and the last figure shows the effects discussed in (B) and (C). The expansion of the outer- and shrinkage of the inner-race in the preloaded bearing, as discussed in (A), tends to relieve some of the preload in the bearing. In figs. 6.18b and 6.19a the point of intersection of the dotted curves (for rigid races) near 90° roller position shows the theoretical preload, but the effective preload is shown by the point of intersection of the solid curves (for fully elastic races) near 90° roller position and depends on the rigidity of the outer and inner races.

The factor $(P_1 Z/F_r)$, where P_1 and Z are the peak roller load, and number of rollers in the bearing respectively, depends on the extent of loaded zone factor (ϵ), as shown in chapters 2 and 3 for rigid races. It was found that $(P_1 Z/F_r)$ for fully elastic races also depends to some extent on ϵ (calculated assuming rigid races from equation 2.43). The variation of $(P_1 Z/F_r)$ for both rigid and fully-elastic races is shown in fig. 6.16. The difference between the two curves in regions A, B and C is due to the effects discussed in (A), (B) and (C) respectively.

Fig. 6.14 shows the variation of non-dimensional equivalent radial load (P_r/F_r) with radial clearance at a radial load of F_r = 9.5 lbs. Both the curves for rigid and fully-elastic races are shown. The curves in general show that (P_r/F_r) decreases rapidly with reduction in interference in the bearing, due to reduction in the preload component of the roller loads. With further reduction in interference, (P_r/F_r) becomes less than 1.0 and attains

a minimum, due to more even roller load distribution compared with rigid race zero clearance bearing. With any further reduction in interference, and then with increase in positive clearance, (P_r/F_r) increases due to increase in the 'peakiness' of roller load distribution.

The difference between the two curves for rigid and fully-elastic races is the following,

(a) for $c < -0.0045$ in., (P_r/F_r) for fully-elastic races is less, due to lower level of roller load distribution as discussed in (A).

(b) in the range -0.0045 in. $< c < +0.0028$ in., (P_r/F_r) for fully-elastic races is higher, due to 'peakier' roller load distribution as discussed in (B).

(c) for $c > +0.0028$ in., (P_r/F_r) for fully-elastic races is lower due to less 'peaky' roller load distribution as discussed in (C).

(P_r/F_r) for rigid races is less than 1.0 at $F_r = 9.5$ lbs. in the range of $c = 0$ to -0.005 in. but, for fully-elastic races and the type of housing under consideration, the range is shifted to $c = -0.0018$ to -0.0063 in. It may be noted here that, (P_r/F_r) greater than, equal to, or less than 1.0, mean that the dynamic life of the bearing is respectively less than, equal to, or greater than the dynamic life of a rigid race zero clearance bearing.

Fig. 6.15 shows the variation of the non-dimensional equivalent radial load (P_r/F_r) with radial load at different radial clearances, for both rigid and fully-elastic races. The explanation of the differences between the corresponding curves for rigid and fully elastic races is similar to that discussed in (A), (B) and (C). The curves, excepting those for zero clearance bearings, show that (P_r/F_r) decreases with increase in radial load. For pre-loaded bearings (P_r/F_r) decreases rapidly with increase in radial load, mainly due to reduction in load of the top half of rollers. For positive clearance bearings (P_r/F_r) decreases with increase in radial load due to more uniform roller load distribution as more and more rollers become loaded. For zero-clearance bearings (P_r/F_r) remains constant for rigid races, and almost constant for fully-elastic races, with increase in radial load.

The values of the non-dimensional equivalent radial load of figs. 6.14 and 6.15 can be generalised as in fig. 6.17. This shows that (P_r/F_r) for rigid races depends on the extent of loaded zone factor ϵ. (P_r/F_r) for fully-elastic races also is found to depend to a large extent on ϵ which is calculated on the basis of rigid race assumption. The difference between the curves for rigid and fully-elastic races can be explained in the same way as for fig. 6.14, using the effects discussed in (A), (B) and (C). Fig. 6.17

has also similar regions A, B and C as in fig. 6.16, though they are not in the same range of ϵ. The ratios of (P_r/F_r), presented in fig. 6.17, may also be expected in similar actual steel bearing applications having similar boundary conditions.

Fig. 6.11 shows the variation in the total radial and component deflections of the Araldite radial roller bearing with radial clearance, at a radial load of 9.5 lbs. The radial deflection, (δ_r) for fully-elastic races is considerably larger than δ_r for rigid races. However, both the curves have similar shapes. The main increase is due to the body deflection of the outer race (δ_b). The outer race deflection for fully elastic races (δ_{or}) is larger than the inner race deflection (δ_{ir}) for fully-elastic or rigid races. δ_{ir} for fully-elastic races is nearly of the same order of magnitude as δ_{ir} for rigid races.

Fig. 6.12 shows the variation in the total radial and component deflections of the bearing with radial load at different radial clearances. Though the radial deflection (δ_r) curves for flexible races run considerably above the corresponding δ_r curves for rigid races, they have more or less similar shapes. The body deflection of the outer race (δ_b) increases almost linearly with radial load. The outer race deflections (δ_{or}) are larger than inner race deflections (δ_{ir}) at all radial loads for fully-elastic races, and both deflections (δ_{or} and δ_{ir}) for positive clearance are higher than for zero clearance. Race deflections for preloaded bearings are higher than for zero (or positive) clearance, due to the preload component of radial load, up to a certain load, after which the deflections become smaller.

The values of K_t and K_b are given in figs. 6.11 and 6.13. K_t and K_b lie in the ranges of about 1.4 to 1.95 and 0.2 to 0.64 respectively, depending on radial clearance and radial load. Similar range of K_t and K_b may also be expected in resembling steel bearing applications having similar boundary conditions. K_t curves for preloaded bearings in both the above figures show a peak, due to the difference in radial clearance (in fig. 6.11) and radial load (in fig. 6.13), between fully-elastic and rigid race cases, at which the top roller is released. The variation in K_b for preloaded bearings is mainly due to the variation in δ_r for rigid-race bearings. The variation in K_t and K_b for zero or positive clearance bearings is very much smaller than that for preloaded bearings.

6.7.2 THE EFFECT OF ROTATIONAL SPEED ON BEARING WITH FULLY-ELASTIC RACES

The range of shaft speeds has been deliberately chosen to be large, to give centrifugal force of roller to maximum roller load ratios larger than normally occurs in actual steel radial roller bearing applications.

The effect of shaft speed on bearing radial and component deflections, and non-dimensional equivalent radial load, are shown in figs. 6.20 and 6.21 respectively. Figs. 6.22 and 6.23 show the effect of shaft speed on roller load distribution. The deflected shapes of races for a bearing with preload and a bearing with zero clearance are shown in figs. 6.35 and 6.36 respectively.

In a preloaded bearing with all rollers loaded, increasing the shaft speed causes an increase in roller load at the outer race, and a decrease at the inner race, as may be seen from fig. 6.22a. The difference in roller loads at the outer and inner races is of course equal to the centrifugal force of the roller. The changes in load at the races cause an increase in outer race diameter, and a decrease in the shrinkage of inner race. This may be seen by comparing the deflected shape of the races of a preloaded bearing at high speed in fig. 6.35, with that at static condition in fig. 6.30. As the inner race (which in this case is solid) is stiffer than the outer race, the reduction in shrinkage of the inner race is less than the expansion of the outer race. As a result the effective preload in the bearing decreases with increase in speed as can be seen from fig. 6.23b, which gives the roller load distribution at the inner race. As the shaft speed is increased, the level of roller load distribution at the inner race decreases, and if all the rollers are loaded at static condition some of the top rollers may be released at the inner race with sufficient increase in speed. If the preload in the bearing is small at static condition, the bearing may have positive clearance at sufficiently high speed.

For zero or positive clearance bearings also, the roller loads at the outer race are increased due to the centrifugal force of the rollers, as may be seen from fig. 6.22b. This tends to expand the outer race diameter as may be seen by comparing the deflected outer race shape at high speed in fig. 6.36 with that at static condition in fig. 6.32. The bearings in both of these figures have the same radial clearance (zero) and the same radial load. The roller load at the inner race is changed only slightly, compared with the increase in roller load at the outer race, and hence, the shape of tne inner race is almost unchanged as may be seen from the deflected shapes of inner

race in the above figures. The expansion of the outer race tends to increase the clearance in the bearing, and hence tne peakiness of roller load distribution, as can be seen in fig. 6.23a.

Fig. 6.21 shows the effect of shaft speed on non-dimensional equivalent radial load (P_r/F_r). For the preloaded bearing, where for most of the speed range all the rollers are loaded, (P_r/F_r) decreases with increase in speed due mainly to the decrease in preload. The curve for the preloaded rigid-race bearing is higher than that for fully-elastic races, due to the higher actual preload. For the zero-clearance bearing, (P_r/F_r) increases with speed, due mainly to the increase in roller loads at the outer race. The curve for the rigid race zero clearance bearing is below the fully elastic case, because of the less peaky roller load distribution for the rigid race bearing, as shown in fig. 6.22b.

Fig. 6.20 shows the effect of shaft speed on the total radial and component deflections of the Araldite bearing. For the preloaded bearing the radial deflection (δ_r) for rigid races remains unchanged with speed. For flexible races δ_r decreases slightly with increase in speed and then starts increasing slowly as the top rollers are released at the inner race. For the zero clearance bearing δ_r increases with speed. The increase is more rapid for fully-elastic races than for rigid races. The body deflection of outer race (δ_b) for both preloaded and zero clearance bearings decreases with increase in speed and the decrease for zero clearance is more than that for preload. For both preloaded and zero clearance bearings the outer race deflection (δ_{or}) increases with increase in speed due to the increase in roller loads. The increase in δ_{or} for zero clearance bearing is greater due to the increase in the 'peakiness' of roller load distribution. The inner race deflection (δ_{ir}) for the preloaded bearing decreases with increase in speed due to the decrease in the roller loads at the inner race. For the zero clearance bearing δ_{ir} increases with increase in speed due to the increase in the 'peakiness' of roller load distribution.

6.7.3 THE EFFECT OF RELIEVED OUTER RACE ON BEARINGS WITH FULLY-ELASTIC RACES

It was shown in the previous sections that the major axis of deflected outer race shape for bearings with low clearance is perpendicular to the direction of the radial load, due to the rigid support of the lower edge of the housing. This makes the roller load distribution peakier. This is

true for many other types of housing. It is possible for these housings, and also for bearings having housing with high rigidity, to modify artificially the roller load distribution to obtain a better bearing performance. This is done by relieving the outer race in the direction of action of the radial load, so that the rollers in this direction carry less load. With the appropriate shape and amount of relief, a more uniform roller load distribution is obtained. Two types of relieved outer race shapes have been investigated:

(a) Tri-lobed relief: The outer race has three uniformly spaced lobes, one being in the direction of radial load. Curve 4 of fig. 6.24a shows the shape of the outer race on a magnified scale for this type of relief.

(b) Bi-lobed relief: In this case the bearing outer race has two lobes, one in the direction of the radial load and the other diametrically opposite to it. Curve 4 of fig. 6.24b shows the shape of the outer race on a magnified scale for this type of relief.

The relieved shapes of the outer race were designed so that they can be machined easily. The procedure of obtaining the relief in the outer race is shown in fig. 6.24. The final and the intermediate shapes drawn in this figure are according to the results obtained by the calculation procedure given in Appendix 6.1. Outer race relief is produced as follows:

(1) For tri-lobed or bi-lobed outer race relief, the outer race ring is held in a three jaw or four jaw chuck, respectively.

(2) All three jaws in case of three jaw chuck, and only two opposite jaws in case of four jaw chuck, are tightened until the radial height difference between the peak and the valley of the deflected outer race shape is equal to the amplitude of relief desired. The remaining two jaws of the four jaw chuck are then used only to lightly locate the ring in position without applying appreciable load. Care must be taken to ensure that the centre of the deflected shape coincides with the axis of the machine tool spindle.

(3) The deflected outer race track is machined to a circular form just touching the valleys of the deflected outer race.

(4) On removal the outer race ring springs back to the original form, producing the desired relief at outer race track.

The effect of relieved outer race on bearing radial deflection and equivalent radial load is given in figs. 6.25 to 6.27, and on the roller load distribution in figs. 6.28 and 6.29. The deflected shapes of races for two tri-lobed relief cases are given in figs. 6.37 and 6.38 and for a bi-lobed relief case in fig. 6.39.

Fig. 6.28a shows the roller load distribution in three Araldite radial roller bearings having radial clearance, c = -0.006 in. (0.152 mm.), one with no outer race relief and the other two with tri-lobed and bi-lobed outer race relief having amplitude of 0.003 in. (0.076 mm.). This figure shows that bearing with relieved outer race gives more uniform roller load distribution. Of the three cases given, the bearing with tri-lobed relieved outer race gives most uniform roller load distribution.

Fig. 6.29a and b give the comparison of roller load distribution, at different radial loads, between Araldite bearings with tri-lobed and bi-lobed outer race relief of amplitude 0.002 in. (0.051 mm.), and with no outer race relief. All the bearings in these figures have radial clearance of c = -0.006 in. (0.152 mm.). These figures also show that tri-lobed relief gives the best roller load distribution at all the radial loads. The deflected shapes of races for bearings with tri-lobed and bi-lobed relief in the outer races having the radial clearance and amplitude of relief as above at a radial load of 9.5 lbs. (42.26 N) are given in figs. 6.37 and 6.39 respectively. The inner curves in the outer race deflected shapes show the initial shape of races on a magnified scale (which is not the same as the scale given in these figures for the deflection). The deflected shapes of the outer race are drawn with respect to these initial shapes. The influence of outer race relief on the deflected shapes of races can be seen by comparing these figures with fig. 6.31.

The roller load distribution obviously depends on the amplitude of race relief. Thus for relatively large relief amplitudes and low radial loads, the maximum load may be carried by some roller other than the normal 'peak' roller (in line with the radial load) as shown in fig. 6.28b. The nature of the roller load distribution for the bearing in this figure at a radial load of 4 lbs. (17.8 N) can be inferred from the deflected shapes of races given in fig. 6.38.

For a low preloaded or positive clearance bearing, at a relatively large amplitude of relief and small radial load, the (two) peak loads now occurring due to race relief may adversely affect the life of the bearing. It is important, therefore, to ascertain the correct amplitude of relief.

Fig. 6.25 shows the effect of the amplitude of relief on the radial deflection and non-dimensional equivalent radial load. In general, radial deflection (δ_r) increases, and non-dimensional equivalent radial load (P_r/F_r) decreases, with increase in relief amplitude, within the range considered. For

radial clearance, c = -0.01 in. (0.254 mm.), the factor (P_r/F_r) decreases rapidly with increase in amplitude of relief, due mainly to the reduction of the preload component of roller loads at the relieved parts of the bearing track. For this clearance the radial deflection is lower for tri-lobed relief case at any amplitude of relief, at the cost of higher (P_r/F_r), compared to bi-lobed relief case. At radial clearance, c_1 = -0.006 in. (0.152mm.) both radial deflection and (P_r/F_r) are lower for tri-lobed case at any amplitude of relief, compared to the bi-lobed case. This shows the distinct advantage of tri-lobed relief. From the bolt and spacer analogy of radial roller bearings given in chapter 3 (figs. 3.3 and 3.4) it can be shown that radial deflection of the preloaded bearing with tri-lobed relief will be lower (mainly due to higher stiffness of the upper half of rollers) than that of the bearing with bi-lobed relief.

Fig. 6.26 gives a comparison between Araldite bearings with preload and race relief, and a bearing having only preload. The bases of comparison are non-dimensional decrease in radial deflection, and non-dimensional decrease in equivalent radial load, compared with a bearing with fully elastic races having zero clearance and no relief (RN-110000). Considering the curves for bearings without relief and having radial clearances, c = -0.006 in. (0.152 mm.) and c = -0.004 in. (0.102 mm.), it is seen that up to a radial load of 11 lbs. (48.9 N), the radial deflection for the former case can be decreased further only at the expense of (P_r/F_r). After this load the decrease in radial deflection for the former case is greater, and also the decrease in (P_r/F_r) is slightly greater than the latter case (having c = -0.004in.). The bearings (RN-110602) with amplitude of relief of 0.002 in. (0.051 mm.) and radial clearance c = -0.006 in., have the actual radial clearance at a different roller position, which varied between c = -0.006 in. to c = -0.004 in. So it might appear that the curves for RN-110602 should lie somewhere between the curves discussed above (for bearings without relief). Considering the bearing with tri-lobed relief the decrease in radial deflection curve lies between them, but the curve for decrease in (P_r/F_r) for radial load above about 6.1 lbs. is well above the curves for the bearings with no relief. Thus considering the bearing (RN-110400) having radial clearance c = -0.004 in. and no relief, it is possible to reduce radial deflection and (P_r/F_r), by having bearing with the correct amount of preload and amplitude of tri-lobed relief. It is interesting to note that it is possible to reduce (P_r/F_r) by increasing the preload alone, even when the radial deflection is decreased. This can be seen from

the curves for bearings without relief above F_r = 11 lbs. However, the decrease in (P_r/F_r) in this case is much smaller than that obtained for bearing with tri-lobed relief.

Similar arguments apply for the case of the bearing with bi-lobed relief (RN-110602), but in this case the decrease in radial deflection and (P_r/F_r) is smaller than is possible with tri-lobed relief case, and hence bi-lobed relief is a less attractive proposition.

From the equivalent radial loads calculated and given in table 6.3, it is possible to compare (P_r/F_r) and hence the percentage increase in bearing dynamic life, as compared with a zero clearance rigid race bearing having no relief (RN-110000) at the same radial load. From this table it is found that the minimum value of (P_r/F_r) among the none, tri-lobed and bi-lobed relief cases considered occurred at the following condition:

Bearing Type	Amplitude and type of relief (in.)	Radial Clearance (in.)	Radial Load, F_r (lb.)	Minimum (P_r/F_r)	Percentage increase in life compared with a zero clearance rigid race bearing having no relief (RN-110000) at the same F_r
RN-110600	None	-0.006	12.0	0.9801	8.35%
RN-110604	0.004 (tri-lobed)	-0.006	9.5	0.9558	19.8%
RN-110603	0.003 (bi-lobed)	-0.006	9.5	0.9674	14.17%

The percentage increase in life given above for the different cases appears to be at or near the ceiling attainable for the corresponding cases. Thus the percentage increase in life possible is maximum for the bearing having tri-lobed outer race relief, with the appropriate amplitude.

Fig. 6.27 gives the non-dimensional decrease in radial deflection and equivalent radial load for an Araldite radial roller bearing having radial clearances, c = - 0.010 in. (0.254 mm.) and c = 0 in. for different amplitudes of relief. Up to the range of load (12 lbs.) of the figure, $(P_r/F_r)_A$ for c=-0.01in bearing decreases with increase in load, but the actual advantage of relieving starts to appear only at the end of the scale. Relieving a zero clearance bearing (or positive clearance bearing) by the proper amount, decreases (P_r/F_r) to some extent throughout the range of the radial load scale. However, the radial deflection of a

zero or positive clearance bearing is higher than for a preloaded bearing, and relieving the races increases the deflection still more.

Though the life of the bearing is increased (or the capacity is increased for the same life) and the deflection can be decreased by proper choice of preload and amplitude of relief, bearing relief has two main practical difficulties:

(1) The relieved bearing can be used effectively only if the direction of radial load is the same or varies only by a small amount: the radial load should act in the direction of a lobe. If the direction of radial load encroaches on, or acts in a direction between two lobes, it will very adversely affect the dynamic life of the bearing due to very much peakier roller load distribution.

(2) The other difficulty concerns assembly. In an actual steel bearing application the amplitude of relief would be only a fraction of a thousandth of an inch. Thus the position of the lobes would be virtually invisible, and would have to be marked and carefully assembled with respect to the eventual loading direction on the bearing.

It will be shown in the next chapter that with some housings it may be possible to arrange that the deflected shapes of the races approximate to the forms of relief discussed in this section, and the foregoing considerations will then apply in that case also. For example, the deflected shape of the outer race may approach tri-lobed relief, if a circular housing of suitable wall thickness is supported with diagonal cruciform ribs.

6.7.4 THE EFFECT OF PARABOLIC SHEAR STRESS DISTRIBUTION IN THE INNER RACE

The external load applied on the shaft is transmitted at any cross section as shear stress. The shear stress distribution from elementary beam theory is parabolic due to the variation of bending moment along the length of the shaft. In the finite-element model for the Araldite radial roller bearing the external load was applied on the shaft as uniform shear stress distribution. The results presented so far are obtained on this basis. However, the effect of parabolic shear stress distribution on the bearing was also studied, case no. 73 of table 6.3 representing this situation. This may be compared with case no. 7 of the same table, in which the inner race shear stress distribution is uniform. The difference in roller load distribution, and bearing radial and component deflections between the two cases is insignificant. Furthermore, no noticeable difference was observed in the deflected shapes of the races for the two cases.

CHAPTER 7 COMPUTED RESULTS FOR BEARINGS WITH FULLY-ELASTIC SUPPORTS, WITH THE ELASTIC PROPERTIES OF STEEL

7.1 GENERAL

The procedure used to investigate the effect of the supporting structure (i.e. housing and shaft) on the steel radial roller bearing characteristics by the finite-element method is the same as that developed in chapter 5. However, one major difference between the housings used in this chapter and that used in chapter 6 (for Araldite bearings) is the method of support of the housings themselves. The housings of chapter 6 rested on a rigid support, whereas in this chapter, for most of the cases, the housing is considered to be the end wall of a cantilevered box structure, thus the somewhat artificial rigid boundary condition of the former is replaced by a more realistic assumption. The finite-element mesh developed and reported in this chapter for the housing can be used to investigate a large number of types of housings, although certain typical configurations were chosen for investigation here. The effect of hollowness of shaft was also considered. Shear-stress distribution in the outer races (where necessary) and inner races, for the cases considered in this chapter, are parabolic.

7.2 CALIBRATION OF ROLLERS ON PLATENS

In section 2.9.1 it was found that, the maximum rolling element load P_{max} at basic static capacity for the roller bearing dimension chosen in section 2.2 is 2185 lbs. (9.73 kN) considering the inner race (which is weaker). Fig. 2.2 gives the width of contact area 2b for this load to be 0.015 in. (0.38 mm). The finite-element mesh for 'calibration' of steel rollers between flat platens shown in fig. 7.1 was designed taking the maximum width of contact area, 2b to be 0.020 in. (0.51 mm). However, a width of contact area somewhat greater than 0.020 in. can also be considered with the mesh. The contact area mesh was made continuous and compatible with that for the complete bearing, and the dimensions for this region are given in figs. 7.4 and 7.5. The width of contact area taken is as given by Hertz's formula. Table 7.1 gives the results for total deflection, given by the approach of the two flat steel platens when a steel roller is loaded between them and, also, roller and platen deflections as obtained by the finite-element method. These results may be compared with the results given by the different formulae,

given in table 2.2. The finite-element results and also the results given by some of the formulae are plotted in fig. 7.2. The agreement between the finite-element result and those from the different formulae is comparable to the agreement between the formulae themselves.

The finite-element results for total, roller and platen deflections were fitted by the method of least squares to curves of the form

$$\delta = A \times P^N$$

using the computer, and the values of A and N are also given in table 7.1. Subscripts 1 and 2 of A indicate the value of the constant for one and two contact areas, respectively. The values of A and N for total and platen deflections are used in the computer program FINELM (as the values of CON1, AAN1 and CON2, AAN2 respectively) for solving complete steel radial roller bearing problems.

7.3 FINITE - ELEMENT MESH FOR STEEL RADIAL ROLLER BEARING WITH HOUSING AND SHAFT

Fig. 7.3 shows the mesh used for finite-element analysis of steel radial roller bearings in housings. Figs. 7.4 and 7.5 show the detail of the mesh near the contact areas in the outer and the inner races respectively. About 70% of all the nodal points are concentrated near the contact areas (in the race rings), because these regions are subjected to the maximum variation of stresses.

The number of elements and nodal points present in the shaft and inner race ring and the housing and outer race ring are given in the following table,

	No. of nodal points	No. of elements
Inner race ring and shaft	401	613
Outer race ring and housing	462	720

Nodal point co-ordinates very near the race tracks (where the mesh is very fine) was found by using the computer.

The mesh is divided into many regions, which are assigned numbers as shown in fig. 7.6. Elements within each region were given constant elastic properties, constant thicknesses and constant body forces per unit volume. These are stored in the computer core as separate arrays with the argument of each given by the number of the region. To change these variables

for any region it is necessary only to change one card containing their values for that particular region. Thus by assigning appropriate values for each region it is possible to consider many different types of housings and shafts. For instance, by assigning very low values of Young's modulus* to regions 1,2,3 etc., making them incapable of transmitting any significant load, it is possible to consider hollow shafts of differing wall thickness. Similarly, a very low Young's modulus in regions 10, 11, 17 and 18, simulates the existence of other openings, which can be in the direction of radial load, at right angles to it, and so on.

The finite-element analysis used represents a two-dimensional case. To take into account the presence of ribs and bosses of thickness greater than the plate it was assumed that the ribbed or bossed portions could be replaced by elements of the same thickness as the plate, but of appropriately higher Young's modulus.

Varying the element Young's modulus E is equivalent in the computer program, to varying the element thickness t by the same factor, as in the element stiffness matrix they occur as a linear product (Ext, see appendix 5.1). For computation, thickness was increased by a factor of 3.0 for the cases with ribs and bosses. This plane-stress computer model of housings with ribs and bosses on the plates (cases S 6 to 8 and R 2 to 7 of figs. 7.9 and 10) is thus slightly more rigid than a three-dimensional model, and of course the actual case. A three-dimensional finite-element model would be feasible, but hardly justified in view of the considerable additional computer time and storage required, for a slight increase in accuracy of the results.

The inner race core axial thickness taken was twice the length of the rollers, was determined for and used in the cases of Araldite bearings, considered in chapter 6.

The basic external dimensions of the finite-element mesh are given in fig. 7.3. The other dimensions are given in sec. 7.3.2.

7.3.1 SOME DESIGN CONSIDERATIONS OF THE FINITE-ELEMENT MODEL MESH

The semi-width of contact area b, at static capacity of the steel radial roller bearing is 0.0075 in. (0.19 mm). The mesh near the contact areas

---

* The actual values of Young's modulus and Poisson's ratio assigned to the regions where there is supposed to be no material are 30 lbs/in.^{2} (which gives a ratio of 10^6 with the Young's modulus for steel) and 0.5 respectively. It should be noted E=0 cannot be used, because it will make the stiffness matrix singular.

(figs. 7.4 and 7.5) was designed considering maximum semi-width of contact area to be 0.010 in. (0.25 mm). However, this mesh can also be used for semi-width of contact area somewhat greater than 0.010 in., because the nodal point load distribution at the contact area given by subroutine NPF is valied if b exceeds the maximum designed value by a small amount. However, in actual analysis the static capacity of the bearing was never exceeded.

As mentioned in the introduction to this chapter, in the case of the 'Araldite' bearings, the housing was supported on an infinitely rigid base, constituting an artificial boundary condition. In this chapter the housings of steel bearings, with the exception of cases T 2 to 9, are considered as the end wall of a cantilevered box structure. Housings are joined to the side walls of the box at their periphery, denoted by areas 13, 20, 28, 31, 37, 43, 44 and 54 in fig. 7.6, where the shear-stress due to the external load is distributed in a parabolic form. This method of boundary support is considered to be more realistic, and is somewhat more flexible than the effect of the rigid base of the Araldite housings (both experimental and computer-simulated). In practice the support may lie between these two cases, but is more likely to approximate to the box-supported configuration.

The shear-stress at any section of the box side walls (which forms a cantilever beam) is constant, thus the length of the side walls considered, from the point of view of shear-stress, is immaterial. Alternatively the housing itself is subjected to a bending moment acting in its own plane, due to the roller loads and supports on the opposite walls. In this case the housing acts as the web, and any of the side walls as the flange, of a beam to support the bending moment. As the width of the flange (which is equal to the length of the cantilever beam) is very large, parts of the flange at a distance from the web (i.e. the housing) do not take a full share in resisting the bending moment, which makes the beam weaker than the elementary theory of bending indicates. Usually the actual width of the flange is replaced in such beams by a certain reduced width, such that the elementary theory of bending, applied to such a transformed beam cross section, gives the correct value of maximum bending stress. This reduced width of flange is called the 'effective width'. The effective width of the flange (side walls) to be considered with the housing was calculated for the probable bending moment distribution in a way similar to that given by Timoshenko and Goodier in ref. 46 (page 262-268), and is given in appendix 7.1. The effective width of the flange was found to be 1.35 in. (34.3 mm, including the thickness of the plate, which is 0.45 in.).

The effects of variation of the width of the 'flange' (i.e. the side walls), considered as the thickness of the elements of the outer race shear area, are shown in figs. 7.7 and 7.8. The variation of thickness of the outer race shear area has comparatively small effect on the bearing as may be seen from fig. 7.7. Increasing this thickness has the greatest effect on the body deflection of the outer race, but the change in deflection of the inner or outer race is comparatively small. For example, if the thickness is increased from 0.45 in. (11.4 mm) to 1.35 in. (34.3 mm), the total bearing deflection decreases from 685 μin. (17.4 μm) to 633 μin. (16.1 μm), out of which 84.6% is due to the decrease in body deflection of the outer race, and only 15.4% is due to the other components of the bearing deflection. As the thickness of the outer race shear area is increased, its support rigidity increases, which tends to make the roller load distribution peakier. But this increase is also small as is evident from the small increase in the equivalent radial load in fig. 7.7.

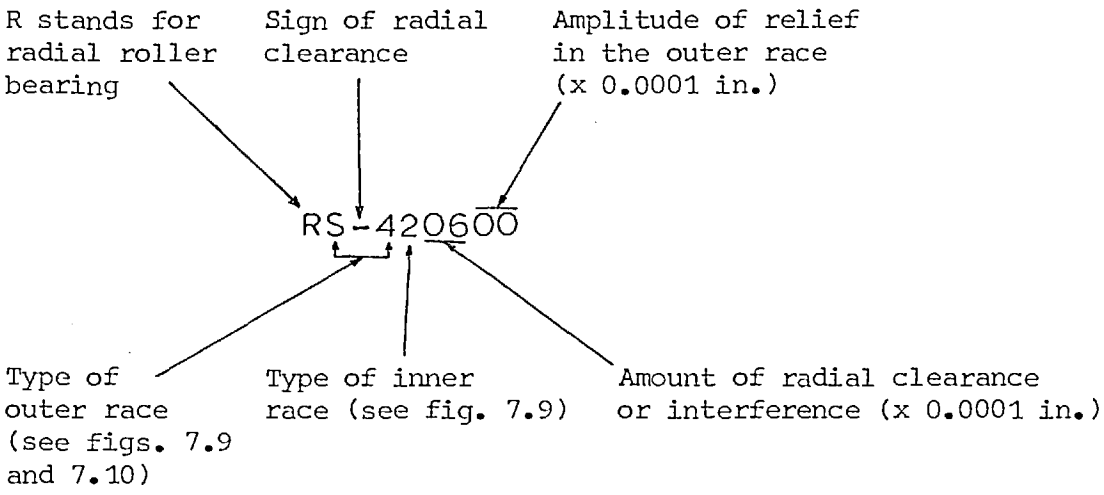
Fig. 7.8 shows the variation of K_t, K_b, and the ratio of outer to inner race deflection (δ_{or}/δ_{ir}) with the thickness of outer race shear area. The factor (δ_{or}/δ_{ir}) decreases slightly with increase in the thickness, due to the increase in stiffness of the outer race and peakiness of the roller load distribution.

In case of Araldite bearings, where the base was infinitely rigid, the major axis of the deflected outer race curve was perpendicular to the direction of radial load. In the present case (for steel) the major axis is in direction of the radial load (see fig. 7.78) due to the reduction in the support rigidity. This is advantageous for the fatigue life of the bearing, because the roller load distribution is more uniform. Comparison of the deflected shape of the outer race with the case of relieved races in chapter 6, indicate the reason for the decrease in peakiness of the load distribution.

The effect of the increase in thickness of the outer race shear area on the deflected shape of the races was also found to be very small.

7.3.2 CODING OF THE STEEL RADIAL ROLLER BEARINGS IN HOUSINGS

A numbering system similar to that of the Araldite bearings is also used for steel bearings. A typical example is,



Thus, the bearing number in the example represents a steel radial roller bearing, the outer race ring of which is mounted in a housing (S 4) which is in the form of a plate (0.45 in. thickness) having a hole at 45^{o} to the direction of radial load (fig. 7.9) and the inner race ring is mounted on a solid shaft (no.2). The bearing has a preload equivalent to c=-0.0006 in. (15.24 μm) interference and the outer race has no relief.

In graphical presentation, if any of the above characters is a variable, it is replaced by 'x'.

Housings and shafts illustrated in figs. 7.9 and 7.10 have all been obtained from the same mesh of fig. 7.3 by assigning the appropriate values of elastic properties, element thicknesses, and body forces, for each region (shown in fig. 7.6). The thickness of the outer and inner race rings have been taken as equal to the length of the rollers (i.e. 0.45 in.) for all the cases. The dimensions of the other parts of the races which have been used* are given below.

Shafts

Shaft no. (see fig. 7.9)	Outside diameter, OD (in.)	Inside diameter, ID (in.)	ID/OD
2	2.15	0.00	0.000
3	2.15	0.80	0.372
4	2.15	1.40	0.651
5	2.15	1.80	0.837

* Three configurations provided in the finite element mesh, were not used in the analysis.

Bosses and Circular housings

Housing nos. (see figs. 7.9 and 7.10)	Outside diameter, OD (in.)	Inside diameter, ID (in.)	OD/ID
S 8,R 4,R 7,T 4,T 7	6.00	3.25	1.847
S 7,R 3,R 6,T 3,T 6	4.50	3.25	1.385
S 6,R 2,R 5,T 2,T 5,T 8,T 9	3.72	3.25	1.145
S 2	3.25	3.25	1.000

Other openings in housings S 3,S 4 and S 5

Diameter, 1.5 in.

Radial distance, 3.0 in.

Disposition with respect to radial load, 0^{o}, 45^{o} and 90^{o}

Breadths of the ribs and the outer race shear area, 0.5 in.

Radial thickness of the inner and outer race rings, 0.125 in.

7.4 CONVERGENCE OF ROLLER LOAD DISTRIBUTION FOR STEEL RADIAL ROLLER BEARINGS

The values of FCTR for convergence* of roller load distribution depend on the type of housing and shafts. For less rigid housing or shaft a lower value of FCTR is required for rapid convergence. For a solid shaft (no.2) with a rigid housing (no. S 2) fig. 7.11 shows the rate of convergence with different values of FCTR. Plotting the number of iterations required for convergence to a certain RMS error in roller load distribution against FCTR in fig. 7.13a, it is found that the value of FCTR for maximum convergence for this case is 3.0.

Fig. 7.12 shows the rate of convergence for a hollow shaft (no.5), and the same rigid housing as in the previous case, for different values of FCTR. Fig. 7.13b shows that the maximum rate of convergence is near a value of FCTR=0.25 and that above the value of FCTR=0.4 the roller load distribution does not converge at all. It was found that FCTR1 has little influence on the rate of convergence.

For a shaft with inside-to-outside diameter ratio of 0.651 (no.4) with rigid housing the value of FCTR taken was 1.0, and for most of the cases of this combination the number of iteration required to converge (below RMS error of 1.0 lb.) was 7.

The limiting RMS error to stop iteration for the results of all the cases given in table 7.2 was 1.0 lb., excepting for the cases of circular

*The explanation of this has been given in step no.24 of section 5.4.1

housings (T-series), for which the limiting RMS error was set at 2.0 lb.

7.5 RESULTS AND DISCUSSION OF THE EFFECTS OF DIFFERENT TYPES OF HOUSING AND SHAFT ON THE PERFORMANCE OF STEEL RADIAL ROLLER BEARINGS

A summary of results obtained by finite-element analysis for steel radial roller bearings having different combinations of shaft and housing is given in table 7.2.

The effect of variation of radial load on the bearing performance is studied only in section 7.5.1. In the later sections, as the effect of variation of radial load is found to be more predictable (from results of section 7.5.1) than the other variables, and also as the number of variables under consideration is large, the radial load, F_r is kept constant at 5000 lbs. (22.24 kN).

The body deflection of the outer race for all the cases in this chapter, with the exception of the cases of circular housings (T-series), is measured with respect to two datum points, each at the opposite edges of the housing and at the same height as the centre of the races. For the T-series housings the body deflection of outer race is the absolute body deflection of it.

7.5.1 BEARINGS WITH HOLLOW SHAFTS

Figs. 7.14 to 7.25 show the variation of radial deflection, non-dimensional equivalent radial load, roller load distribution etc. and figs. 7.78 to 7.91 show the deflected shape of the races for different shaft hollowness, radial clearances and radial loads. In all the cases under consideration in this section the housing is of the type S 2 (fig. 7.9).

The total and different component deflections of the bearing with fully elastic housing and shaft (solid), and the corresponding deflections assuming rigid races are compared in fig. 7.14. The body deflection considering rigid races is obviously zero. The total bearing deflection for elastic races is more than that for rigid races, mainly due to the larger outer race deflection and the body deflection of the outer race. As the shaft is solid, the inner race deflections for elastic and rigid races are nearly the same.

Fig. 7.15 shows the variation of the total, and the different component deflections, with radial load for different degrees of shaft hollowness, for a radial clearance of c= -200 μin. (-5.08 μm). The body deflection of the outer race is nearly the same for all shaft hollowness and

the curves are almost linear. The total radial deflection increases with decreasing wall thickness of shaft, lowest deflection occuring with a solid shaft. The main increase in bearing deflection for a hollow shaft is, as expected, due to the increase in the inner race deflection. For hollow shafts, the peakiness of roller load distribution (and also the peak roller load) is less than that for solid shafts, as may be seen from figs. 7.24 and 7.25. Due to this, the outer race deflection decreases with increase in hollowness of the shaft (fig. 7.15). This may also be seen from the deformed shape of the races for solid and hollow shafts at the same radial load and clearance, e.g. figs. 7.78 and 7.89.

Fig. 7.16 shows the variation of total bearing deflection with radial clearance for different hollowness of the shaft. The linear portion of the curves for preloaded bearings increases with increase in the shaft hollowness. This is because, for a hollow shaft, the preload required at a particular radial load for the top roller to be just loaded is greater (due to the lower shaft radial stiffness) than that required for a solid shaft, or less hollow shaft. The difference between the total deflection curves for shafts of different radial stiffness increases with increase in radial clearance. This is because the hollow shaft, which is succeptible to more deformation, is held more securely by the rollers when the radial clearance is lower. For heavily preloaded bearings the deflected shape of inner races for a hollow shaft is nearly circular, as may be seen from fig. 7.89. However, as the preload is decreased, or the bearing is given some positive clearance, the shaft is held by fewer rollers, and there is less restriction on shaft deflection. Hence the inner race deflects laterally, as may be seen from figs. 7.90 and 7.91.

Fig. 7.17 shows the variation of total, and different component deflections, with increase in the hollowness of the shaft. The fact that the outer race deflection decreases and the total and inner race deflection increases with increase in the shaft hollowness, can be seen more readily from this figure. The rate of increase in inner race deflection increases with increase in radial clearance in the bearing (from negative to positive). This is also due to the lower lateral restriction with increase in clearance. The rate of decrease in outer race deflection increases after a certain increase in shaft hollowness (see the curve for c= +600 μin., above a shaft diameter ratio of 0.5). This is due to the decrease in peak roller load with increase in shaft hollowness; maximum roller load actually starts to move from the line

of action of the radial load after a certain hollowness is reached (see fig. 7.25b for bearing no. RS+240600, and for bearing no. RS+250600, the position of maximum roller load is actually at about, $\psi_j=45^o$).

Fig. 7.18 shows the variation of non-dimensional equivalent radial load (P_r/F_r) with radial clearance for different hollowness of the shaft. The (P_r/F_r) curves become progressively more flat with the increase in shaft hollowness. It may be recalled here that, a ratio of $P_r/F_r=1.0$ means that the life of the bearing is equal to that for a rigid race zero clearance bearing, and when (P_r/F_r) is more or less than 1.0 the life is less or more, respectively. (P_r/F_r) for even some positive clearance bearings with solid shaft is lower than 1.0, which is unlike the cases considered in Araldite bearing section. The reason for this is that the major axis of the deflected shape of outer race for the present cases is in the direction of radial load due to the less rigid support (which is effectively equivalent to having relieved races), giving a more uniform roller load distribution. In addition to the above reason, (P_r/F_r) for hollow shafts is lower than 1.0 for positive clearance, and for a larger range, due to even more uniform roller load distribution (as may be seen in fig. 7.25), than for solid shaft.

The ratio (P_r/F_r) for heavily preloaded bearings with solid shaft is high, due to the preload component of roller load distribution. However as the shaft becomes hollow the preload component decreases due to the shrinkage of the shaft and this effect increases with increase in shaft hollowness. For this reason, the factor (P_r/F_r) decreases with increase in shaft hollowness for high preload.

The minimum value of (P_r/F_r) at which the life is maximum, occurs at or near a radial clearance of c= -200 μin. (-5.08 μm) for F_r= 5000 lbs. and is almost independent of shaft hollowness for less hollow shafts.

Between the range of clearance of about c= 0 to c= -400 μin. (-10.16 μm), which is desirable in the bearing (the actual desirable value of c depends on F_r), the ratio (P_r/F_r) is minimum at a particular shaft hollowness as may be seen from fig. 7.19. The value of inner to outer diameter ratio* of shaft at which (P_r/F_r) is minimum is about 0.65 (for c= -200 μin.) to 0.75 (for c= 0 μin.). Shaft number 4 has inner to outer diameter ratio of 0.651. It may be seen from figs. 7.24 and 7.25 that the roller load distribution at this shaft

---

* Note that the equivalence of these inner-to-outer diameter ratios for shafts, with those of an actual application will strictly depend on taking appropriate values for the equivalent core thickness for both.

hollowness is also most uniform, and the roller in direction of radial load is just carrying maximum load, and the peak is just on the point of moving from this roller.

Fig. 7.20 shows the variation of (P_r/F_r) with radial load for different hollowness of the shaft at c= -200 μin. The factor (P_r/F_r) is large at low value of radial load, due to comparatively large preload components of the roller loads. With increase in radial load (P_r/F_r) decreases rapidly and eventually becomes almost constant.

Figs. 7.21 and 7.22 give the variation of the values of K_t and K_b for different hollowness of the shaft with radial clearance and radial load, respectively.

The effect of high speed on non-dimensional equivalent radial load (P_r/F_r), the ratio of outer to inner race deflection $(\delta_{or}/\delta_{ir})$, K_t and K_b for bearing number RS-250200 at radial load F_r= 2000 lbs. (8.9 kN) is shown in fig. 7.23. It may be seen from this figure that the factors (P_r/F_r), $(\delta_{or}/\delta_{ir})$ and K_t increase and K_b remains constant with increase in speed.

Figs. 7.24 and 7.25 show the roller load distribution for different shaft hollowness and radial clearances. These figures show the more uniform roller load distribution for reasonably hollow shafts, and also the fact that, if the bearing clearance is sufficiently high and the shaft is sufficiently hollow, maximum roller load may be carried by some roller other than that in line with the external load. For positive (or zero) clearance bearings the loaded zone increases with increase in shaft hollowness.

Figs. 7.78 to 7.81 show the deformed shape of the races on loading for the steel bearings with solid shafts having radial clearances c= -600, -300, 0 and +600 μin. respectively. The local deformations in these figures are much 'sharper' than for the Araldite bearings, because of the smaller width of contact area for steel. Figs. 7.78, 7.82, 7.84 and 7.89 show the deflected shape of races with increasing shaft hollowness at high interference (-600 μin.). In these figures the increasing shrinkage of the inner race, and small decrease in expansion of the outer race, can be observed.

Figs. 7.81, 7.83, 7.88 and 7.91 show the deflected race shapes at c= +600 μin. with increasing hollowness. These figures illustrate the fact that as the shaft becomes more hollow for a high-clearance bearing, the inner race tends to 'flatten out' over the rollers, increasing the loaded zone of the bearing. The large deflection for hollow shafts around the peak roller position is responsible for the low load on these rollers.

The deflected shapes of races at three different radial loads for

a bearing with hollow shaft and radial clearance of c= -200 μin. are given in figs. 7.85 to 7.87. At low load all, or nearly all, the rollers are loaded and hold the inner race securely so that it is circular. But as the radial load is increased the number of rollers carrying load decreases and the inner race starts to expand in a direction perpendicular to the radial load.

7.5.2 BEARINGS IN HOUSINGS WITH OTHER HOLES

Figs. 7.26 to 7.30 show the effect of angular position with respect to the external radial load, of other holes in the housing, on the deflections, non-dimensional equivalent radial loads (P_r/F_r), K_t, K_b and load distribution, for a bearing with solid shaft (no.2), and at different radial clearances. Figs. 7.31 to 7.34 show similarly effects of holes for a hollow shaft (no.4). Figs. 7.92 to 7.95 show the deflected shape of races for holes at different angular positions, for a solid shaft, and figs. 7.96 and 7.97 for hollow shaft.

The outer race deflection is greater in the direction of an opening in the housing wall, as may be seen from figs. 7.92 to 7.97. All these figures, excepting fig. 7.94, are for radial clearance c= -300 μin. The deflected shape of races for solid and hollow shafts are given in figs. 7.92 and 7.96 when there is a hole at 0°, and in figs 7.93 and 7.97 for holes at 45° to the radial load, and on either side of it. For holes at 90° to the radial load (on either side) the effect on the deflected shape of races is more pronounced for a high preload e.g. equivalent to c= -600 μin. (fig. 7.94), than for a lower preload, e.g. equivalent to c= -300 μin. (fig. 7.95). Rollers at 90° to the radial load carry more load with greater preload. The effect of other holes will obviously increase with their size and proximity to the bearing.

Figs. 7.26 and 7.31 show the variations in total and component deflections of the bearing with radial clearance, for different positions of holes in the housing, and for solid and hollow shafts. Total radial deflection is larger for housings with additional holes in any position, but it is largest for holes at 45° to the radial load on each side of it. Outer race deflection for a hole at 0° is greatest, as it is directly in the line of radial load; the peak roller load for this case is lower than for the other positions of holes (as may be seen from figs. 7.29, 7.30 and 7.34), and consequently the inner race deflection is a minimum. The peakiness of roller load distribution is greatest for holes at 45°, hence the inner and outer race deflections are comparatively larger. Body deflection of outer race is also largest for holes at 45°. The effect of holes at 90° is much less pronounced.

Figs. 7.27 and 7.32 show the variation of non-dimensional equivalent radial load (P_r/F_r) with radial clearance for the same arrangements of holes and shafts as previously. At high preload the presence of any hole near the bearing tends to relieve the preload in the direction of the hole. This reduces the equivalent radial load at high preload. At about C =-450 μ in. (for F_r = 5000 lbs.) the (P_r/F_r) curve for holes at 45° crosses the curve for housing without holes, and remains above it for any further increase in clearance. The non-dimensional equivalent radial load (P_r/F_r) for holes at 0° and 90° is lower than for the no-hole case. The curves for holes at 90° and 0° are virtually coincident at high preload. They become separate at lower preload, the curve for 90° holes being lower than for 0° holes with increase in clearance. At further clearance still the curves cross over, and the equivalent radial load for a 0° hole position becomes least. The change of non-dimensional equivalent load difference for cases with and without holes is also plotted in fig. 7.32, for the case of hollow shafts.

From the evidence of deflection and equivalent radial load, the preferred situation is to have no additional holes at all, but then to dispense them at 90°, 0° and 45° to the radial load, in order of decreasing preference.

It should be noted that in the above cases the number of holes in the housing for 45° and 90° positions are two in each case and for 0° position it is one. If there is only one hole in the housing at 45° or 90° position, some estimate of deflection and equivalent radial load may be obtained by taking average of the curves for two holes at 45° or 90° position, and no-hole case. This will still make the equivalent radial load for a housing with a hole at 45° position maximum, and that for hole at 90° will be lower than the no-hole case. However the radial deflection for one hole at 45° or 90° position will be smaller than the corresponding two-hole cases. Overall, if an additional hole is necessary, it is always safer to position it at 90° to the radial load. If the direction of radial load is non-reversing, the holes can be safely placed at the 180° position.

Fig. 7.28 and 7.33 show the variation of K_t and K_b with radial clearance for different positions of holes in the housing for bearings with solid and hollow shafts, respectively.

Figs. 7.29(a) and (b) and 7.30(a) and (b) show the roller load distribution in the bearings with solid shafts for different positions of holes, at radial clearances -600, -300, 0 and +600 μin. Figs. 7.34(a) and (b) show the similar roller load distributions for a hollow shaft at radial clearances

-600 and +600μin. It may be seen that the roller loads in the direction of holes are smaller than they would be in the absence of holes, due to the increased local flexibility of the outer race (as may be seen from figs. 7.92 to 7.97).

7.5.3 BEARINGS IN BOSSED HOUSINGS

The effect of boss radial thickness on bearing deflection, K_t, K_b, non-dimensional equivalent radial load (P_r/F_r) and roller load distribution in a steel radial roller bearing with solid shaft at different radial clearances, is given in figs. 7.35 to 7.39. Similar effects on bearings having a hollow shaft (no. 4) is given in figs. 7.40 to 7.43. The deflected shape of races for bearings with hollow shafts, for different boss radial thicknesses, is given in figs. 7.98 to 7.103; fig. 7.101 is for a solid shaft.

The outer race expansion of a bearing under heavy preload reduces as the boss radial thickness is increased. This may be seen from the deflected shape of outer races given in figs. 7.84, 7.98 and 7.102; these are for housings with no boss, a thin boss and the thickest boss used, for a bearing with radial clearance C = -600μin. As this 'expansion' decreases, the level of roller load increases for highly preloaded bearings, and tends to approach the distribution obtained for 'rigid races', as may be seen from figs. 7.39a and 7.43a. This increase roller load level is greater for solid shafts (fig. 7.39a) than for hollow shafts (fig. 7.43a), as the relatively flexible hollow shaft is more readily compressed (see the deflected shapes of the inner races in the figures mentioned above). This also tends to decrease the level of roller load distribution to some extent.

The outer race retains its circular shape better as the boss radial thickness is increased, as may be seen from figs. 7.99, 7.100, and 7.103 (which are for boss outer-to-inner diameter ratios 1.145, 1.385 and 1.847, respectively), for a radial clearance of C = -300μin., and hollow shaft. For a solid shaft, figs. 7.79 and 7.101 illustrate the situation for the 'no-boss' and the thickest boss, respectively, at the same radial clearance. The tendency of the outer race to remain circular produces a 'peakier' roller load distribution, which approaches that obtained from 'rigid races'. Figs. 7.39b and 7.43b show the roller load distribution for solid and hollow shafts respectively in bearings with high radial clearance (c = +600μin). The roller load distribution becomes peakier with increasing boss thickness, but the effect is much smaller with a hollow shaft (fig. 7.43b), than with a solid shaft (fig. 7.39b).

Fig. 7.35 and 7.40 show the variation of total radial and component deflections with increasing thickness of the boss, at different clearances, for solid and hollow shafts. The outer race deflection decreases (first rapidly) with increase in boss outside diameter, with consequent increase in peakiness of roller load distribution. This increases the inner race deflection. Also the body deflection of outer race decreases as boss outside diameter rises. The overall effect is that the total radial deflection of the bearing decreases with increasing boss outer diameter, but this is subject to diminishing returns.

Fig. 7.36 for a solid shaft, shows the percentage decrease in total radial and body deflection compared with a housing with no boss (no.S 2) plotted against radial clearance, for different boss thickness. At a preload of about $c = -400\,\mu$in. for $F_r = 5000$ lbs. (possibly when the top roller is just released) the decrease in total radial and body deflection is at a maximum.

Figs. 7.38 and 7.42 show the variation of K_t and K_b with increase in boss radial thickness for solid and hollow shafts respectively, at different radial clearances. K_t decreases, at first rapidly, with increase in boss outside diameter, whereas K_b remains almost constant at first, and then decreases with further increase in boss diameter.

Figs. 7.37 and 7.41 show the effect of boss thickness on non-dimensional equivalent radial load (P_r/F_r). Equivalent radial load increases with boss outside diameter due to the increasing peakiness of roller load distribution. At high preload (e.g. when $c = -600\,\mu$in.) the increase in equivalent radial load is rapid, particularly at the start, as the rising radial stiffness of the boss restricts radial expansion of the outer race.

7.5.4 BEARINGS IN HOUSINGS WITH BOSSES AND RIBS

Ribs are normally employed to increase the rigidity of the housing plate in bending, nevertheless they have some effect on the bearing. Two classes of ribbed housings have been considered:

(a) Upright cruciform ribs, with the ribs disposed at 0° and 90° to the radial load. Housings R2, R3 and R4 have this form of ribs. Symbol used to denote this form of ribbed housing is ⊕.

(b) Diagonal cruciform ribs, with the ribs disposed at 45° to the radial load. Housings R5, R6 and R7 have this form of ribs. The symbol used is ⊠.

In both the classes the outer diameter of the boss have been varied.

The deflected shapes of races for bearings with the thinnest boss and hollow shaft are given in figs. 7.104 and 7.105 for housings with upright and diagonal cruciform ribs respectively. Figs. 7.44 to 7.49 show the excess deflections K_t, K_b, excess non-dimensional equivalent radial load, and excess roller load distribution, for a bearing with housing having upright cruciform ribs. Similar graphs for the case of a bearing with diagonal cruciform ribs are given in figs. 7.50 to 7.55. The first three figures, and the last three figures, are for bearings with solid and hollow shafts, respectively. The excess deflection etc. are for housings with and without ribs and a particular boss outside diameter. The excess deflection, excess non-dimensional equivalent radial load, and excess roller load distributions plotted show clearly the effect of the ribs. In general this is small in comparison to the total values and decrease with increase in boss outside diameter. The effect of ribs will obviously depend on their thickness and that of the plate. However, these values are kept constant here. The variation of relative thickness of ribs and plate would affect only the magnitude of the effects on the bearing, whilst the trends would be virtually the same as presented here.

The deflected shapes of races of figs. 7.104 and 7.105 are for hollow shafts and housings with upright and diagonal cruciform ribs, and may be compared with the equivalent 'non-ribbed' case of fig. 7.99. Overall deflection of outer race is lower in the direction of the ribs, and as a result, there is an increase in roller load in this direction, as may be seen from figs. 7.46, 7.49, 7.52 and 7.55 (b and c in each figure). The first two figures are for upright ribs, and the last two for diagonal ribs. The increase in roller load in the direction of ribs is greater in case of a solid shaft (figs. 7.46 and 7.52) than for the hollow shaft (figs. 7.49 and 7.55). However, with increasing boss outside diameter, the effect of the ribs on roller load distribution decreases, as may be seen from part (c) of the above four figures.

This can also be seen from the excess non-dimensional equivalent radial load, shown in figs. 7.46a, 7.49a, 7.52a and 7.55a. The non-dimensional equivalent radial load (P_r/F_r) for upright ribs (figs. 7.46a and 7.49a) is higher than for a housing with no ribs, at all radial clearances. This is because the roller load distribution for a housing with upright ribs is peakier than the 'no-rib' case, as is evident from positive values of excess peak roller loads shown in parts b and c of the same figures. The rollers at 90° to the radial load (which do not share the radial load)also have positive excess roller load for preloaded bearing and this also causes some increase in the equivalent

radial load.

For diagonal ribs and small preload or positive clearance, the non-dimensional equivalent radial load (P_r/F_r) actually decreases compared with the 'no-rib' case, as may be seen from figs. 7.52a and 7.55a. This is because the rollers at 45° to the radial load carry positive excess roller loads, and those at 0° carry negative excess roller load (as shown in parts b and c of the above figures). Thus due to this increase and relief of load in the right positions, the roller load distribution is more uniform than for a housing without ribs. However, non-dimensional equivalent radial load for very high preloaded bearings ($\epsilon > 1.0$) is always greater than the no-ribbed case, even with diagonally ribbed housings. This is because ribs introduce additional rigidity and tend to raise the whole roller load distribution curve as all the rollers are loaded, though the curves may still be less peaky for diagonal ribs.

Figs. 7.44 and 7.47 show the excess radial and component deflections for a housing with upright cruciform ribs over the corresponding deflections without ribs. The outer race deflection for this position of ribs decreases due to the rigidity of the ribs (as may also be seen from the deflected shape of outer race in fig. 7.104). This reduced outer race deflection increases the peakiness of roller load distribution curve and this in turn increases the inner race deflection. The body deflection also decreases due to the rigidity of the ribs. All these give rise to a lower radial deflection for upright ribs compared with the 'no-ribs' case. Again, the effect of the ribs in terms of the decrease in outer race and total radial deflections and the increase in inner race deflection, decreases with increasing boss outside diameter.

The excess body deflection of the outer race is almost constant for both solid and hollow shaft cases. Though the outer race deflection may be less by as much as 8% for the thinnest boss, the decrease in total radial deflection for the position of ribs under discussion is less than 3%.

Figs. 7.50 and 7.53 show the excess radial and component deflections of a bearing having housing with diagonal cruciform ribs over the corresponding 'no-ribs' case. In this case the inner race deflection decreases due to less peaky roller load distribution as explained earlier. The outer race deflection may increase or decrease, depending on radial clearance and boss outside diameter. The maximum decrease occurs in the body deflection of the outer race (which may be as much as 10 - 12% for the thinnest boss used). The total radial deflection for a housing with diagonal ribs also decreases in comparison

with the 'no-ribs' case (maximum about 5% decrease for the thinnest boss), most of this decrease being due to the decrease in body deflection of the outer race. These figures also show that the effect of ribs decreases as boss thickness is increased.

Figs. 7.45 and 7.48 give the value of K_t and K_b for a housing with upright cruciform ribs and with solid and hollow shafts respectively. Figs. 7.51 and 7.54 are the similar graphs for a diagonally ribbed housing. These values are lower than the 'no-ribs' case, due to the lower bearing radial deflection, as explained earlier. K_t and K_b for a housing with diagonal ribs are lower than those for upright ribs.

From the above results it is found that for a housing with diagonal cruciform ribs, the bearing deflection and the equivalent radial load decreases compared with the 'no-ribs' case. Upright ribs give rise to increased equivalent radial load (i.e. less bearing life) and slightly less decrease in bearing radial deflection (less decrease than the case of diagonal ribs), with respect to a housing without ribs. Thus the diagonal cruciform configuration of ribs is preferable to the upright form.

7.5.5 CIRCULAR (BOSSED) HOUSINGS ON RIB SUPPORTS ONLY

The three outside-to-inside diameter ratios of the circular housings used are the same as those used for the bosses (i.e. 1.145, 1.385 and 1.847). Four types of support configurations of the circular housing have been considered:

(a) Upright cruciform support; with the supports disposed at 0° and 90° to the radial load. Housings T2, T3 and T4 have this form of support, denoted by the symbol .

(b) Diagonal cruciform support; with the supports disposed at 45° to the radial load. Housings T5, T6 and T7 have this form of support, denoted by the symbol .

(c) Upright part-cruciform support, having three supports - one in the direction of radial load and the other two on either side of it at 90° (i.e. the same as (a) without the top support). Housing T8 has this form of support, denoted by the symbol .

(d) Diagonal part-cruciform support, have two supports at 45° to the radial load on either side (i.e. the same as (b) without the top two supports). Housing T9 has this form of support, denoted by the symbol .

The outer ends of the supports are fixed and the body deflection

of the outer race, δ_b is the absolute deflection of the two points on the outer race track at 90^o to the radial load on either side. The bearing deflections, non-dimensional equivalent radial load (P_r/F_r), K_t, K_b and roller load distributions for housings with upright cruciform support are given in figs. 7.56 to 7.59 for a solid shaft, and in figs. 7.60 to 7.63 for a hollow shaft (no. 4). For a housing with diagonal cruciform support they are given in figs. 7.64 to 7.67 for a solid shaft, and in figs. 7.68 to 7.71 for a hollow shaft (no. 4). The effect of shaft speed on the bearing with the thin circular housing, is given in fig. 7.72 for upright support, and in fig. 7.73 for diagonal support.

The bearing deflections, non-dimensional equivalent radial load (P_r/F_r), K_t, K_b and roller load distribution for a bearing with thin circular housing having part-cruciform supports, and hollow shaft are given in figs. 7.74 to 7.77. The deflected shapes of races for different cases are given in figs. 7.106 to 7.121.

Upright cruciform support ⊹ :

Figs. 7.107 to 7.110 show the deflected shape of races with thin circular housing having upright cruciform support, and hollow shaft at radial clearances -600, -300, 0 and +600 μin. Fig. 7.106 is for the solid shaft at a radial clearance of -300μin. The outer race deflected shapes have three lobes. The lower two lobes are formed by the roller loads acting on the span of the outer race, which is acting as a beam, between the two supports. The top lobe is formed by the tension in the upper support. Due to the roller loads on either side of the bottom support (which are responsible for the lower two lobes), the points on the outer race track at 90^o to the radial load on either side are deflected downwards. As the outer race deflection (δ_{or}) is measured with respect to these two points, δ_{or} decreases and may, in fact, be negative as may be seen from figs. 7.106 to 7.110. The body deflection of the outer race comprises two parts:

(1) due to the deflection of the lower supports, and

(2) due to the deflection of the above two points with respect to the top of the lower supports.

Part (2) is large for this housing compared with other types. Inner race deflection is greater in the directions of the supports, due to larger roller loads in these directions.

Figs. 7.108, 7.111 and 7.112 show the deflected shapes of the bearing races with a hollow shaft, for increasing outside diameter of the

housing at a radial clearance of -300 μin. The figures show that the size of the lobes decreases, and hence the effect of the supports decreases, with increase in the housing outside diameter.

Figs. 7.59 and 7.63 show the roller load distribution in the bearing with solid and hollow shafts. The roller loads in the direction of supports, excepting the top one, increases. Rollers in the direction of the top support do not carry load, as the outer race in this region deflects outwards due to tension in this support. The roller load distribution in the above figures is for different radial clearance with the thinnest housing in parts (a), and for different housing outer diameter at a radial clearance of -300 μin. in parts (b). From parts (b) it is clear that as the housing outer diameter increases, the peakiness of roller load distribution decreases, and it tends to approach the curve obtained by assuming rigid races.

Figs. 7.57 and 7.61 show the non-dimensional equivalent radial load (P_r/F_r) for a bearing with circular housing having upright cruciform support, for solid and hollow shafts. For the case of highly preloaded bearings (e.g. for c = -600 μin.), the (P_r/F_r) curves exhibit a minimum due to two opposing effects:

(i) factor (P_r/F_r) tends to decrease with increasing housing outside diameter due to the reducing effects of supports (supports increase the peakiness of roller load distribution curve).

(ii) factor (P_r/F_r) tends to increase with increasing outside diameter of housing, due to the increase in the preload component of the roller loads (as shown in section on effects of boss thickness).

The combination of the above effects produces a minimum value of (P_r/F_r) at high preloads. For the curves at other clearances only effect (i) is present and hence (P_r/F_r) decreases with increase in the housing outside diameter. The decrease in (P_r/F_r) is rapid up to a diameter ratio of about 1.5 but is thereafter subject to diminishing returns. This value of 1.5 could therefore be taken as the value of outer to inner diameter ratio of housing where the effect of support is quite small.

The radial and component deflections of the bearing with circular housing having upright cruciform supports for solid and hollow shafts are shown in figs. 7.56 and 7.60 respectively and, K_t and K_b in figs. 7.58 and 7.62. From these figures it may be seen that body deflection of the outer race (δ_b) is a substantial part of the total radial deflection. A part of δ_b, as mentioned earlier is due to the compression of the lower support, which depends on the length of

the support. For a housing with different lengths of support, if the compression of the lower support is calculated, then, δ_b (and K_b) and hence δ_r (and K_t) can be altered easily from the values given in the above mentioned figures to obtain an estimate of their actual values for these lengths of supports. It may be seen from figs. 7.56 and 7.60 that, δ_r, δ_b and δ_{ir} decrease and δ_{or} increases with the increase in housing outer diameter. Inner race deflection (δ_{ir}) decreases due to the decrease in peakiness of roller load distribution. Body deflection of the outer race (δ_b) decreases, due mainly to the lower deflection of the two points on the outer race tracks at 90^o to the radial load on either side, with respect to the top of the lower support (and also, to some extent due to shorter length of the lower support). Total radial deflection (δ_r) decreases due to the decrease in δ_{ir} and δ_b. The outer race deflection (δ_{or}) increases with increase in the housing outer diameter mainly due to the reduction in deflection of the above mentioned two points, with respect to which the outer race deflection is measured.

Diagonal cruciform support ⌘ :

Figs. 7.113 to 7.116 show the deflected shape of the races for bearing with thin circular housing having diagonal cruciform support, and hollow shaft at radial clearances -600, -300, 0 and +600μin. The outer race deflected shapes for these cases has also three lobes. One downwards in the direction of radial load formed by the roller loads acting on the span of the outer race, between the two lower supports. The upper two lobes are formed by the tension in the upper supports. The inner race deflection is greater in the direction of supports (at 45^o to the radial load on either side) due to larger roller loads in these directions. Figs. 7.114, 7.118 and 7.119 show the deflected shapes of bearing races with hollow shaft, for increasing housing outside diameter, at a radial clearance of -300μin. These figures show that, as before, the size of the lobes decreases, thus the effect of the supports decreases, with increase in the housing outside diameter.

Figs. 7.67 and 7.71 show the roller load distribution in the bearing with solid and hollow shafts. Roller loads in the direction of the lower supports increase due to the reduced outer race deflection in these directions. Roller loads in the direction of top supports decrease, due to the 'outward' race deflection in these regions, caused by the tension in these supports. Parts (a) of the above figures are for the roller load distribution for different radial clearances with the thinnest housing used. The maximum roller load in these figures is at 45^o to the radial load. Parts (b) of the

above figures are for the roller load distribution in bearings with housing having different outside diameters, and a radial clearance of -300 μin. As the housing outside diameter increases the peakiness of roller load distribution decreases and tends to approach the theoretical roller load distribution curve obtained by assuming rigid races.

Figs. 7.65 and 7.69 show the non-dimensional equivalent radial load (P_r/F_r) for a bearing with circular housing having diagonal cruciform supports, for solid and hollow shafts. At the smaller outside diameter of the housing factor (P_r/F_r) is high due to the effect of support. With increase in housing diameter this effect decreases and (P_r/F_r) falls. Further increase in housing diameter causes (P_r/F_r) to increase (especially for large clearance bearings) due to the peakier roller load distribution as the housing rigidity is increased, and also for large preloads (e.g. for c = -600 μin.) due to the increase in the preload component of the roller loads. The minimum value of (P_r/F_r) is at an outer-to-inner diameter ratio of about 1.5 (for bearings not having very large preload). At this value the roller load distribution tends to be uniform, but below or above this point the roller load distribution curve becomes 'peakier' due to support, and clearance, respectively.

The lower lobe formed due to the roller loads may be considered as relief in the outer race as considered in chapter 6. The three lobes in the outer race may be compared to the tri-lobed relief considered in that chapter. Proper amplitude of this relief, which is controlled by the housing outside diameter, gives rise to uniform roller load distribution and hence lower (P_r/F_r). Lower or higher amplitude of relief given by higher or lower housing outside diameter gives rise to peakiness in the roller load distribution curve with the peaks at 0^o and 45^o to the radial load respectively, which gives rise to increased (P_r/F_r). The optimum amplitude is given for this bearing at outer-to-inner diameter ratio of the housing of about 1.5, if the bearing is not heavily preloaded.

From the discussion above, and in the previous section, it may be stated that upright cruciform support is to be avoided, as it tends to make the roller load distribution peakier. If it must be used the housing outer-to-inner diameter ratio should be about 1.5, or greater. Diagonal cruciform support is preferable as it tends to produce a more uniform roller load distribution for the correct housing radial thickness; an optimum outer-to-inner diameter ratio of the housing attained is at about 1.5.

The radial and component deflections for a bearing with circular

housing having diagonal cruciform support for solid and hollow shafts are given in figs. 7.64 and 7.68, and the values of K_t and K_b in figs. 7.66 and 7.70. The body deflection of the outer race (δ_b) for this case also is a substantial part of the total radial deflection. A part of δ_b is due to the compression of the lower supports which depends on the length of the supports. For a housing with different length of supports, if the deflection due to the compression of the lower supports is calculated then δ_b (and K_b) and hence, δ_r (and K_t) can be altered easily from the values given in the above mentioned figures to obtain an estimate of their actual values for these new lengths of supports. With increase in the housing outer diameter δ_r, δ_b and δ_{or} decrease and δ_{ir} increases. Inner race deflection (δ_{ir}) increases due to the increase in roller loads at, and near, 0^o, and the decrease in roller loads at, and near, 45^o to the radial load on either side, with increase in the bearing outer diameter. Outer race deflection (δ_{or}) decreases due to greater rigidity of the span of housing between the supports. Body deflection of the outer race (δ_b) decreases due to the increase in overall rigidity of the housing and support structure. It may be seen from figs. 7.64 and 7.68 (for ⌑) that δ_b curves are flatter than the δ_b curves in figs. 7.56 and 7.60 (for ⌖). This is because a substantial part of δ_b in the later cases is due to the deflection of the two points on the race tracks at right angles to the radial load on either side, with respect to the top of the lower support.

Effect of shaft speed on bearings with thin circular housing having cruciform supports (⌖ and ⌑)

Figs. 7.72 and 7.73 show the effect of shaft speed on radial deflection (δ_r), non-dimensional equivalent radial load (P_r/F_r) and excess roller load distribution at the outer race for a bearing with thin circular housing having upright and diagonal cruciform supports, and for solid and hollow shafts at a radial clearance of -300μin. Fig. 7.117 shows the deflected shape of races for a bearing with hollow shaft and thin circular housing having diagonal cruciform support at a radial clearance of -300μin. and shaft speed of 30,000 r.p.m.

The deflected shape of races at 30,000 r.p.m., fig. 7.117, may be compared with fig. 7.114, which is for zero r.p.m. Little difference is evident in the shape of the curves, except that the local deformations at the contact areas are slightly higher in the outer race due to the increased roller load at 30,000 r.p.m. The excess roller loads at high speed (shown in figs.

7.72 and 7.73(c)), which are mainly due to the centrifugal force of the rollers, is not uniform over all the rollers, but the increase is greater in the directions of the supports.

The bearing radial deflection (δ_r) increases with increase in the speed of the shaft as shown in figs. 7.72a and 7.73a. The increase in δ_r in case of diagonal supports is almost totally due to the increase in δ_{or} (δ_{ir} and δ_b remain virtually unchanged), and in case of upright support increase in δ_r is mainly due to δ_{or} and also to some extent due to δ_b.

The non-dimensional equivalent radial load (P_r/F_r) also increases with increase in shaft speed as shown in figs. 7.72b and 7.73b.

Upright and diagonal part-cruciform supports (⊹ and ⍝)

Figs. 7.120 and 7.121 shows the deflected shapes of races for a bearing with hollow shaft and housing having upright and diagonal part-cruciform supports at $c = -300\mu$in. These figures may be compared with figs. 7.108 and 7.114, which are for the corresponding cases of upright and diagonal full-cruciform supports, at the same radial clearance. In the first two figures the top lobes are not present in the outer race deflected shapes, as there are no top supports. The loop in the outer race deflected shape of fig. 7.120 is due to comparatively large deflections for the magnification used in plotting.

The roller load distribution in the bearings for upright and diagonal part-cruciform support cases is given in figs. 7.77a and b, and may be compared with the corresponding full-cruciform support cases of figs. 7.63a (for ⊹) and 7.71a(for ⍁). The peakiness of roller load distribution is greater in the part-cruciform support cases. This peakier roller load distribution gives rise to higher non-dimensional equivalent radial load, as may be seen from fig. 7.75, compared with the corresponding cases of cruciform support configurations (figs. 7.61 and 7.69).

The radial and component deflections, and K_t and K_b, for the upright and diagonal part-cruciform support cases are given in figs. 7.74 and 7.76. These values may be compared with the corresponding values of deflection (in figs. 7.60 and 7.68) and, of K_t and K_b (in figs 7.62 and 7.70) for cruciform support configurations. The deflections δ_r, δ_b and δ_{ir} for the case of upright part-cruciform support, and δ_r and δ_b for the case of diagonal part-cruciform support are larger than the corresponding values for the full-cruciform support configurations. The increase is mainly in δ_b (about double the value of the corresponding full-cruciform support configuration). The outer race deflection

(δ_{or}) for the upright part-cruciform support case decreases (i.e. the negative value increases) due to greater deflection of the two points on the outer race track at right angles to the radial load, compared with the full-cruciform support case. The inner race deflection δ_{ir} for the diagonal part-cruciform support case decreases, due to lower roller loads at, and near 0° and greater roller loads at, and near, 45° to the radial load, compared with the corresponding full-cruciform configuration. The values of K_t and K_b for the upright and diagonal part-cruciform support cases increases due to the increase in δ_r and δ_b compared with the corresponding full-cruciform support configuration.

CHAPTER 8 CONCLUSIONS AND SUGGESTIONS FOR FURTHER WORK

8.1 CONCLUSIONS

1. Using the assumption of rigid races, calculations have shown that the stiffness of a bearing can be considerably increased by imposing a fairly low degree of preloading. An increase in stiffness by a factor of up to two, compared with that for a zero clearance bearing, can be achieved by imposing a relatively small amount of preload. Small preloads also increase bearing life.

2. Even using the 'rigid race' assumption, determination of the deflection of a rolling bearing by considering the radial clearance present in it can be time consuming. Thus nomograms for radial roller and ball bearings have been constructed to enable the radial deflection to be found quickly and easily.

3. The modified stress-freezing technique is a useful method for determining the various components of bearing deflection, roller load distribution, and the deflected shapes of the races. This enables the model to be dismantled while frozen in the loaded state; the information thus gained would be difficult to obtain by any other method. The main disadvantage is the time required in the manufacture and testing of models.

4. Good agreement was found between the experimental results (using the modified stress-freezing technique) for load-deflection characteristics of a roller loaded between two flat platens, and that obtained by finite-element analysis. Agreement was also good between the experimental results for total and components of bearing deflections, roller load distribution and the deflected shapes of the races, and those obtained by finite-element analysis.

5. The finite element program together with the mesh for the races (especially for steel bearings) enables the consideration of a number of types of housings and shafts. By using zones within the complete mesh, having constant elastic properties, thicknesses and densities, a range of different housing and shaft configurations has been evaluated using the same basic finite-element network. It has been possible to conserve computing time by storing the intermediate matrices of a bearing with a particular combination of housing and shaft on a magnetic tape.

6. The deflected shapes of the races calculated by the program and drawn by the calcomp graph plotter were found to be of great assistance in explaining physically the effect of the different types of housings and shafts

on the bearing performance. It was found that the deflected shape of the races influences the roller load distribution and hence, life of the bearing. Support conditions which give rise to adverse profiles, by increasing the peakiness of the roller load distribution, lower the life of the bearing, and vice-versa. As a unifying factor in evaluation of bearing life, the equivalent radial load, calculated from the roller load distribution, was found to be very useful.

7. The general trends of the deflection vs. radial clearance curves for different types of housings and shafts for fully-elastic races, are similar to those obtained with the 'rigid race' assumption*, although they are bodily shifted in the direction of increased flexibility. A small preload for fully-elastic races also reduced bearing deflection considerably, and it was also found that light preloads for fully-elastic races improved bearing life.

8. The actual bearing radial deflection for fully-elastic races has been found to be larger than the theoretical radial deflection assuming rigid races, by a factor of 1.3 to 2.0 for the combination of comparatively rigid housings and shafts, up to 2.8 for very hollow shafts (e.g. no. 5), and up to 5.3 for weak housings (e.g. thin circular housing with part cruciform support. The radial deflection of the bearing includes the body deflection of the outer race, which largely depends upon the rigidity of the housing. For the housings studied, the body deflection has been found to be 13% to 35% of the bearing radial deflection for the comparatively rigid housings, and up to 85% for the weak housings (e.g. thin circular housing with part-cruciform support).

9. At a certain value of shaft 'hollowness' the roller load distribution attains its most uniform condition, and gives the lowest equivalent radial load (i.e. maximum life) for the bearing. This condition was found to be at an inner-to-outer shaft diameter ratio of about 0.7.

10. Ribs in the housing have been found to have comparatively little effect on radial roller bearing performance, and their effect decreases with increase in the boss outer diameter.

11. Increasing speed has the effect of increasing the radial clearance in the bearing.

12. Artificially modifying the roller load distribution by relieving the outer race of a bearing in comparatively rigid housings, has been found to be effective in reducing bearing deflection and also increasing life to a greater extent than is possible by preloading alone. Tri-lobed relief is more effective than the bi-lobed form. The use of race relief is suitable

* which, to a first approximation, is reasonably justified for rigid housings

only for bearings having a constant, or fairly constant, direction of the external radial load.

13. From the point of view of life it is found to be better to design the housing in such a way that the major axis of the deflected outer race shape is in the direction of radial load. Stiffening the housing (i.e. by using ribs) at and around 45° positions to the radial load is found to be more effective than stiffening at the 0° position. A housing which is relatively stiff at the 0° position and weak at about the 45° position is found to have an adverse effect on the bearing life due to very peaky roller load distribution.

14. From the analysis of a circular housing on rib supports it was found that an upright cruciform support should be avoided; if it must be used, the housing outer-to-inner diameter ratio should be equal to or greater than about 1.5. Diagonal cruciform support is found to be preferable, and the optimum outer-to-inner diameter ratio is about 1.5, for lowest equivalent radial load (i.e. highest life). For very heavily preloaded bearings this ratio is somewhat lower. The deflected shape of outer race for diagonal cruciform support is found to be similar to the case of tri-lobed relief.

15. The 'correction' factors K_t and K_b for different types of housing and shaft combinations are plotted in the respective sections. Actual bearing radial deflection and body deflection of the outer race for bearings with fully-elastic races can be found by multiplying the theoretical bearing deflection assuming rigid races (which can be obtained by calculation or by using the nomograms), by the appropriate value of K_t and K_b respectively.

8.2 SUGGESTIONS FOR FURTHER WORK

The following are the suggestions of the author for further investigation in this field.

(1) The radial clearance of a bearing under actual operating conditions depends upon the temperature distribution in the bearing and its immediate surroundings. Usually the shaft and inner race ring of a bearing operate at a higher temperature than the outer race ring and housing. This temperature gradient between the inner and outer race causes a reduction of the radial clearance in the bearing. In an experiment Opitz et al.(3) found that an operating radial clearance of $-5\ \mu m$ (-0.2 thou) to be equivalent to a mounting setting of $+5\ \mu m$ (+0.2 thou) radial clearance. Therefore, it is important to consider the temperature distribution in the bearing assembly to find its

characteristics under actual operating conditions.

Temperature distribution in a bearing application under steady-state conditions can be calculated from the heat generation due to frictional losses and the heat transfer analysis. A numerical method of calculating the temperature distribution has been produced by Harris (e.g. reference 12) and a computer program based on this method has been developed by SKF (The Skefko Ball Bearing Co., Ltd.) and described in reference 47 by Fernlund et al. After finding the temperature distribution it can be introduced into the finite element program FINELM (which will require some small additions) to find the performance of the bearing under actual operating conditions.

(2) It is difficult to know the exact radial clearance present in a bearing when mounted. If the outer and inner race rings are considered separately from the housing and shaft respectively in the finite-element program, and the interference between the housing and outer race ring, and that between the shaft and inner race ring, are supplied as data, it would be possible to find the actual radial clearance in the bearing and also the bearing radial and component deflections, roller load distribution, and the deflected shapes of the races. This form of computer program would be of more practical use. Another advantage of this form of computer program is that it will be possible to consider the geometrical imperfections of the bearing races, shaft and housing. The chief drawback will be in the time required by the computer. This would be greater than that required in the present investigation, because iterations would be necessary at three boundaries, instead of one, namely:

(a) between the housing and the outer race ring

(b) between the shaft and the inner race ring

(c) between the two races separated by the rolling elements.

(3) It would be interesting to consider the shaft as an axi-symmetric body in the finite element analysis. It is possible to consider the axi-symmetric body with non-axisymmetric load distribution (i.e. each individual rolling element loads) by employing Fourier series to distribute the load and deflection of the nodal points in the finite-element analysis.

REFERENCES

1. Opitz, H. "Performance Testing of Machine Tools". Inst. Mech. Eng. Proc. Conf. on Tech. of Manufacture. 1958, pp.440-454.

2. Koenigsberger, F. "Design Principles of Metal-Cutting Machine Tools". Springer-Verlag, 1964.

3. Opitz, H., Günther, D., Kalkert, W. and Kunkel, H. "The Study of the Deflection of Rolling Bearings for Machine Tool Spindles". Proc. Mach. Tool Des. Res. Conf. 1965, pp. 257-269.

4. Stansfield, F.M. and Bell, I.F. The Machine Tool Industry Research Association. "Notes for Designers":
   No.3. "Design of Two-bearing Spindles"
   (for varying external diameter between bearings).
   No.4. "Design of Two-bearing Spindles"
   (for constant external diameter between bearings and smaller diameter overhang).
   No.5. "The Optimum Position for the Driving Gear or Pulley on a Two-bearing Spindle".
   No.6. "The Stiffness of Machine Tool Spindles".

5. "Machine Tool Spindle Supported at Three Positions". The Ball Bearing Journal No. 145, 1966, pp.17.

6. Holdsworth, H.W. "Procedure in Preloading". American Machinist, 21st March, 1931, Vol.74, pp. 269-272.

7. "Preloaded Ball and Roller Bearings". Engineering, 3rd April, 1936, Vol.141, pp. 370-372.

8. Swanson Jr.,S. "Basic Theory and Application of Preload in Bearings". Machine Design, July 22, 1965, pp.174-179.

9. Harris, T.A. "How to Compute the Effects of Preloaded Bearings". Product Engineering, 19th July, 1965, pp.84-93.

10. Dowson, D. and Higginson, G.R. "Theory of Roller-bearing Lubrication and Deformation". Lubrication and Wear Convention,(Inst. Mech. Eng.) Bournbouth 1963, Paper 19, pp.216-227.

11. Rumbarger, J.H. "How Clearance Affects Life of Rolling Bearings". Machine Design, 8th June, 1961, pp.145-149.

12. Harris, T.A. "Rolling Bearing Analysis". John Wiley and Sons, Inc., 1966.

13. Münnich, H., Erhard, M. and Niemeyer, P. "The Effect of Elastic Deformation on Load Distribution in Rolling Bearings". The Ball Bearing Journal, No.155, 1968, pp.3-12. The same paper was also published

in Design and Components in Engineering, Vol.10, 21st May, 1969, under the heading, "Elastic Deformation in Rolling Bearings".

14. Peters, W.E. "Thin-bearing Performance". Machine Design, V.39, No.24, 12th October, 1967, pp176-179.
15. Crookall, J.R. "The Rigidity of Bosses on Flat Plates". Ph.D. Thesis, 1966, University of Nottingham.
16. Datta, P.N. "Deformation of Race Bearing". M.Sc. Thesis, September, 1966, University of London, Imperial College of Science and Technology.
17. Jones, A.B. "A General Theory for Elastically Constrained Ball and Radial Roller Bearings Under Arbitrary Load and Speed Conditions". ASME Journal of Basic Engineering, June, 1960, pp 309-320.
18. El Tamimi, A.M.A. "Study of Gear Box Elements". M.Sc. Thesis, October, 1969, University of Manchester Institute of Science and Technology.
19. Stansfield, F.M. "The Use and Construction of Models for the Experimental Analysis of Machine Tool Structures". M.T.I.R.A. Machine Tool Research, Vol.2, No.3, July 1963.
20. D'Souza, A.C. "Models as Aids to Design". Engineering Materials and Design, Vol.7, No.5, May 1964, pp.316-322.
21. Opitz, H. and Döpper, W. "Development of Digital Computer Programs for the Analysis of Machine Tool Structures and Elements". 9th. M.T.D.R. Conference, M.S. No.48.
22. Taylor, S. "Computer Aided Design of a Planing Machine Structure". 9th M.T.D.R. Conference, Sept. 1968.
23. Stephen A.C. and Taylor, S. "Computer Analysis of Machine Tool Structures by the Finite Elememt Method". 9th M.T.D.R. Conference, September 1968.
24. Taylor, S. and Tobias, S.A. "Computer Methods for the Structural Analysis of Machine Tools". C.I.R.P. General Assembly, September 1968.
25. Cowley, A. and Hinduja, S. "The Finite Element Method for Machine Tool Structural Analysis". Annals of the C.I.R.P. Vol.XVIII, 1970. MS24.
26. Lundberg, G. and Palmgren, A. "Dynamic Capacity of Rolling Bearings". Acta Polytechnica, Mechanical Engineering Series, Vol.1, No.3, 1947.
27. Lundberg, G. and Palmgren, A. "Dynamic Capacity of Rolling Bearings". Acta Polytechnica, Mechanical Engineering Series, Vol.2, No.4, 1951.
28. Allan, R.K. "Rolling Bearings". Sir Isaac Pitman and Sons, Ltd., London, 1960.
29. Goodman, J. "The distribution of Load on the Ball and Rollers of Ball and Roller Bearings". Engineering, Vol.119, 19th June, 1925, pp.753-754.

30. Goodman, J. "The Approach of Flat Elastic Plates Under Load When Separated by a Ball of Similar Material". Engineering, 24th. August, 1923, pp. 244-245.

31. Goodman, J. "The Contact Area of an Elastic Sphere When Compressed Between Flat Elastic Plates". Engineering, 3rd August, 1923, pp.133.

32. Palmgren, A. "Ball and Roller Bearing Engineering". S.K.F. Industries, 1945.

33. "Rolling Bearing Calculations". The Hoffmann Manufacturing Co. Ltd.

34. Morley, A. "Strength of Materials" Longmans Green and Co. Ltd., and The English Language Book Society, 1962.

35. Roark, R.J. "Formulas for Stress and Strain". McGraw-Hill Book Company, Inc. 1943.

36. Scarborough, J.B. "Numerical Mathematical Analysis". Sixth Edition, John Hopkins.

37. Levens, A.S. "Nomography". John Wiley and Sons, Inc., New York, Second edition, 1959.

38. Zienkiewicz, O.C. "The Finite Element Method in Structural and Continuum Mechanics". McGraw-Hill Book Co. Inc., New York and London, 1967.

39. Wilson, E.L. "Finite Element Analysis of Two-dimensional Structures". Ph.D. Dissertation, University of California.

40. Zienkiewicz, O.C. and Holister, G.S. "Stress Analysis". John Wiley and Sons Ltd., 1965. Chapters 7 and 8 .

41. Fox, L. "Practical Solution of Linear Equations and Inversion of Matrices". Applied Mathematics Series 39, U.S. Dept. of Commerce, Washington, D.C. 1954.

42. Clough, R.W., Wilson, E.L. and King, I.P. "Large Capacity Multistorage Frame Analysis Programs". Proceedings of the American Society of Civil Engineers, Structural Division, August 1963, Vol.89, No.ST4, pp.179-204.

43. McCormick, C.W. "Plane Stress Analysis". Journal of the Structural Division, American Soc. of Civil Engrs., Vol.89, No.ST4, Proc. Paper 3581, August 1963, pp. 37-54.

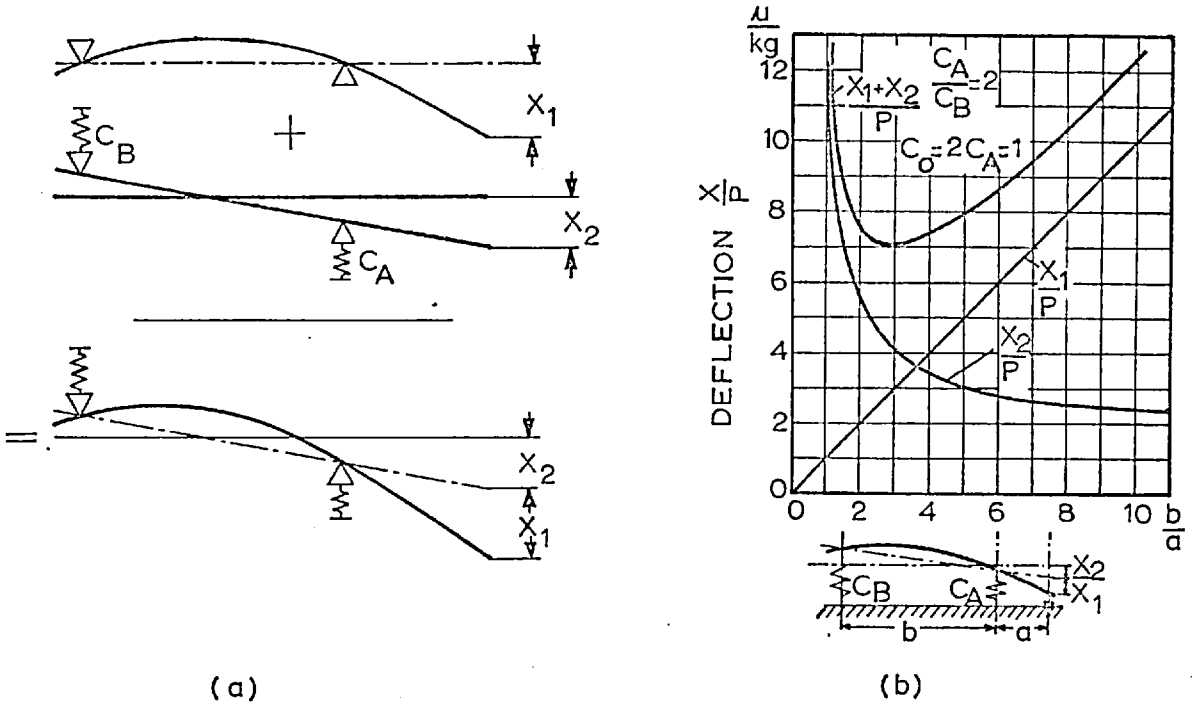
44. Fernlund, I. "Equivalent Bearing Load for an Arbitrary Rolling Element Load". The Ball Bearing Journal, No.143, 1965, pp.2-7.

45. Conte, S.D. "Elementary Numerical Analysis, an Algorithmic Approach". McGraw-Hill Book Company, 1965.

46. Timoshenko, S.P. and Goodier, J.N. "Theory of Elasticity". Third Edition, McGraw-Hill Book Company, Inc., 1970.

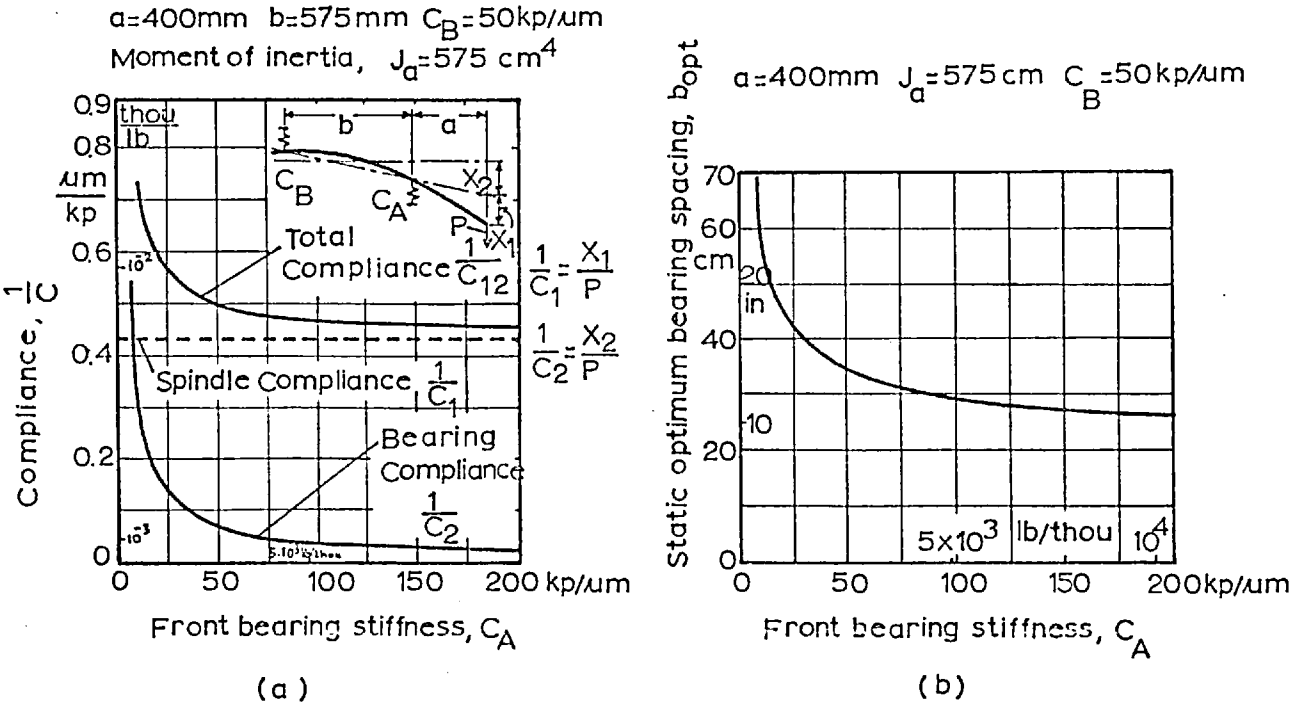
47. Fernlund, I. and Anderéason, S. "Bearing Temperature Calculated by Computer". The Ball Bearing Journal, No.156.

Fig. 1.1 (a) Deflection of a beam on elastic supports.
(b) Deflection of the beam-on-elastic-supports plotted as a function of the distance between bearings.
(from Opitz(1))



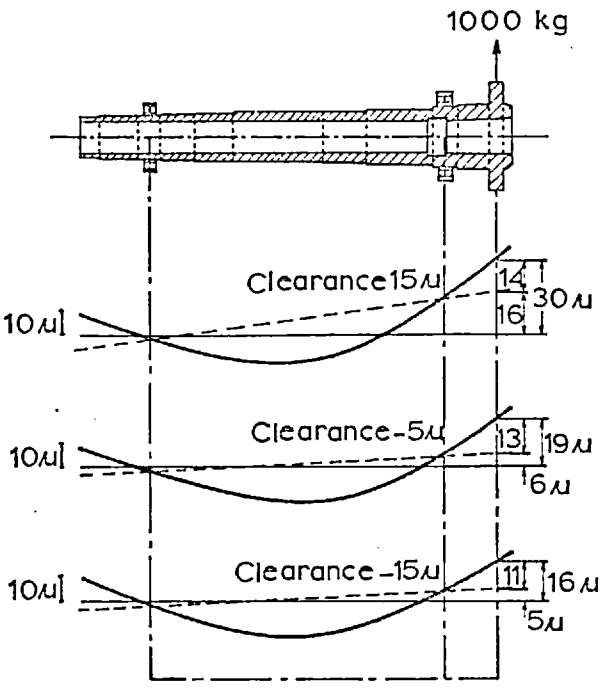
(a) (b)

Fig. 1.2 (a) Effect of bearing stiffness on the compliance of a spindle-bearing system.
(b) Front bearing stiffness-optimum bearing spacing relationship.
(from Opitz et al.(3))

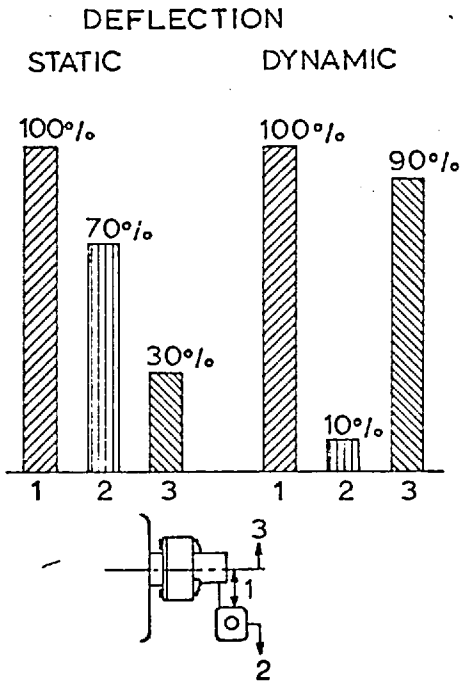


(a) (b)

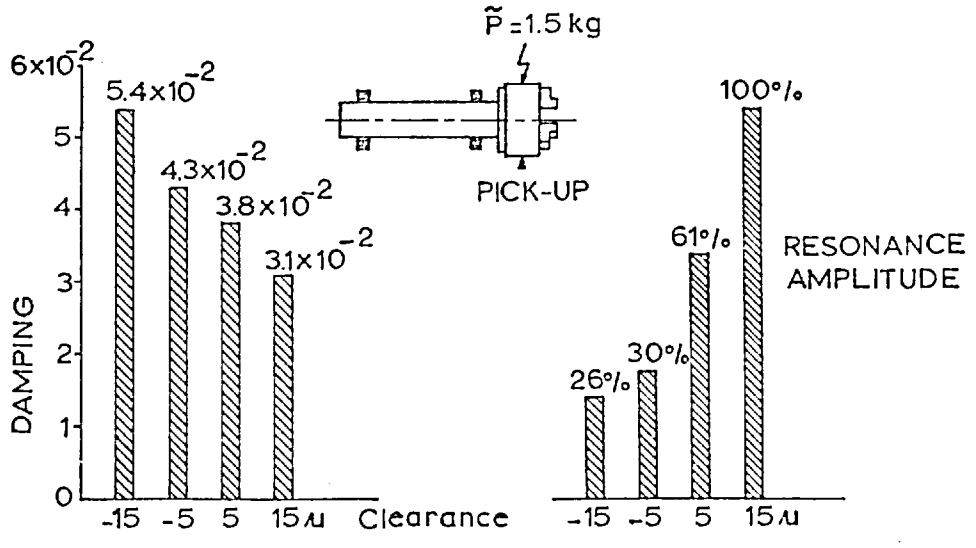
Fig. 1.3 (a) Static spindle deflection as a function of clearance. Radial clearance of rear bearing is constant at 2μ.
(b) Static and dynamic deflection of a lathe.
(c) Damping and resonance amplitude against clearance.
(from Opitz(1))



(a)



(b)



(c)

Fig.2.1 Surface stress distribution between two cylindrical bodies in contact.

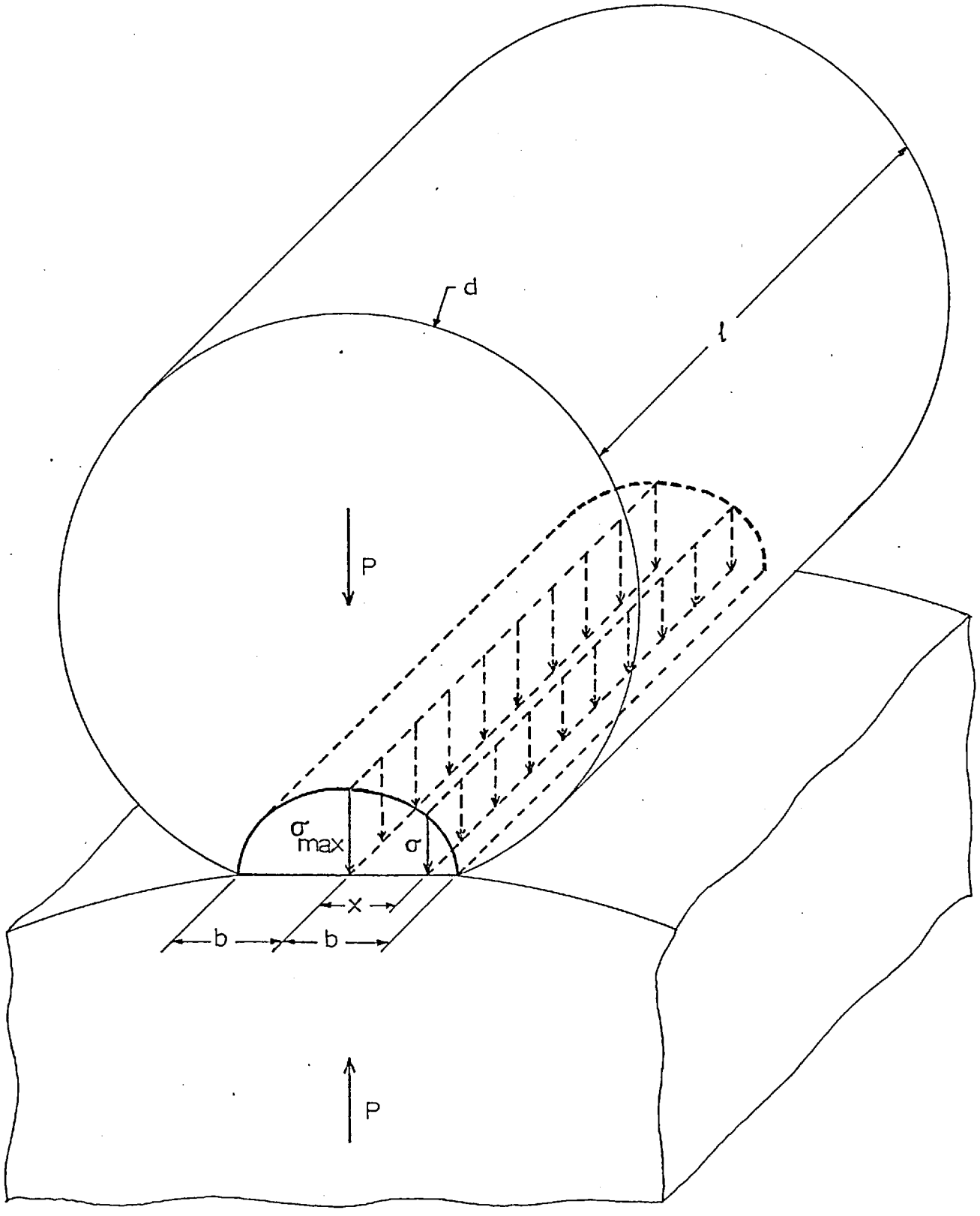


Fig. 2.2 Width of contact area for steel roller loaded between flat steel platens, by Hertz's formula.

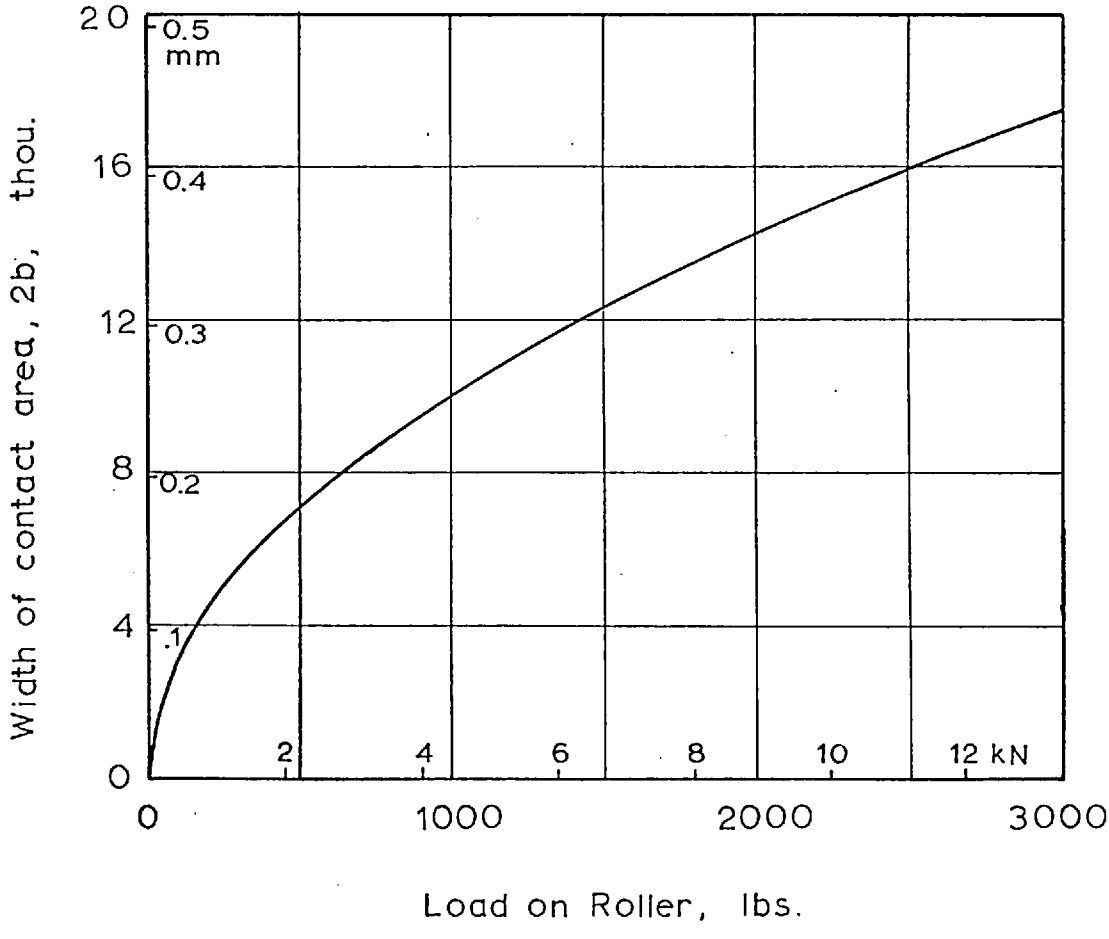


Fig.2.3 Width of contact area for Araldite roller loaded between flat Araldite platens, by Hertz's formula.

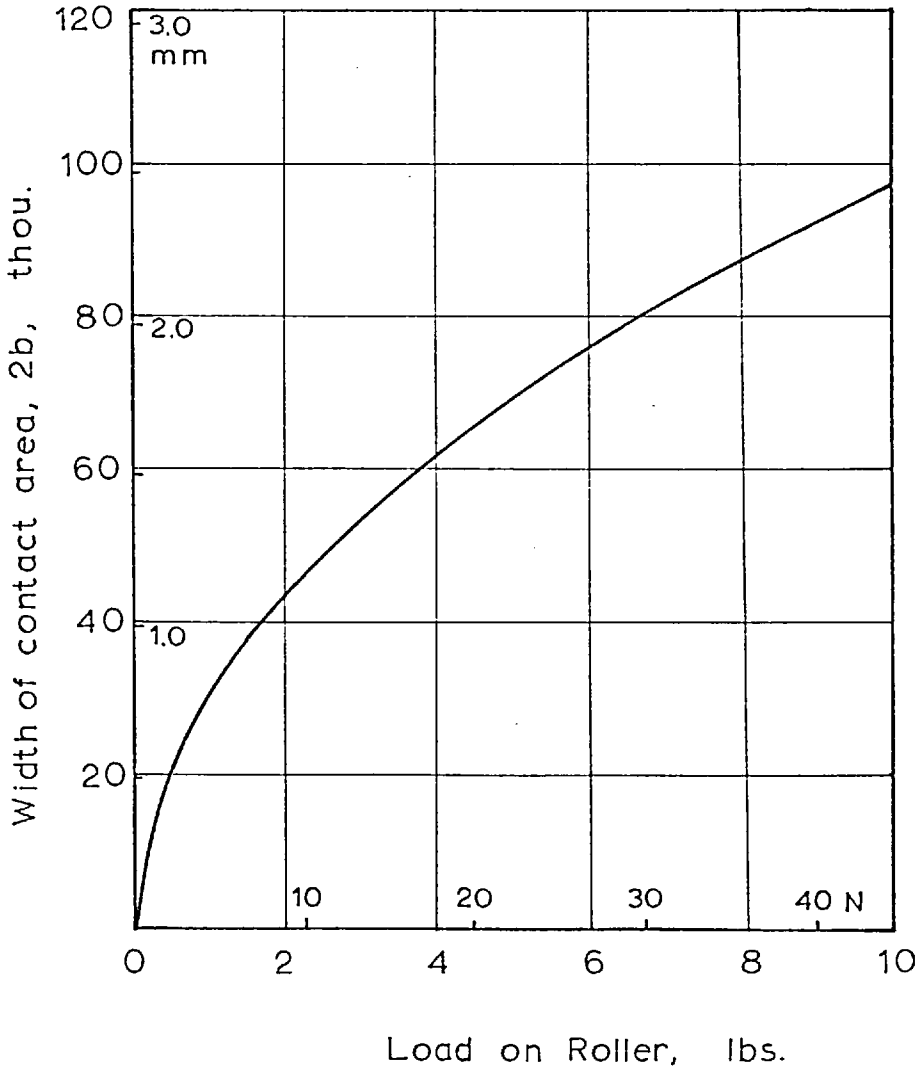


Fig. 2.4 Comparison of different deflection formulae for line contact. Deflection given by the approach of two flat steel platens when a steel roller is loaded between them.

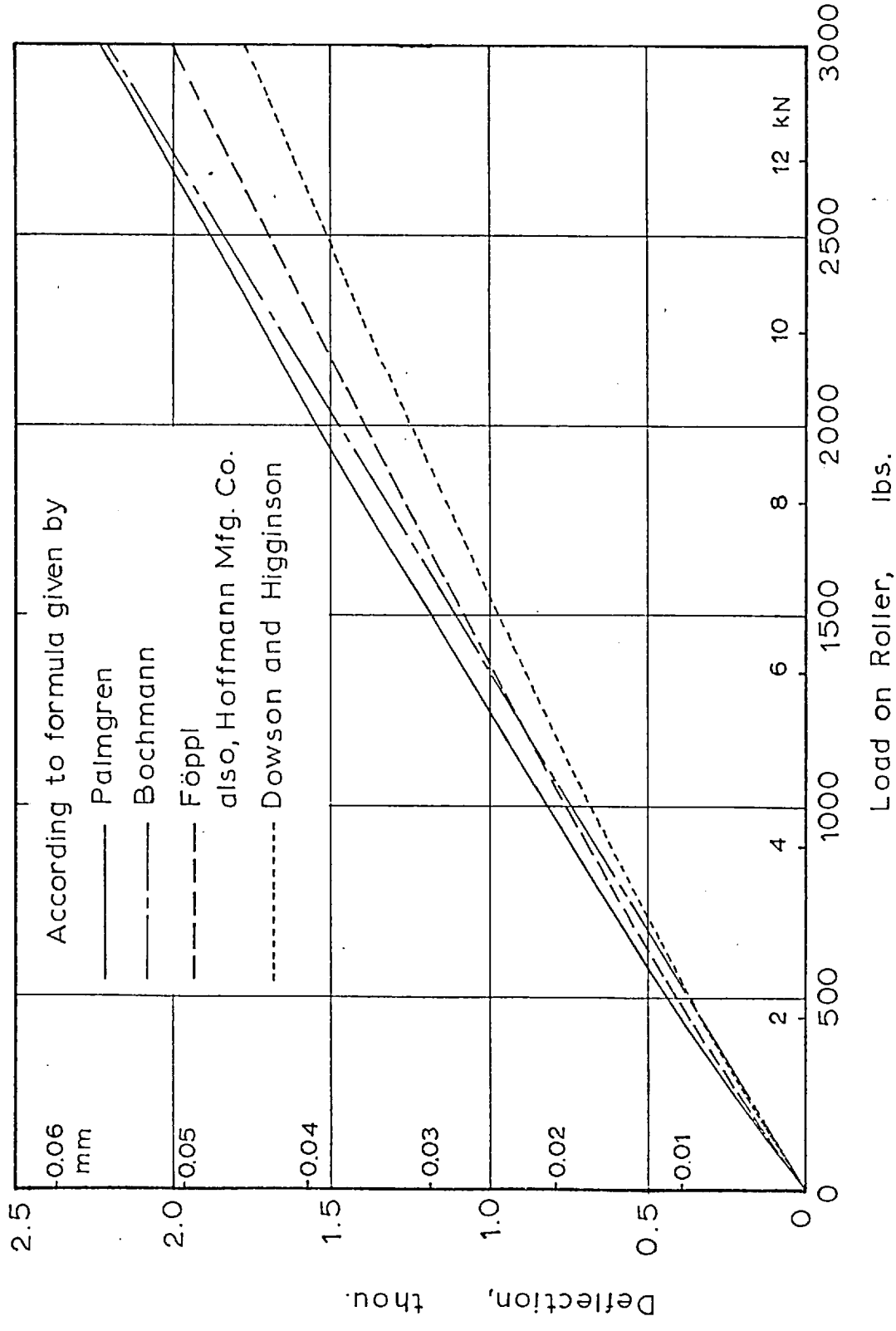


Fig. 2.5 Comparison of different deflection formulae for line contact. Deflection given by the approach of two flat Araldite platens when an Araldite roller is loaded between them.

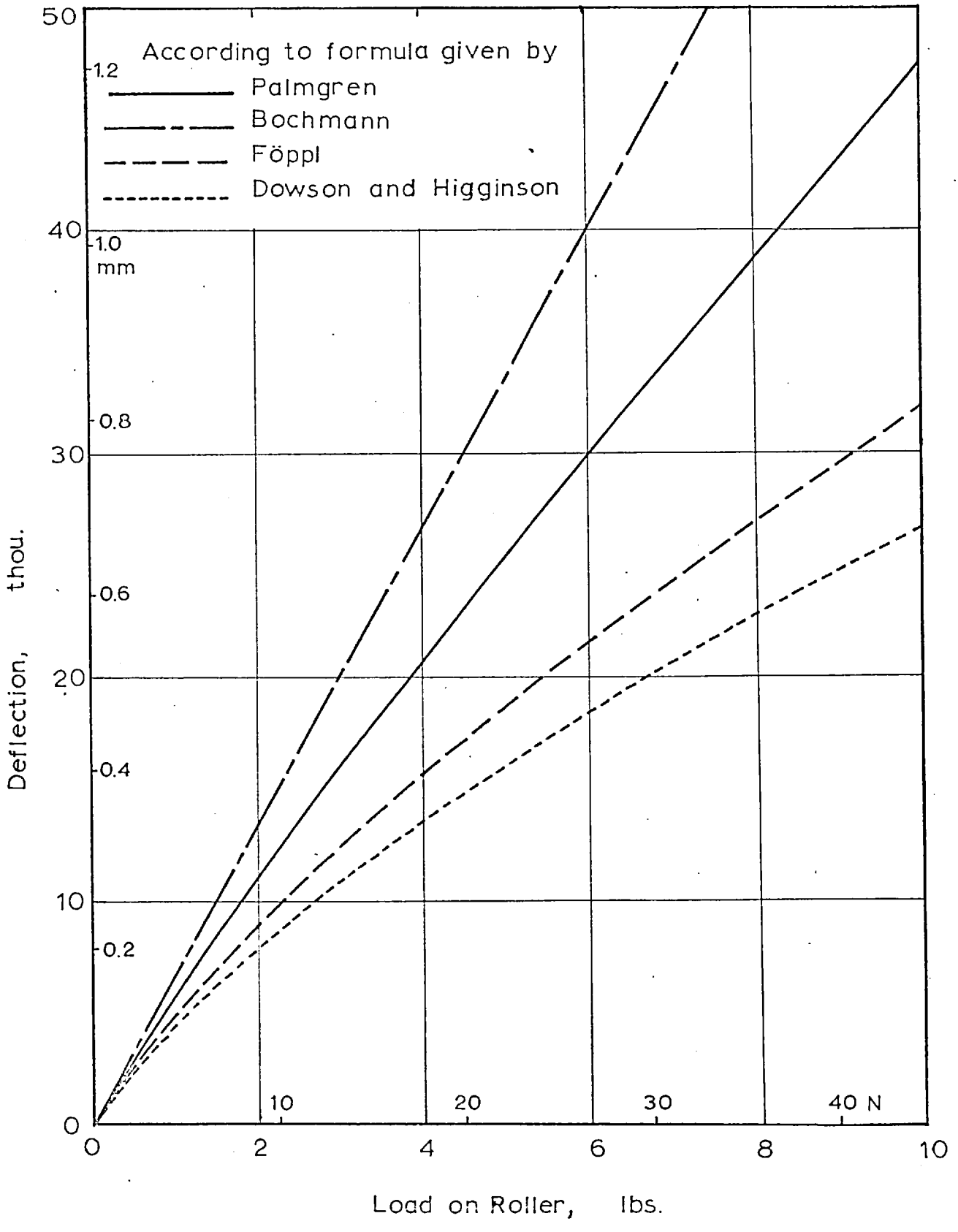


Fig. 2.6 Deflection of hollow rollers;
(a) deflection of a hollow roller as a cylinder,
(b) total deflection given by the mutual approach of two flat platens, when a hollow roller is loaded between them.

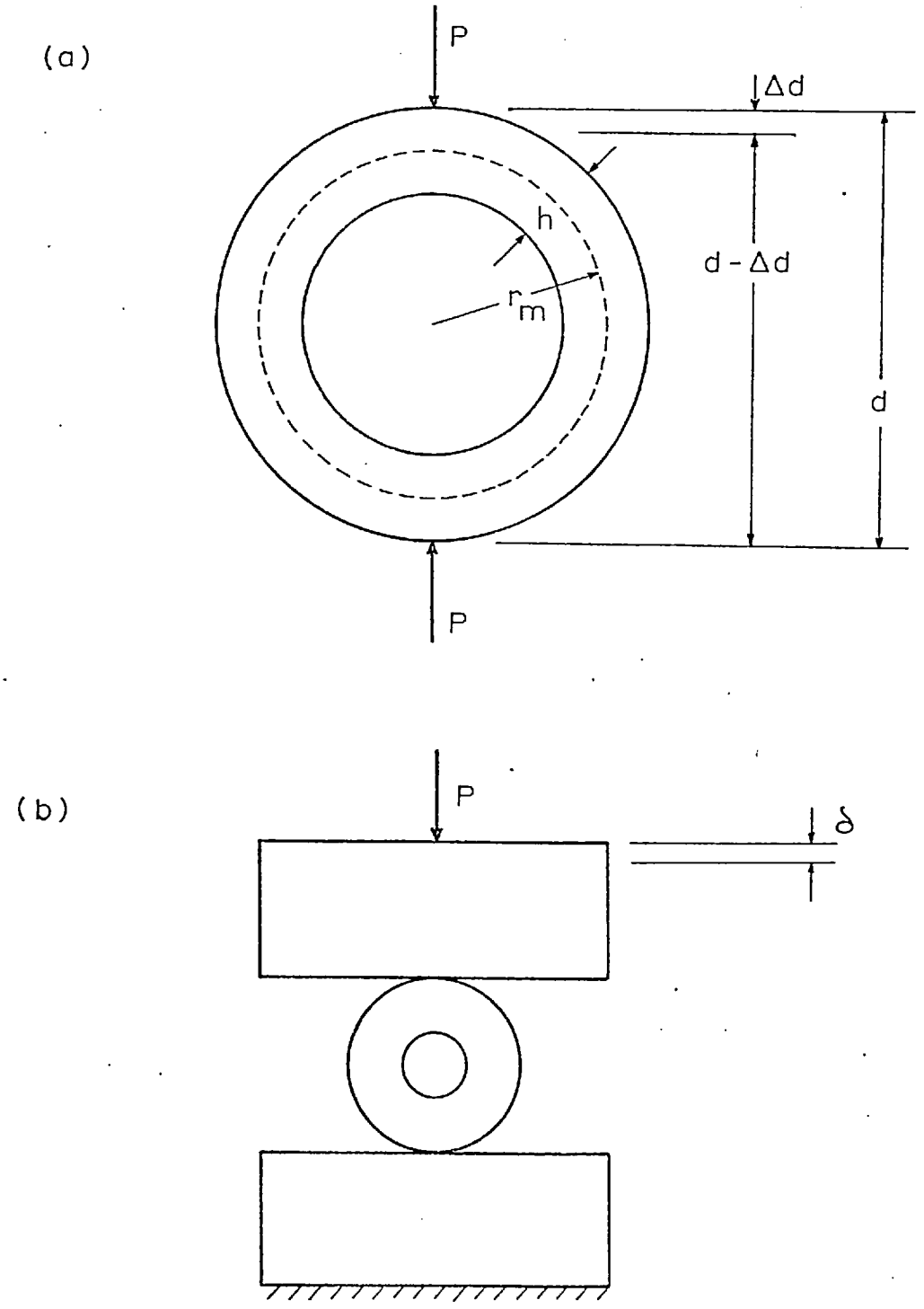


Fig. 2.7 Comparison of total deflection of hollow and solid Araldite rollers pressed between two flat Araldite platens, using Föppl's formula.

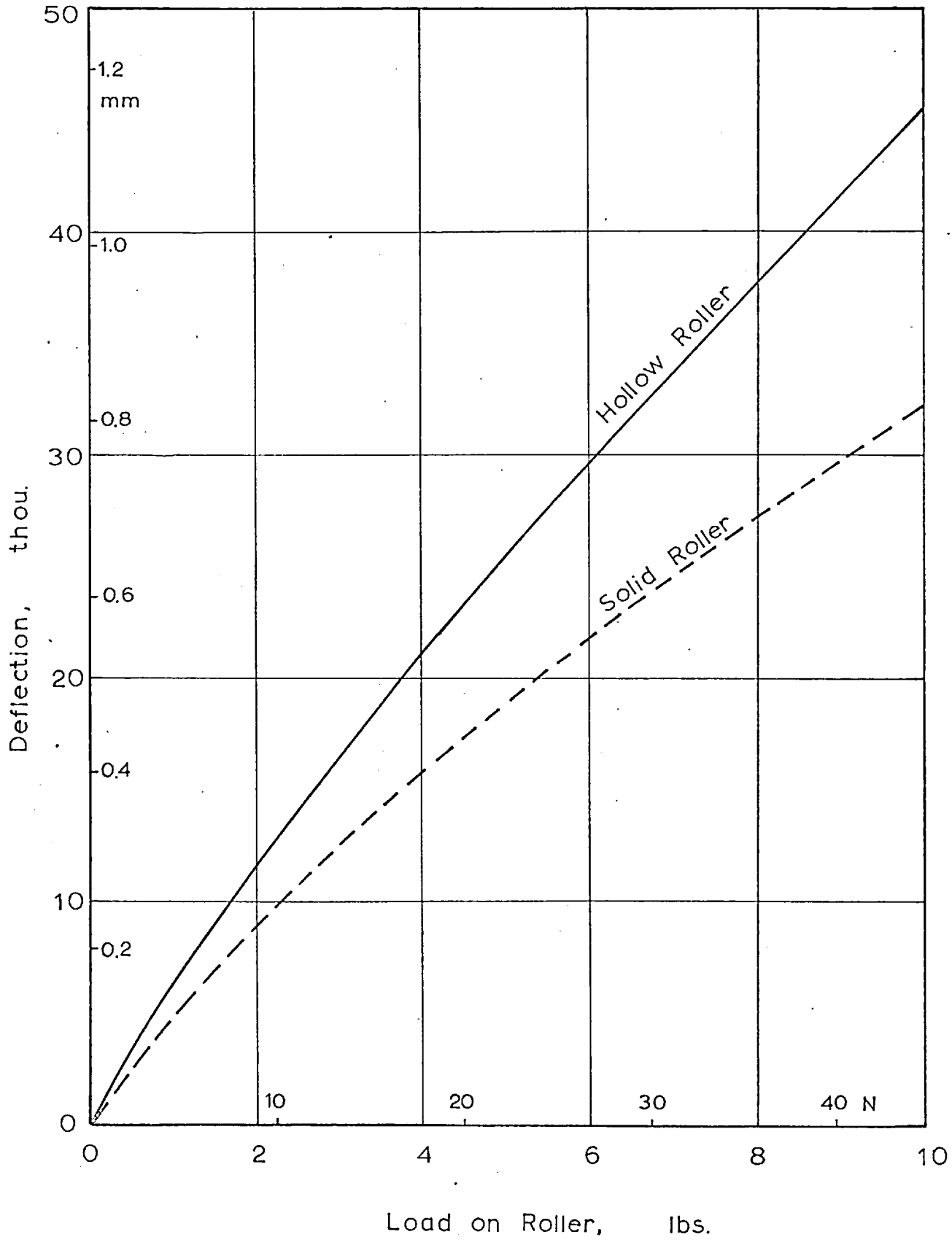


Fig. 2.8 (a) Bearing with positive clearance.
(b) Bearing with interference (preload).

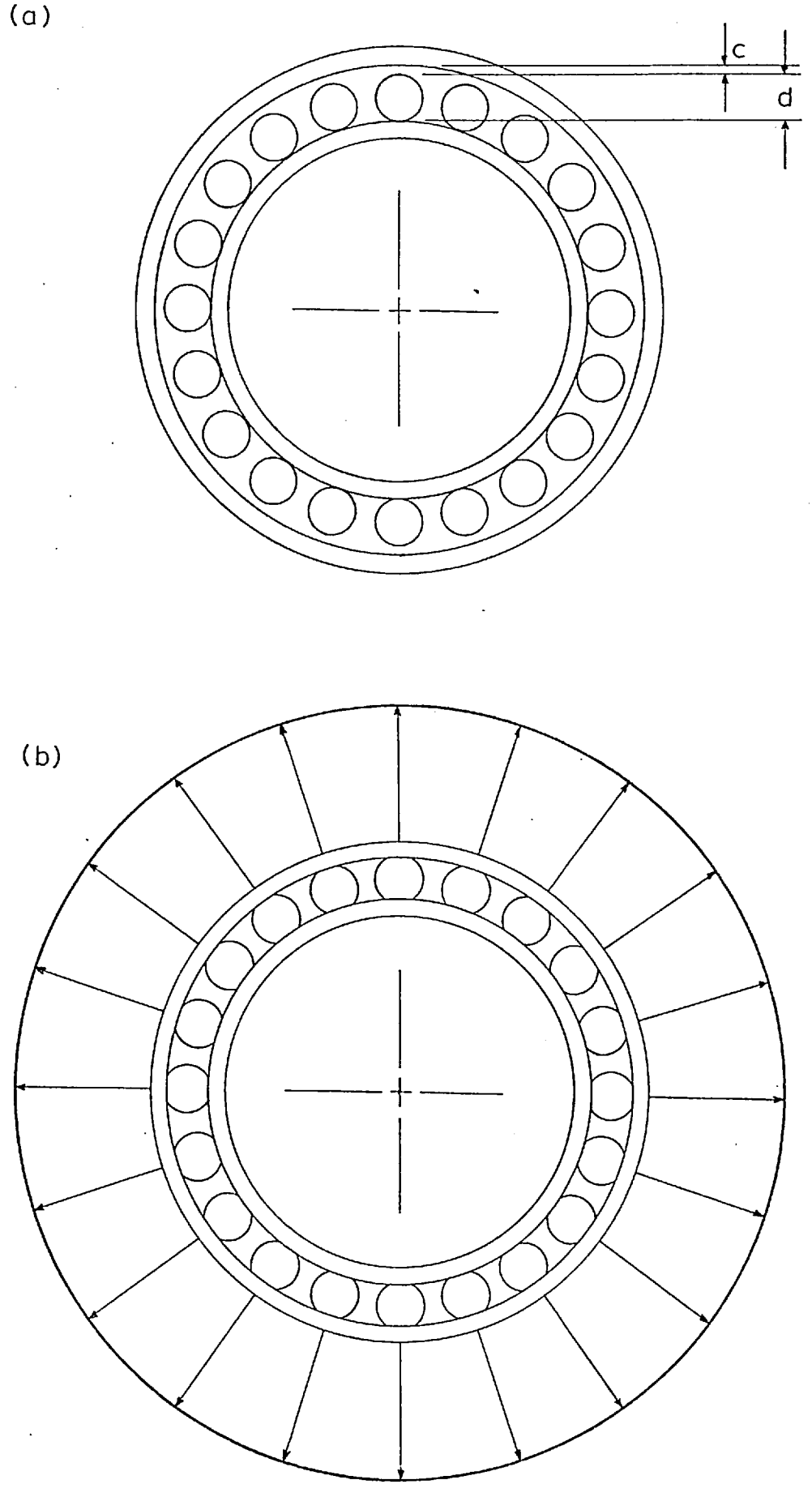


Fig. 2.9 Deflection and load distribution in a radial rolling bearing with zero clearance and ideal geometry.

According to Stribeck,

$$F_r/P_1 = 1 + 2(\cos^{t+1}\phi + \cos^{t+1}2\phi + \cdots\cdots) = Z/S_f$$

where, $\phi = 2\pi/Z$, Z = number of rolling elements,

S_f = load sharing factor.

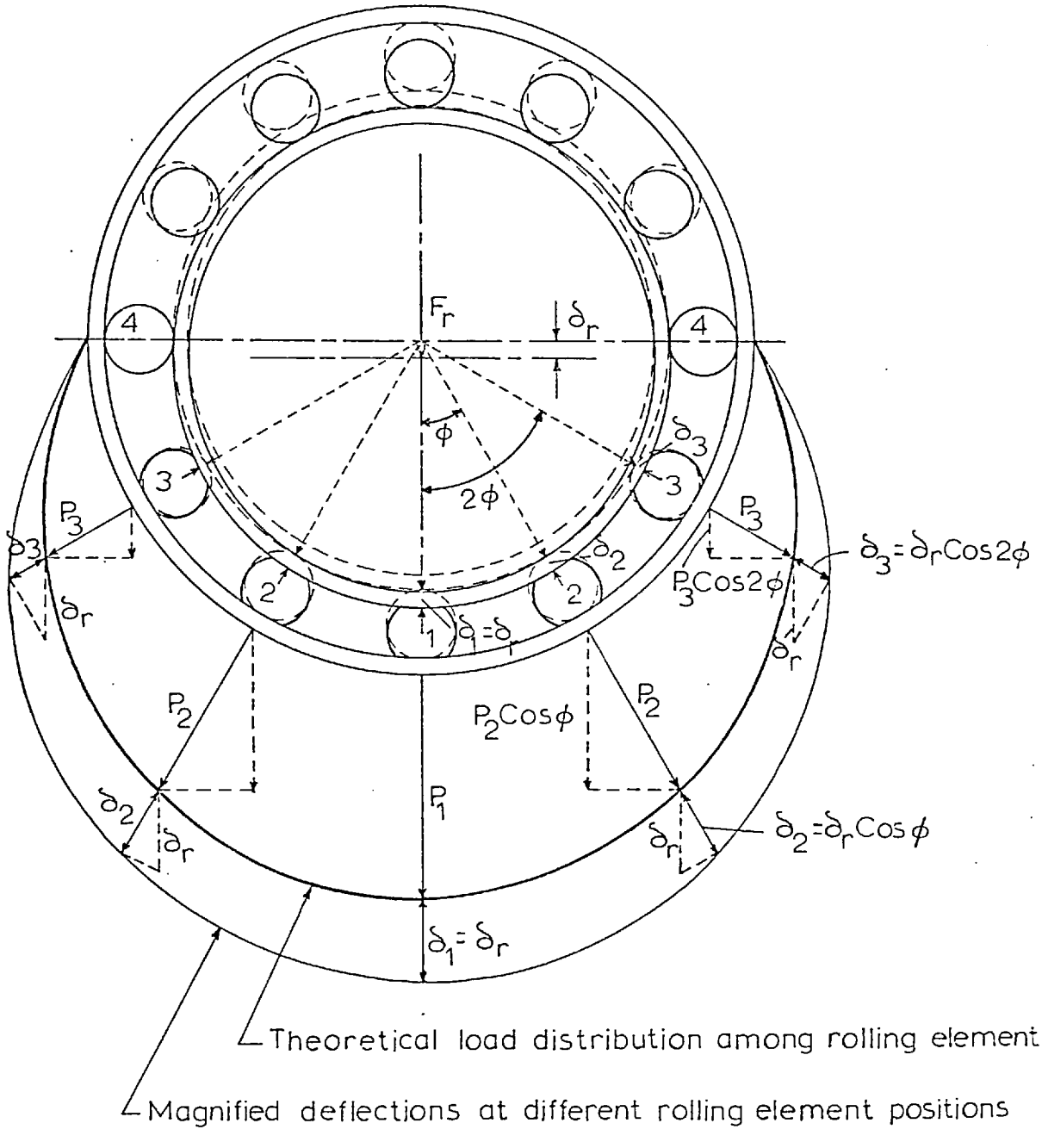


Fig. 2.10 Roller load distribution in a radial rolling bearing with play or interference, assuming the geometry to be otherwise perfect.

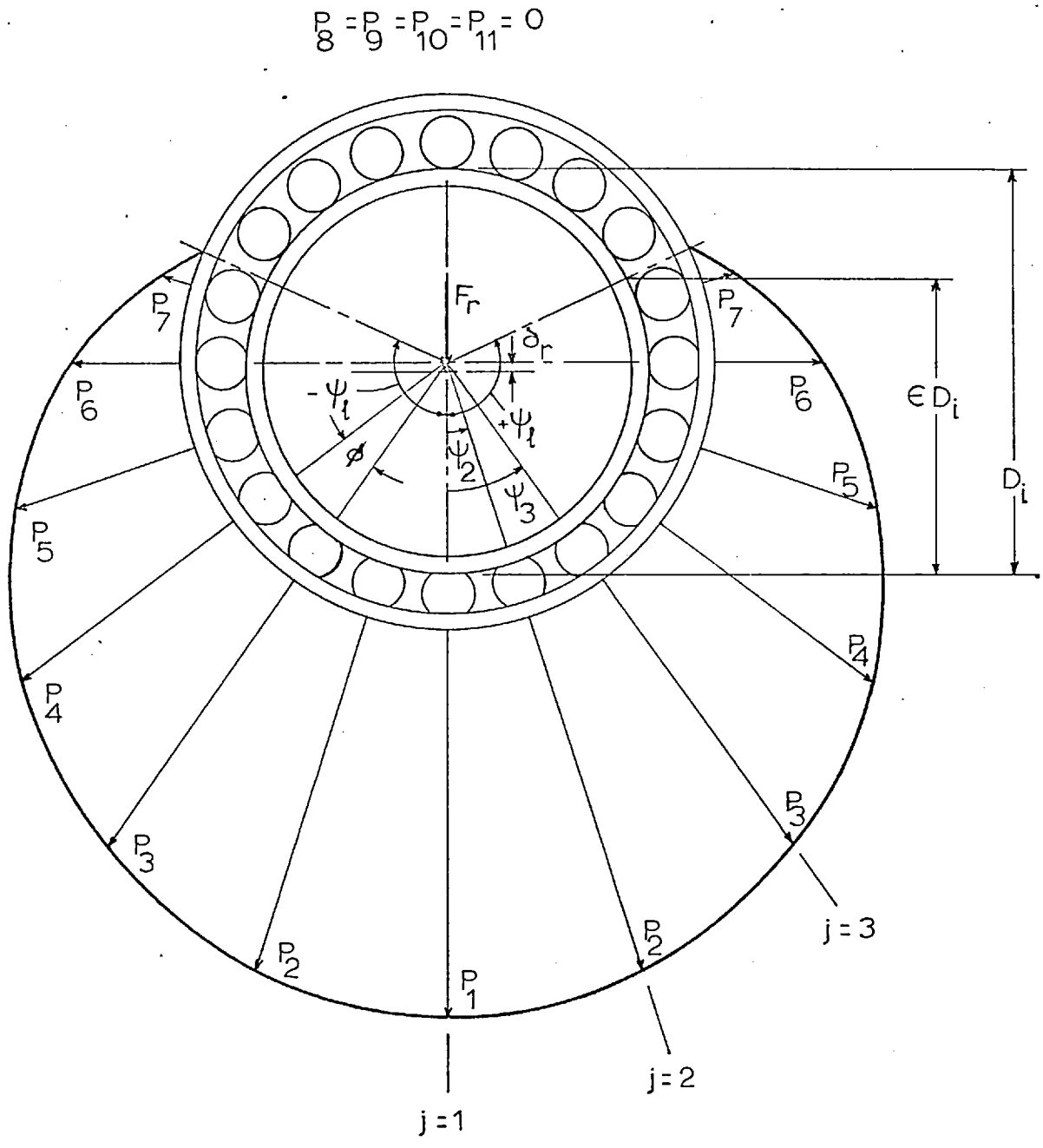


Fig.2.11 General case of imperfect geometrical shape and dynamic loading due to high speed condition in a radial rolling bearing.

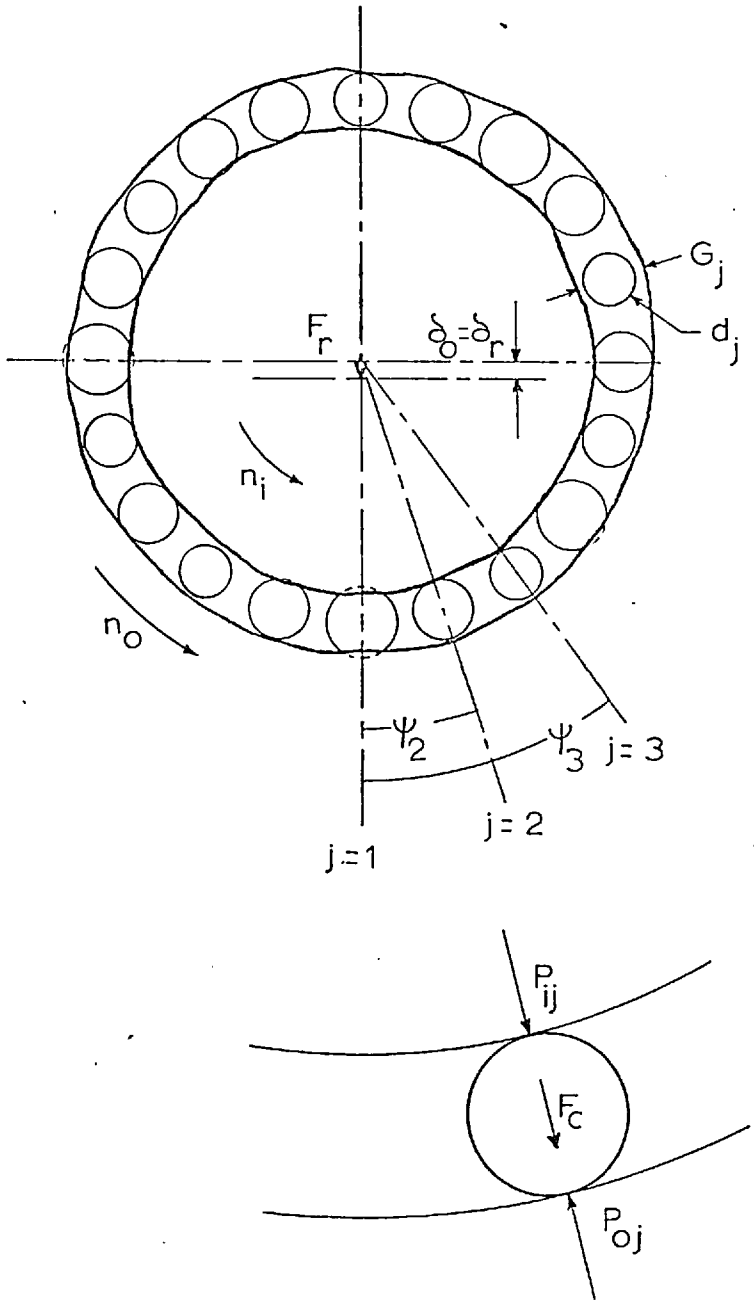


Fig. 3.1 Variation of load zone factor ϵ with radial load for different radial clearances of a radial roller bearing with rigid races. Number of rollers, Z=20.

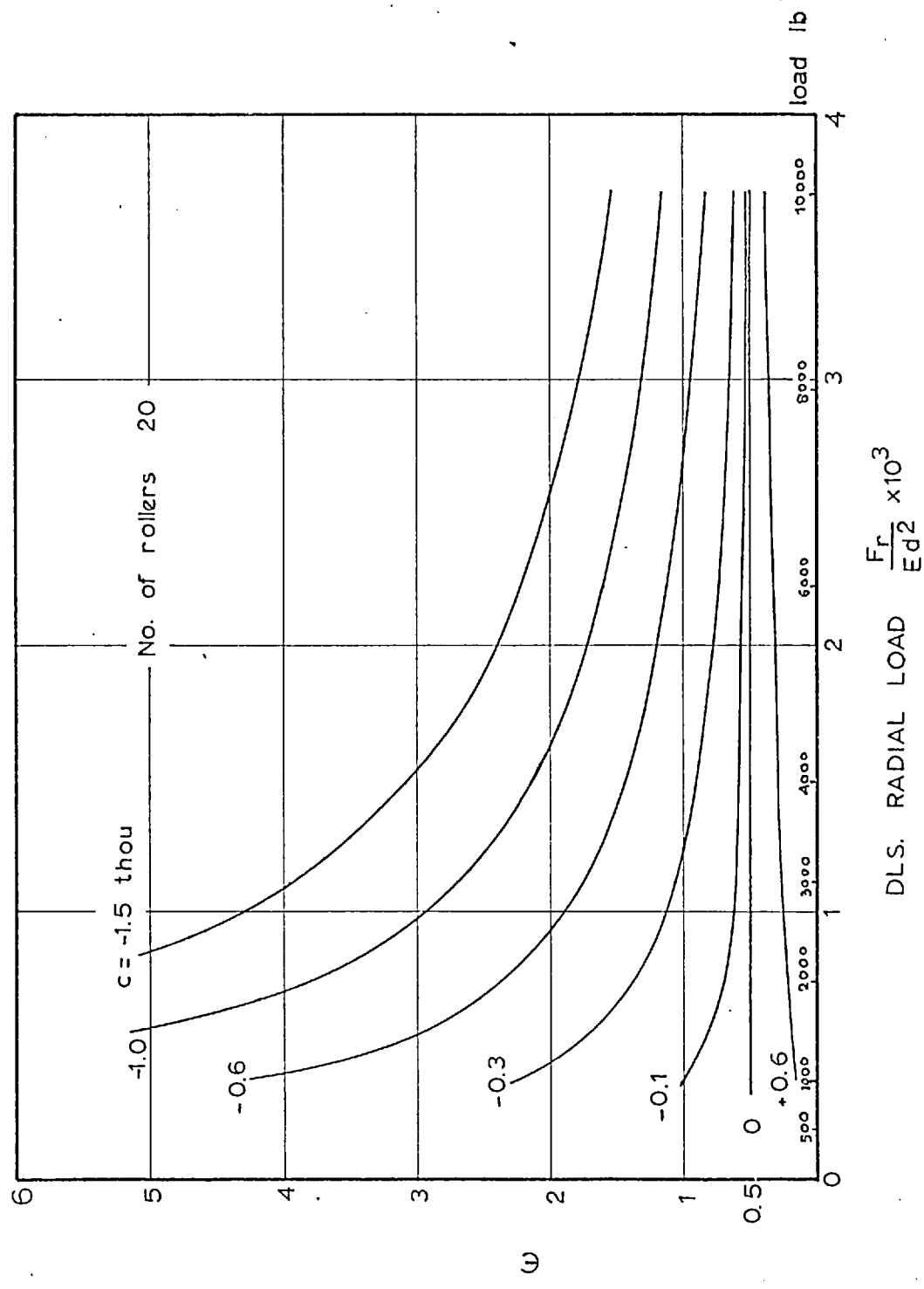


Fig. 3.2 Variation of load zone factor ϵ with radial clearance for different radial loads of a radial roller bearing with rigid races. Number of rollers, Z=20.

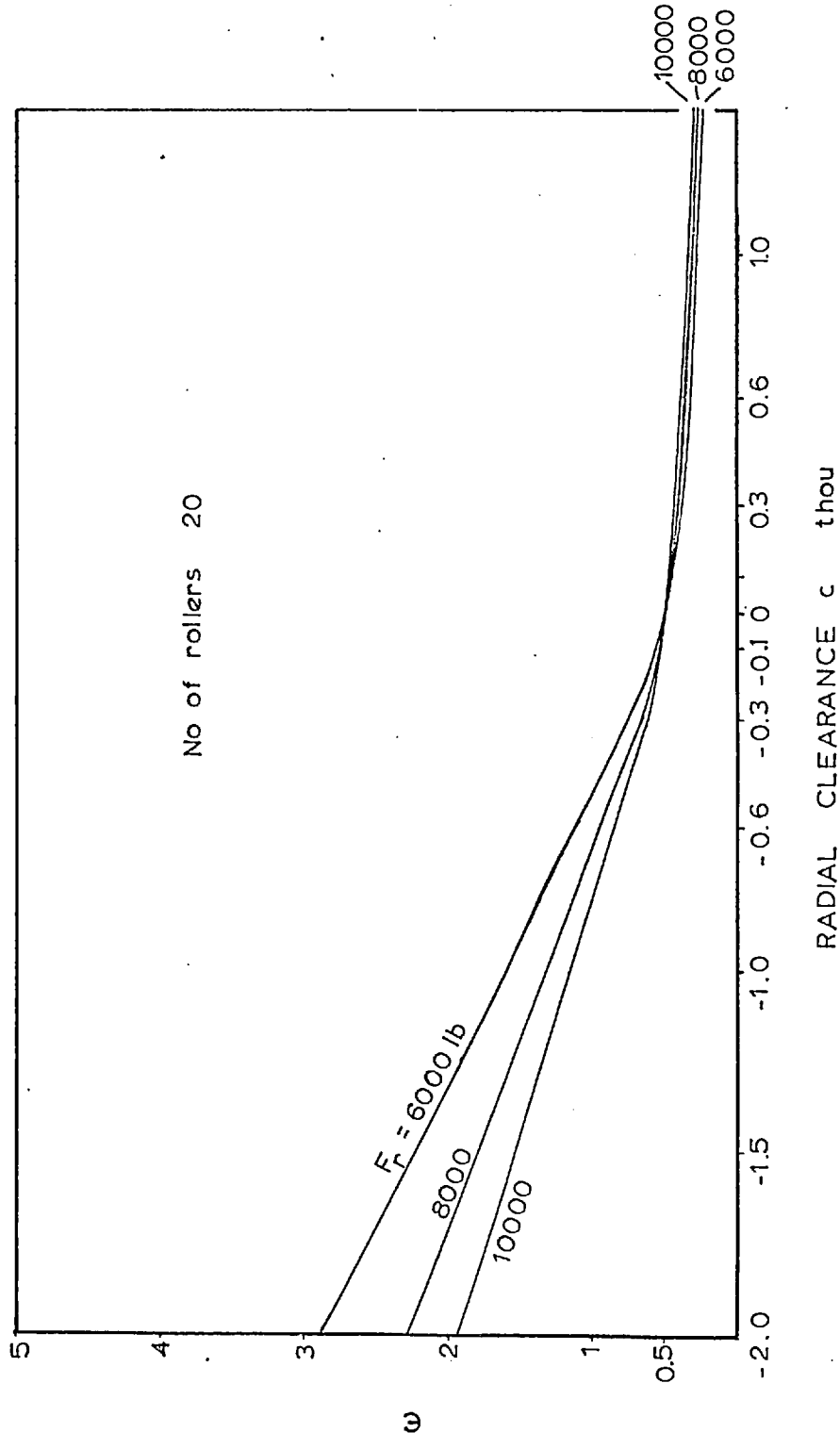
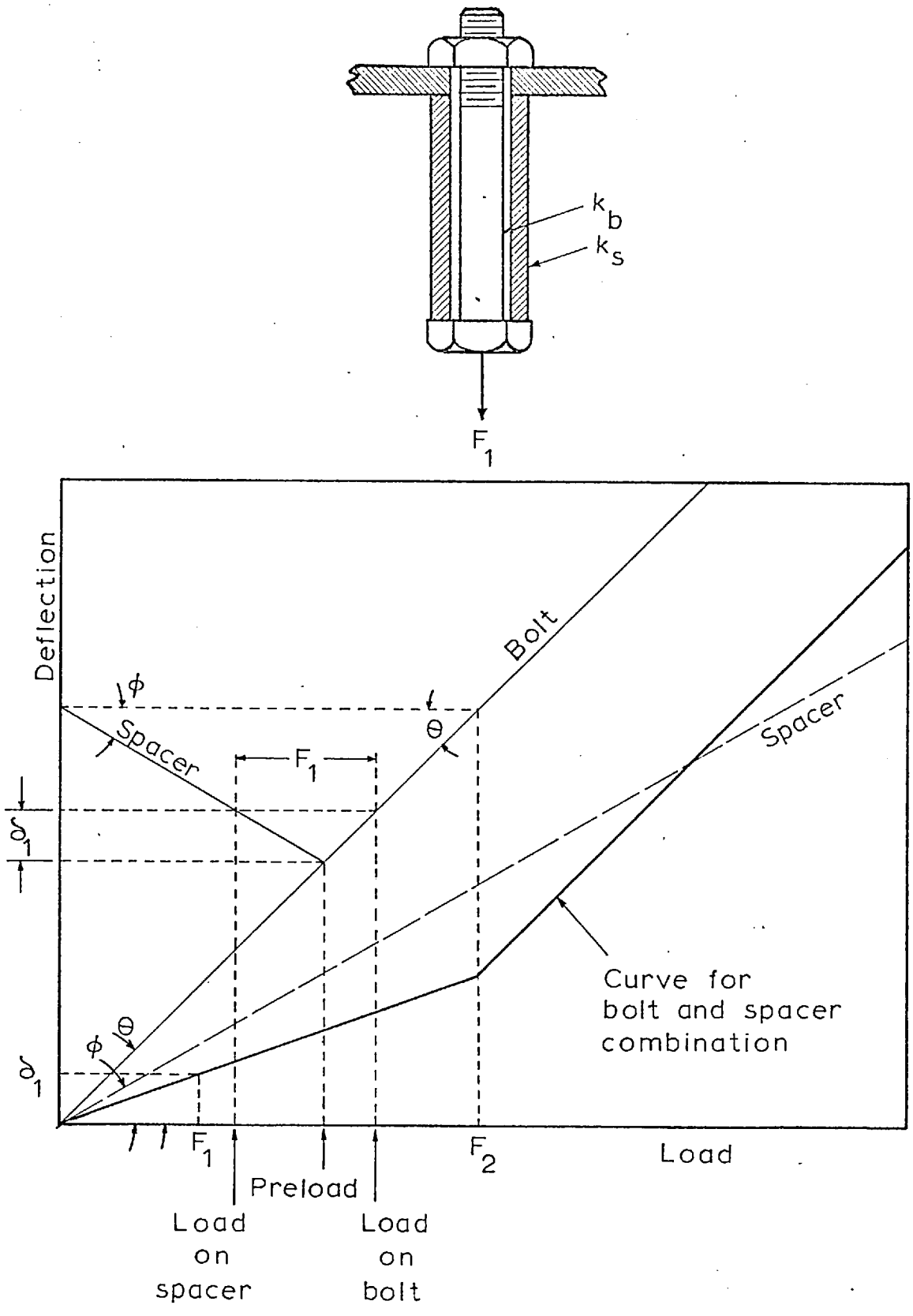


Fig. 3.3 Deflection vs. load curve for bolt and spacer system.



Stiffness of the bolt and spacer system upto an external load of F_2,

$= F_1 / \delta_1 = (\delta_1 \text{Cot}\theta + \delta_1 \text{Cot}\phi)/\delta_1 = \text{Cot}\theta + \text{Cot}\phi$

= bolt stiffness + spacer stiffness.

Fig. 3.4 Deflection vs. load curve for a preloaded radial roller bearing as obtained by bolt and spacer analogy.

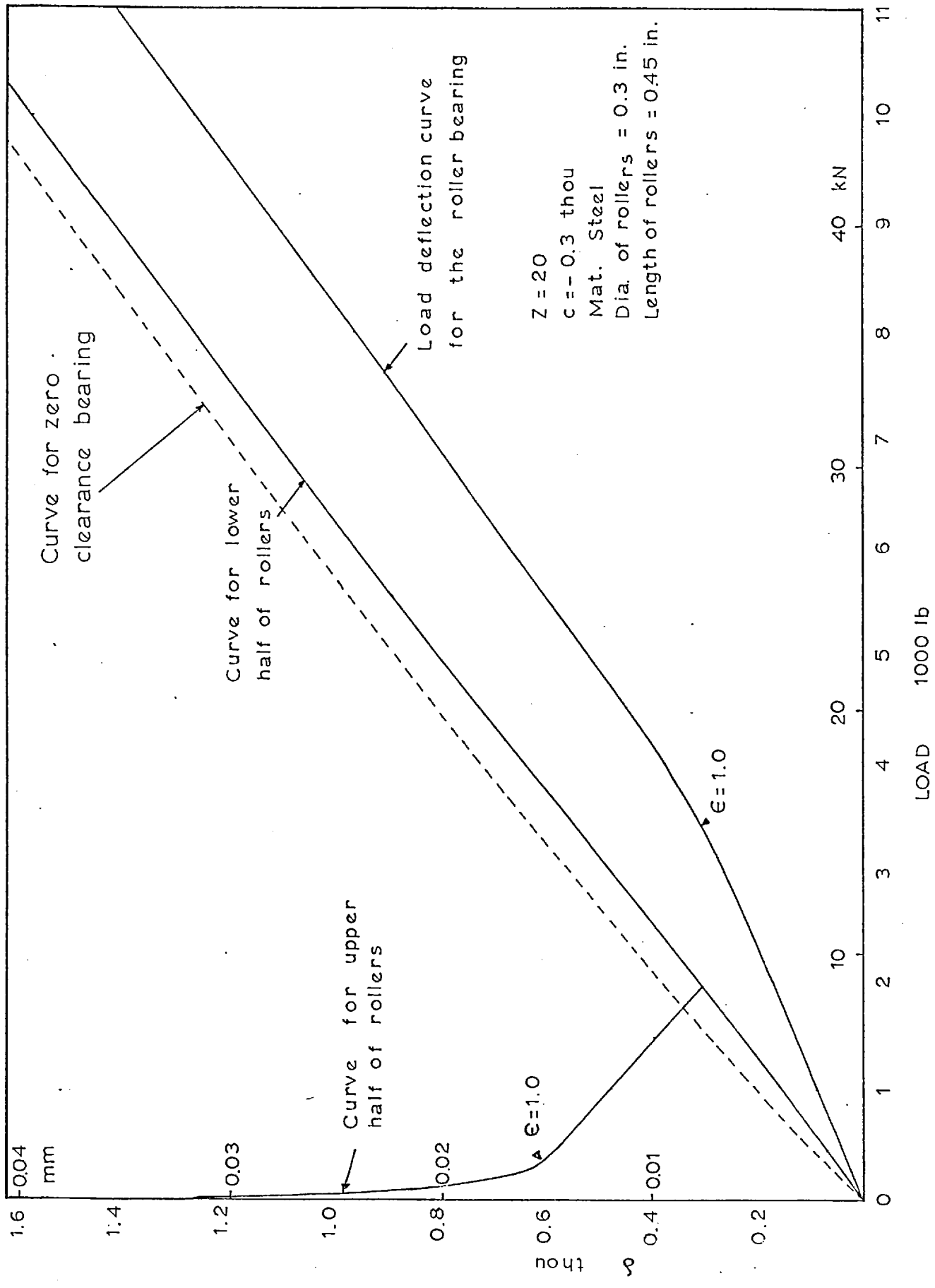


Fig. 3.5 Dimensionless deflection against dimensionless radial load for different radial clearances of a radial roller bearing with rigid races. Number of rollers, Z=20.

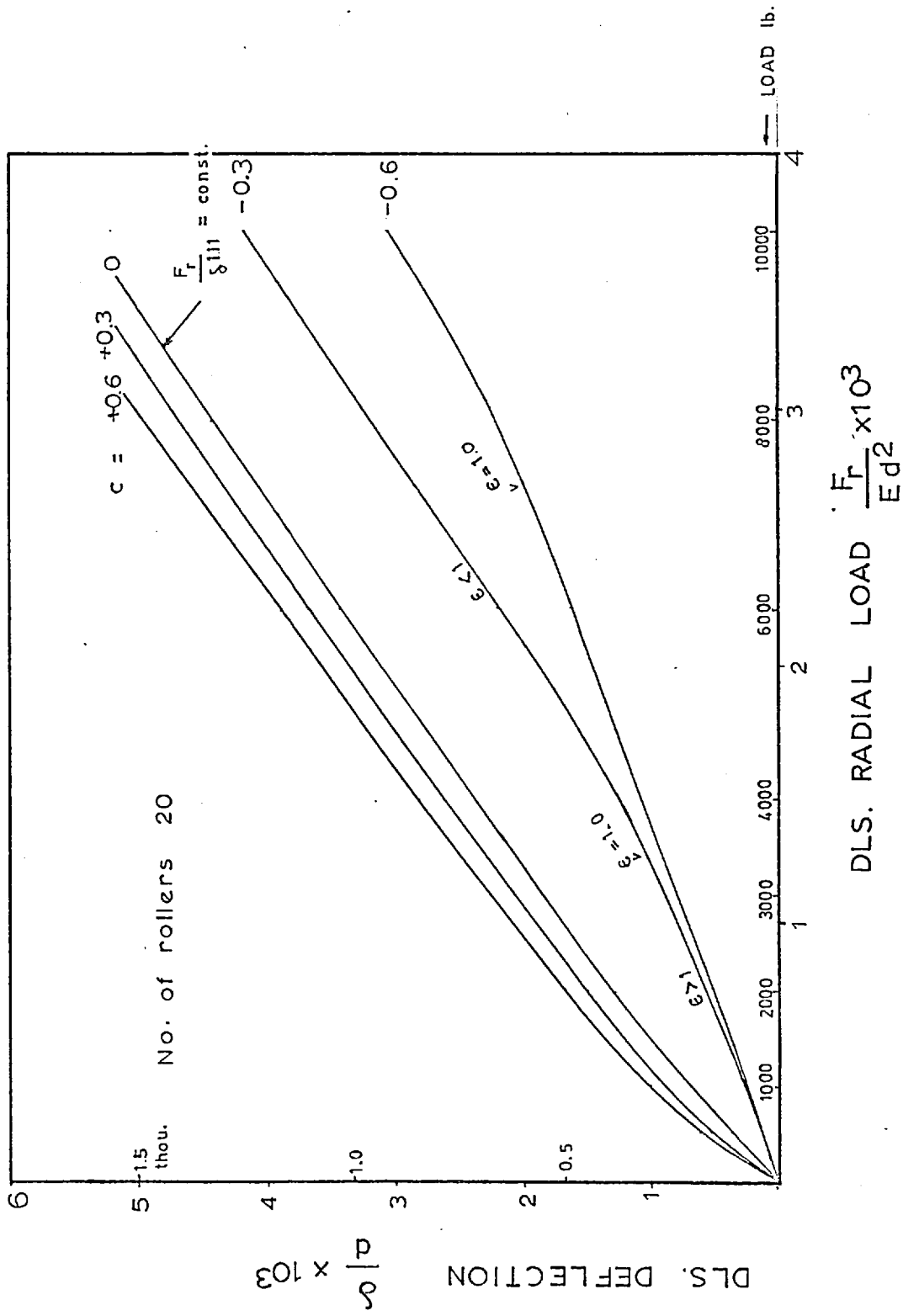


Fig. 3.6 Variation of dimensionless deflection of a radial roller bearing having rigid races with dimensionless radial clearance and dimensionless radial load.

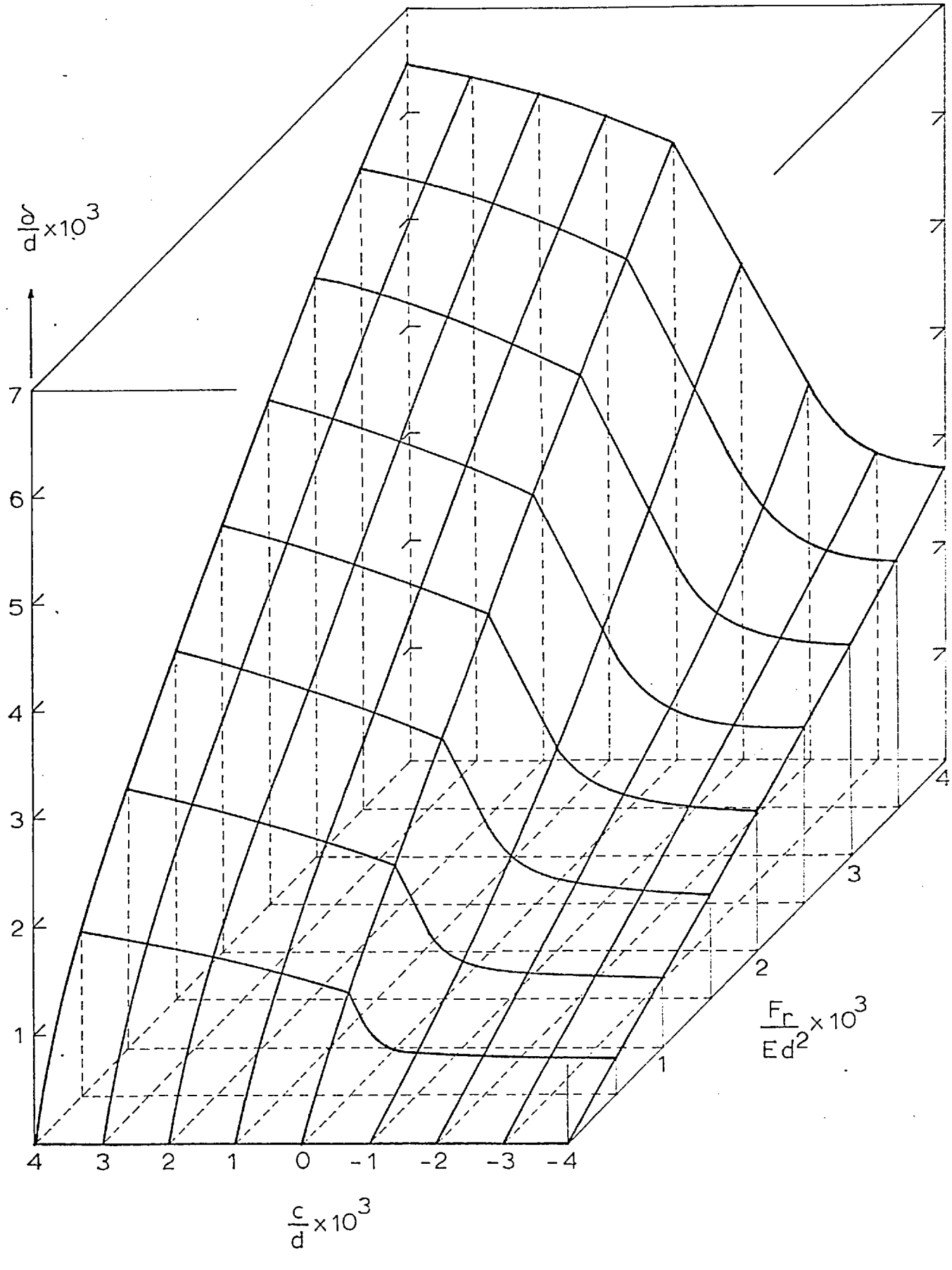


Fig. 3.7 Dimensionless deflection against dimensionless radial clearance for different numbers of rollers of a radial roller bearing with rigid races. Radial load, F_r=4000 lbs.

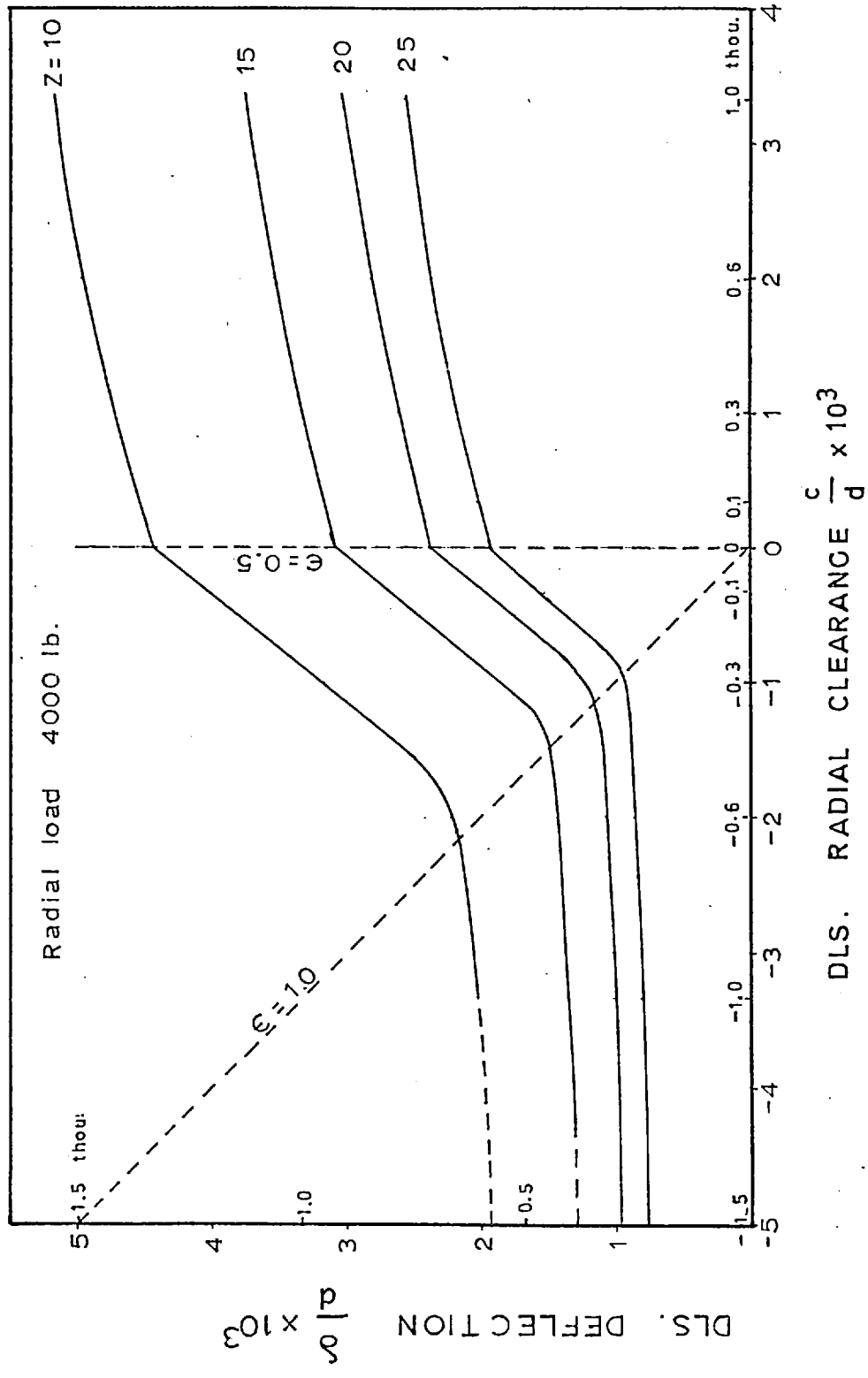


Fig. 3.8 Dimensionless deflection against number of rollers for different radial loads of a radial roller bearing with rigid races. Radial clearance, c=0.

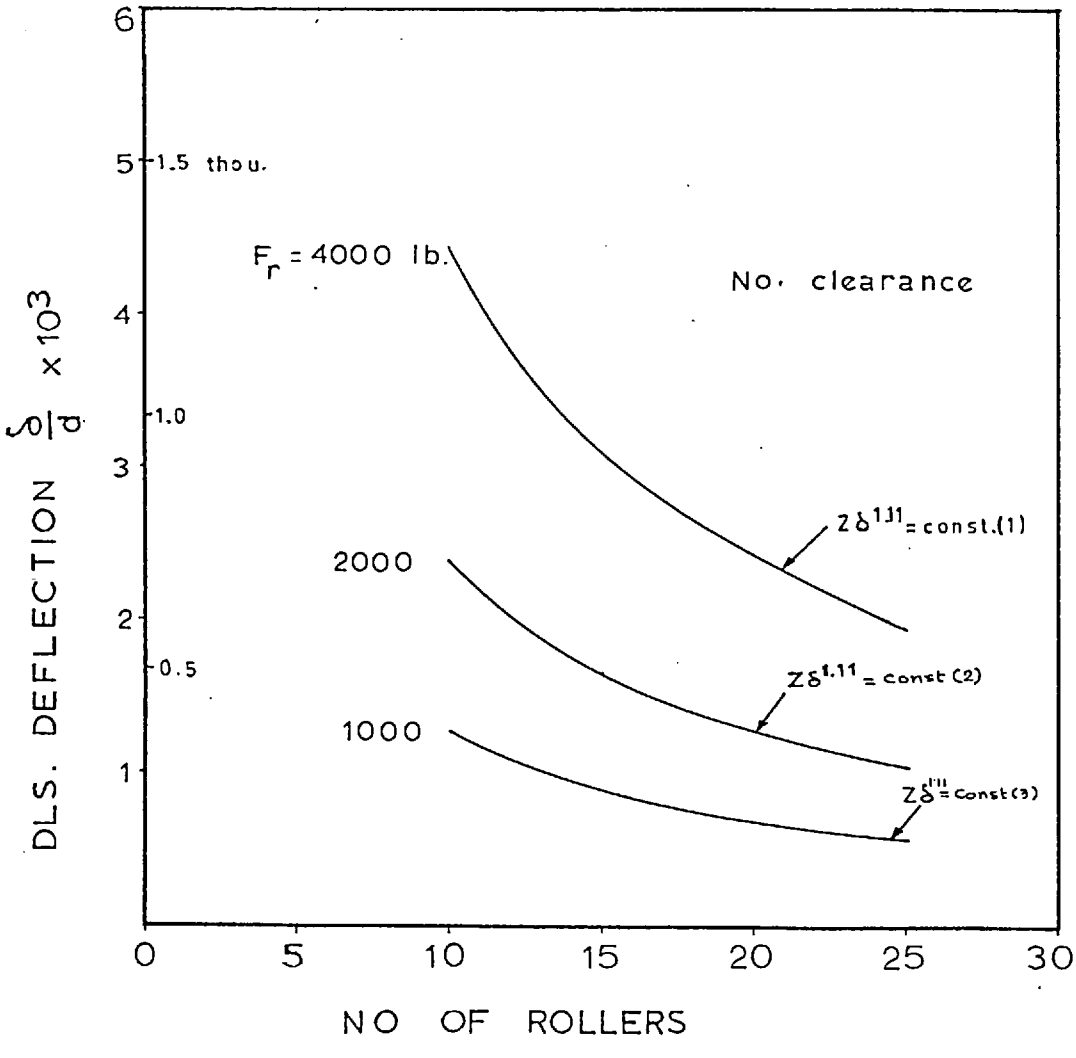


Fig. 3.9 Roller load distribution in radial roller bearings having rigid races with different radial clearances.

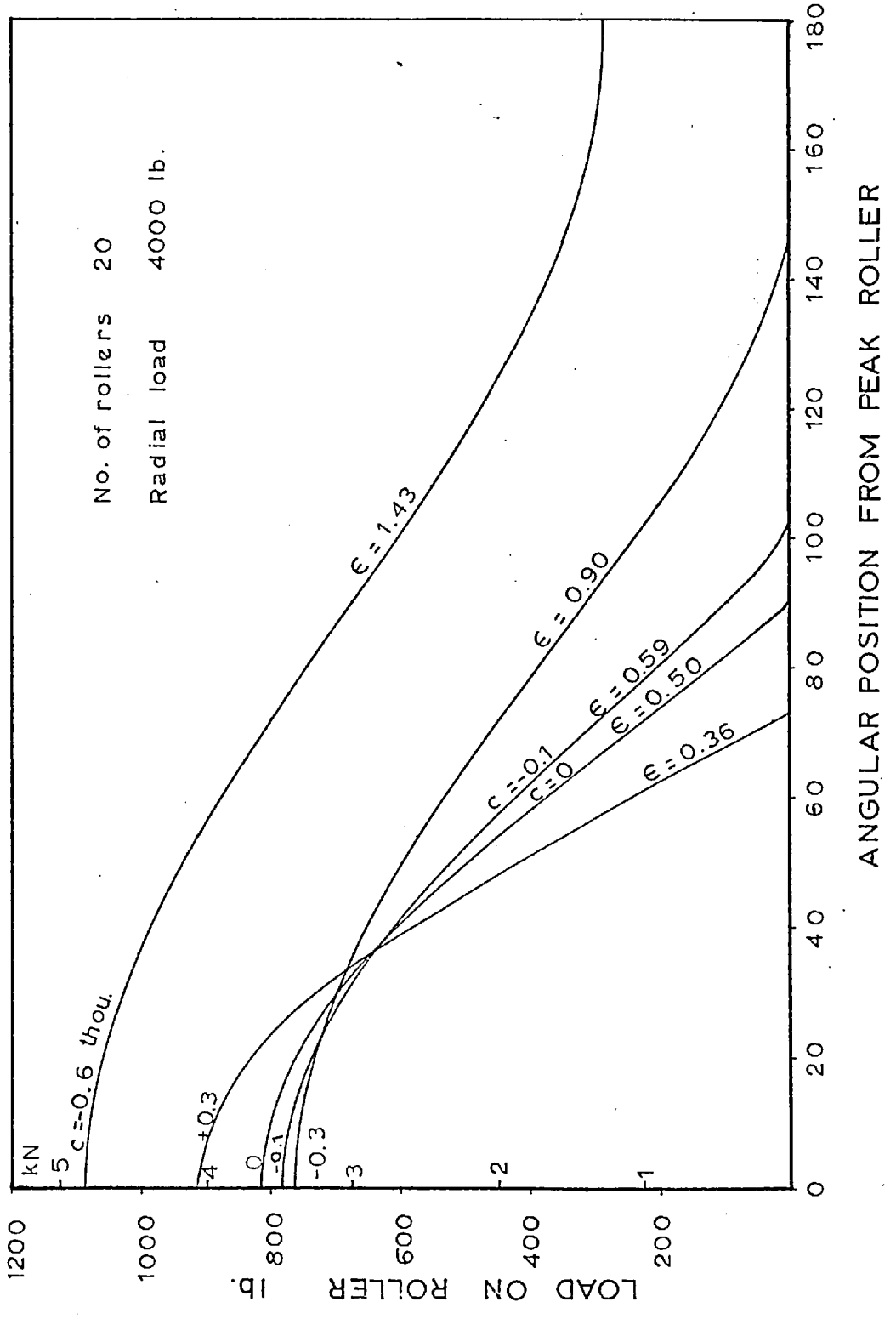


Fig. 3.10 Variation of peak roller load with radial load for different radial clearances of a radial roller bearing having rigid races. Number of rollers, Z=20.

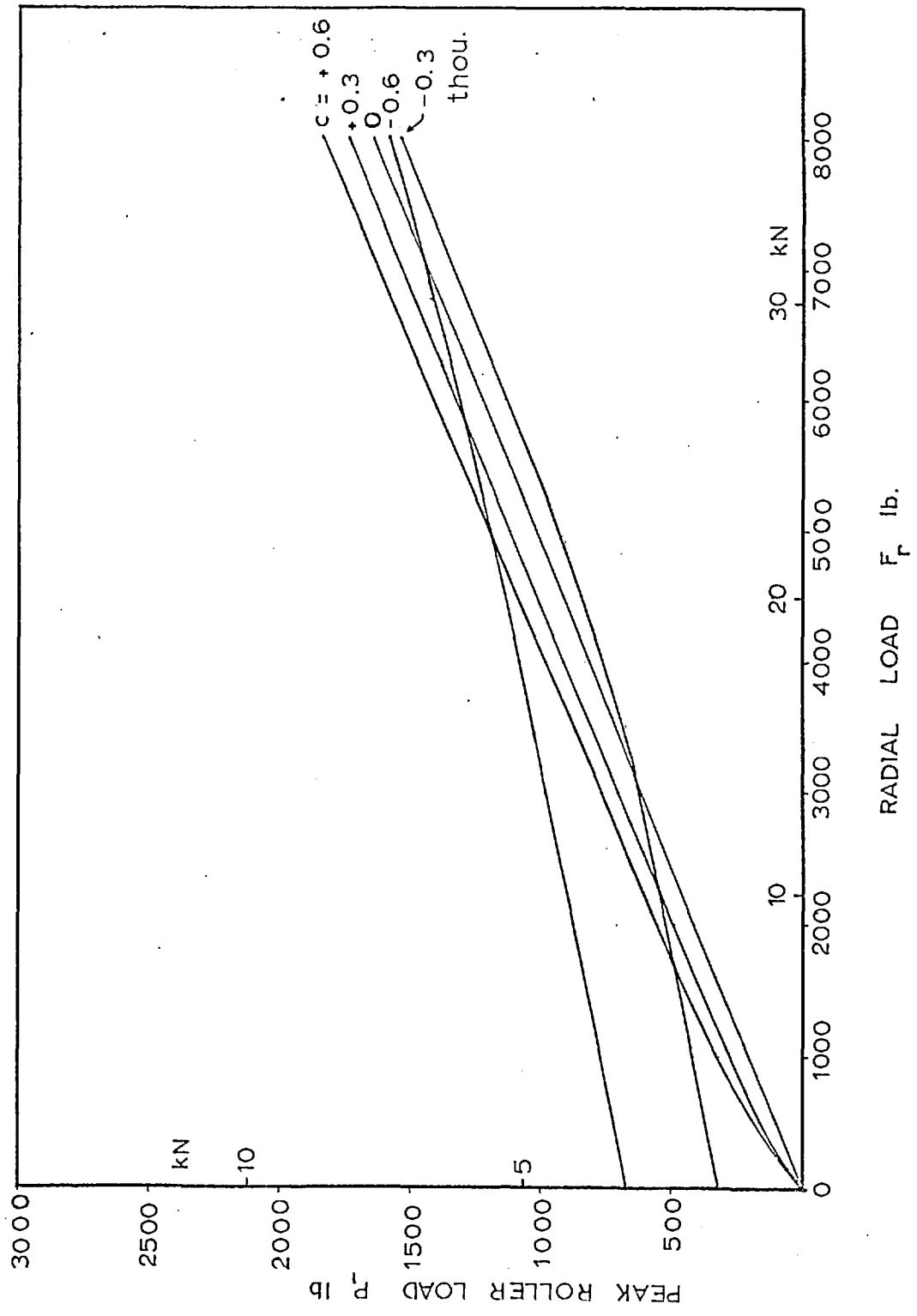


Fig. 3.11 Variation of dimensionless peak roller load with dimensionless radial clearance for different radial loads of a radial roller bearing with rigid races.

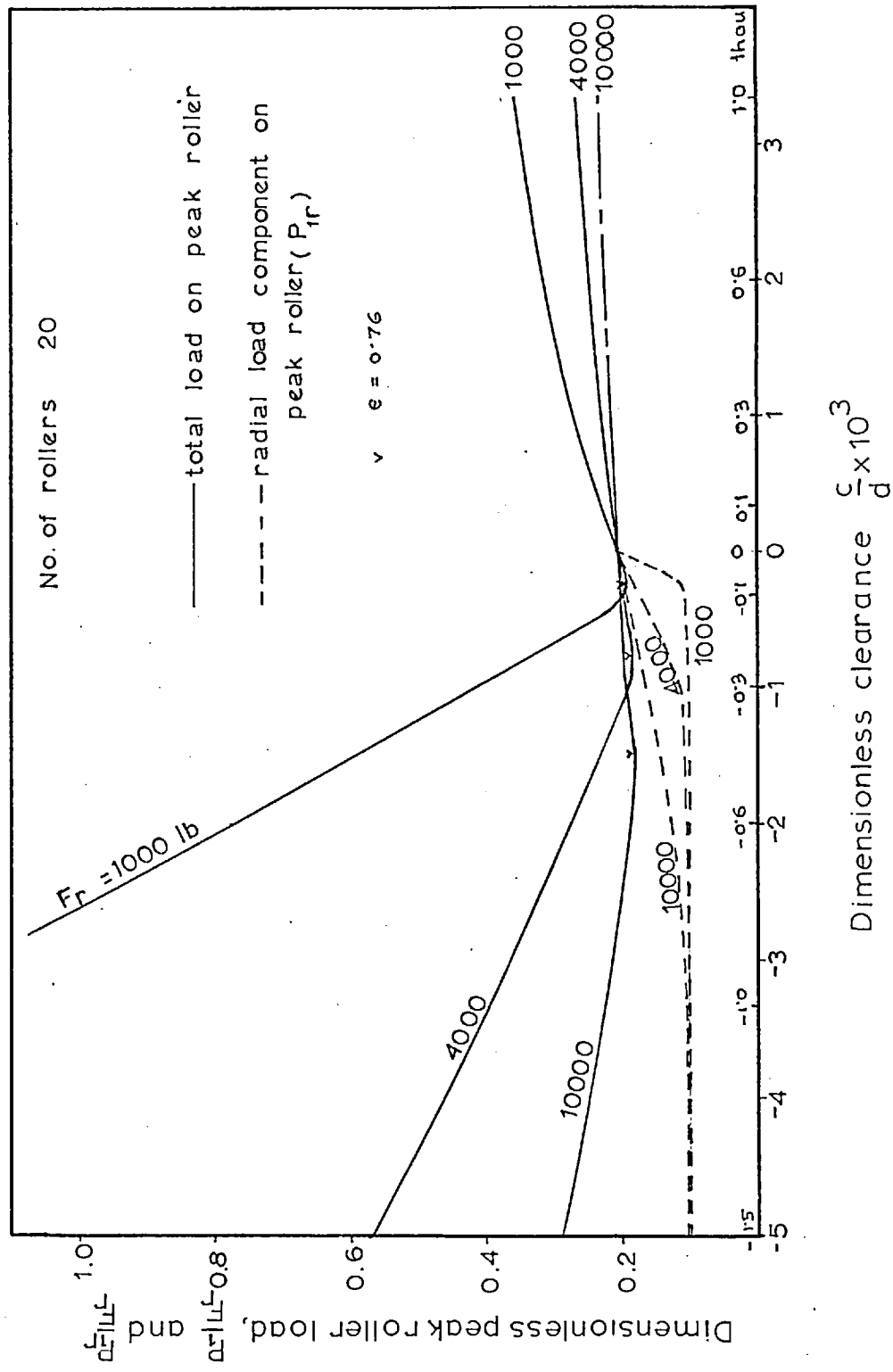


Fig. 3.12 Variation of dimensionless peak roller load with dimensionless radial clearance for different numbers of rollers in a radial roller bearing with rigid races.

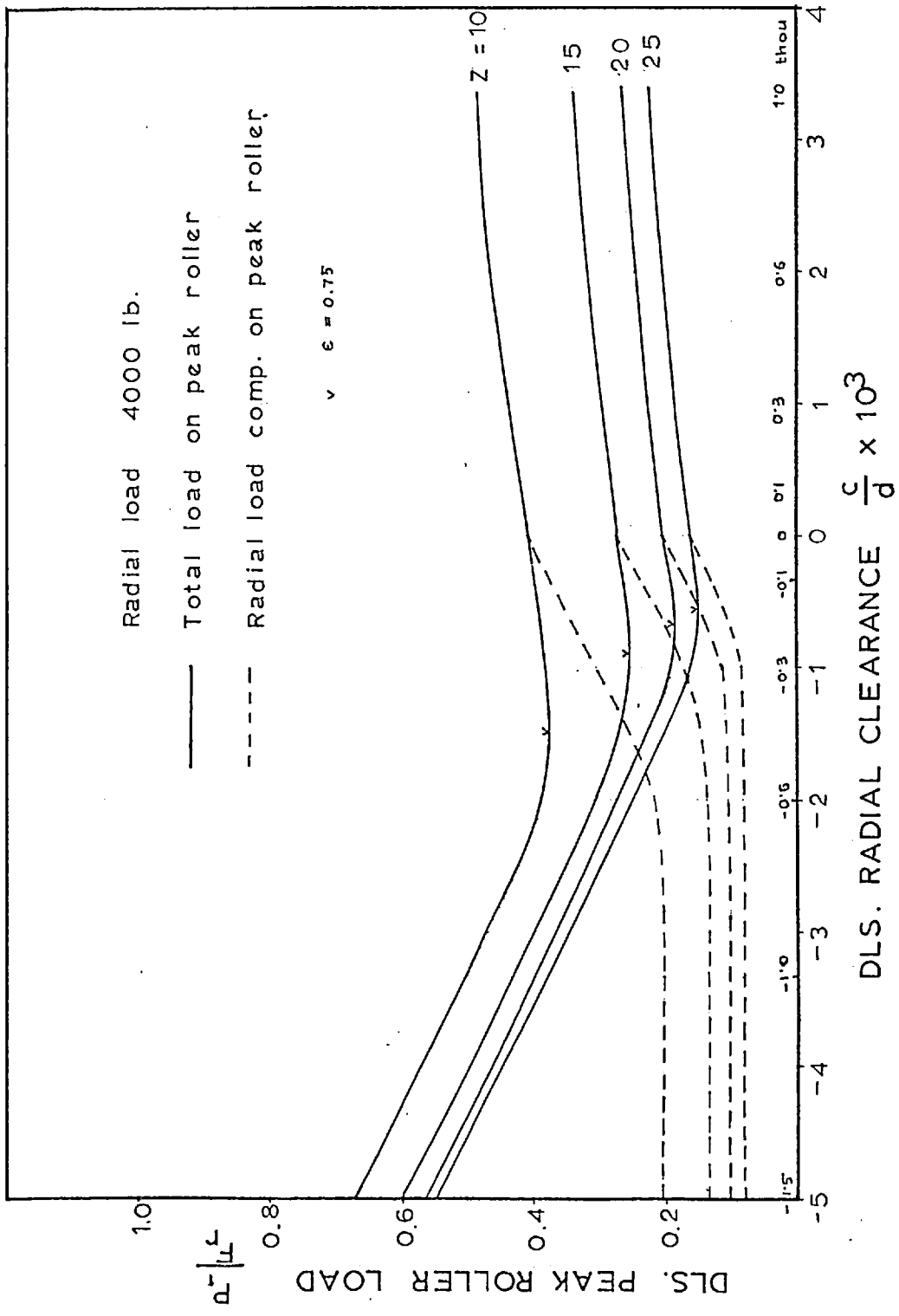


Fig. 3.13 Variation of load sharing factor with dimensionless radial load for different radial clearances in a radial roller bearing with rigid races. Number of rollers, Z=20.

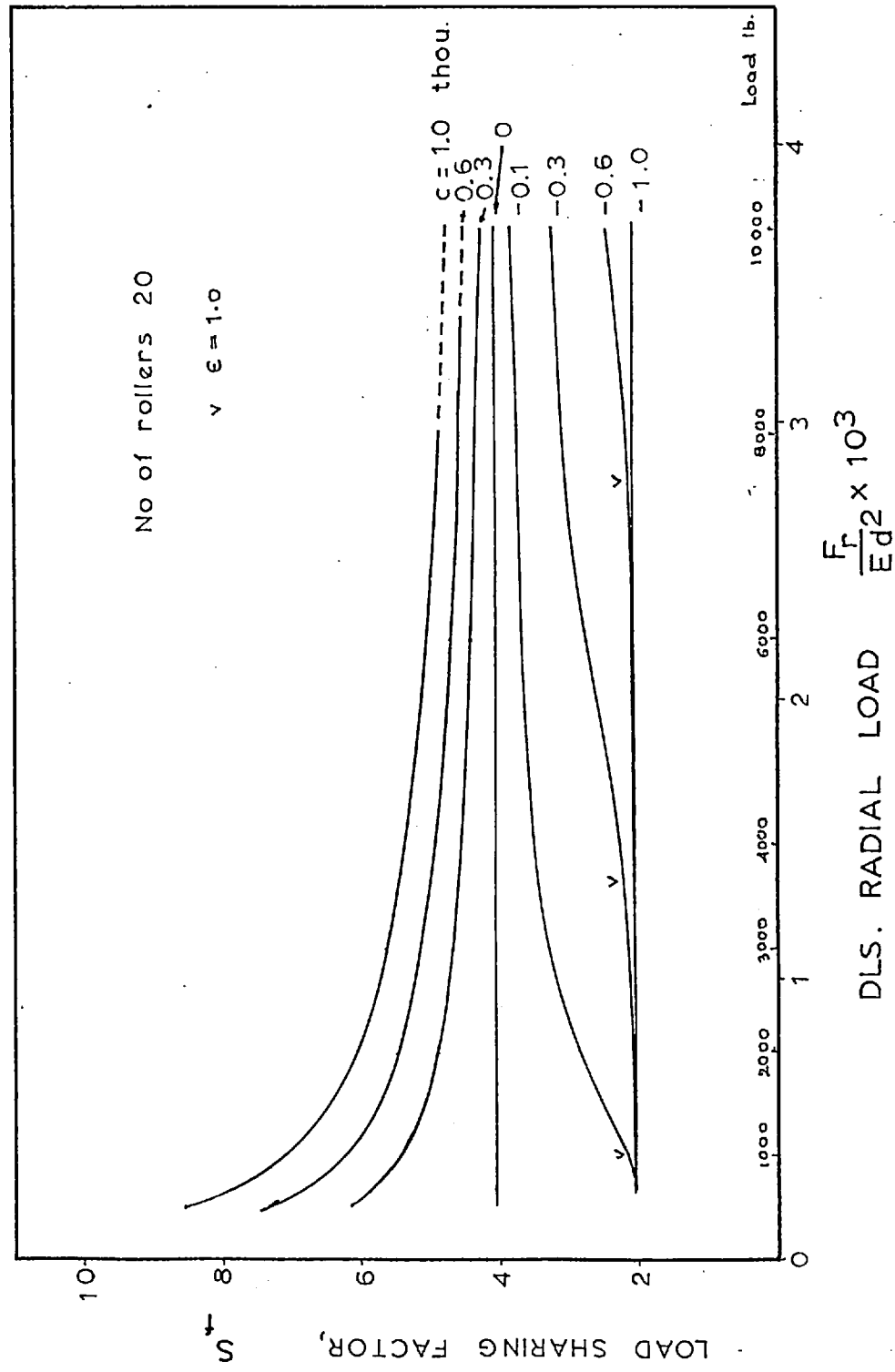


Fig. 3.14 Variation of load sharing factor with dimensionless radial clearance for different numbers of rollers in a radial roller bearing with rigid races.

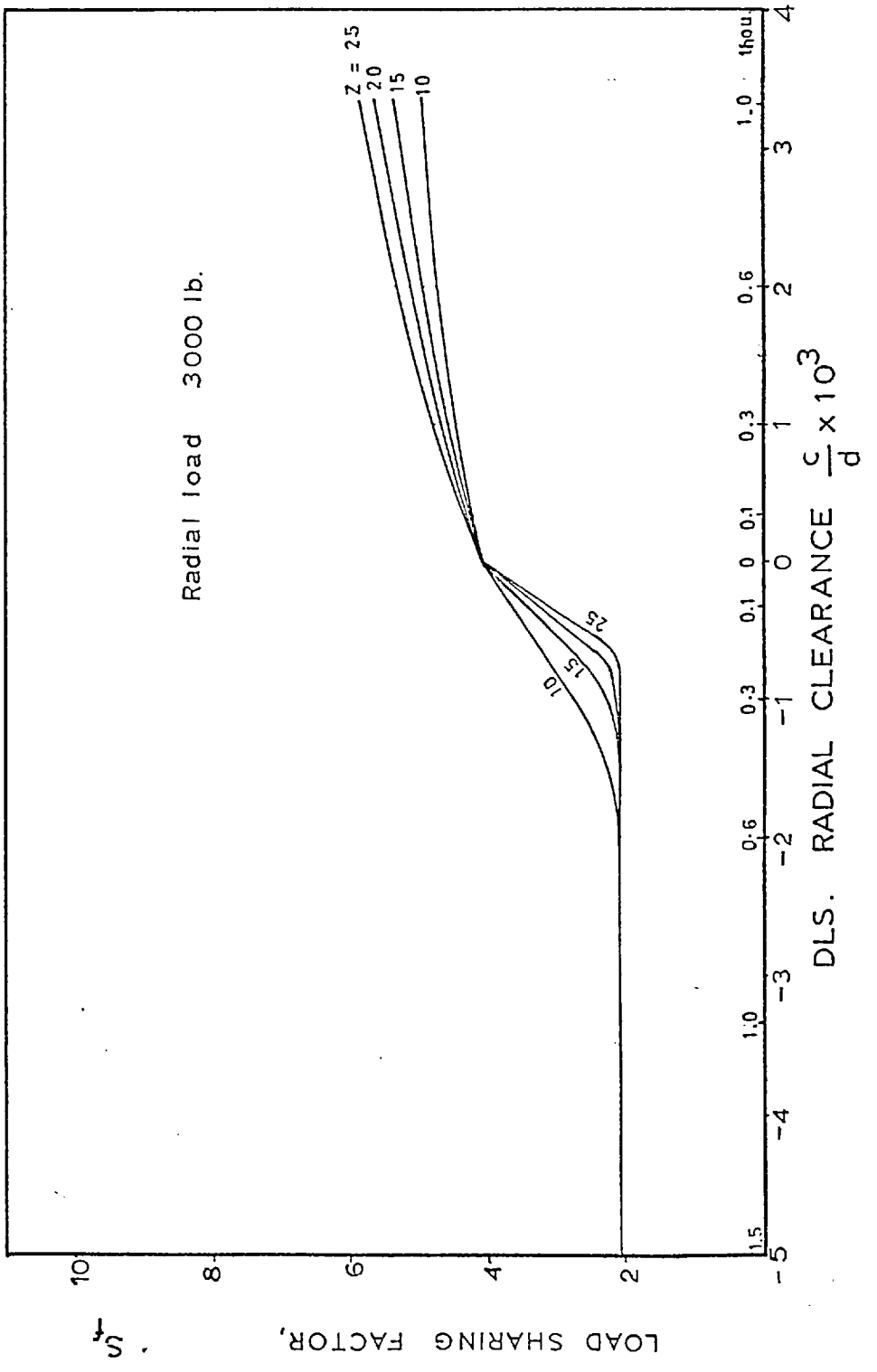


Fig. 3.15 Variation of dimensionless incremental stiffness with dimensionless radial load for different radial clearances in a radial roller bearing with rigid races. Number of rollers, Z=20.

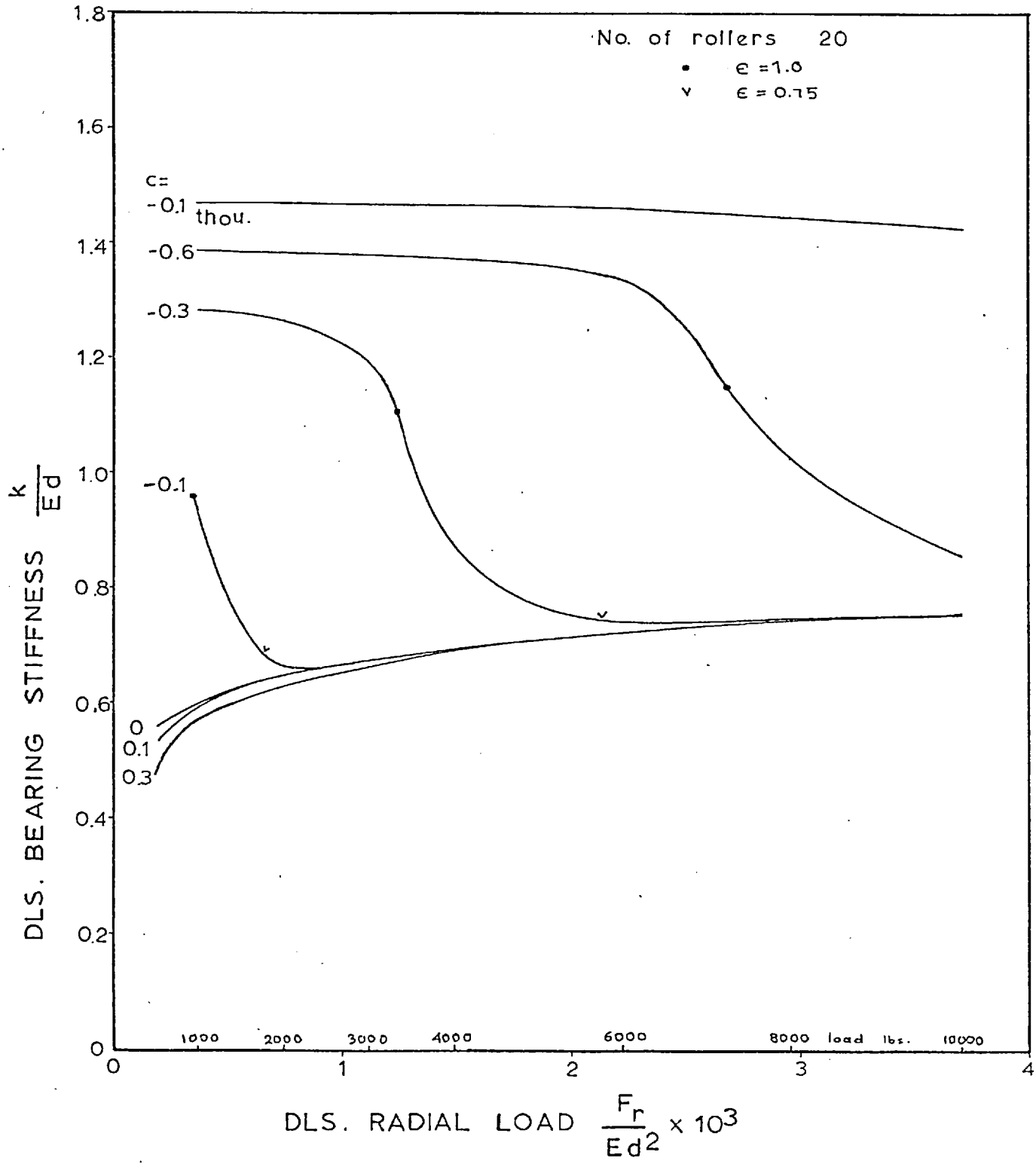


Fig. 3.16 Variation of dimensionless incremental stiffness with dimensionless radial clearance for different radial loads in a radial roller bearing with rigid races. Number of rollers, Z=20.

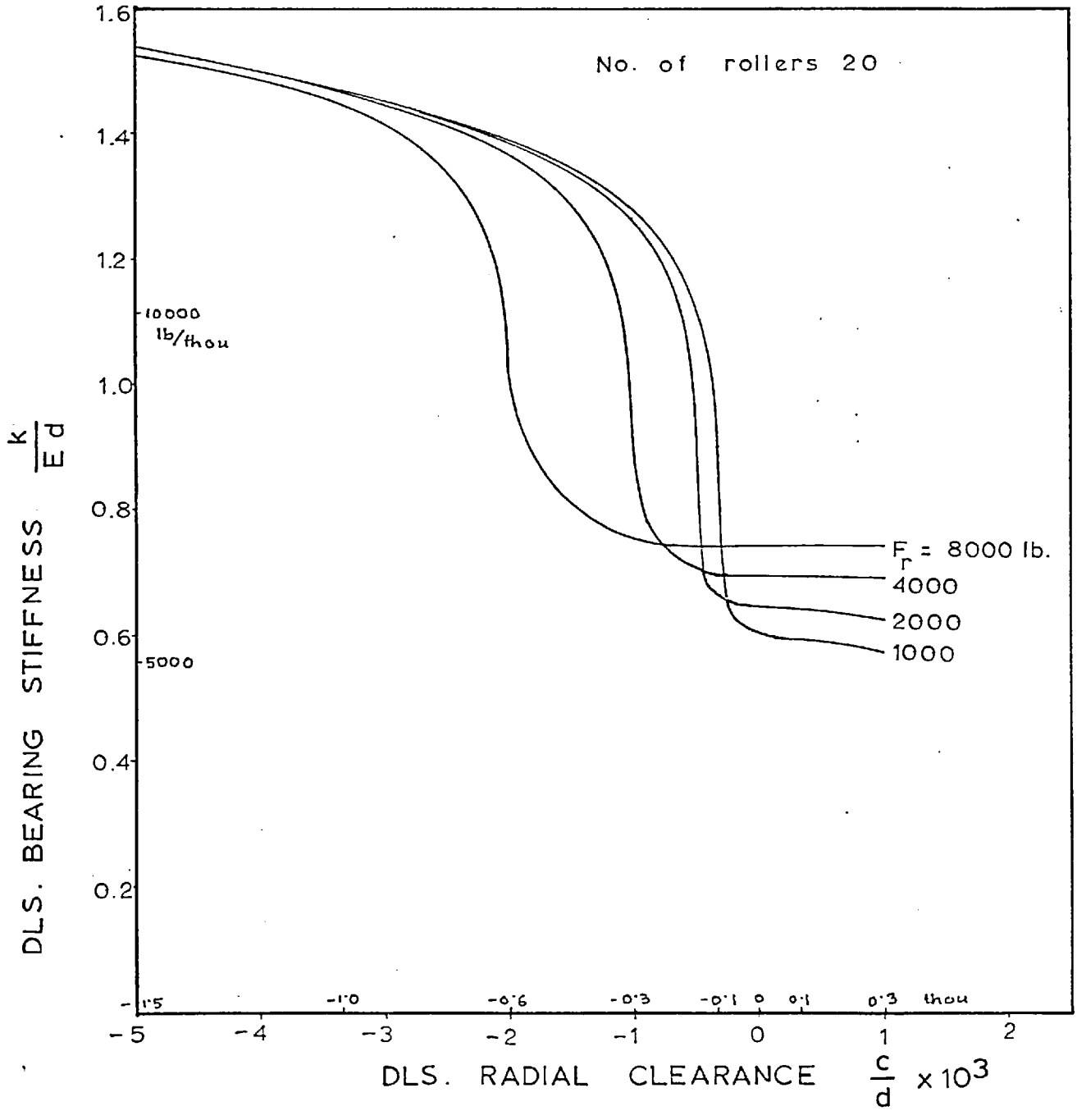


Fig. 3.17 Variation of dimensionless incremental stiffness with dimensionless radial load for different numbers of rollers in a radial roller bearing with rigid races. Radial clearance, c = -0.3 thou.

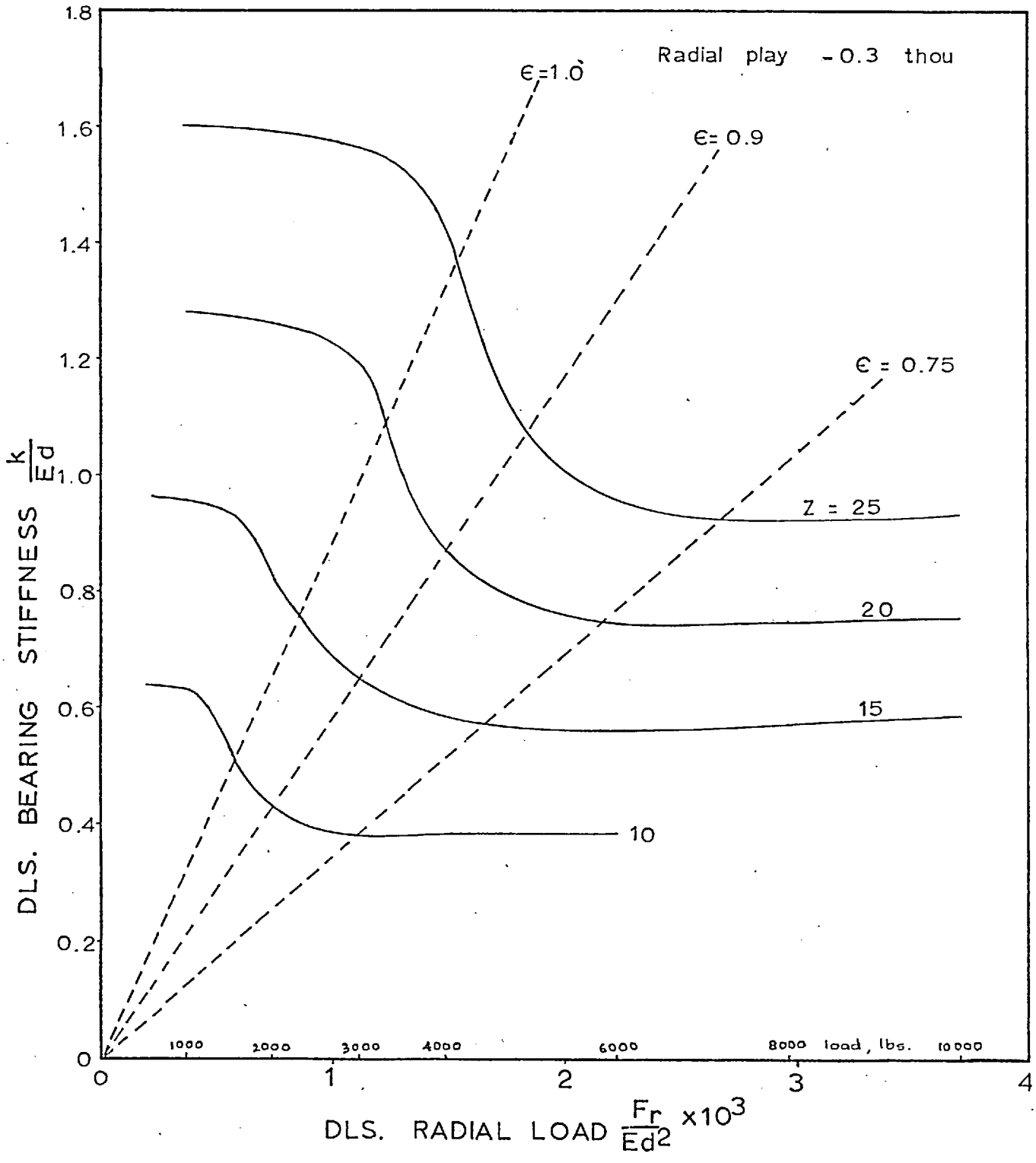


Fig. 3.18 Variation of dimensionless incremental stiffness with dimensionless radial clearance for different numbers of rollers in a radial roller bearing with rigid races. Radial load, F_r= 4000 lbs.

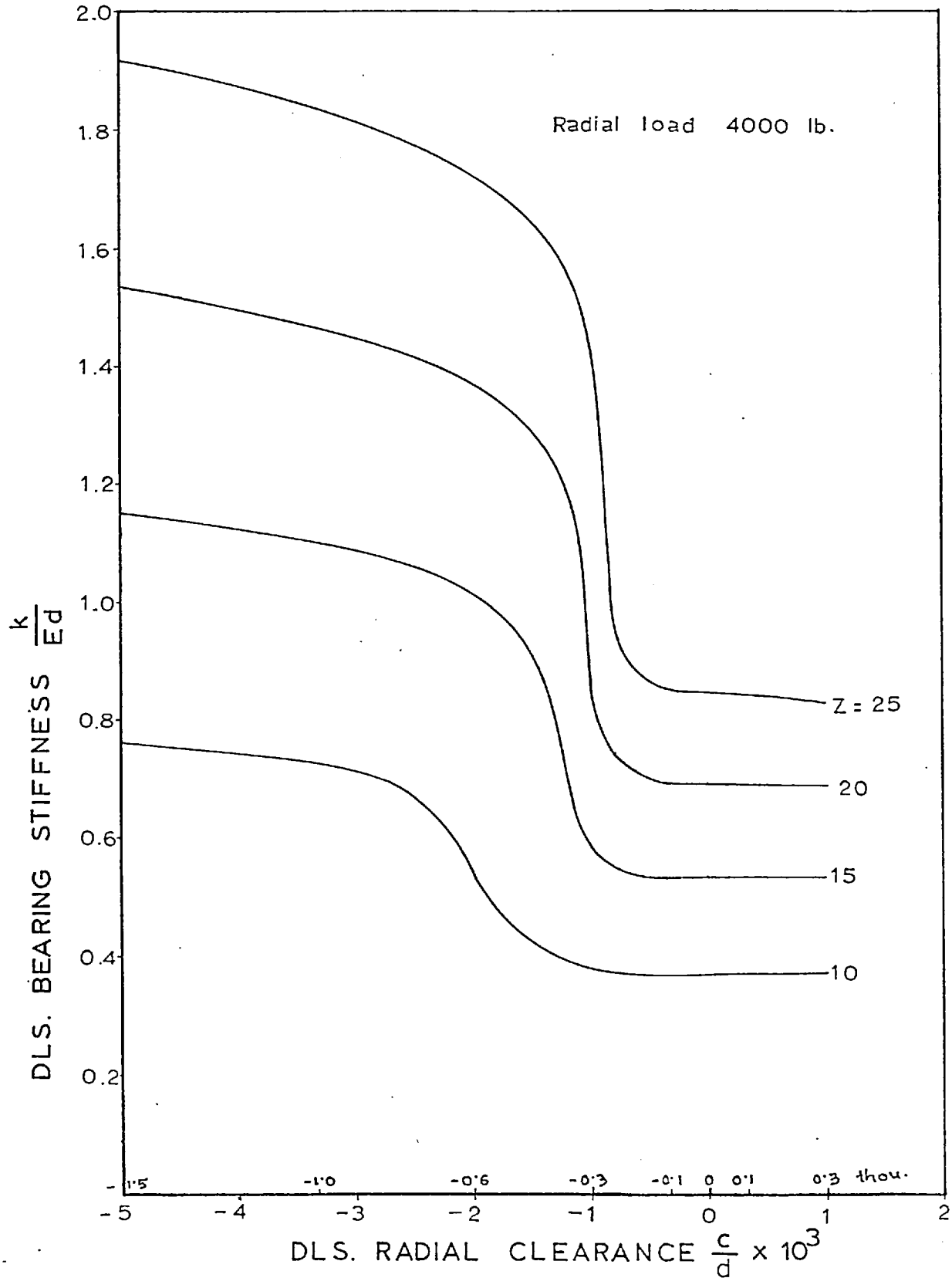


Fig. 3.19 Variation of average stiffness with radial load for different radial clearances in a radial roller bearing with rigid races. Number of rollers, Z = 20.

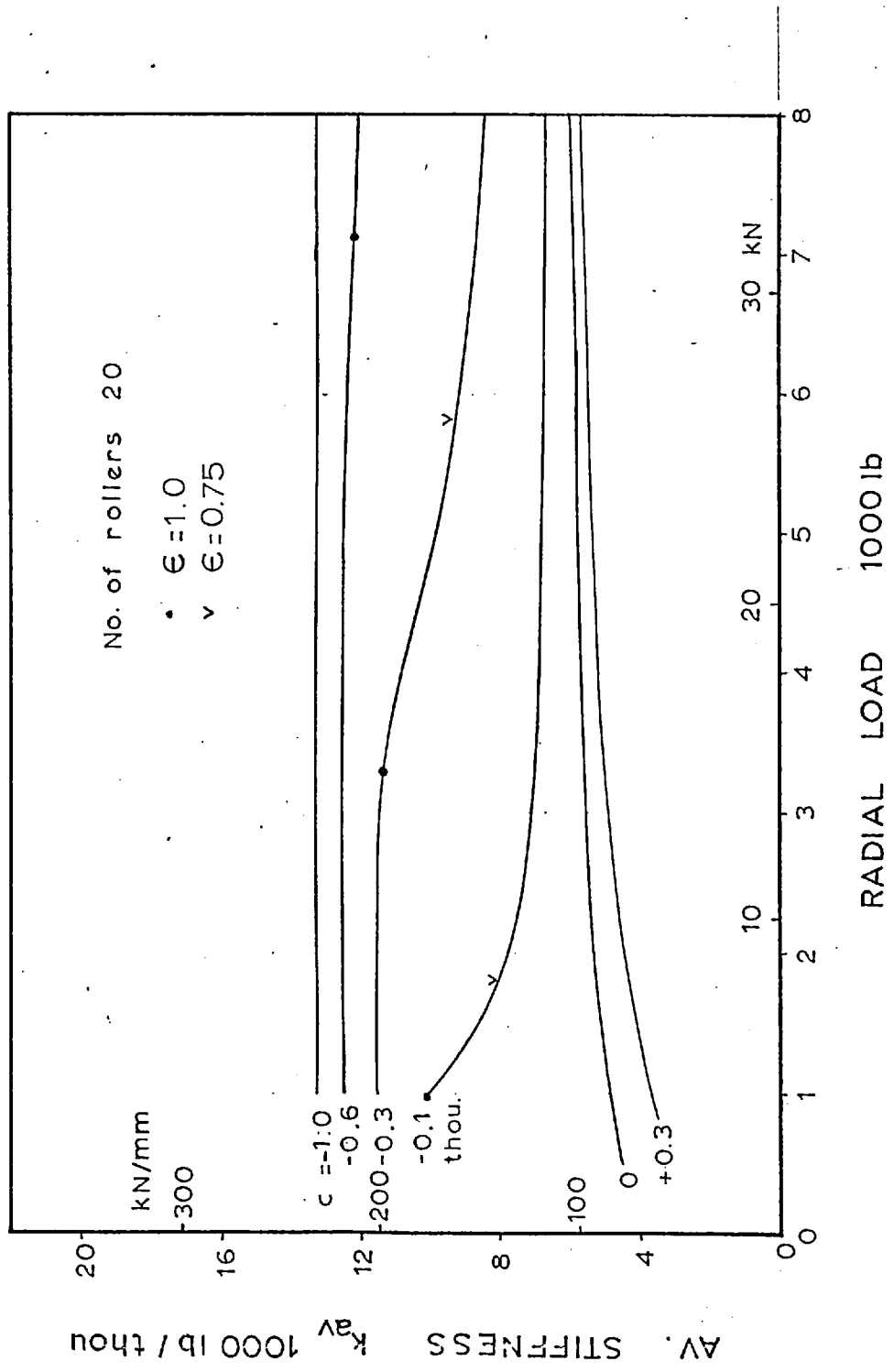


Fig. 3.20 Variation of life with radial load for different radial clearances in a radial roller bearing with rigid races. Number of rollers, Z=20.

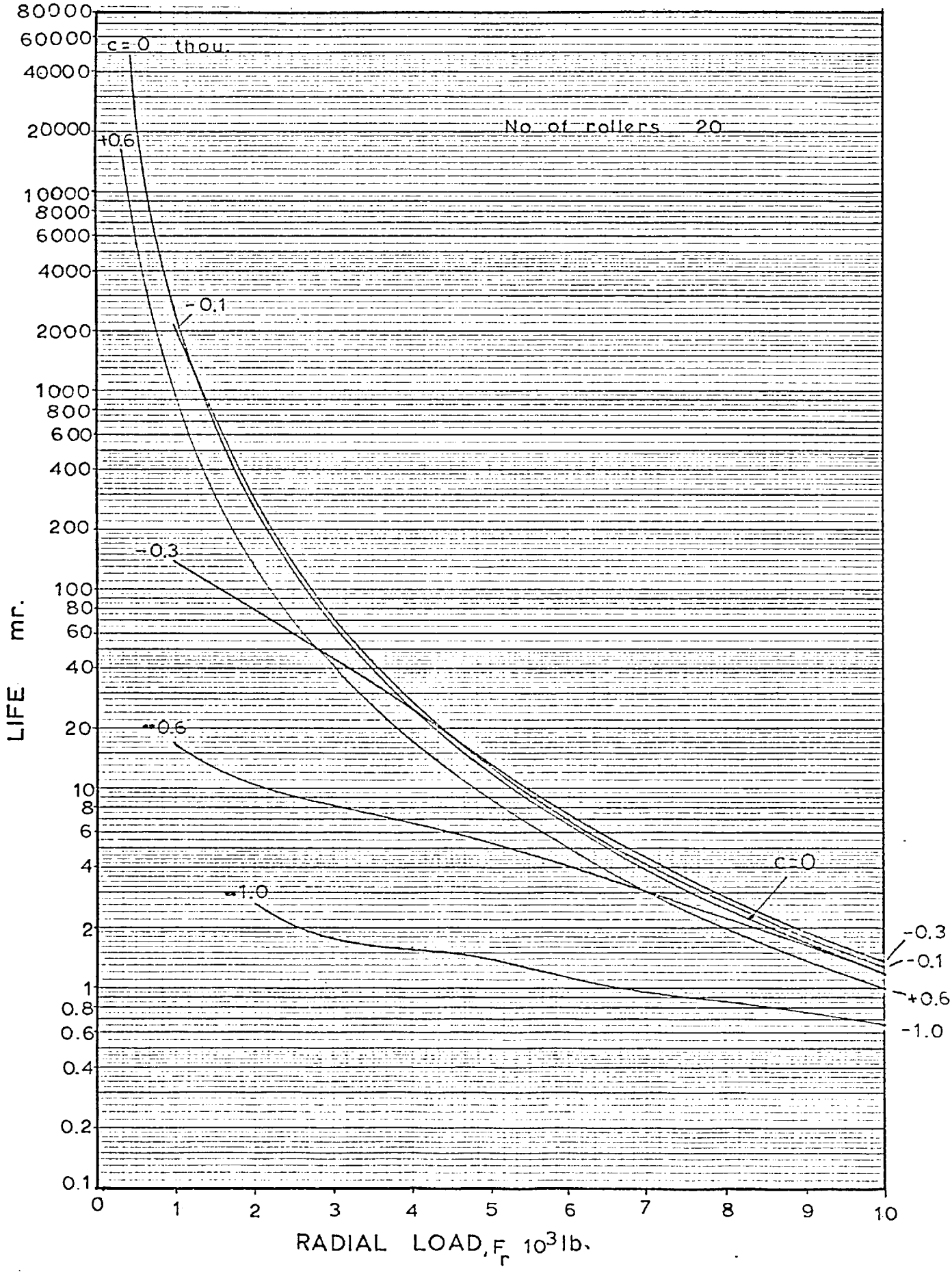


Fig. 3.21 Variation of life with radial clearance for different radial loads in a radial roller bearing with rigid races. Number of rollers, Z=20.

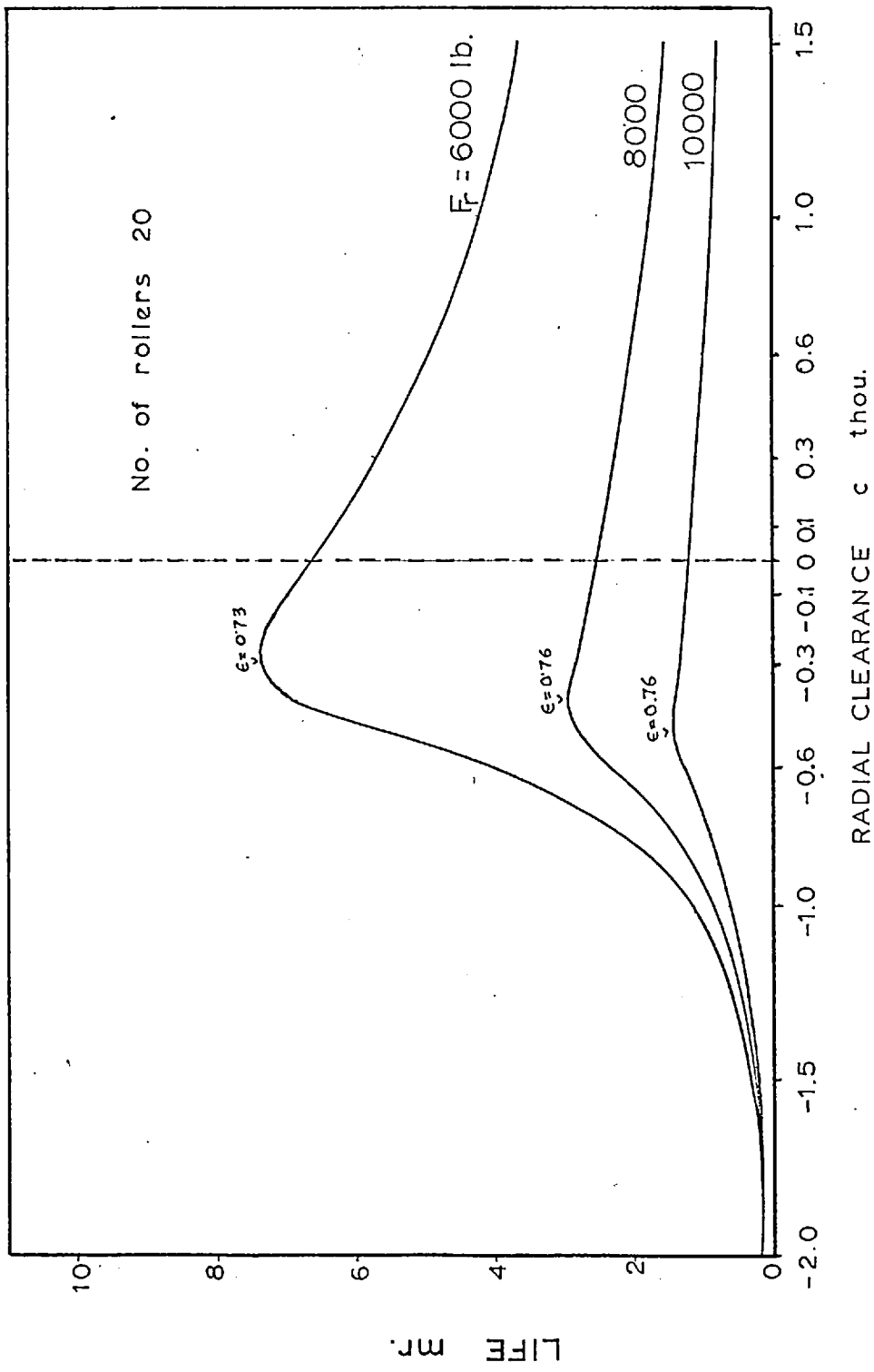


Fig. 3.22 Variation of life with radial clearance for different numbers of rollers in a radial roller bearing with rigid races. Radial load, F_r=6000 lbs.

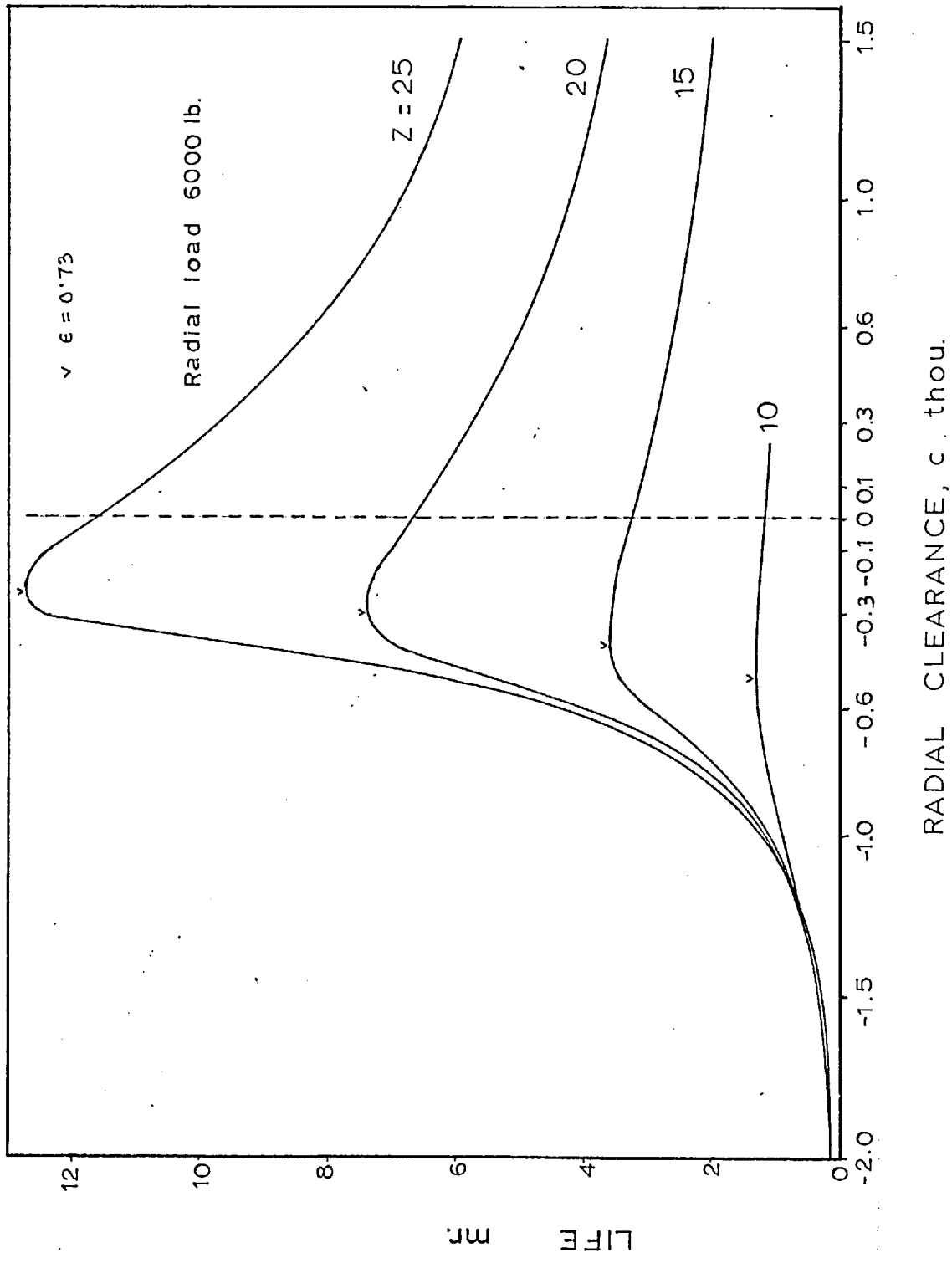


Fig. 3.23 Nomogram for determining F^* from Z, ℓ and F_r for radial roller bearings with rigid races.

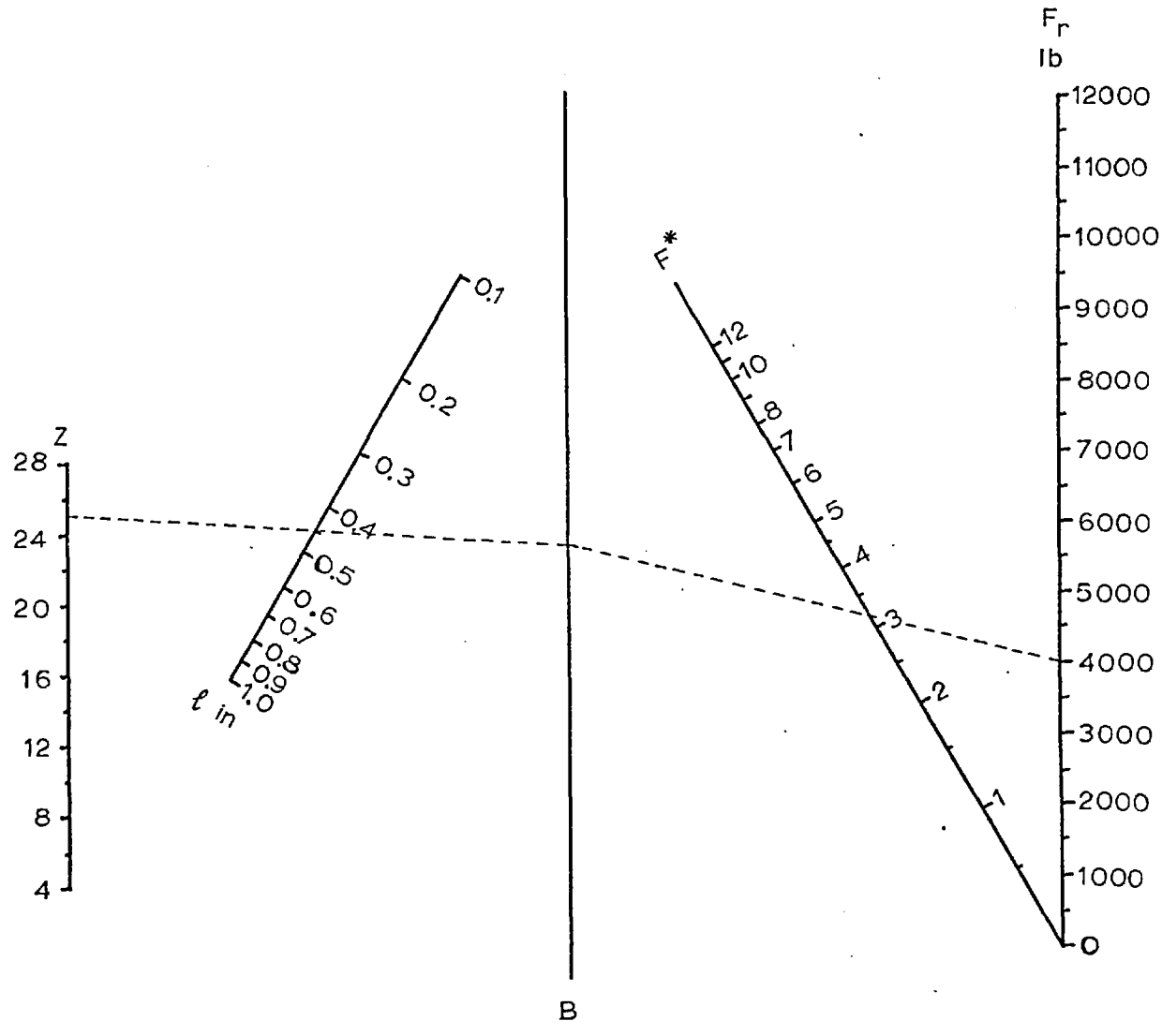


Fig. 3.24 Nomogram for determining the extent of loaded zone factor ϵ, from F^* (found from fig. 3.23) and radial clearance c, of radial roller bearings with rigid races.

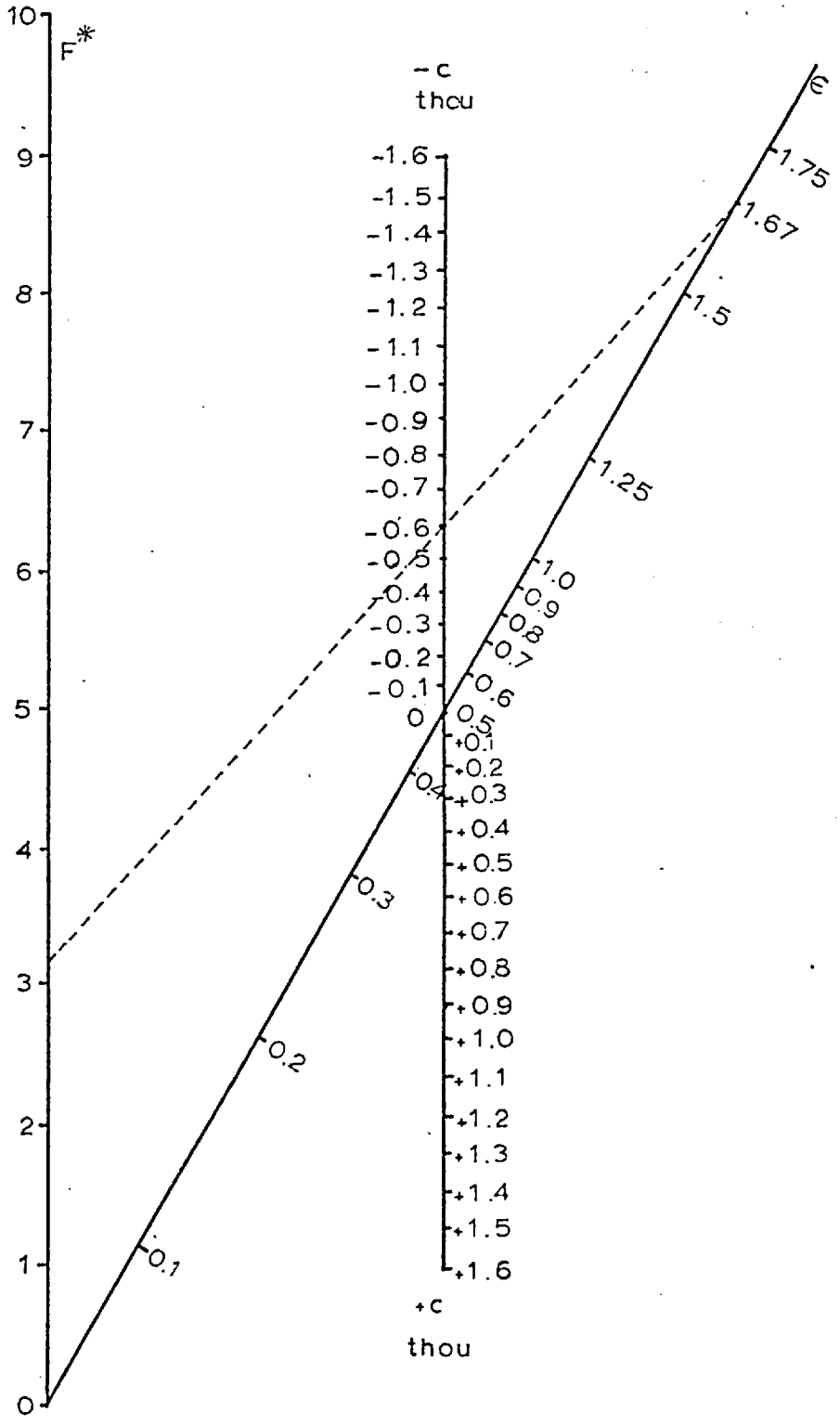
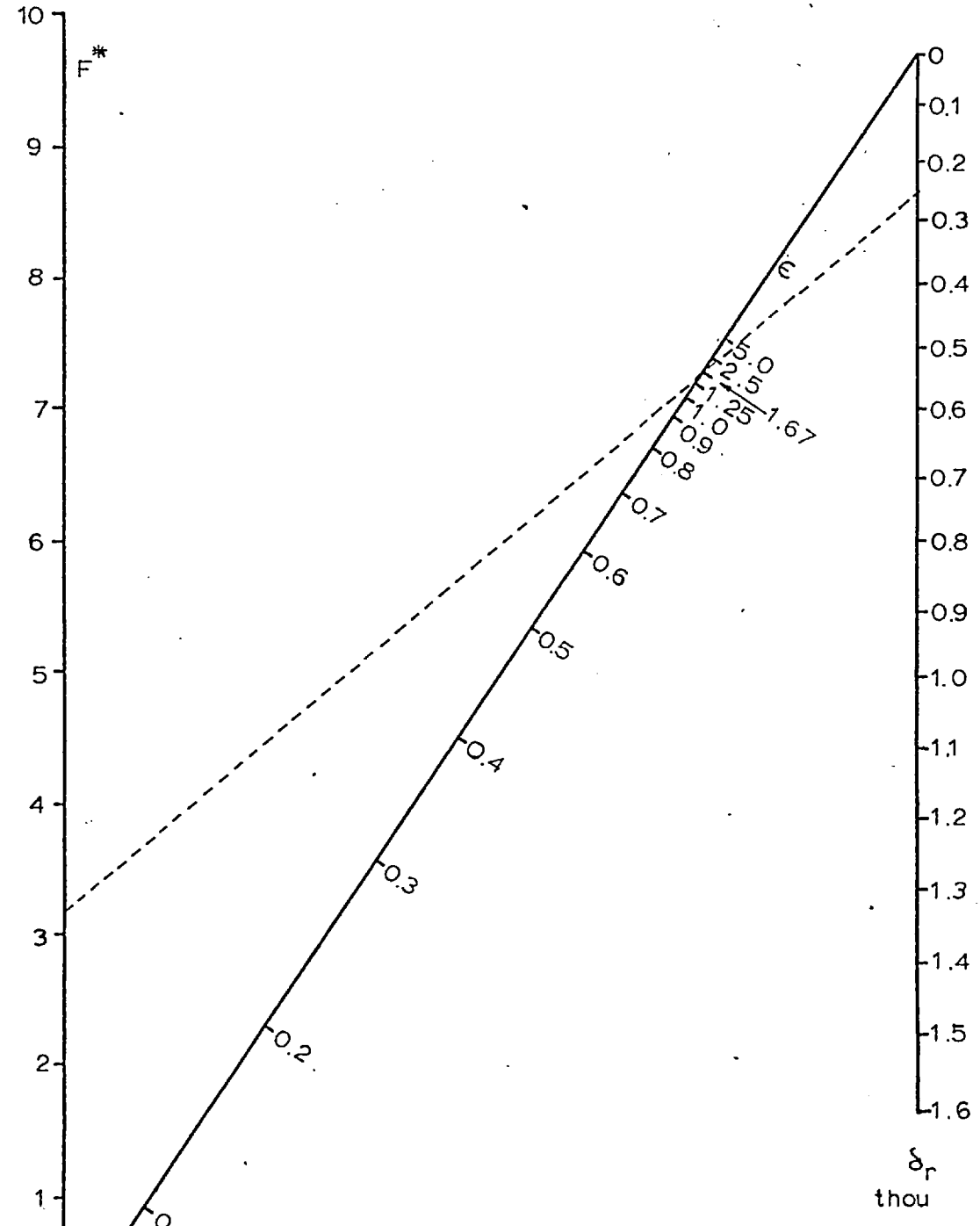


Fig. 3.25 Nomogram for determining the radial deflection δ_r of radial roller bearings with rigid races, from F^* (found from fig. 3.23) and the extent of loaded zone factor ϵ (found from fig. 3.24).



Note: δ_r is the radial deflection of a bearin- given by the deflection of the inner race from centered position in the outer race. For positive clearance bearings, to get the radi- deflection after the peak roller is loaded the radial clearance c is to be subtracted from δ_r obtained from the nomogram.

Fig. 3.26 Variation of load sharing factor S_f and $(P_1 Z/F_r)$ with the extent of loaded zone factor ϵ, of radial roller bearings with rigid races.

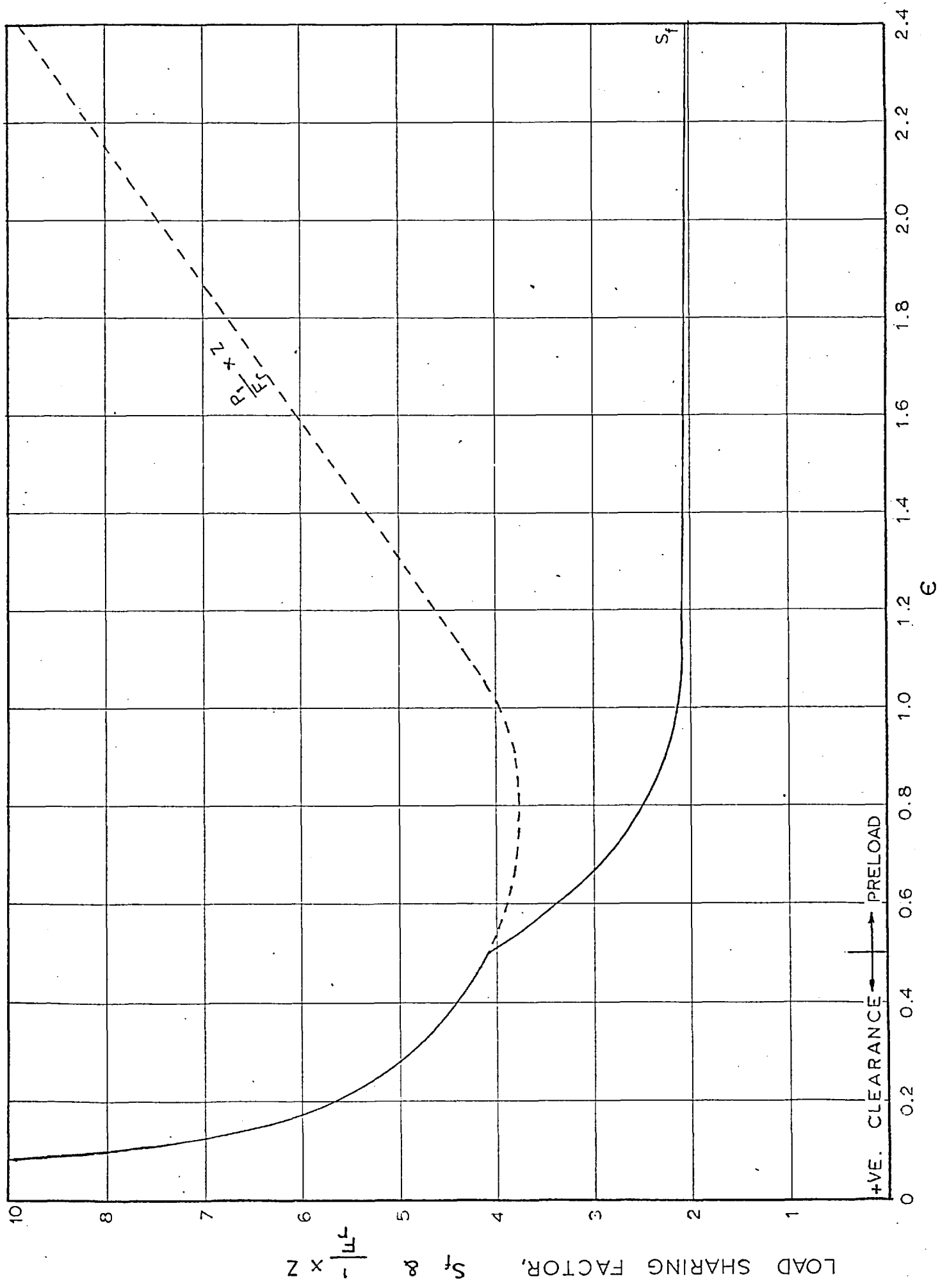
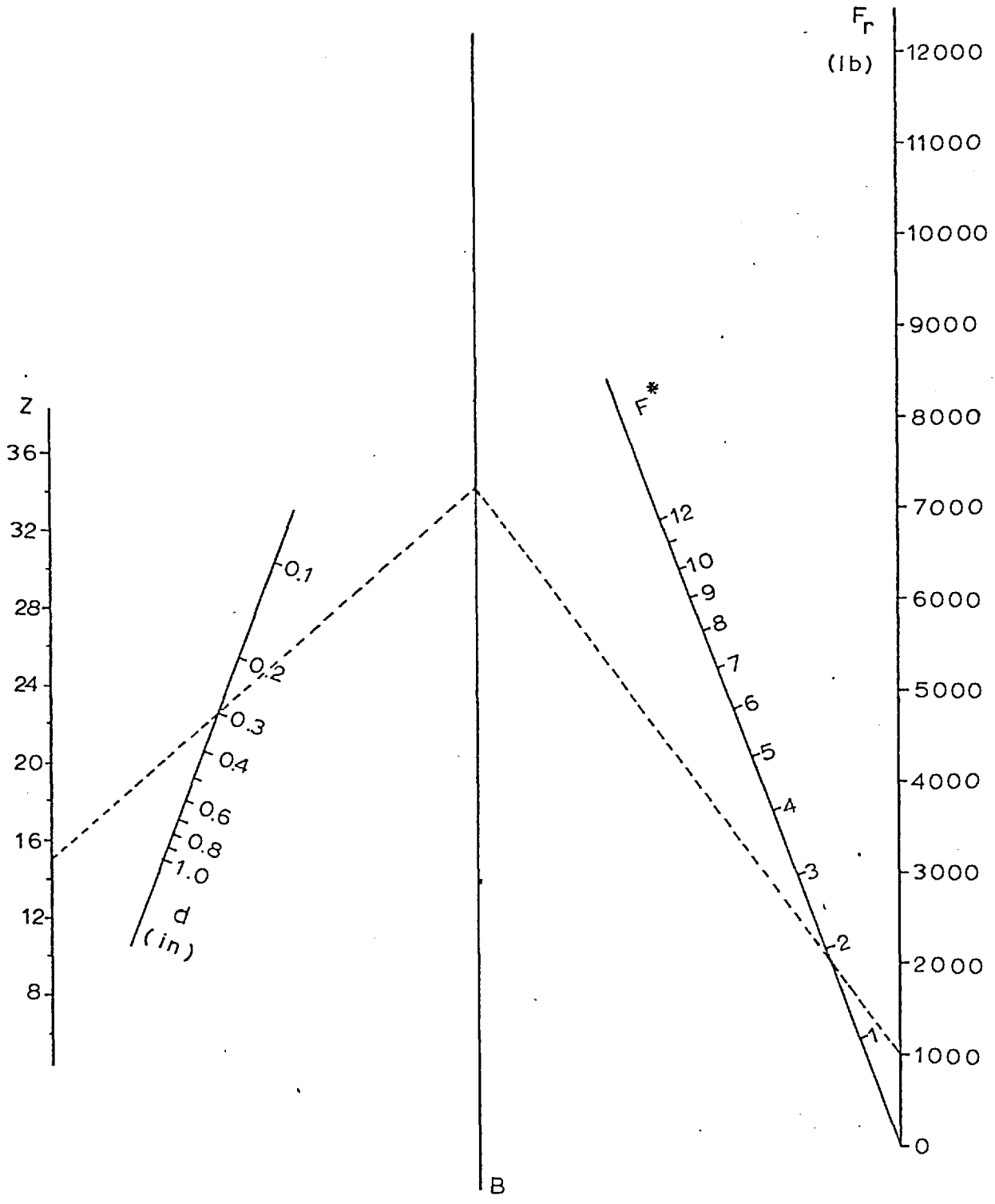


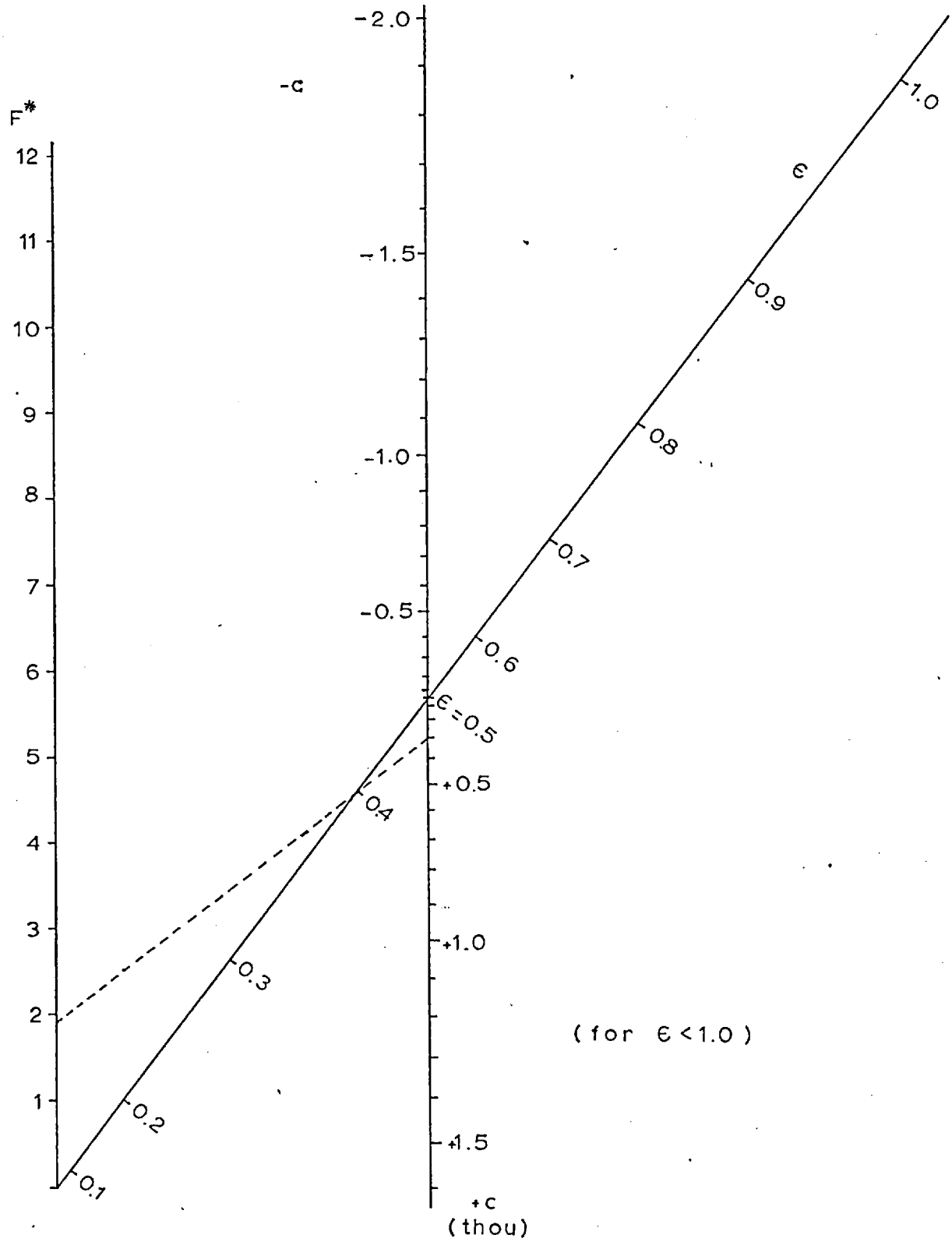
Fig. 3.27 Nomogram for determining F^* from Z, d and F_r for radial ball bearings with rigid races.

d is the diameter of ball.



For Ball Bearings

Fig. 3.28 Nomogram for determining the extent of loaded zone factor ϵ, from F^* (found from fig.3.27) and radial clearance c, of radial ball bearings with rigid races. For $\epsilon < 1.0$.



For Ball Bearings

Fig. 3.29 Nomogram for determining the extent of loaded zone factor ϵ, from F^* (found from fig.3.27) and radial clearance c, of radial ball bearings with rigid races. For $\epsilon > 1.0$.

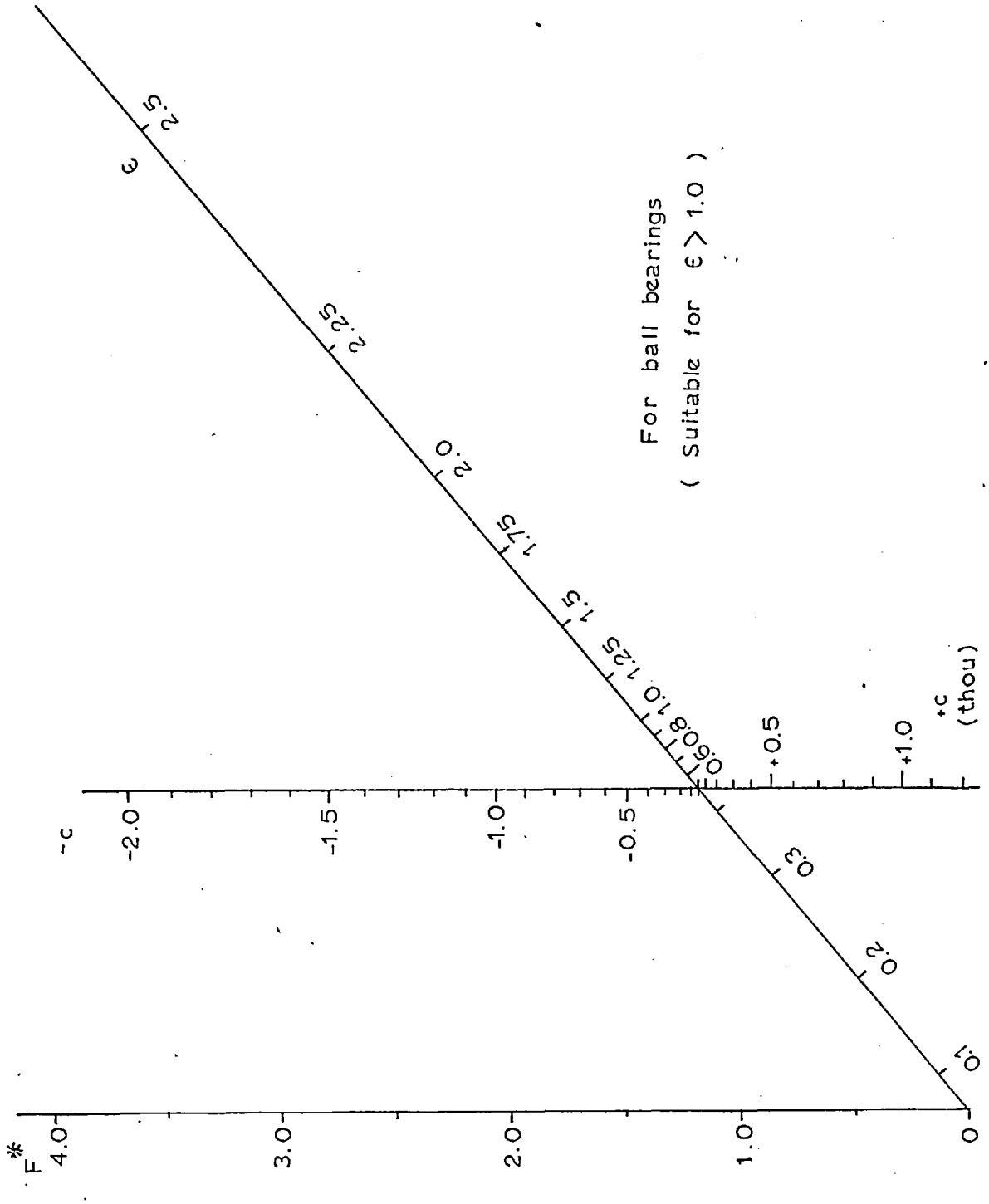
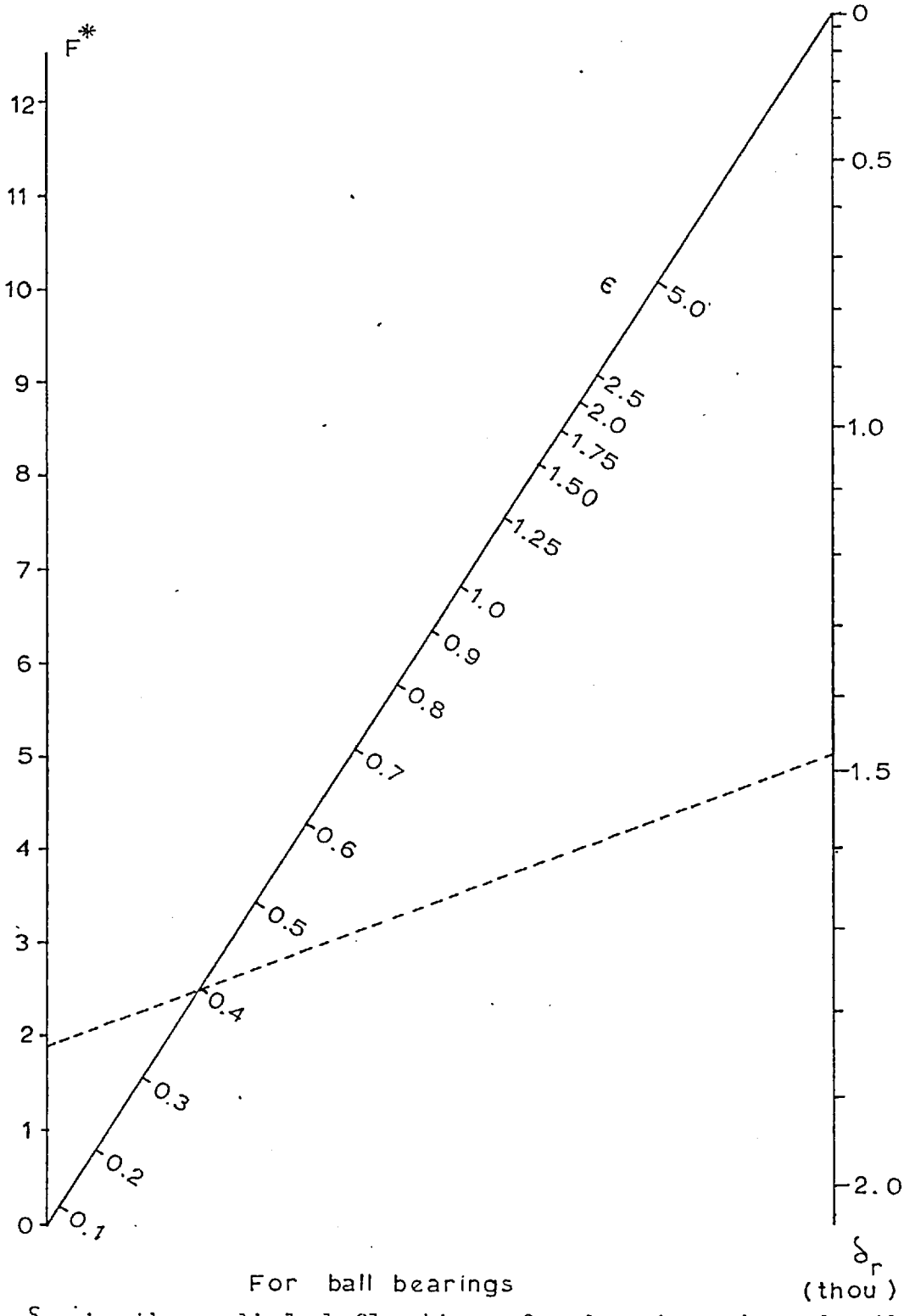
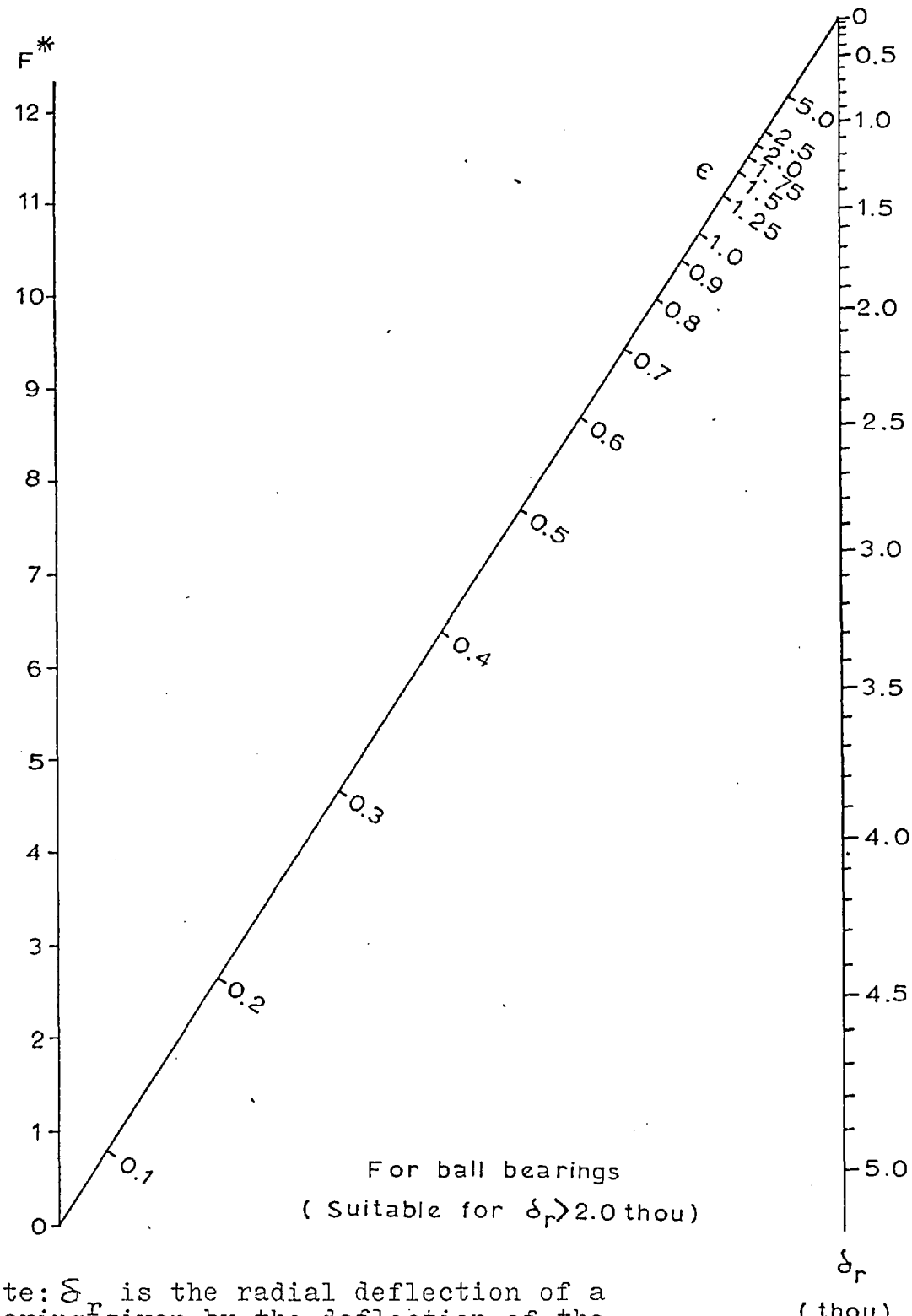


Fig. 3.30 Nomogram for determining the radial deflection δ_r, of radial ball bearings with rigid races from F^* (found from fig.3.27) and the extent of loaded zone factor ϵ, (found from fig.3.28 or 3.29). For $\delta_r < 2.0$ thou.



Note: δ_r is the radial deflection of a bearing given by the deflection of the inner race from centered position in the outer race. For positive clearance bearings, to get the radial deflection after the peak ball is loaded the radial clearance c is to be subtracted from δ_r obtained from the nomogram.

Fig. 3.31 Nomogram for determining the radial deflection δ_r, of radial ball bearings with rigid races from F^* (found from fig.3.27) and the extent of loaded zone factor ϵ, (found from fig.3.28 or 3.29). For $\delta_r > 2.0$ thou.



Note: δ_r is the radial deflection of a bearing given by the deflection of the inner race from centered position in the outer race. For positive clearance bearings, to get the radial deflection after the peak ball is loaded the radial clearance c is to be subtracted from δ_r obtained from the nomogram.

Fig. 3.32 Variation of load sharing factor S_f and $(P_1 Z/F_r)$ with the extent of loaded zone factor ϵ, for radial ball bearings with rigid races.

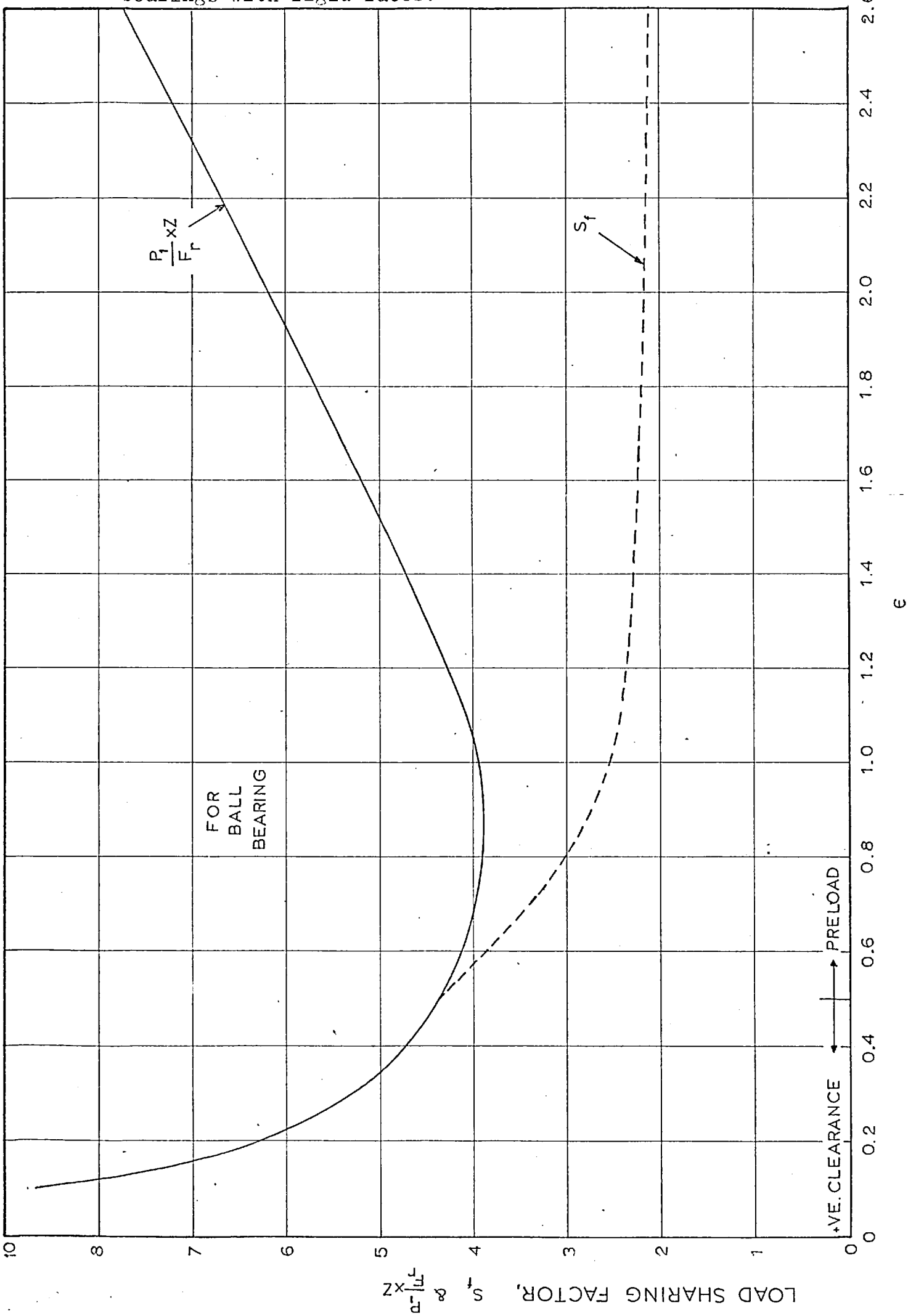


Fig. 4.1 Calibration specimens and gauge lengths.

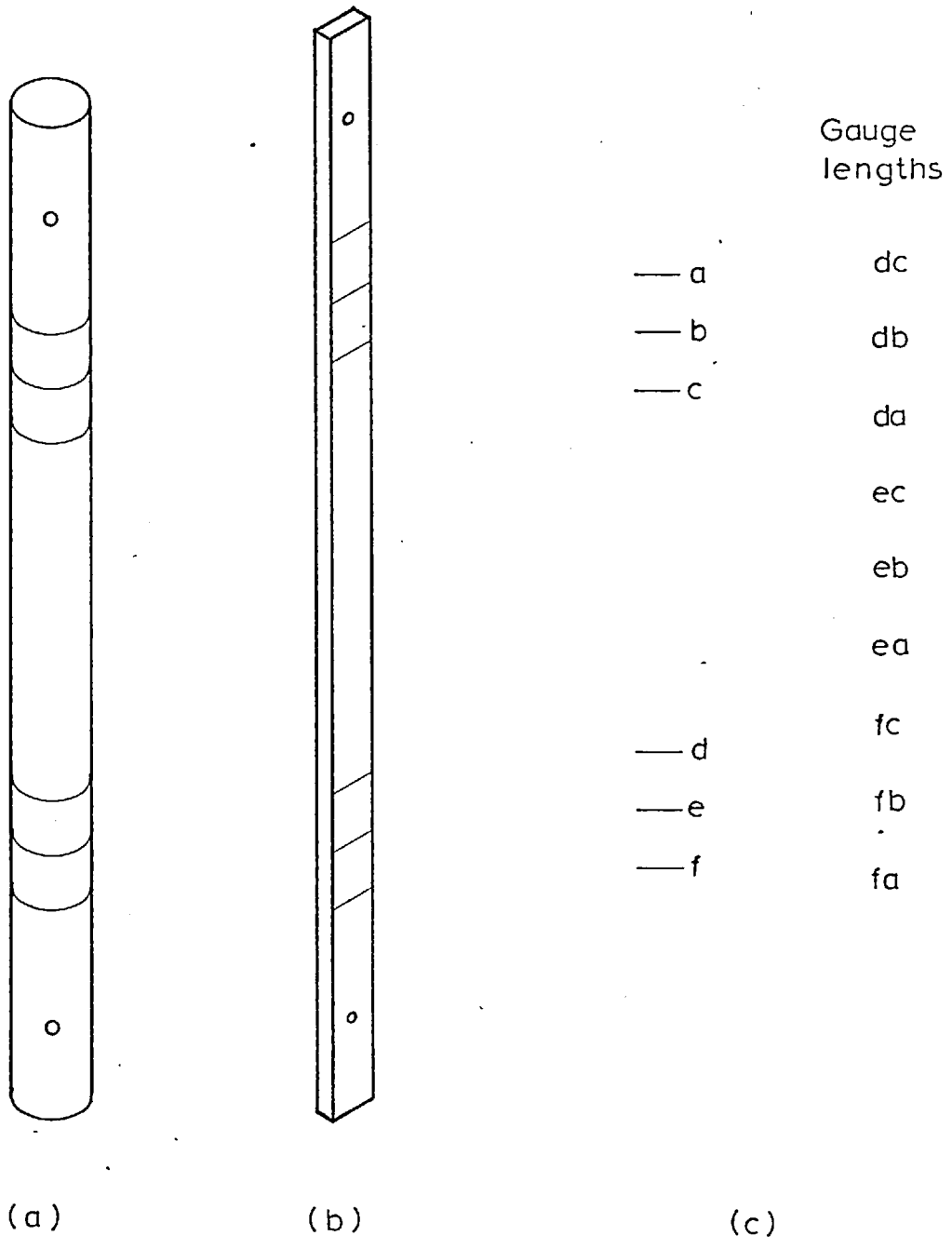


Fig. 4.2 A typical plot of elongation vs. gauge length to find the Young's modulus of the model material.

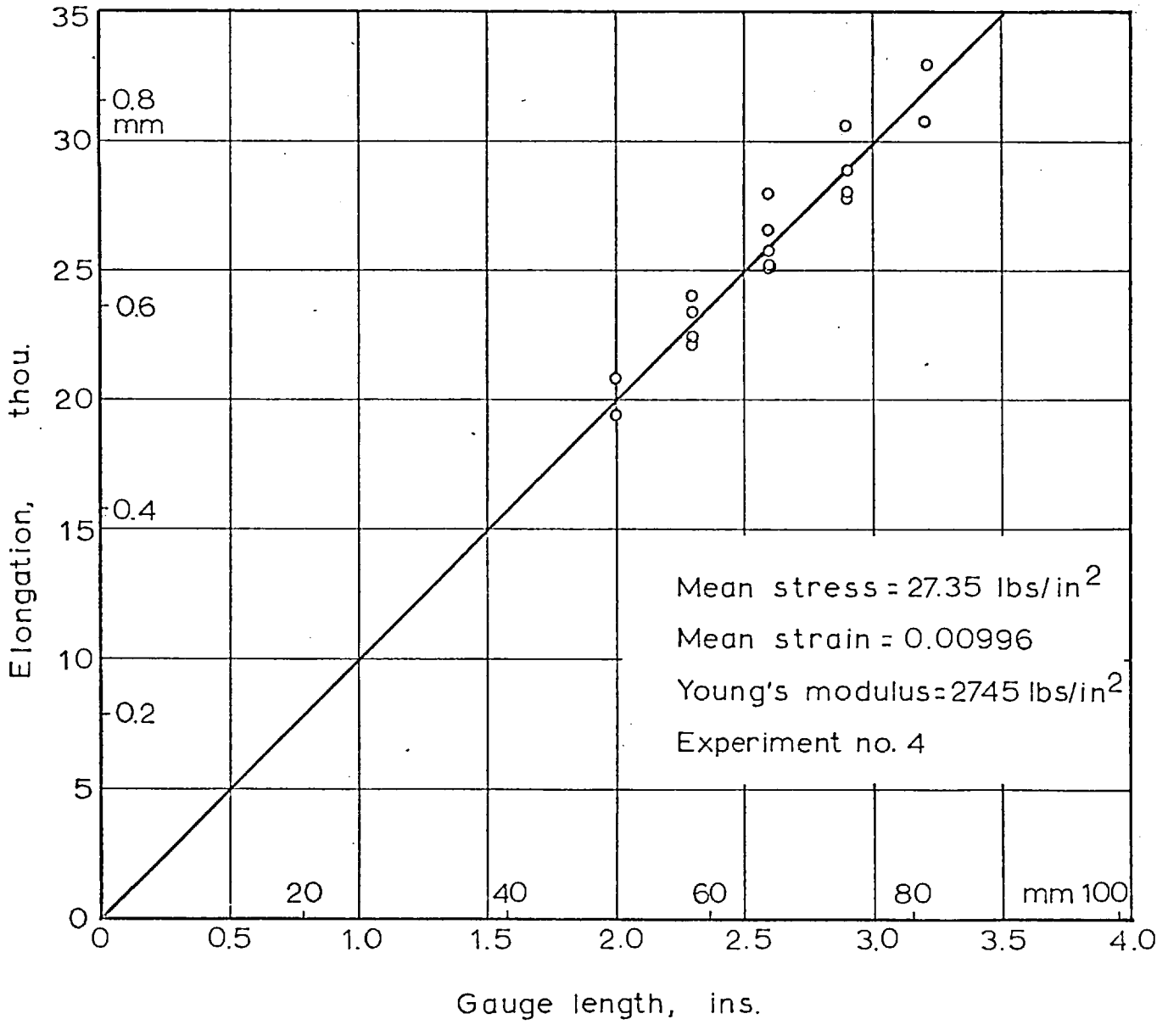


Fig. 4.3 Variation of Young's modulus of roller material with repeated heating. All roller and platen models were previously stabilised.

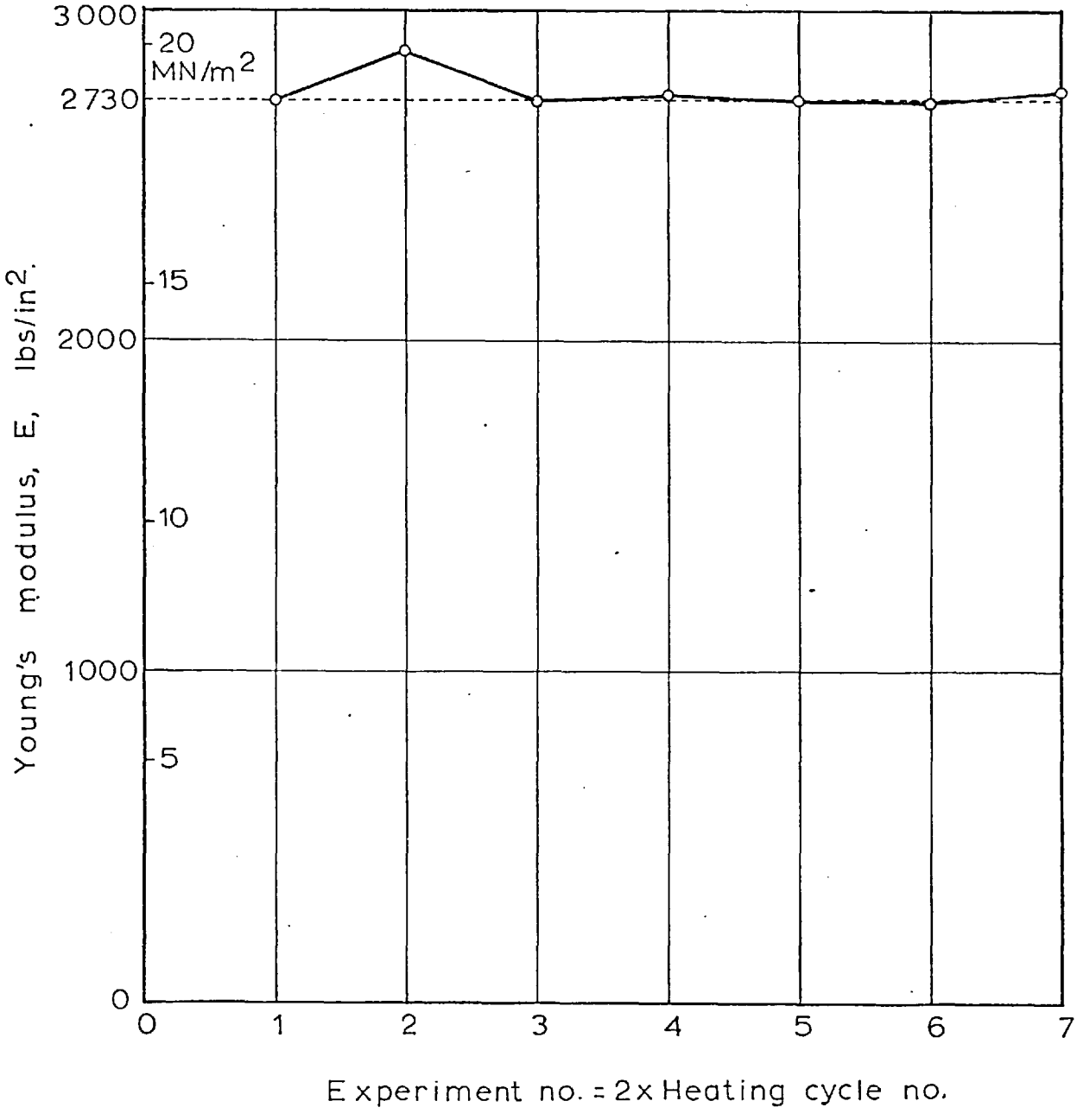
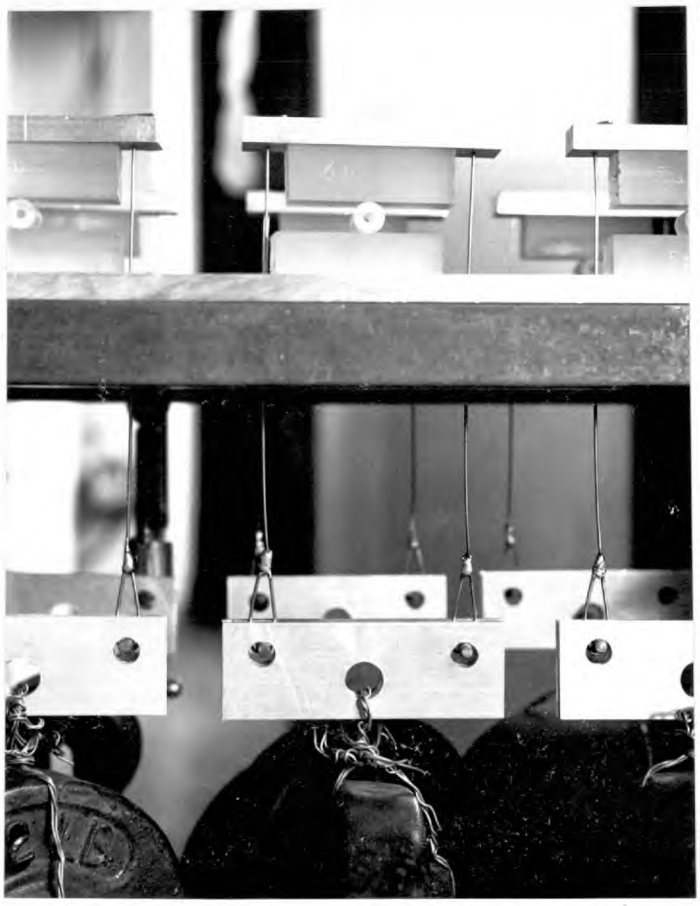
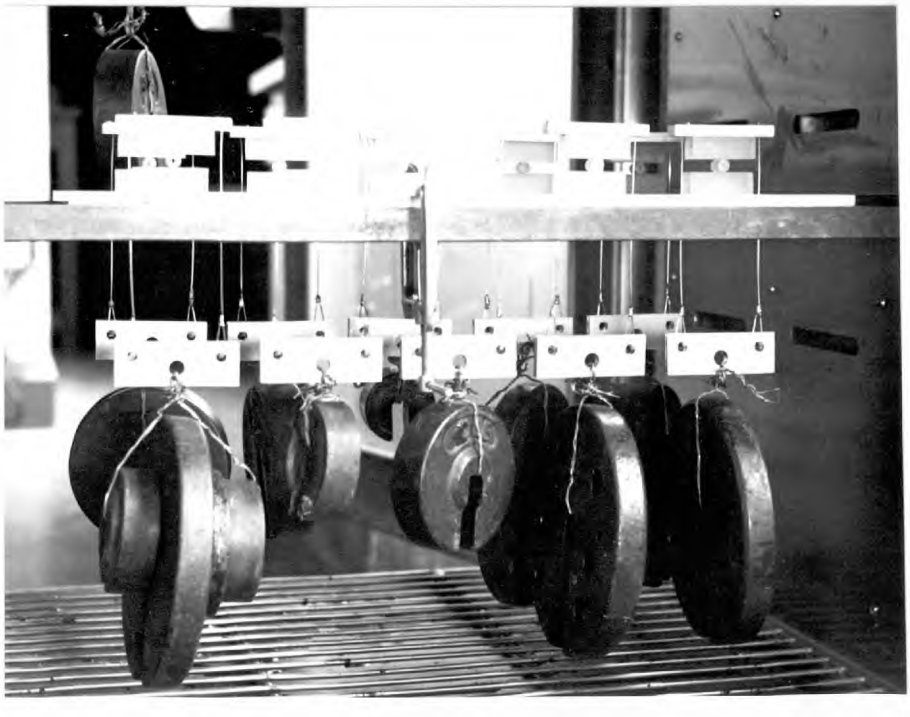


Fig. 4.4 Loading hollow Araldite rollers between Araldite platens.

Dimensions for the rollers and platens,
roller outside diameter= 0.3in. (7.62mm)
roller length=0.45in. (11.43mm)
inside diameter of hollow roller= 0.1in. (2.54mm)
thickness of platen= 0.545in. (13.84mm)
length of platen= about 1.75in. (44.5mm)
widths of platen= 0.616in. (15.65mm) and 0.45in. (11.43mm. i.e. equal to the length of roller)



(a)



(b)

Fig. 4.5 Experimental results for calibration of solid Araldite roller between Araldite platens. (Width of platen= 0.616 in. Thickness of platen= 0.545in.)

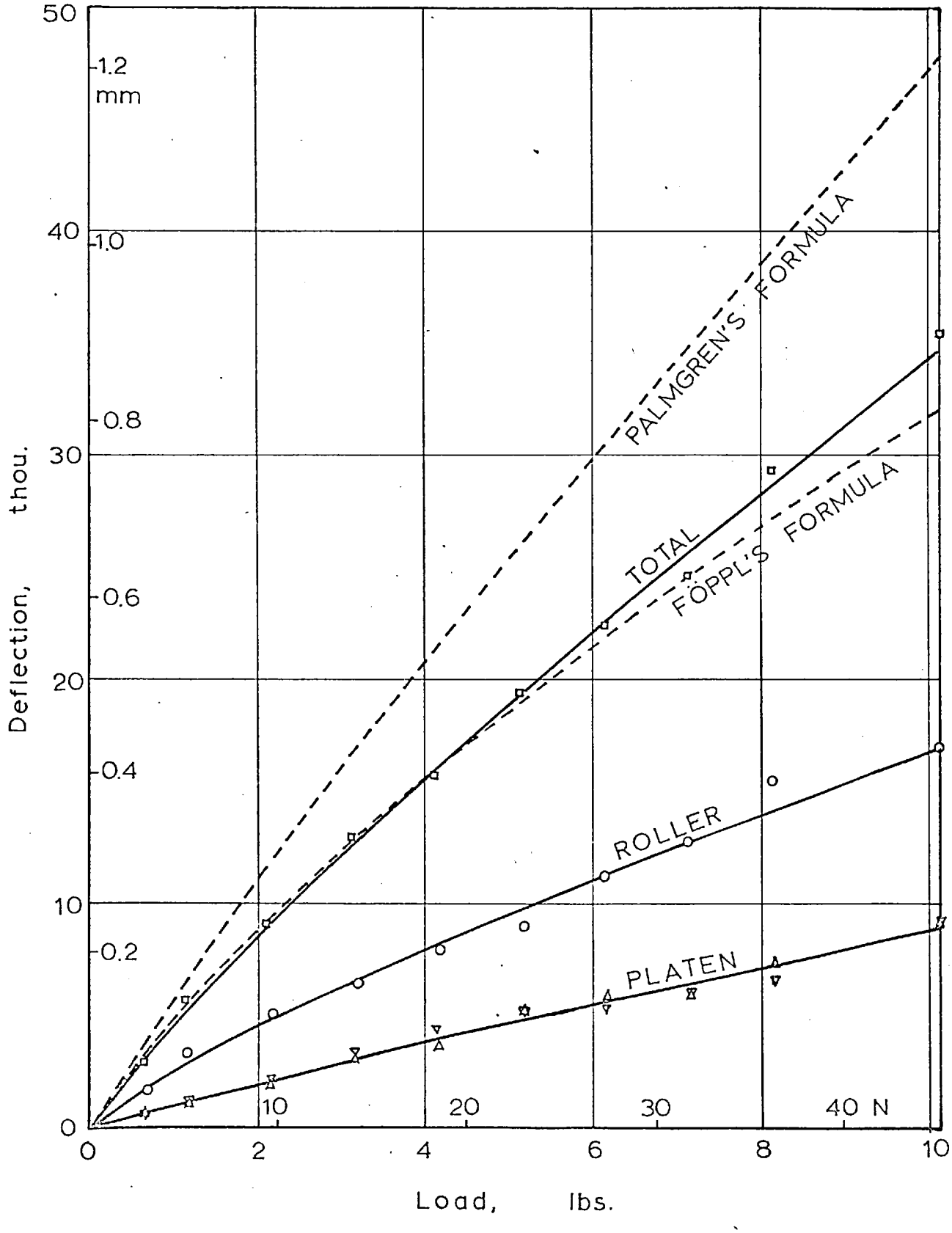


Fig. 4.6 Experimental results for width of contact area for solid Araldite roller loaded between Araldite platens.
(Width of platen= 0.616 in. Thickness of platen=0.545in.)

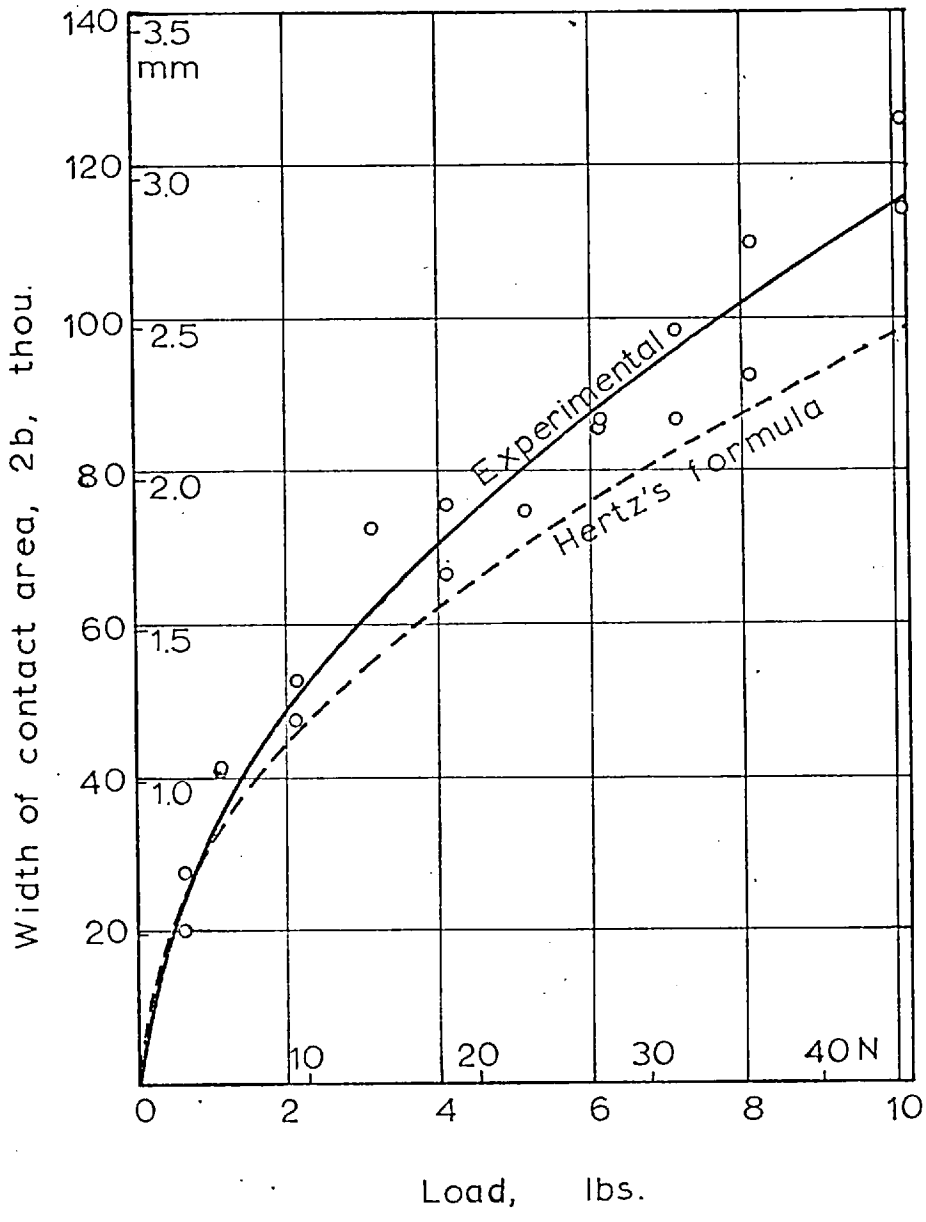


Fig. 4.7 Experimental results for calibration of hollow Araldite roller between Araldite platens.
(Width of platen= 0.616 in. Thickness of platen=0.545in.)

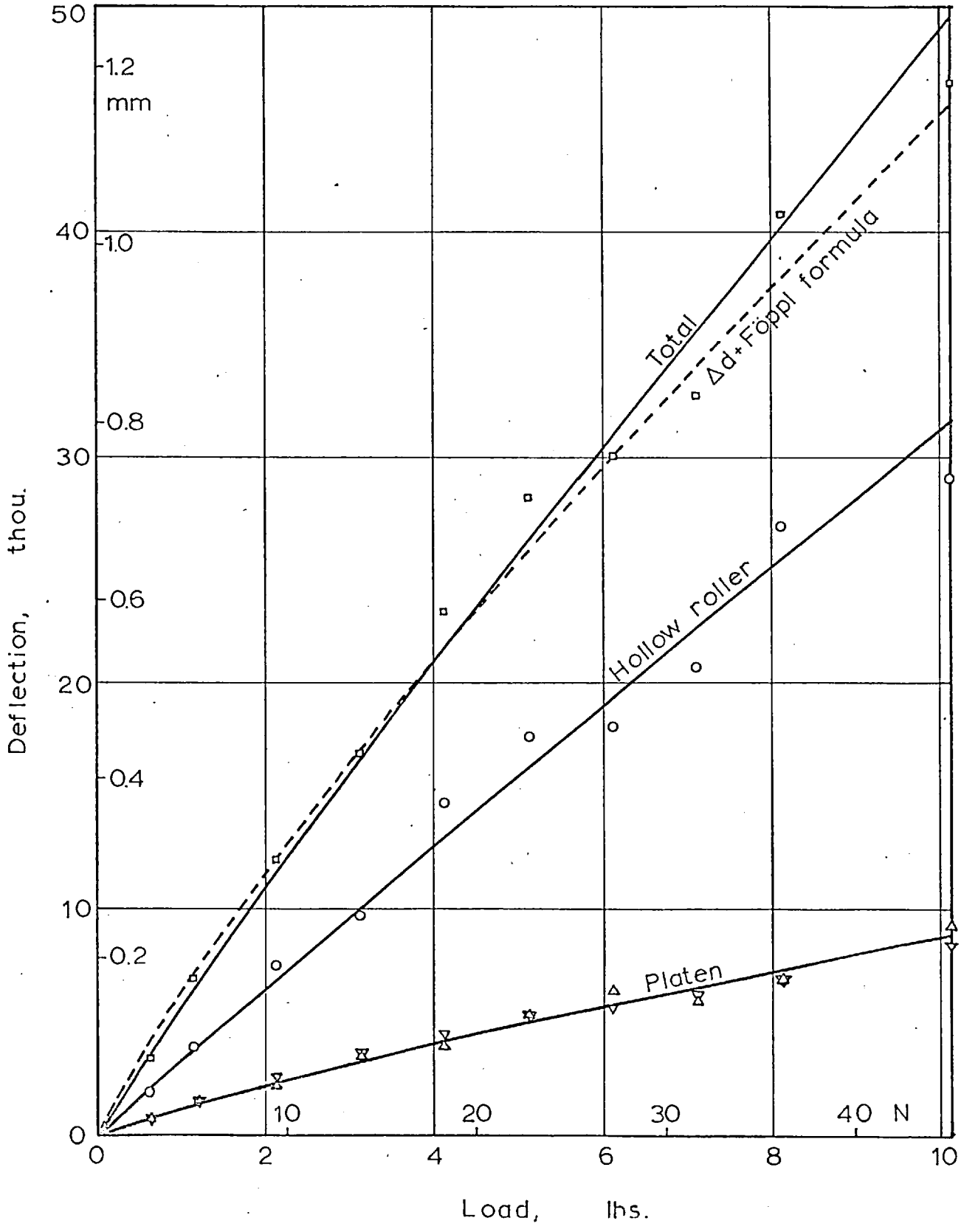


Fig. 4.8 Experimental results for width of contact area for hollow Araldite roller loaded between Araldite platens.
(Width of platen=0.616in. Thickness of platen=0.545in.)

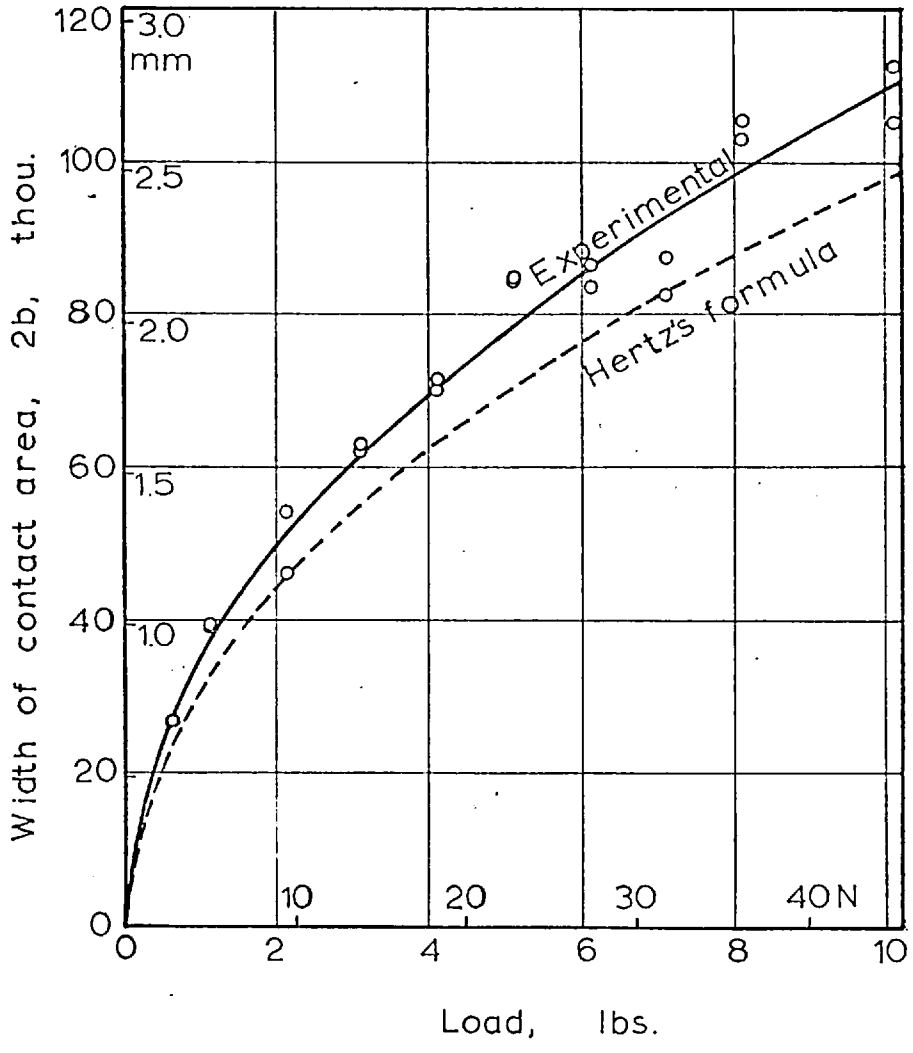


Fig. 4.9 Experimental results for calibration of solid Araldite roller between Araldite platens. (Width of platen=0.450in. Thickness of platen=0.545in.)

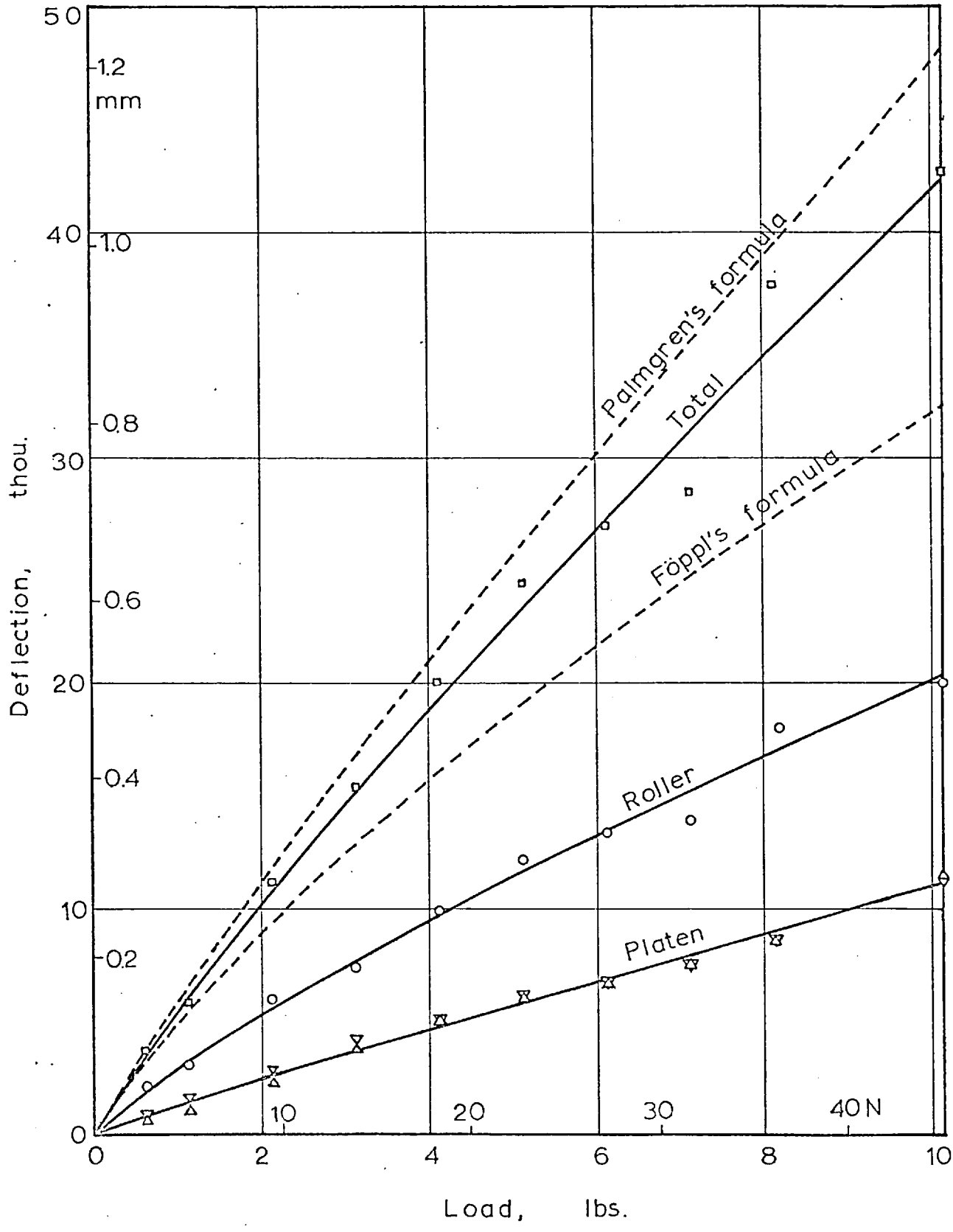


Fig. 4.10 Experimental results for width of contact area for solid Araldite roller loaded between Araldite platens.
(Width of platen=0.450in. Thickness of platen=0.545in.)

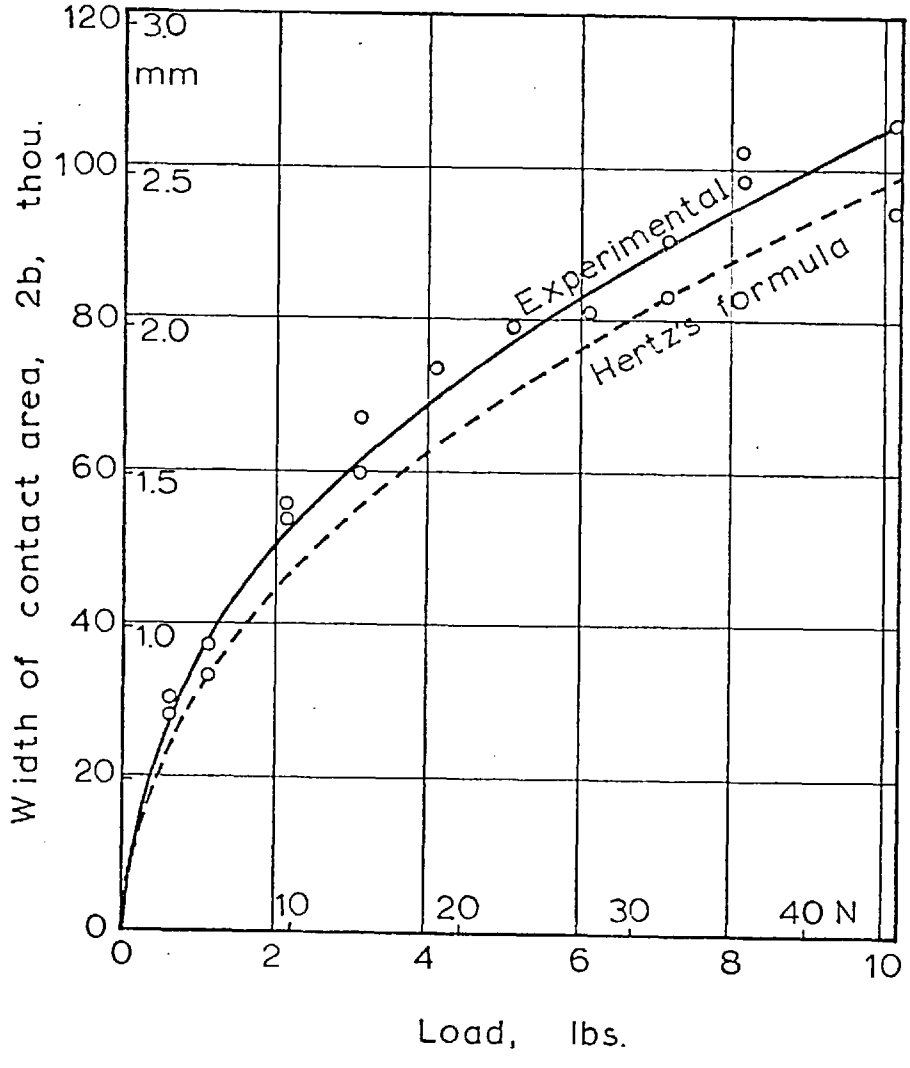


Fig. 4.11 Experimental results for calibration of hollow Araldite roller between Araldite platens. (Width of platen=0.45in. Thickness of platen=0.545in.)

Δd= compression of the diameter of the roller as a cylinder.

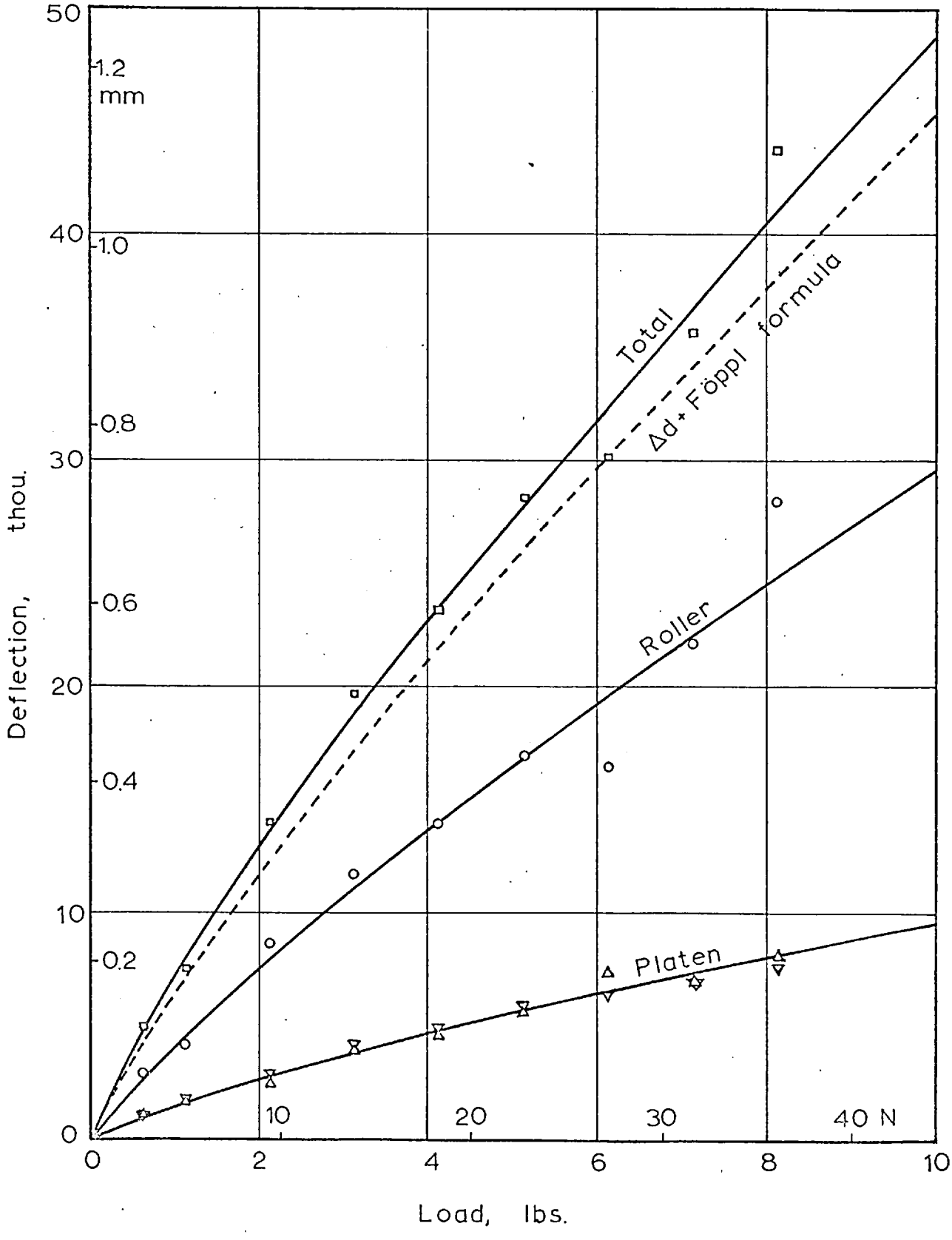


Fig. 4.12 Experimental results for width of contact area for hollow Araldite roller loaded between Araldite platens.
(Width of platen=0.450in. Thickness of platen=0.545in.)

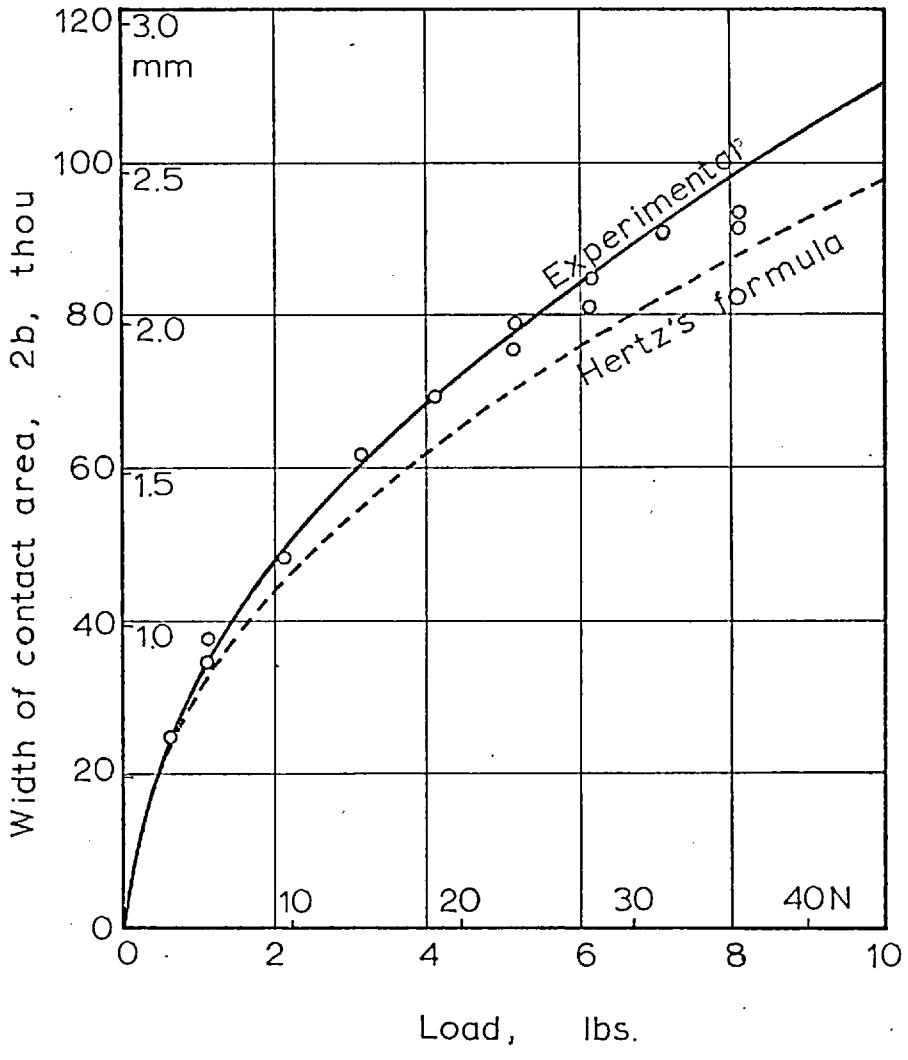


Fig. 4.13 Experimental results for calibration of solid Araldite roller between aluminium platens.

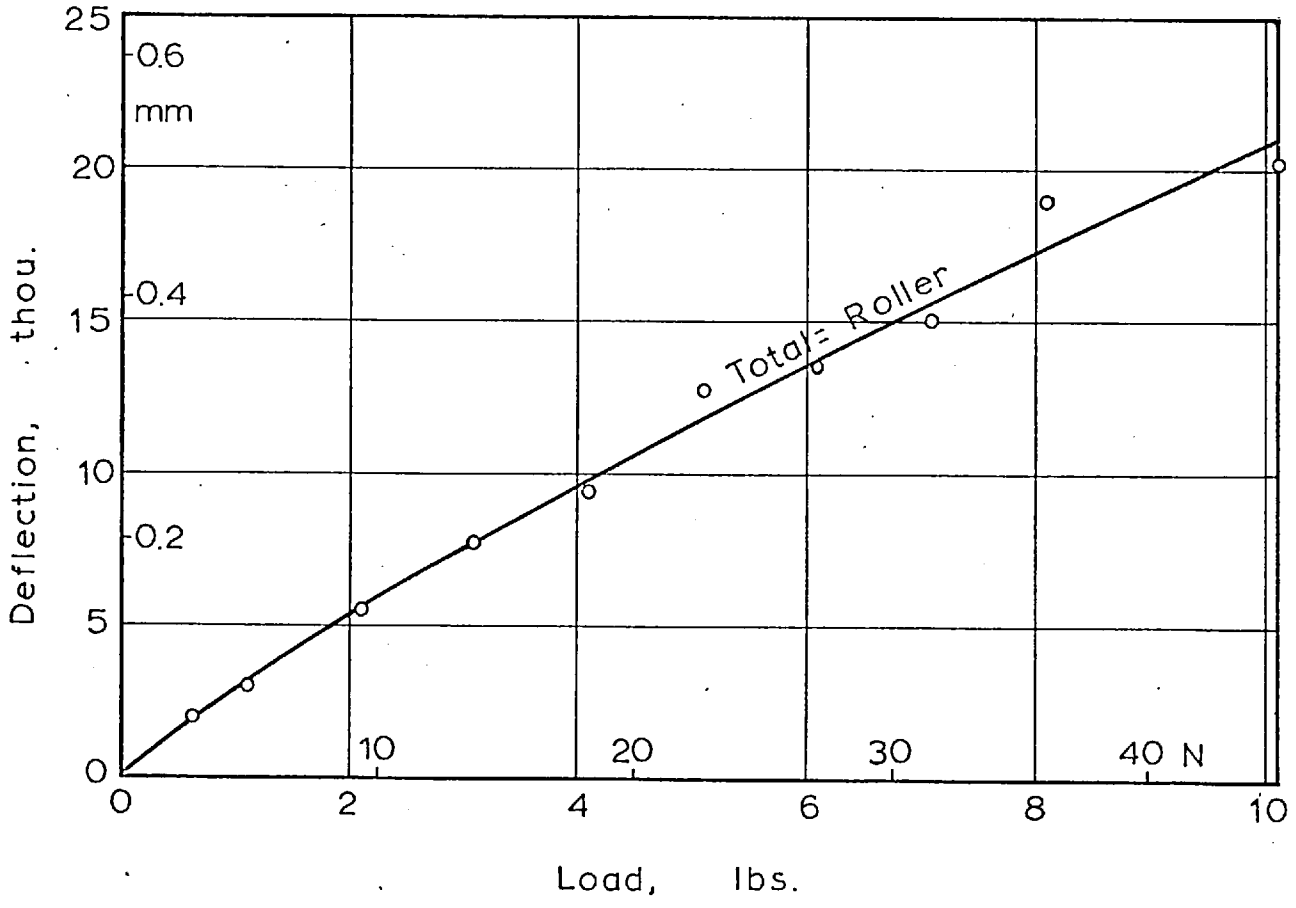


Fig. 4.14 Experimental results for calibration of hollow Araldite roller between aluminium platens.

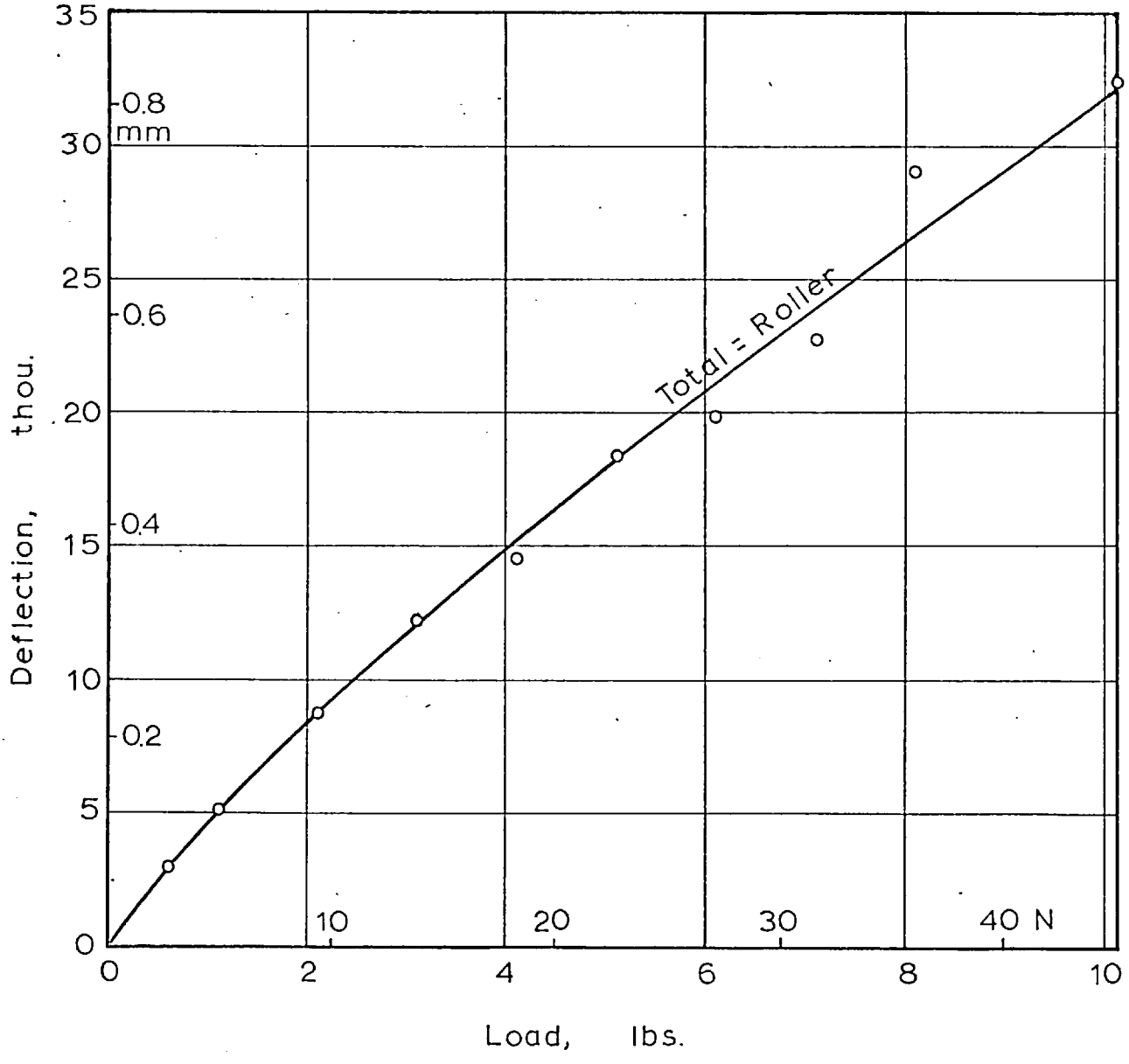


Fig. 4.15 Effect of edge loading of a roller loaded on platen wider than the length of the roller.

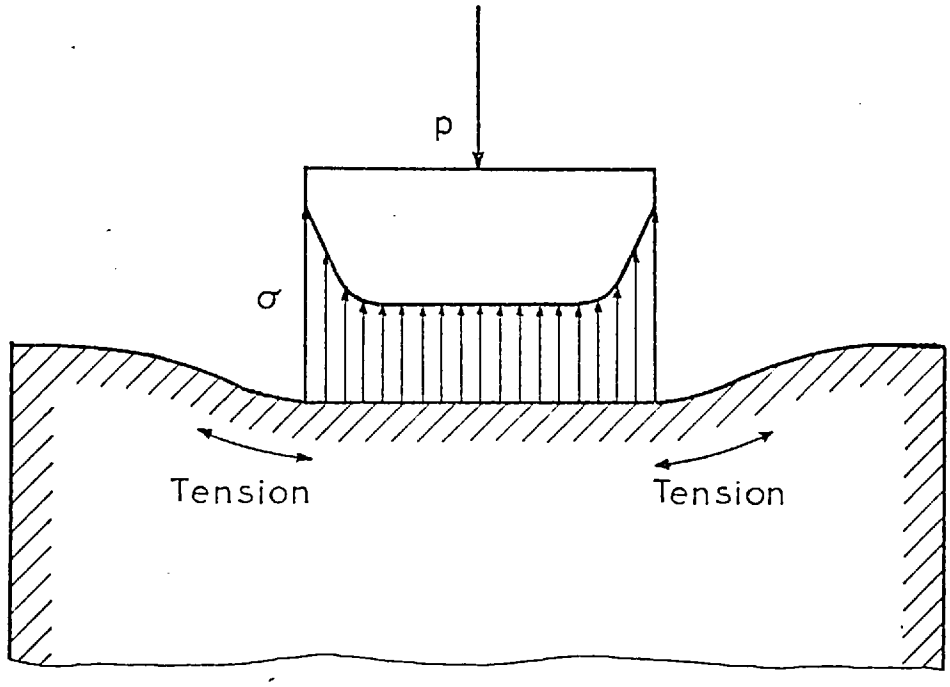


Fig. 4.16 Experimental set-up for loading the complete Araldite radial roller bearing model in a temperature controlled oven.

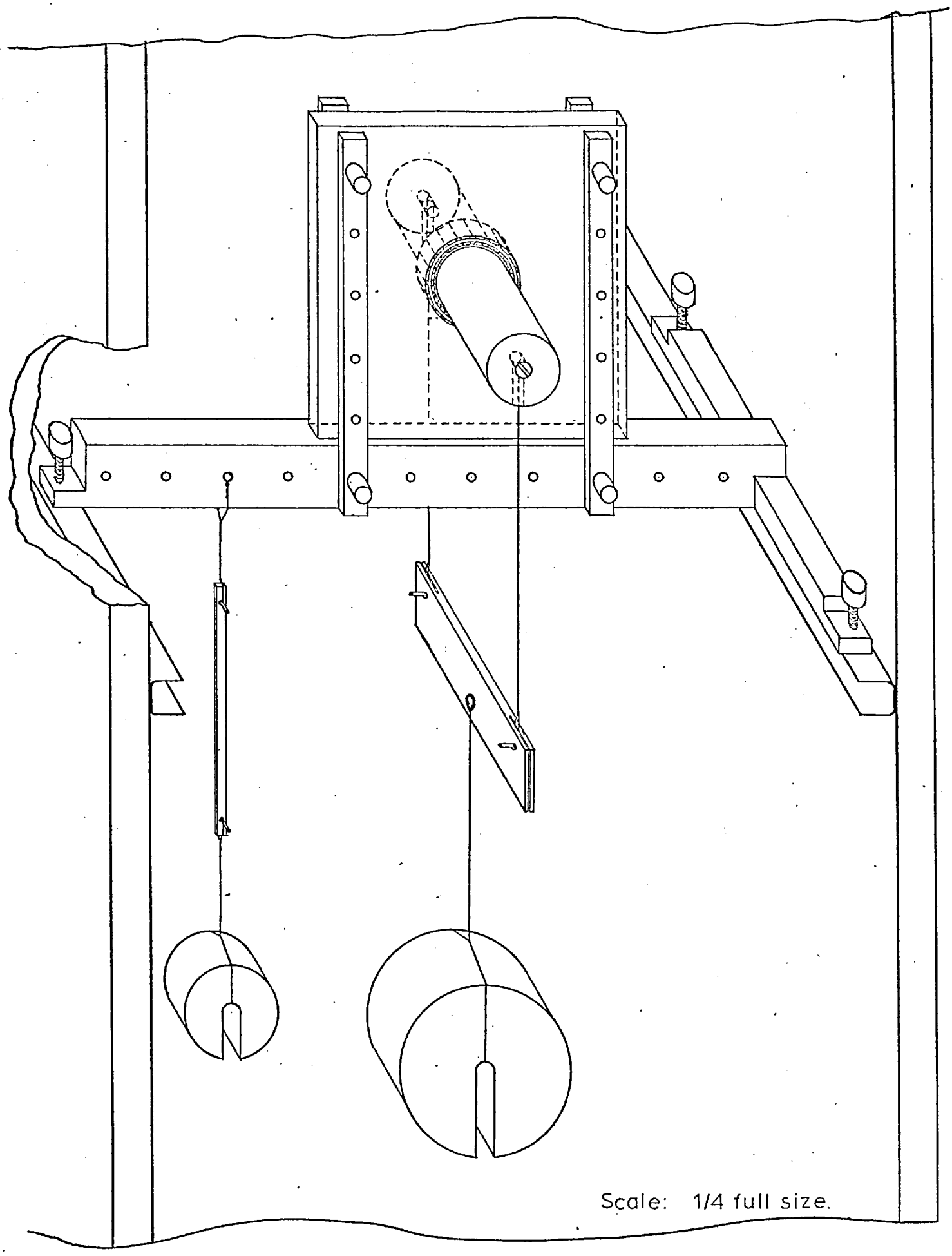
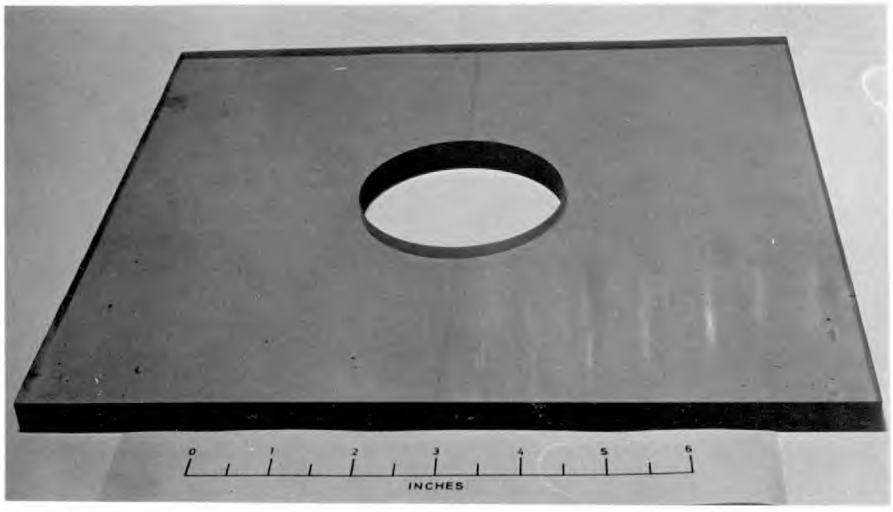
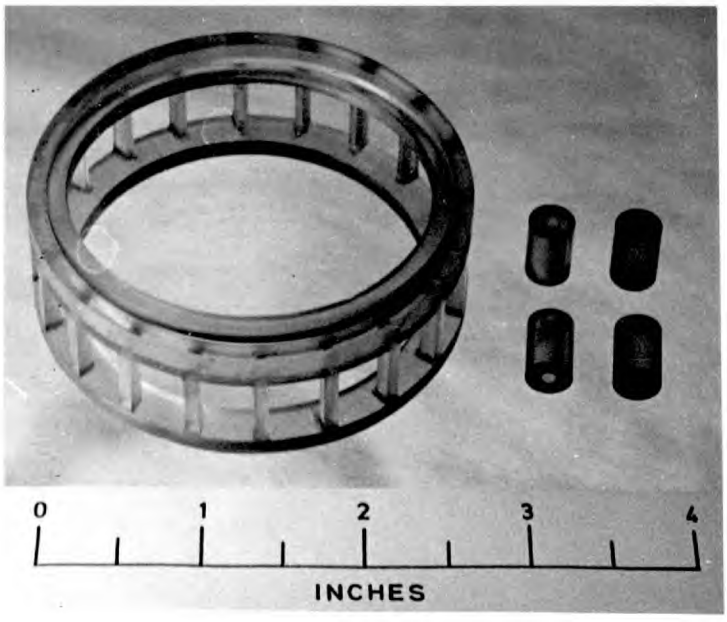


Fig. 4.17 (a) The integral outer race and housing.
(b) The cage and rollers.
(c) The assembly of rollers and cage on the inner race.



(a)



(b)



(c)

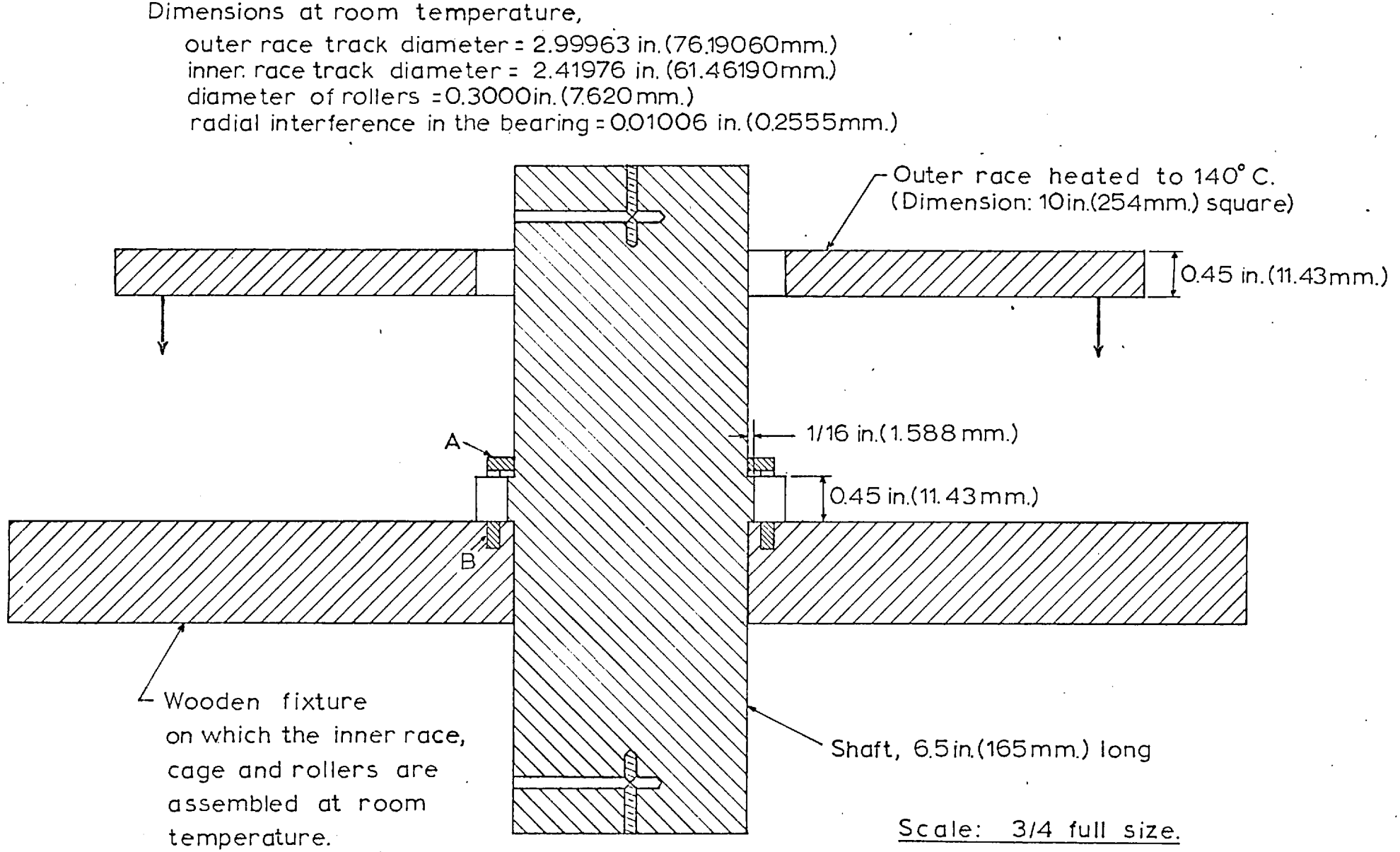
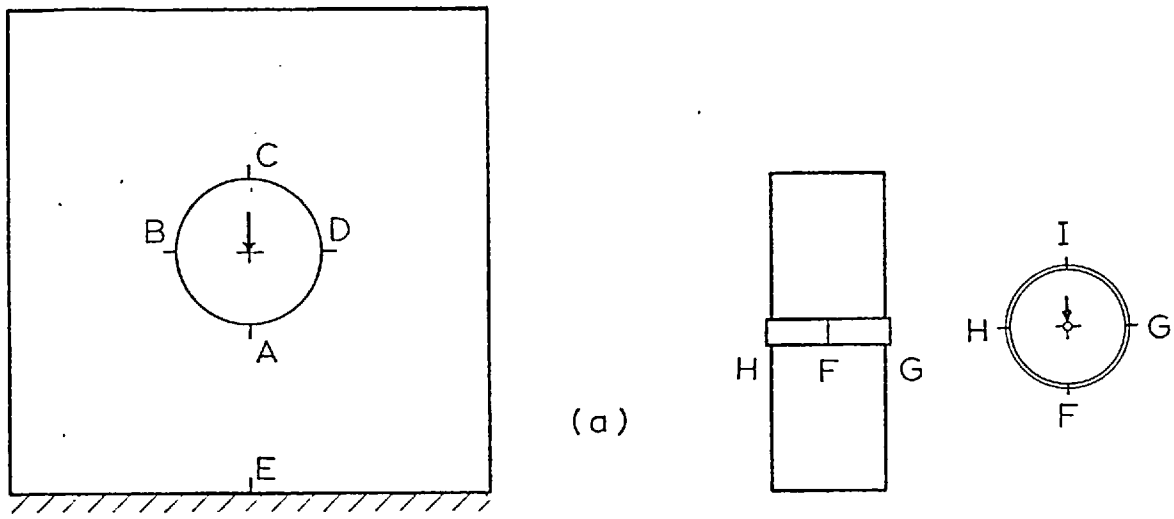
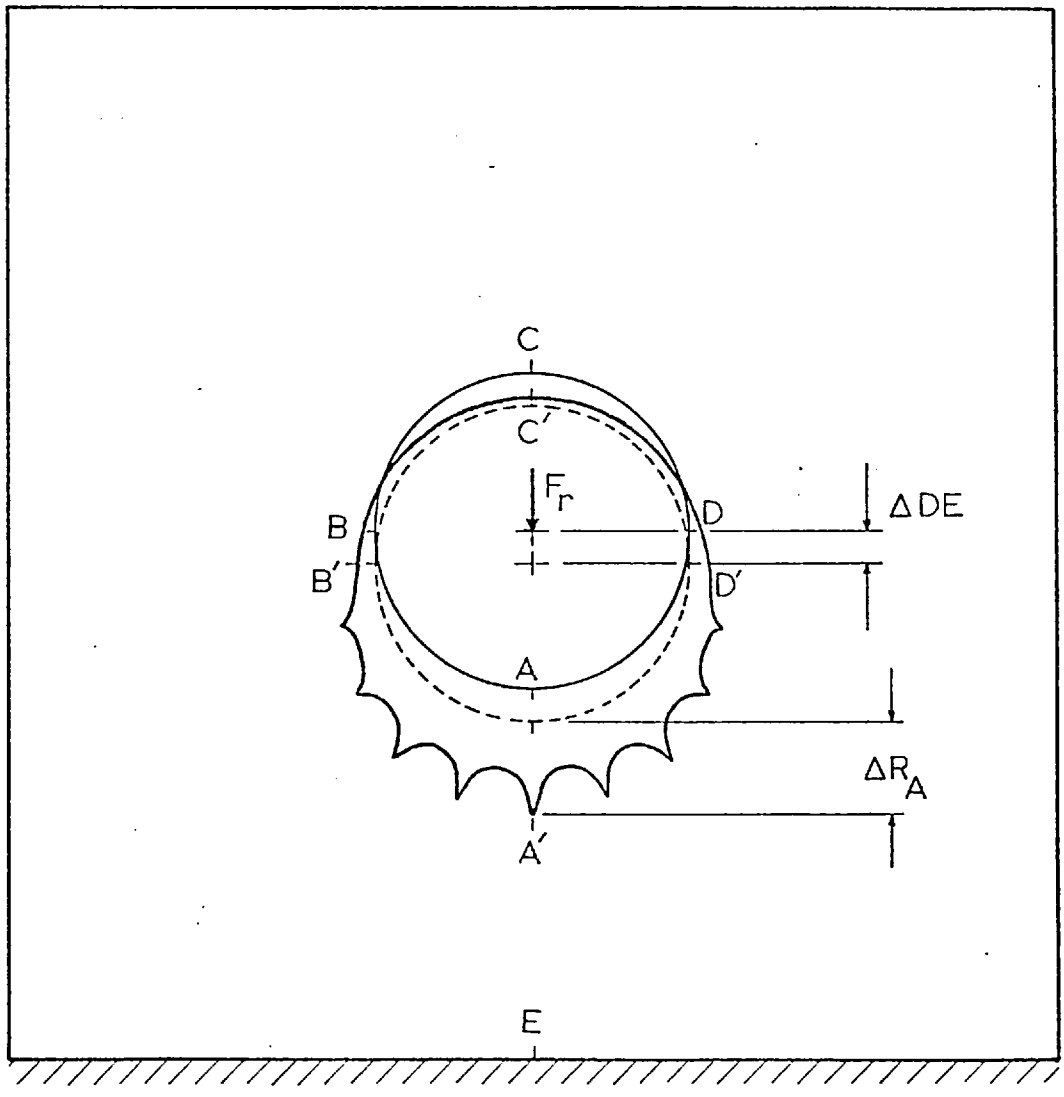


Fig. 4.18 Method of obtaining preload in the Araldite radial roller bearing model.

Fig. 4.19 (a) Markings on the outer and inner races for measurement of deflection of the bearing.
(b) Components of the outer race deflection.





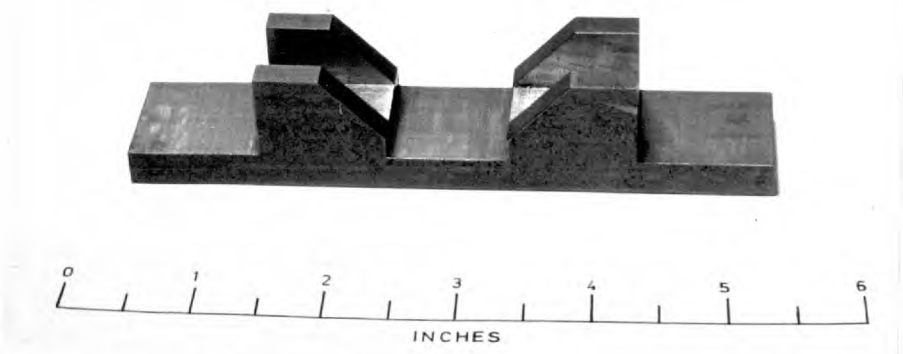
(b) Total deflection of outer race =

$$\delta_A = \delta_D + \delta_{A/D}$$

$$= \Delta DE + \Delta R_A$$

Fig. 4.20 (a) V-block to hold the inner race on the Universal Measuring Machine.

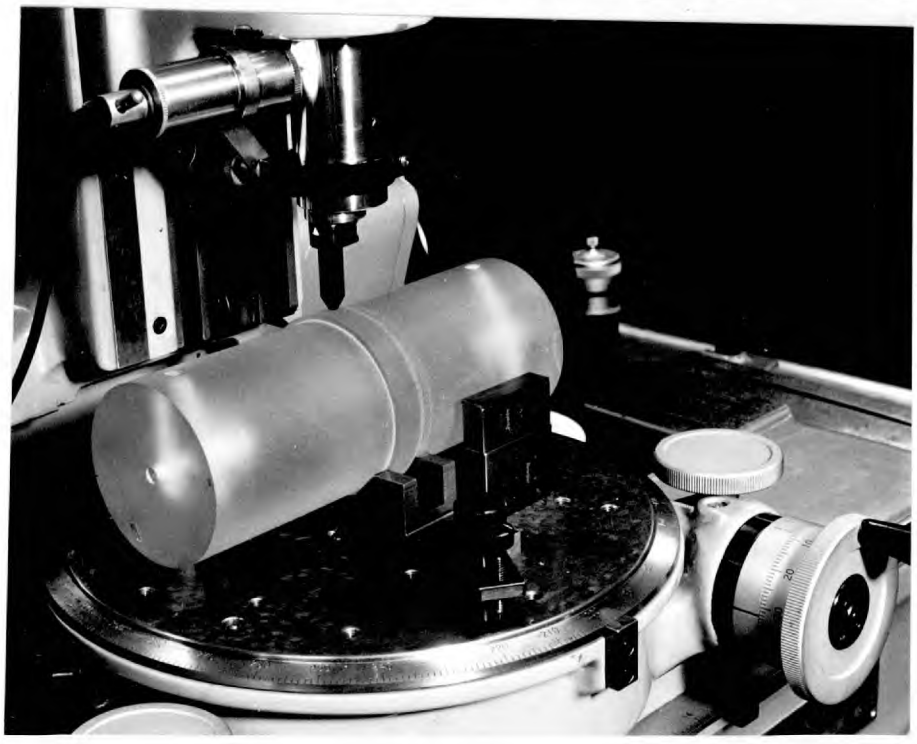
(b) and (c) Procedure of measurement of radius of inner race to find its deflection.



(a)



(b)



(c)

Fig. 4.21 Fixture to hold the bent shaft on the Talyrond table so that, the axis of the inner race track is perpendicular to the table top-surface.

Scale: Full size.

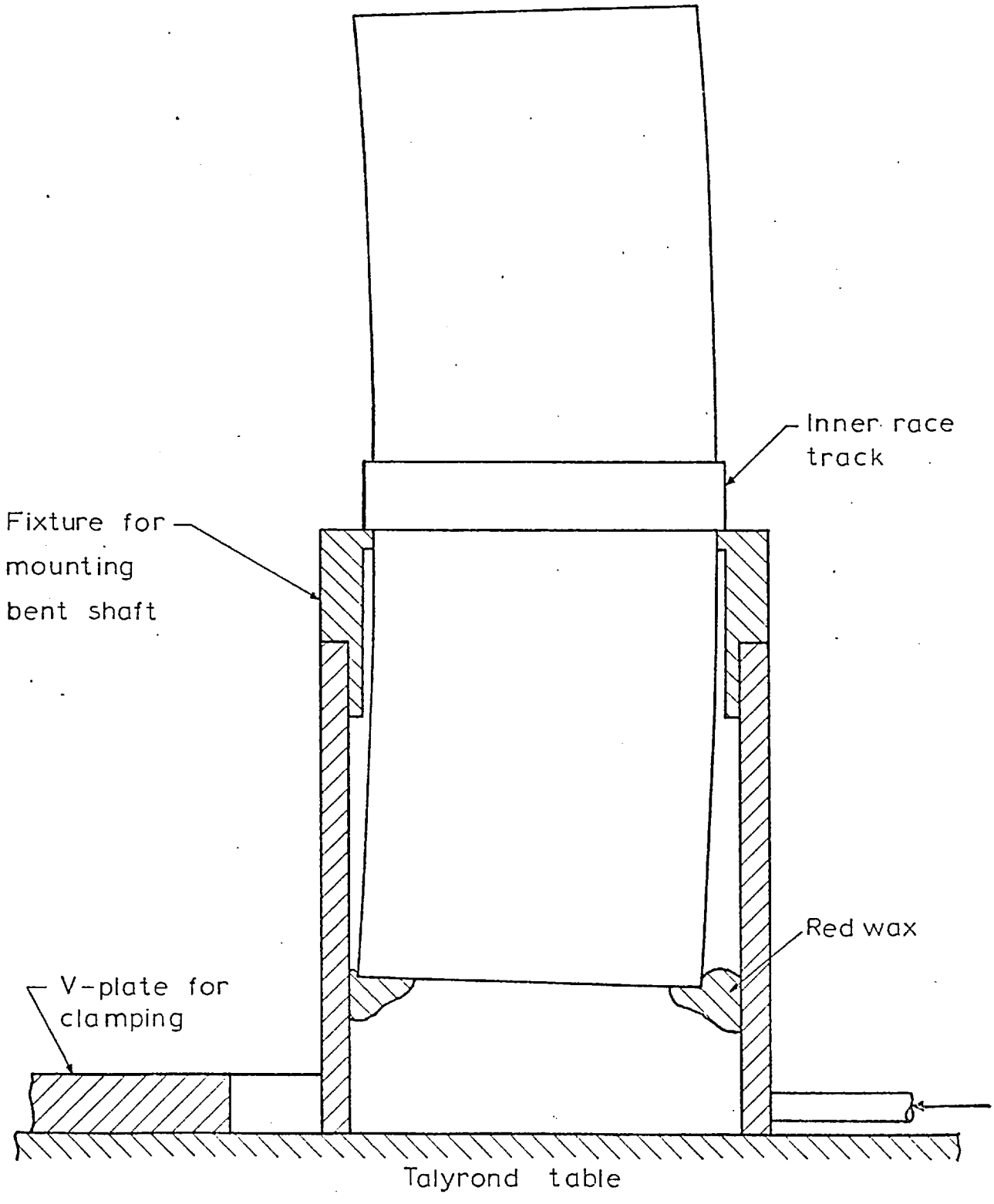


Fig. 4.22 Roller load distribution, as obtained by experiment, in an Araldite radial roller bearing having radial clearance c= -0.010 in., radial load F_r=9.5 lbs. and number of (solid) rollers Z=20.

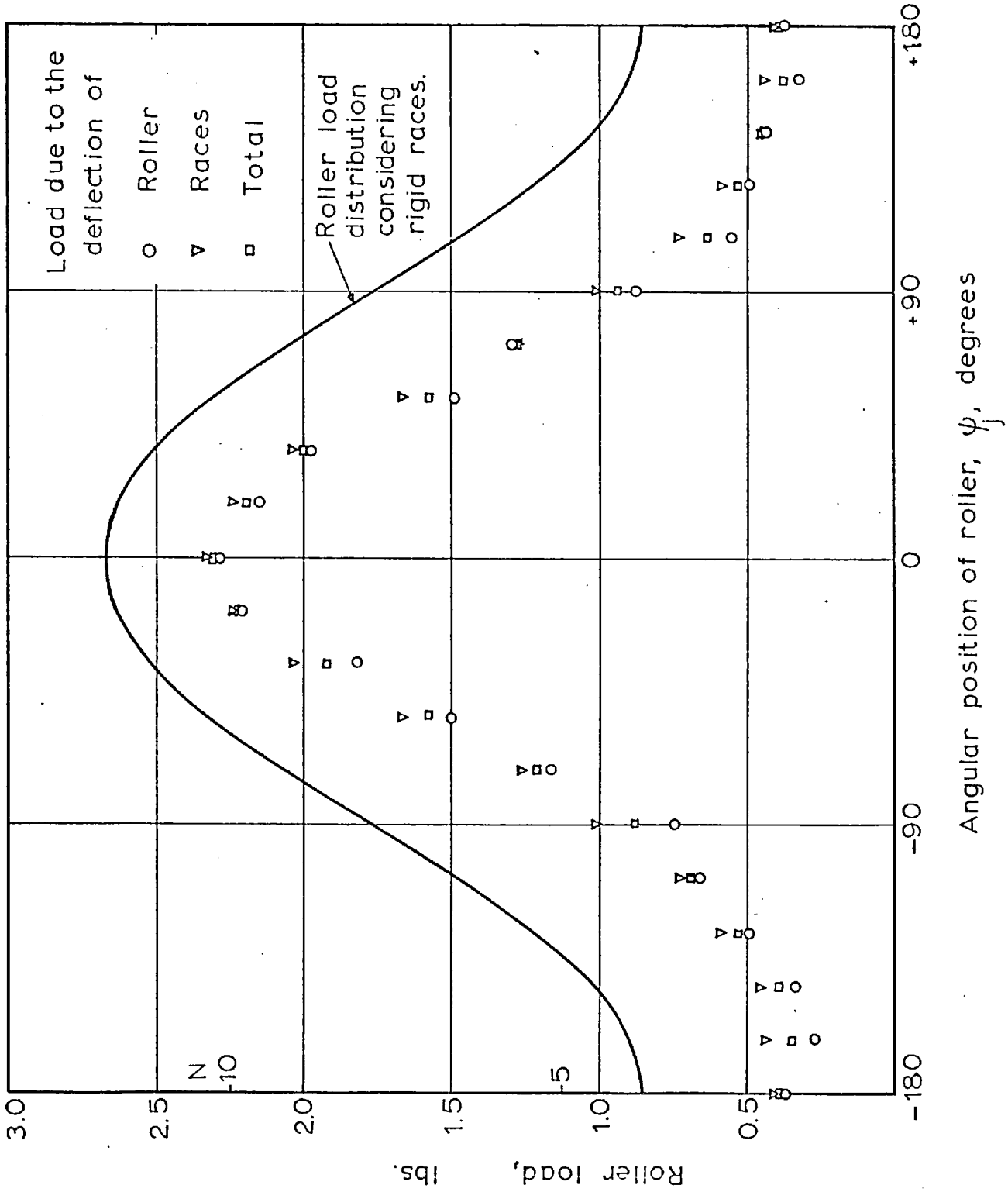
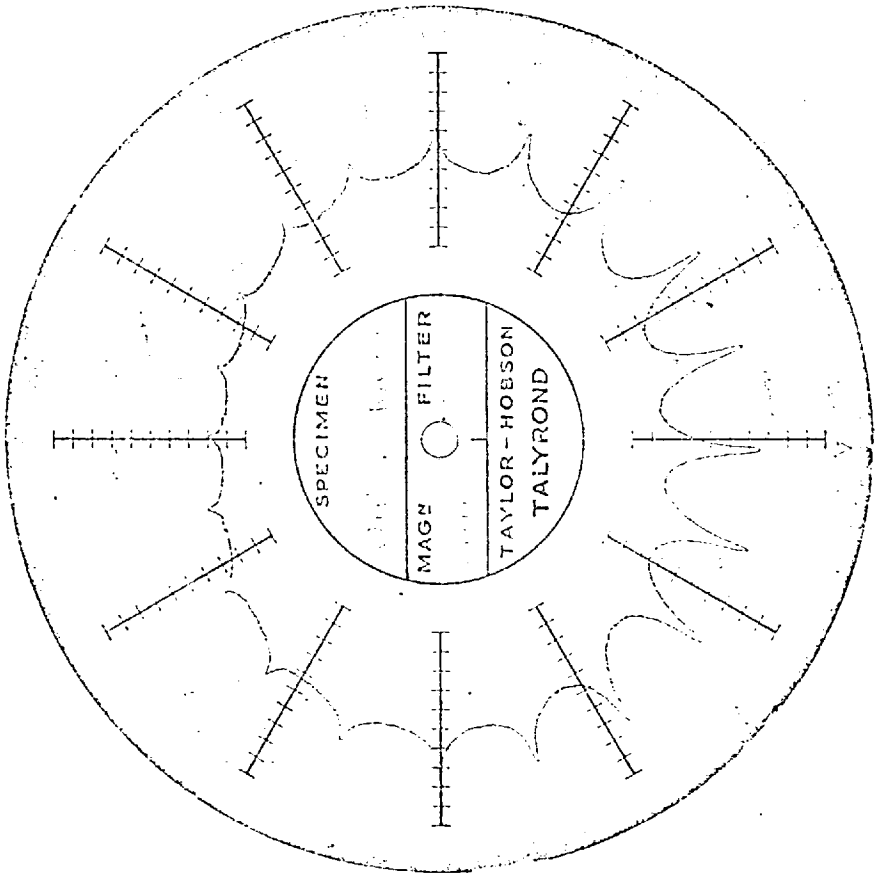
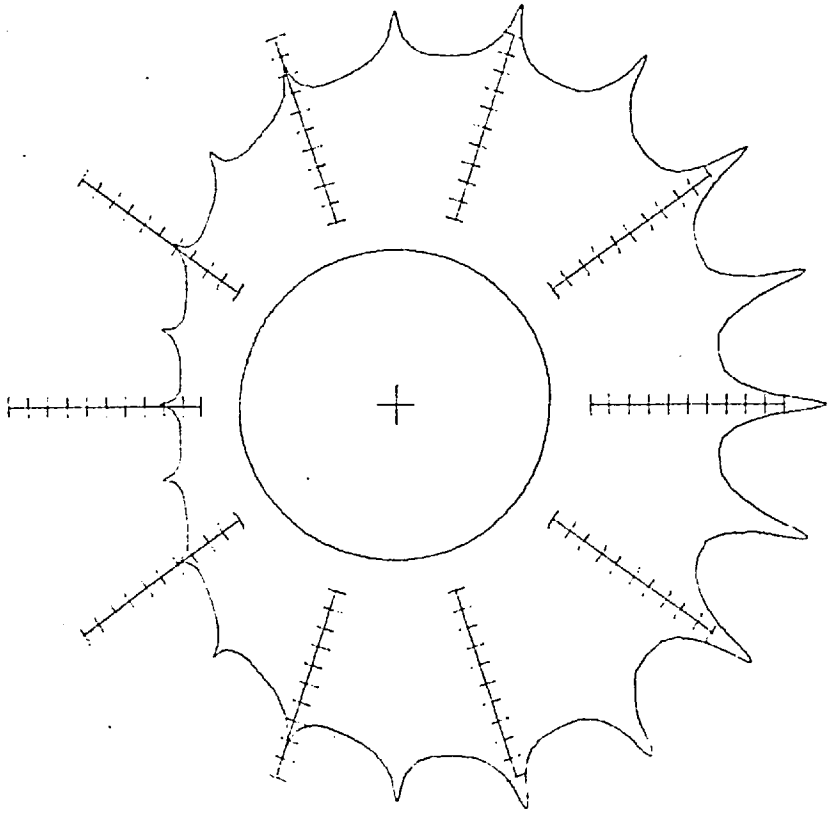


Fig. 4.23 Deflected shape of outer race of an Araldite radial roller bearing with 0.010 in.(0.254mm) interference fit. Radial load F_r= 9.5 lbs.(42.26 N).
(a) Talyrond chart of experimental model.
(b) Calcomp (graph-plotter) chart of finite element model.



(a)

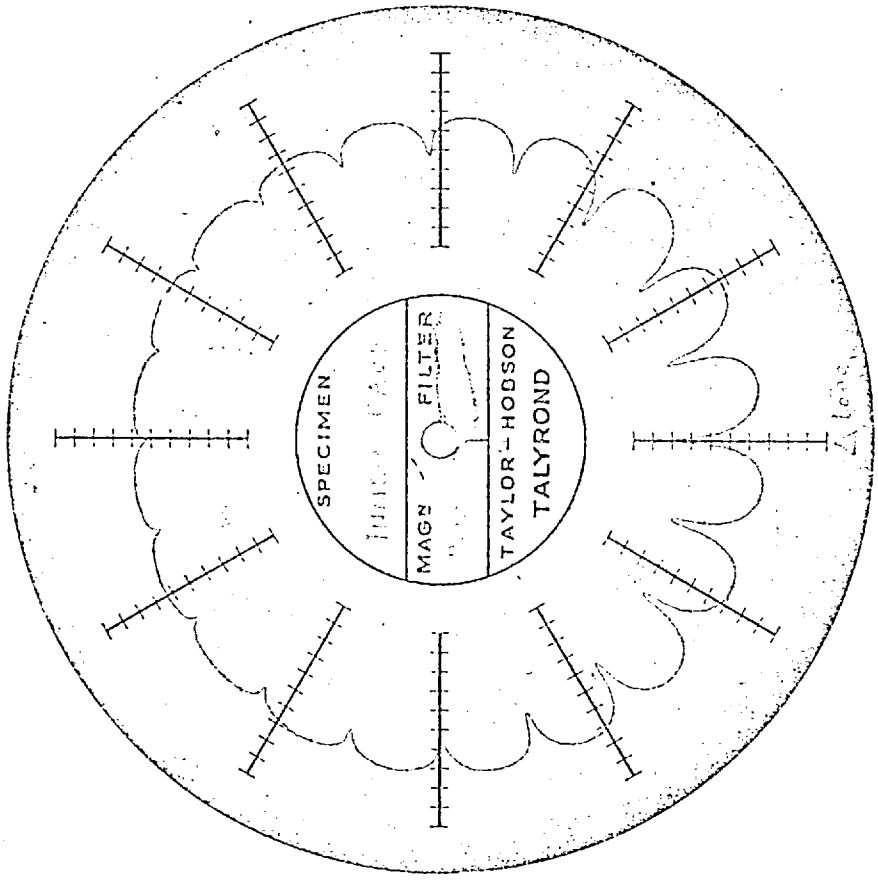
Talyrond chart of the outer race track
One div. represents 0.50 thou.
(experimental)



(b)

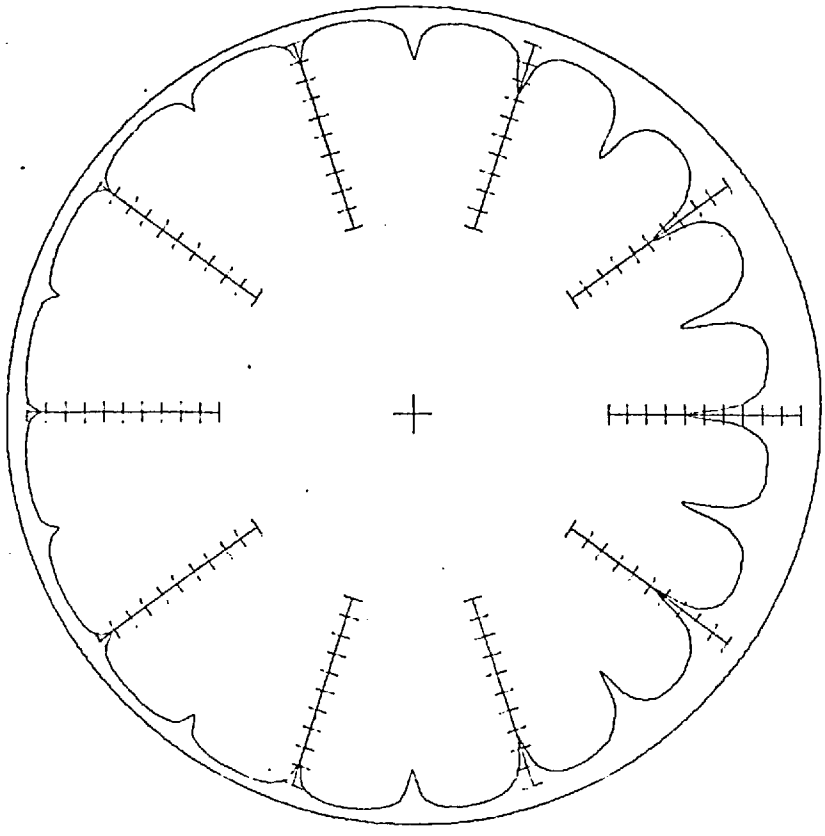
OUTER RACE
ONE DIV REPRESENTS .50 THOU
BEARING NO RN -111000 LOAD= 9.5 LBS RPM= 0

Fig. 4.24 Deflected shape of inner race of an Araldite radial roller bearing with 0.010 in.(0.254mm) interference fit. Radial load F_r= 9.5 lbs.(42.26 N).
(a) Talyrond chart of experimental model.
(b) Calcomp (graph-plotter) chart of finite element model.



(a)

Talyrond chart of the inner race track
One div. represents 0.50 thou.
(experimental)



(b)

INNER RACE
ONE DIV REPRESENTS .50 THOU
BEARING NO AN -111000 LOAD: 9.5 LBS RPM: 0

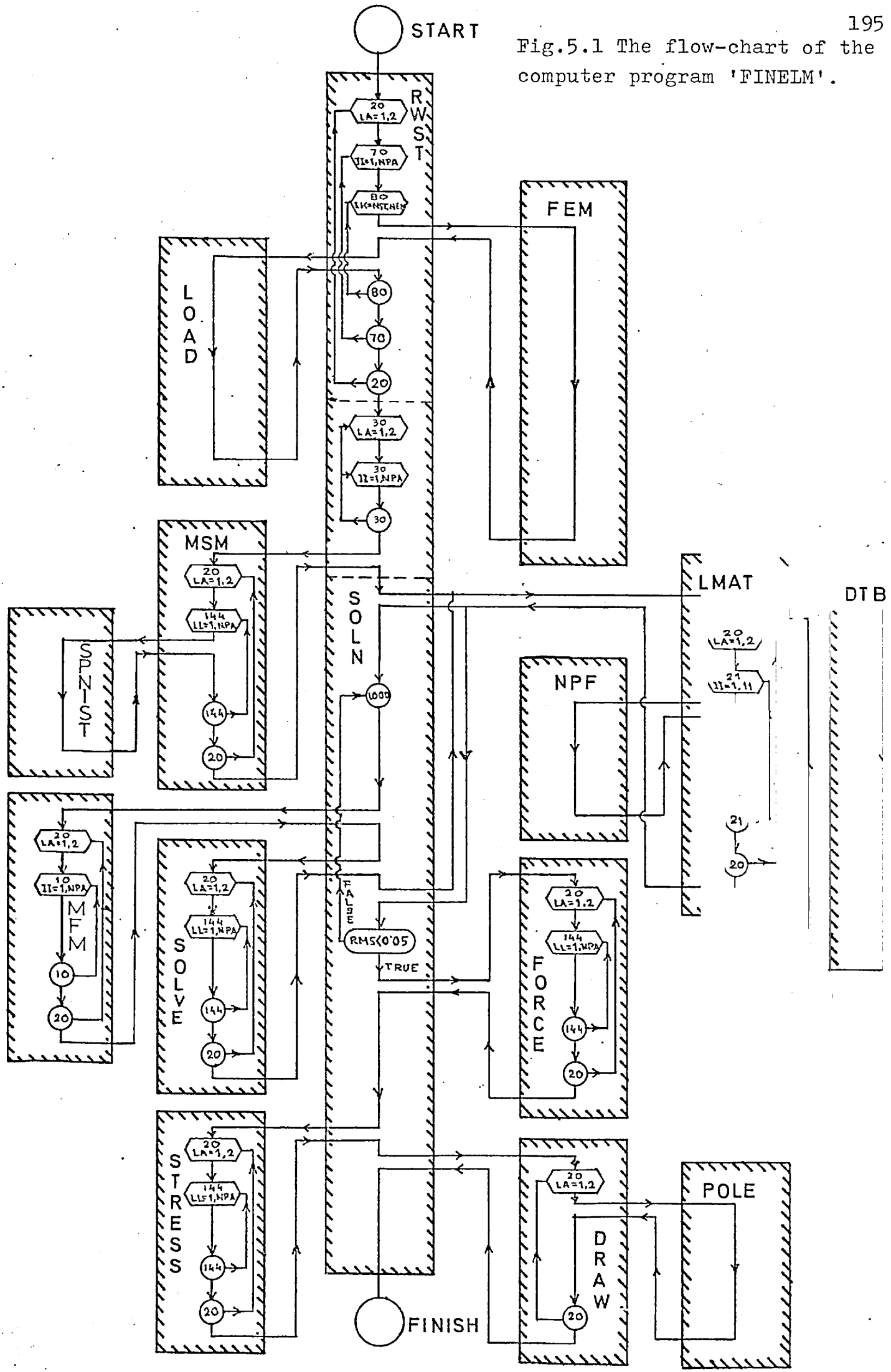
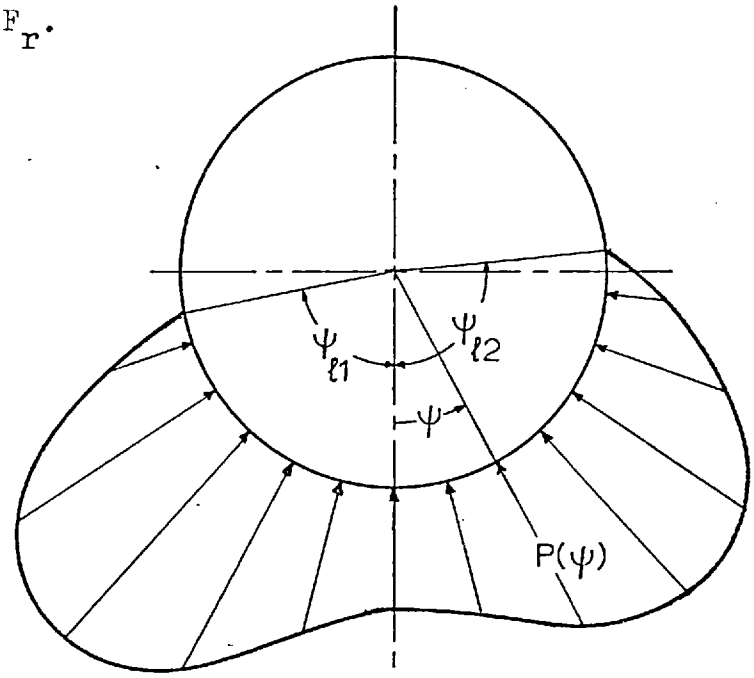
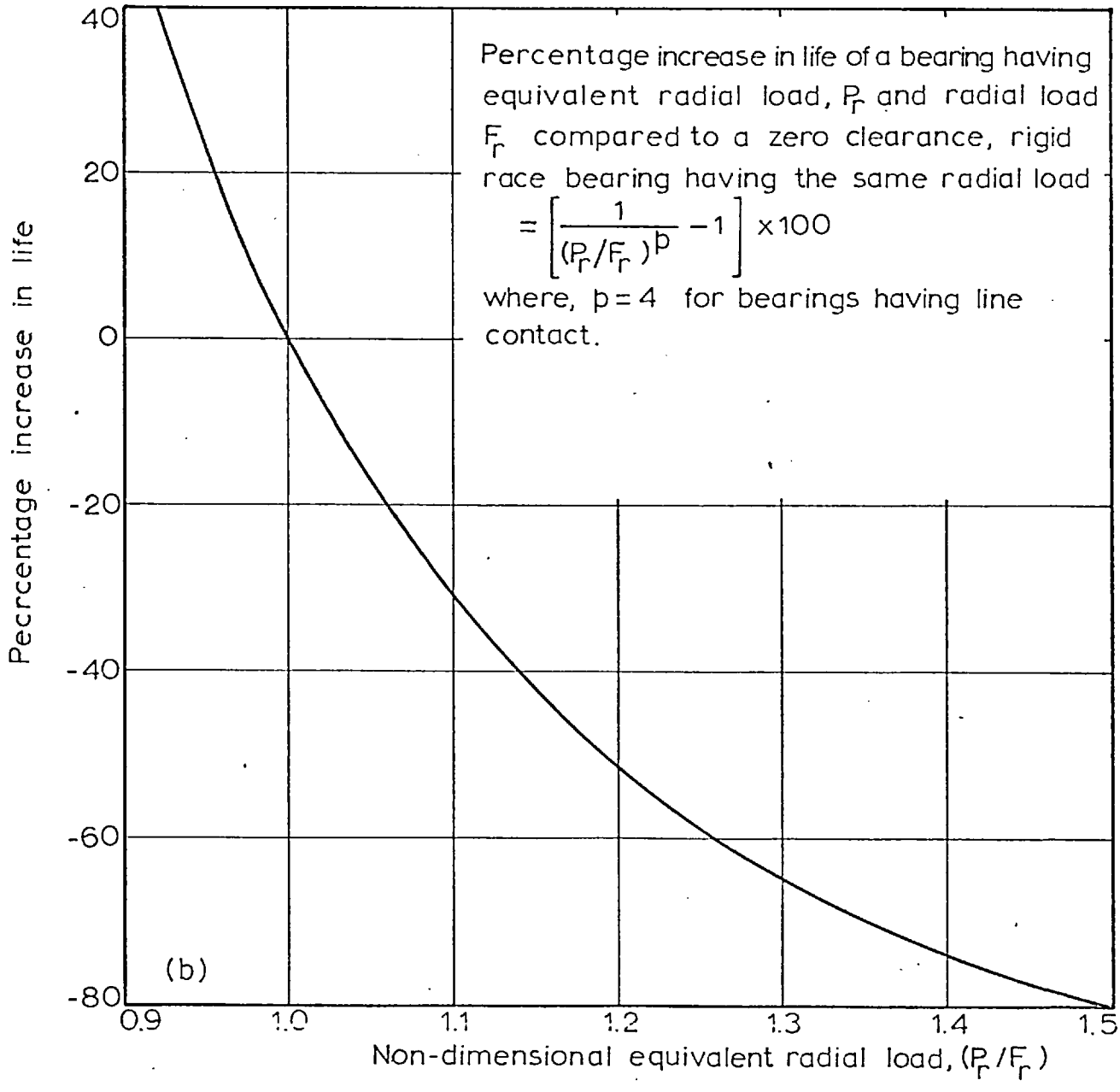


Fig.5.1 The flow-chart of the computer program 'FINELM'.

Fig. 5.2 (a) An arbitrary rolling element load distribution in a radial rolling bearing. (b) Percentage increase in life of a radial roller bearing having equivalent radial load P_r and radial load F_r, compared to a zero clearance, rigid race bearing having the same radial load F_r.



(a)



(b)

Fig. 6.1 Finite-element mesh for calibration of an Araldite roller loaded between two flat Araldite platens.

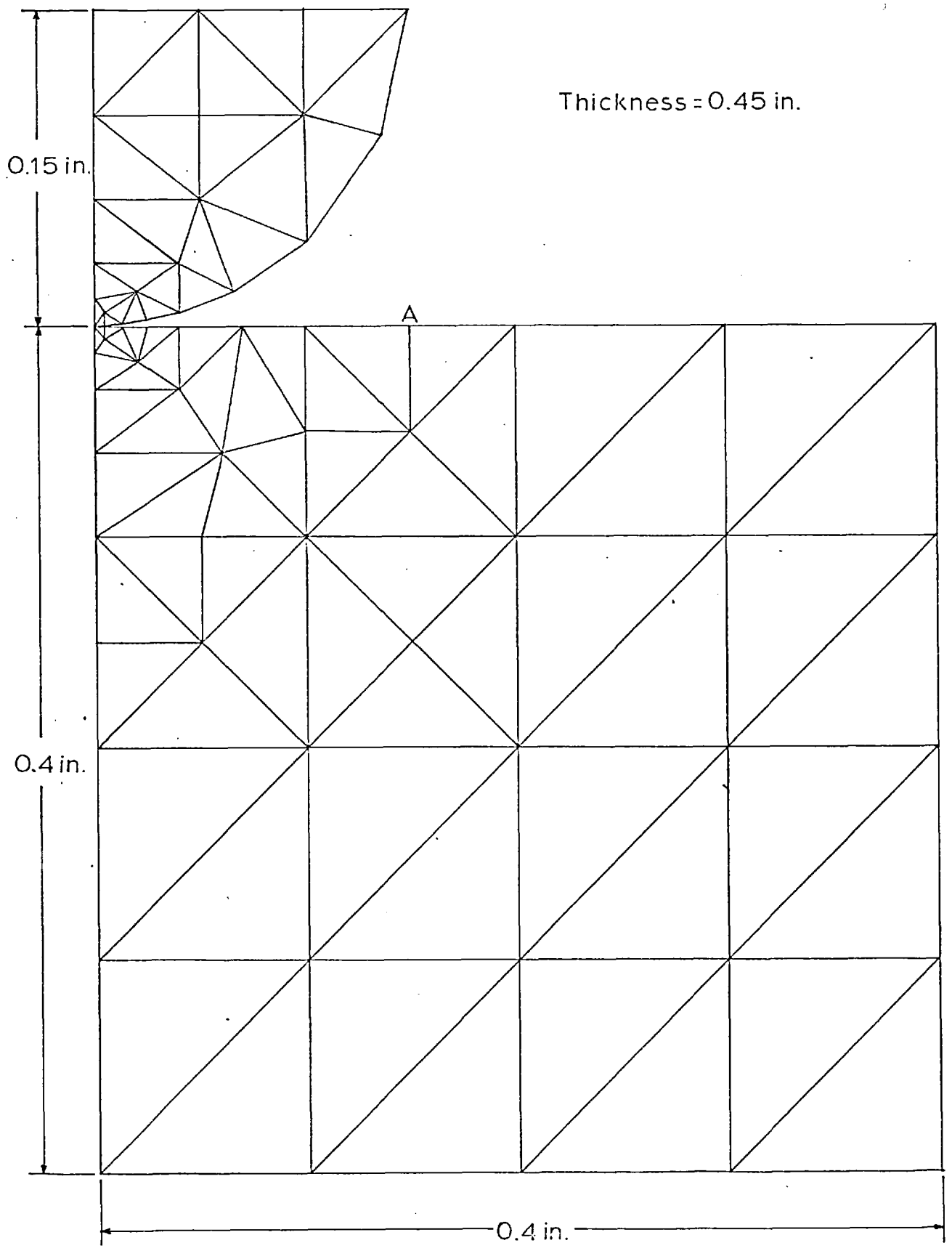


Fig. 6.2 Total deflection given by the approach of two flat Araldite platens when an Araldite roller is loaded between them, and also roller and platen deflections as obtained by finite-element method. Comparison with theoretical (Palmgren's) formula and experimental results.

δ_C deflection of the point at the centre of contact area, on the platen surface.

δ_A deflection of a point at 0.15 in. from the centre of contact area, on the surface of the platen.

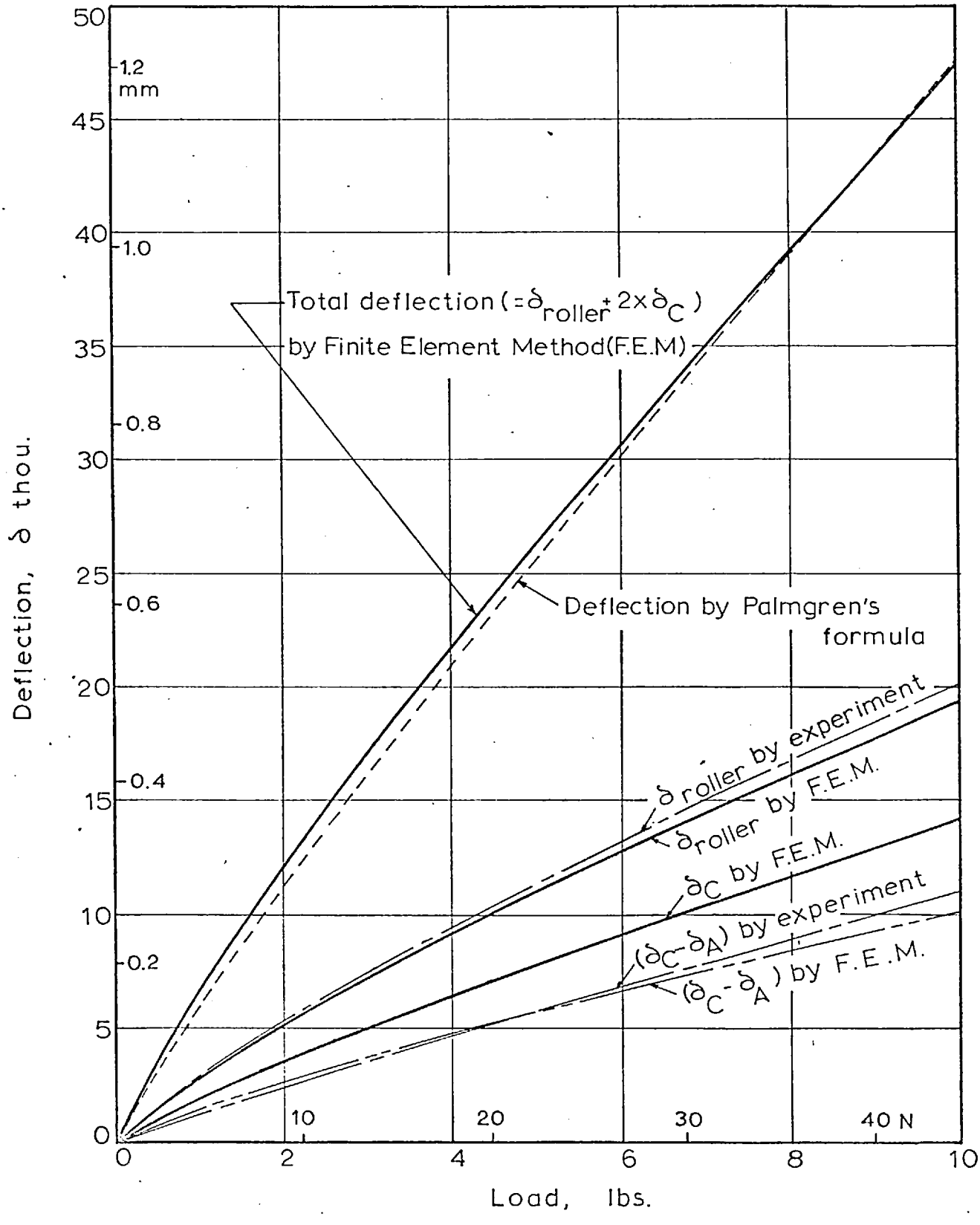
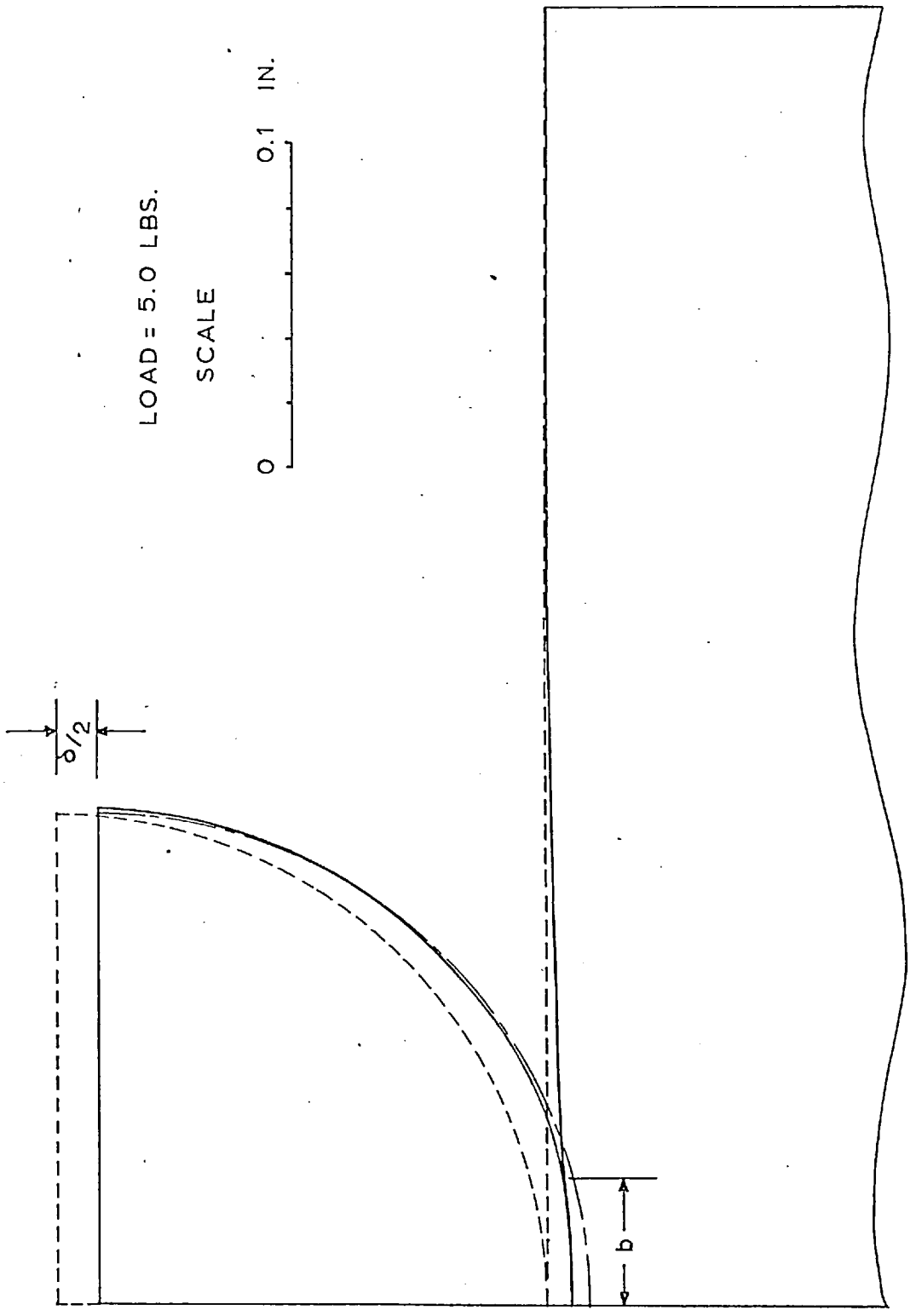


Fig. 6.3 Deflected shape of Araldite roller and platen assembly as obtained by finite-element method for a load of 5 lbs. (22.2 N)



DEFLECTED SHAPE OF ARALDITE ROLLER AND PLATEN ASSEMBLY.

Fig. 6.4 Mesh used in finite-element analysis of Araldite radial roller bearing race rings with housing and shaft. Meshes near contact areas between radial lines a and b on the outer and inner races are shown in the next two pages.

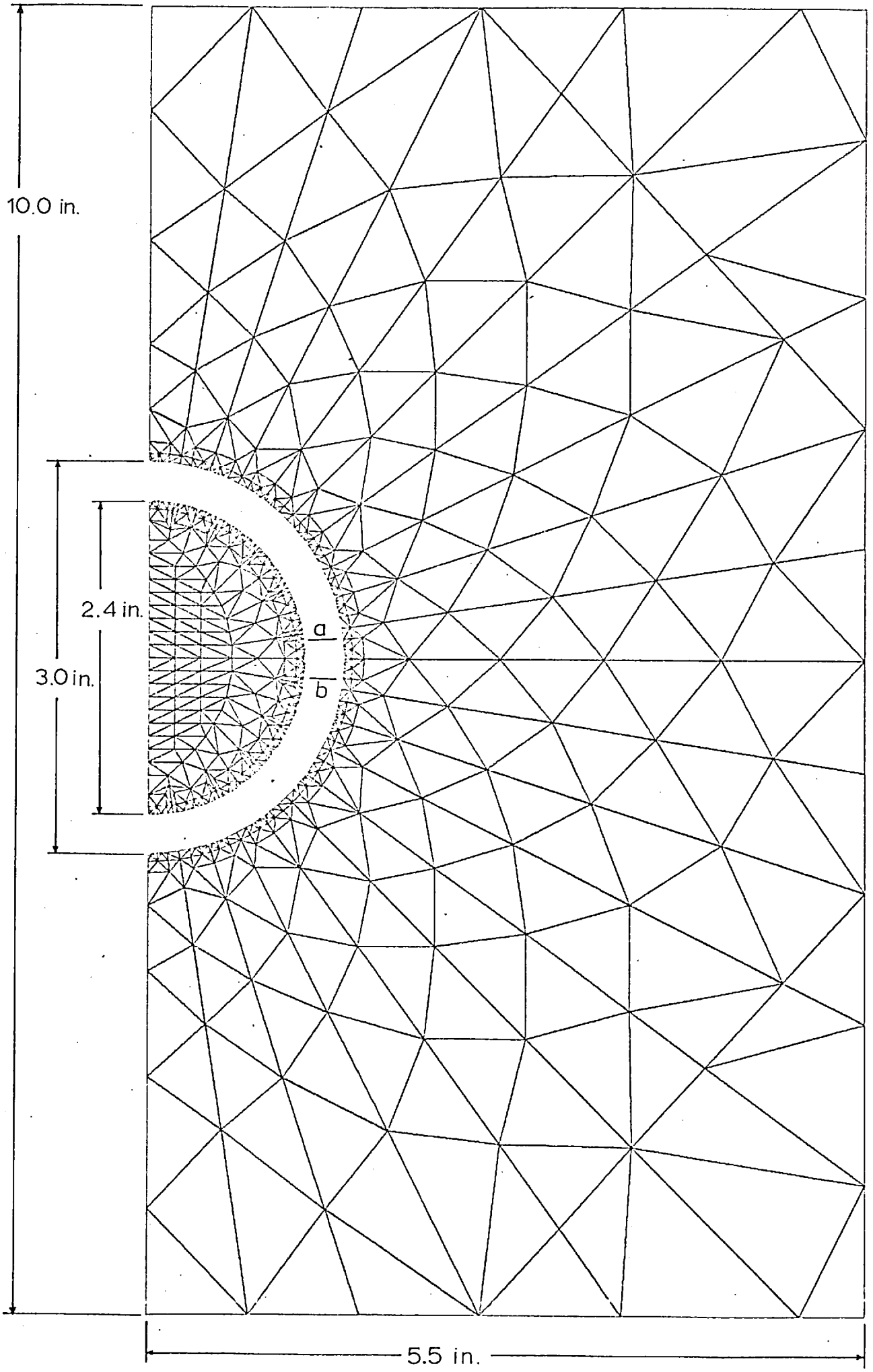


Fig. 6.5 Mesh near a contact area of the outer race between radial lines a and b of fig.6.4 for Araldite radial roller bearing.

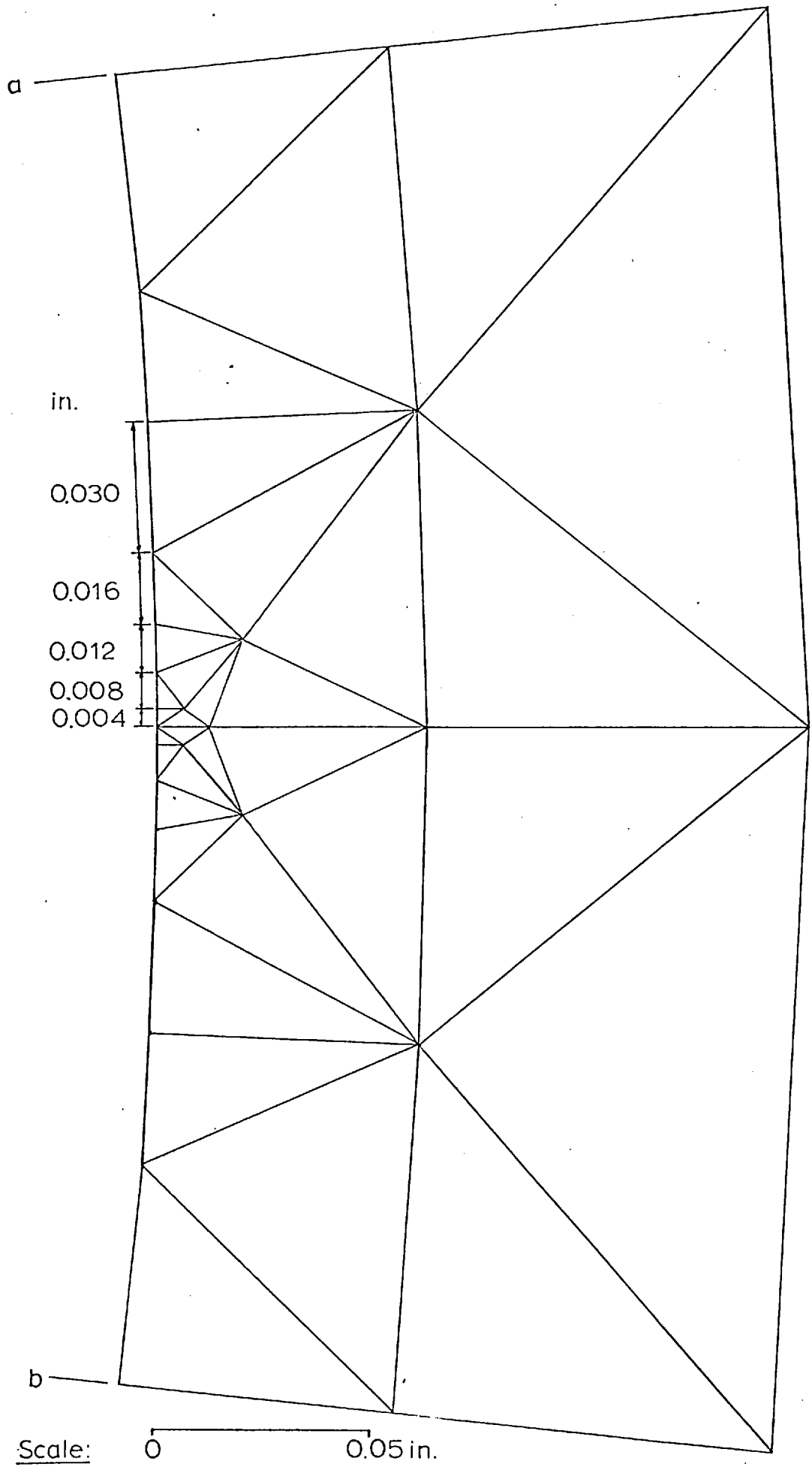


Fig. 6.6 Mesh near a contact area of the inner race between radial lines a and b of fig.6.4 for Araldite radial roller bearing.

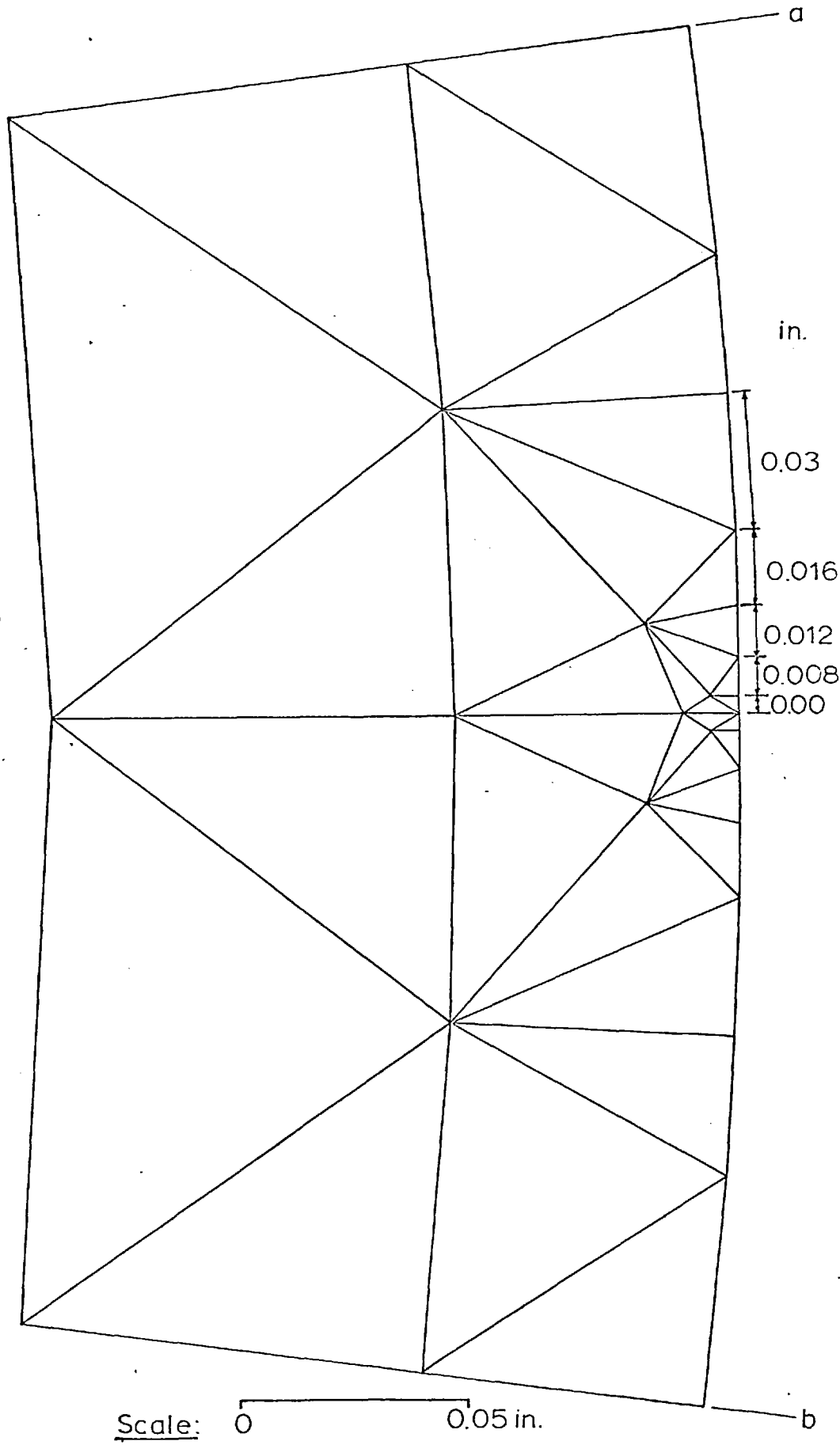
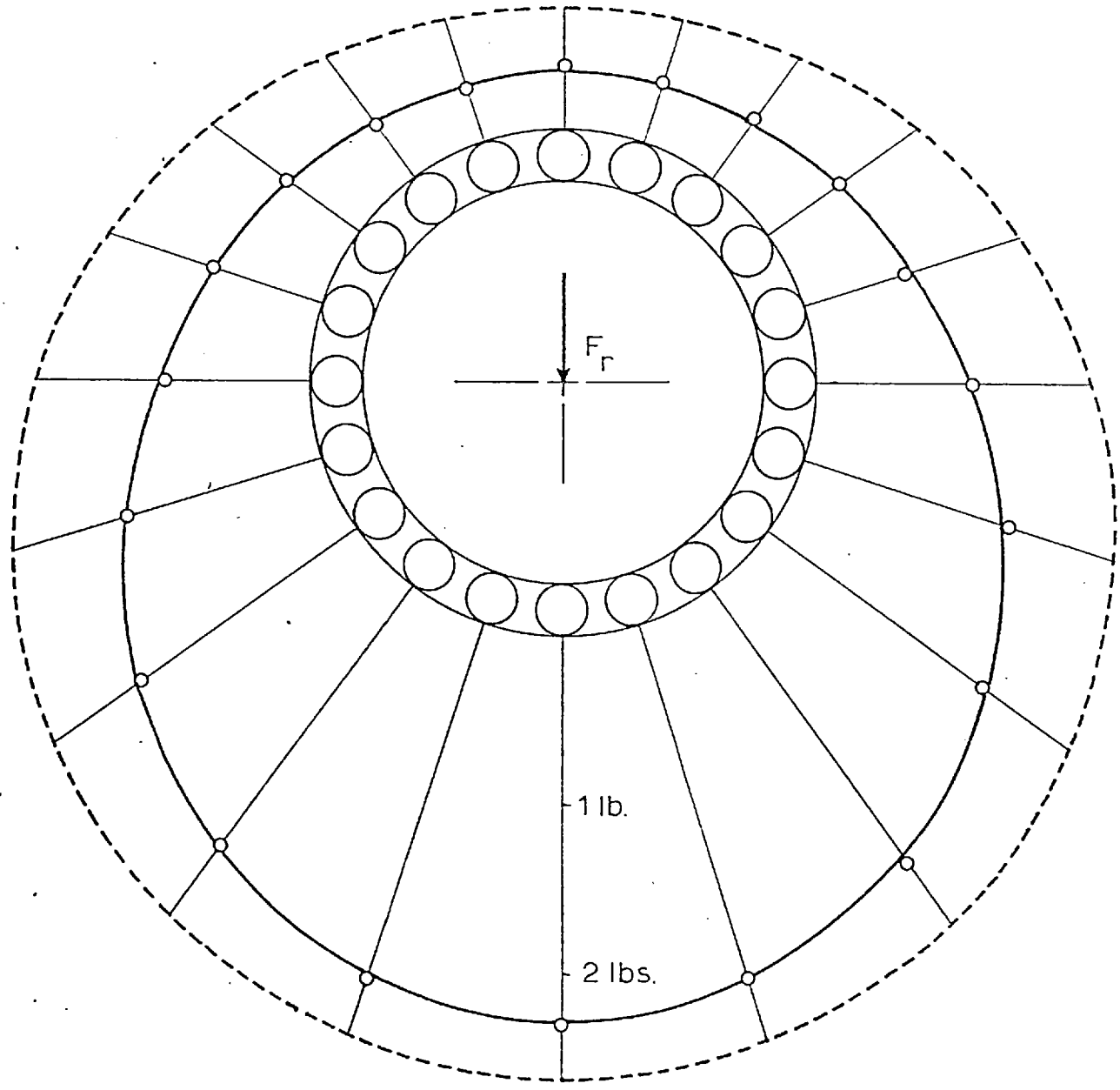


Fig. 6.7 Roller load distribution in the Araldite radial roller bearing with 0.010 in.(0.254mm) interference and a radial load of 9.5 lbs.(42.26 N) acting on it. Figure shows experimentally determined, and calculated load distributions, using normal 'rigid race' assumption, and the fully elastic condition evaluated by finite-element analysis.



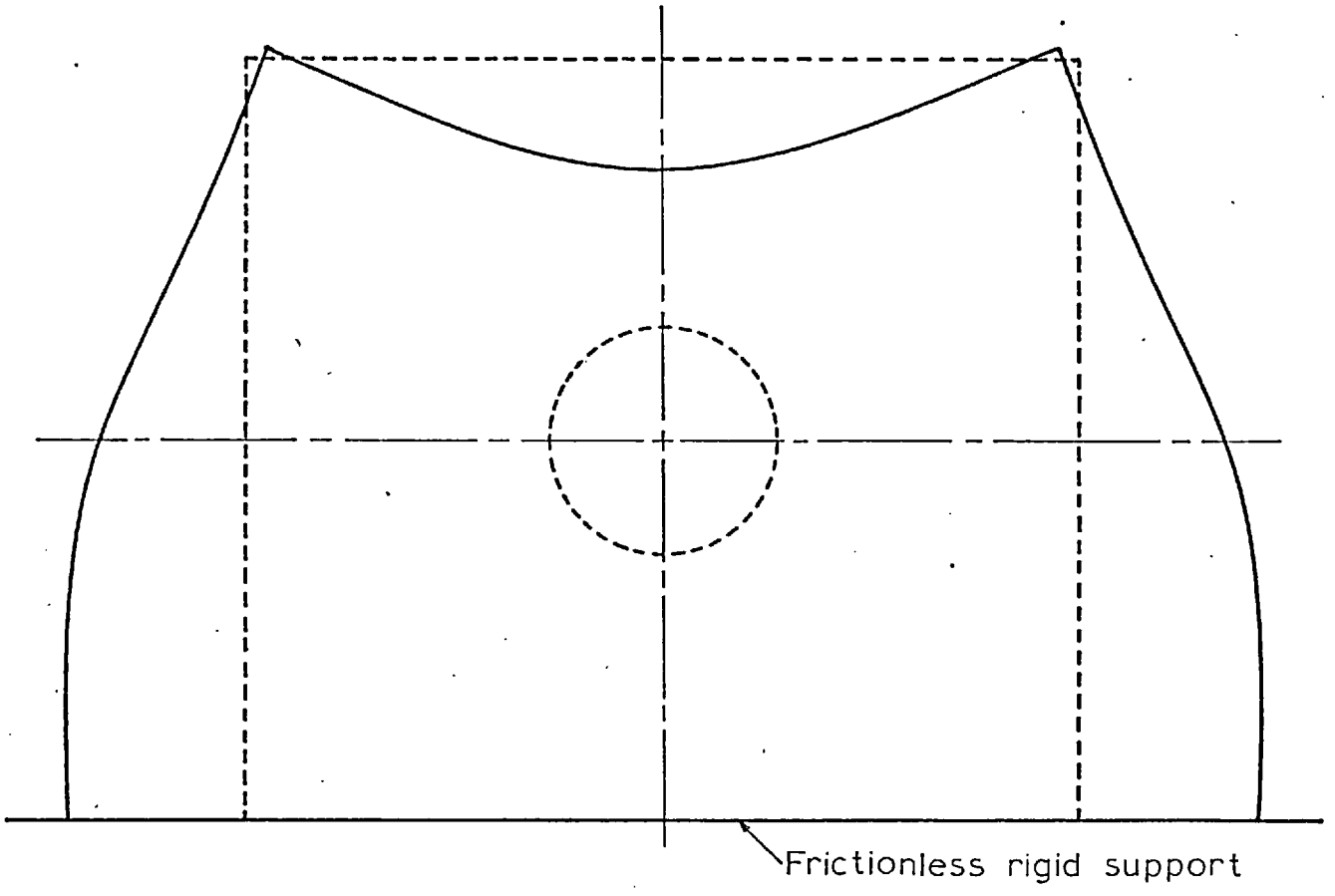
---------- By theory assuming rigid races

o By experiment

———— By finite element method

Bearing no. RN-111000,

Fig. 6.8 Deflected shape of housing outer boundary of the Araldite radial roller bearing with 0.010 in.(0.254 mm) interference and a radial load of 9.5 lbs.(42.26 N) acting on it, as obtained by finite-element analysis.



One inch represents 4.0 thou. deflection

RN-111000 F_r = 9.5 lbs. RPM = 0

(Inner race core thickness=0.9 in.)

Fig. 6.9 Effect of inner race core (i.e. shaft) thickness of an Araldite radial roller bearing having radial clearance c=-0.010 in.(0.254mm) and radial load F_r=9.5 lbs.(42.26 N), on the error in roller load distribution (by finite-element analysis), with respect to experimental results.

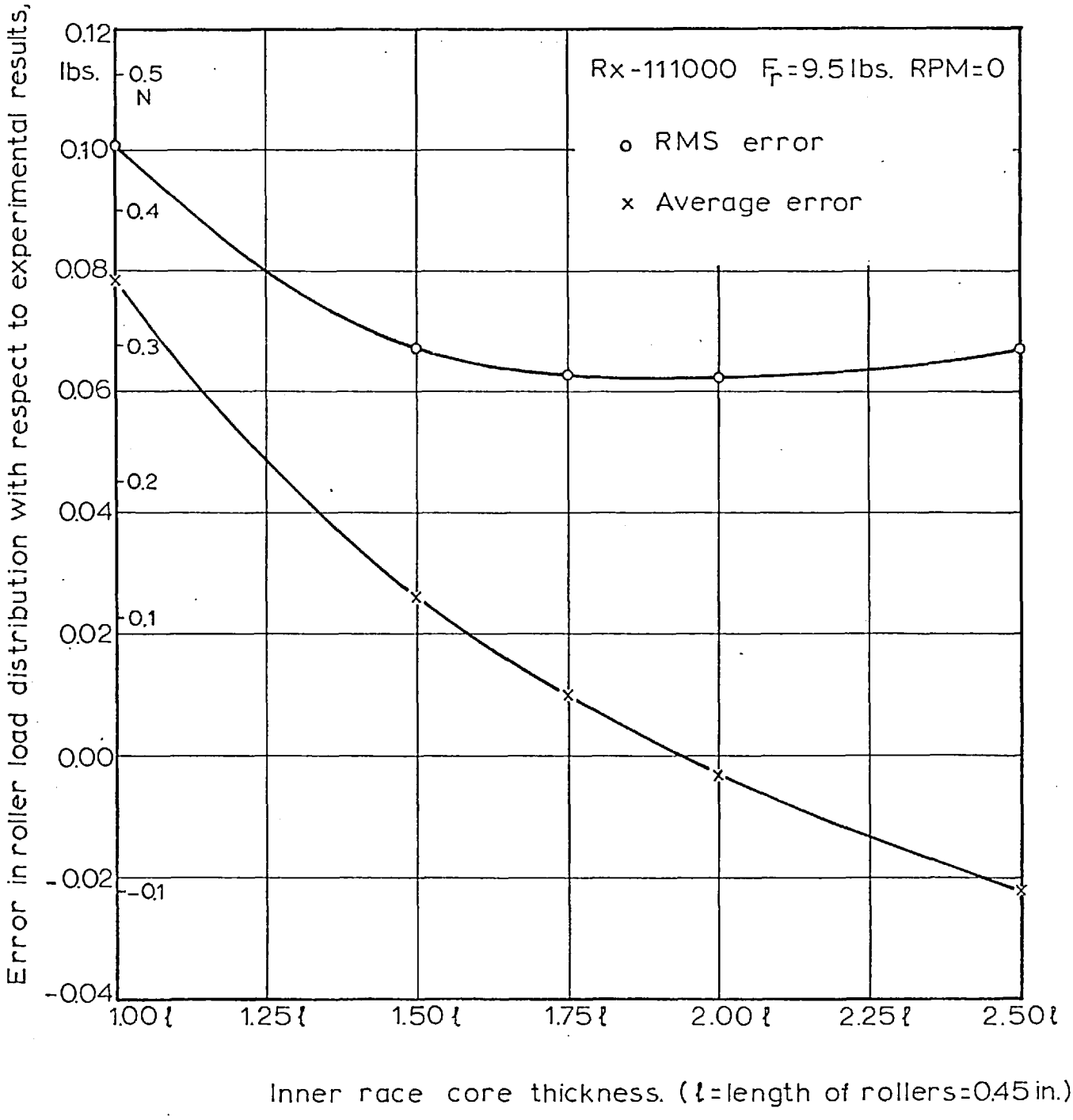


Fig. 6.10 Rate of convergence of roller load distribution for an Araldite radial roller bearing with radial clearance c= -0.008 in. and radial load of F_r= 9.5 lbs.

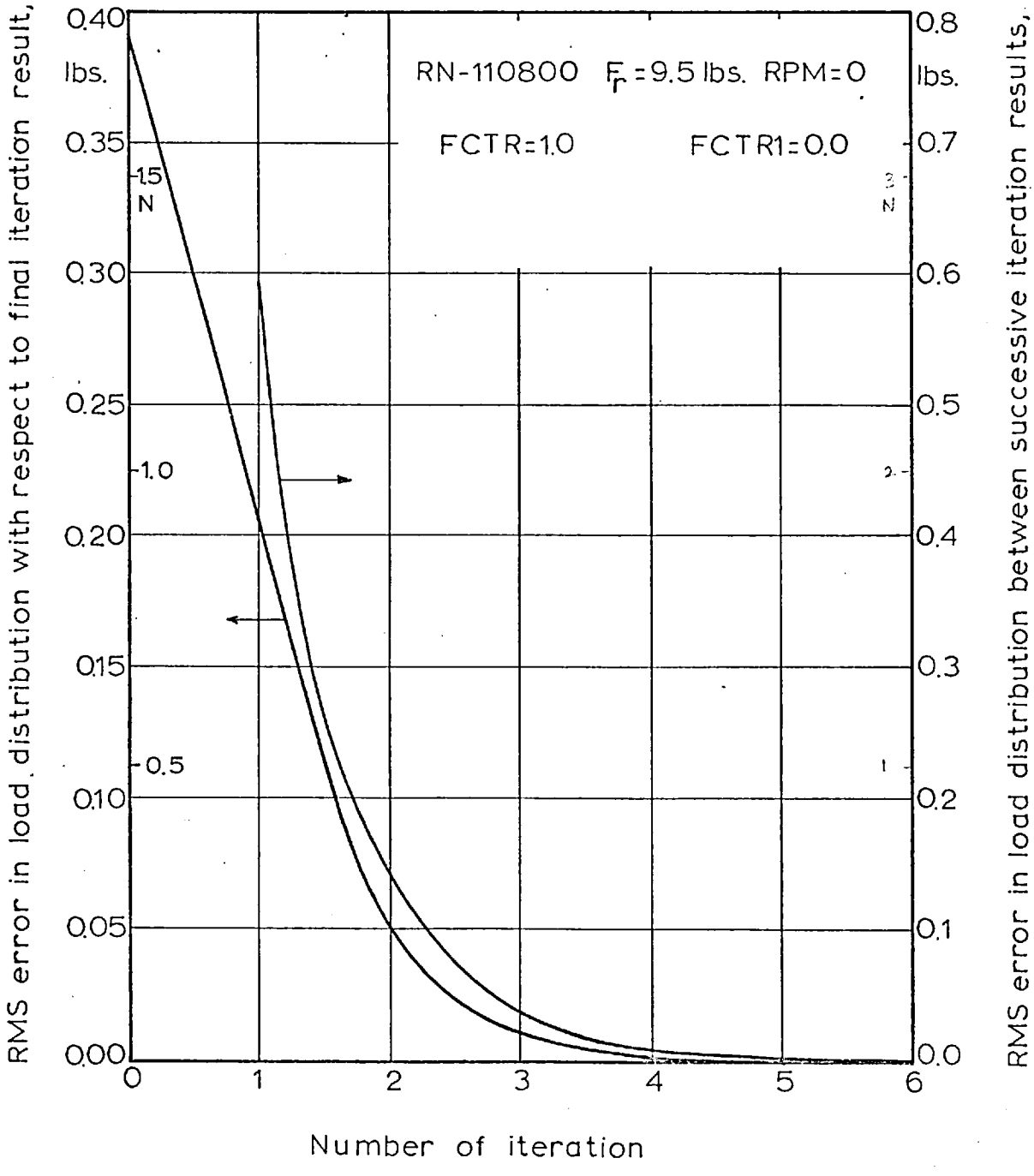


Fig. 6.11 Effect of radial clearance on the total radial and component deflections, and K_t and K_b of an Araldite radial roller bearing having a radial load of F_r= 9.5 lbs.

$$K_t = \frac{\delta_r \text{ for flexible races}}{\delta_r \text{ for rigid races}}, \quad K_b = \frac{\delta_b \text{ for flexible races}}{\delta_r \text{ for rigid races}}.$$

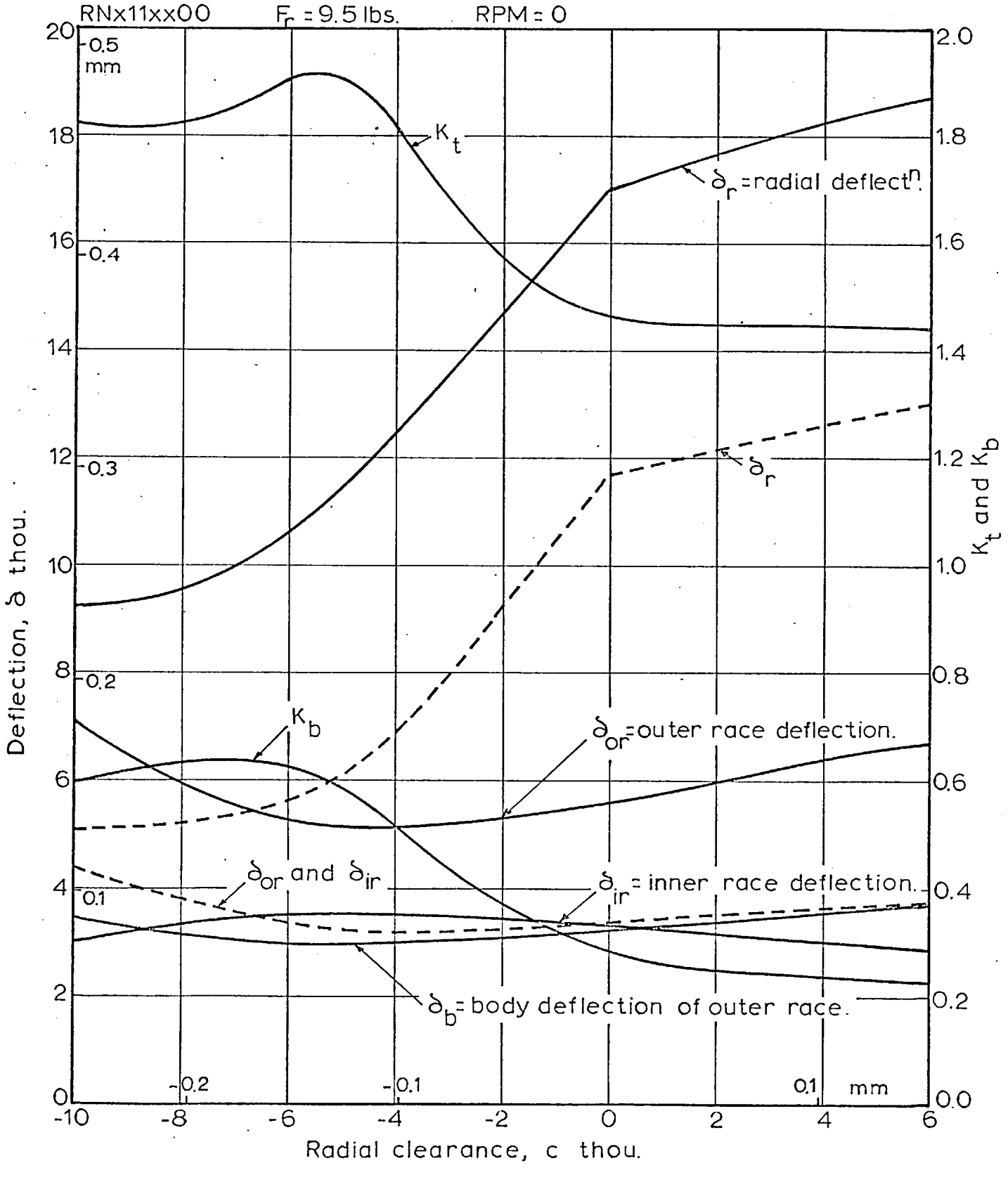


Fig. 6.12 Effect of radial load on the total radial and component deflections of an Araldite radial roller bearing at different radial clearances.

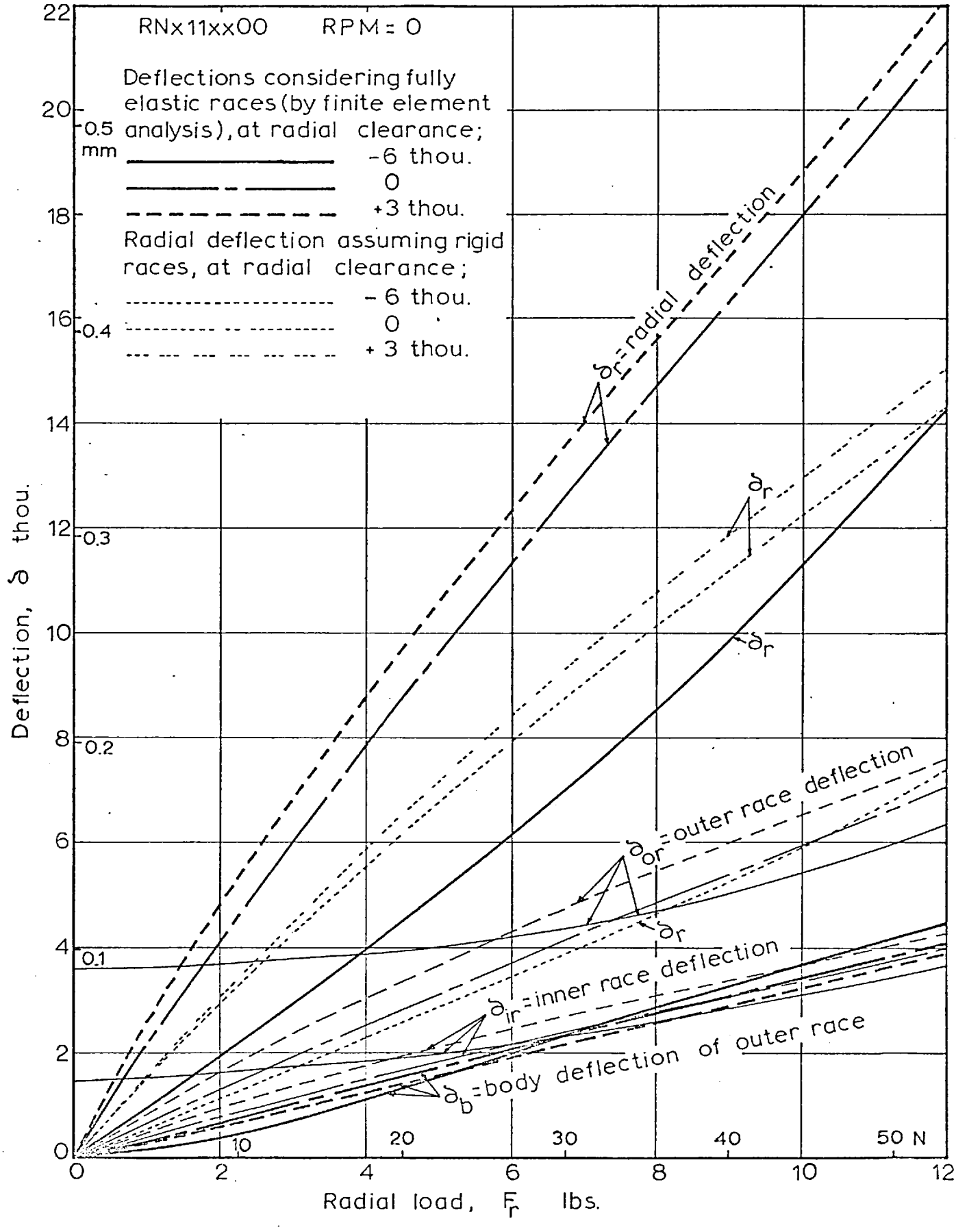


Fig. 6.13 Effect of radial load on the factors K_t and K_b of an Araldite radial roller bearing at different radial clearances.

$$K_t = \frac{\delta_r \text{ for flexible races}}{\delta_r \text{ for rigid races}}, \quad K_b = \frac{\delta_b \text{ for flexible races}}{\delta_r \text{ for rigid races}}$$

where, δ_r=radial deflection, δ_b=body deflection of outer race.

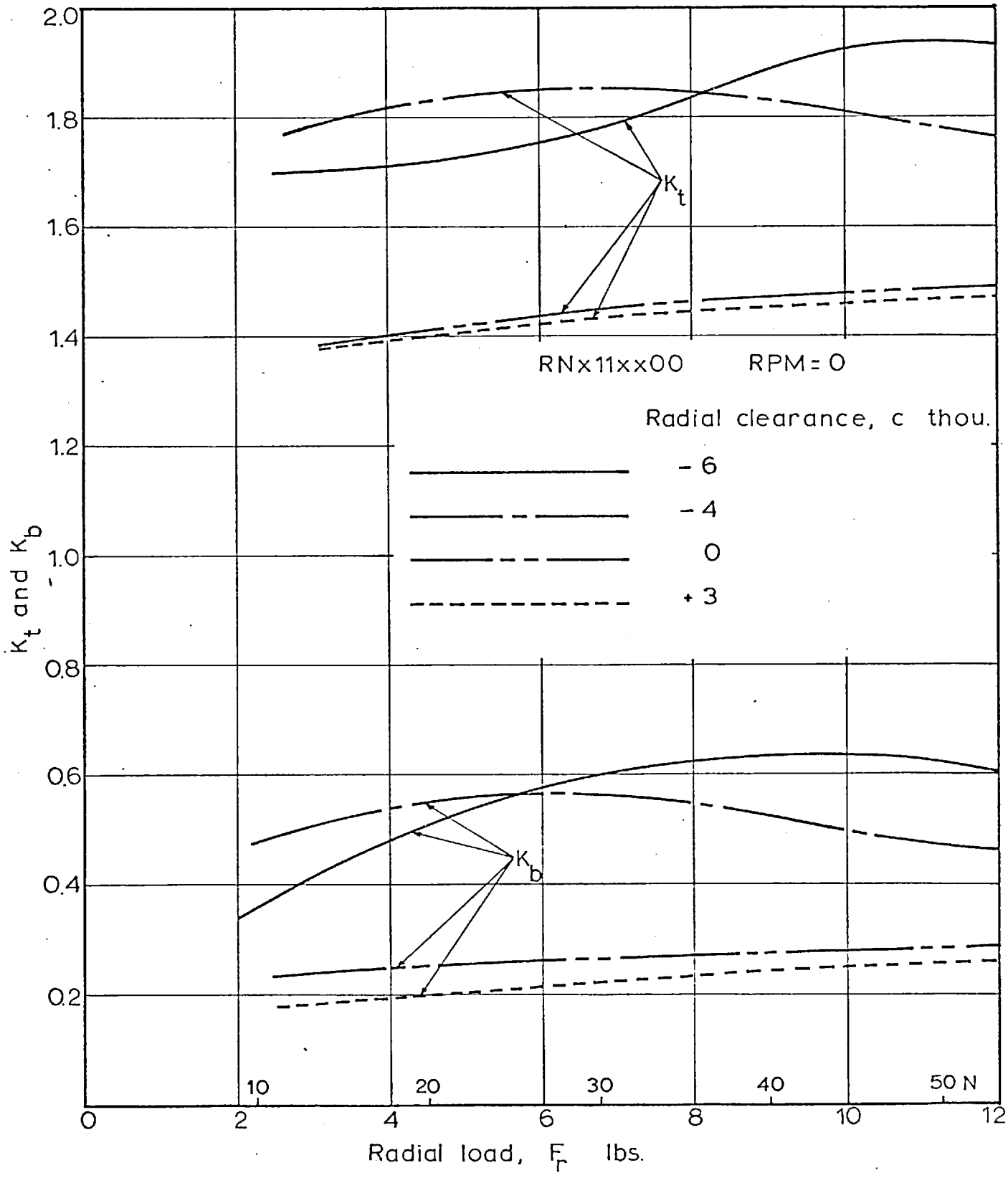


Fig. 6.14 Effect of radial clearance on the non-dimensional equivalent radial load (P_r/F_r) of an Araldite radial roller bearing having a radial load of 9.5 lbs.

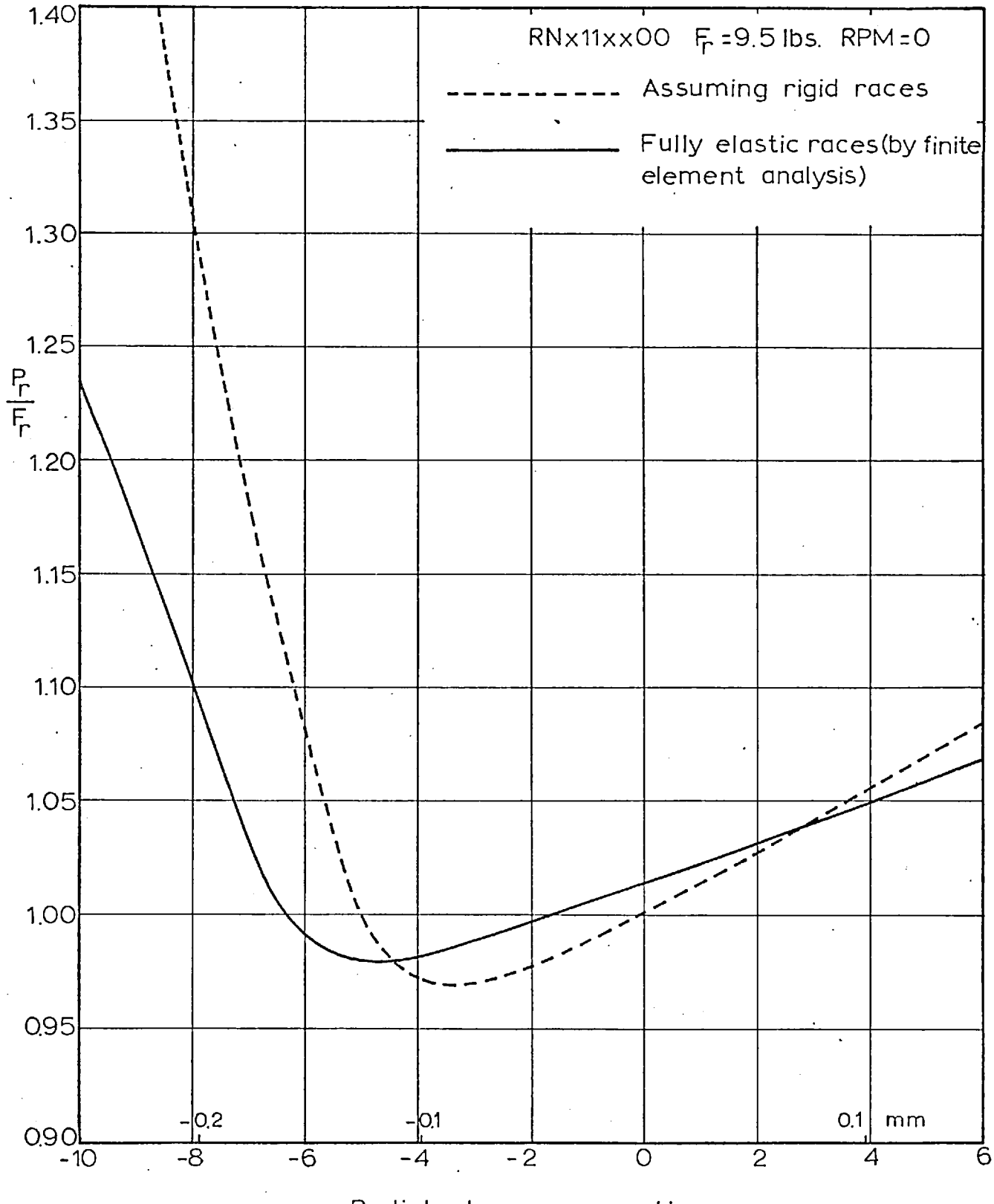


Fig. 6.15 Effect of radial load on the non-dimensional equivalent radial load (P_r/F_r) of an Araldite radial roller bearing at various radial clearances.

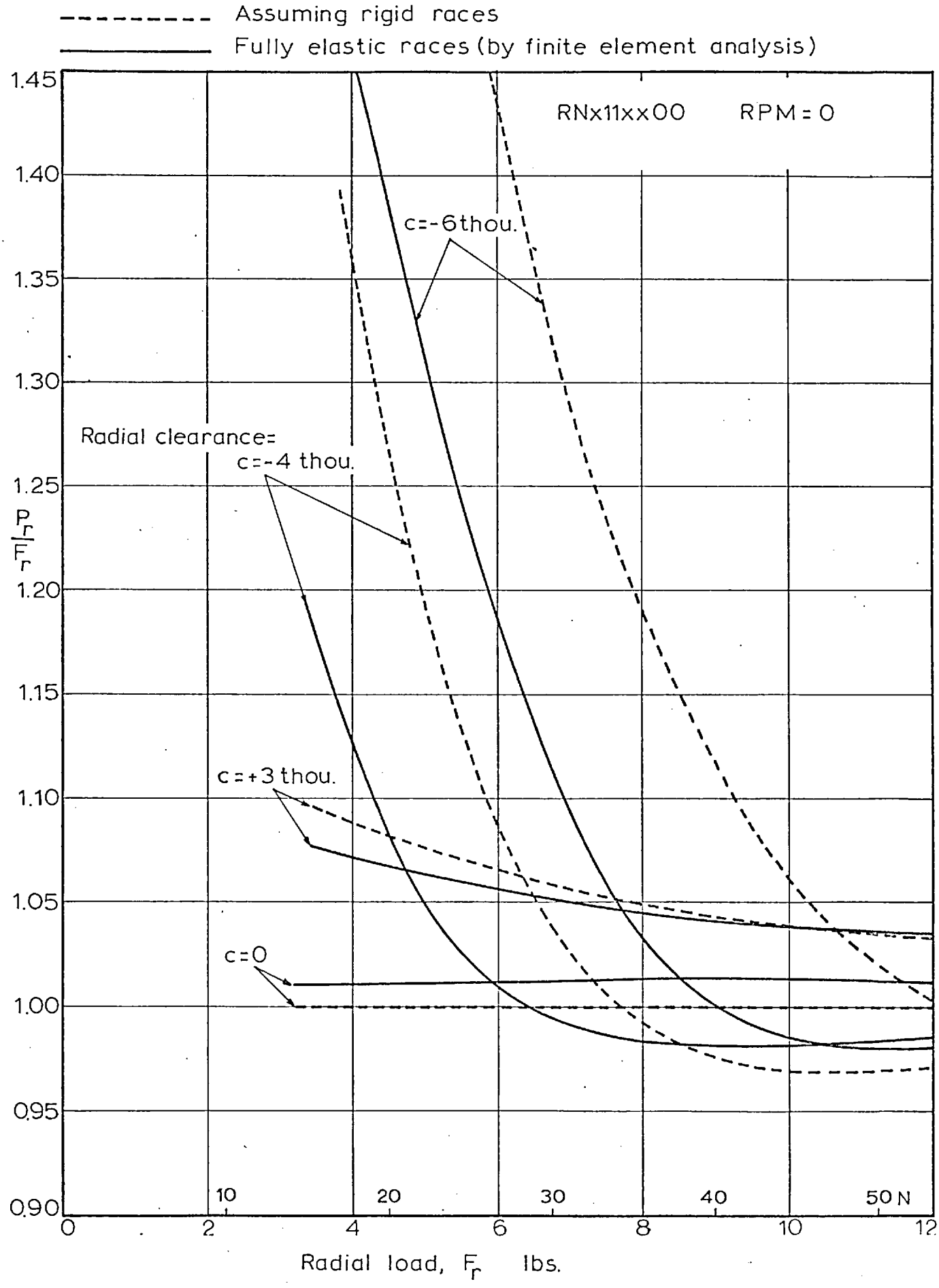


Fig. 6.16 Effect of fully elastic races on the factor $(P_1 Z/F_r)$ of an Araldite radial roller bearing.

P_1 = Peak roller load.
F_r = Radial load on the bearing.
Z = Number of rollers in the bearing.

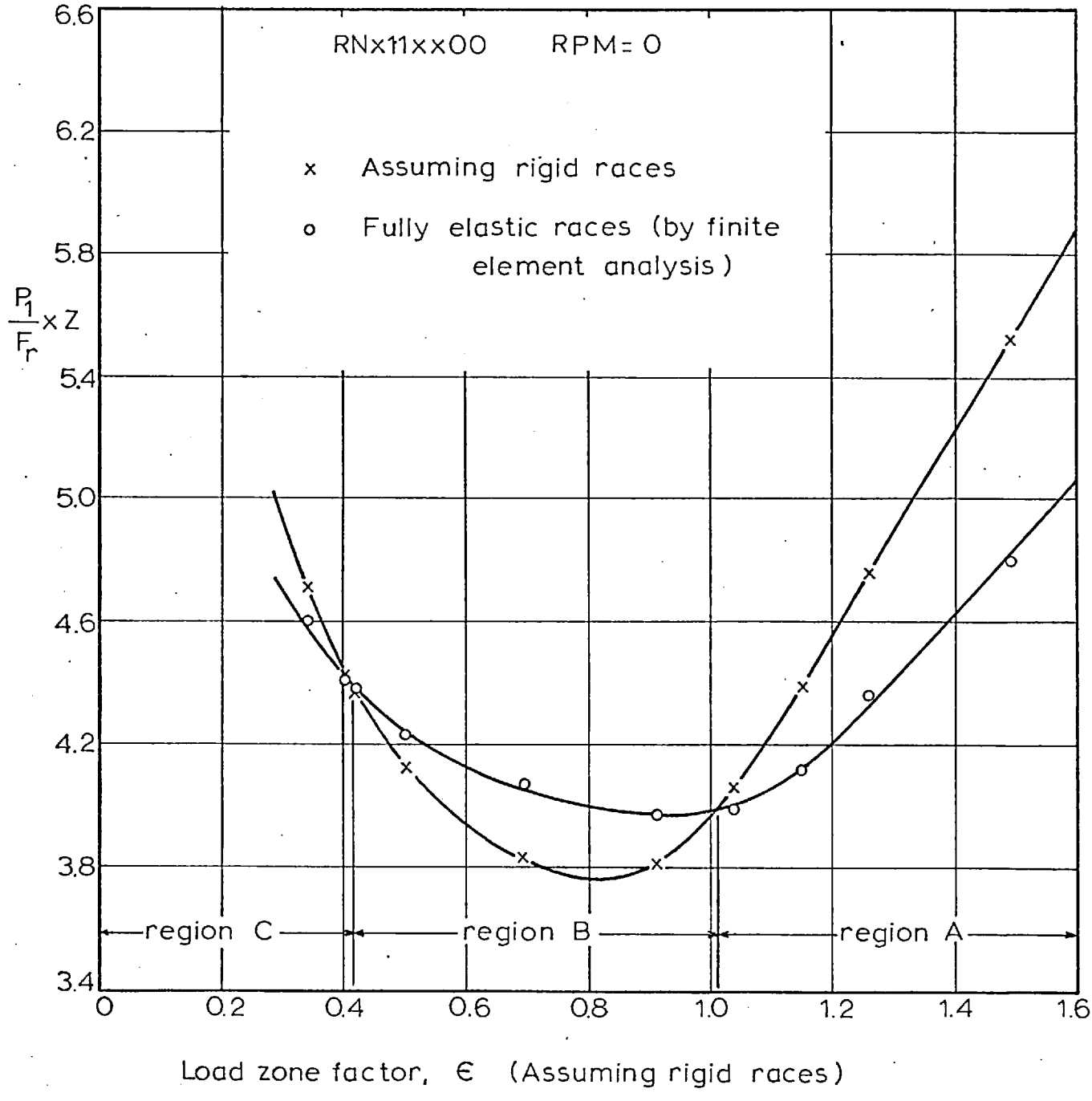


Fig. 6.17 Effect of fully elastic races on the non-dimensional equivalent radial load (P_r/F_r) of an Araldite radial roller bearing.

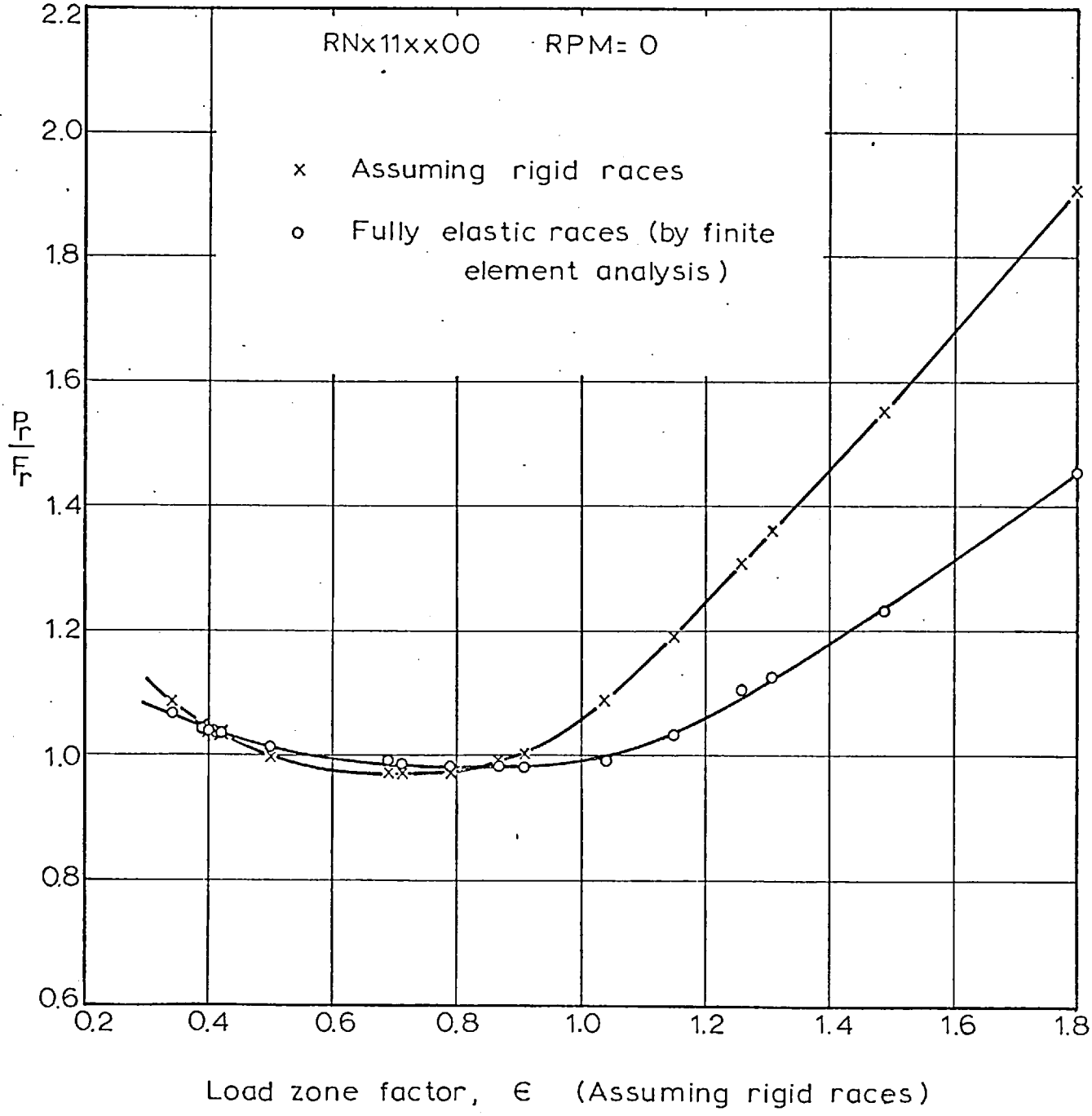


Fig. 6.18 Roller load distribution in an Araldite radial roller bearing having (a) radial load F_r= 9.5 lbs., and (b) radial clearance c= -0.006 in.

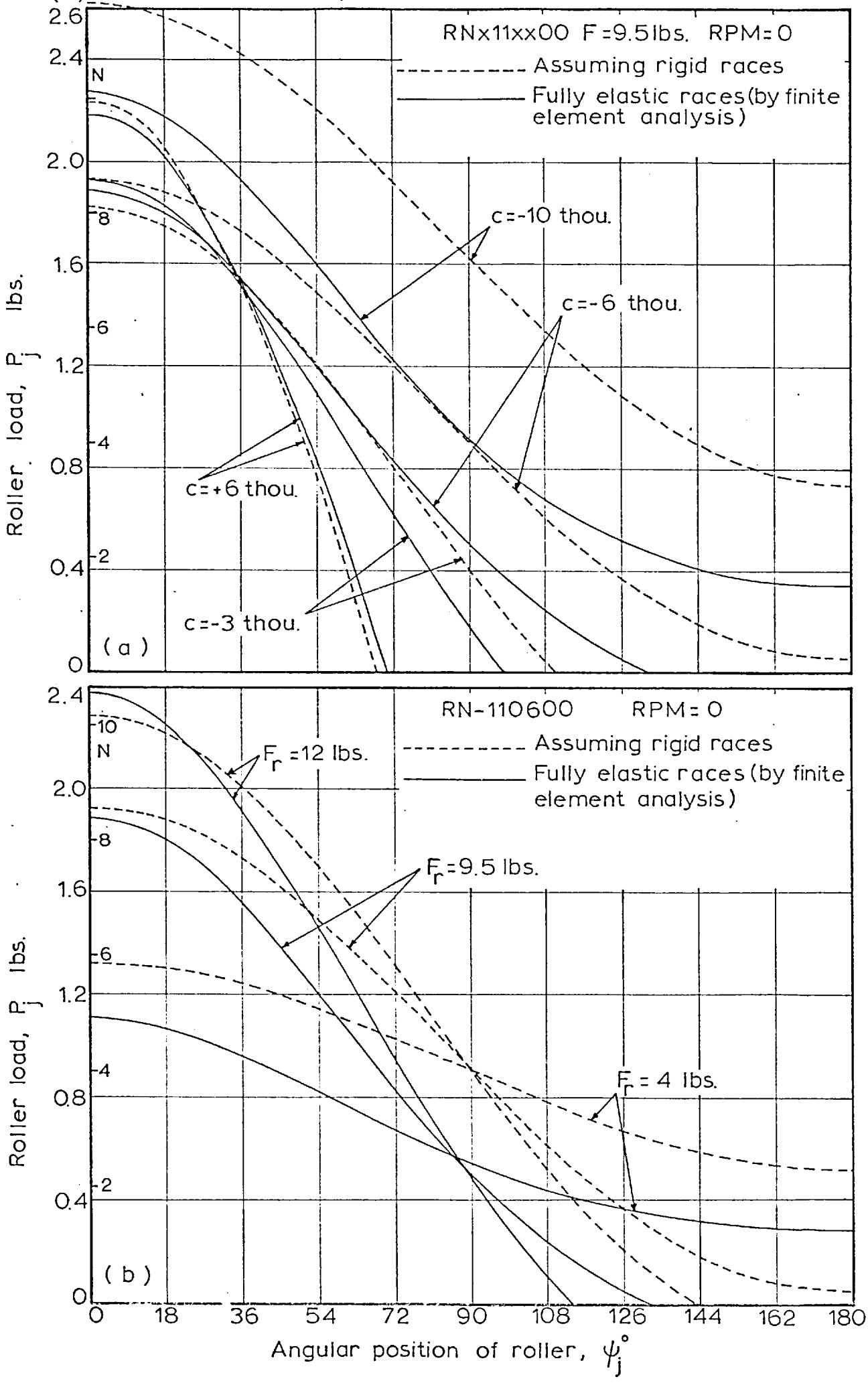


Fig. 6.19 Roller load distribution in an Araldite radial roller bearing having (a) radial clearance c= -0.004 in., and (b) c= +0.003 in.

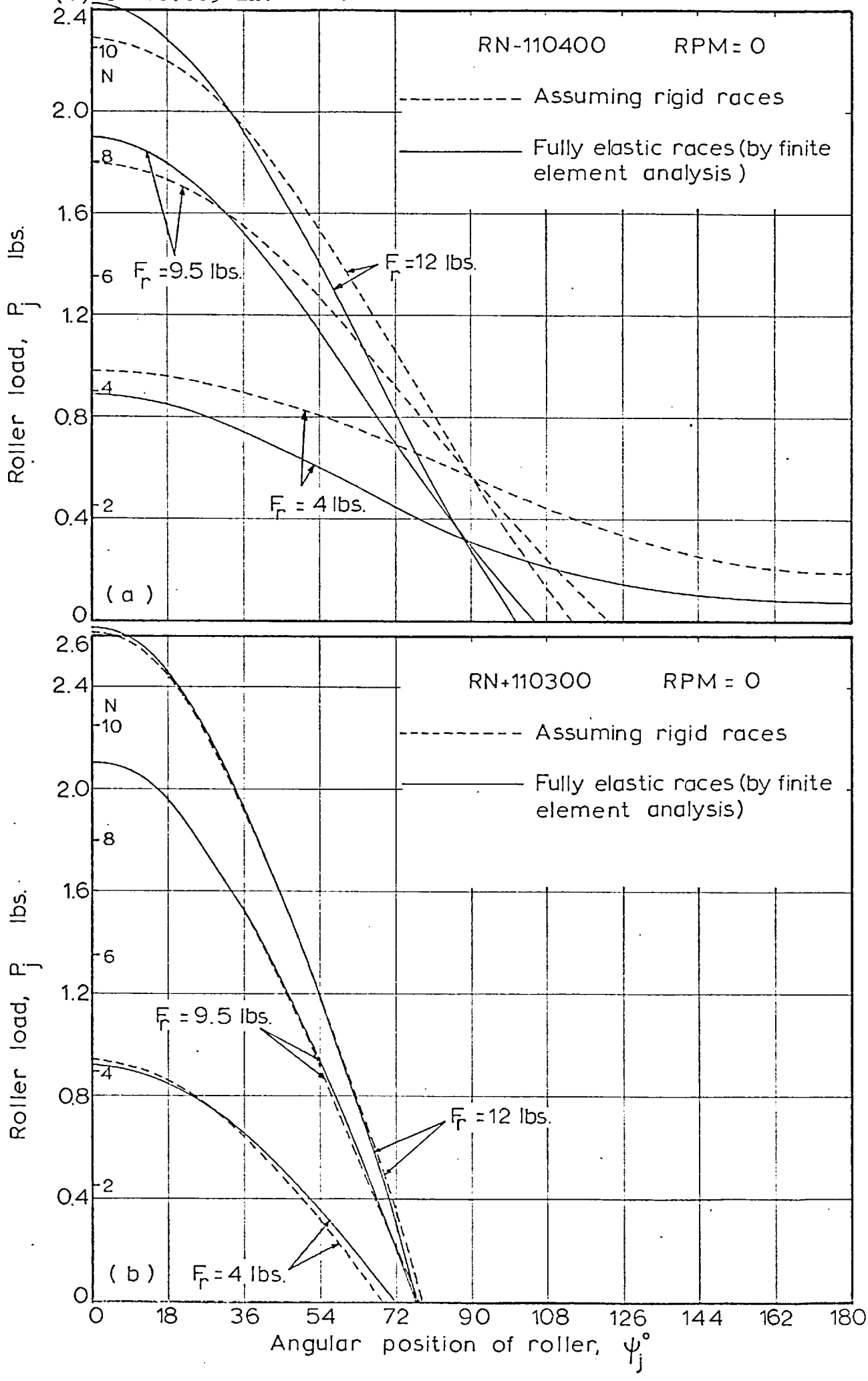


Fig. 6.20 Effect of shaft speed on the total radial and component deflections of an Araldite radial roller bearing.

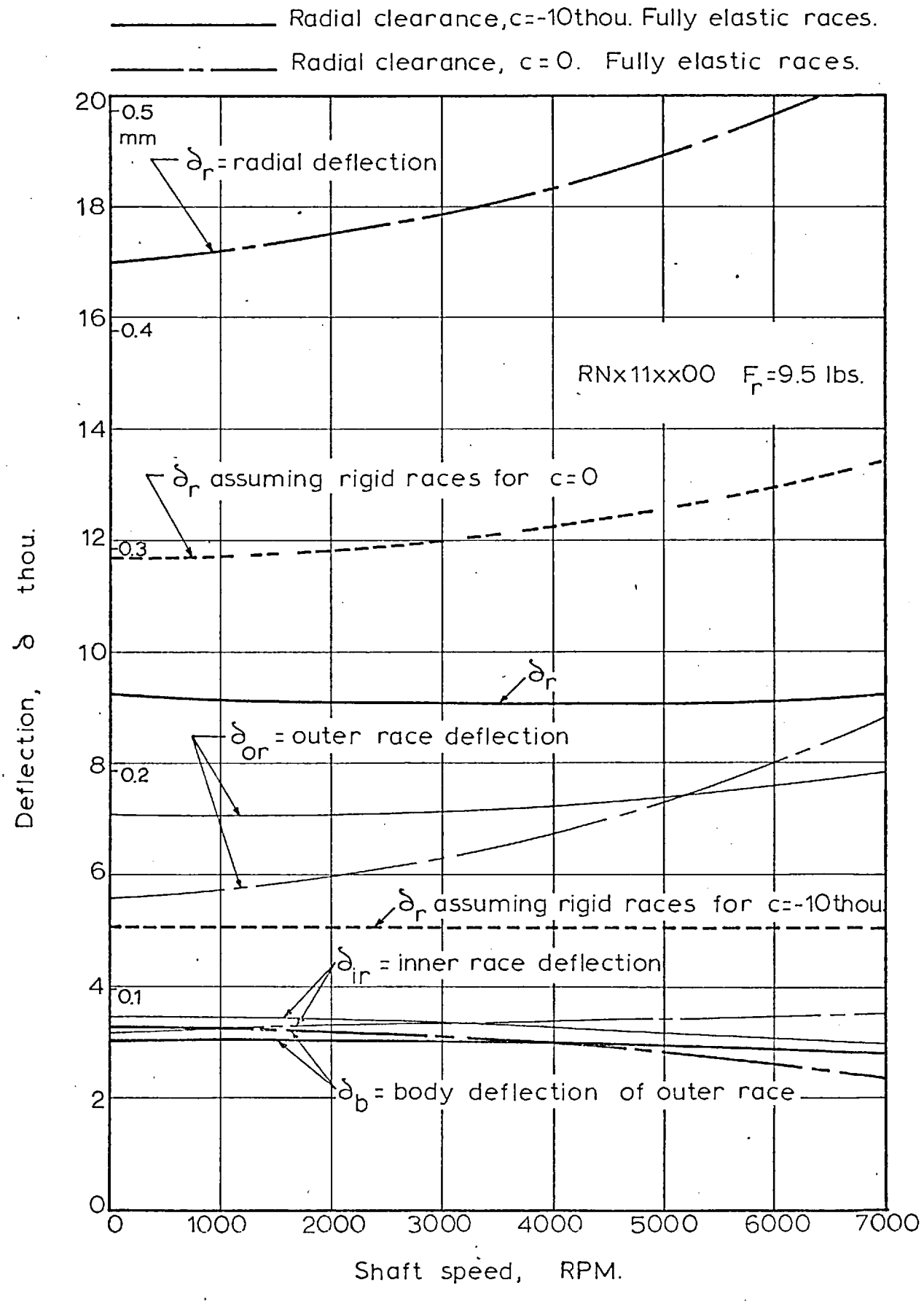


Fig. 6.21 Effect of shaft speed on the non-dimensional equivalent radial load (P_r/F_r) of an Araldite radial roller bearing.

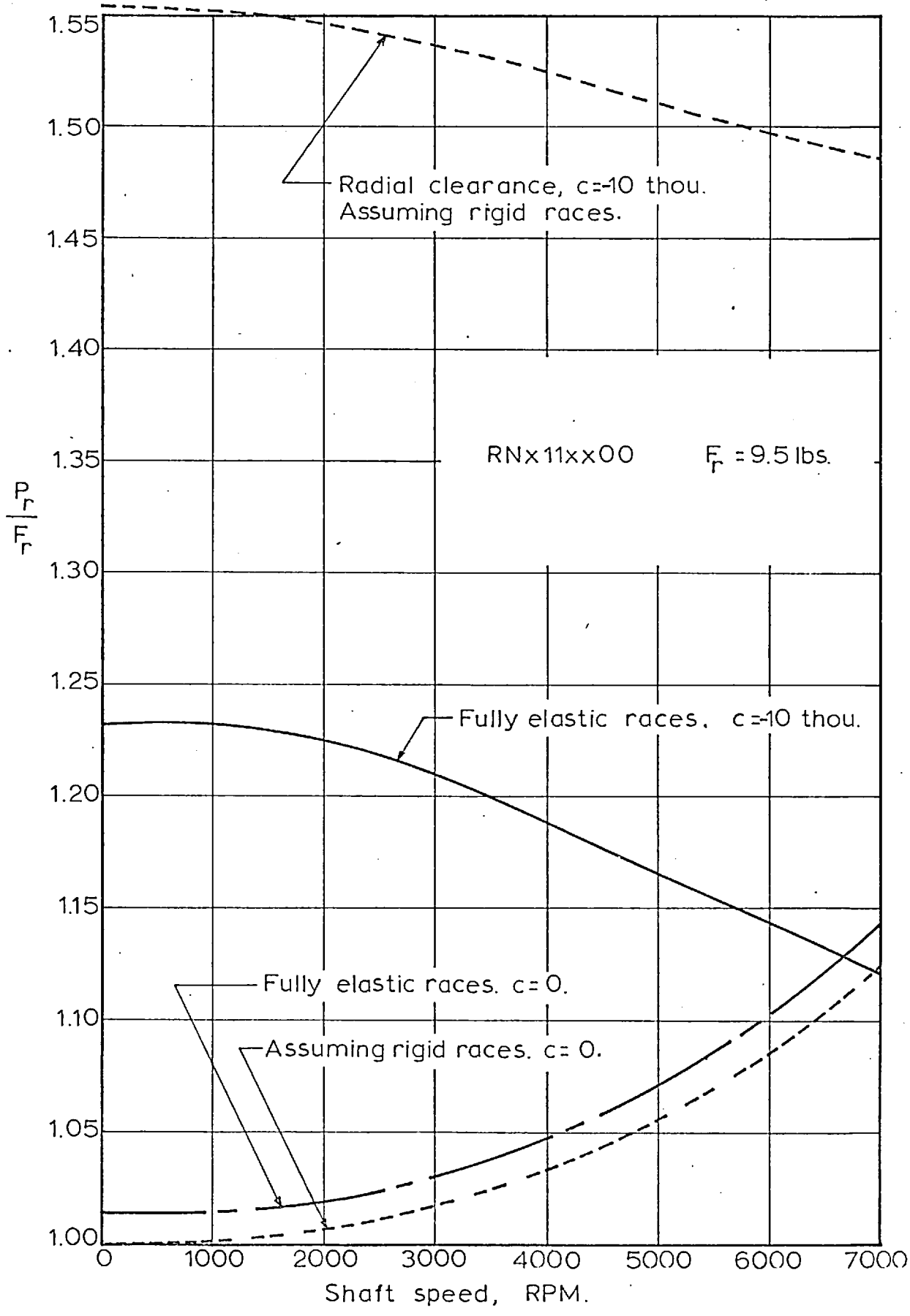


Fig. 6.22 Effect of shaft speed on roller load distribution in an Araldite radial roller bearing having (a) radial clearance c= -0.006 in. and radial load F_r= 4.0 lbs. (b) c= 0 and F_r= 9.5 lbs.

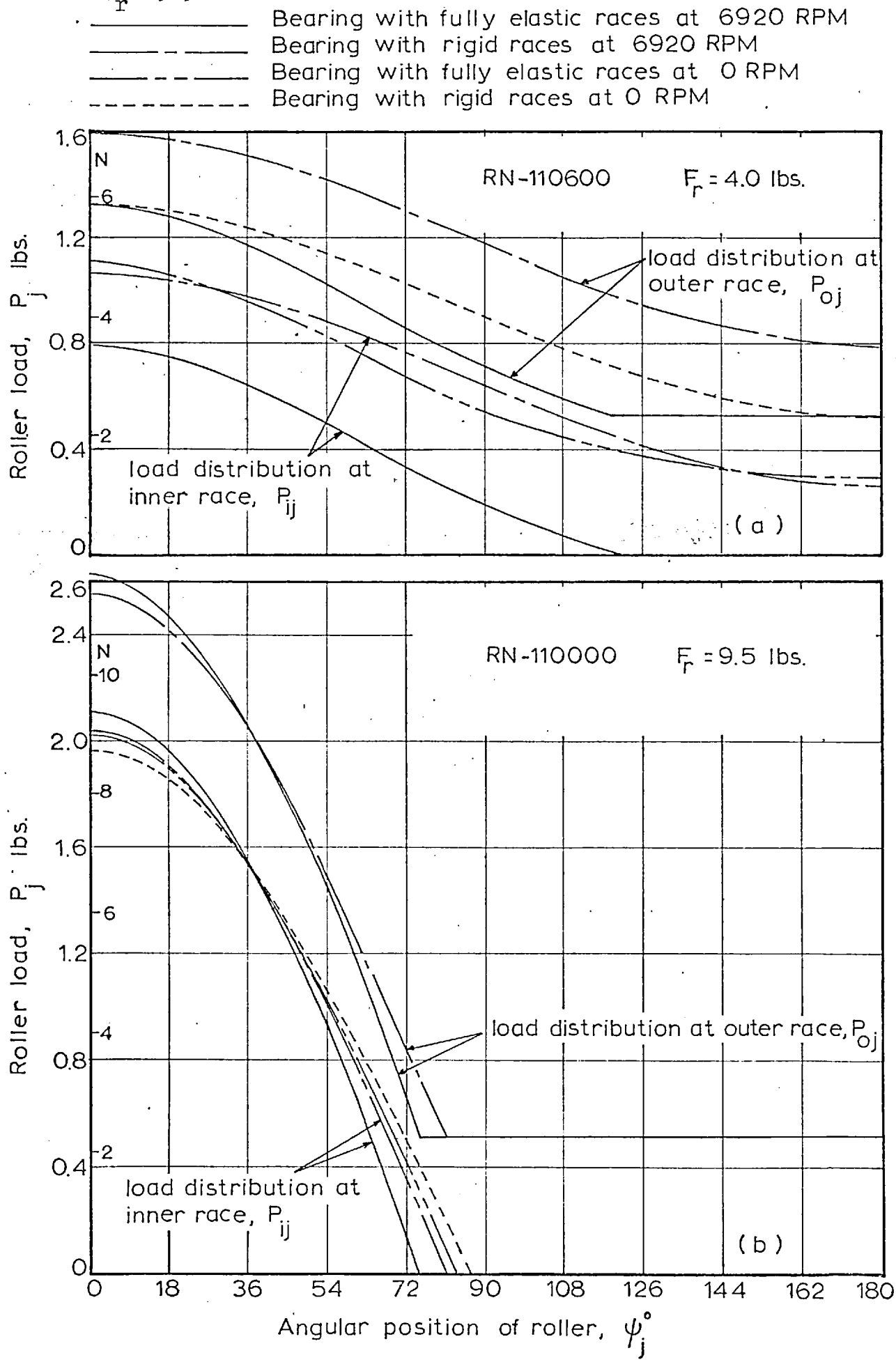


Fig. 6.23 Effect of shaft speed on roller load distribution in an Araldite radial roller bearing having a radial load of 9.5 lbs. and radial clearance (a) c= 0, and (b) c= -0.010in.

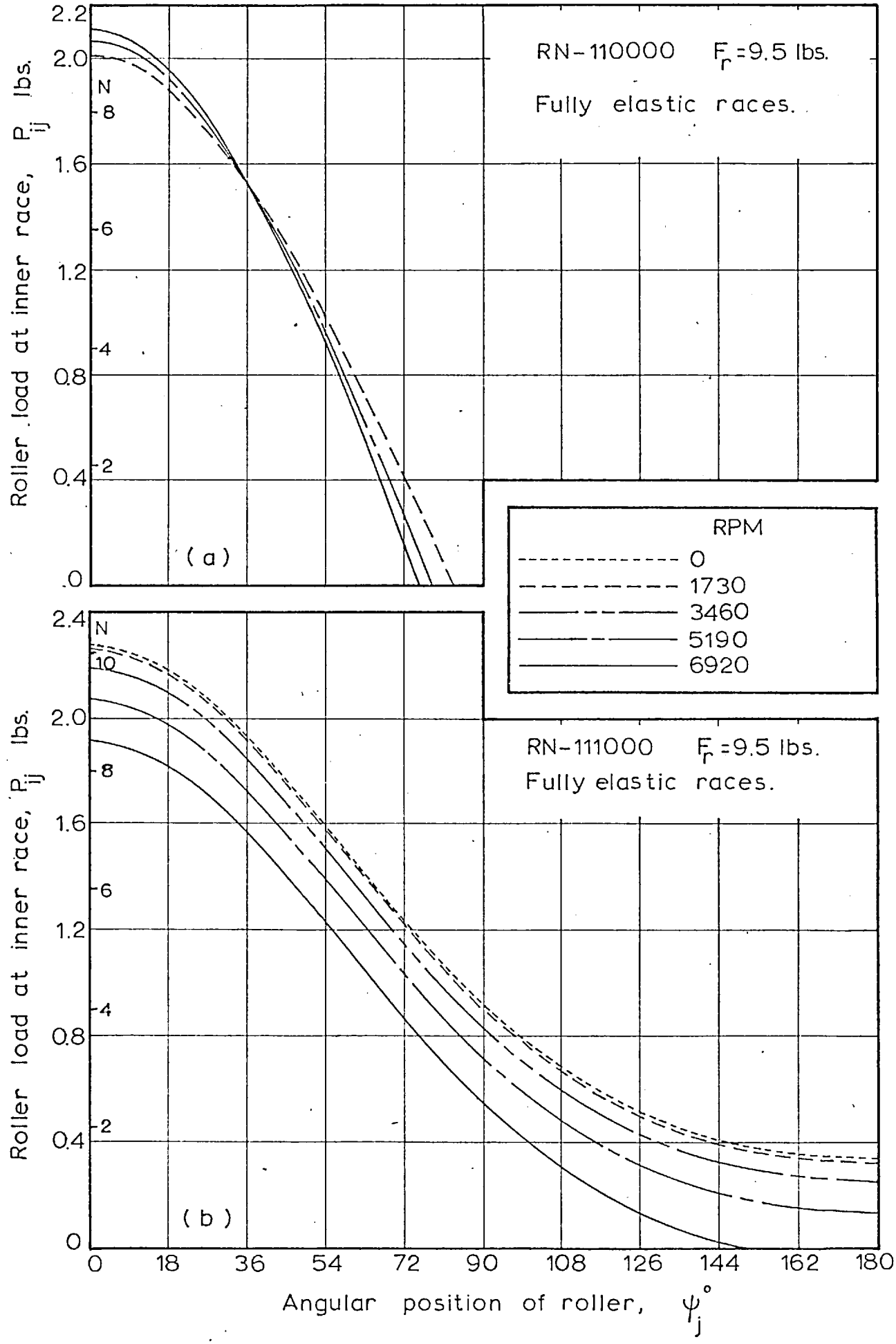


Fig. 6.24 Procedure for obtaining relief in the outer race. (a) Tri-lobed relief, and (b) bi-lobed relief.

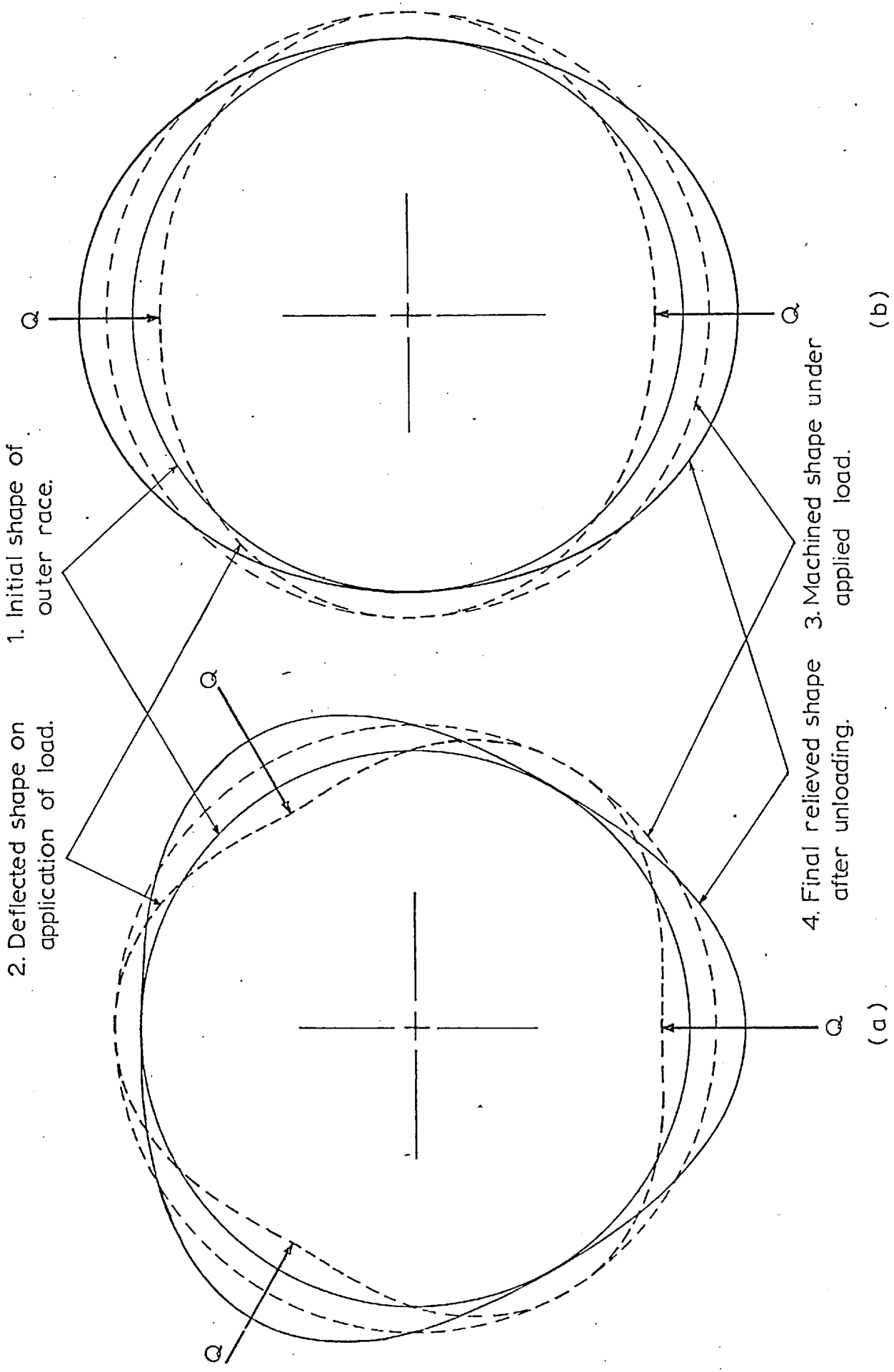


Fig. 6.25 Effect of the amplitude of outer race relief on the radial deflection (δ_r) and non-dimensional equivalent radial load (P_r/F_r) of an Araldite radial roller bearing.

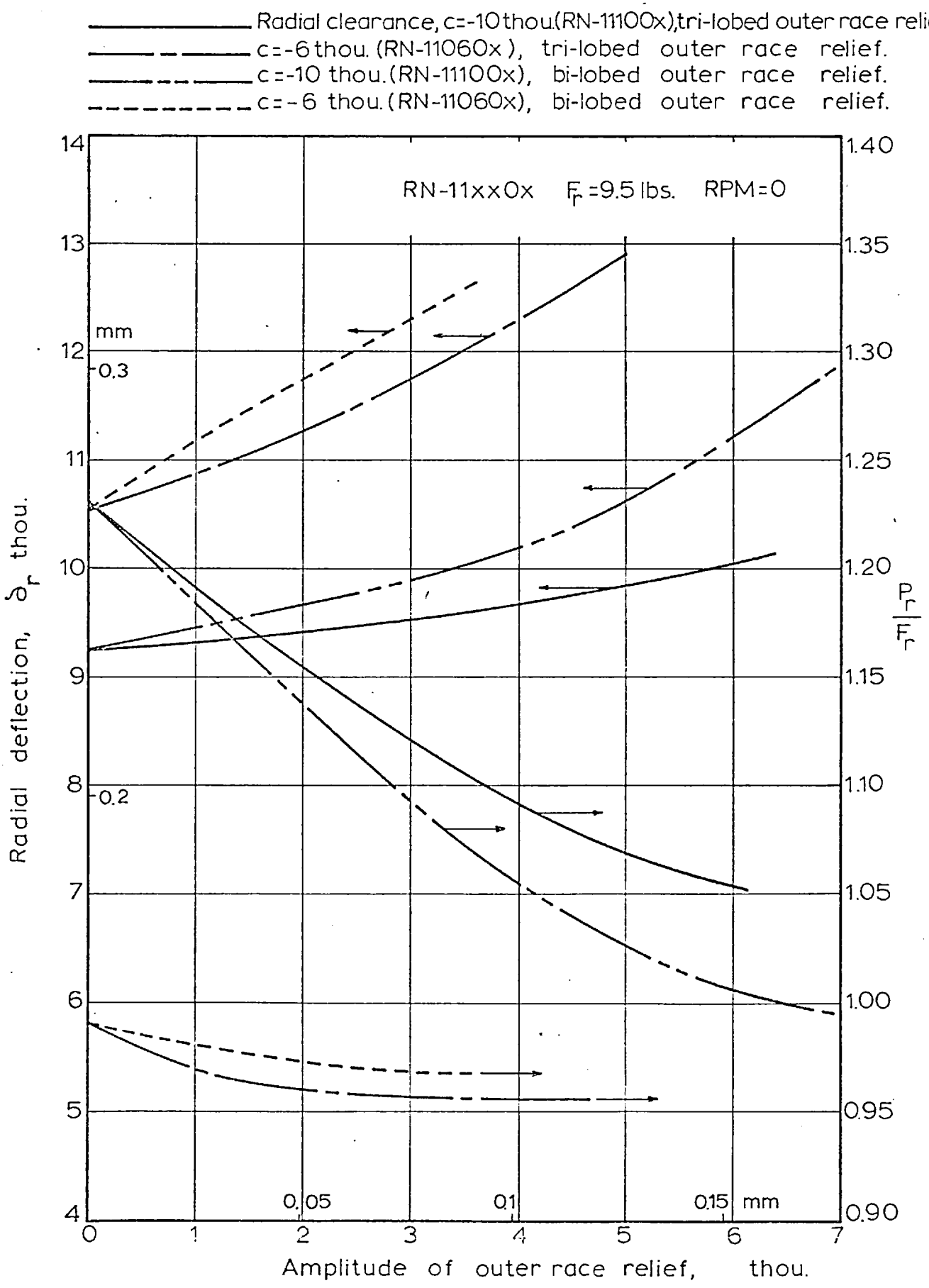


Fig. 6.26 Comparison between Araldite radial roller bearings having preload and relieved outer race and bearings having only preload, on the basis of non-dimensional decrease in radial deflection and equivalent radial load.

Subscript 'A' stands for bearing with fully elastic races having zero clearance and no relief (RN-110000), and 'B' for the following bearing with fully elastic races :

——— RN-110602, outer race relief is tri-lobed.
——— - ——— RN-110602, outer race relief is bi-lobed.
——— — ——— RN-110600.
— — — — — RN-110400.

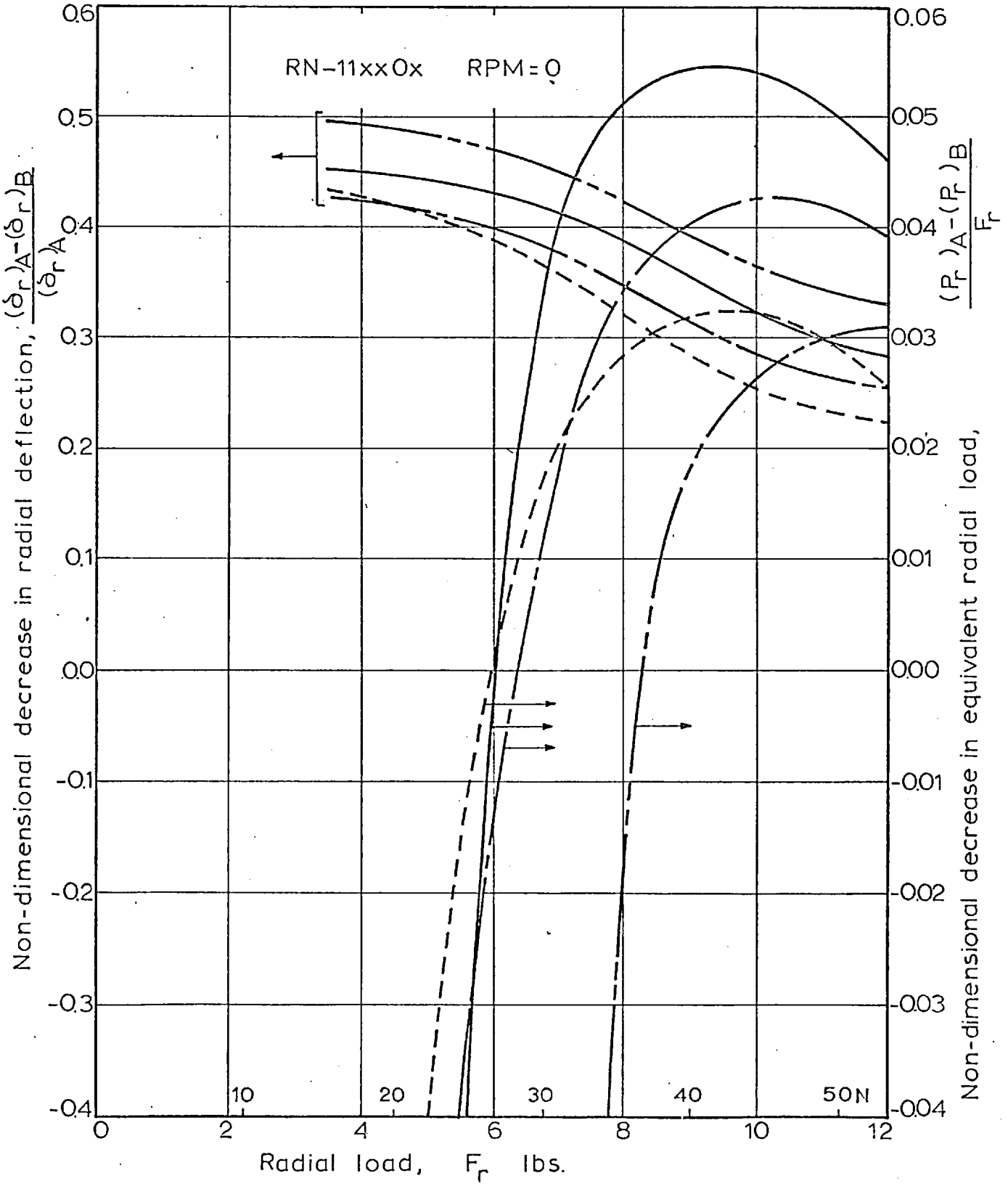


Fig. 6.27 Non-dimensional decrease in radial deflection and equivalent radial load for Araldite radial roller bearings having different radial clearances and amplitude of outer race relief.

Subscript 'A' stands for bearing with fully elastic races having zero clearance and no relief (RN-110000), and 'B' for the following bearing with fully elastic races:

——————— RN-111005, outer race relief is tri-lobed.
——— — ——— RN-111003, outer race relief is tri-lobed.
——— -- ——— RN-110002, outer race relief is tri-lobed.
— — — — — — RN-111003, outer race relief is bi-lobed.
..... RN-110001, outer race relief is bi-lobed.

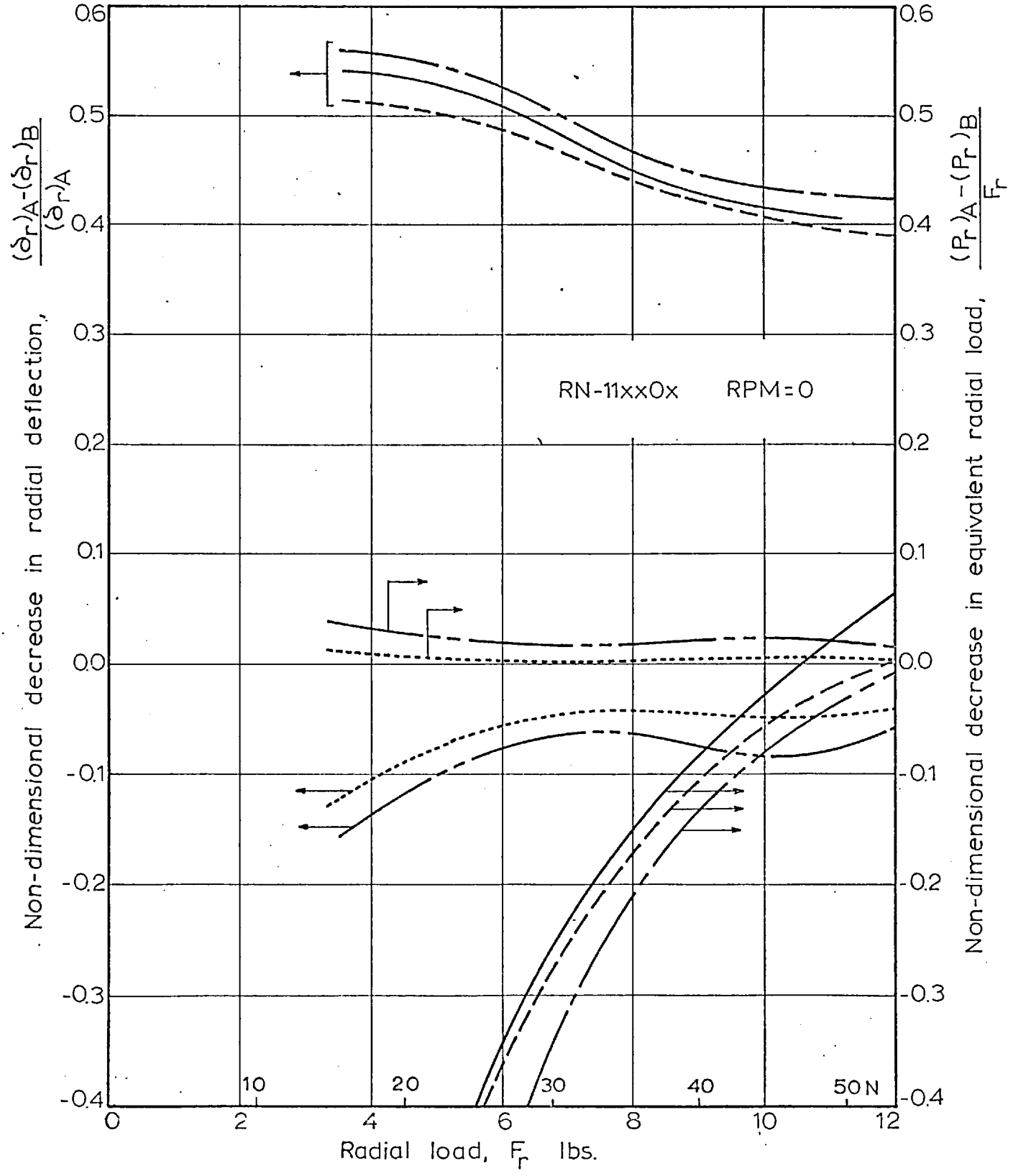


Fig. 6.28 Roller load distribution in (a) three Araldite roller bearings having radial clearance c= -0.006 in., one with no outer race relief and the other two with tri-lobed and bi-lobed outer race relief (amplitude 0.003 in.), (b) a bearing having c= -0.010 in. and tri-lobed outer race relief (amplitude 0.005in.) at different radial loads.

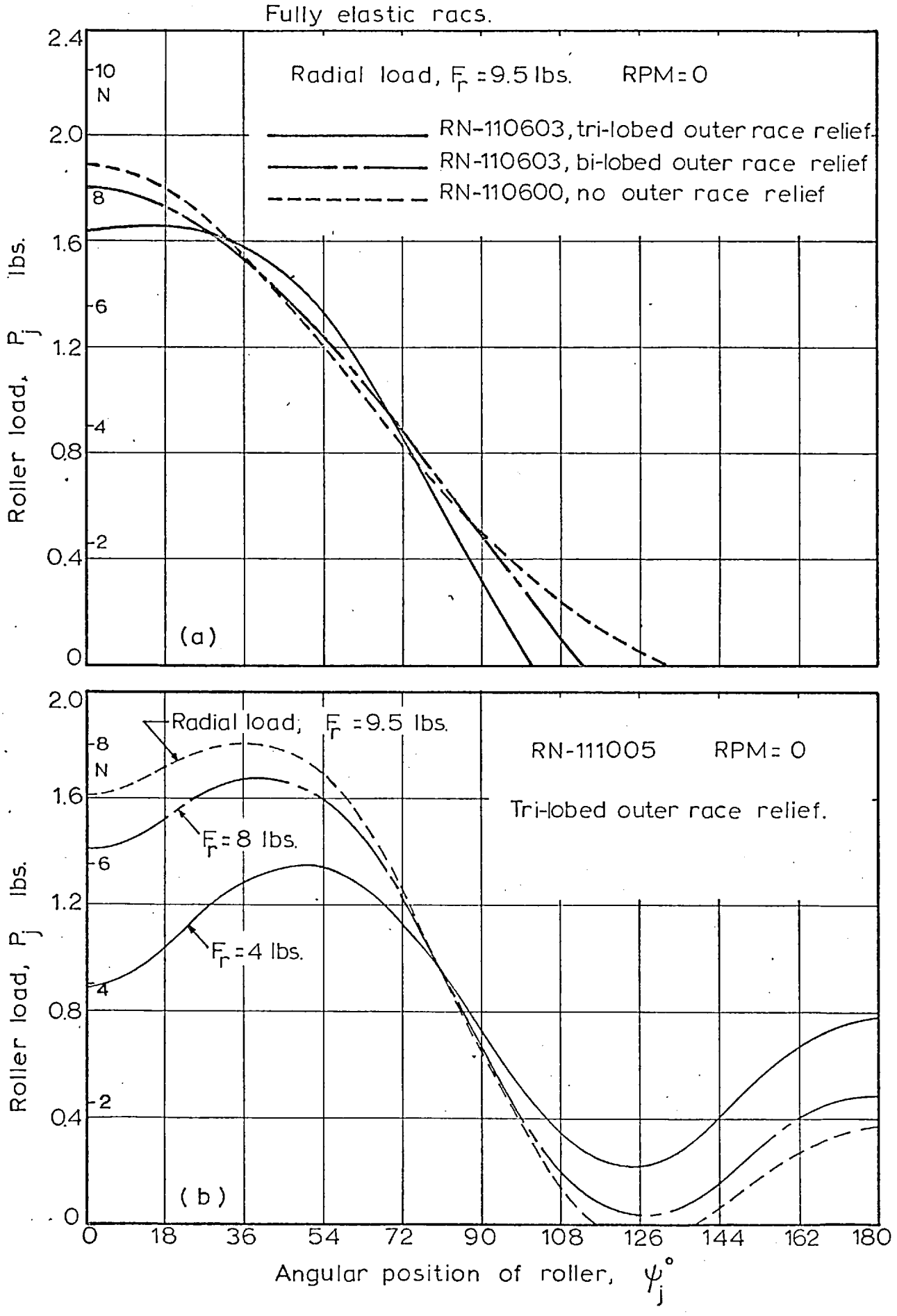


Fig. 6.29 Comparison of roller load distribution between Araldite radial bearings having (a) tri-lobed, (b) bi-lobed outer race relief (amplitude 0.002in.) and bearing having no outer race relief. All the bearings have radial clearance c= -0.006 in.

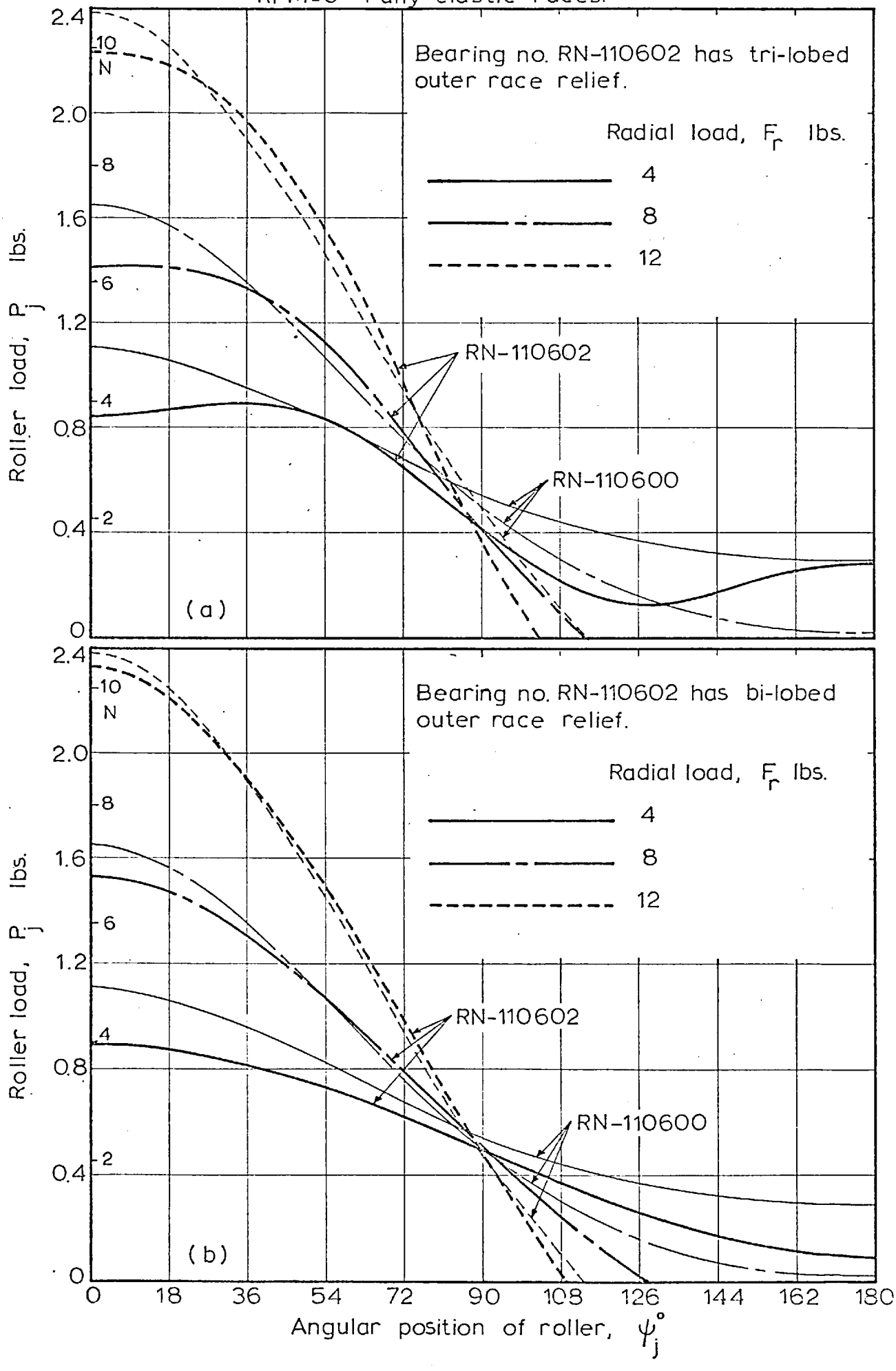
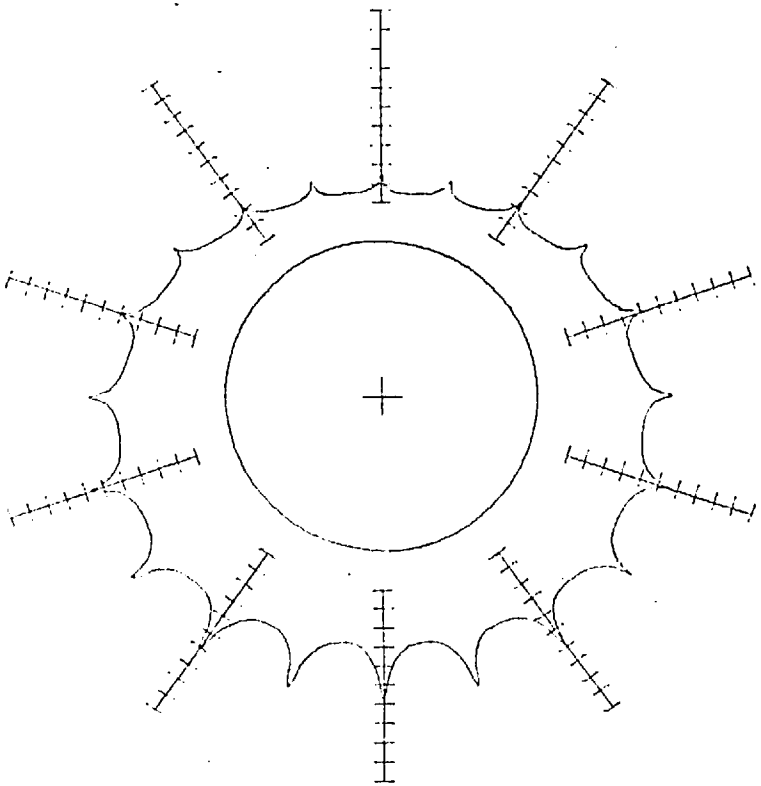


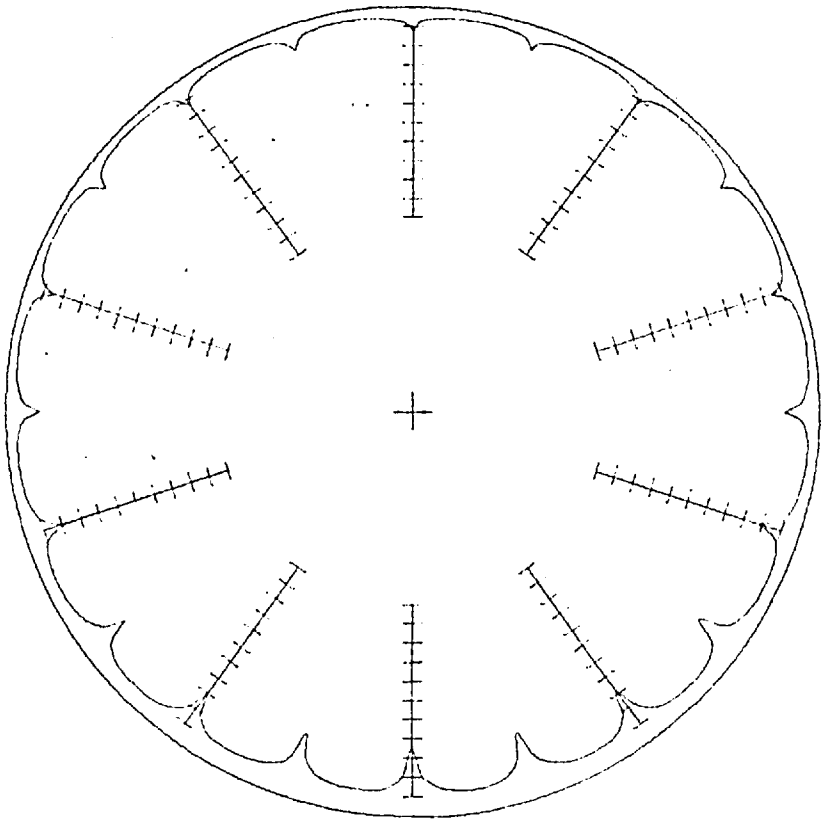
Fig. 6.30 Deflected shapes of the races of an Araldite radial roller bearing having radial clearance c= -0.006 in. and radial load F_r= 4.0 lbs.



OUTER RACE

ONE DIV REPRESENTS .50 THOU

BEARING NO RN--110500 LOAD= 4.0 LBS RPM= 0



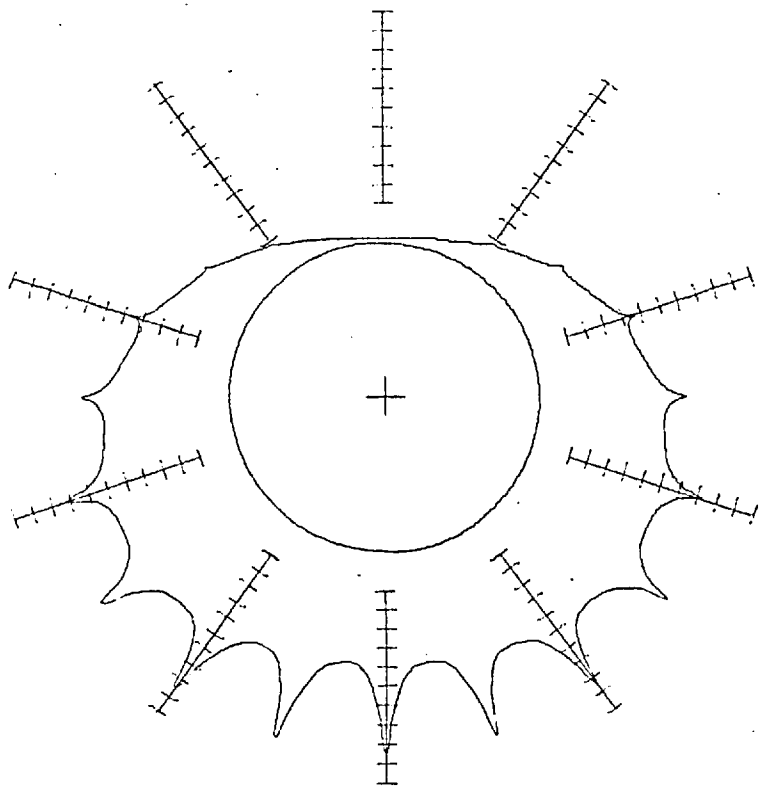
INNER RACE

ONE DIV REPRESENTS .50 THOU

BEARING NO RN -110500 LOAD= 4.0 LBS RPM= 0

Fig. 6.30

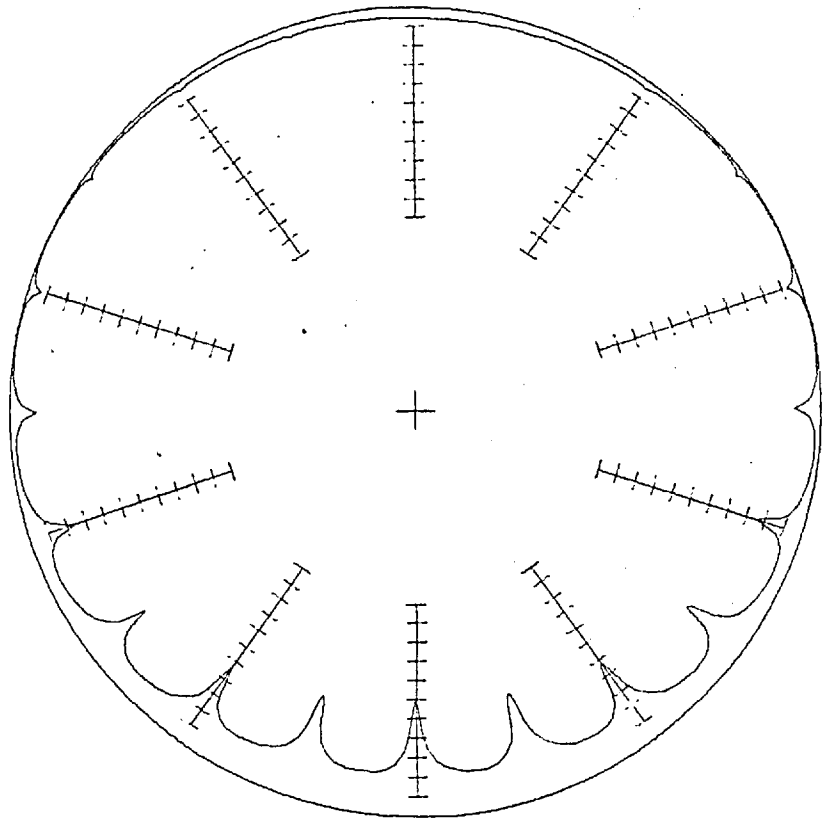
Fig. 6.31 Deflected shapes of the races of an Araldite radial roller bearing having radial clearance c= -0.006 in. and radial load F_r = 9.5 lbs.



OUTER RACE

ONE DIV REPRESENTS .50 THOU

BEARING NO RN -110600 LOAD: 9.5 LBS RPM= 0



INNER RACE

ONE DIV REPRESENTS .50 THOU

BEARING NO RN -110600 LOAD: 9.5 LBS RPM= 0

Fig. 6.31

Fig. 6.32 Deflected shapes of the races of an Araldite radial roller bearing having radial clearance c= 0.0 in. and radial load F_r= 9.5 lbs.

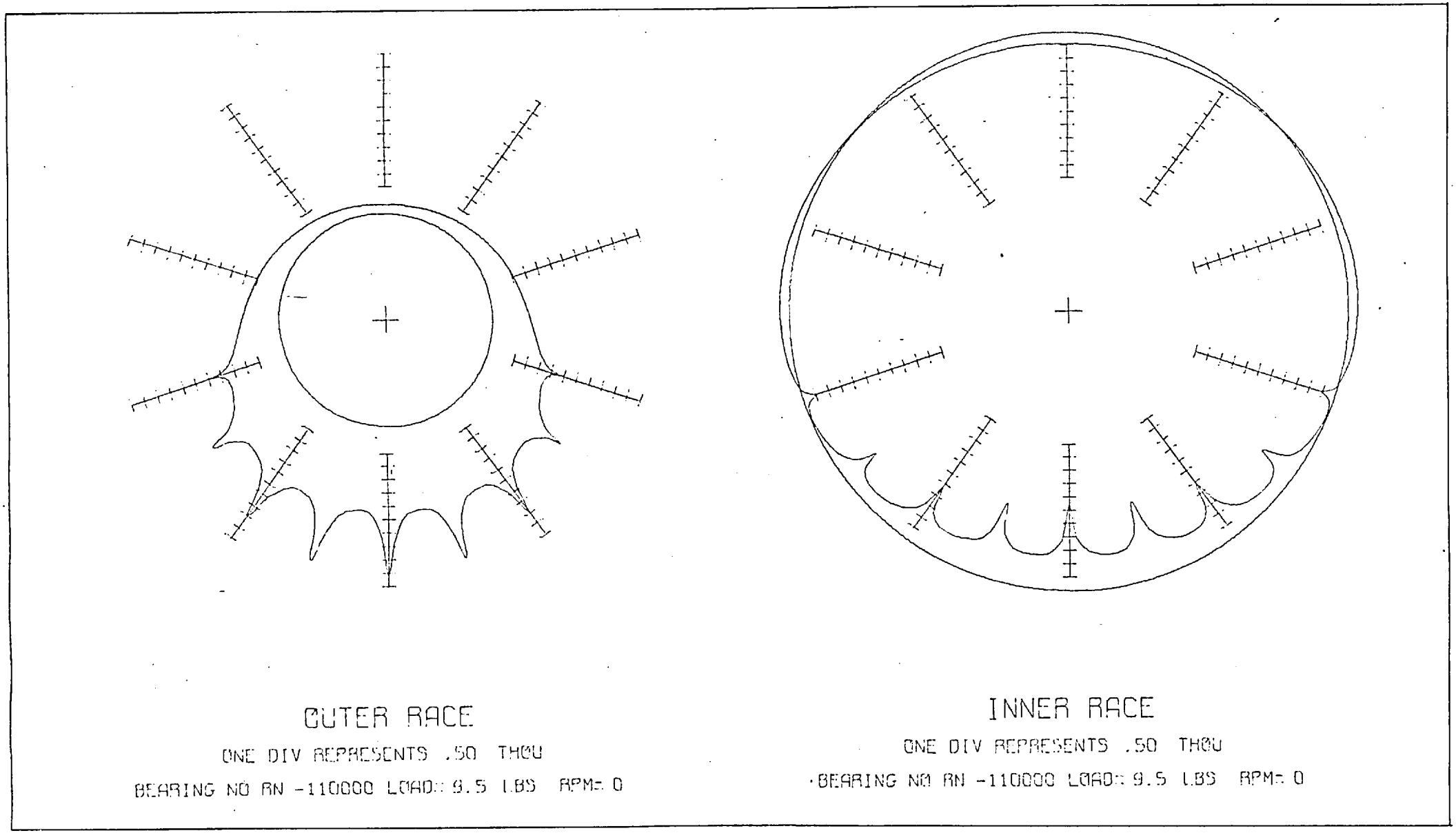
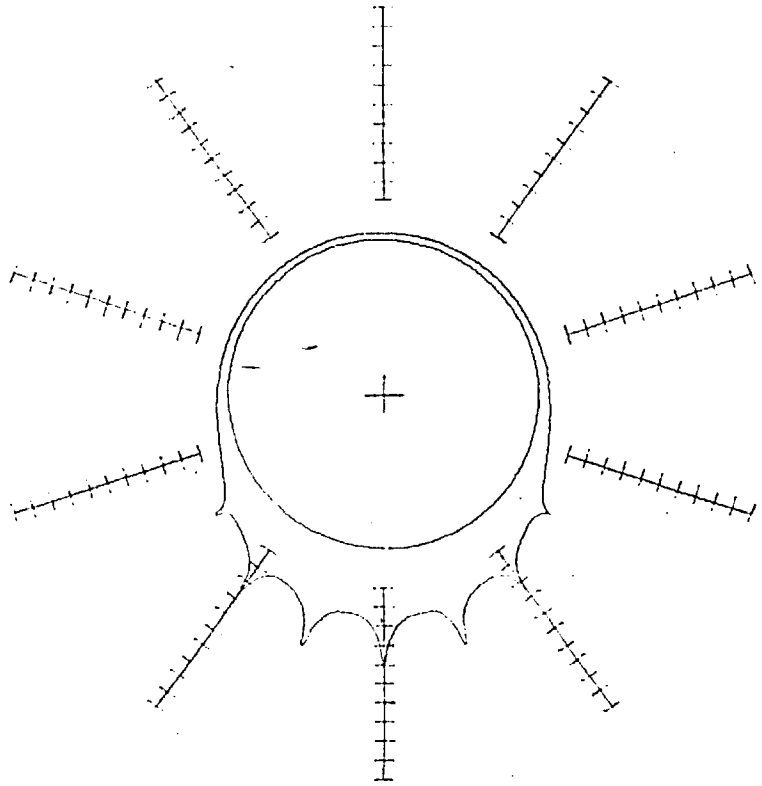


Fig. 6.32

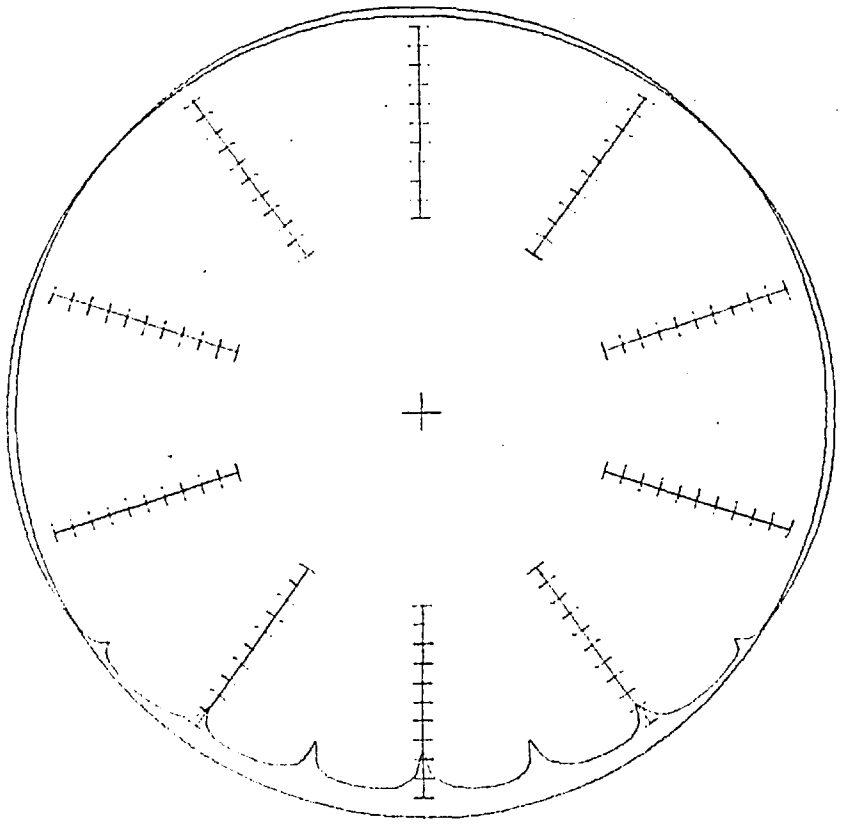
Fig. 6.33 Deflected shapes of the races of an Araldite radial roller bearing having radial clearance c=+0.003 in. and radial load F_r= 4.0 lbs.



OUTER RACE

ONE DIV REPRESENTS .50 THOU

BEARING NO RN 110300 LOAD: 4.0 LBS RPM= 0



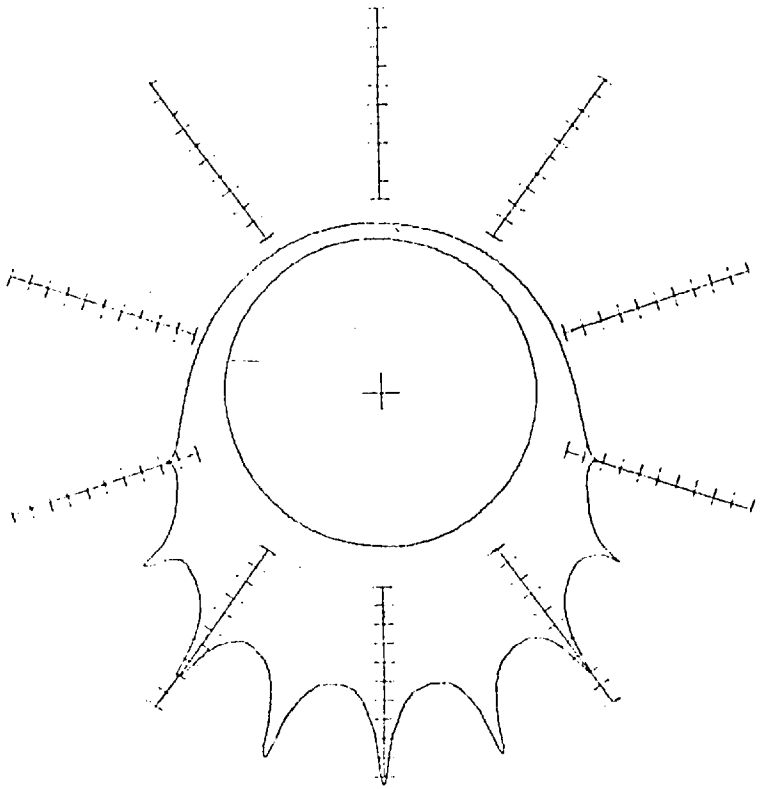
INNER RACE

ONE DIV REPRESENTS .50 THOU

BEARING NO RN 110300 LOAD: 4.0 LBS RPM= 0

Fig. 6.33

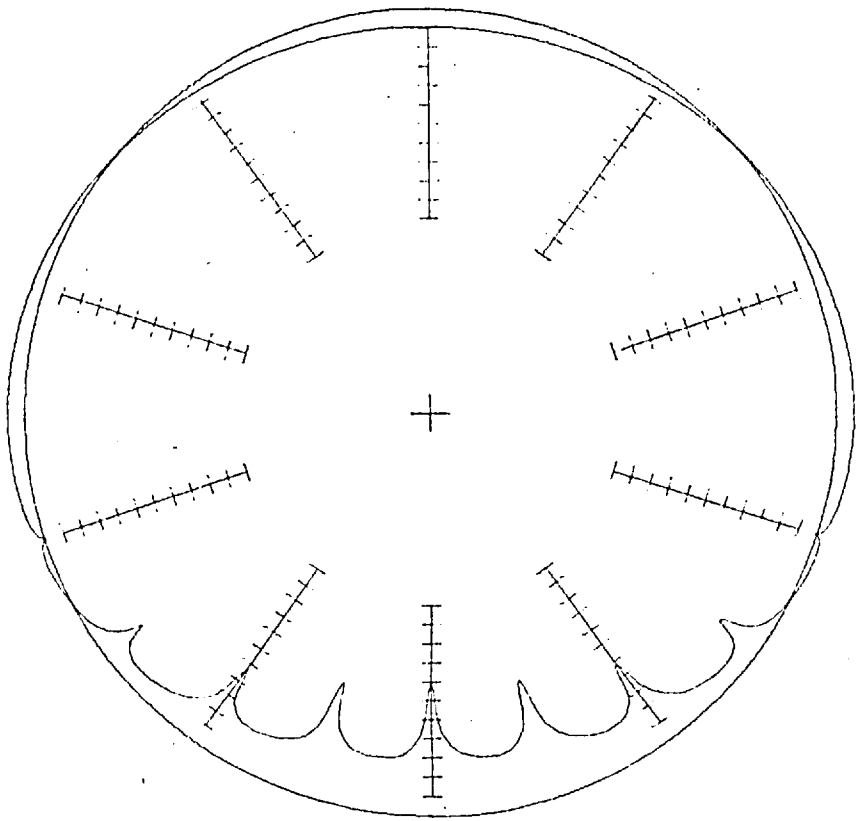
Fig. 6.34 Deflected shapes of the races of an Araldite radial roller bearing having radial clearance c= +0.003 in. and radial load F_r= 9.5 lbs.



OUTER RACE

ONE DIV REPRESENTS .50 THOU

BEARING NO BN 110300 LOAD: 9.5 LBS RPM= 0



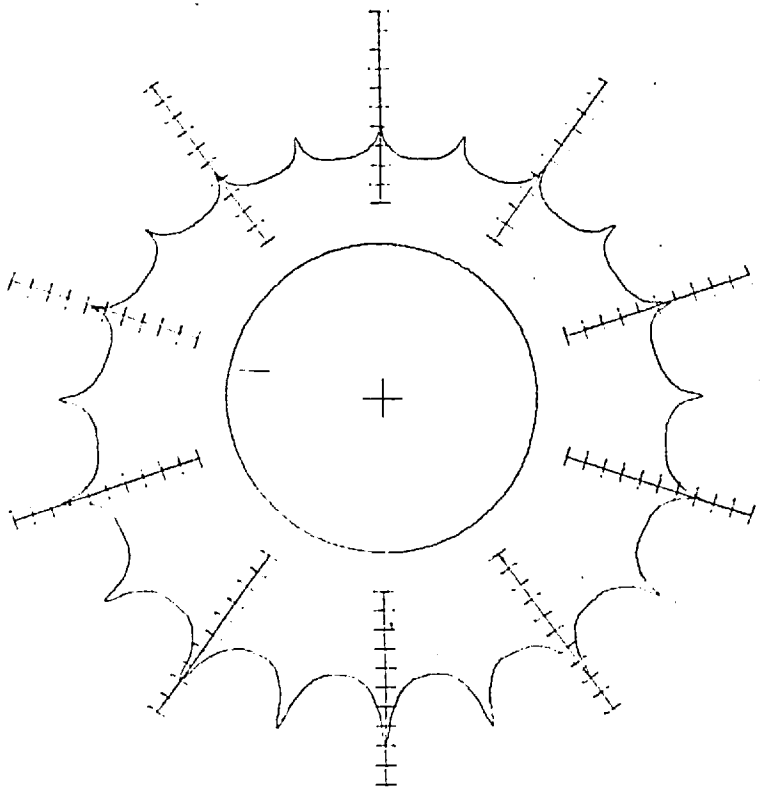
INNER RACE

ONE DIV REPRESENTS .50 THOU

BEARING NO BN 110300 LOAD: 9.5 LBS RPM= 0

Fig. 6.34

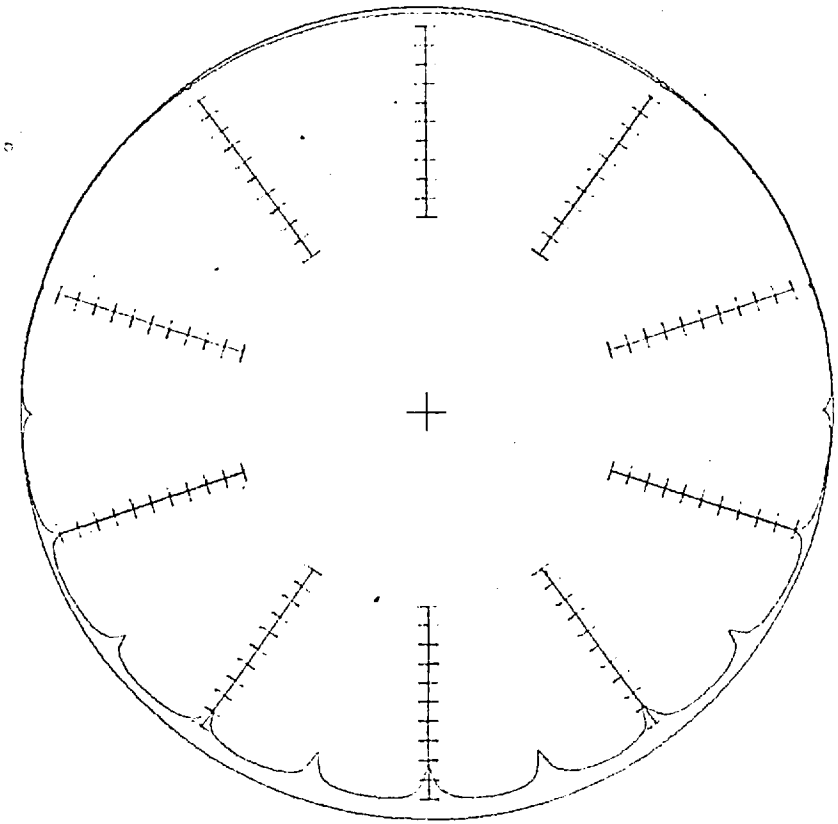
Fig. 6.35 Deflected shapes of the races of an Araldite radial roller bearing having radial clearance c= -0.006 in. and radial load F_r = 4.0 lbs. Shaft speed is 6920 R.P.M.



OUTER RACE

ONE DIV REPRESENTS .50 THOU

BEARING NO RN -110600 LOAD= 4.0 LBS RPM= 6920



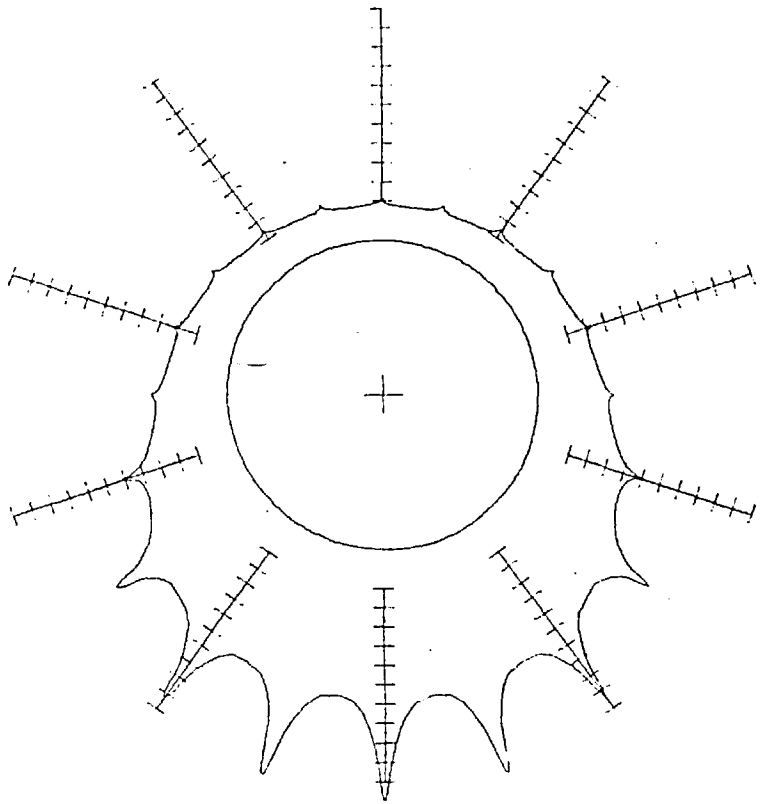
INNER RACE

ONE DIV REPRESENTS .50 THOU

BEARING NO RN -110600 LOAD= 4.0 LBS RPM= 6920

Fig. 6.35

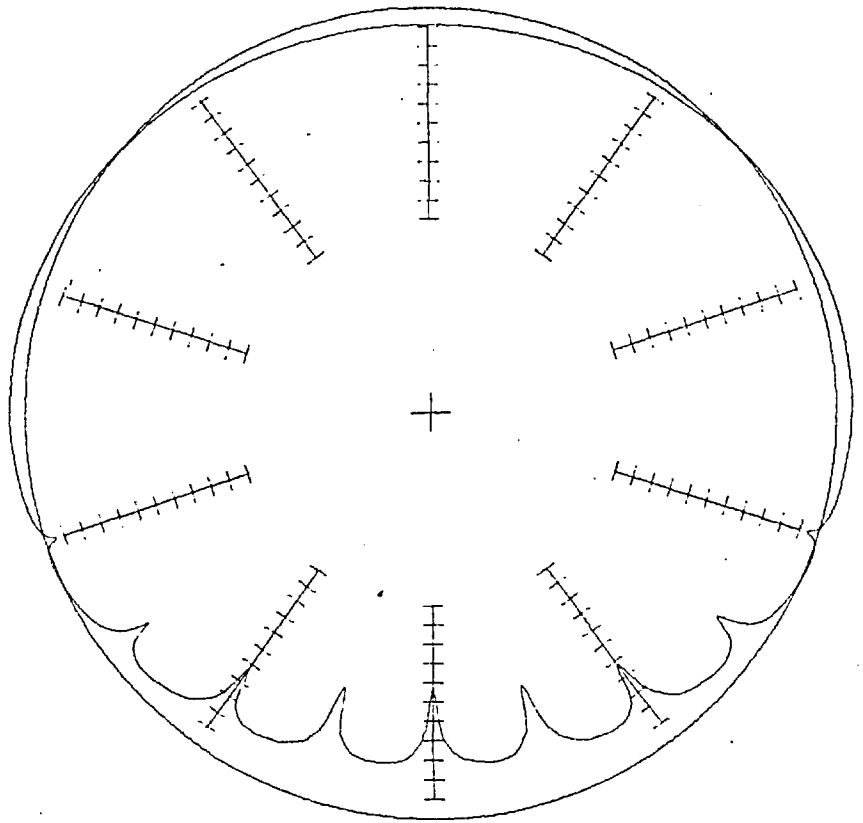
Fig. 6.36 Deflected shapes of the races of an Araldite radial roller bearing having radial clearance c= 0.0 in. and radial load F_r= 9.5 lbs. Shaft speed is 3460 R.P.M.



OUTER RACE

ONE DIV REPRESENTS .50 THOU

BEARING NO RN -110000 LOAD= 9.5 LBS RPM=3460



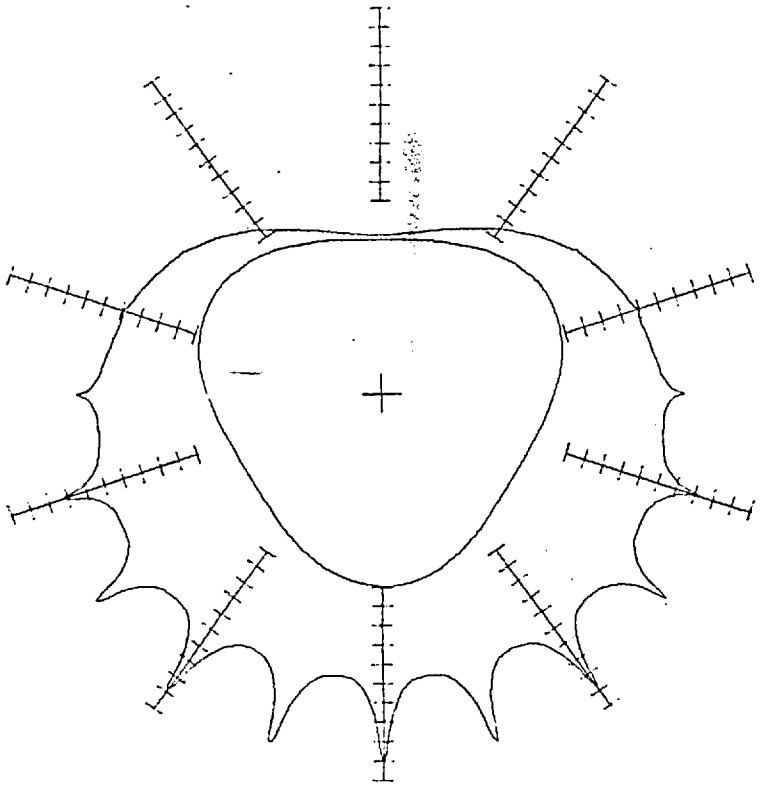
INNER RACE

ONE DIV REPRESENTS .50 THOU

BEARING NO RN -110000 LOAD= 9.5 LBS RPM=3460

Fig. 6.36

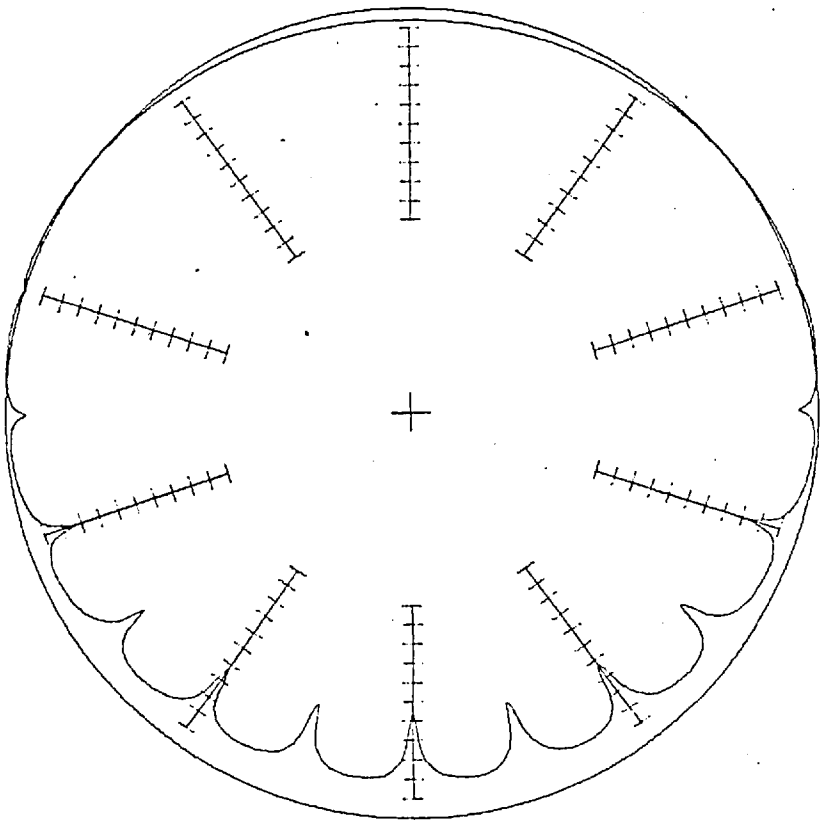
Fig. 6.37 Deflected shapes of the races of an Araldite radial roller bearing having radial clearance c= -0.006 in. and radial load F_r= 9.5 lbs. Outer race has tri-lobed relief with amplitude 0.002 in.



OUTER RACE

ONE DIV REPRESENTS 0.50 THOU

BEARING NO RN-110602 LOAD=9.5 LBS RPM=0



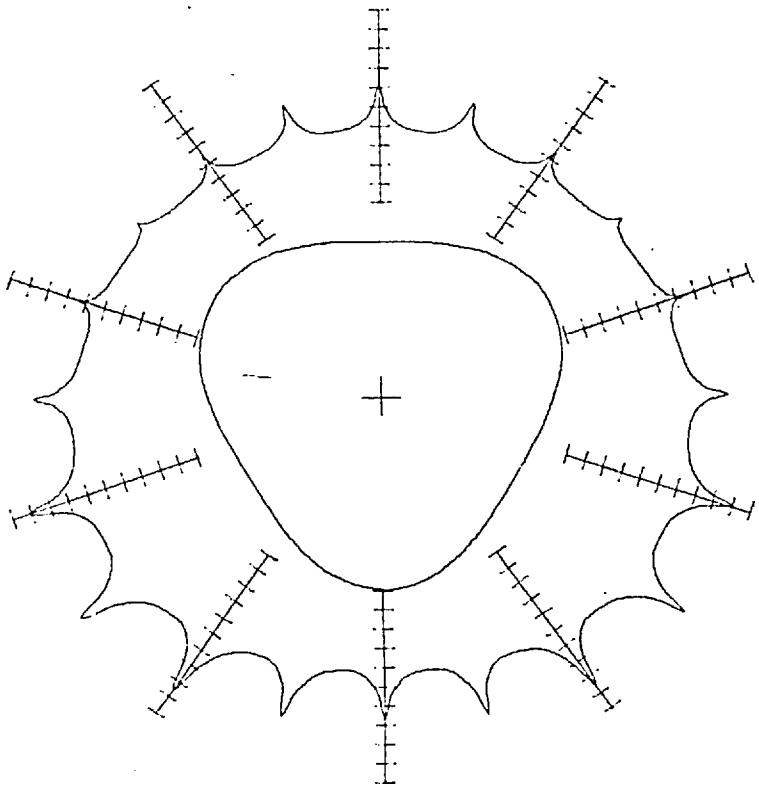
INNER RACE

ONE DIV REPRESENTS 0.50 THOU

BEARING NO RN-110602 LOAD=9.5 LBS RPM=0

Fig. 6.37

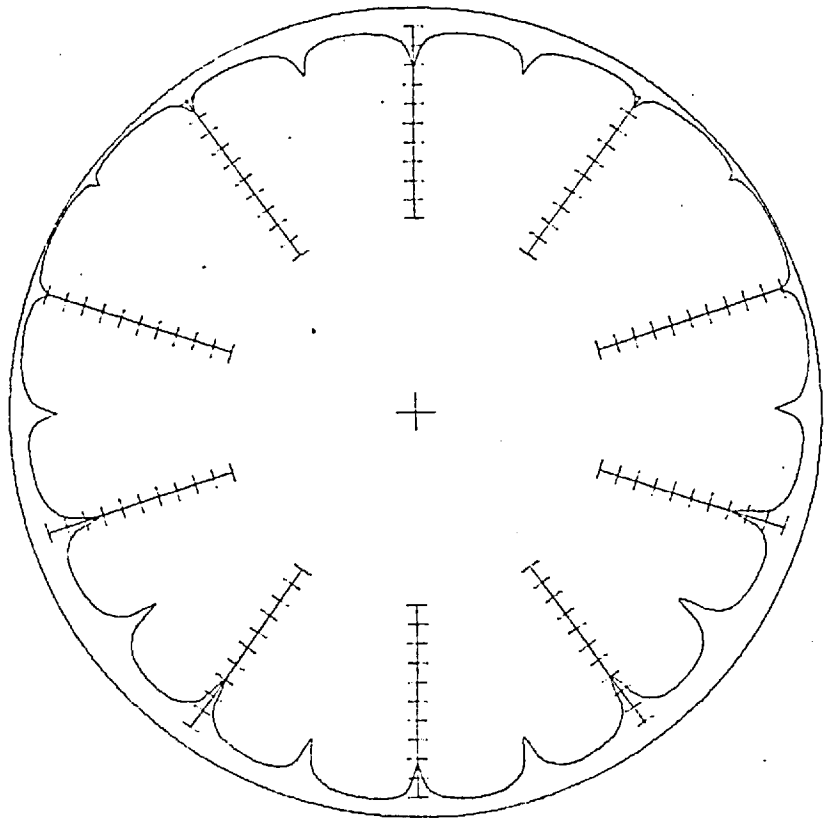
Fig. 6.38 Deflected shapes of the races of an Araldite radial roller bearing having radial clearance c= -0.010 in. and radial load F_r= 4.0 lbs. Outer race has tri-lobed relief with amplitude 0.005 in.



OUTER RACE

ONE DIV REPRESENTS 0.50 THOU

BEARING NO RN-111005 LOAD=4.0 LBS RPM=0



INNER RACE

ONE DIV REPRESENTS 0.50 THOU

BEARING NO RN-111005 LOAD=4.0 LBS RPM=0

Fig. 6.38

Fig. 6.39 Deflected shapes of the races of an Araldite radial roller bearing having radial clearance c= -0.006 in. and radial load F_r= 9.5 lbs. Outer race has bi-lobed relief with amplitude 0.002 in.

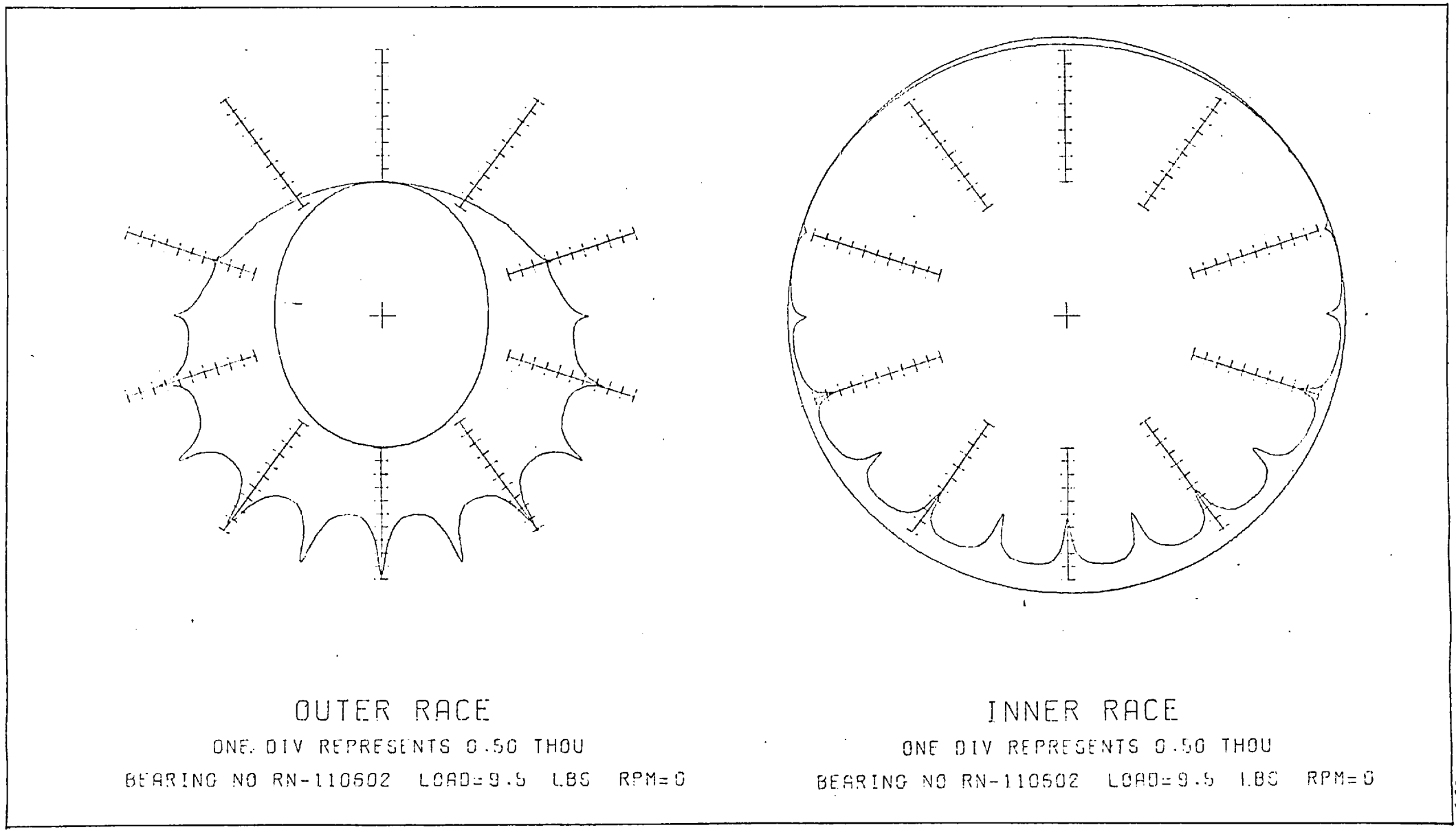


Fig. 6.39

Fig. 7.1 Finite-element mesh for calibration of a steel roller loaded between two flat steel platens.

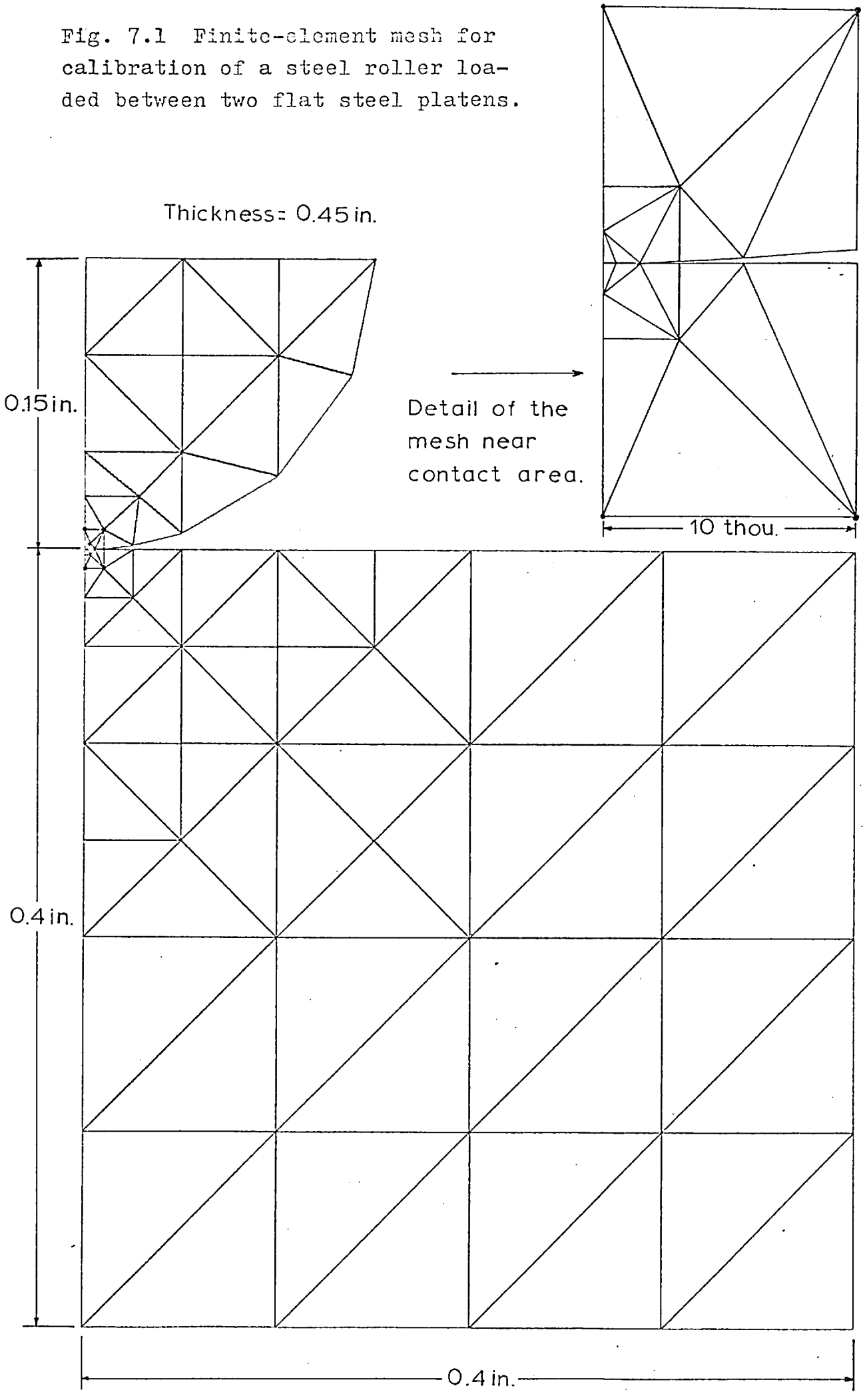


Fig. 7.2 Total deflection given by the approach of two flat steel platens when a steel roller is loaded between them, and also roller and platen deflections as obtained by finite-element method. Comparison of total deflection by finite-element method with different deflection formulae.

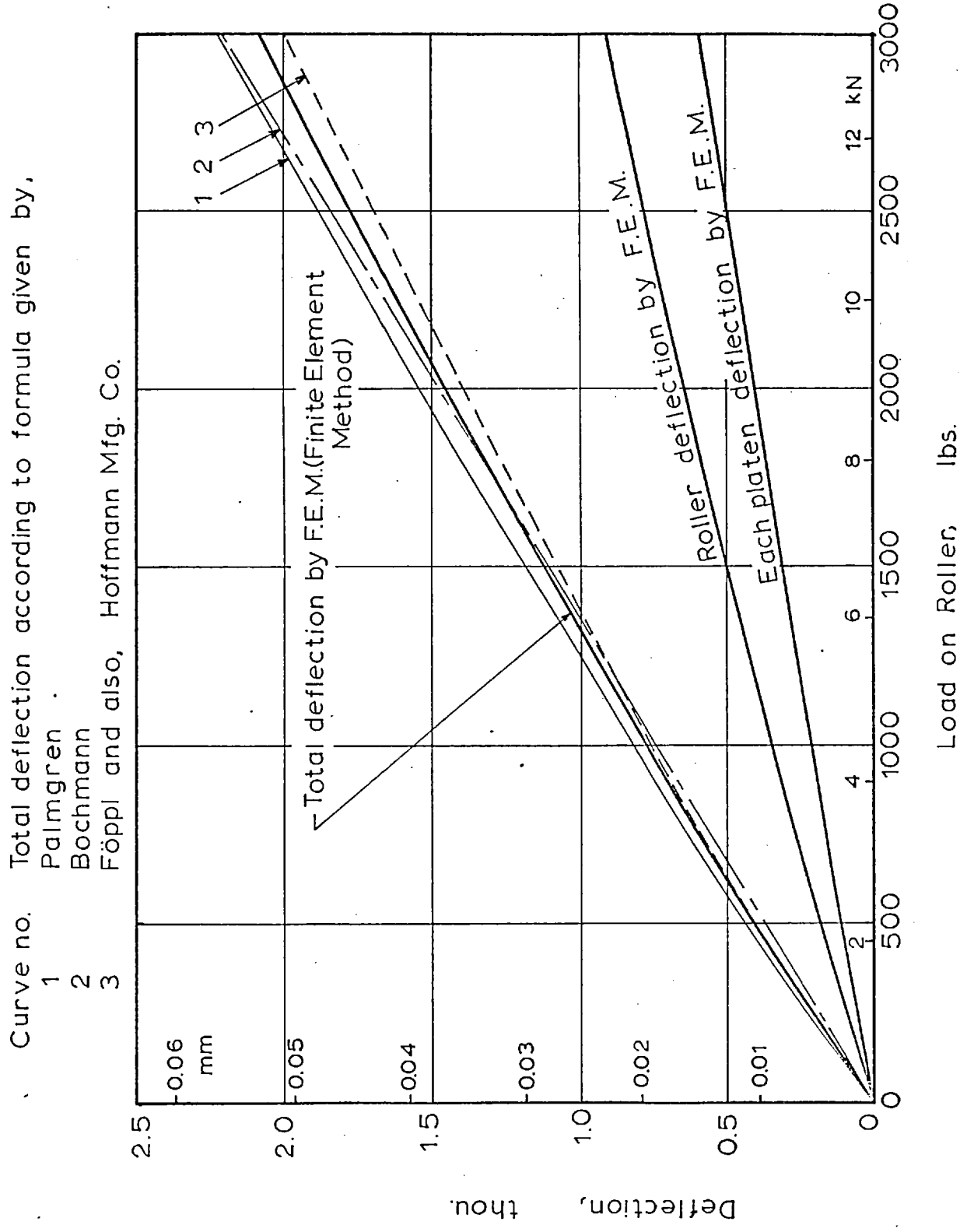


Fig. 7.3 Finite-element mesh for steel radial roller bearing race rings with housing and shaft. Meshes near the contact areas between radial lines a and b on the outer and inner races are shown in the next two pages.

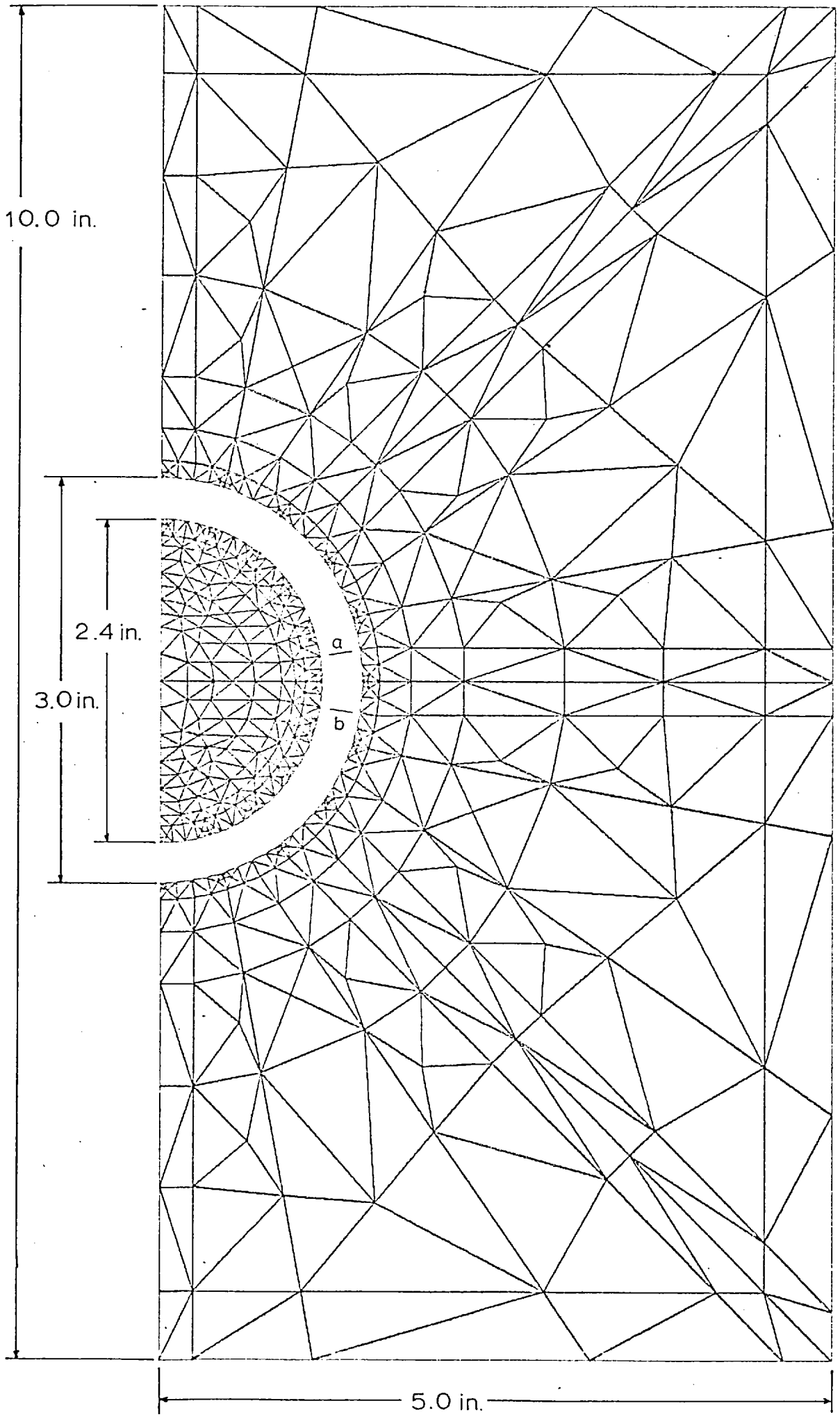


Fig. 7.4 Mesh near a contact area of the outer race between radial lines a and b of fig.7.3 for steel radial roller bearing.

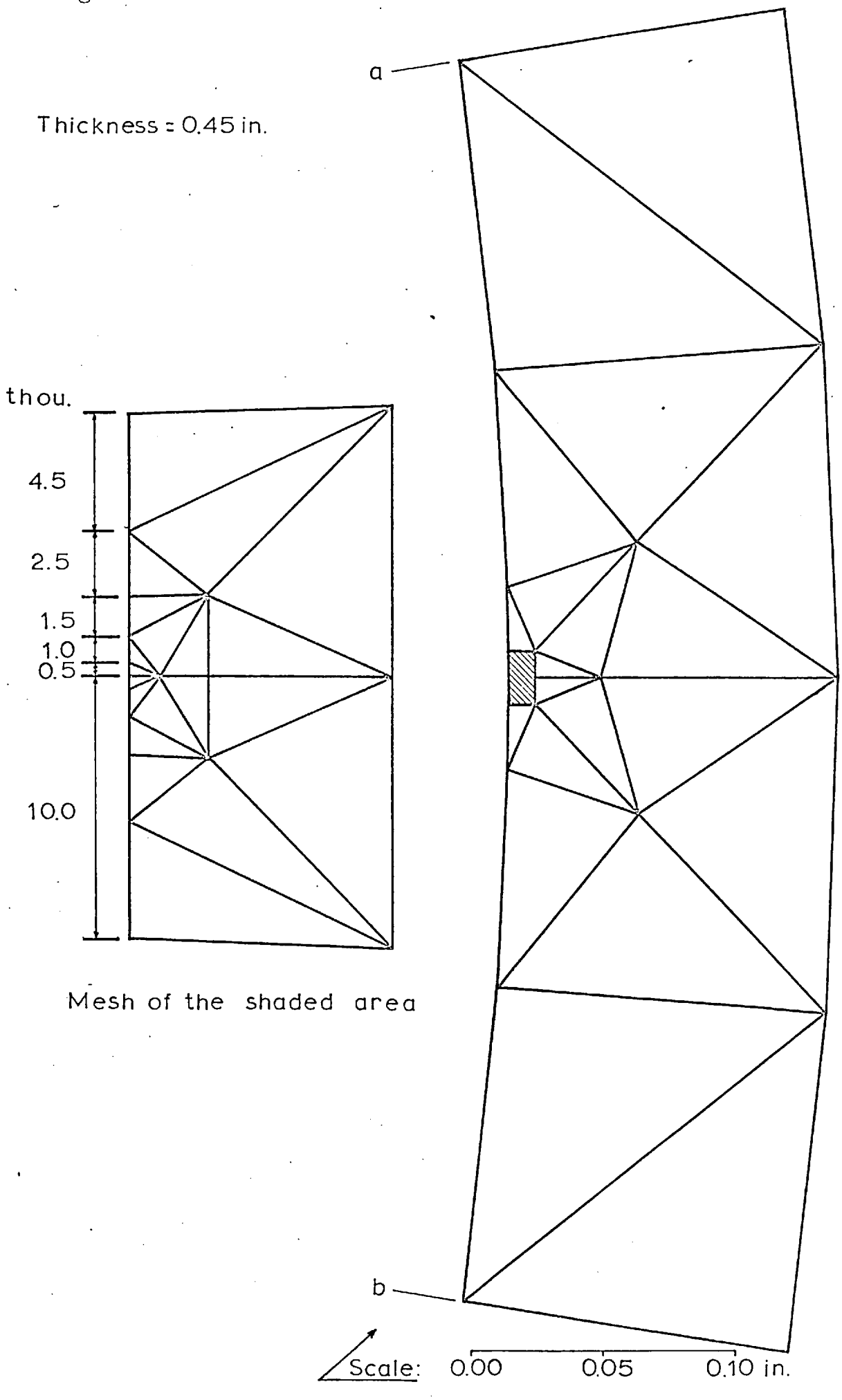


Fig. 7.5 Mesh near a contact area of the inner race between radial lines a and b of fig.7.3 for steel radial roller bearing.

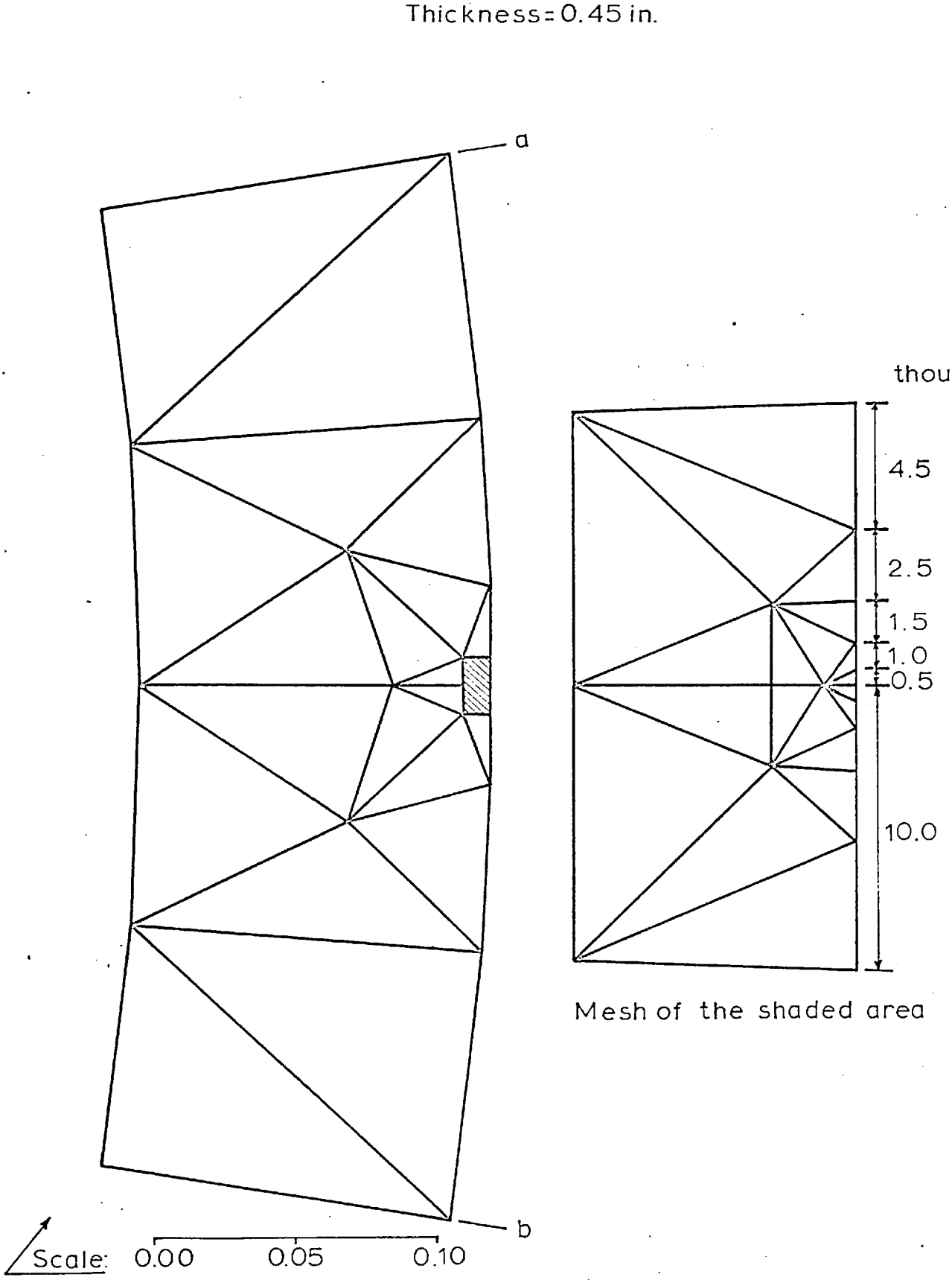


Fig. 7.6 Numbering the regions in the race rings, housing and shaft. Elements within each region have constant elastic properties, thickness and body force per unit volume.

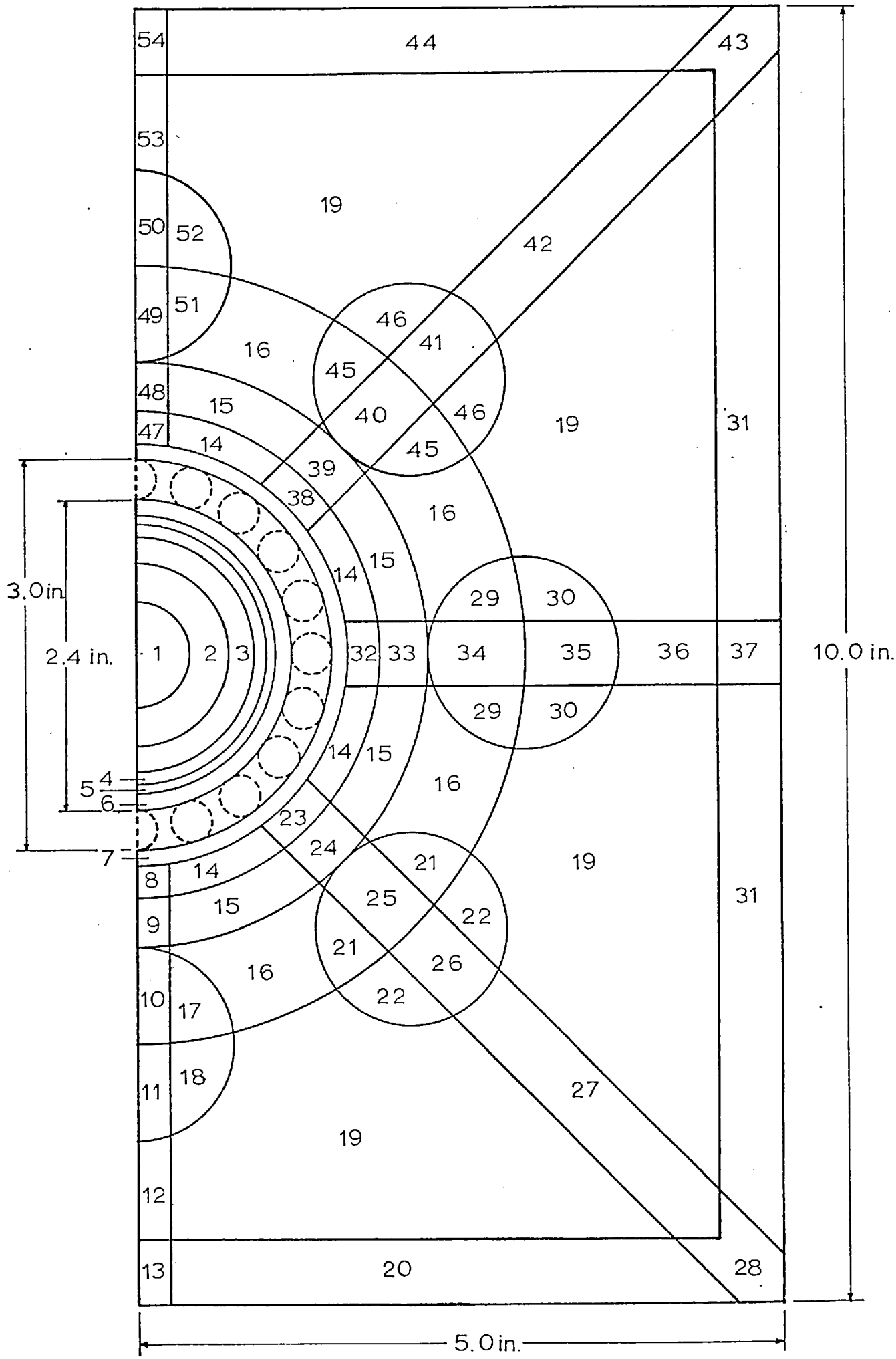


Fig. 7.7 Percentage change of bearing total radial and component deflections, and equivalent radial load vs. the ratio of the thickness of outer race shear area to the length of the rollers.

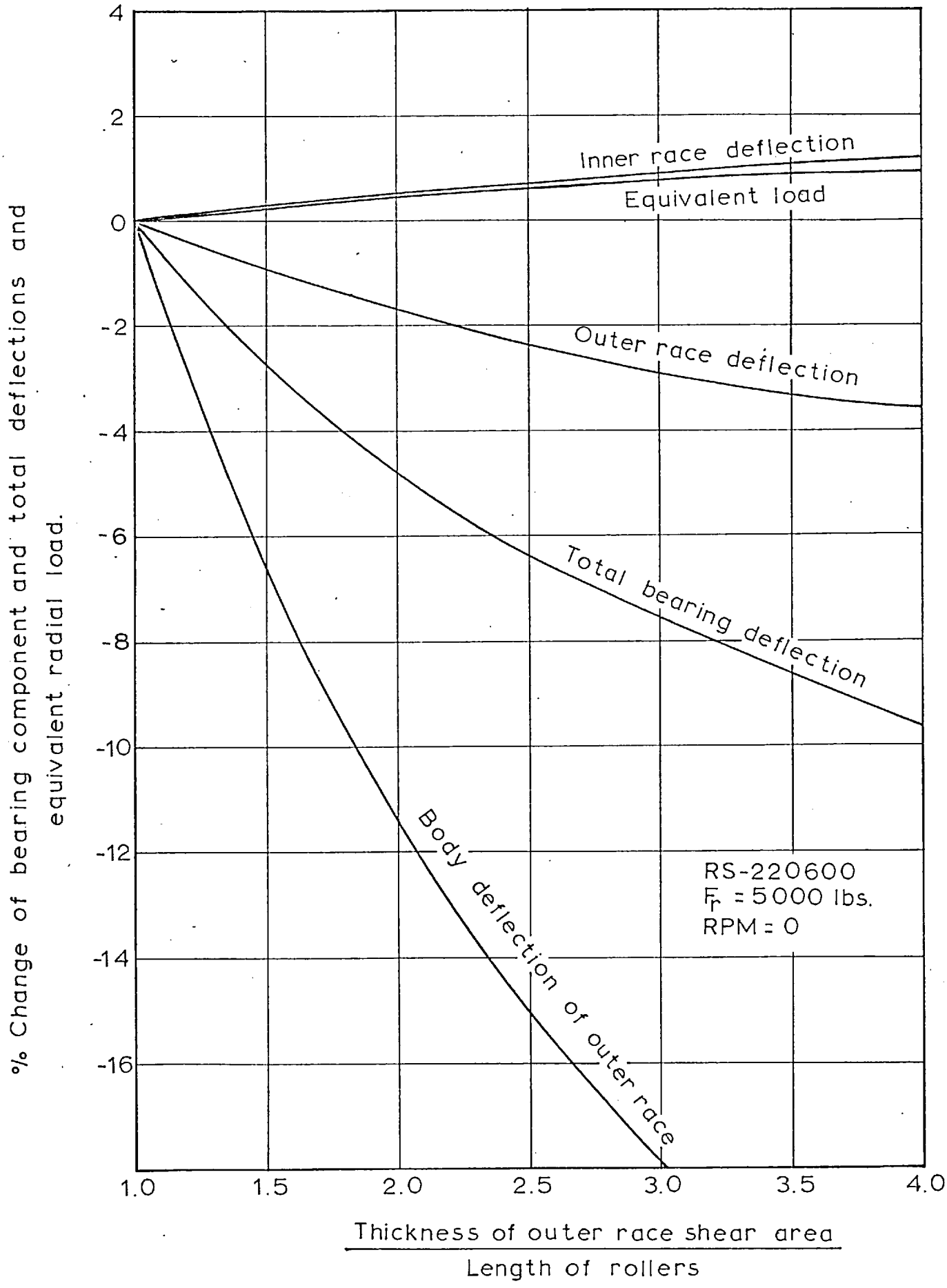


Fig. 7.8 Variation of K_t, K_b and $(\delta_{or}/\delta_{ir})$ with the ratio of the thickness of the outer race shear area to the length of the rollers.

$K_t = \dfrac{\delta_r \text{ for flexible races}}{\delta_r \text{ for rigid races}}$, $K_b = \dfrac{\delta_b \text{ for flexible races}}{\delta_r \text{ for rigid races}}$,

δ_{or}= outer race deflection, δ_{ir}= inner race deflection,

δ_r= radial deflection, δ_b= body deflection of outer race.

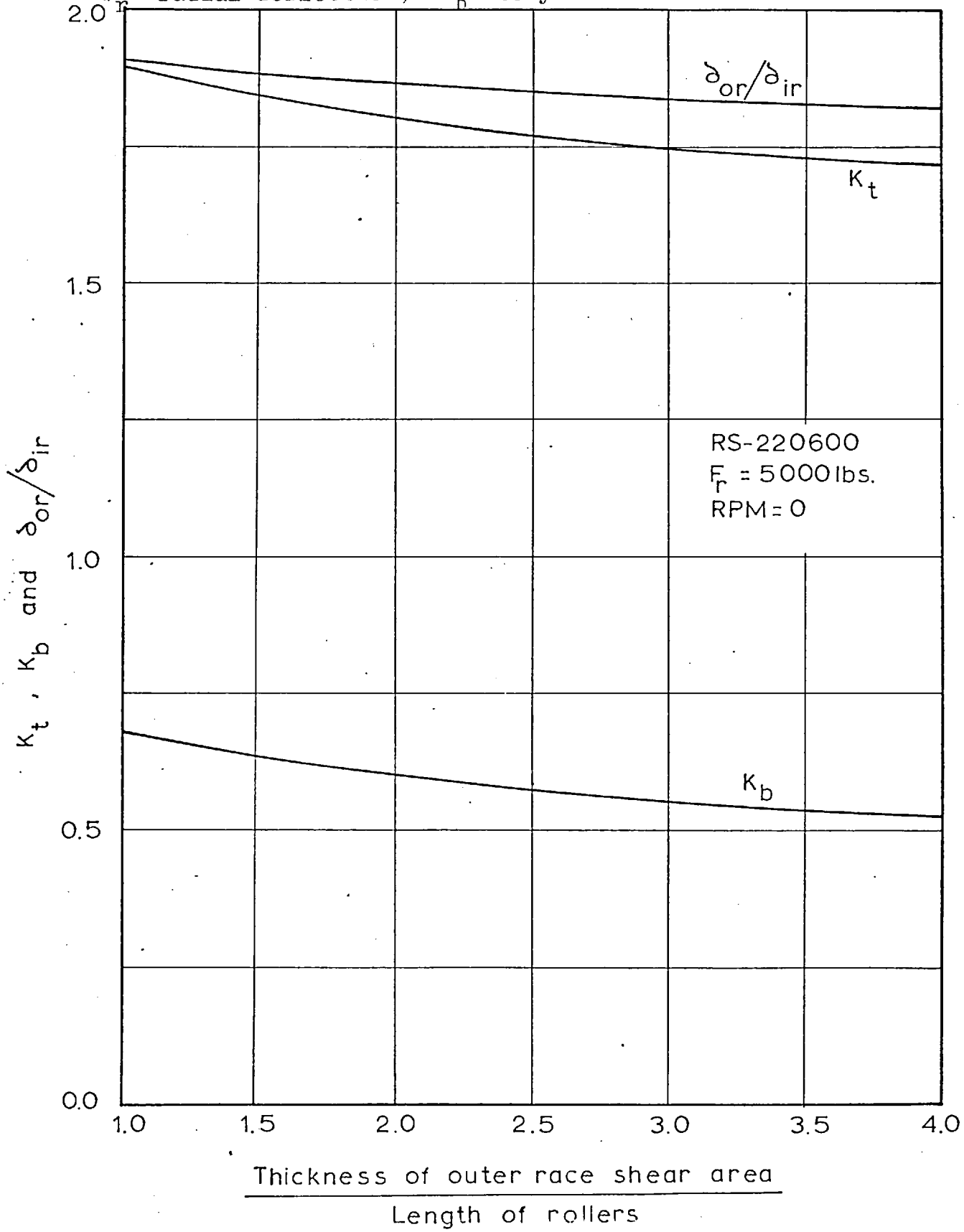


Fig. 7.9 Types of housings with outer race ring and shafts with inner race ring considered for the steel radial roller bearings.

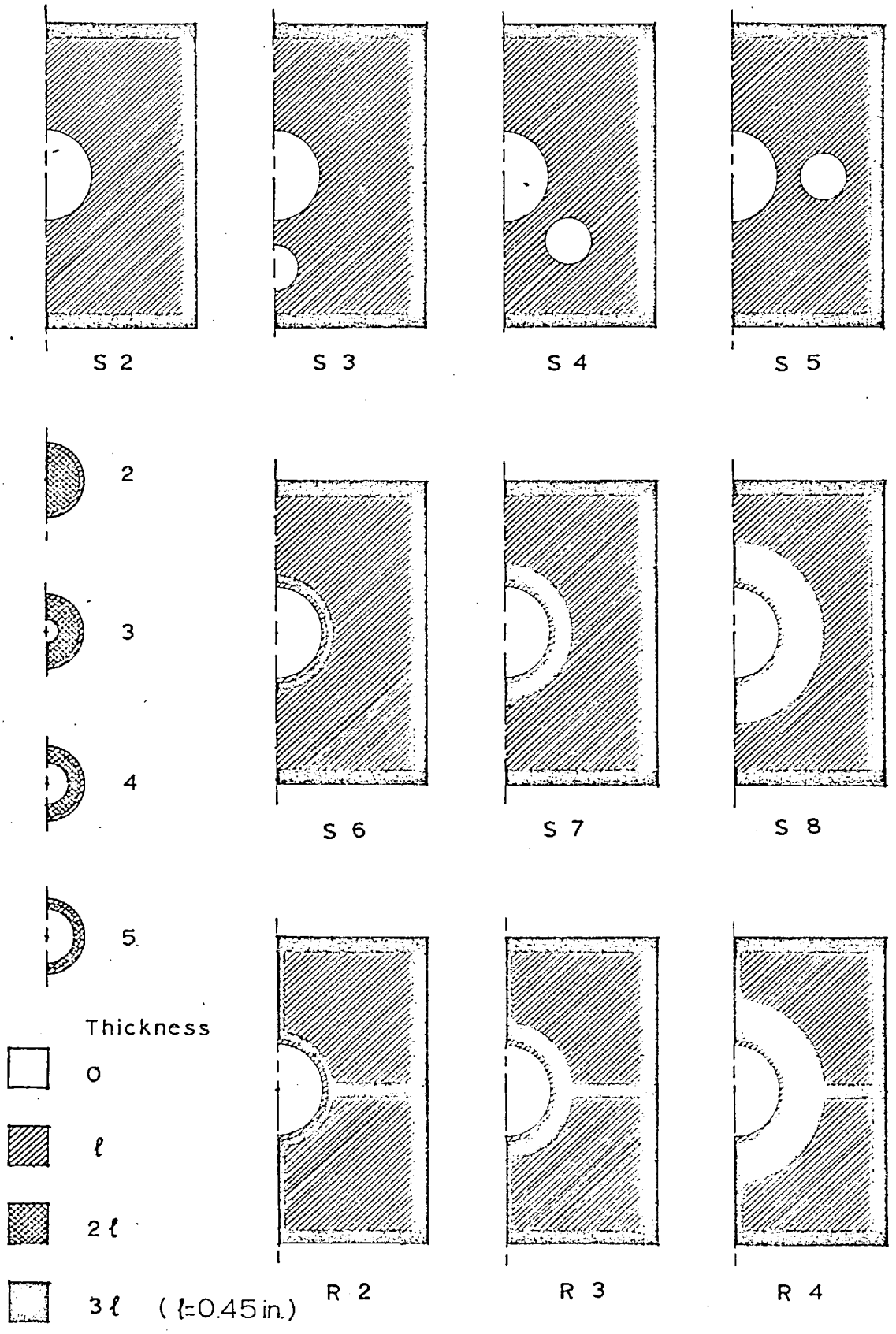


Fig. 7.10 Some other types of housings with outer race ring considered for the steel radial roller bearings.

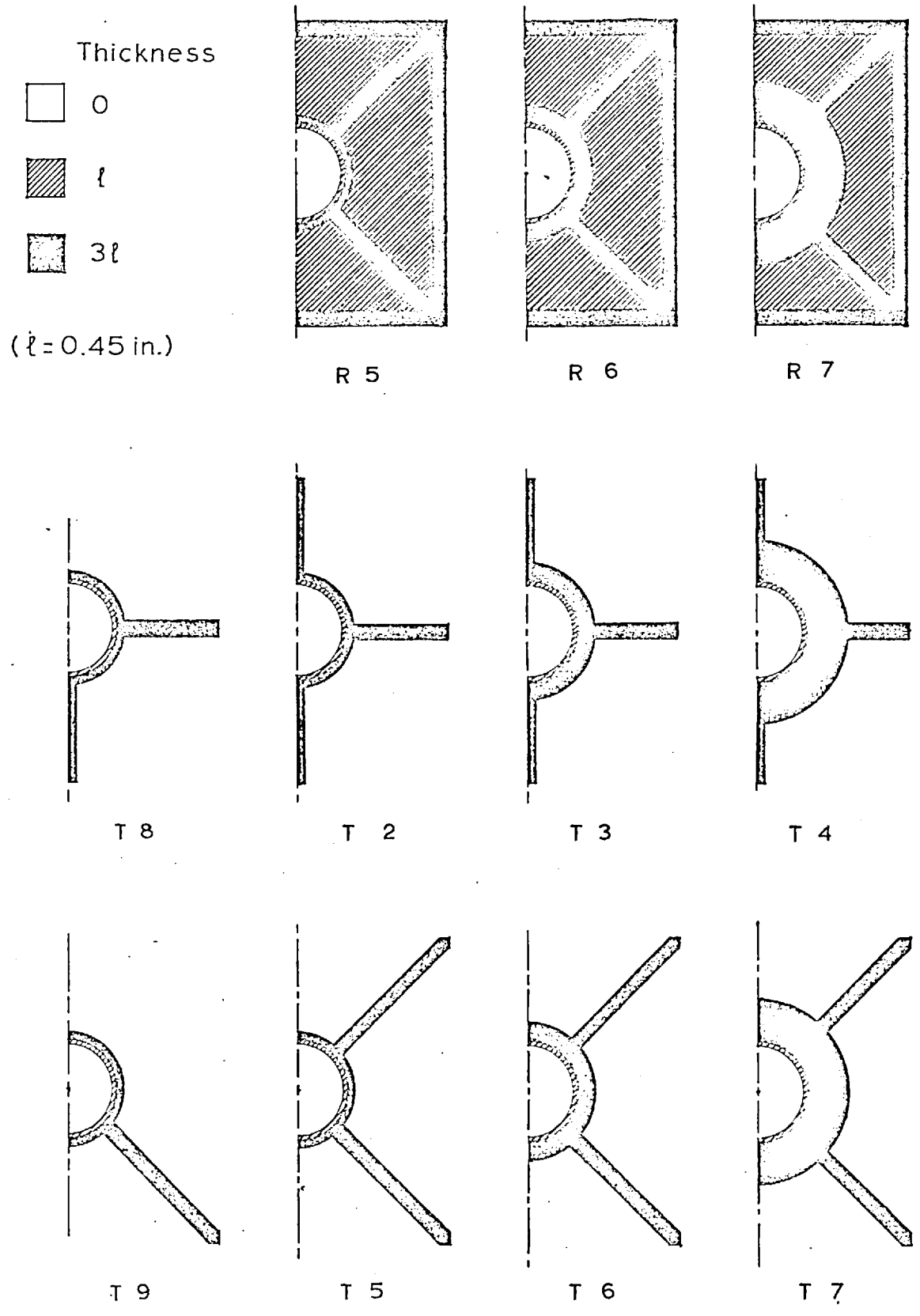


Fig. 7.11 Rate of convergence of roller load distribution for bearing number RS-220600 for different values of FCTR.

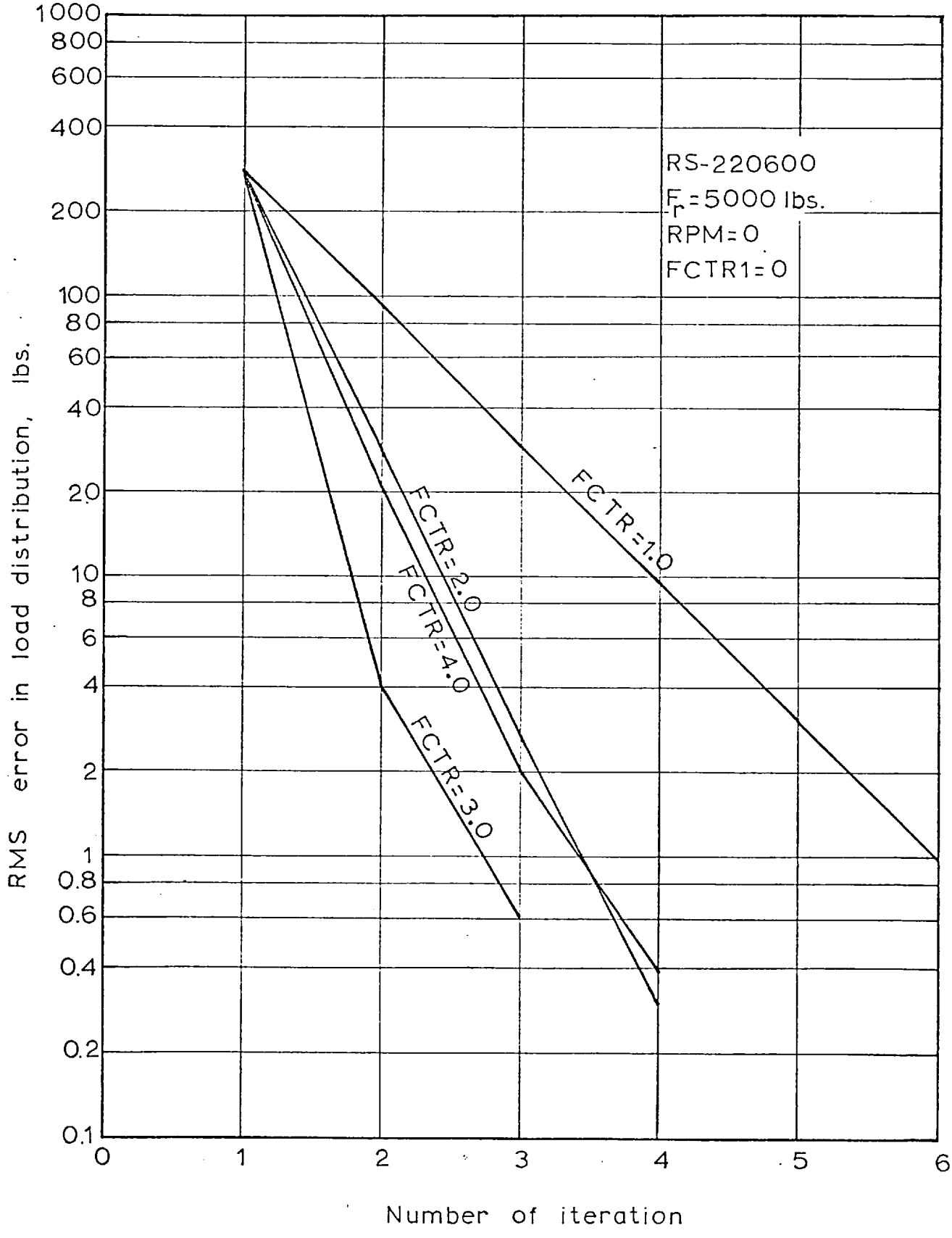


Fig. 7.12 Rate of convergence of roller load distribution for bearing number RS-250600 for different values of FCTR and FCTR1.

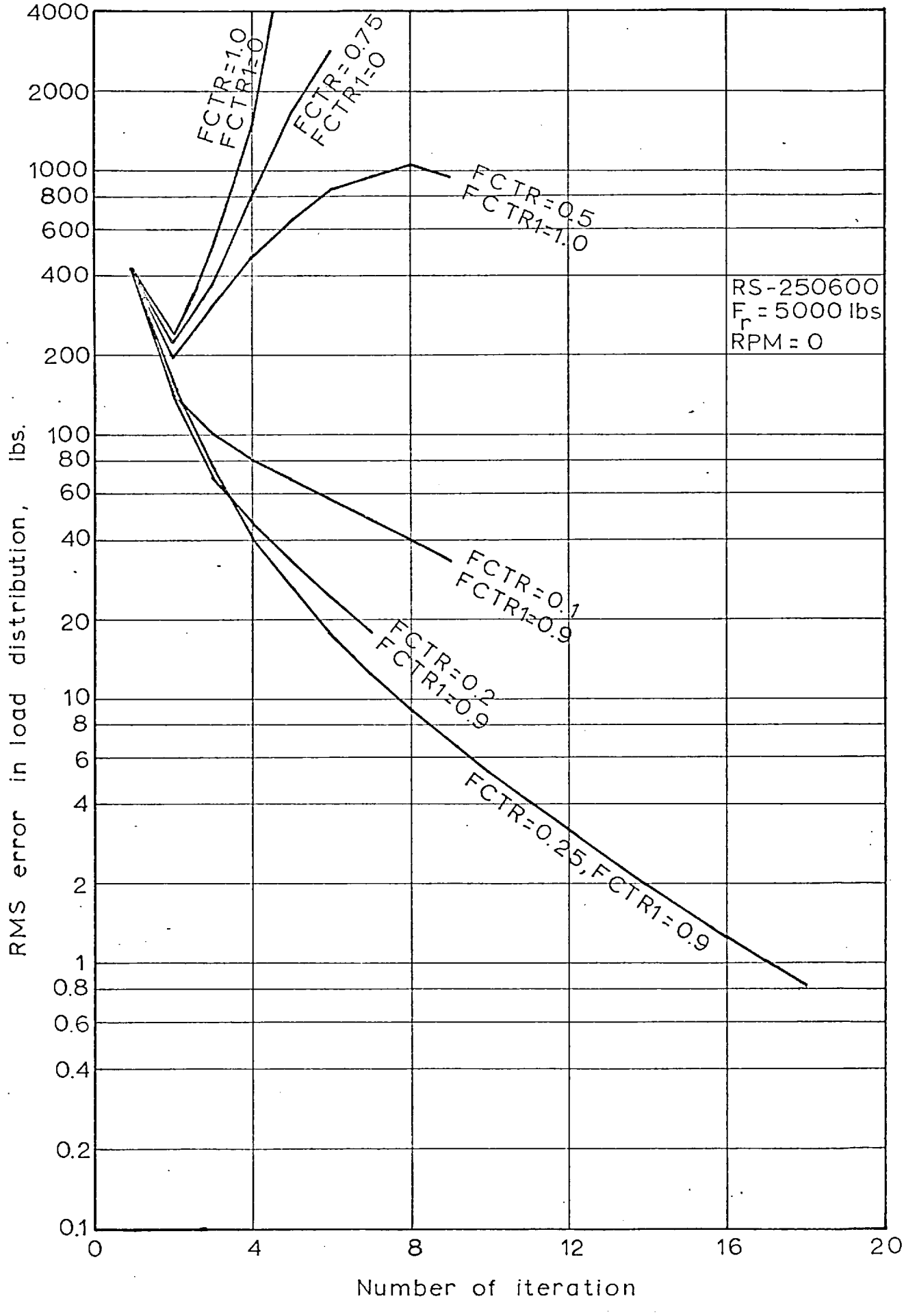
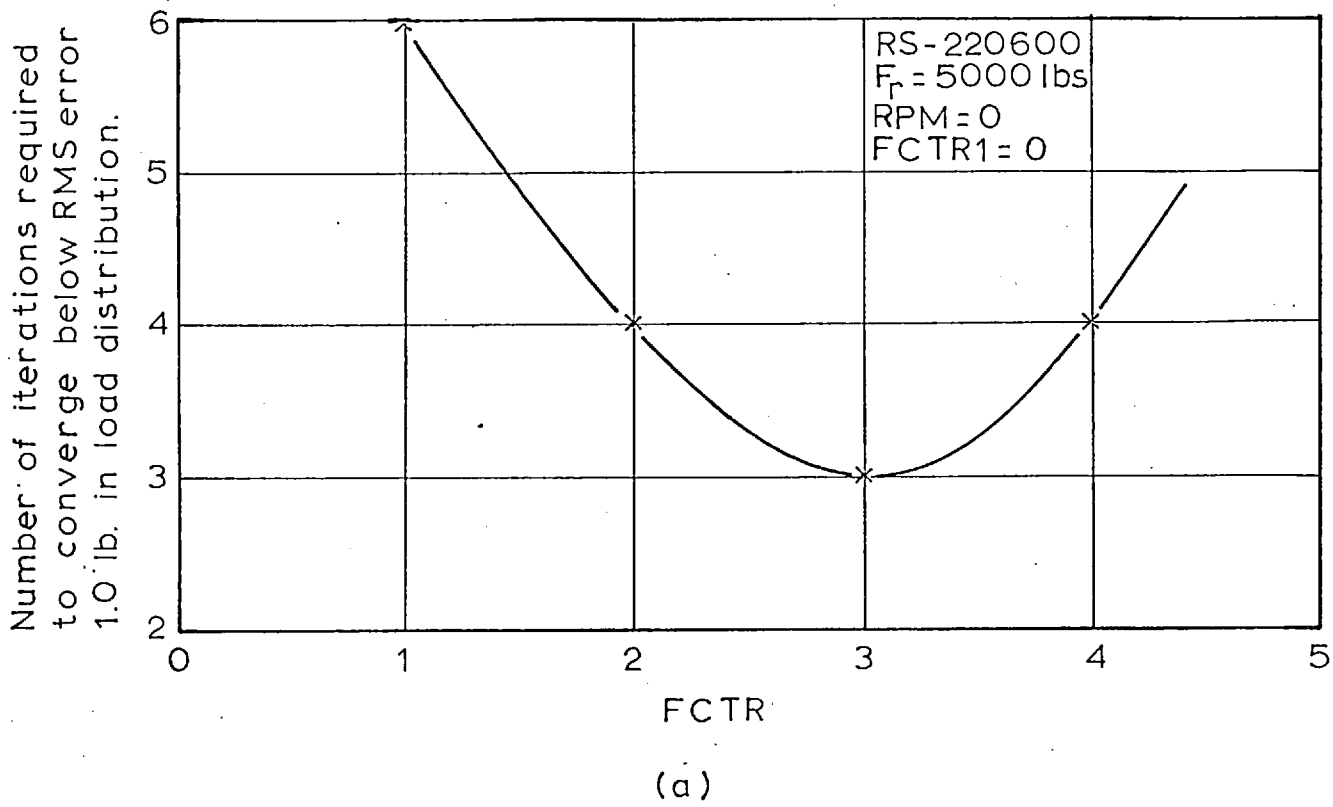
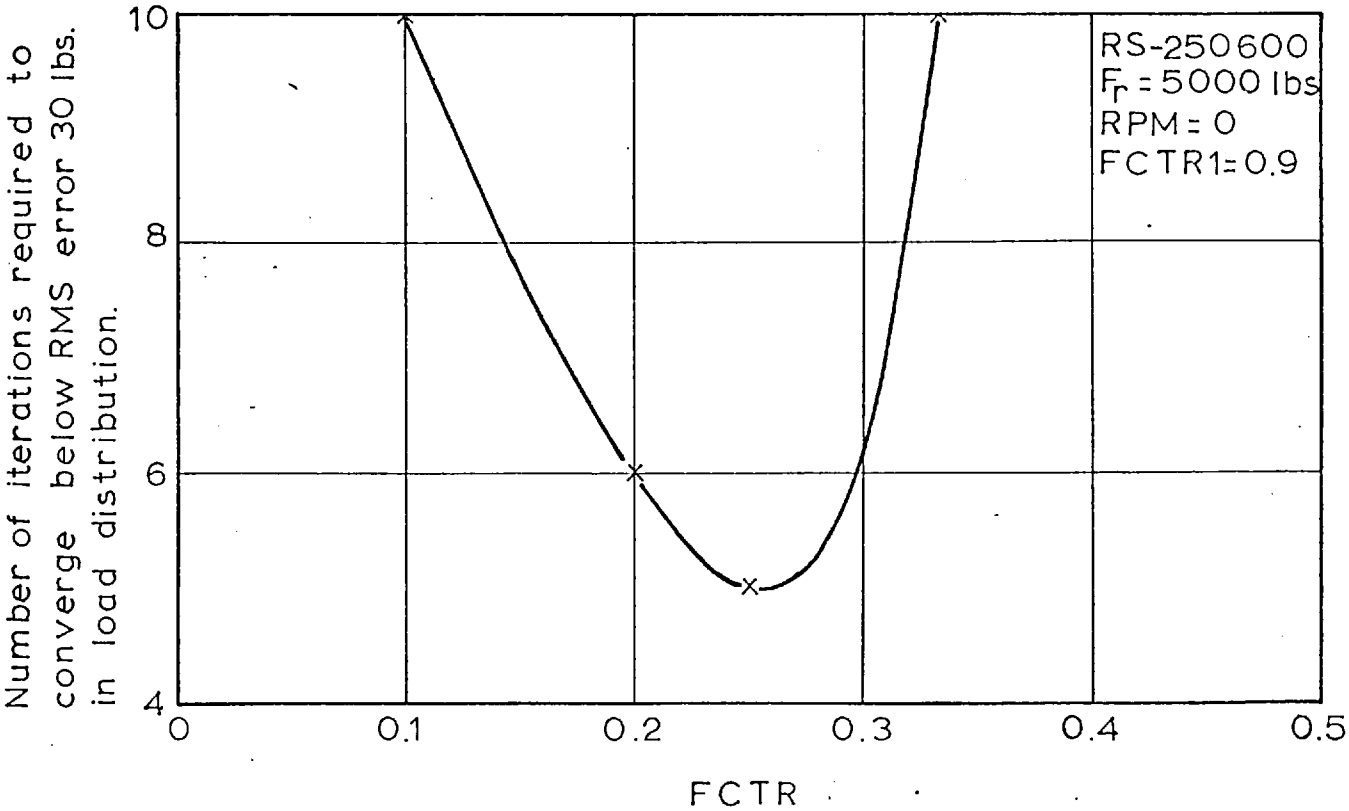


Fig. 7.13 Finding the value of FCTR for most rapid convergence of roller load distribution for bearing numbers (a) RS-220600 and (b) RS-250600.



(a)



(b)

Fig. 7.14 Comparison of total radial and component deflections obtained by finite-element method with those obtained by assuming rigid races, of a steel radial roller bearing (RS-220200).

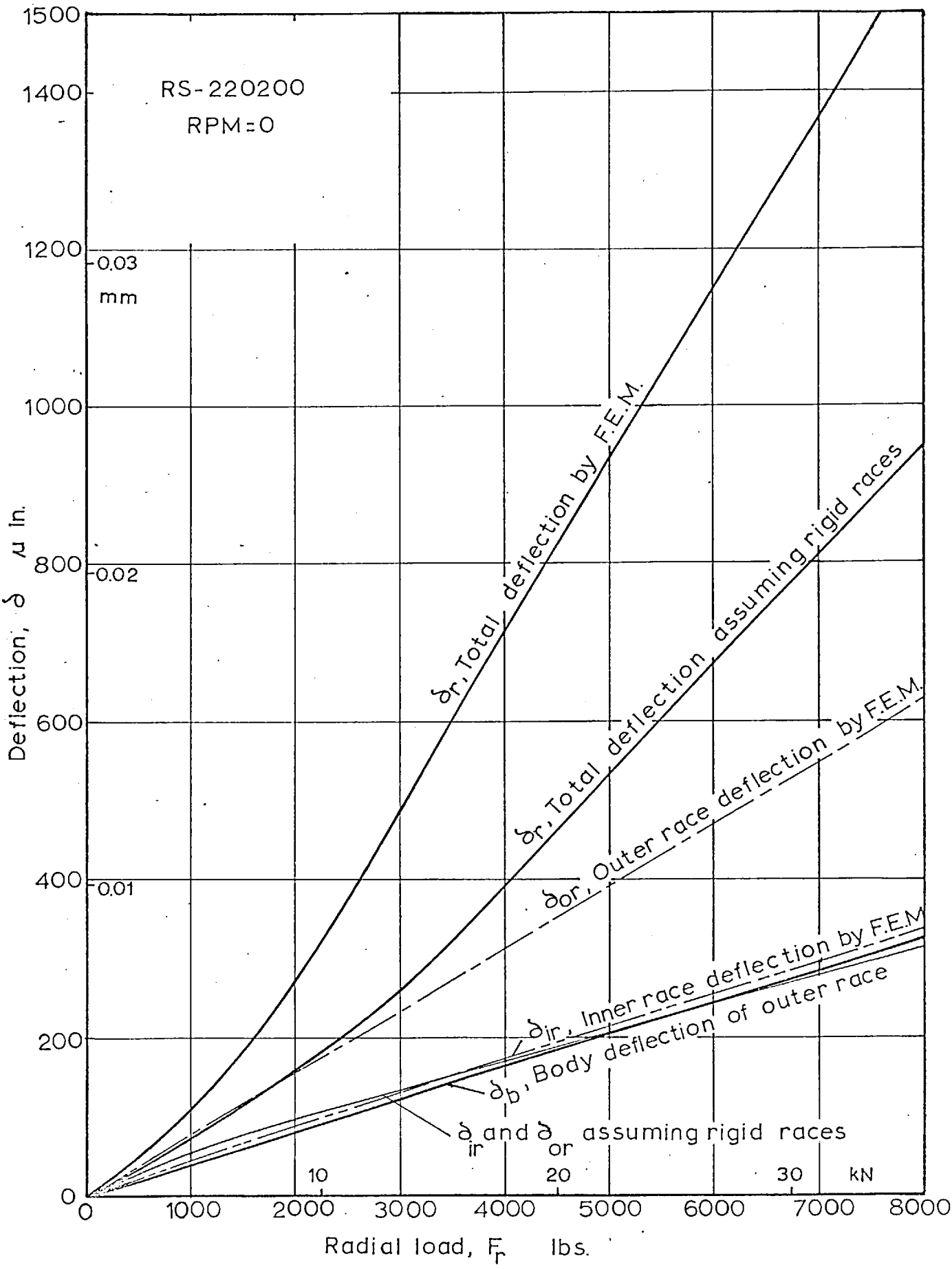


Fig. 7.15 Variation of total radial and component deflections of a steel radial roller bearing with radial load for different hollowness of the shaft.

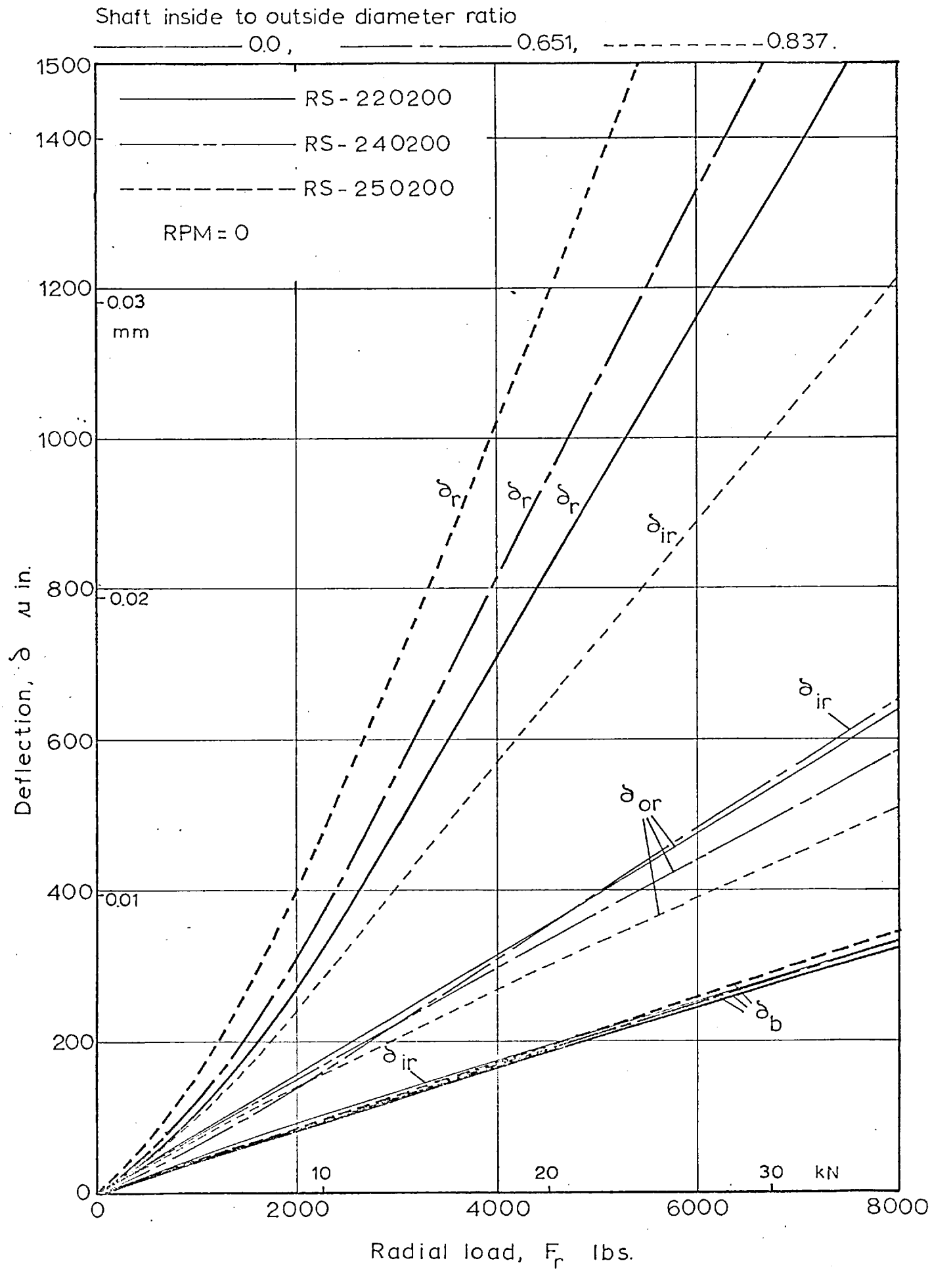


Fig. 7.16 Total radial and body deflections of a steel radial roller bearing with housing number S 2 plotted against radial clearance for different shaft hollowness.

δ_r= radial deflection,
δ_b= body deflection of the outer race.

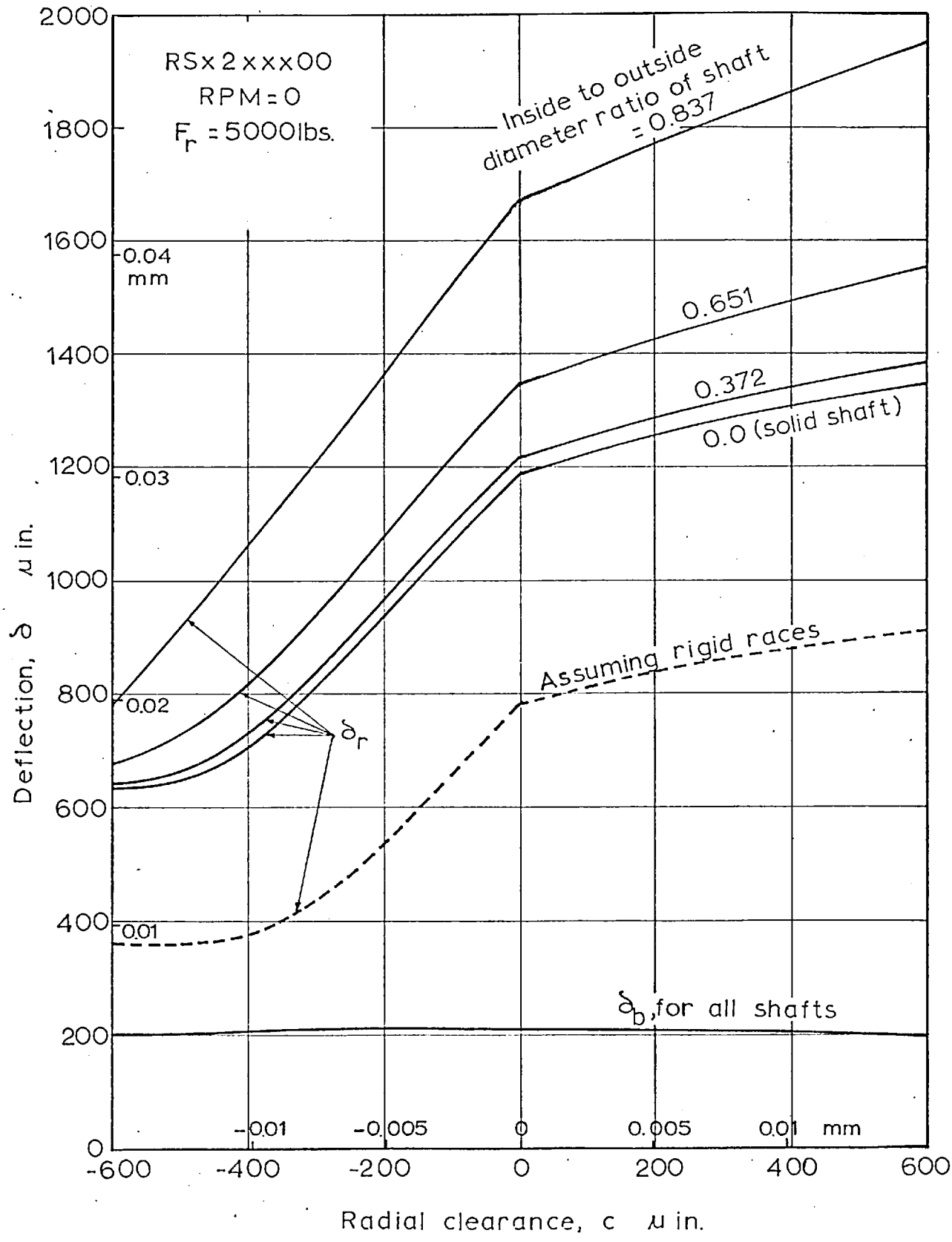


Fig. 7.17 Variation of total radial and component deflections of a steel bearing with the inner to outer diameter ratio of the shaft for different radial clearances.

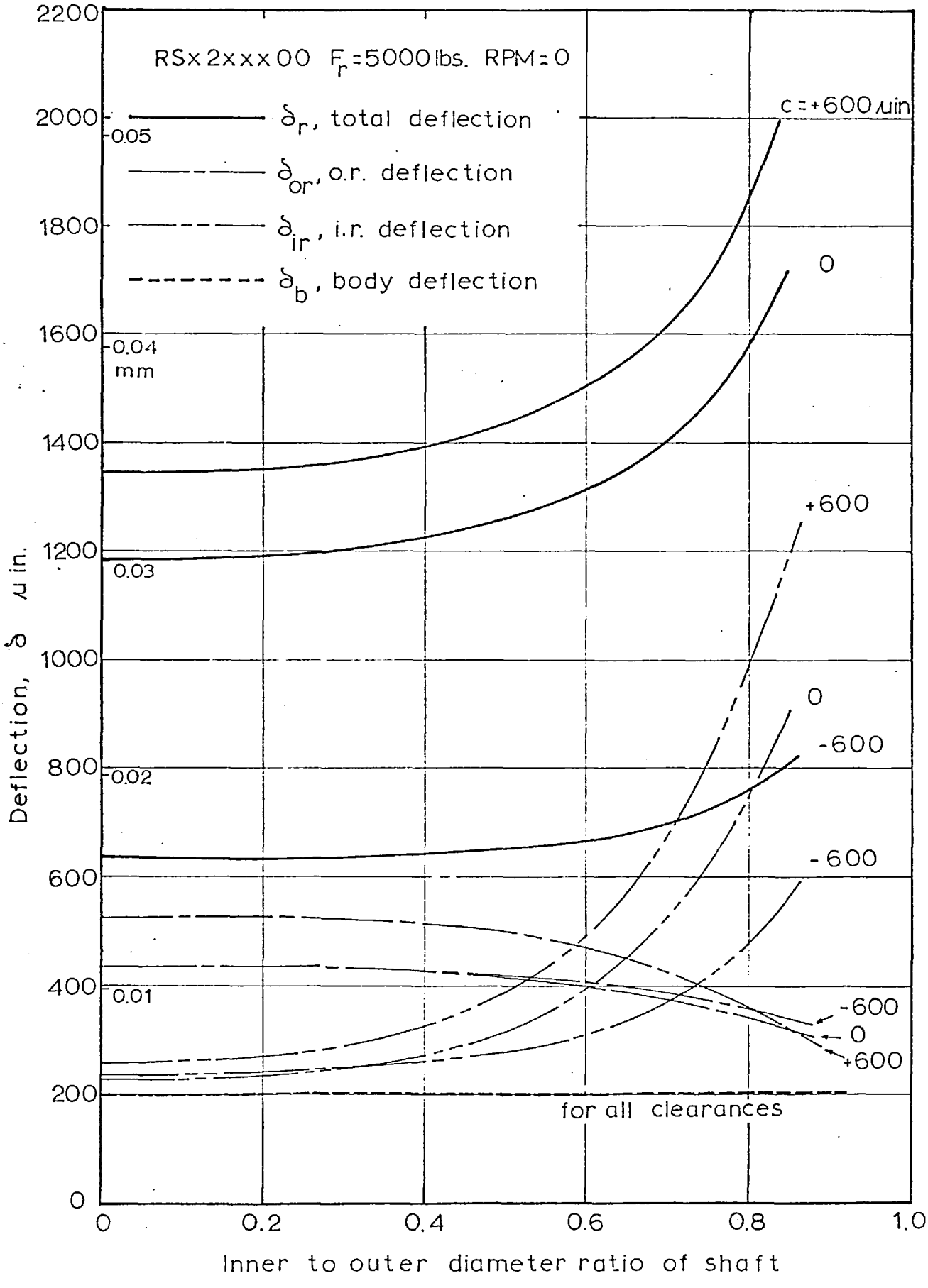


Fig. 7.18 Variation of non-dimensional equivalent radial load (P_r / F_r) of a steel bearing with radial clearance for different shaft hollowness.

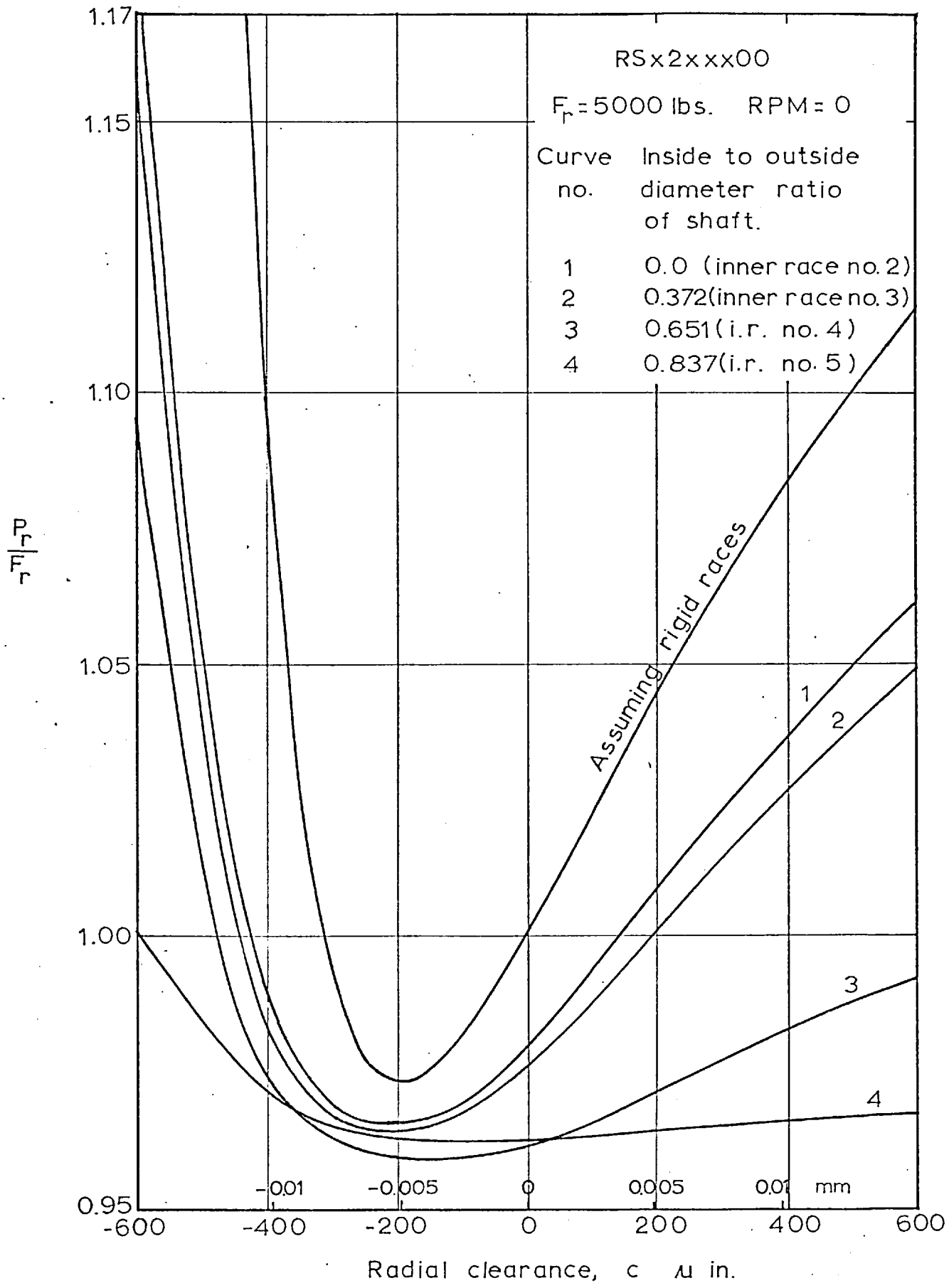


Fig. 7.19 Variation of non-dimensional equivalent radial load (P_r/F_r) of a steel bearing with inner to outer diameter ratio of shaft, for radial clearances c= 0 and -200 μin.

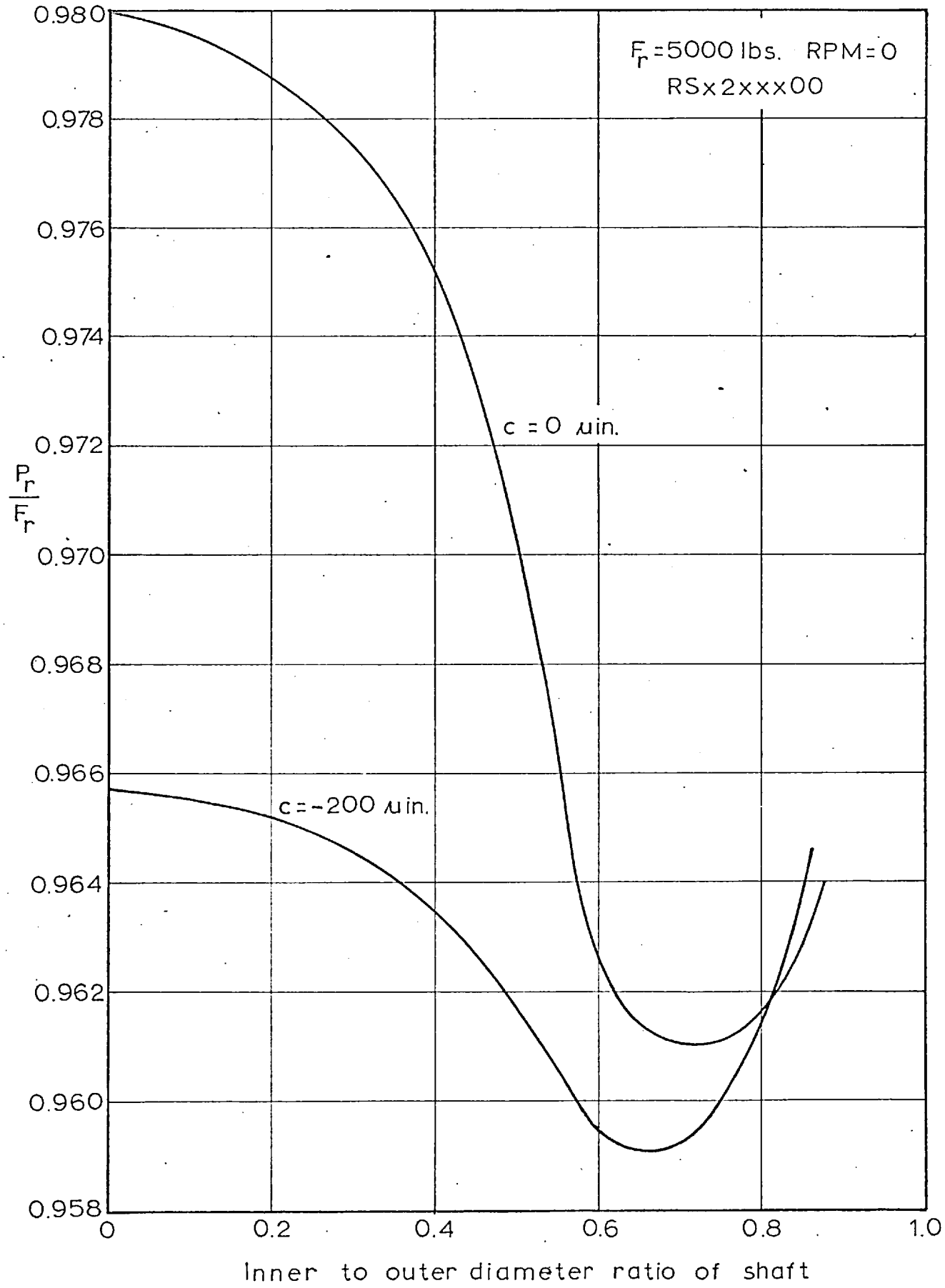


Fig. 7.20 Variation of non-dimensional equivalent radial load (P_r/F_r) of a steel bearing with radial load for different shaft hollowness.

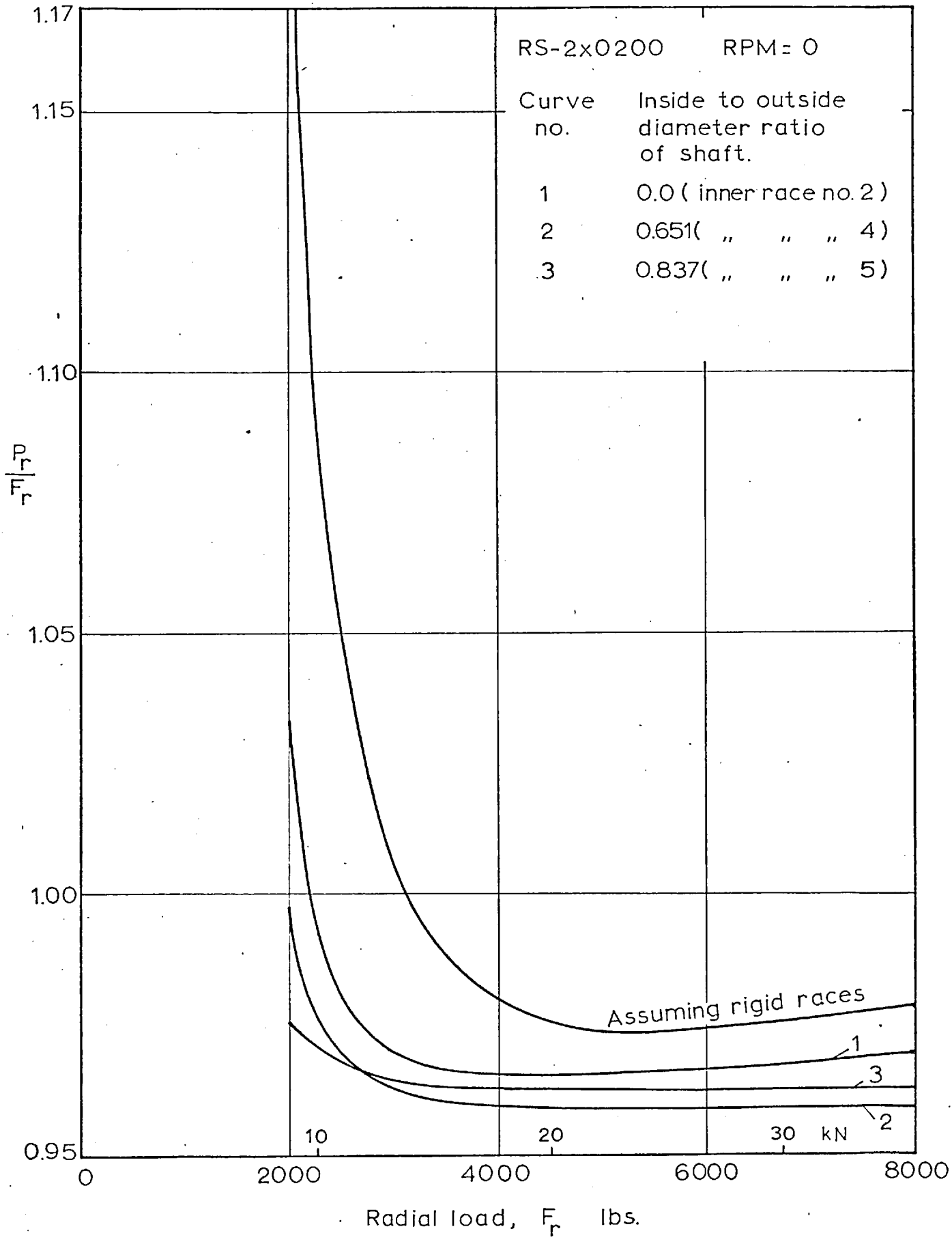


Fig. 7.21 Variation of K_t and K_b for a steel bearing with radial clearance for different shaft hollowness.

$K_t = \frac{\delta_r \text{ for flexible races}}{\delta_r \text{ for rigid races}}$, $K_b = \frac{\delta_v \text{ for flexible races}}{\delta_r \text{ for rigid races}}$.

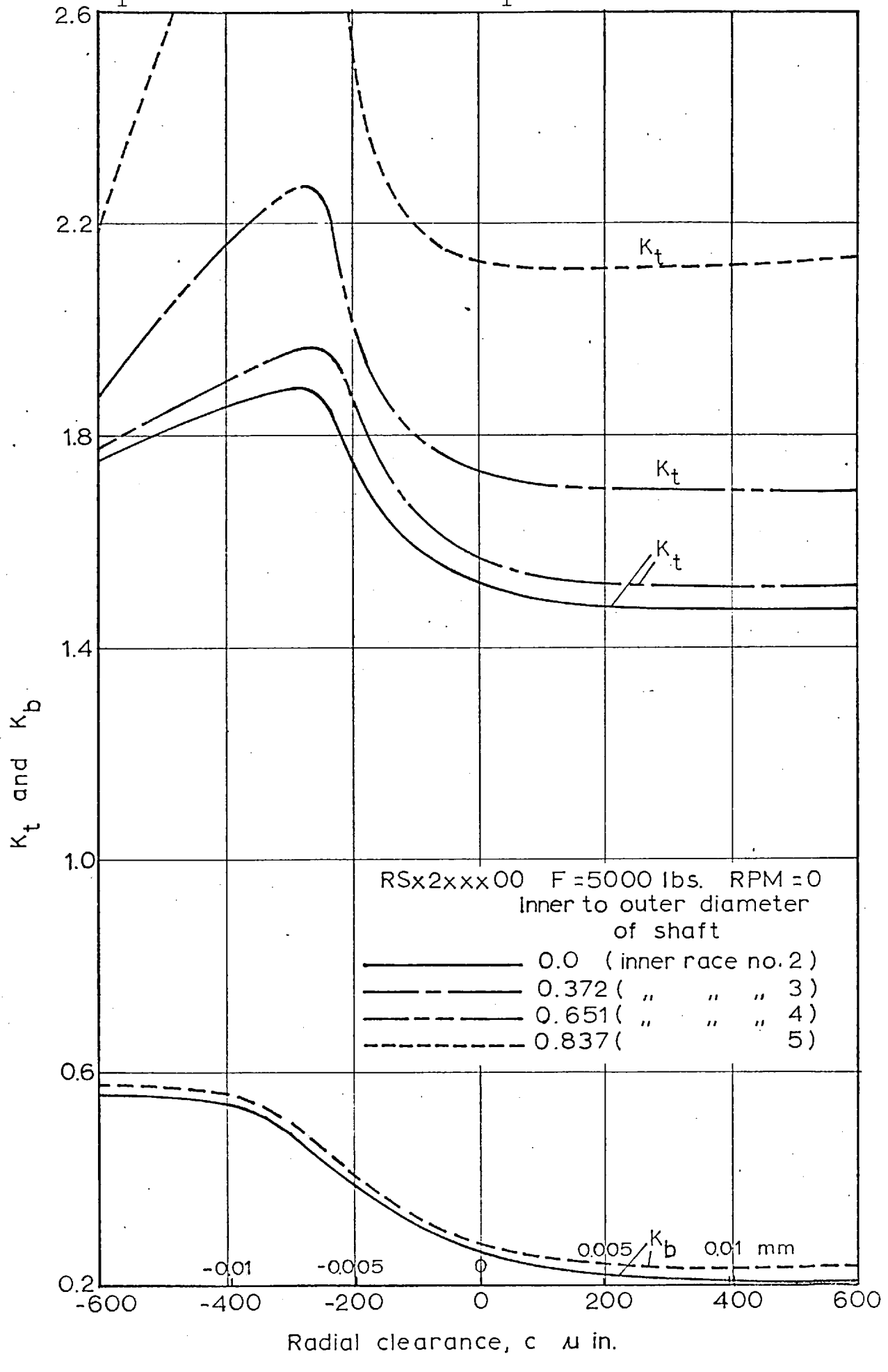
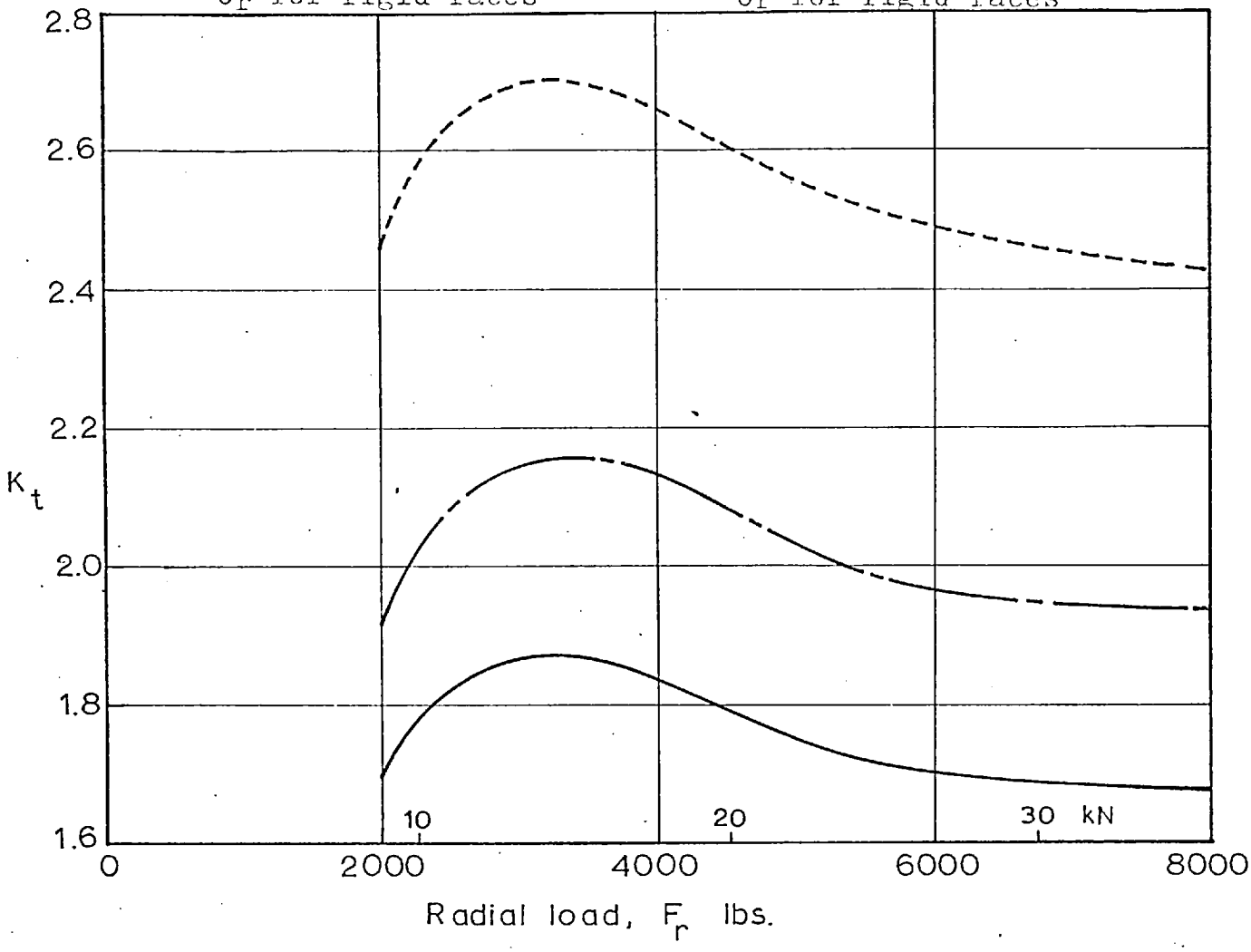
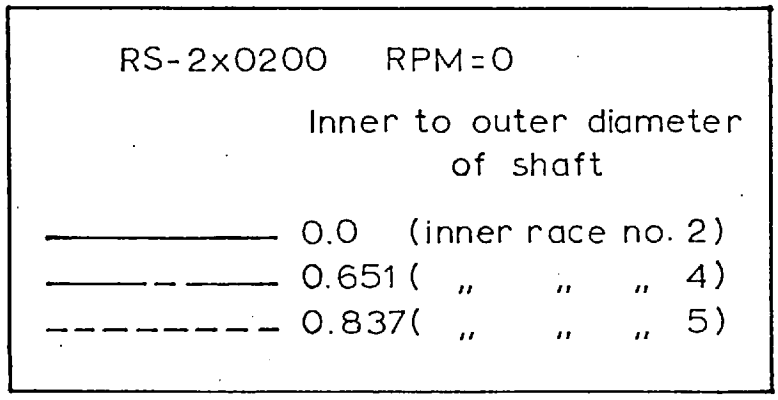


Fig. 7.22 Variation of K_t and K_b of a steel bearing with radial load for different shaft hollowness.

$K_t = \frac{\delta_r \text{ for flexible races}}{\delta_r \text{ for rigid races}}$, $K_b = \frac{\delta_b \text{ for flexible races}}{\delta_r \text{ for rigid races}}$.





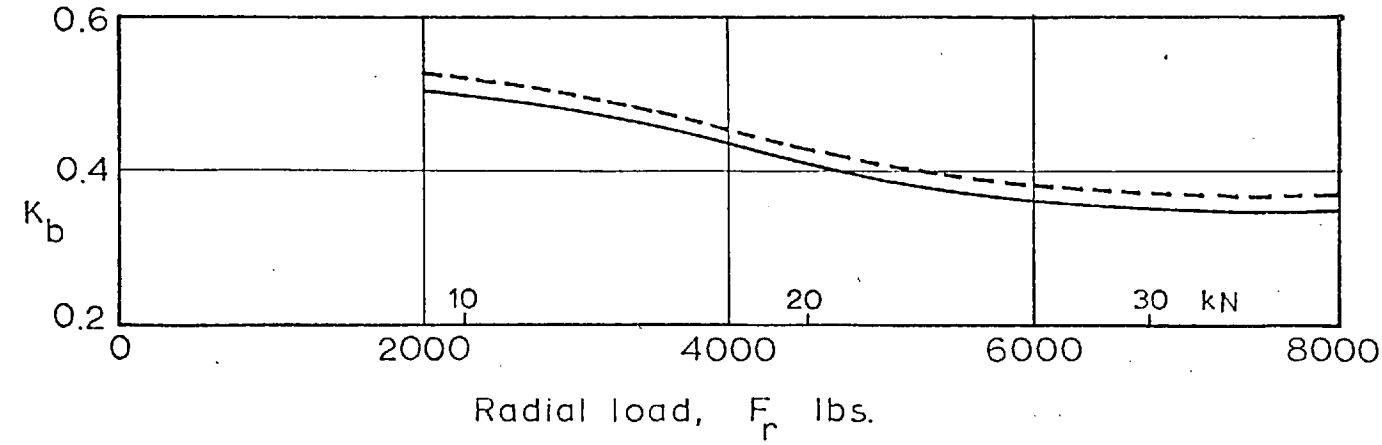


Fig. 7.23 Effect of high speed on non-dimensional equivalent radial load (P_r/F_r), outer to inner race deflection ratio (δ_{or}/δ_{ir}), K_t and K_b of a steel bearing with hollow shaft (inner to outer diameter ratio 0.837).

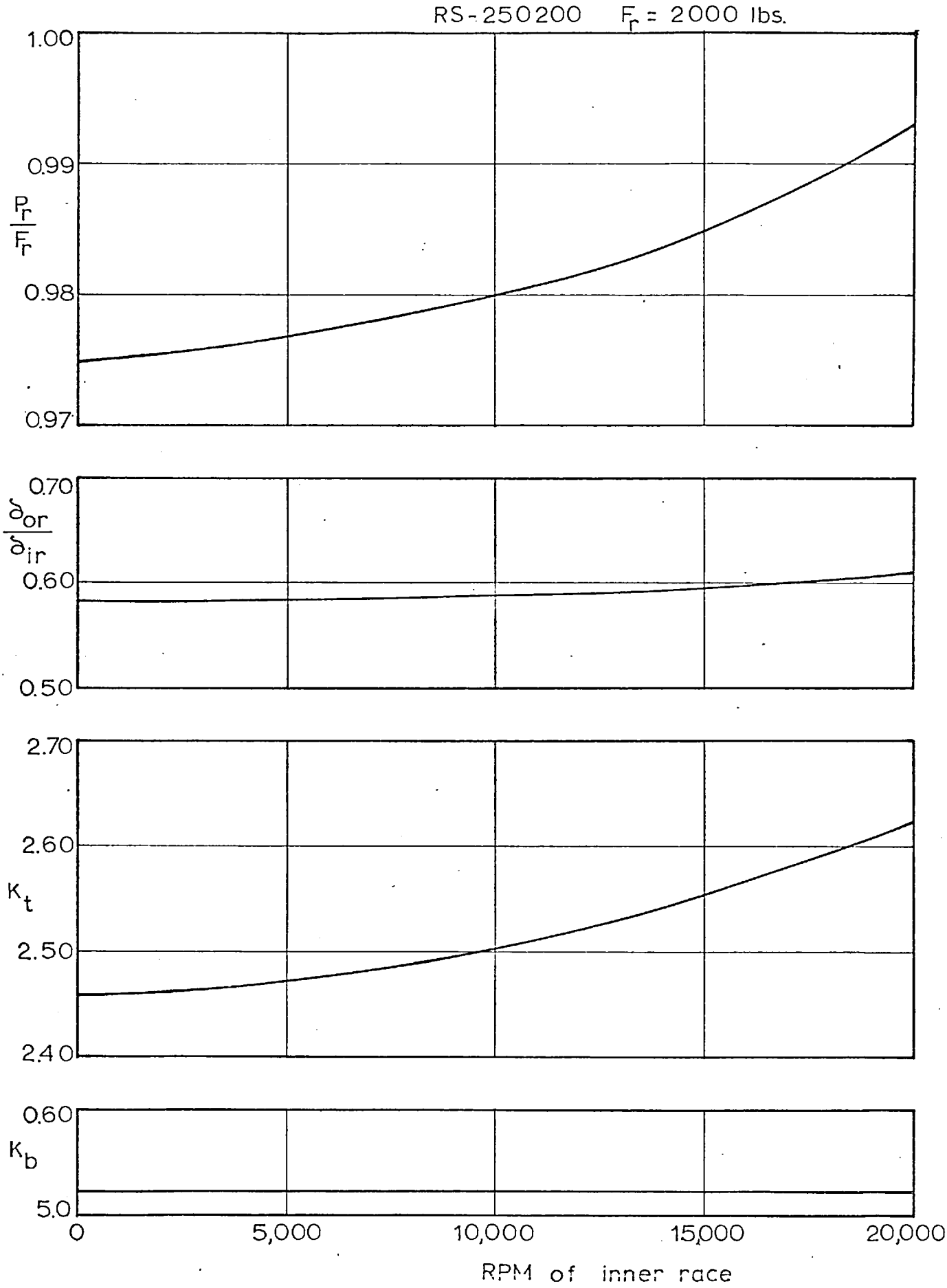
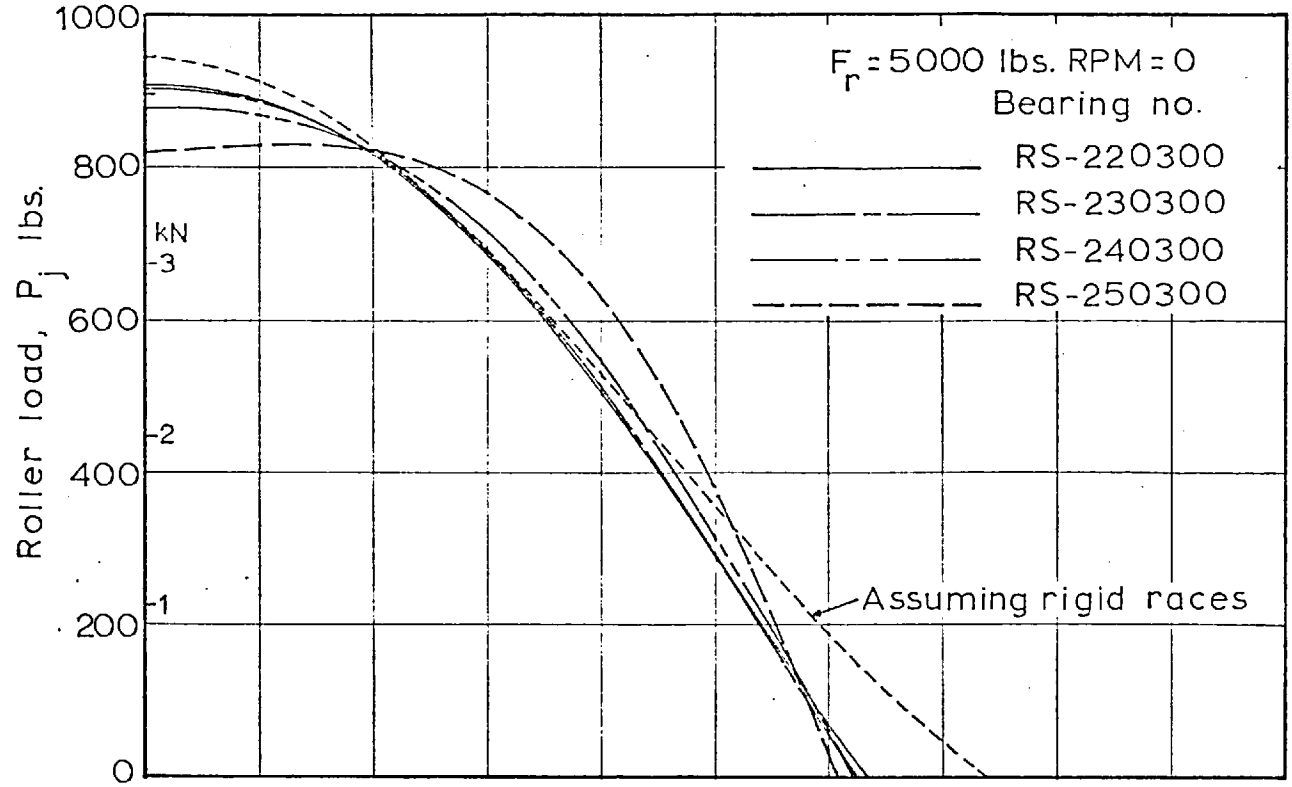
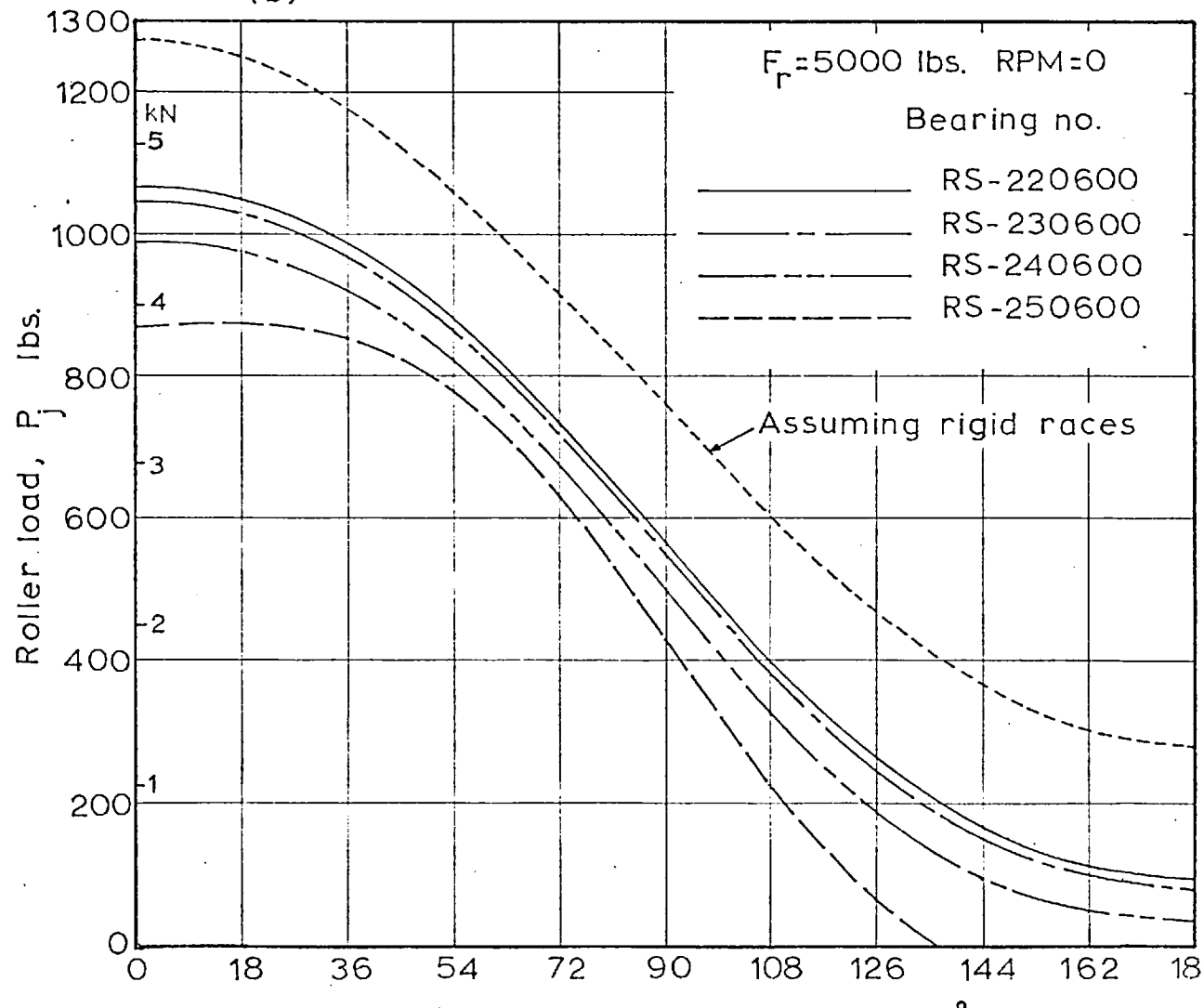


Fig. 7.24 Load distribution among the rollers of a steel bearing with different hollowness of shaft and having radial clearance (a) c= -600 μin., (b) c= -300 μin.

Inner to outer diameter ratio of shaft no. 2 is 0.0, 3 is 0.372, 4 is 0.651 and 5 is 0.837.

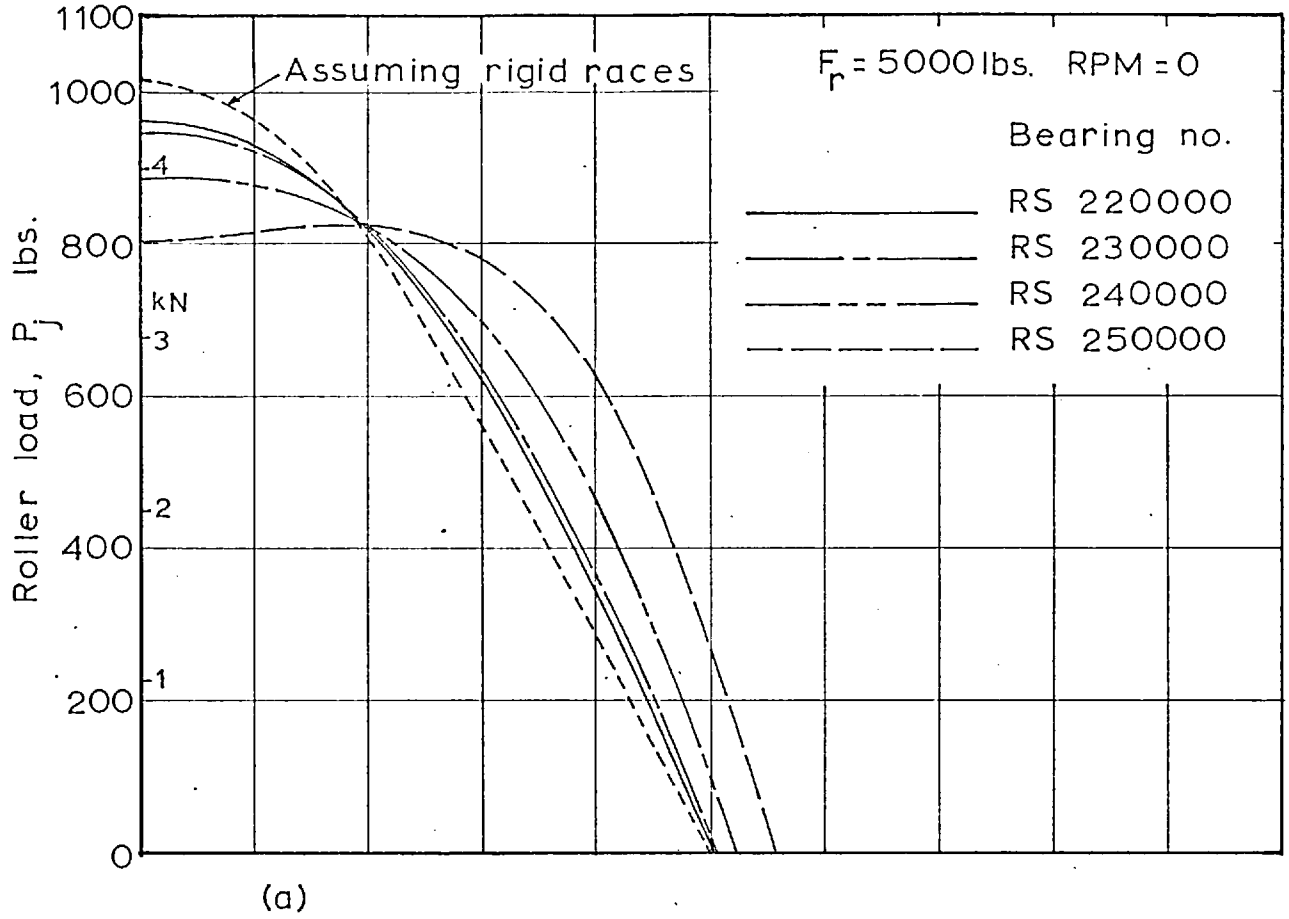


(b)

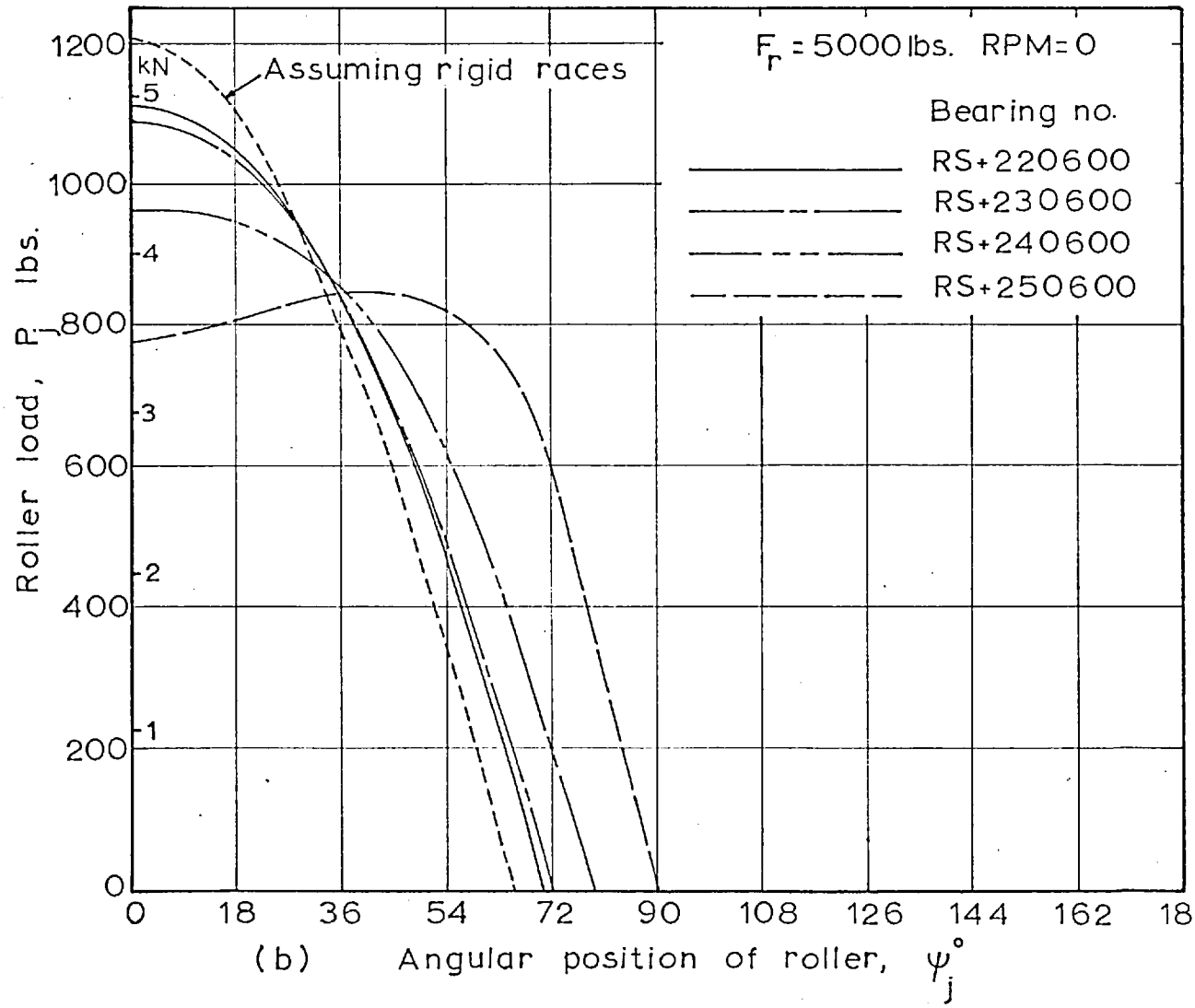


(a)

Fig. 7.25 Load distribution among the rollers of a steel bearing with different hollowness of shaft and having radial clearance (a) c= 0 μin. (b) c= +600 μin.
Inner to outer diameter ratio of shaft no.2 is 0.0, 3 is 0.372, 4 is 0.651 and 5 is 0.837.



(a)



(b) Angular position of roller, ψ_j°

Fig. 7.26 Effect of other holes in the housing on the total radial and component deflections of a steel bearing with solid shaft.

δ_r = bearing radial deflection
δ_{or} = outer race deflection
δ_{ir} = inner race deflection
δ_b = body deflection of outer race.

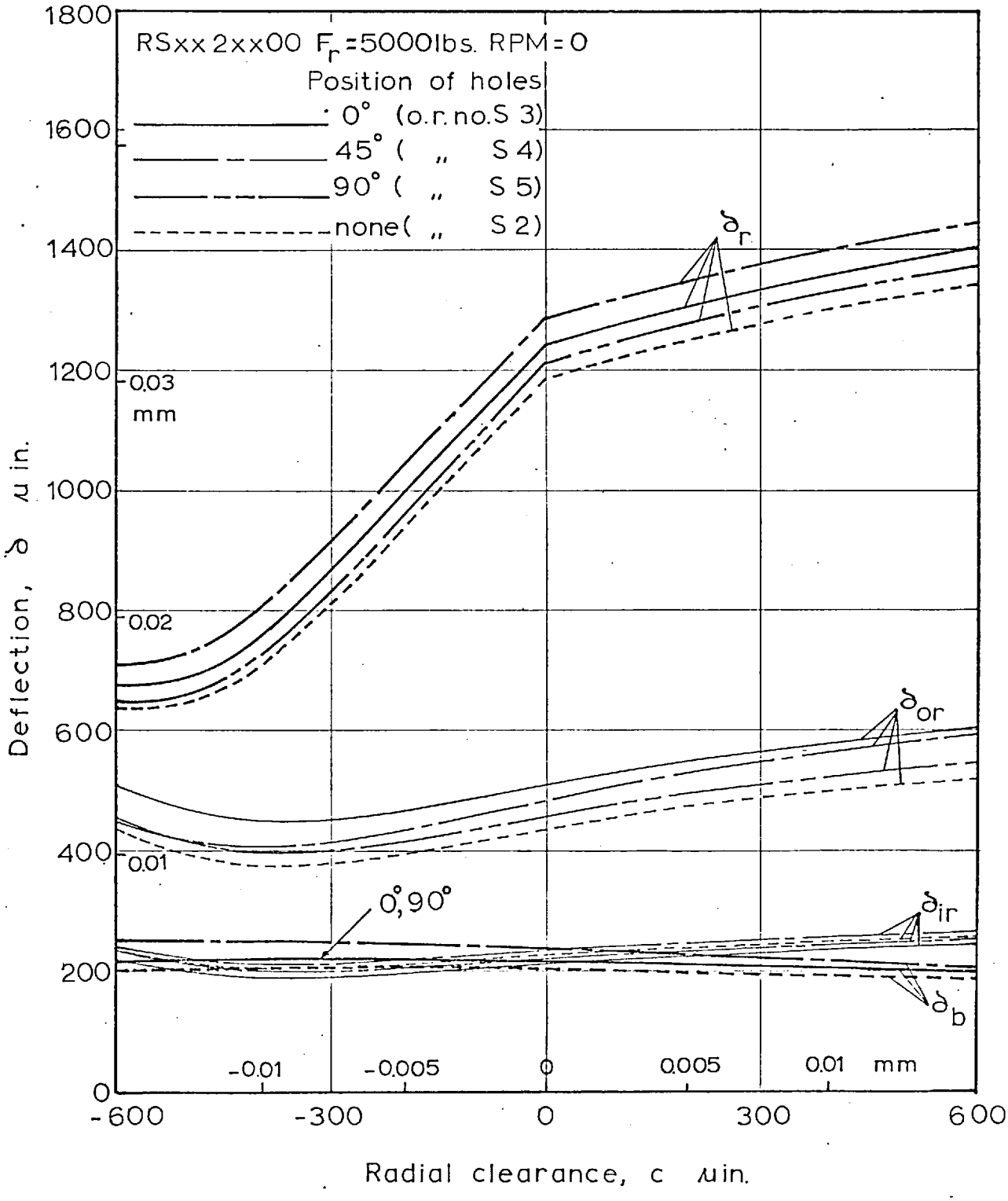


Fig. 7.27 Effect of other holes in the housing on the non-dimensional equivalent radial load (P_r/F_r) of a steel bearing having solid shaft.

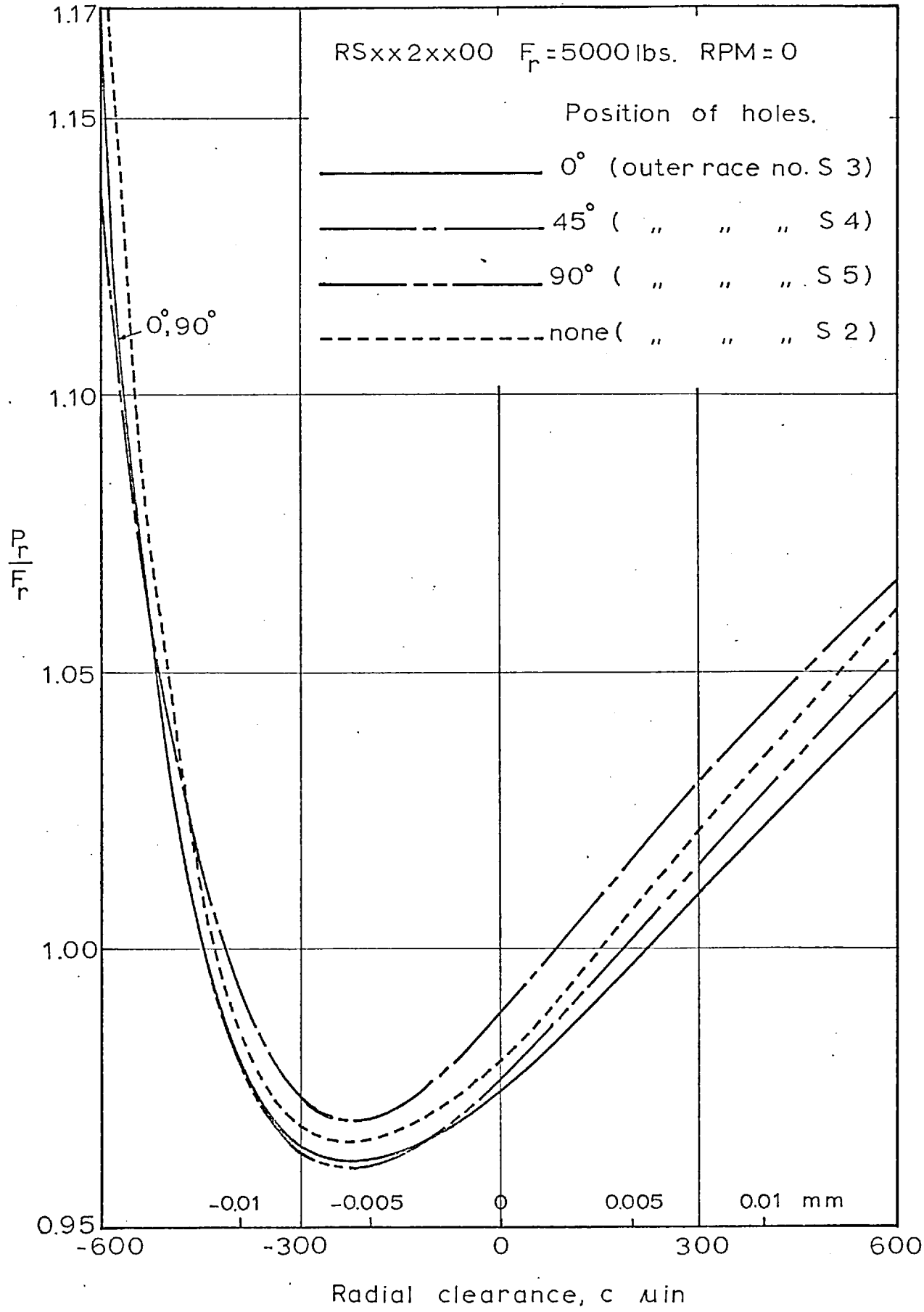


Fig. 7.28 Effect of other holes in the housing on K_t and K_b for a steel bearing with solid shaft.

$$K_t = \frac{\delta_r \text{ for flexible races}}{\delta_r \text{ for rigid races}}, \quad K_b = \frac{\delta_b \text{ for flexible races}}{\delta_r \text{ for rigid races}}$$

where, δ_r = radial deflection and δ_b = body deflection of outer race.

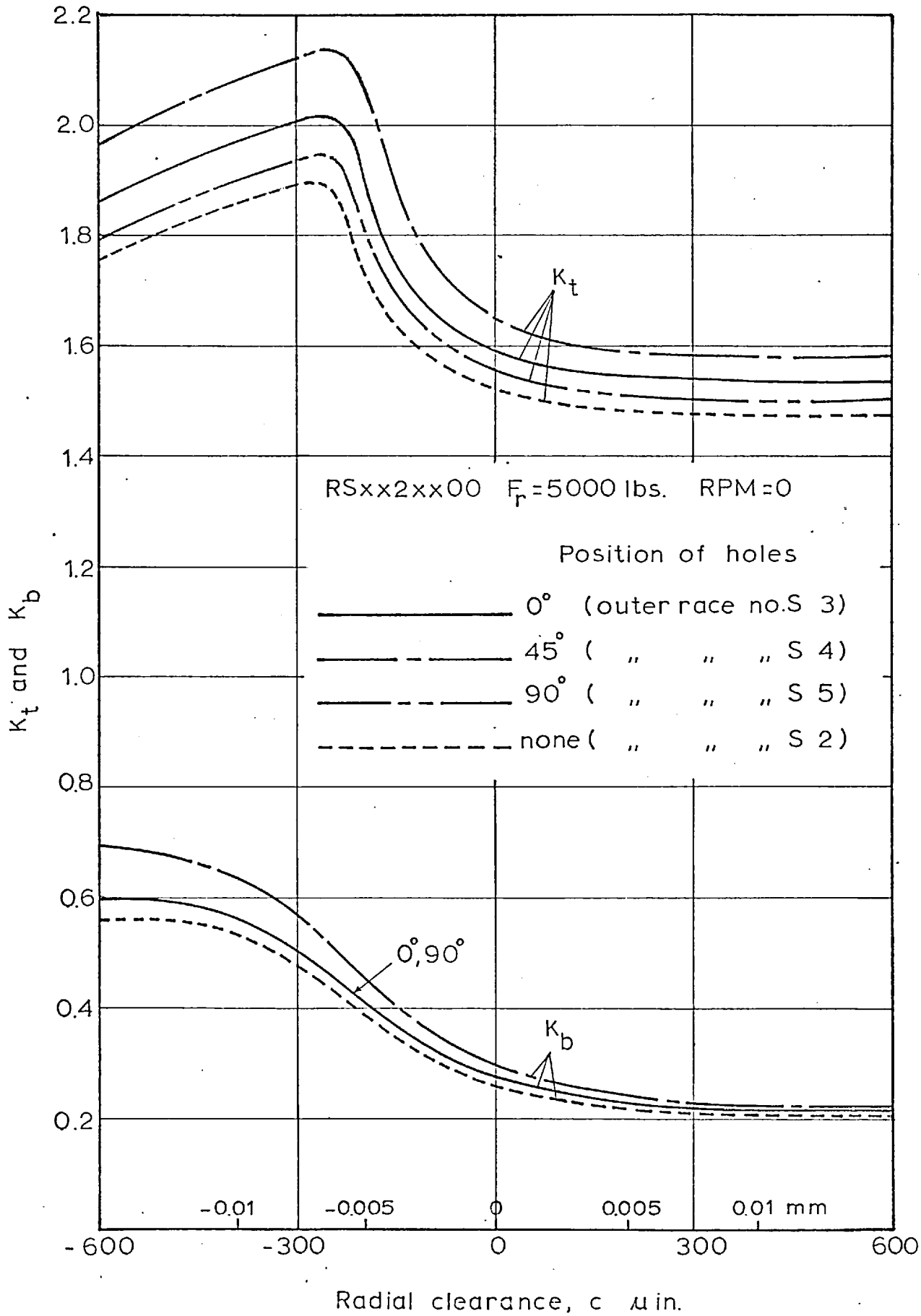


Fig. 7.29 Effect of other holes in the housing on the roller load distribution in a steel bearing with solid shaft and radial clearance (a) c= -600 μin., (b) c= -300 μin.

Housing no. S 2 has no hole, S 3 has hole at 0°, S 4 has holes at 45° and S 5 has holes at 90° to radial load.

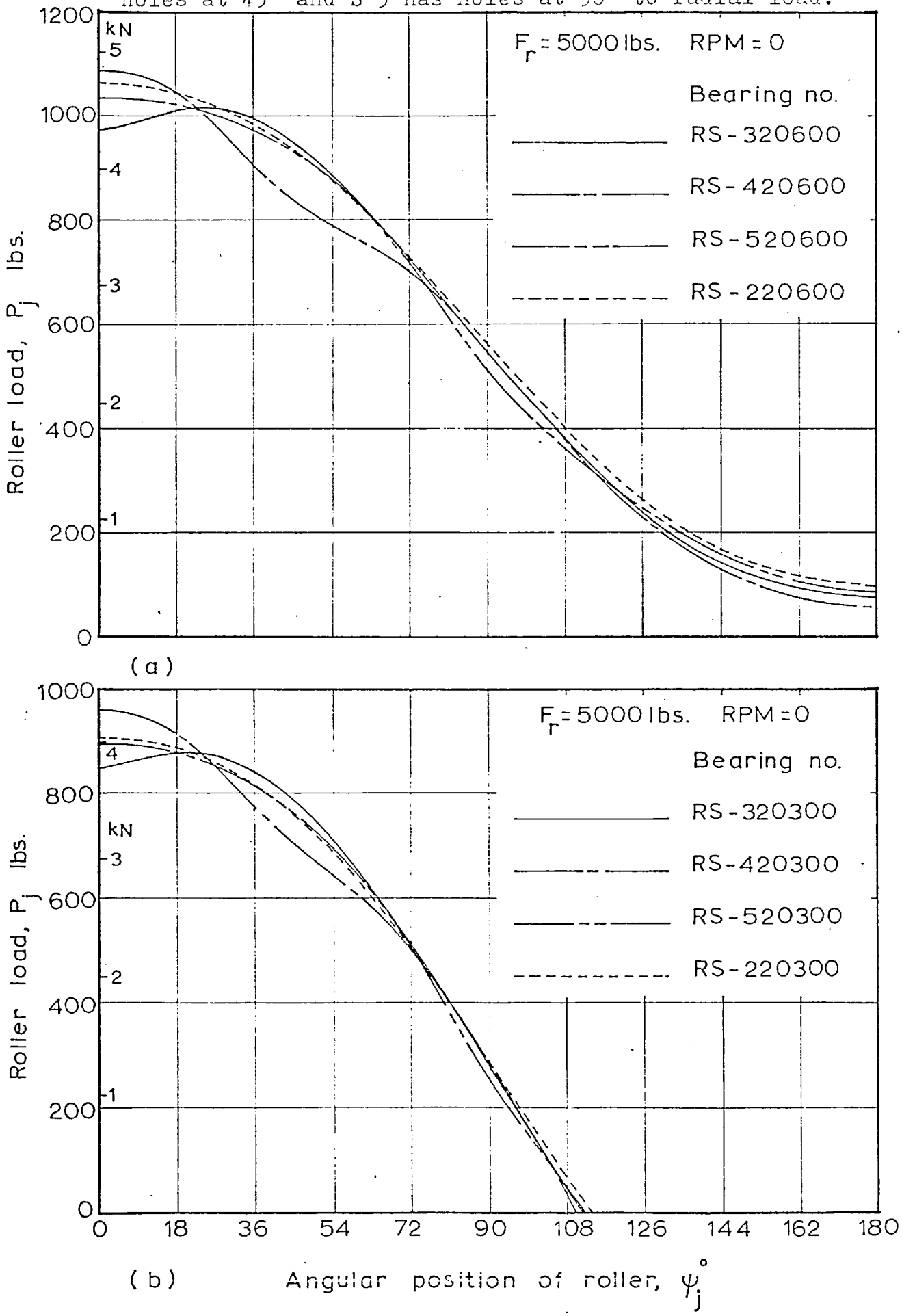


Fig. 7.30 Effect of other holes in the housing on the roller load distribution in a steel bearing with solid shaft and radial clearance (a) c= 0, (b) c= +600 μin.

Housing no. S 2 has no hole, S 3 has hole at 0°, S 4 has holes at 45° and S 5 has holes at 90° to radial load.

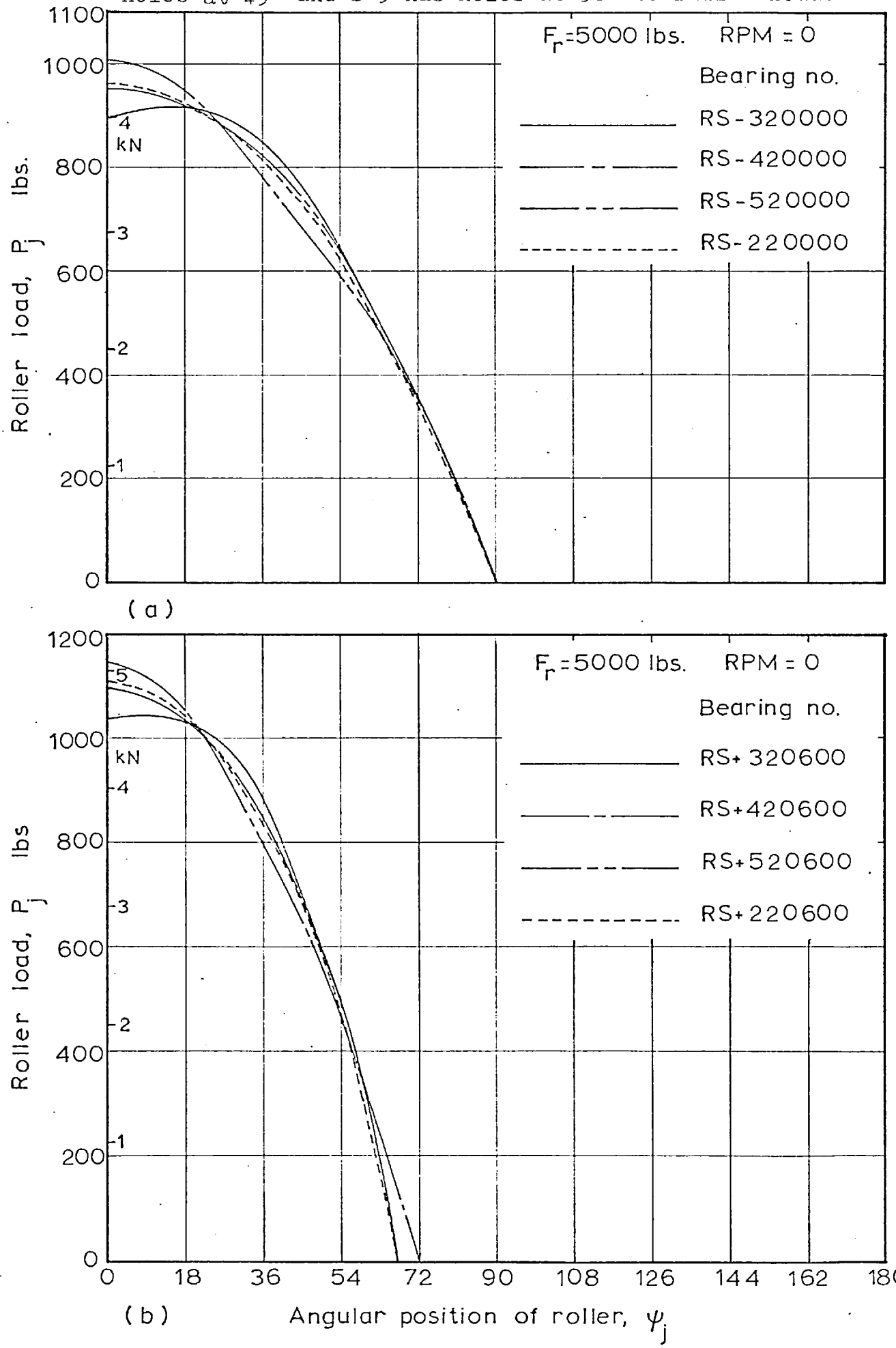


Fig. 7.31 Effect of other holes in the housing on the total radial and component deflections of a steel bearing with hollow shaft (no. 4).

δ_r = bearing radial deflection
δ_{or} = outer race deflection
δ_{ir} = inner race deflection
δ_b = body deflection of outer race

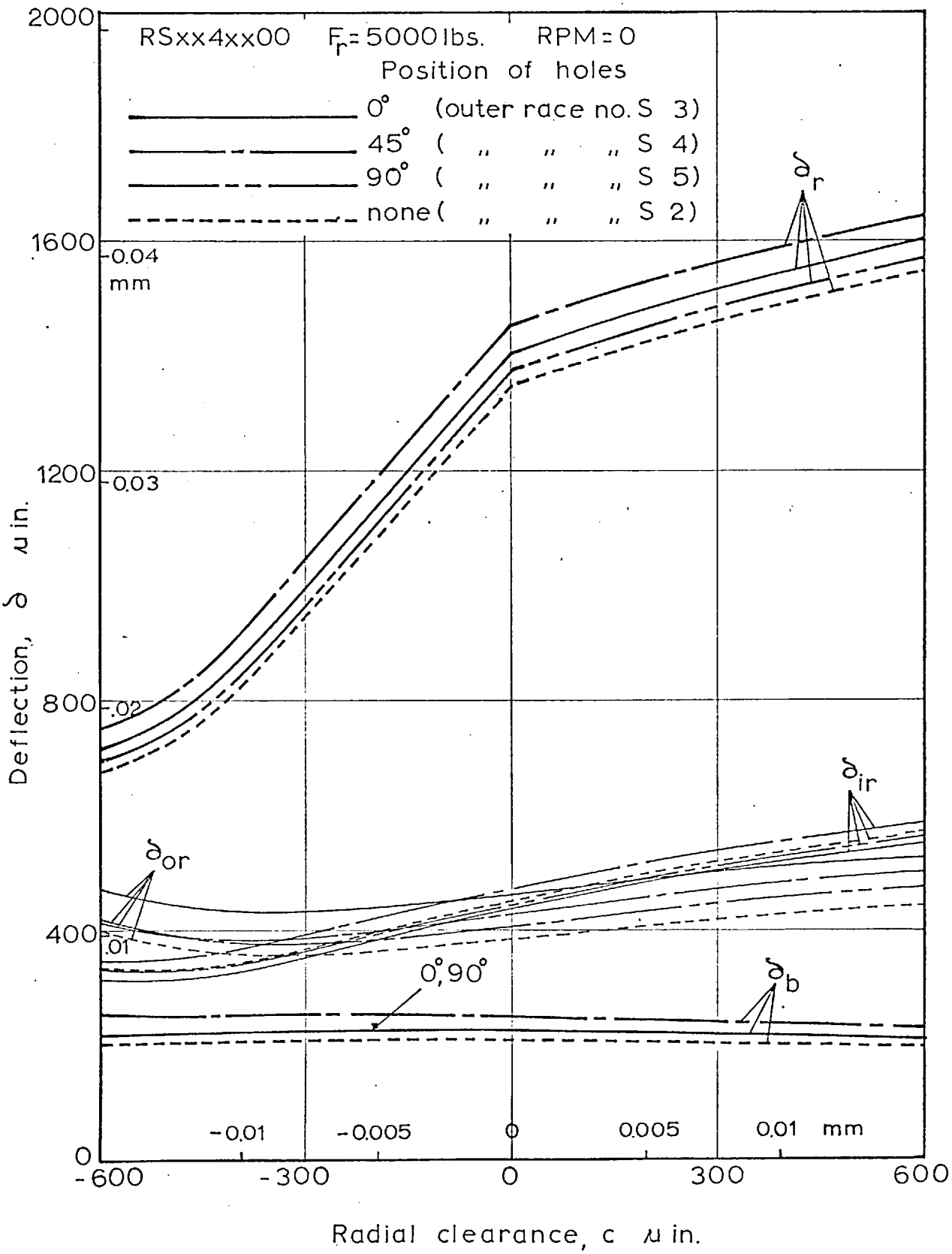


Fig. 7.32 Effect of other holes in the housing on the non-dimensional equivalent radial load (P_r/F_r) of a steel bearing having hollow shaft (no.4).

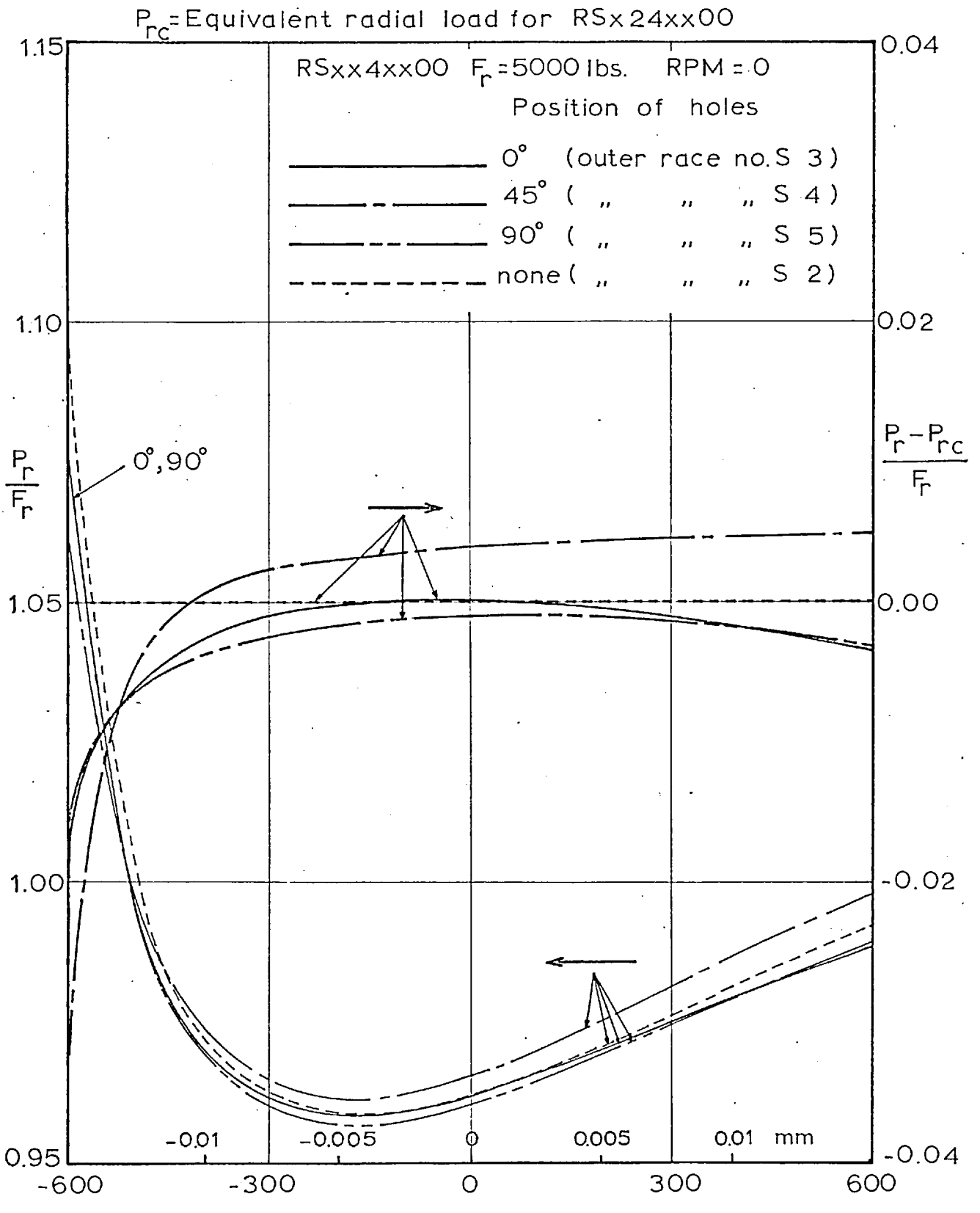
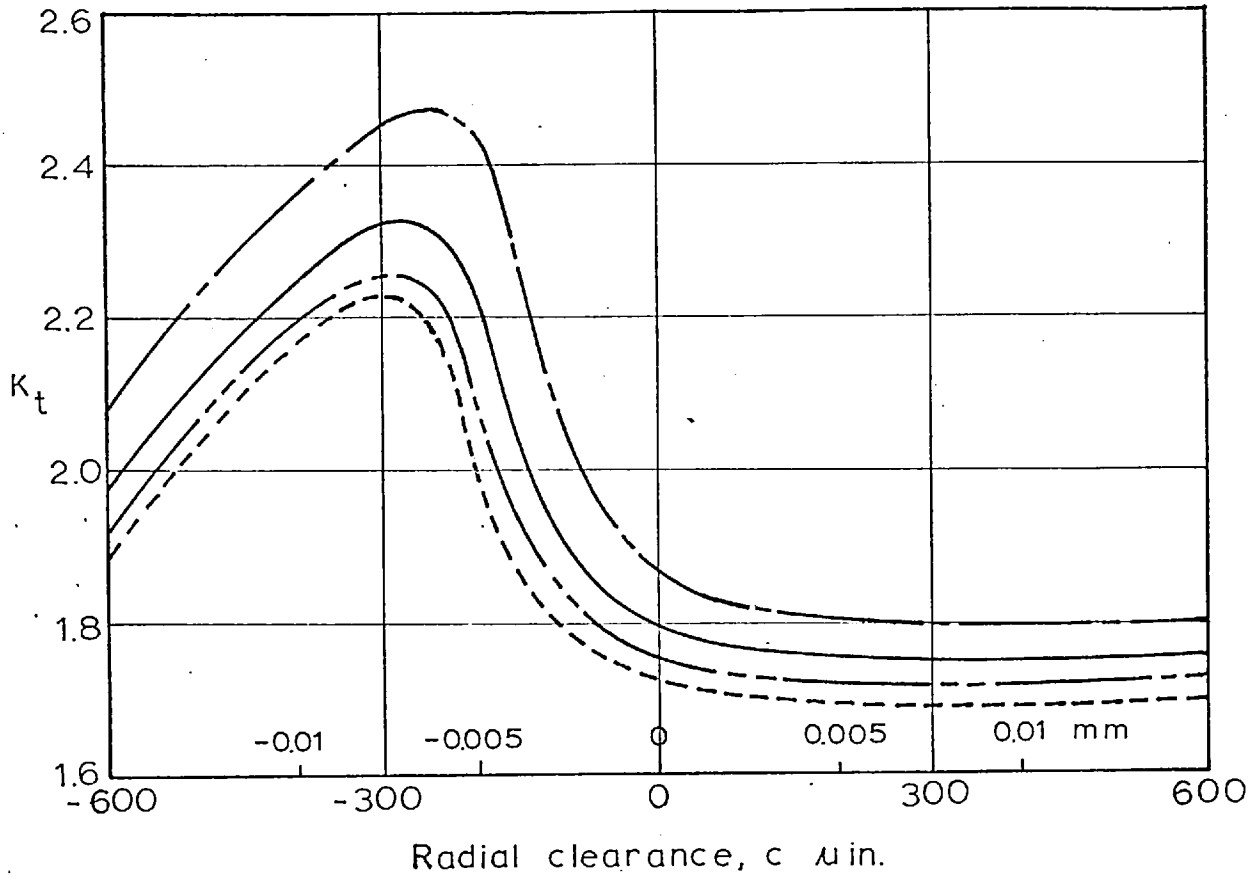


Fig. 7.33 Effect of other holes in the housing on K_t and K_b of a steel bearing with hollow shaft (no.4).

$$K_t = \frac{\delta_r \text{ for flexible races}}{\delta_r \text{ for rigid races}}, \quad K_b = \frac{\delta_b \text{ for flexible races}}{\delta_r \text{ for rigid races}}$$



RSxx4xx00 F_r = 5000 lbs. RPM = 0

Position of holes

0° (outer race no.S 3)

45° (" " " S 4)

90° (" " " S 5)

none(" " " S 2)

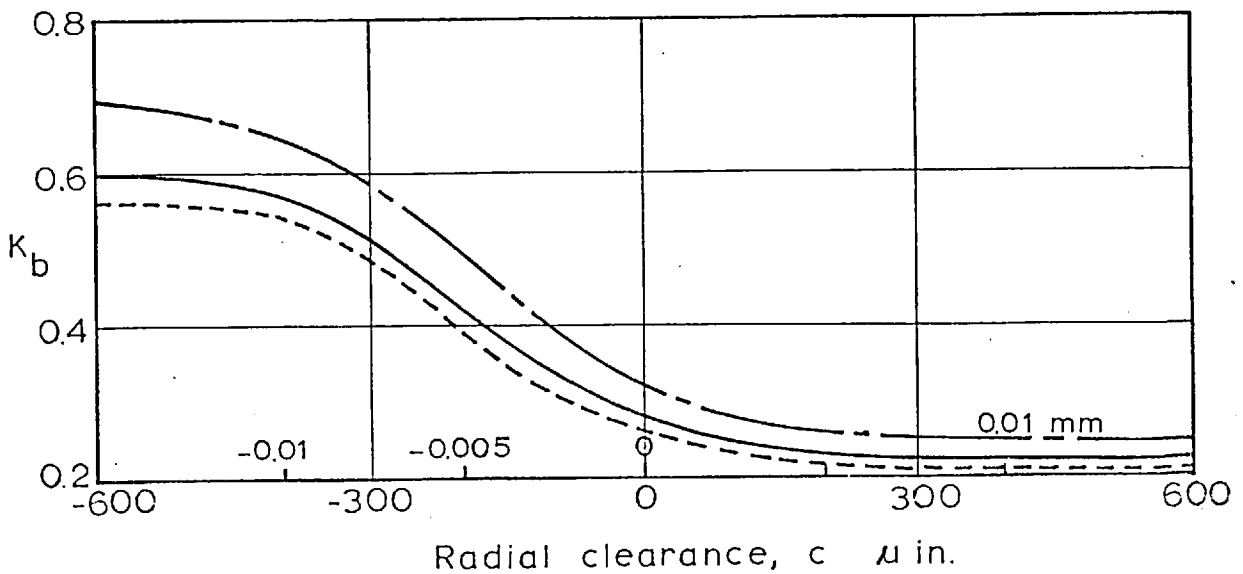


Fig. 7.34 Effect of other holes in the housing on the roller load distribution in a steel bearing with hollow shaft (no.4) and radial clearance (a) c= -600 μin., (b) c= +600 μin.
Housing no.S 2 has no hole, S 3 has hole at 0°, S 4 has holes at 45° and S 5 has holes at 90° to radial load.

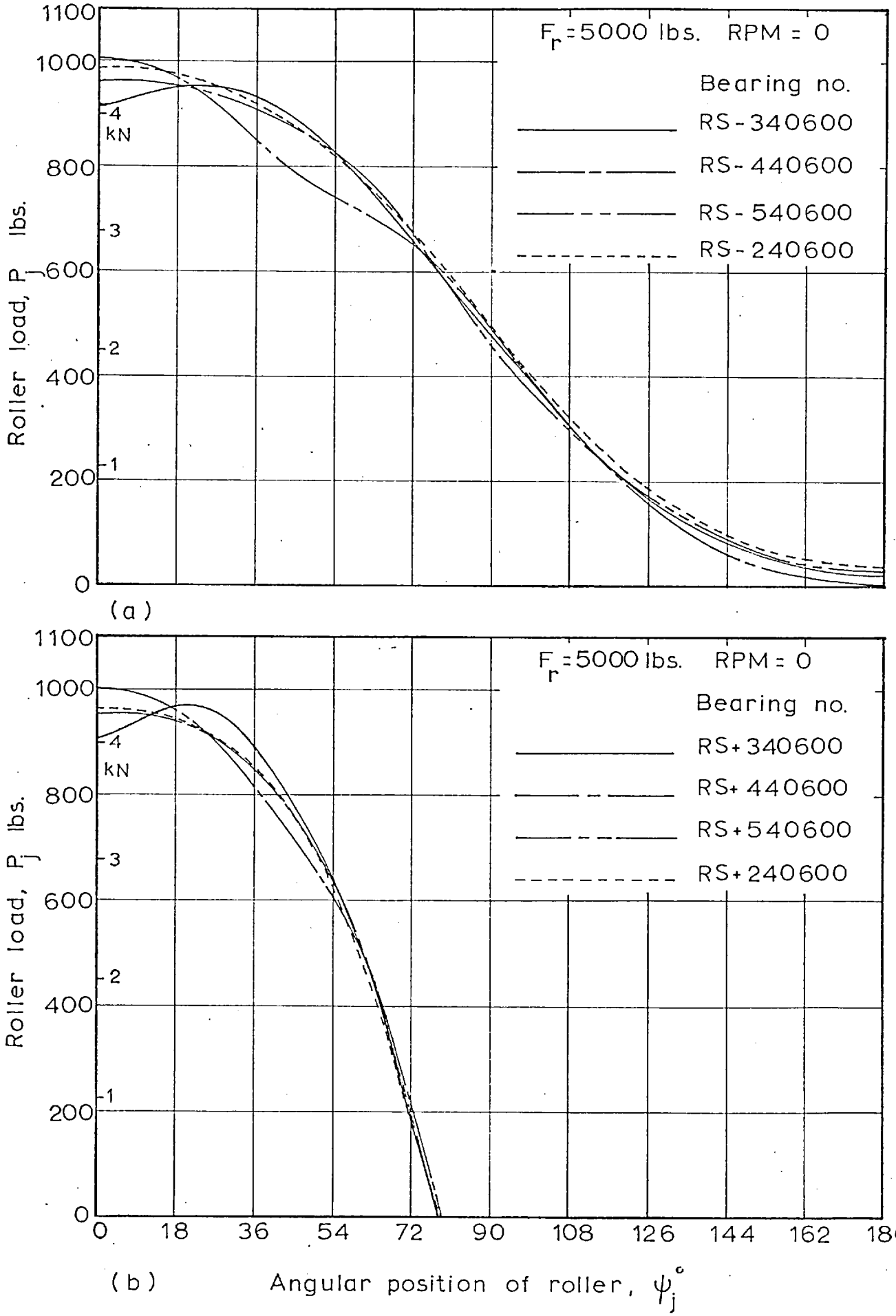


Fig. 7.35 Effect of boss radial thickness on the total radial and component deflections of a steel bearing with solid shaft.

δ_r = bearing radial deflection
δ_{or} = outer race deflection
δ_{ir} = inner race deflection
δ_b = body deflection of outer race.

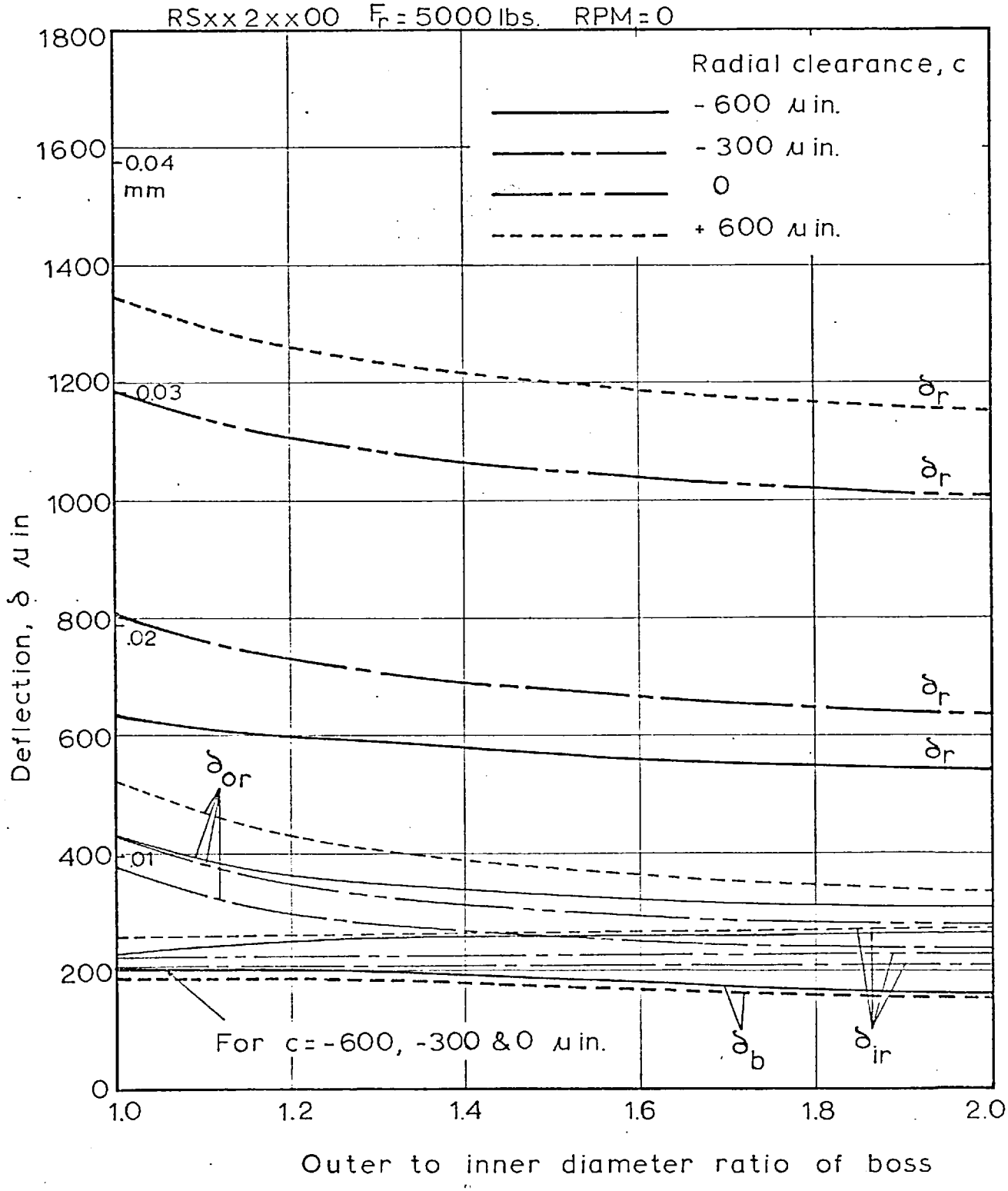


Fig. 7.36 Effect of radial clearance on the decrease in total radial (δ_r) and body deflection of outer race (δ_b) compared with the case of housing with no boss, for a steel bearing having solid shaft, for different outer to inner diameter ratio of boss.

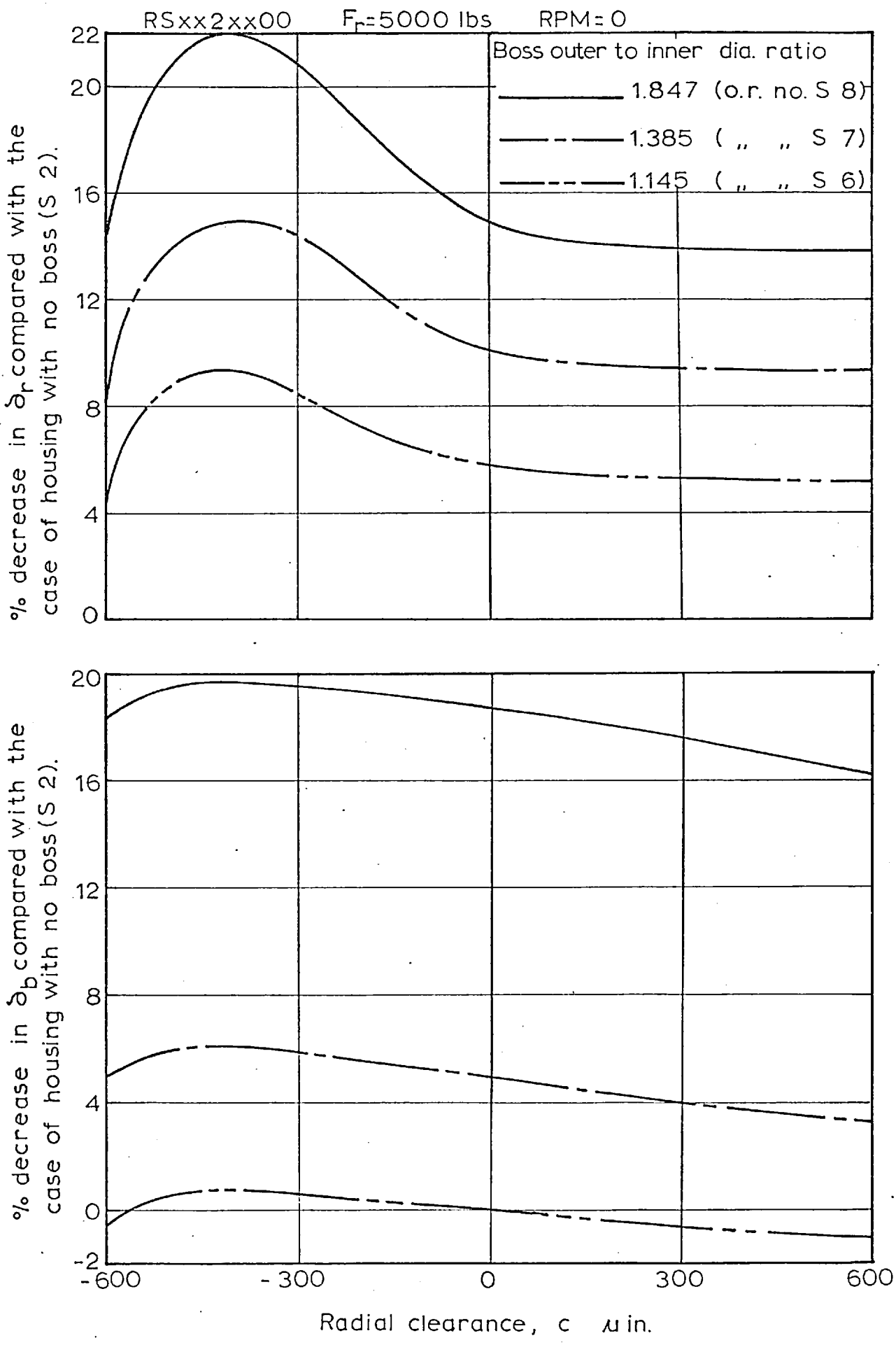


Fig. 7.37 Effect of boss radial thickness on the non-dimensional equivalent radial load (P_r/F_r) of a steel bearing having solid shaft.

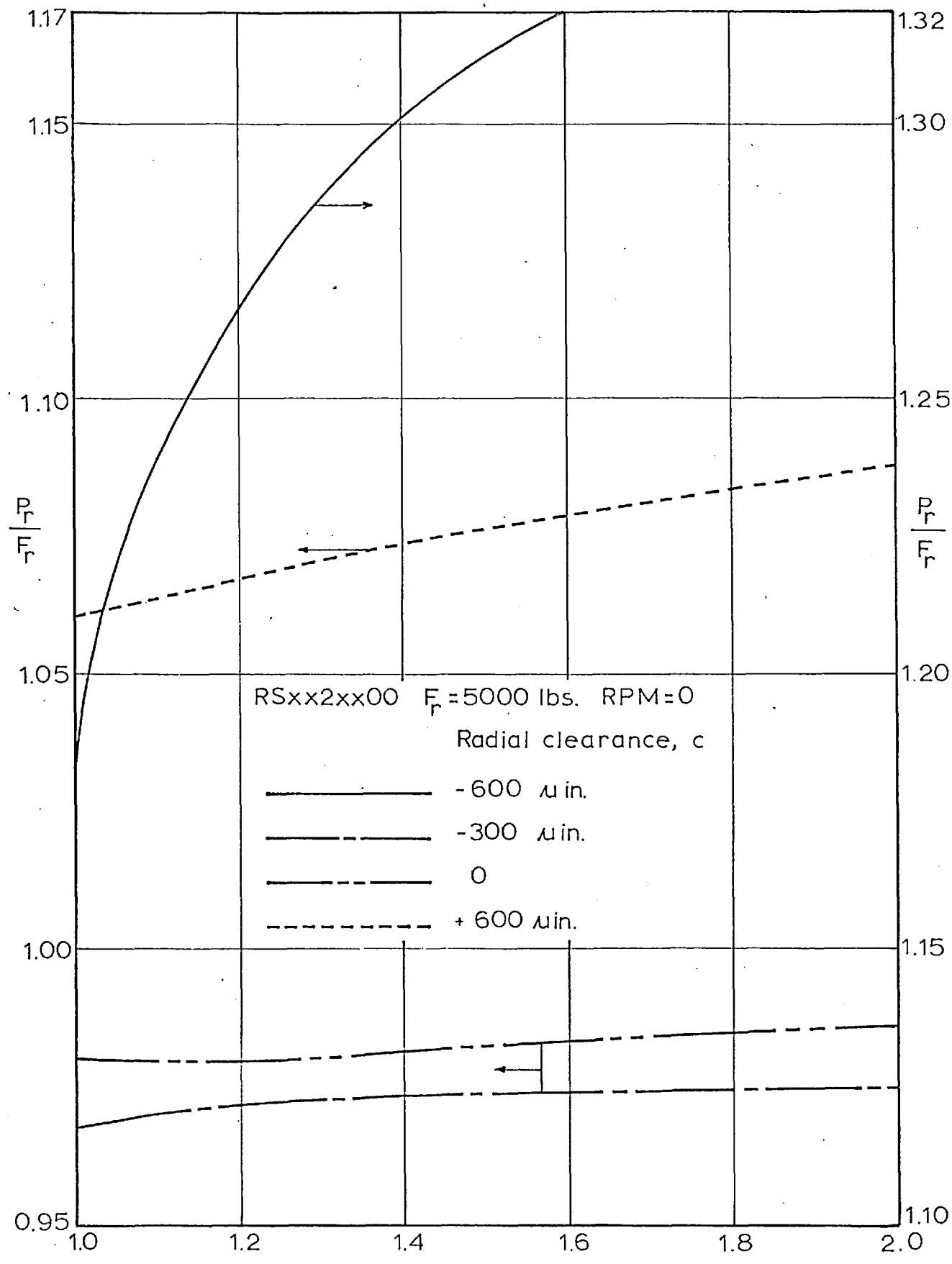


Fig. 7.38 Effect of boss radial thickness on K_t and K_b of a steel bearing with solid shaft.

$$K_t = \frac{\delta_r \text{ for flexible races}}{\delta_r \text{ for rigid races}}, \quad K_b = \frac{\delta_b \text{ for flexible races}}{\delta_r \text{ for rigid races}}$$

where, δ_r=radial deflection, δ_b=body deflection of outer race

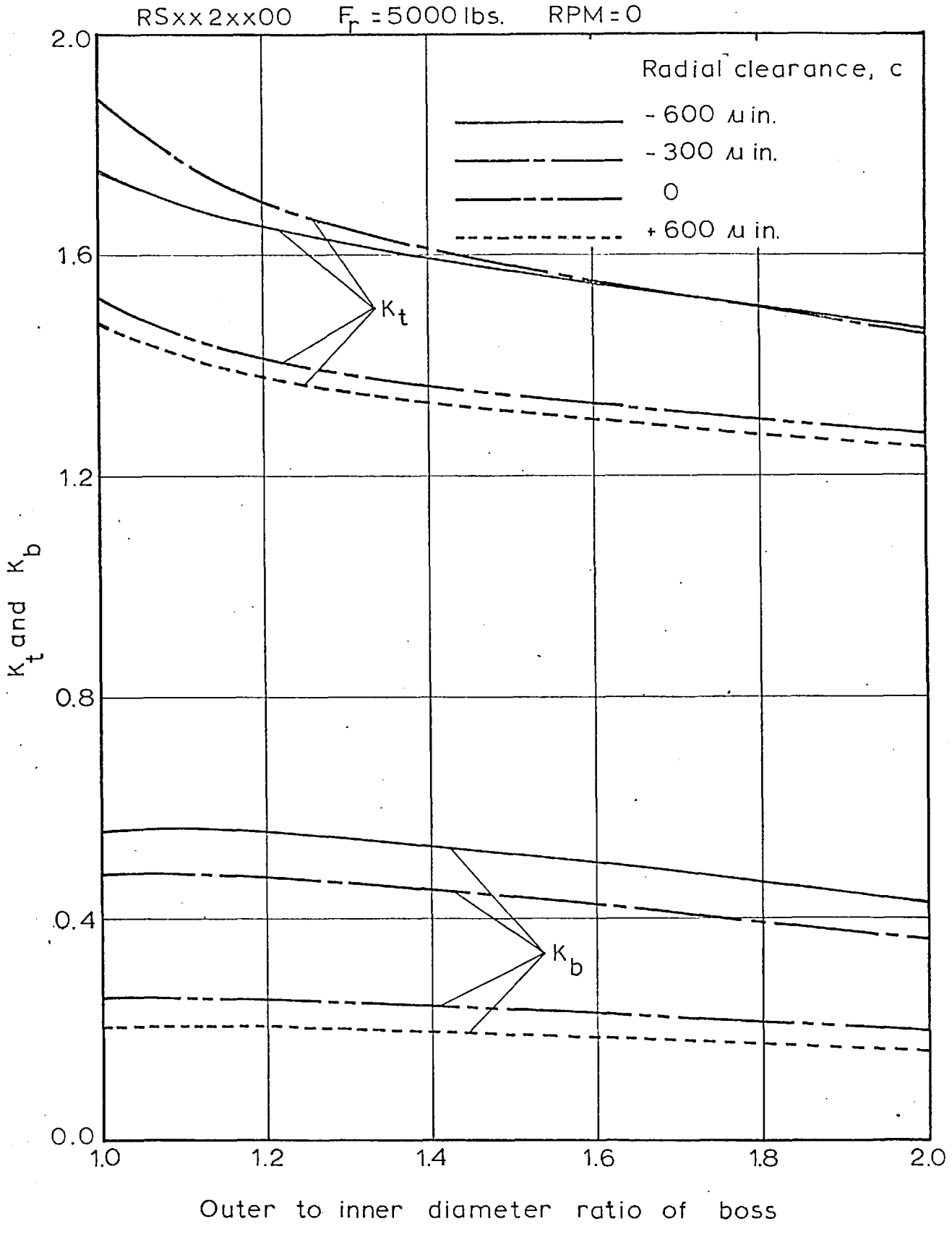


Fig. 7.39 Effect of boss radial thickness on the roller load distribution in a steel bearing with solid shaft and radial clearance (a) c= -600 μin., (b) c= +600 μin.

Boss outer to inner diameter ratio for housing no.S 2 is 1.0, S 6 is 1.145, S 7 is 1.385 and S 8 is 1.847.

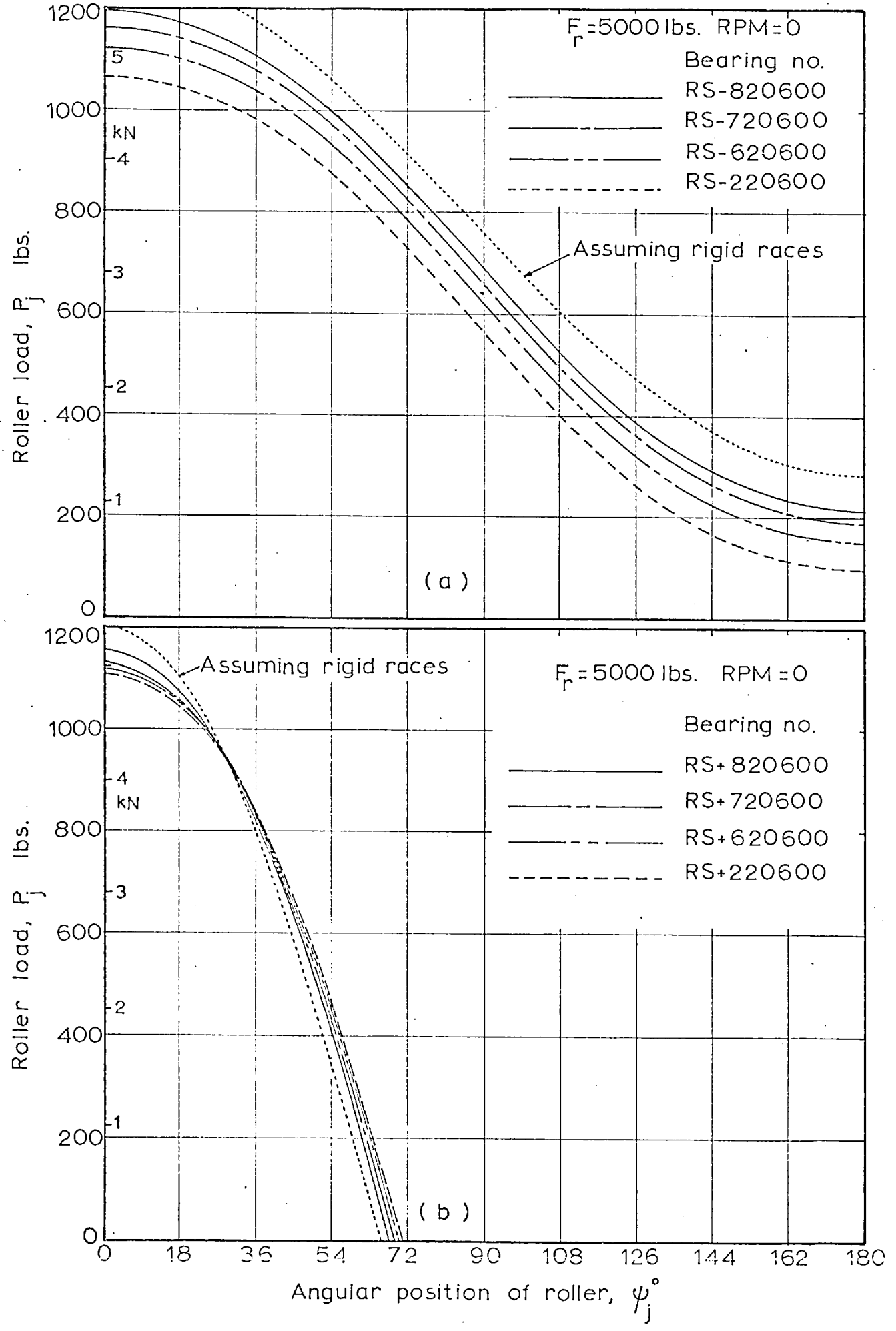


Fig. 7.40 Effect of boss radial thickness on the total radial and component deflections of a steel bearing with hollow shaft (no.4).

δ_r = bearing radial deflection
δ_{or} = outer race deflection
δ_{ir} = inner race deflection
δ_b = body deflection of outer race

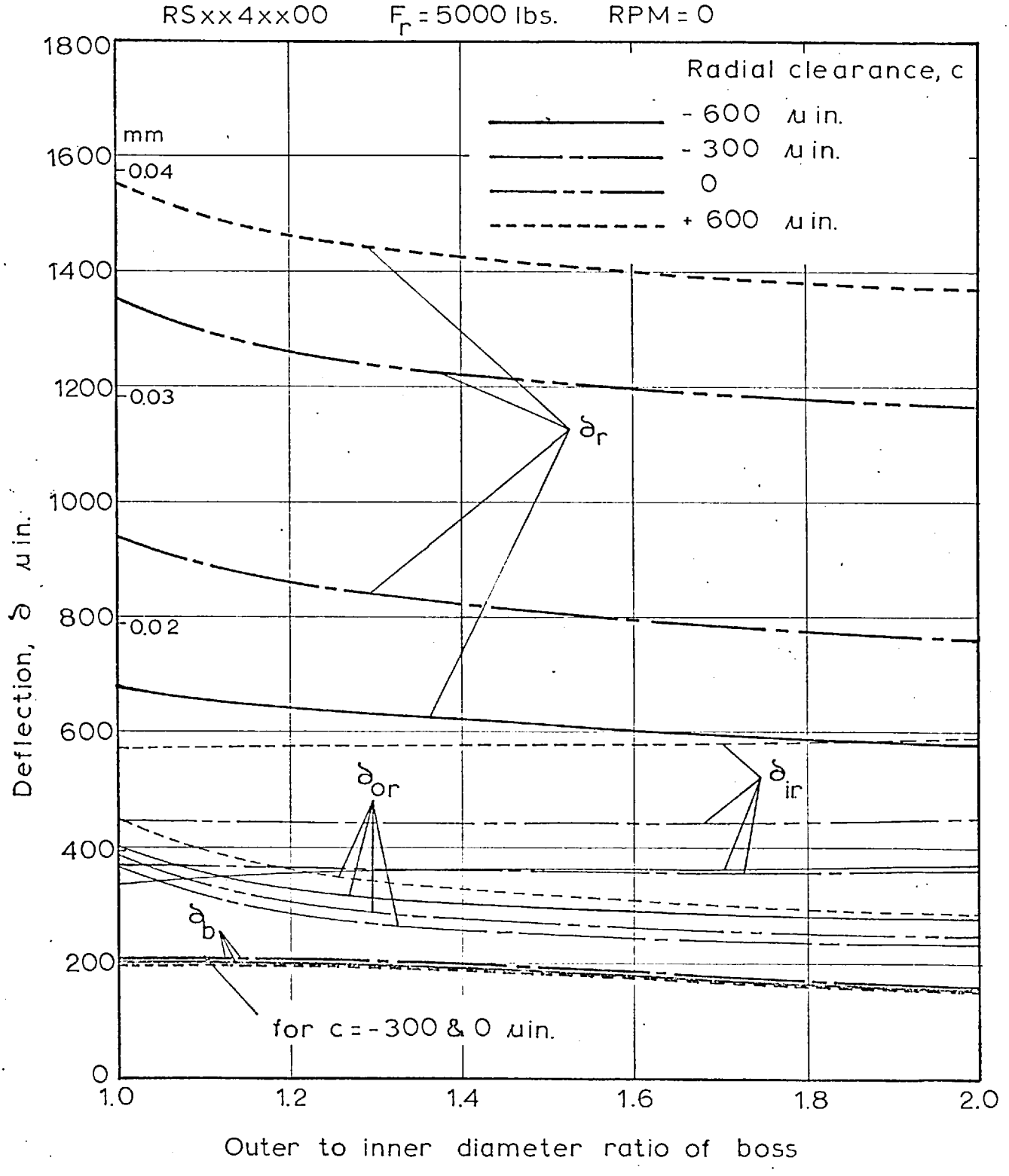


Fig. 7.41 Effect of boss radial thickness on the non-dimensional equivalent radial load (P_r/F_r) of a steel bearing having hollow shaft (no.4).

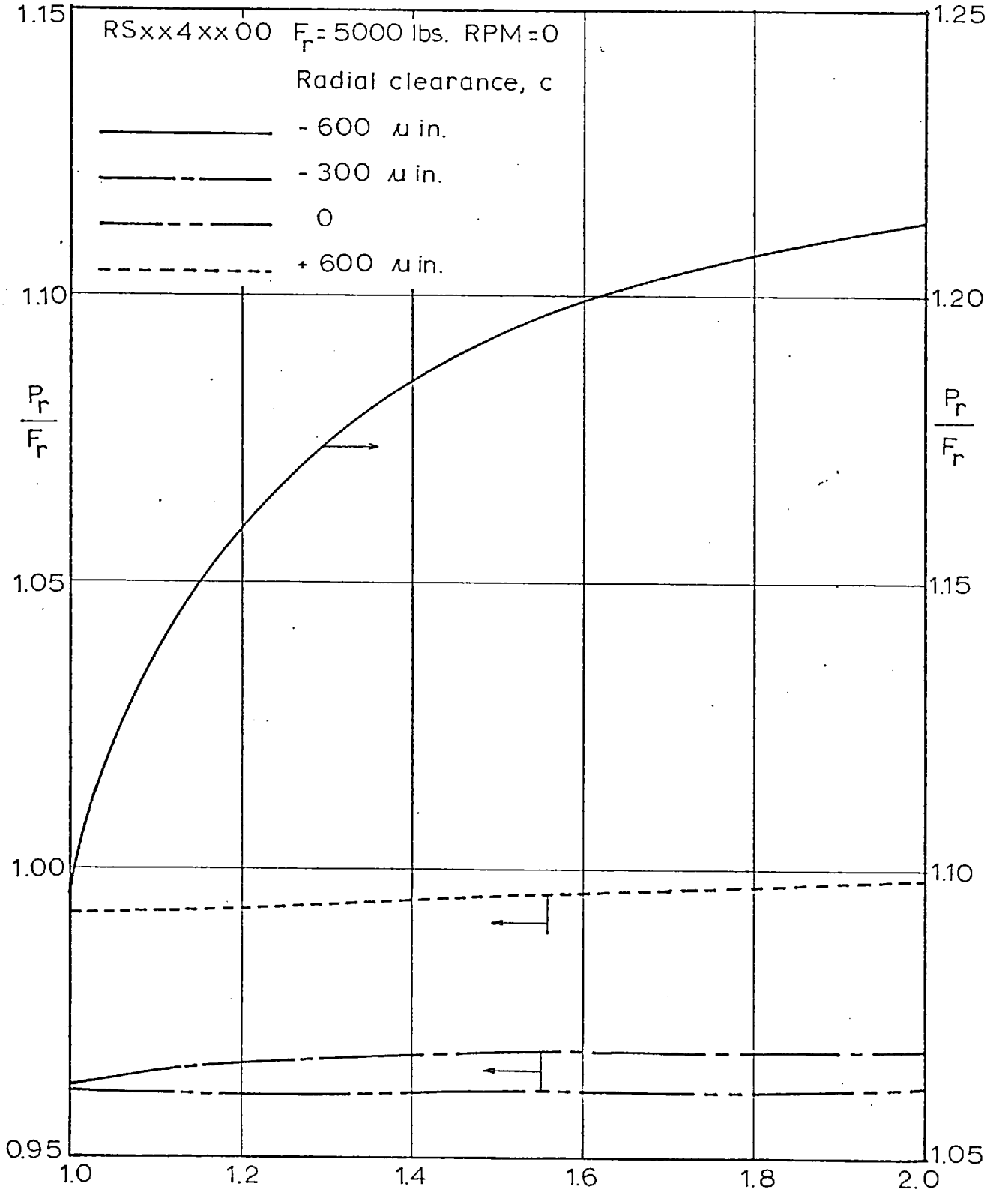


Fig. 7.42. Effect of boss radial thickness on K_t and K_b of a steel bearing with hollow shaft (no.4).

$$K_t = \frac{\delta_r \text{ for flexible races}}{\delta_r \text{ for rigid races}}, \quad K_b = \frac{\delta_b \text{ for flexible races}}{\delta_r \text{ for rigid races}}$$

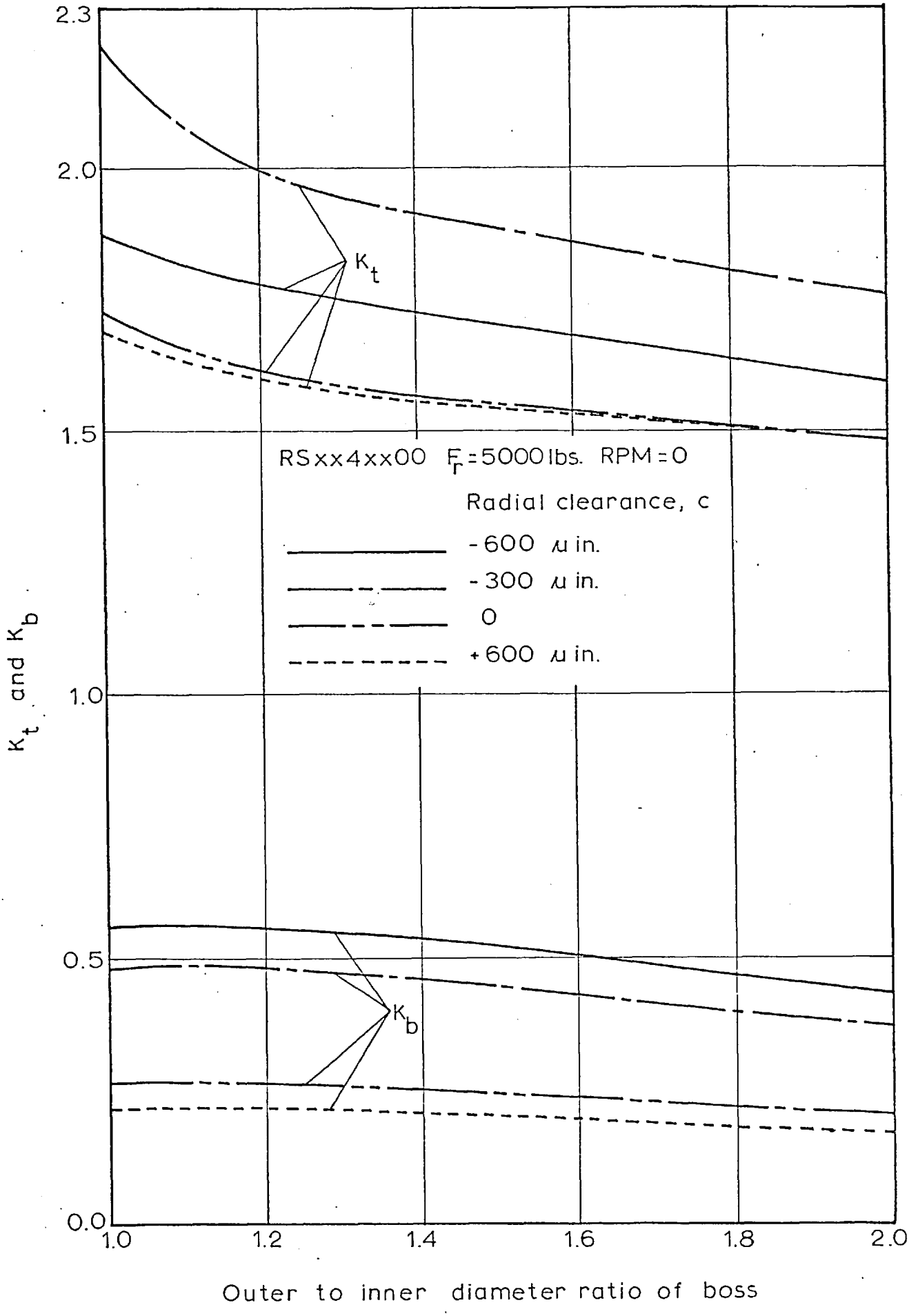


Fig. 7.43 Effect of boss radial thickness on the roller load distribution in a steel bearing with hollow shaft (no.4) and radial clearance (a) c= -600 uin. (b) c= +600 uin.

Boss outer to inner diameter ratio for housing no.S 2 is 1.0, S 6 is 1.145, S 7 is 1.385 and S 8 is 1.847.

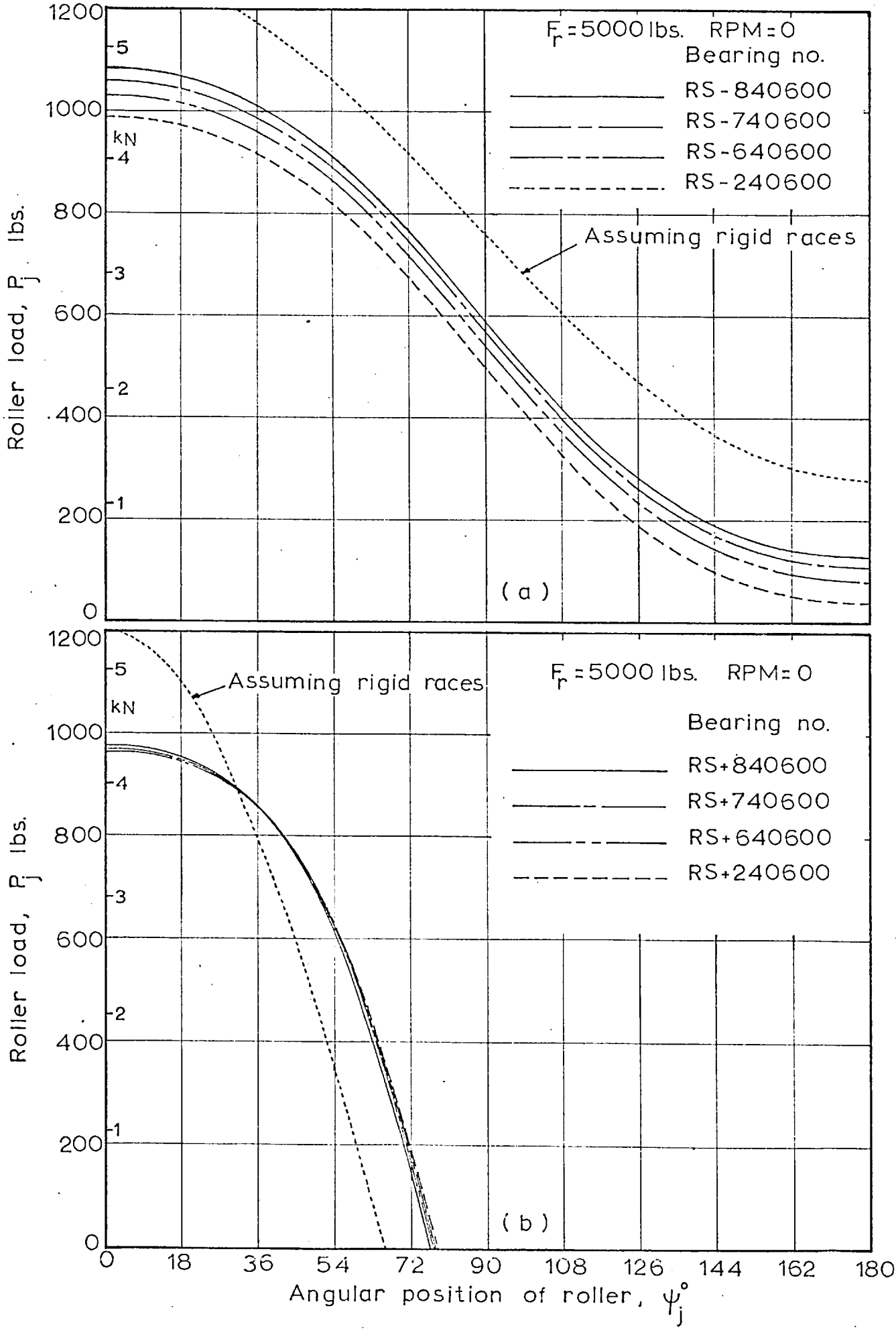


Fig. 7.44 Excess radial and component deflections, for housing with upright cruciform ribs over those for housing without ribs, of a steel bearing with solid shaft.

δ_r= radial deflection, δ_b= body deflection of outer race, δ_{or}= outer race deflection, δ_{ir}= inner race deflection.

Subscripts: A for housing with ribs (R 2, R 3 & R 4) ⊞

B for housing without ribs (S 6, S 7 & S 8)

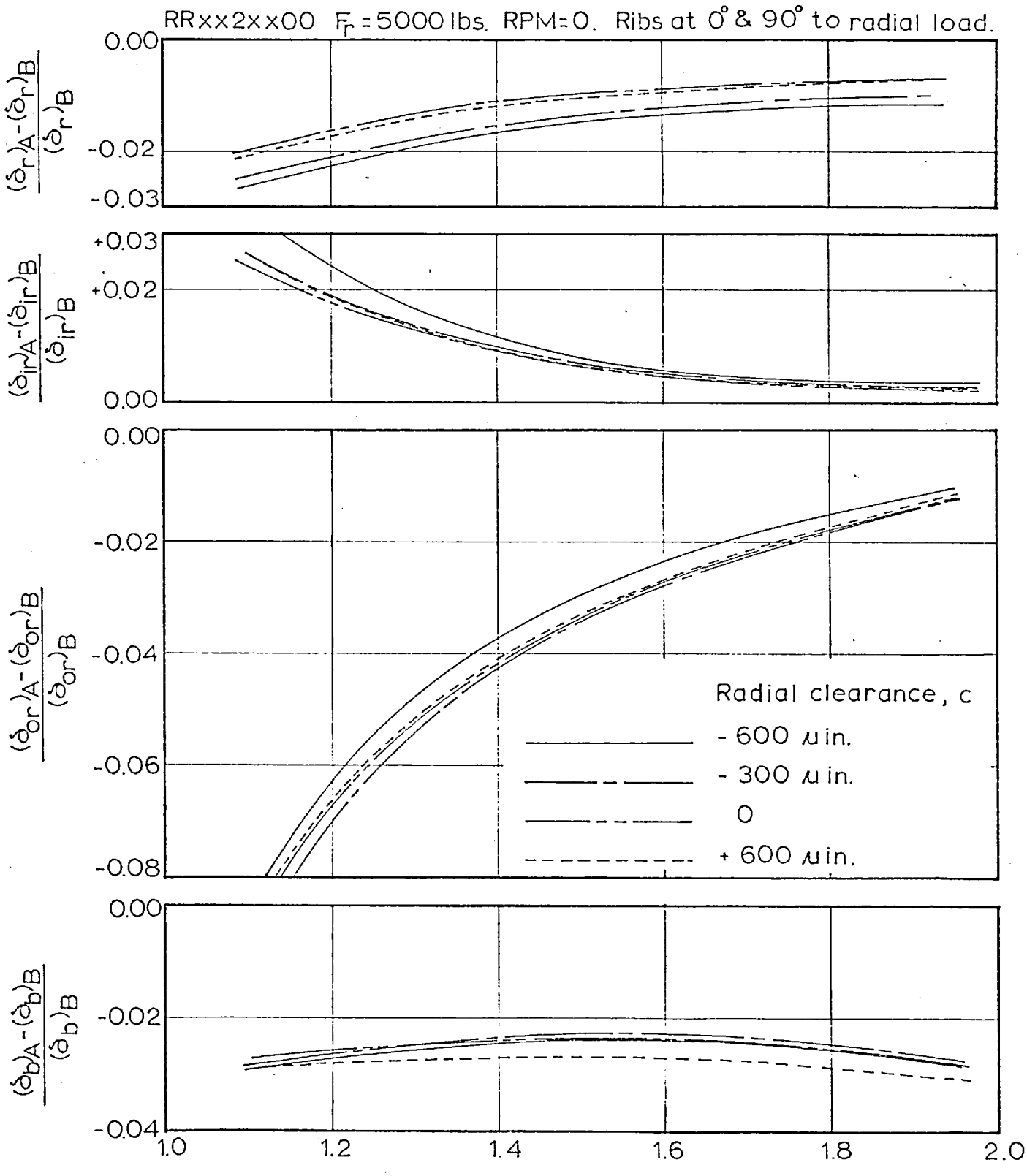


Fig. 7.45 K_t and K_b, for housing with upright cruciform ribs, of a steel radial roller bearing with solid shaft.

$$K_t = \frac{\delta_r \text{ for flexible races}}{\delta_r \text{ for rigid races}}, \quad K_b = \frac{\delta_b \text{ for flexible races}}{\delta_r \text{ for rigid races}}$$

where, δ_r = radial deflection, δ_b = body deflection of outer race.

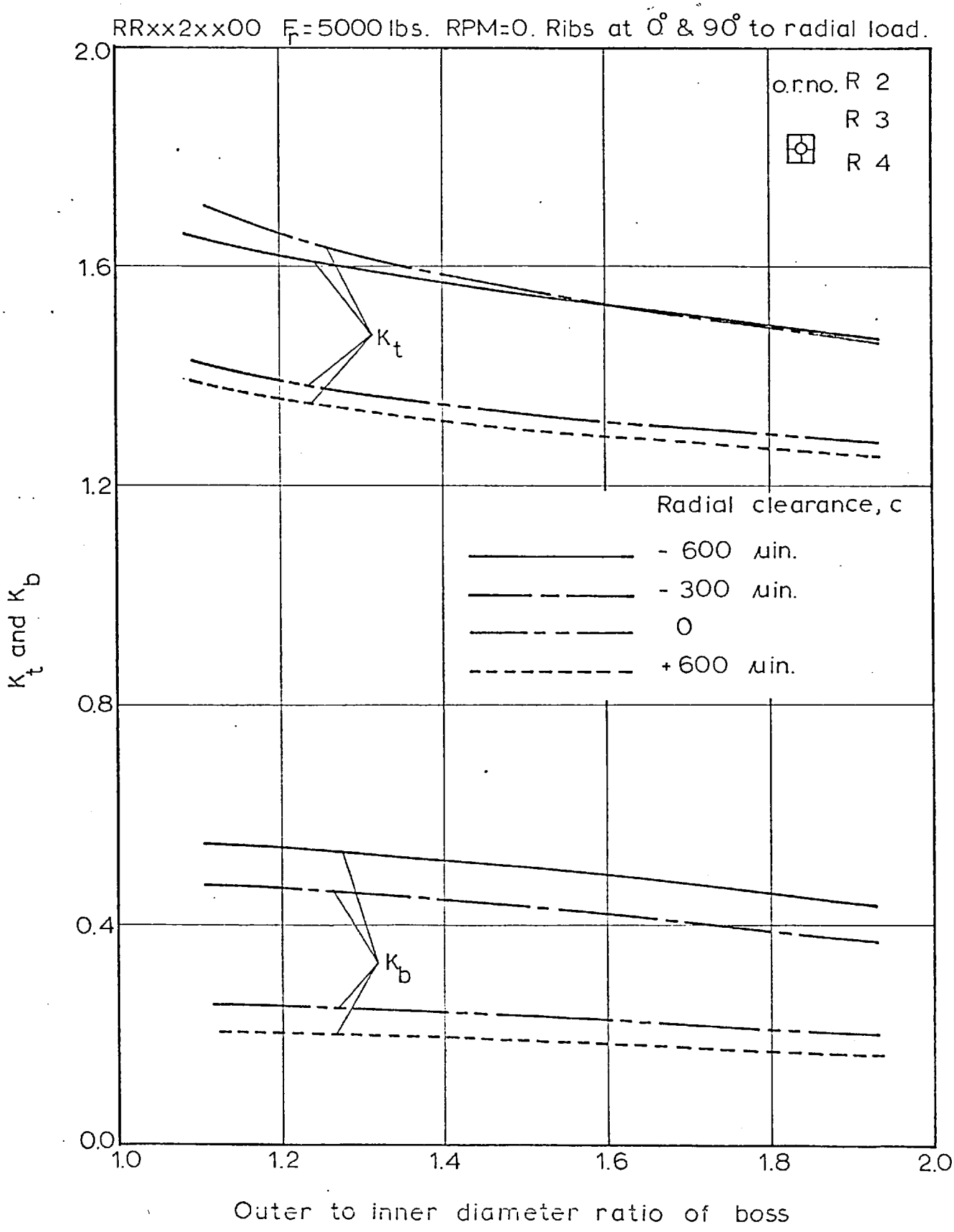
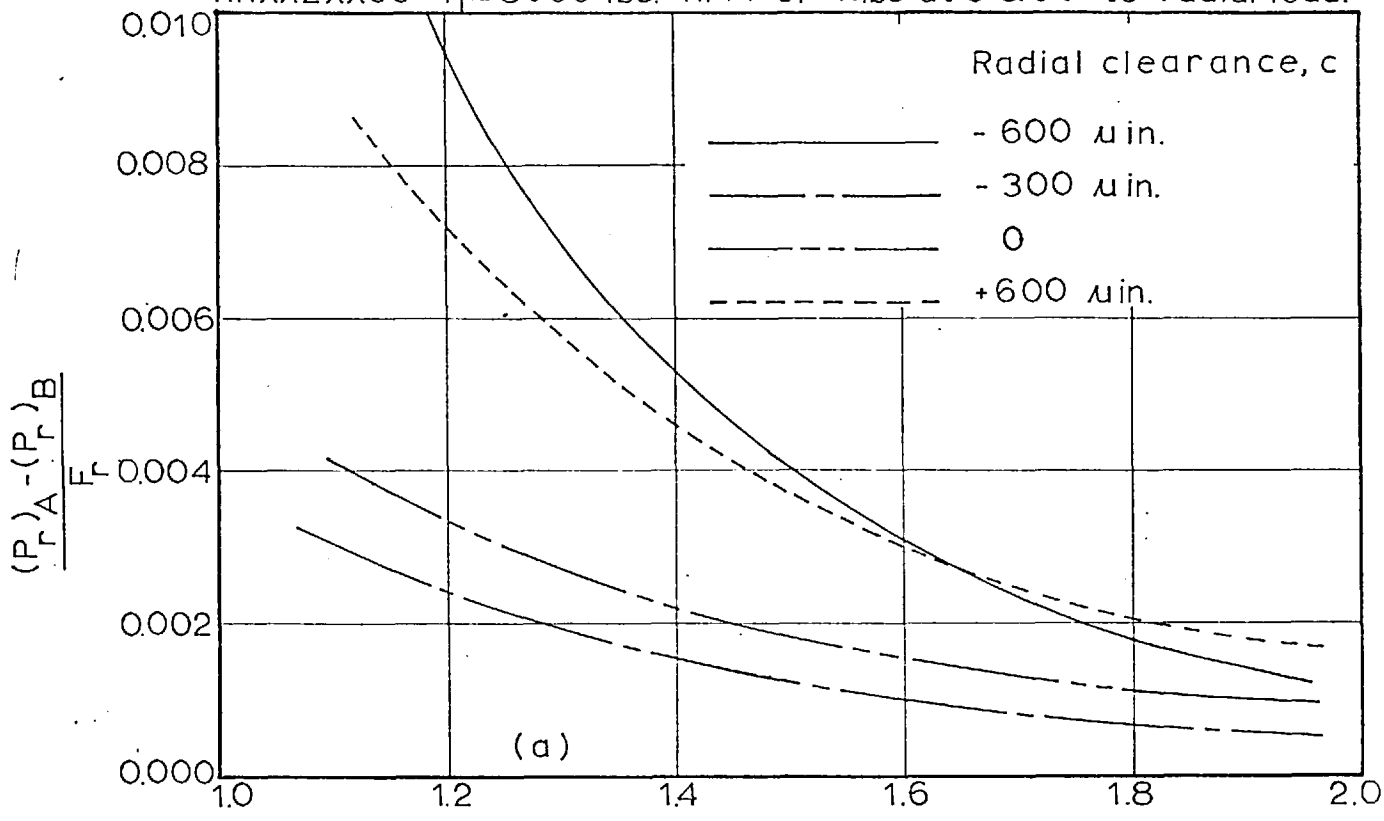
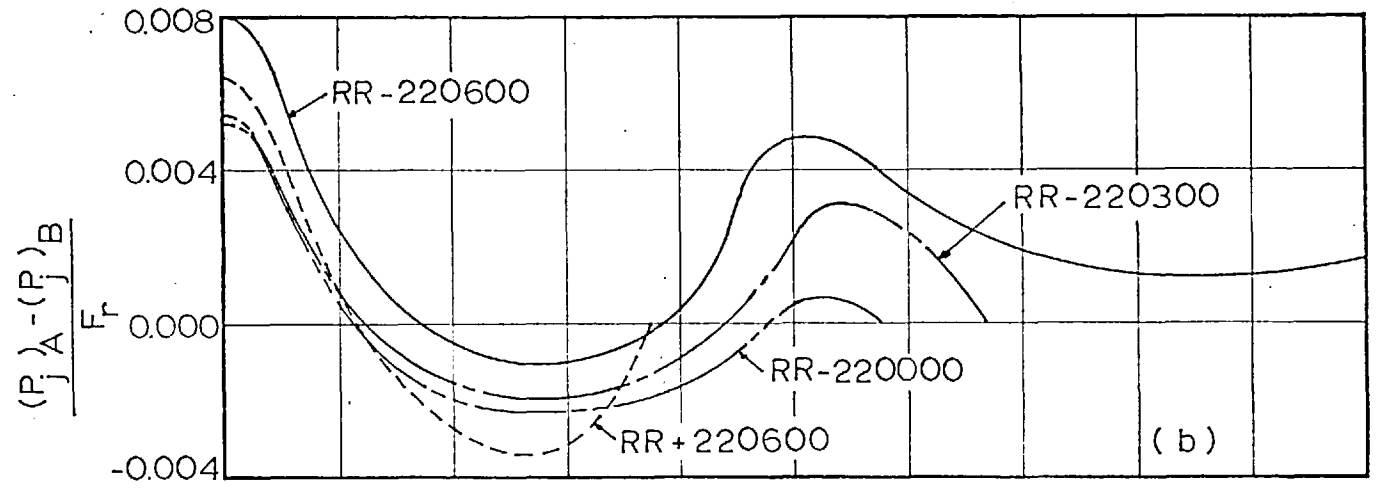


Fig. 7.46 For a steel bearing with solid shaft and housing having upright cruciform ribs,
(a) excess non-dimensional equivalent radial load (P_r/F_r) over non-ribbed case,
and excess roller load distribution over non-ribbed case
(b) for housing with thinnest boss (R 2) at different c,
and (c) for increasing boss thickness at c= -300 μin.

Subscripts: A for housing with ribs (R 2, R 3 & R 4)
B for housing without ribs (S 6, S 7 & S 8)

RRxx2xx00 F_r = 5000 lbs. RPM=0. Ribs at 0° & 90° to radial load.





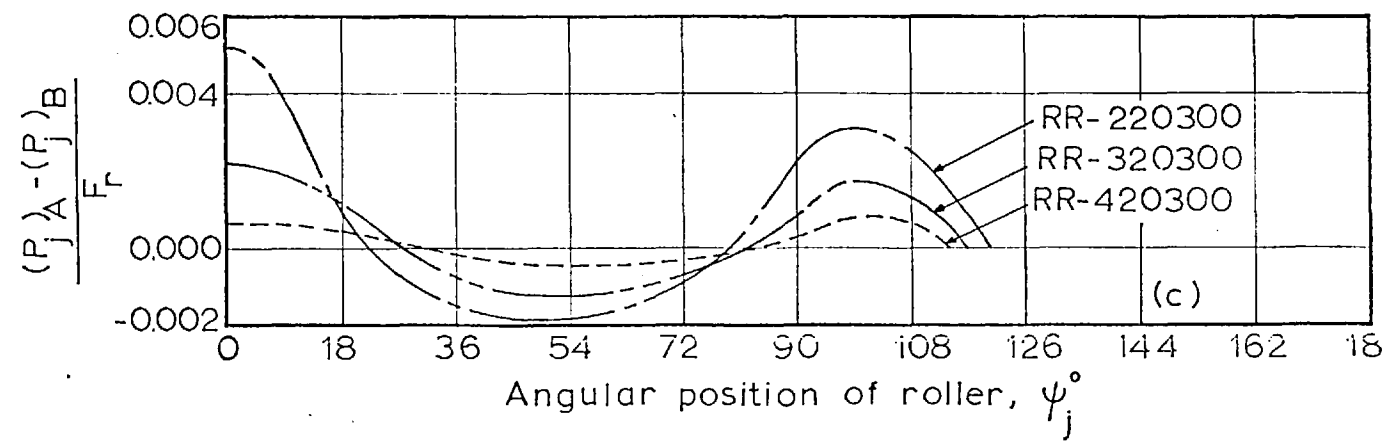


Fig. 7.47 Excess radial and component deflections, for housing with upright cruciform ribs over those for housing without ribs, of a steel bearing with hollow shaft (no.4).

δ_r= radial deflection, δ_b= body deflection of outer race, δ_{or}= outer race deflection, δ_{ir}= inner race deflection.

Subscripts: A for housing with ribs (R 2, R 3 & R 4)

B for housing without ribs (S 6, S 7 & S 8)

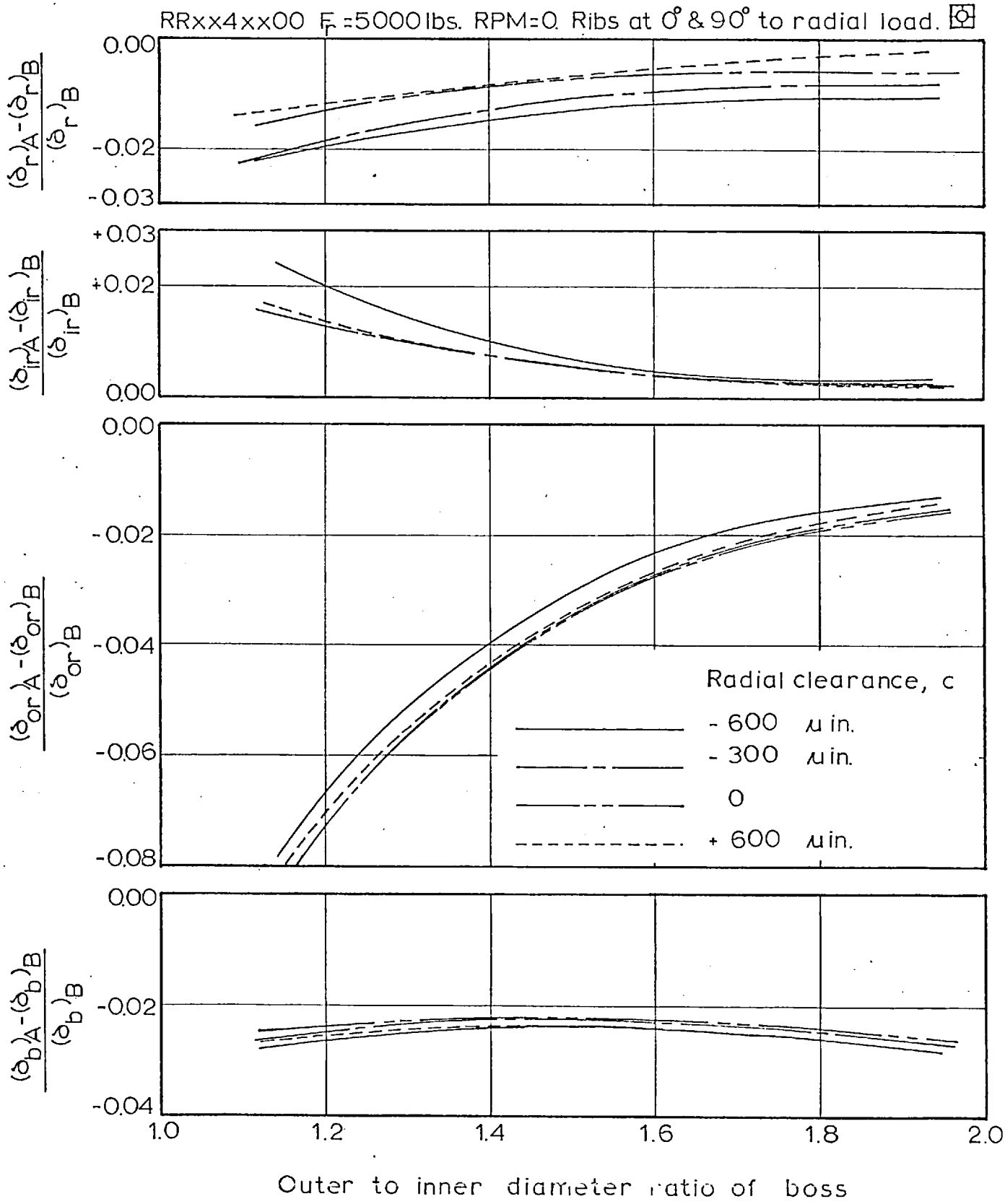


Fig. 7.48 K_t and K_b, for housing with upright cruciform ribs, of a steel radial roller bearing with hollow shaft (no.4).

$$K_t = \frac{\delta_r \text{ for flexible races}}{\delta \text{ for rigid races}}, \quad K_b = \frac{\delta_b \text{ for flexible races}}{\delta_r \text{ for rigid races}}$$

where, δ_r = radial deflection, δ_b = body deflection of outer race

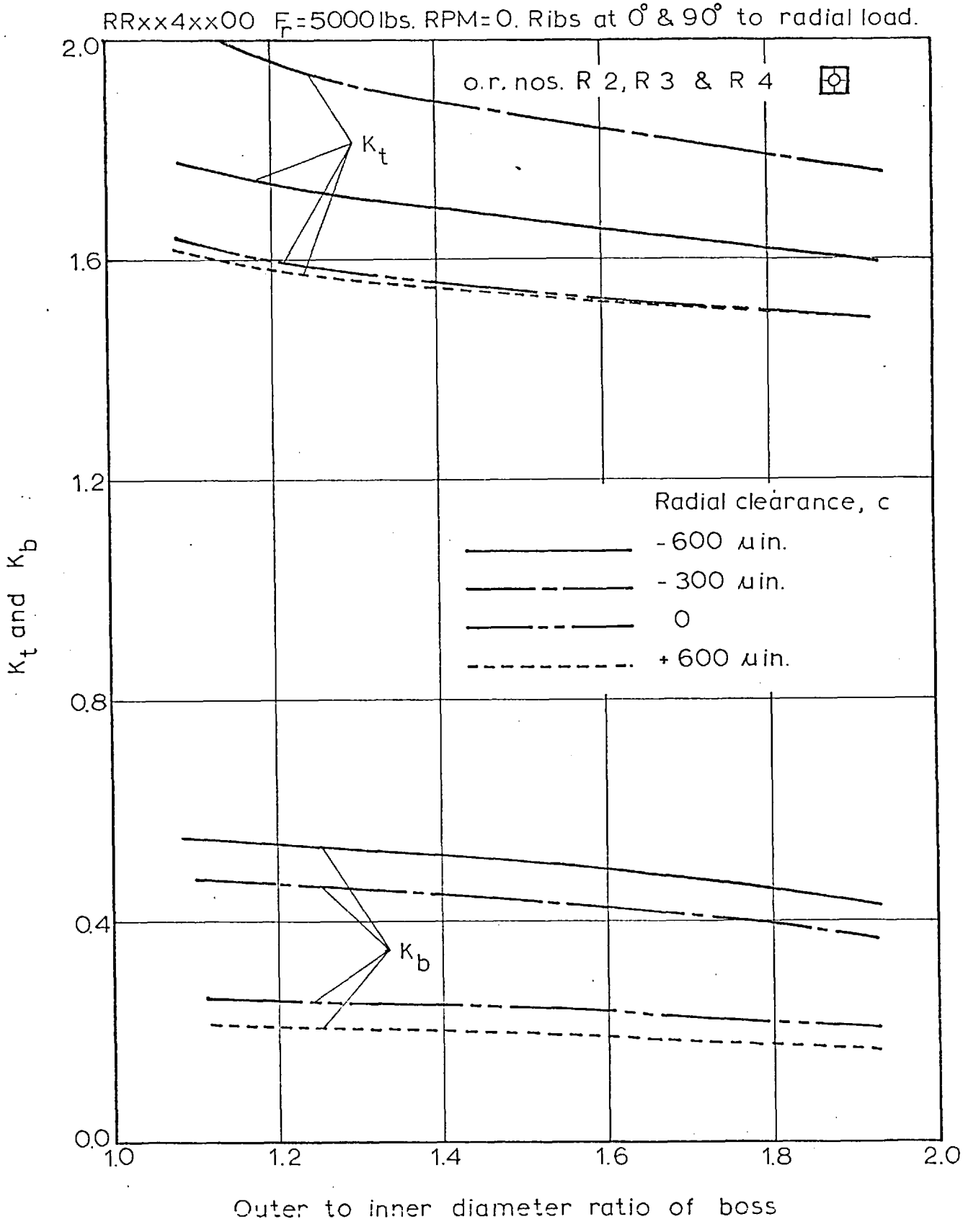
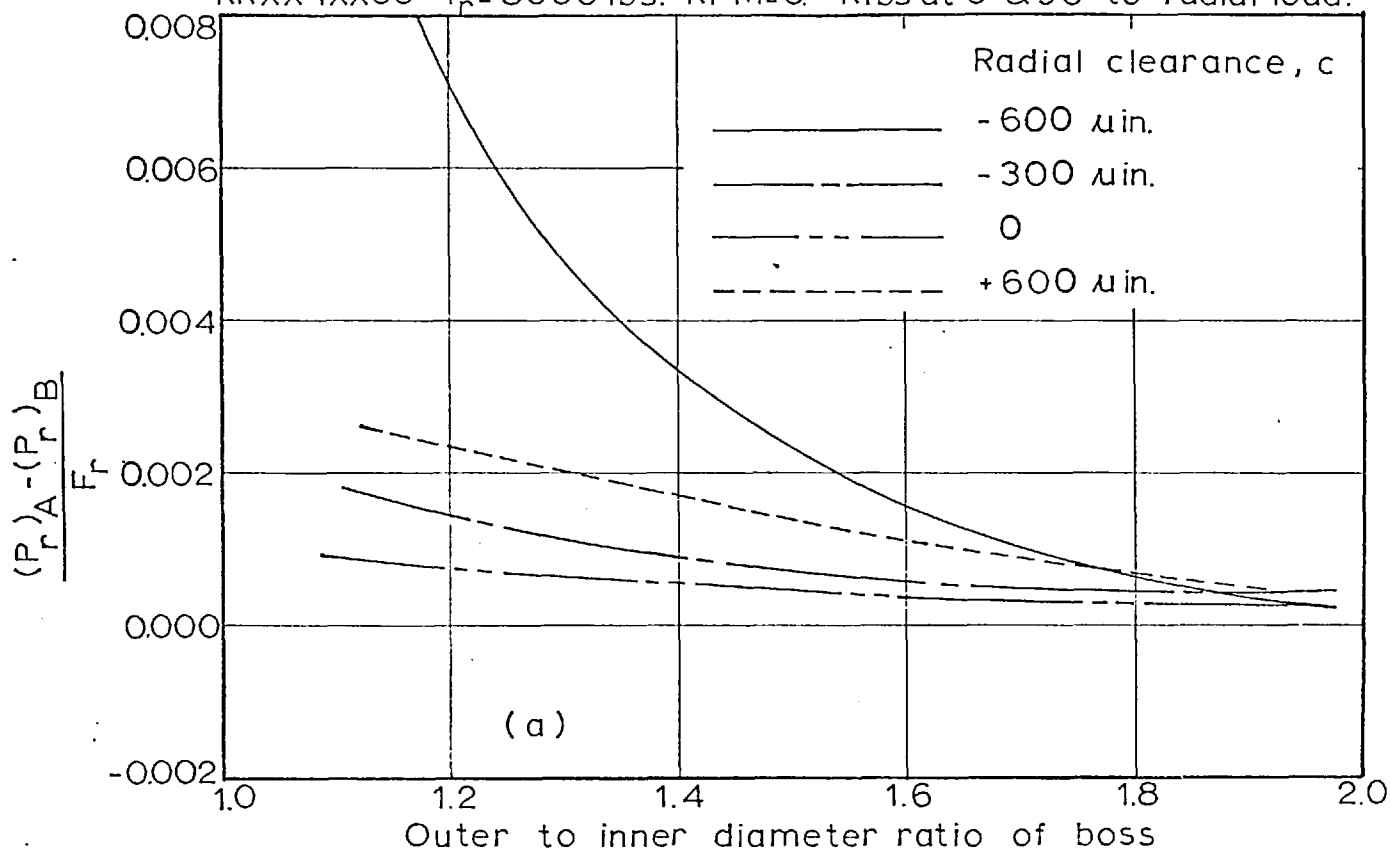
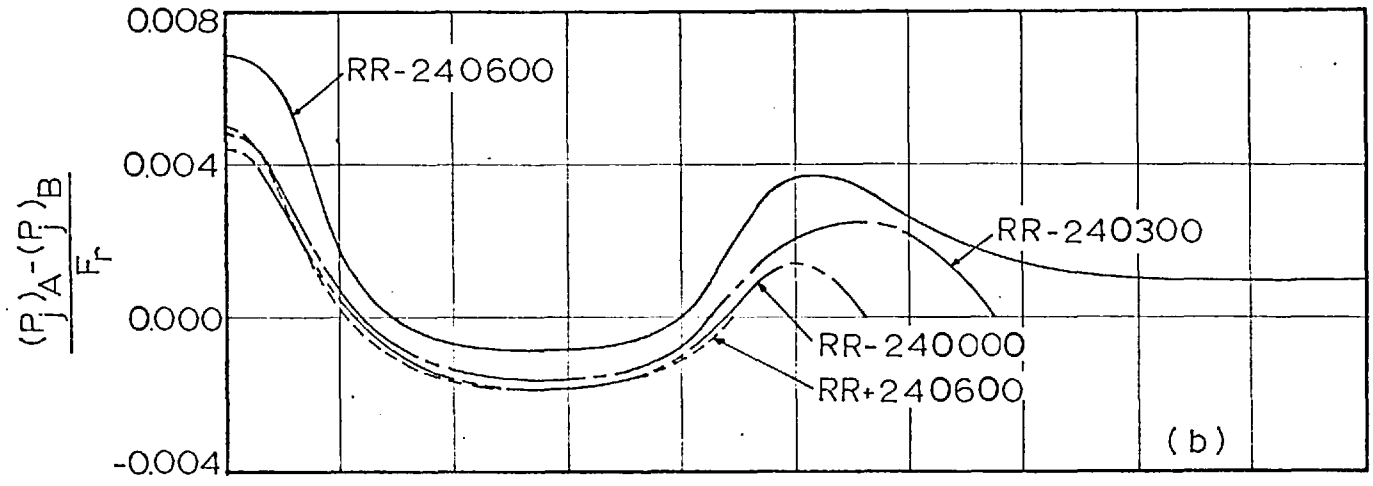


Fig. 7.49 For a steel bearing with hollow shaft (no.4) and housing having upright cruciform ribs,
(a) excess non-dimensional equivalent radial load (P_r/F_r) over non-ribbed case,
and excess roller load distribution over non-ribbed case
(b) for housing with thinnest boss (R 2) at different c,
and (c) for increasing boss thickness at c= -300 μin.

Subscripts: A for housing with ribs (R 2, R 3 & R 4)
B for housing without ribs (S 6, S 7 & S 8)

RRxx4xx00 F_r= 5000 lbs. RPM=0. Ribs at 0° & 90° to radial load.





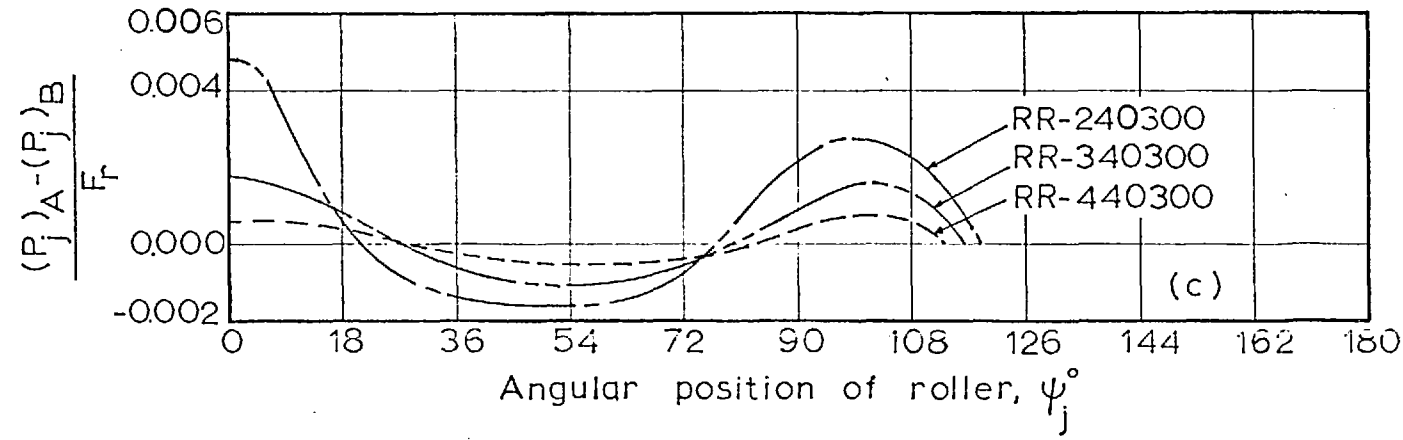


Fig. 7.50 Excess radial and component deflections, for housing with diagonal cruciform ribs over those for housing without ribs, of a steel bearing with solid shaft.

δ_r= radial deflection, δ_b= body deflection of outer race, δ_{or}= outer race deflection, δ_{ir}= inner race deflection.

Subscripts: A for housing with ribs (R 5, R 6 & R 7)

B for housing without ribs (S 6, S 7 & S 8)

RRxx2xx00 F_r=5000 lbs. RPM=0. Ribs at 45° to radial load.

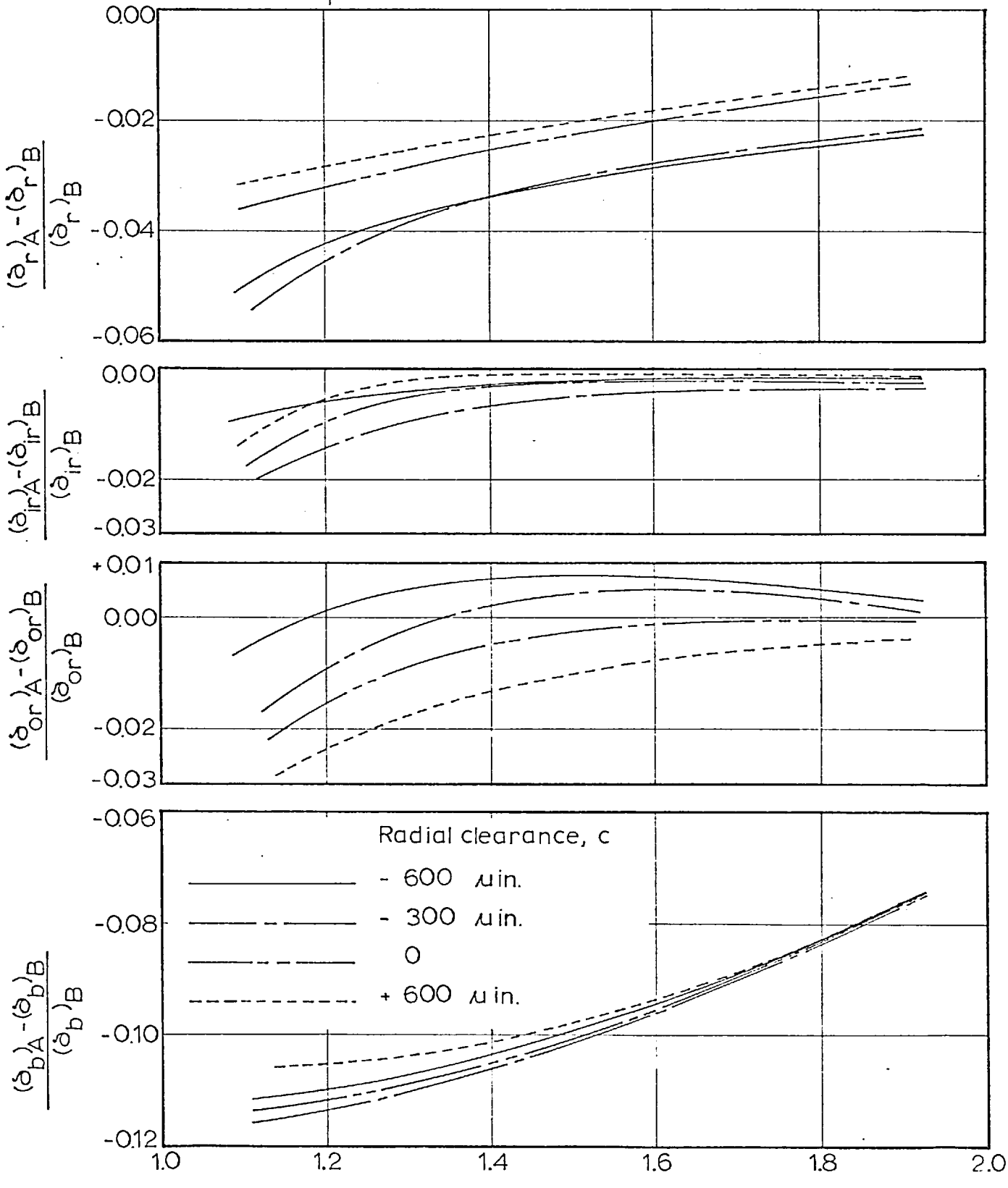


Fig. 7.51 K_t and K_b, for housing with diagonal cruciform ribs, of a steel radial roller bearing with solid shaft.

$$K_t = \frac{\delta_r \text{ for flexible races}}{\delta_r \text{ for rigid races}}, \quad K_b = \frac{\delta_b \text{ for flexible races}}{\delta_r \text{ for rigid races}}$$

where, δ_r= radial deflection, δ_b=body deflection of outer race

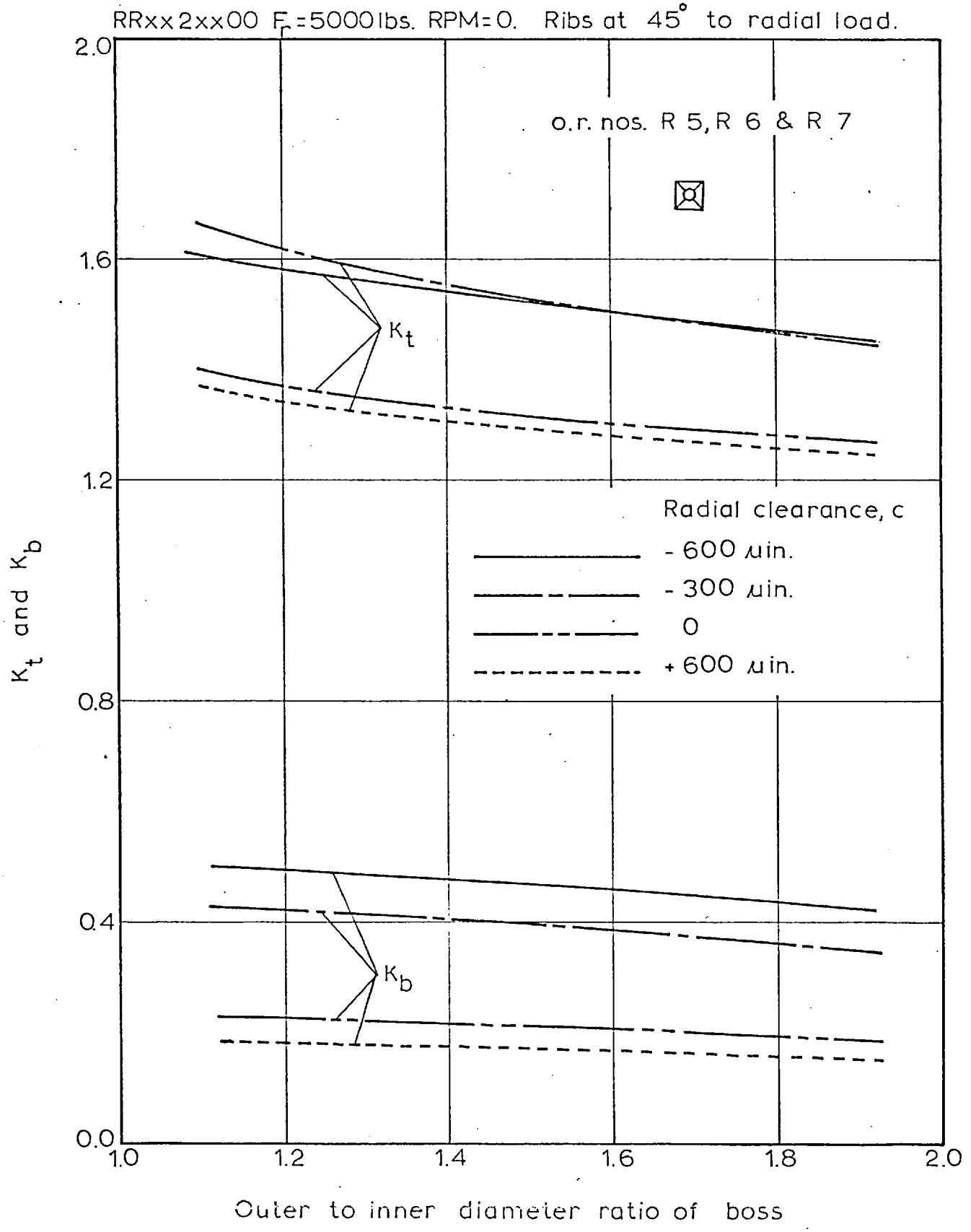


Fig. 7.52 For a steel bearing with solid shaft and housing having diagonal cruciform ribs,
(a) excess non-dimensional equivalent radial load (P_r/F_r) over non-ribbed case,
and excess roller load distribution over non-ribbed case
(b) for housing with thinnest boss (R 5) at different c,
and (c) for increasing boss thickness at c= -300 μin.

Subscripts: A for housing with ribs (R 5, R 6 & R 7)
B for housing without ribs (S 6, S 7 & S 8)

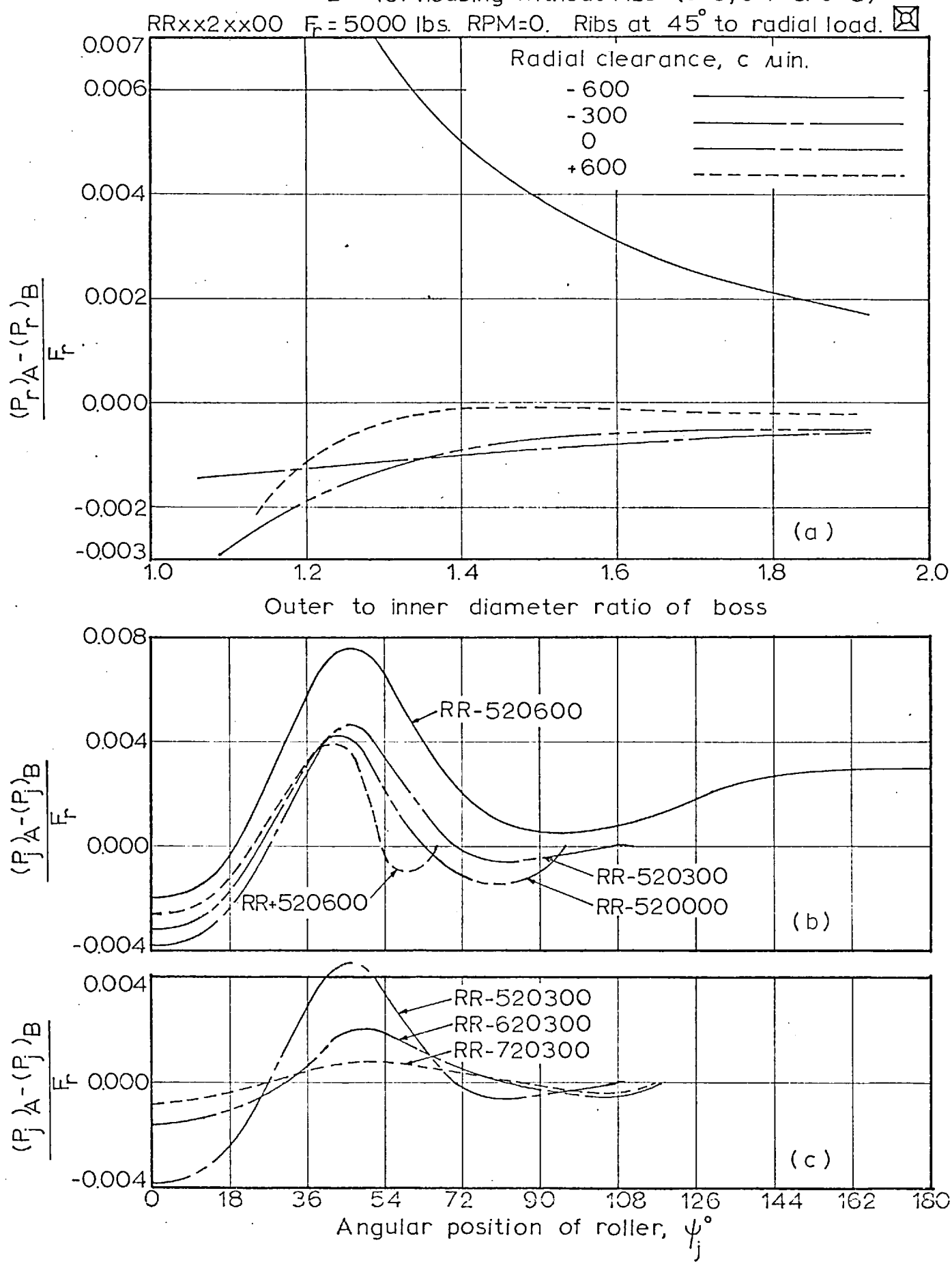


Fig. 7.53 Excess radial and component deflections, for housing with diagonal cruciform ribs over those for housing without ribs, of a steel bearing with hollow shaft (no.4).

δ_r= radial deflection, δ_b= body deflection of outer race
δ_{or}= outer race deflection, δ_{ir}= inner race deflection.

Subscripts: A for housing with ribs (R 5, R 6 & R 7)
B for housing without ribs (S 6, S 7 & S 8)

RRxx4xx00 F_r=5000 lbs. RPM=0. Ribs at 45° to radial load.

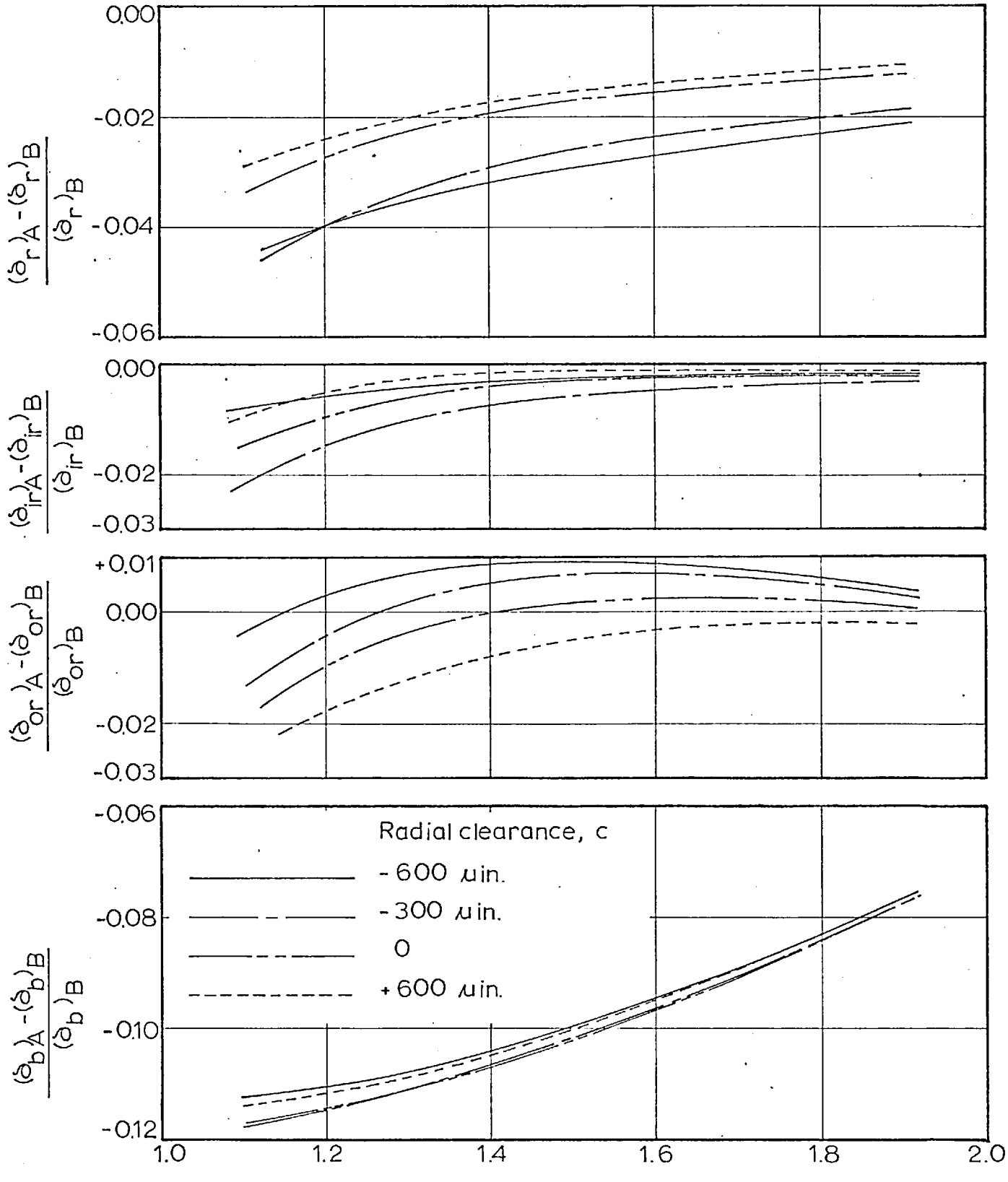


Fig. 7.54 K_t and K_b, for housing with diagonal cruciform ribs, of a steel radial roller bearing with hollow shaft (no.4).

$$K_t = \frac{\delta_r \text{ for flexible races}}{\delta_r \text{ for rigid races}}, \quad K_b = \frac{\delta_b \text{ for flexible races}}{\delta_r \text{ for rigid races}}$$

where, δ_r=radial deflection, δ_b=body deflection of outer race.

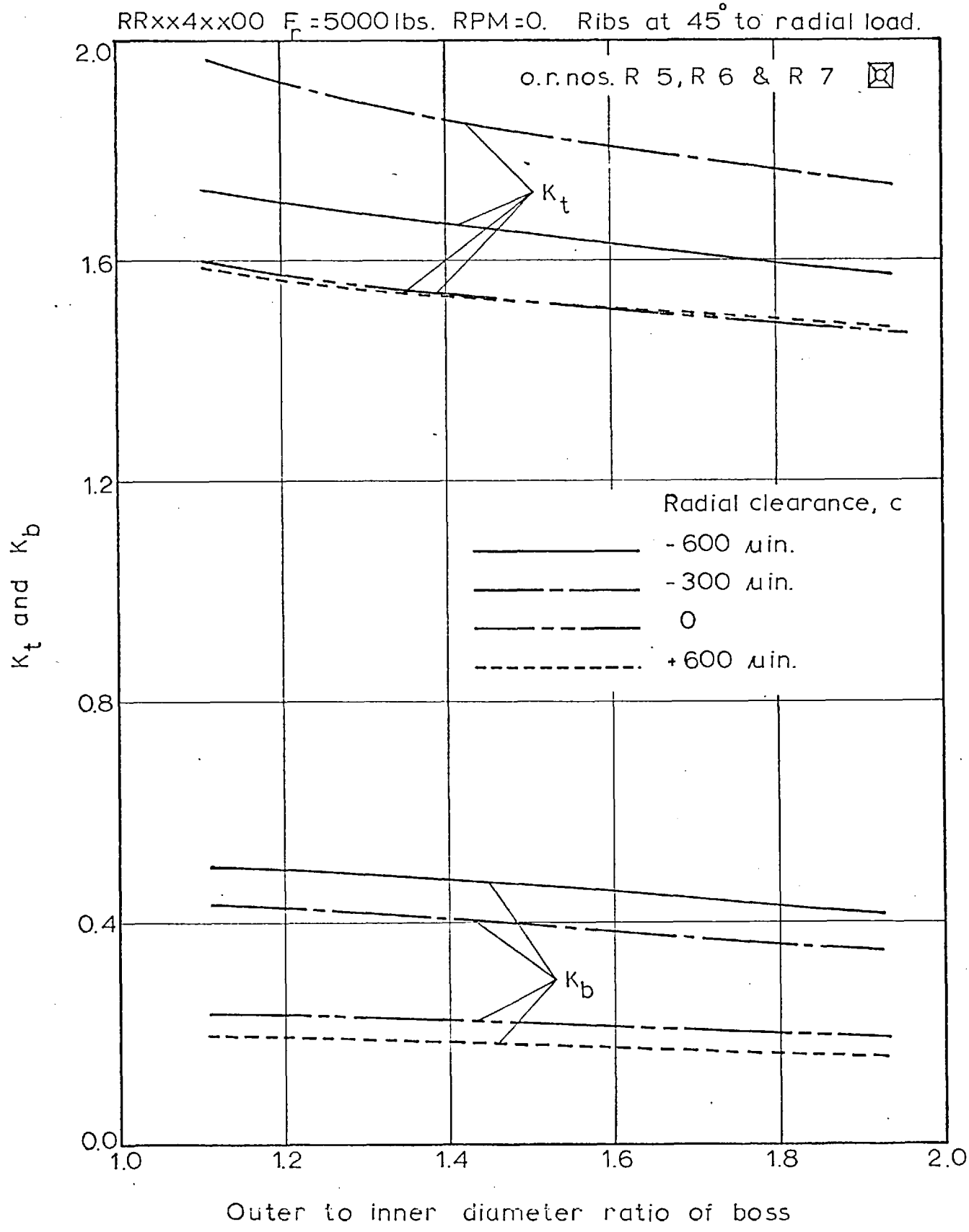


Fig. 7.55 For a steel bearing with hollow shaft (no.4) and housing having diagonal cruciform ribs,
(a) excess non-dimensional equivalent radial load (P_r/F_r) over non-ribbed case,
and excess roller load distribution over non-ribbed case
(b) for housing with thinnest boss (R 5) at different c,
and (c) for increasing boss thickness at c= -300 μin.

Subscripts: A for housing with ribs (R 5, R 6 & R 7)
B for housing without ribs (S 6, S 7 & S 8)

RRxx4xx00 F_r = 5000 lbs. RPM=0. Ribs at 45° to radial load.

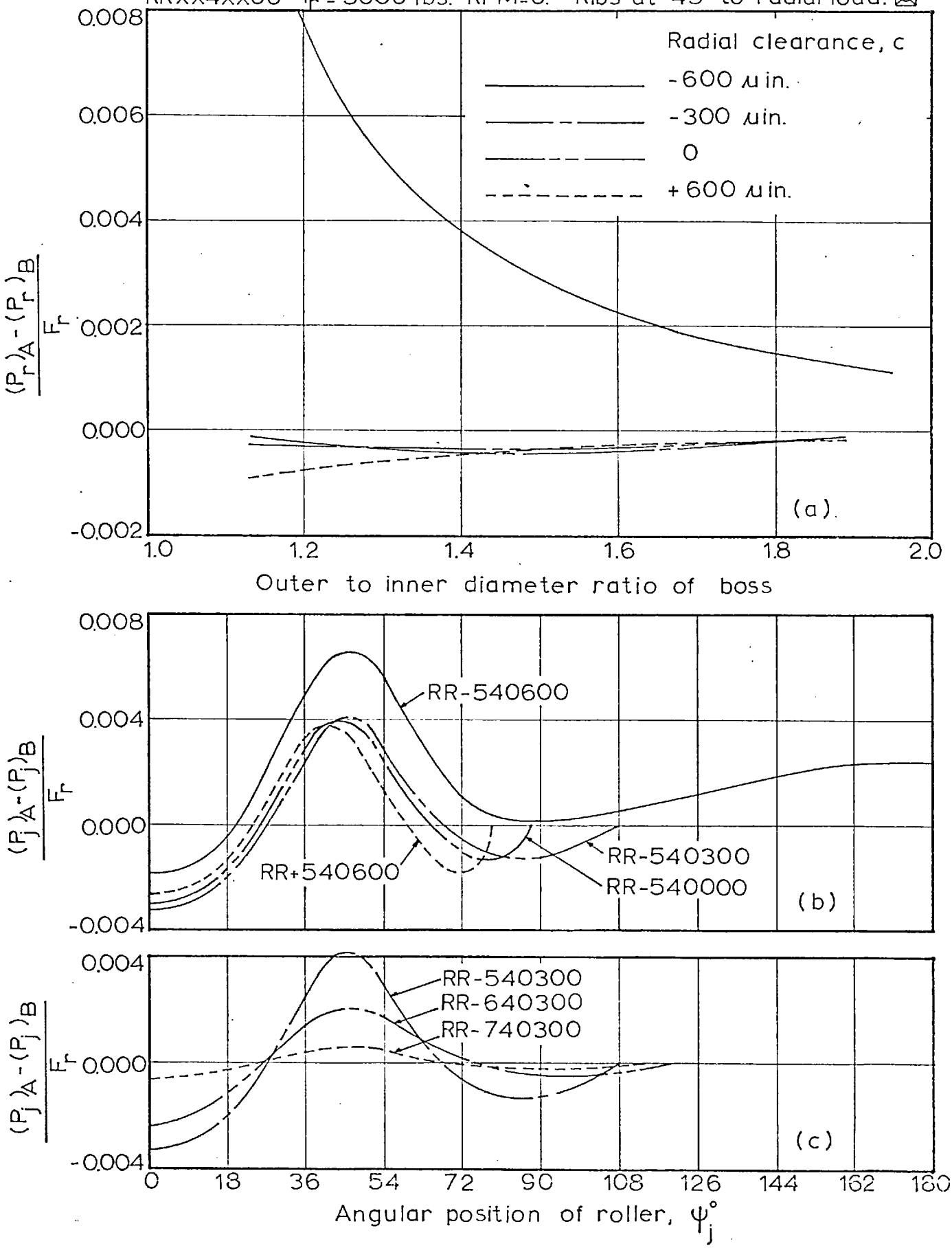


Fig. 7.56 Radial and component deflections of a steel bearing having solid shaft and circular housing with upright cruciform support.

δ_r= radial deflection, δ_b= body deflection of outer race, δ_{or}= outer race deflection, δ_{ir}= inner race deflection.

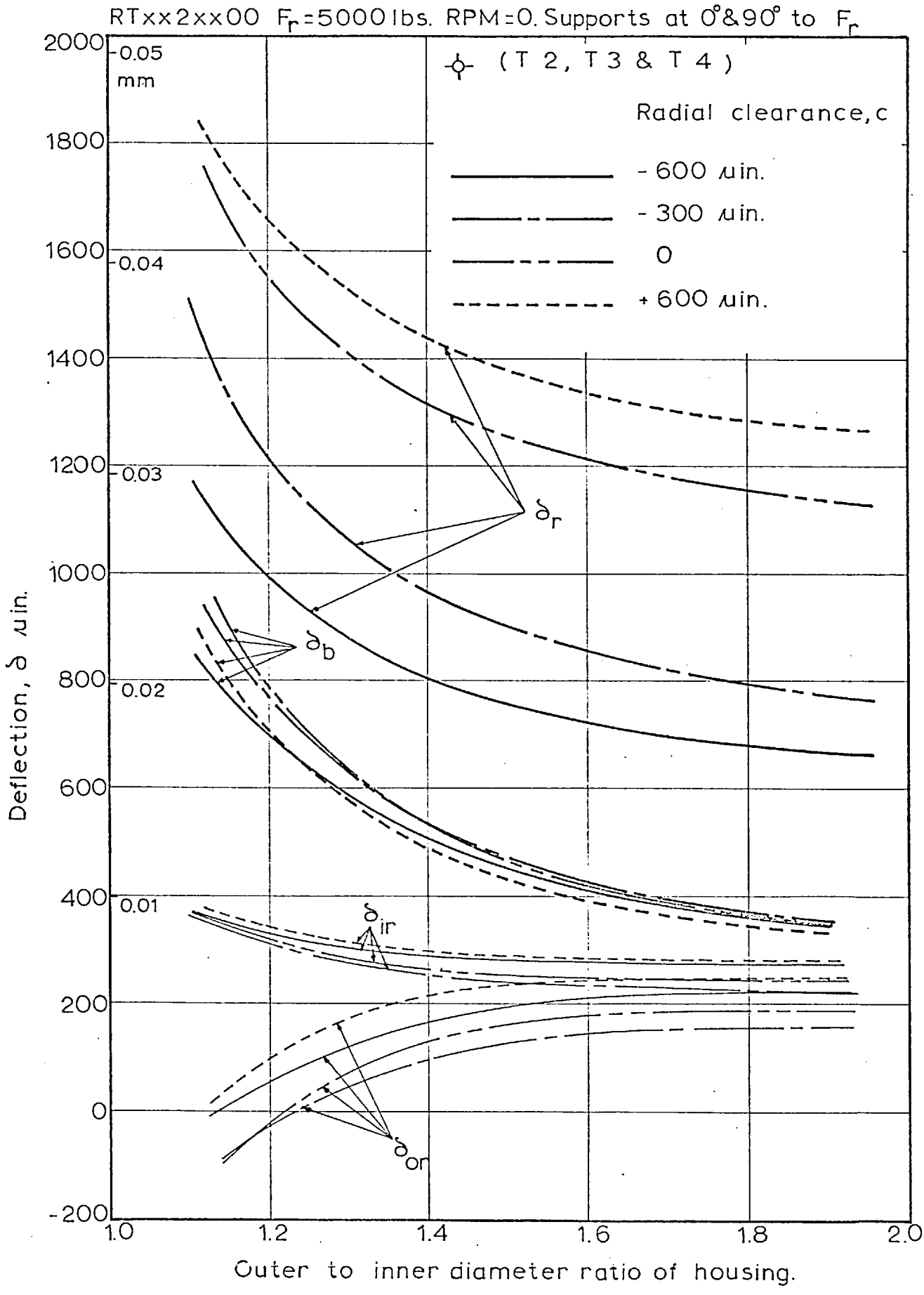


Fig. 7.57 Non-dimensional equivalent radial load (P_r/F_r) of a steel bearing having solid shaft and circular housing with upright cruciform support.

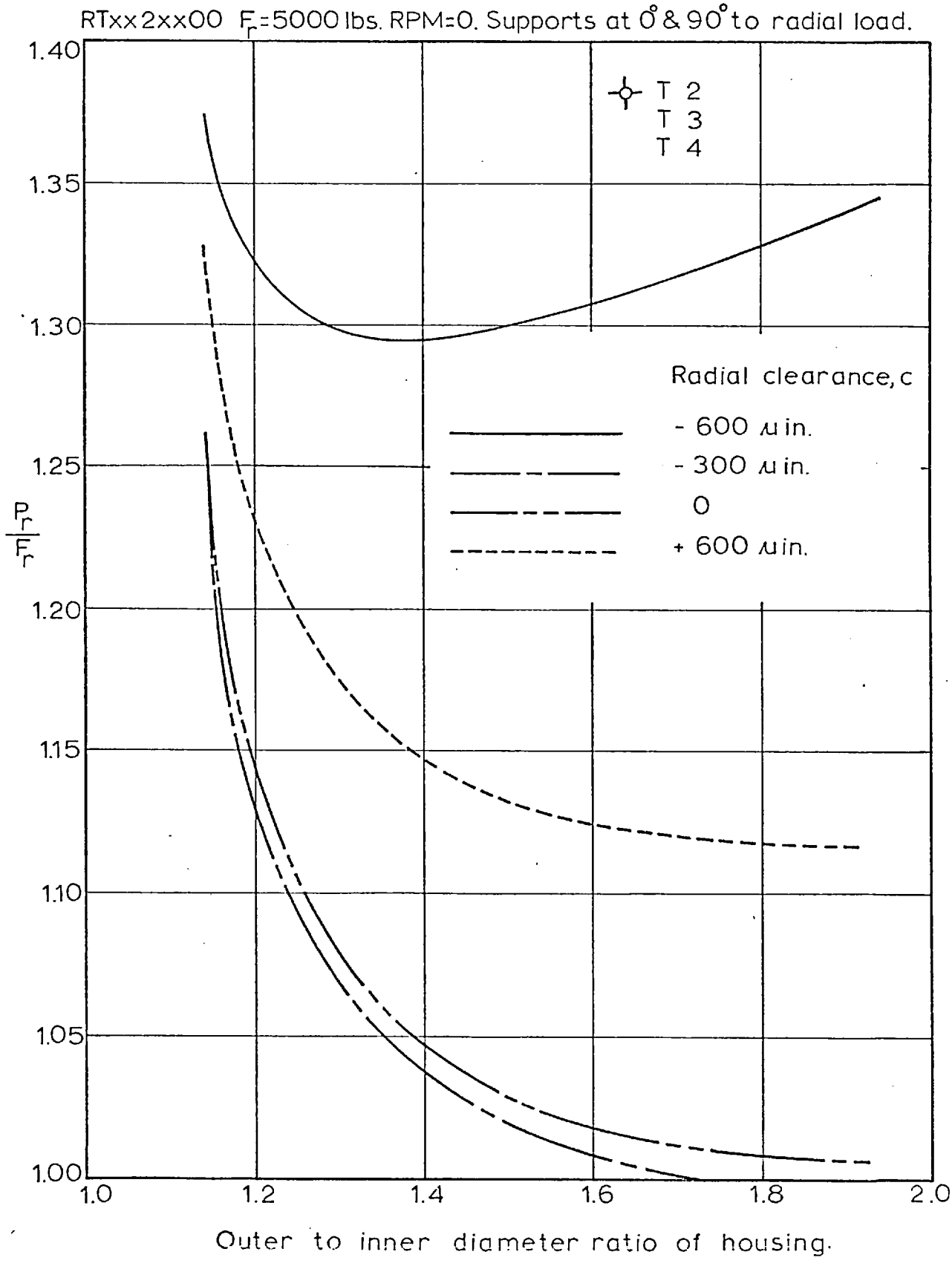


Fig. 7.58 K_t and K_b of a steel bearing having solid shaft and circular housing with upright cruciform support.

$$K_t = \frac{\delta_r \text{ for flexible races}}{\delta_r \text{ for rigid races}}, \quad K_b = \frac{\delta_b \text{ for flexible races}}{\delta_r \text{ for rigid races}}$$

where, δ_r= radial deflection, δ_b=body deflection of outer race.

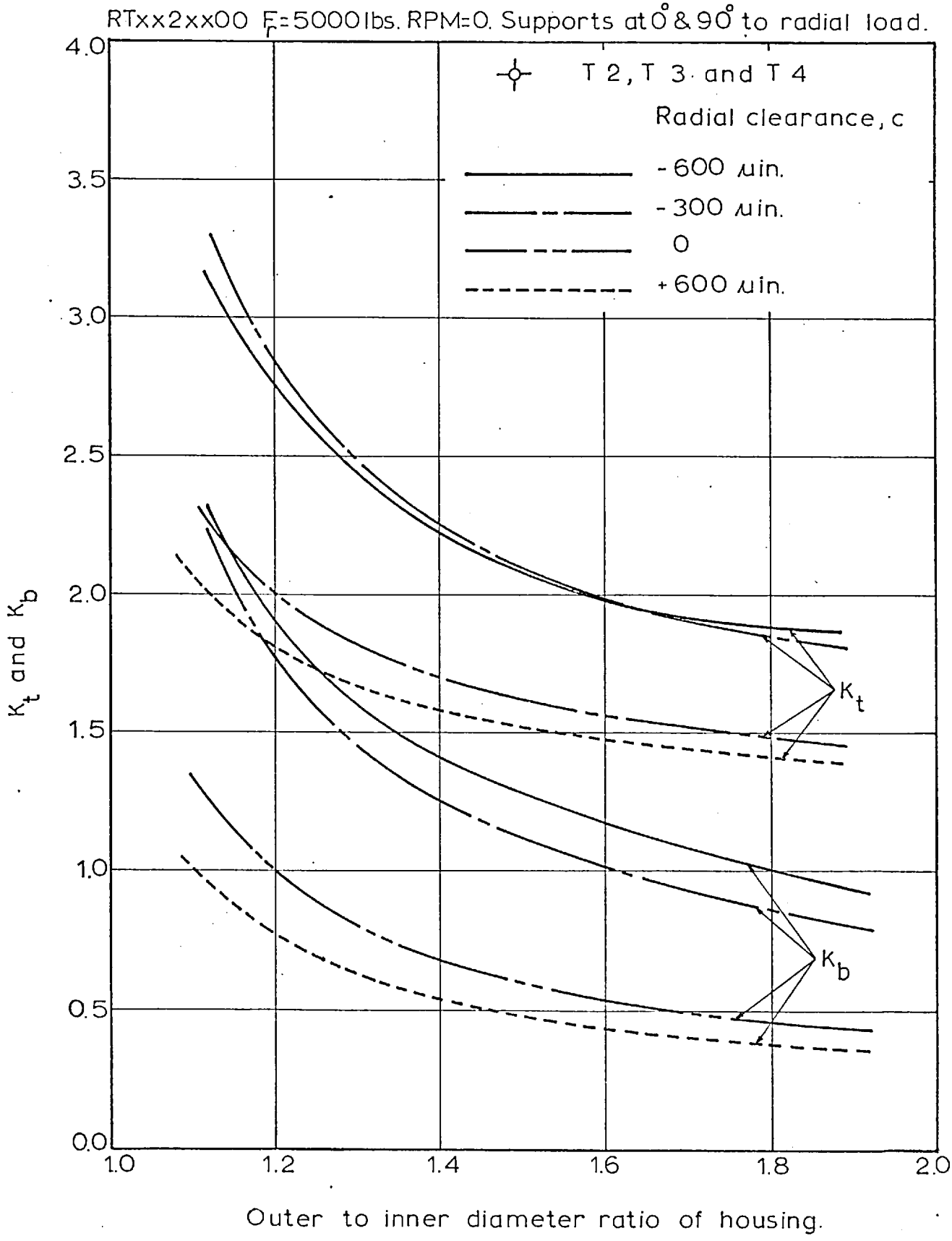


Fig. 7.59 Roller load distribution in a steel bearing having solid shaft and circular housing with upright cruciform support.

Outer to inner diameter ratio of housing no. T 2 is 1.145, T 3 is 1.385 and T 4 is 1.847.

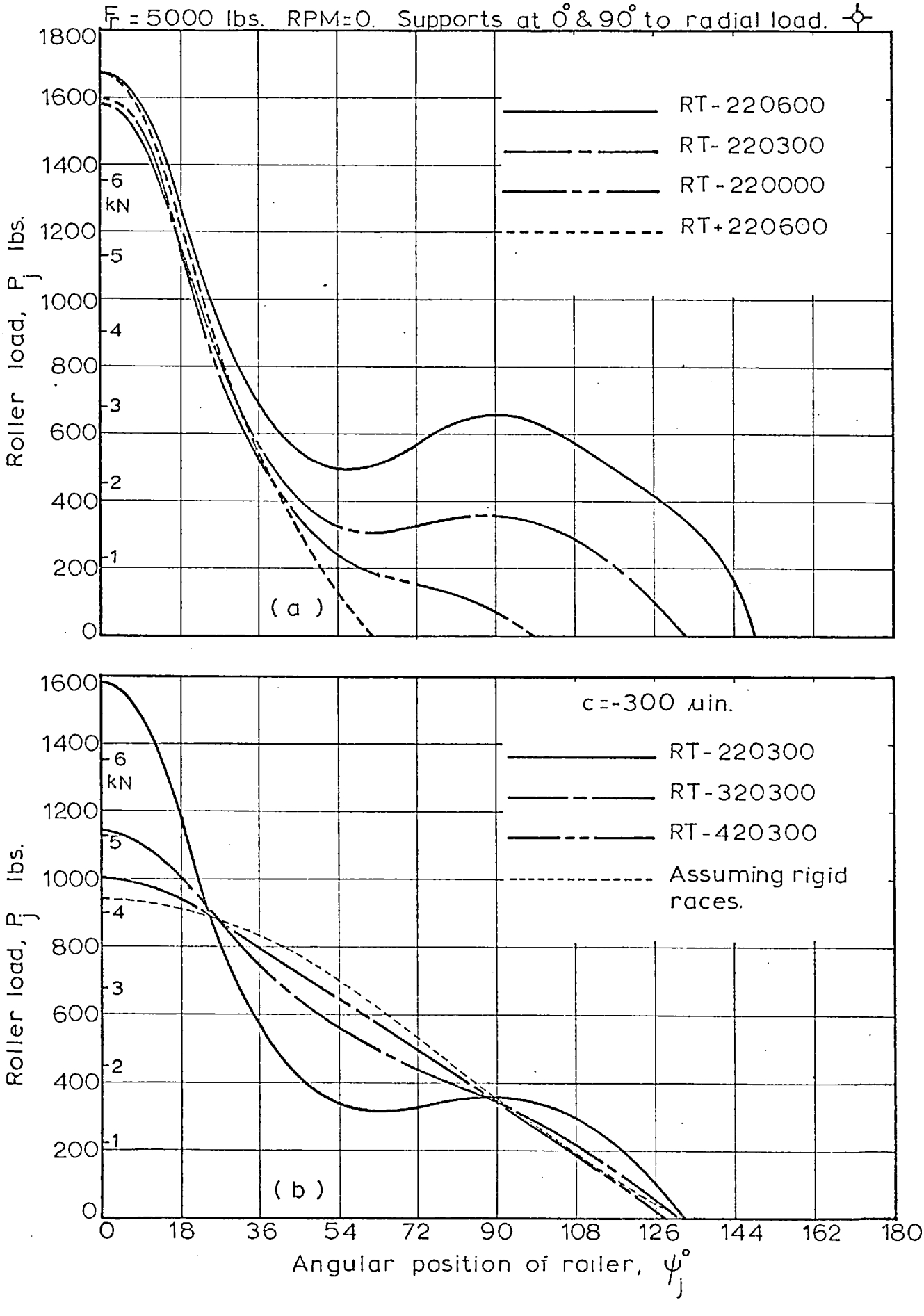


Fig. 7.60 Radial and component deflections of a steel bearing having hollow shaft (no.4) and circular housing with upright cruciform support.

δ_r= radial deflection, δ_b= body deflection of outer race, δ_{or}= outer race deflection, δ_{ir}= inner race deflection.

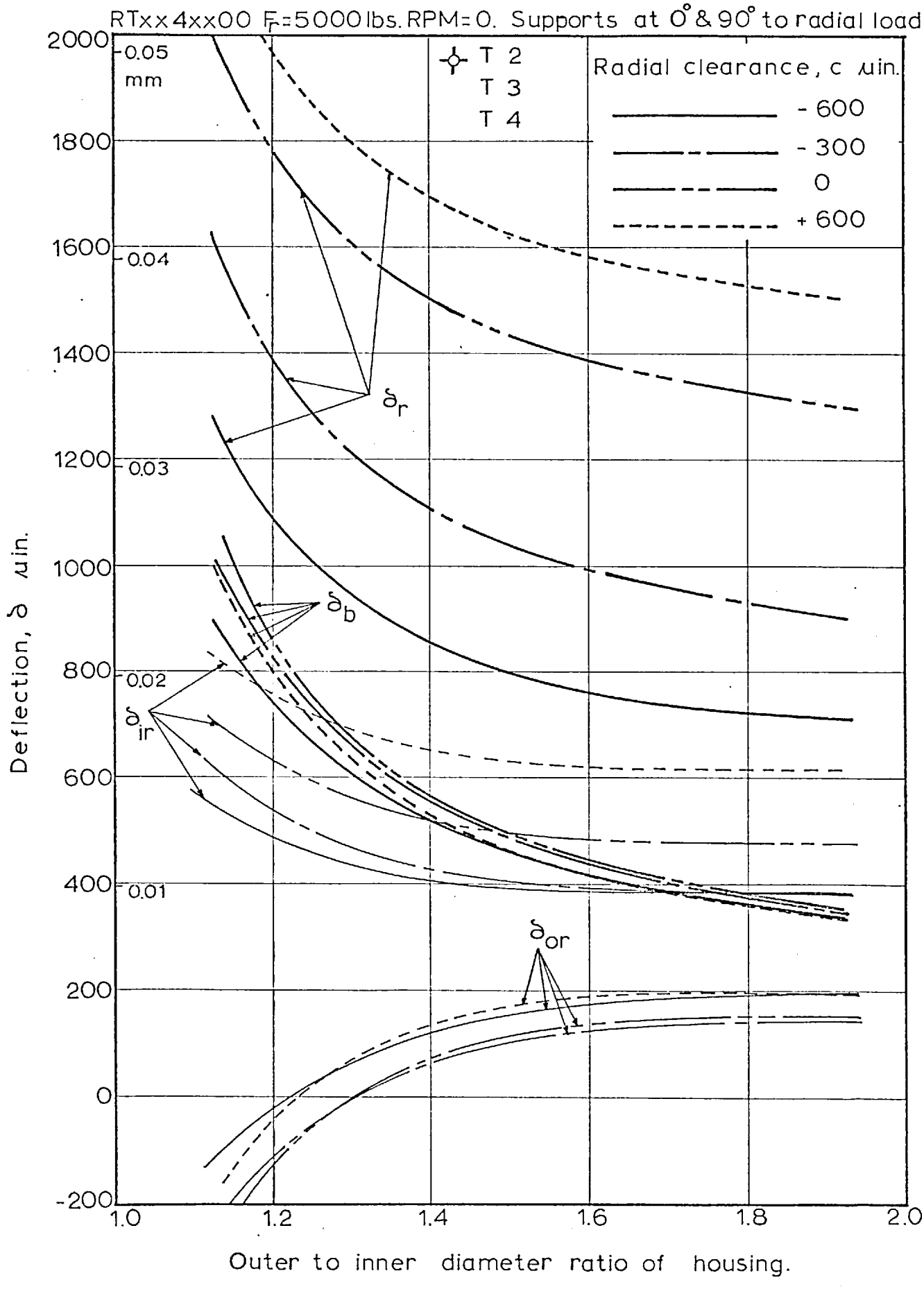


Fig. 7.61 Non-dimensional equivalent radial load (P_r/F_r) of a steel bearing having hollow shaft (no.4) and circular housing with upright cruciform support.

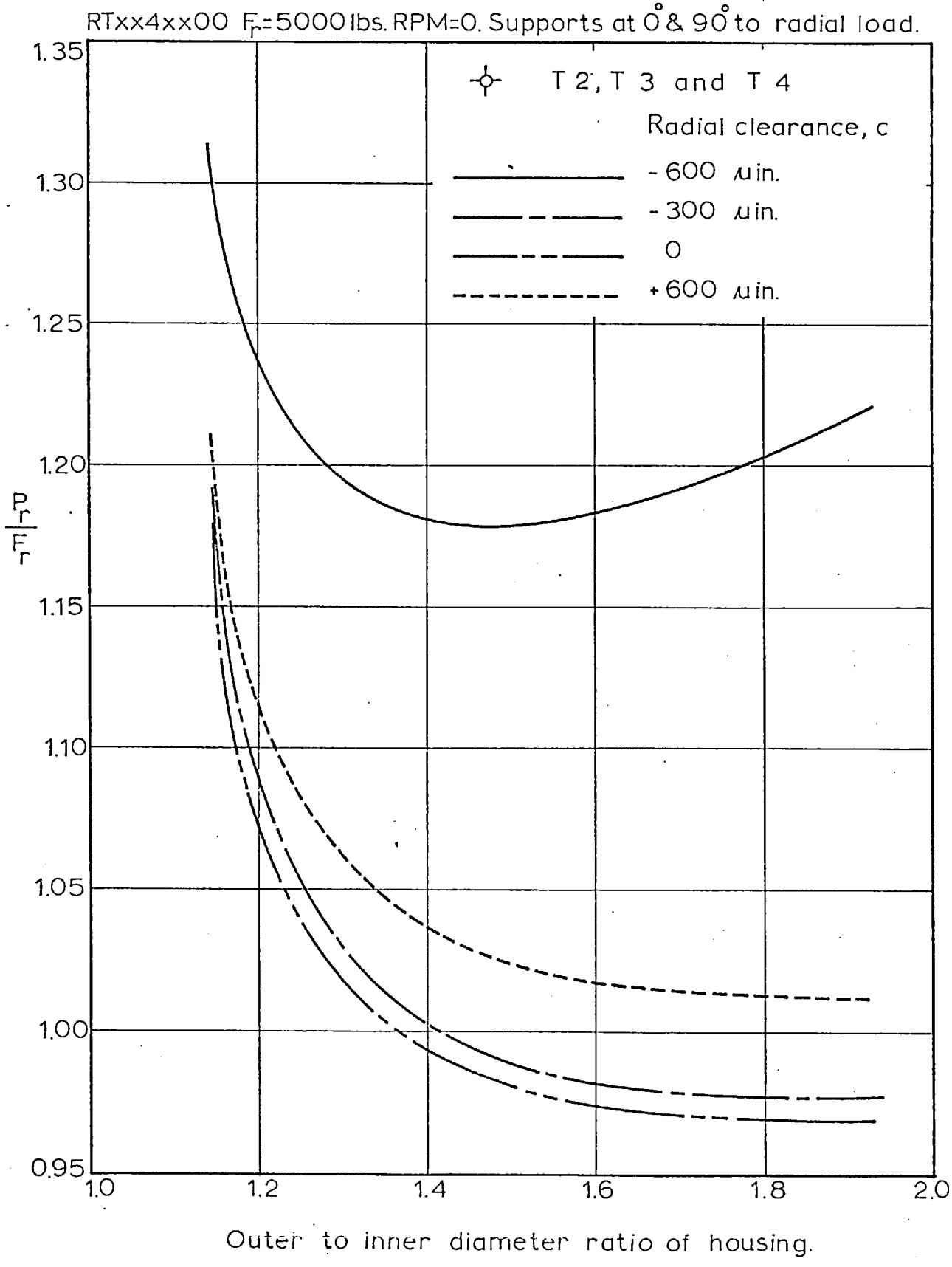


Fig. 7.62 K_t and K_b of a steel bearing having hollow shaft (no.4) and circular housing with upright cruciform support.

$$K_t = \frac{\delta_r \text{ for flexible races}}{\delta_r \text{ for rigid races}}, \quad K_b = \frac{\delta_b \text{ for flexible races}}{\delta_r \text{ for rigid races}}$$

where, δ_r=radial deflection, δ_b=body deflection of outer race.

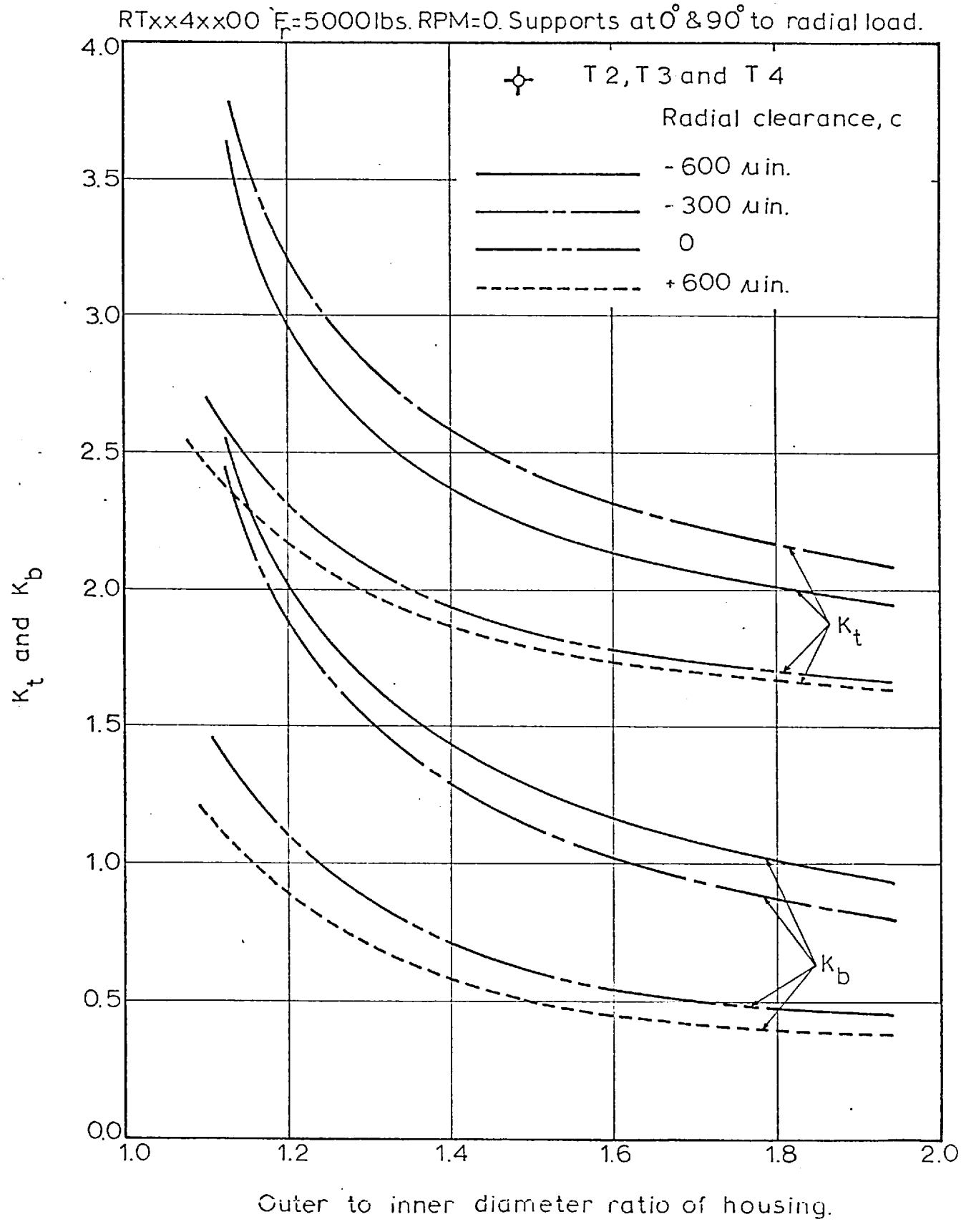


Fig. 7.63 Roller load distribution in a steel bearing having hollow shaft (no.4) and circular housing with upright cruciform support.

Outer to inner diameter ratio of housing no.T 2 is 1.145, T 3 is 1.385 and T 4 is 1.847.

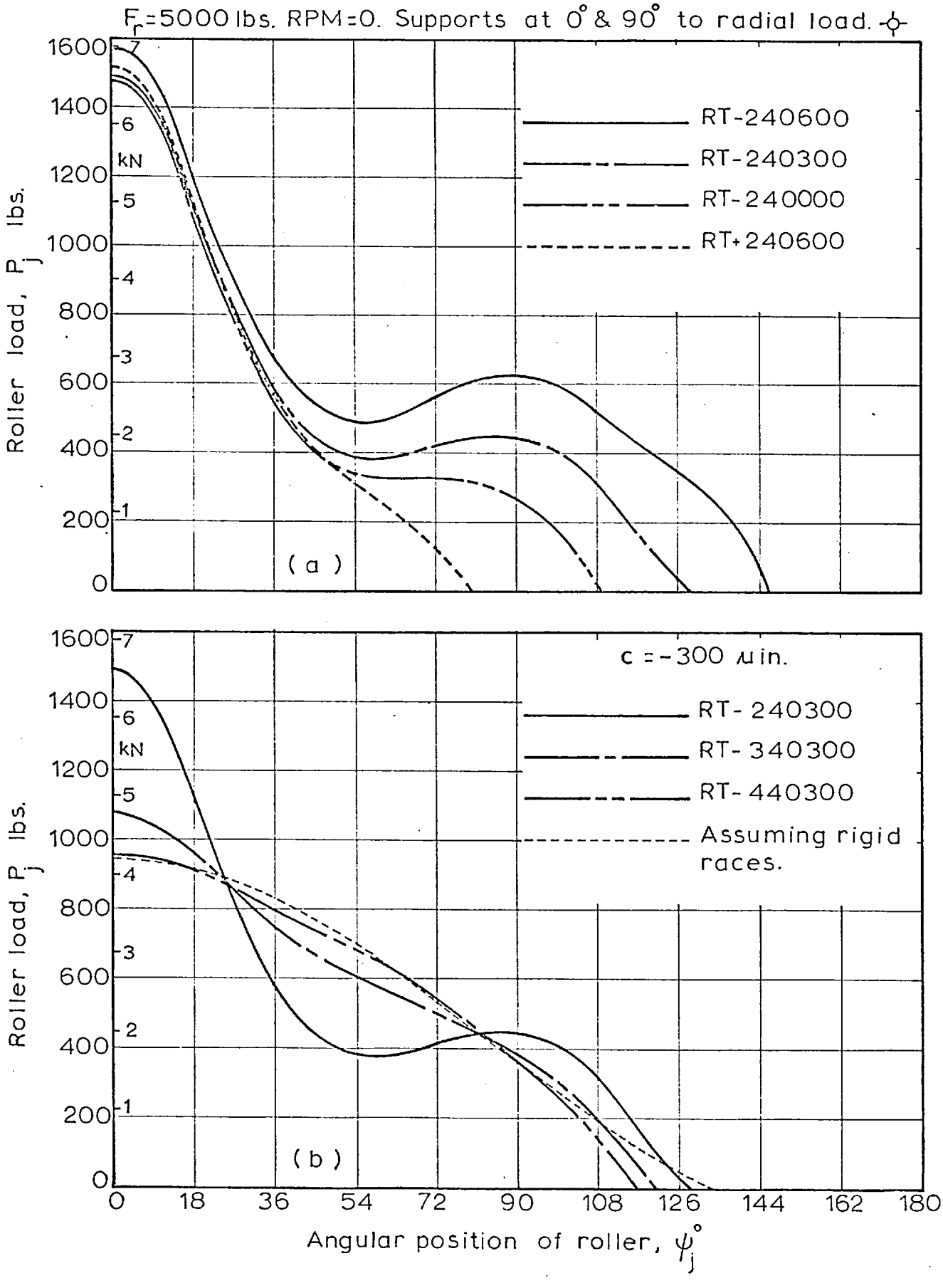


Fig. 7.64 Radial and component deflections of a steel bearing having solid shaft and circular housing with diagonal cruciform support.

δ_r= radial deflection, δ_b= body deflection of outer race
δ_{or}= outer race deflection, δ_{ir}= inner race deflection.

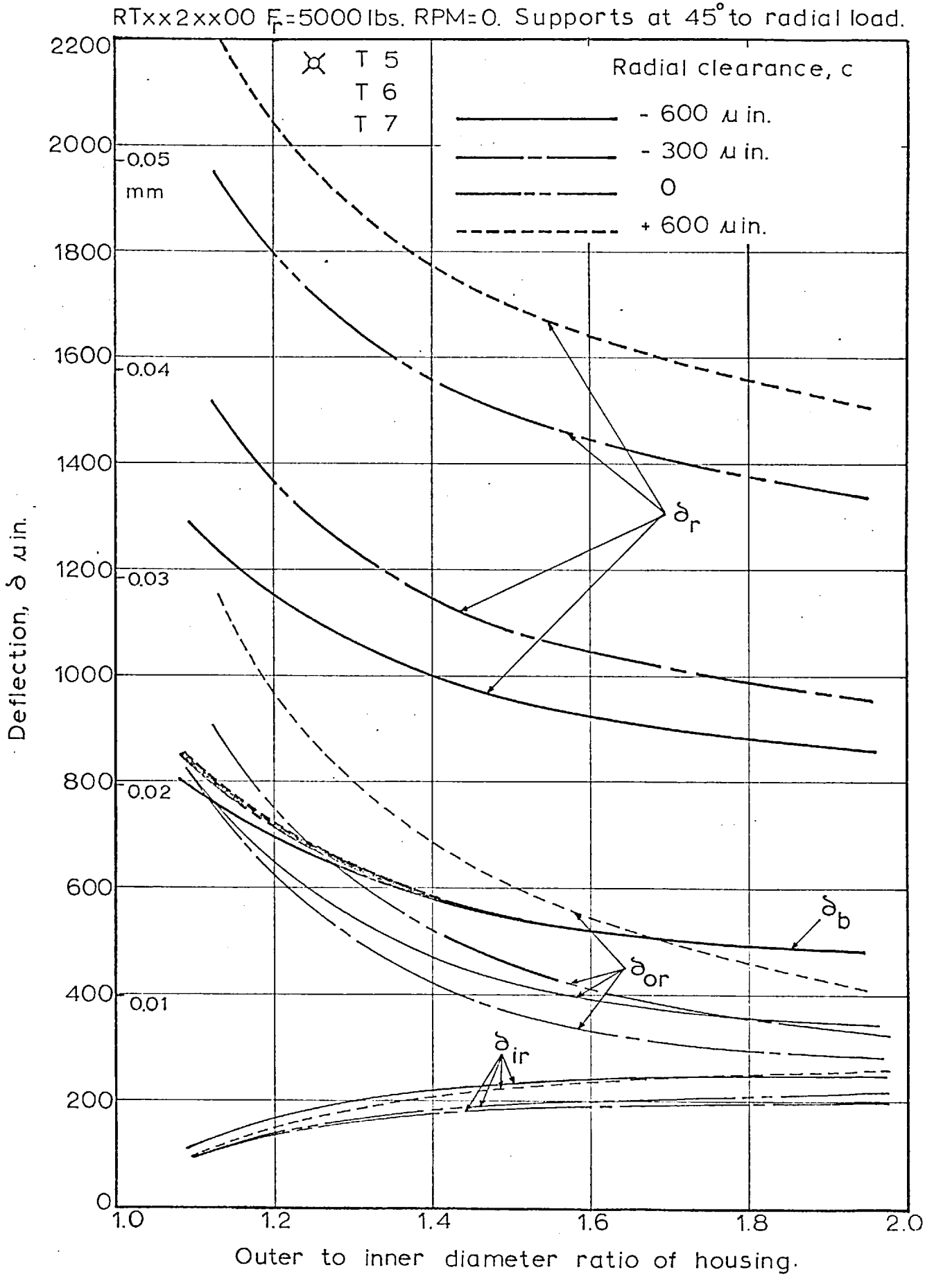


Fig. 7.65 Non-dimensional equivalent radial load (P_r/F_r) of a steel radial roller bearing having solid shaft and circular housing with diagonal cruciform support.

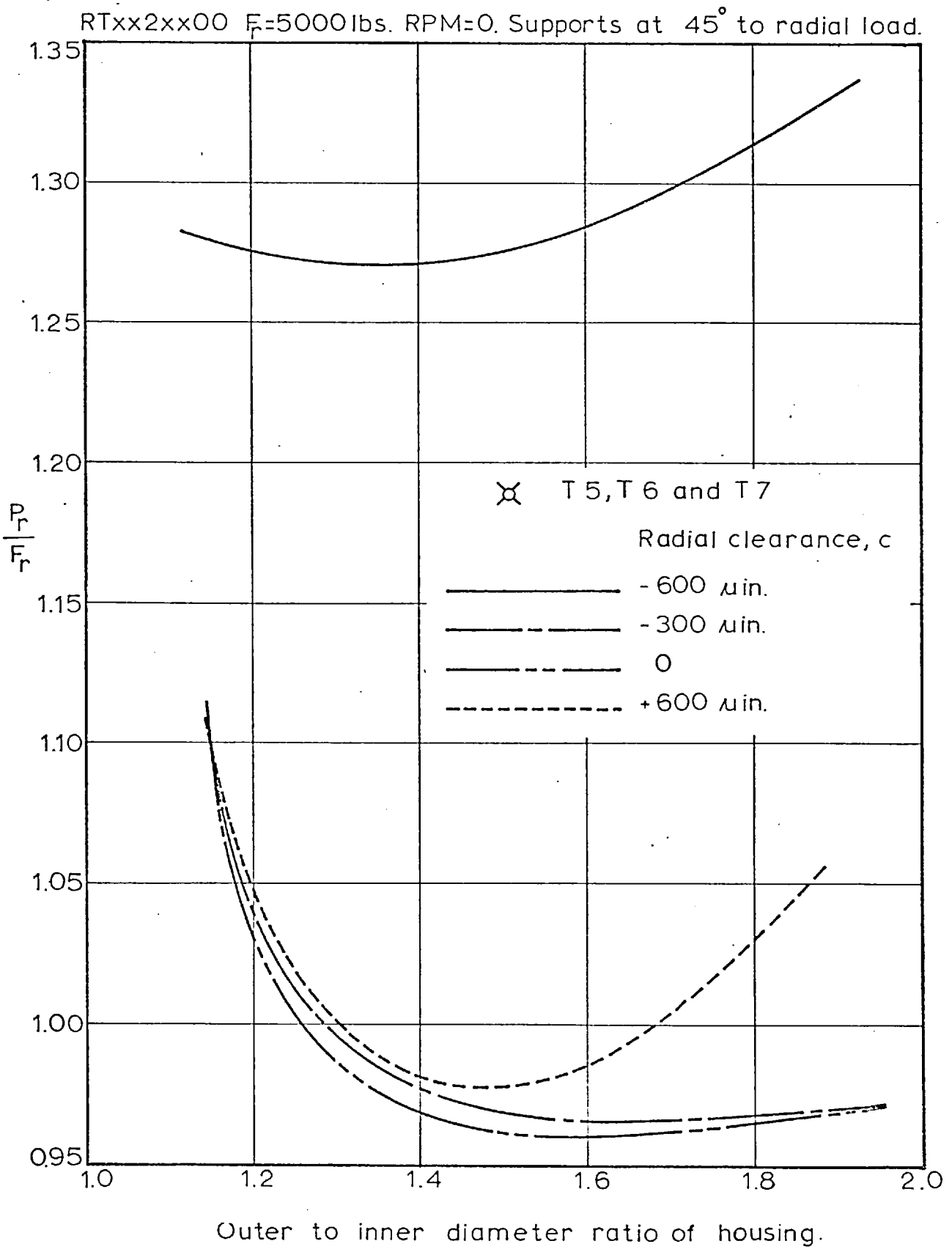


Fig. 7.66 K_t and K_b of a steel bearing having solid shaft and circular housing with diagonal cruciform support.

$$K_t = \frac{\delta_r \text{ for flexible races}}{\delta_r \text{ for rigid races}}, \quad K_b = \frac{\delta_b \text{ for flexible races}}{\delta_r \text{ for rigid races}}$$

where, δ_r=radial deflection, δ_b=body deflection of outer race.

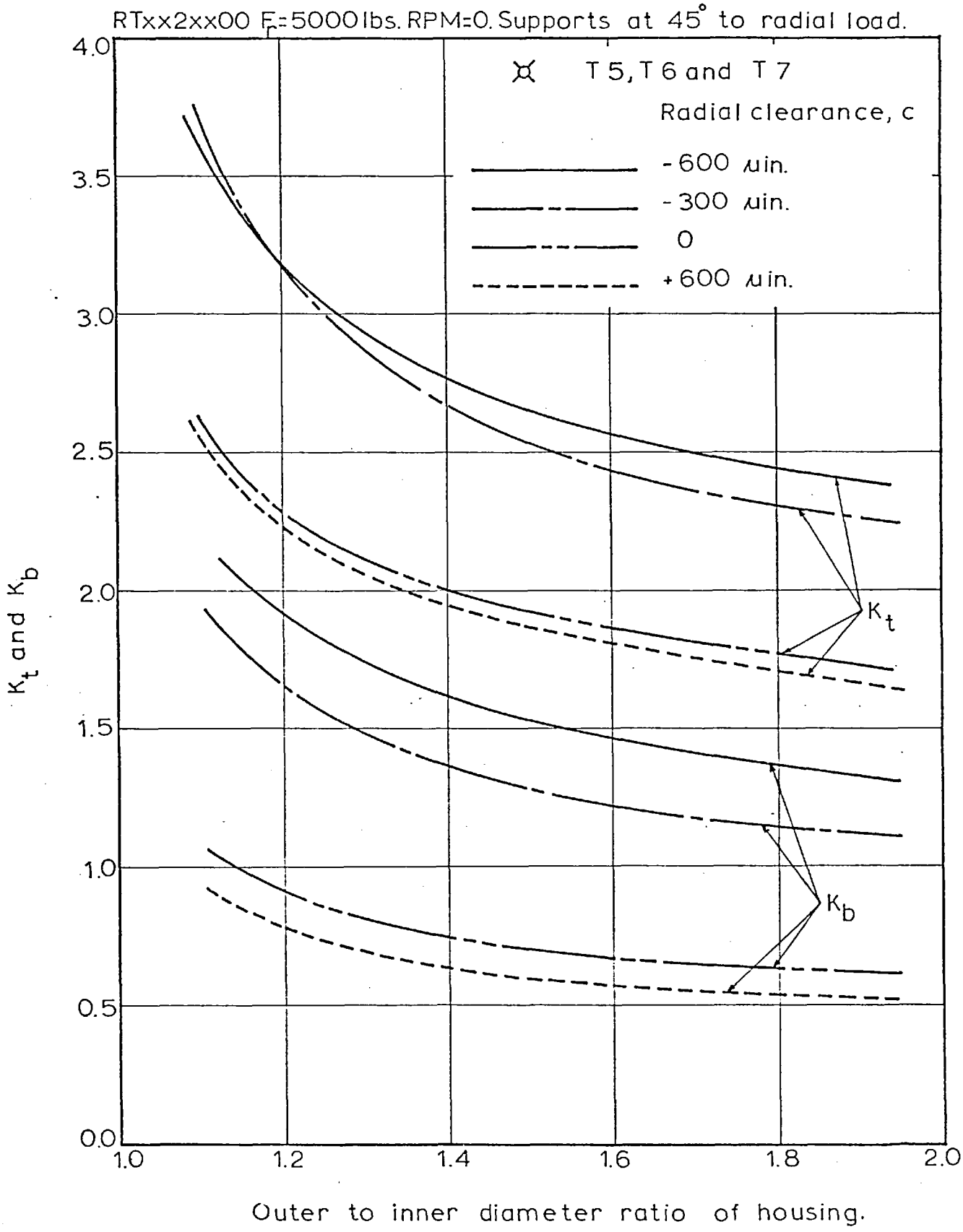


Fig. 7.67 Roller load distribution in a steel bearing having solid shaft and circular housing with diagonal cruciform support.

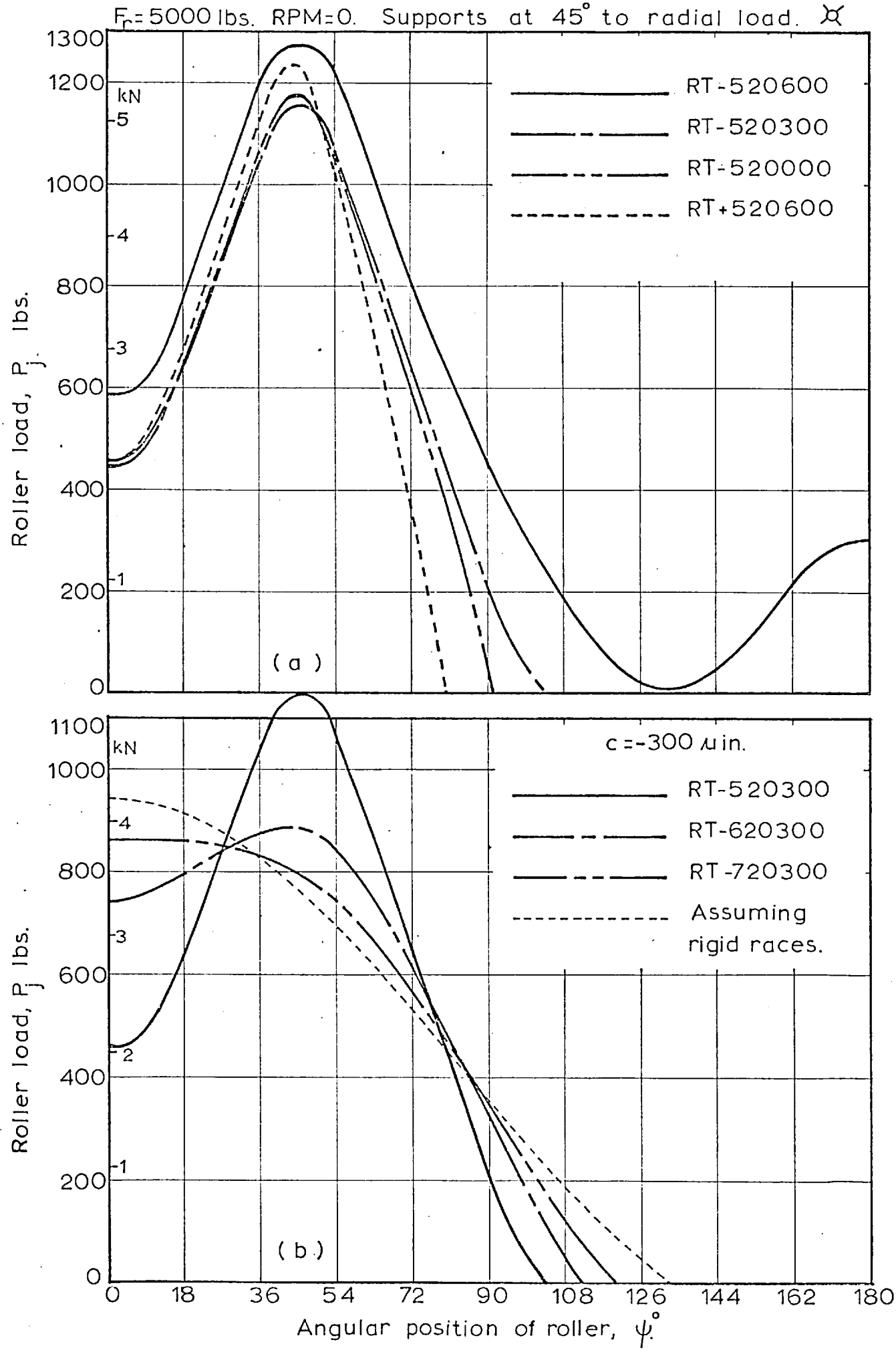


Fig. 7.68 Radial and component deflections of a steel bearing having hollow shaft (no.4) and circular housing with diagonal cruciform support.

δ_r = radial deflection, δ_b = body deflection of outer race
δ_{or} = outer race deflection, δ_{ir} = inner race deflection.

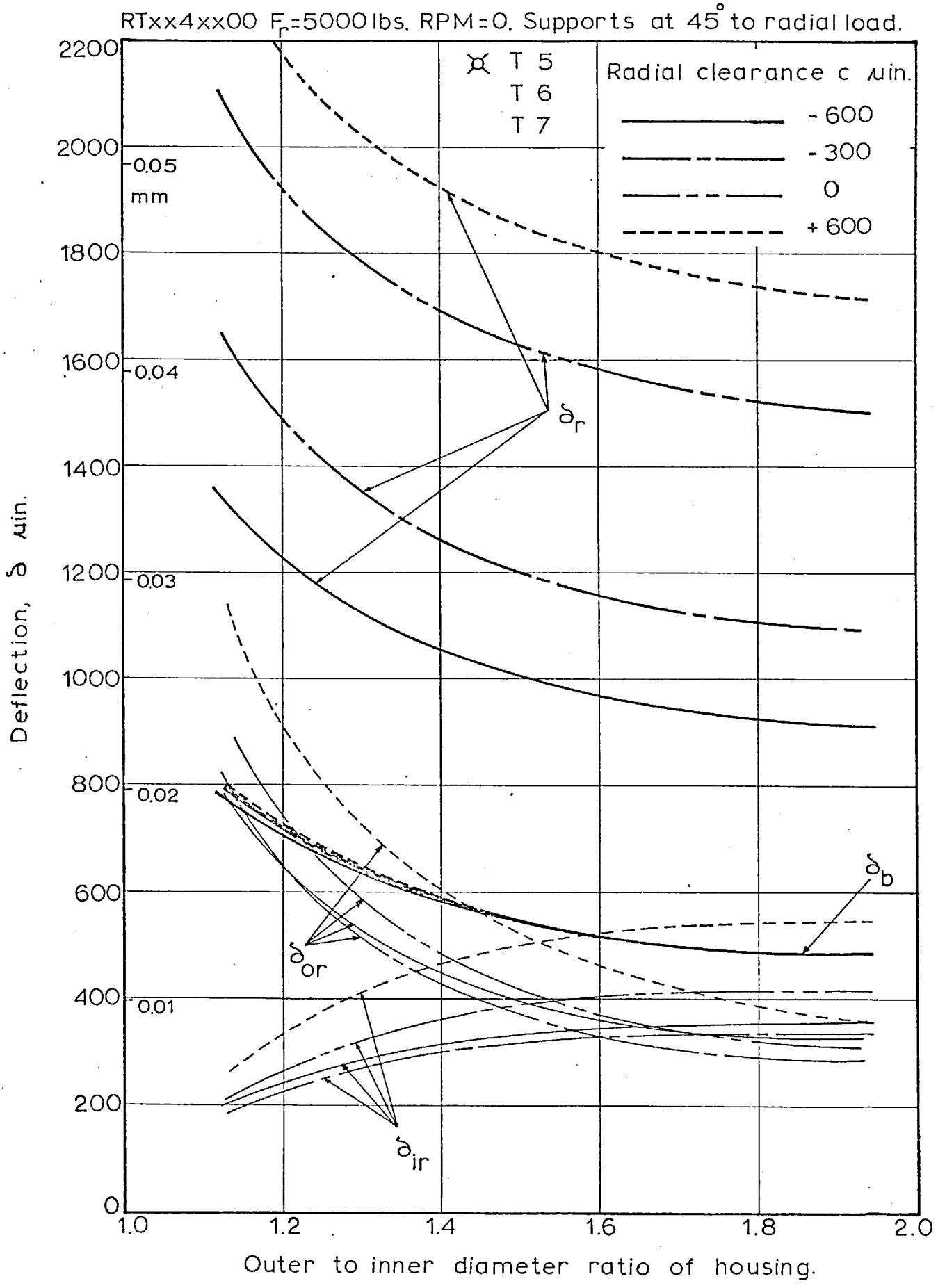


Fig. 7.69 Non-dimensional equivalent radial load (P_r/F_r) of a steel radial roller bearing having hollow shaft (no.4) and circular housing with diagonal cruciform support.

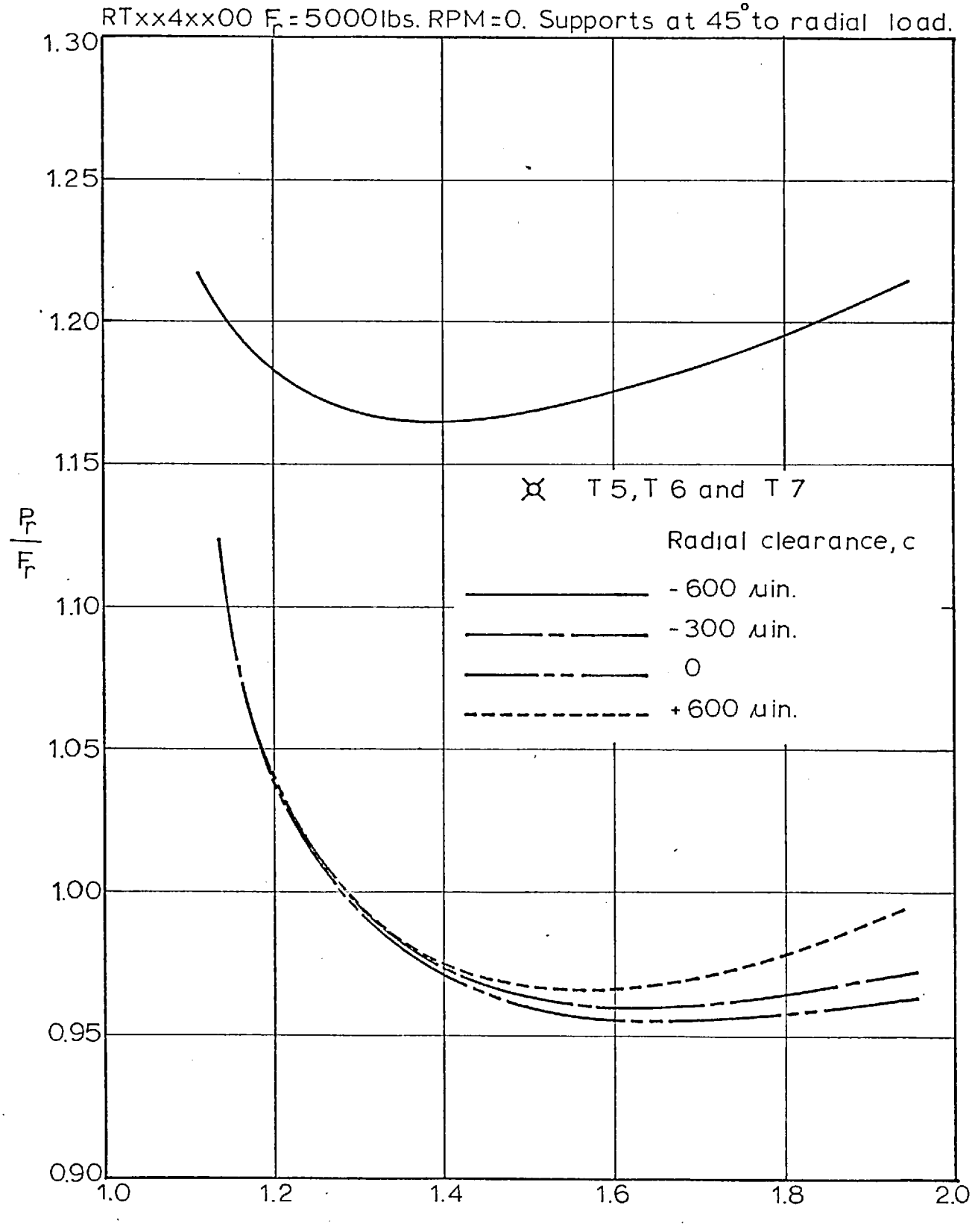


Fig. 7.70 K_t and K_b of a steel bearing having hollow shaft (no.4) and circular housing with diagonal cruciform support.

$$K_t = \frac{\delta_r \text{ for flexible races}}{\delta_r \text{ for rigid races}}, \quad K_b = \frac{\delta_b \text{ for flexible races}}{\delta_r \text{ for rigid races}}$$

where, δ_r = radial deflection, δ_b = body deflection of outer race.

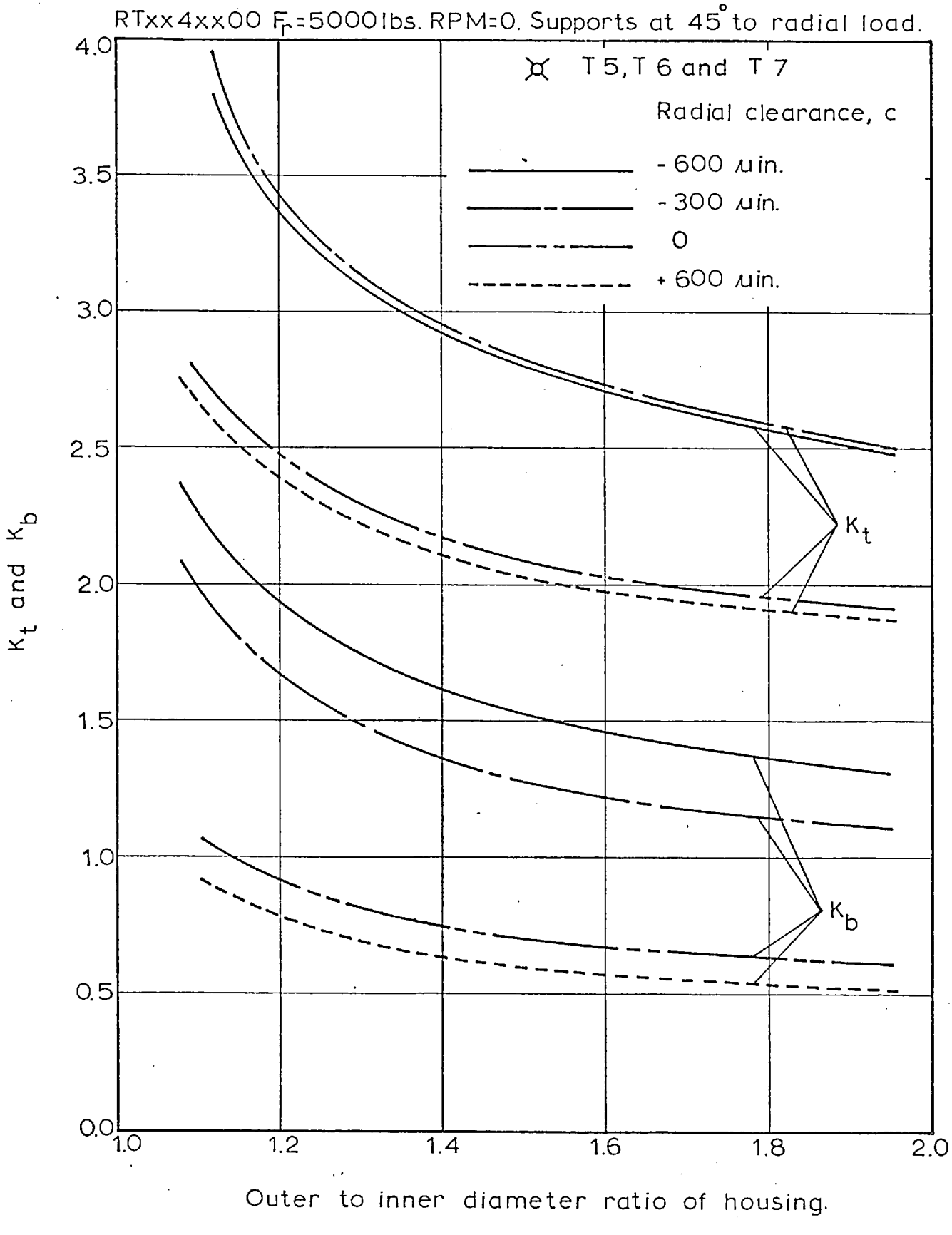


Fig. 7.71 Roller load distribution in a steel bearing having hollow shaft (no.4) and circular housing with diagonal cruciform support.

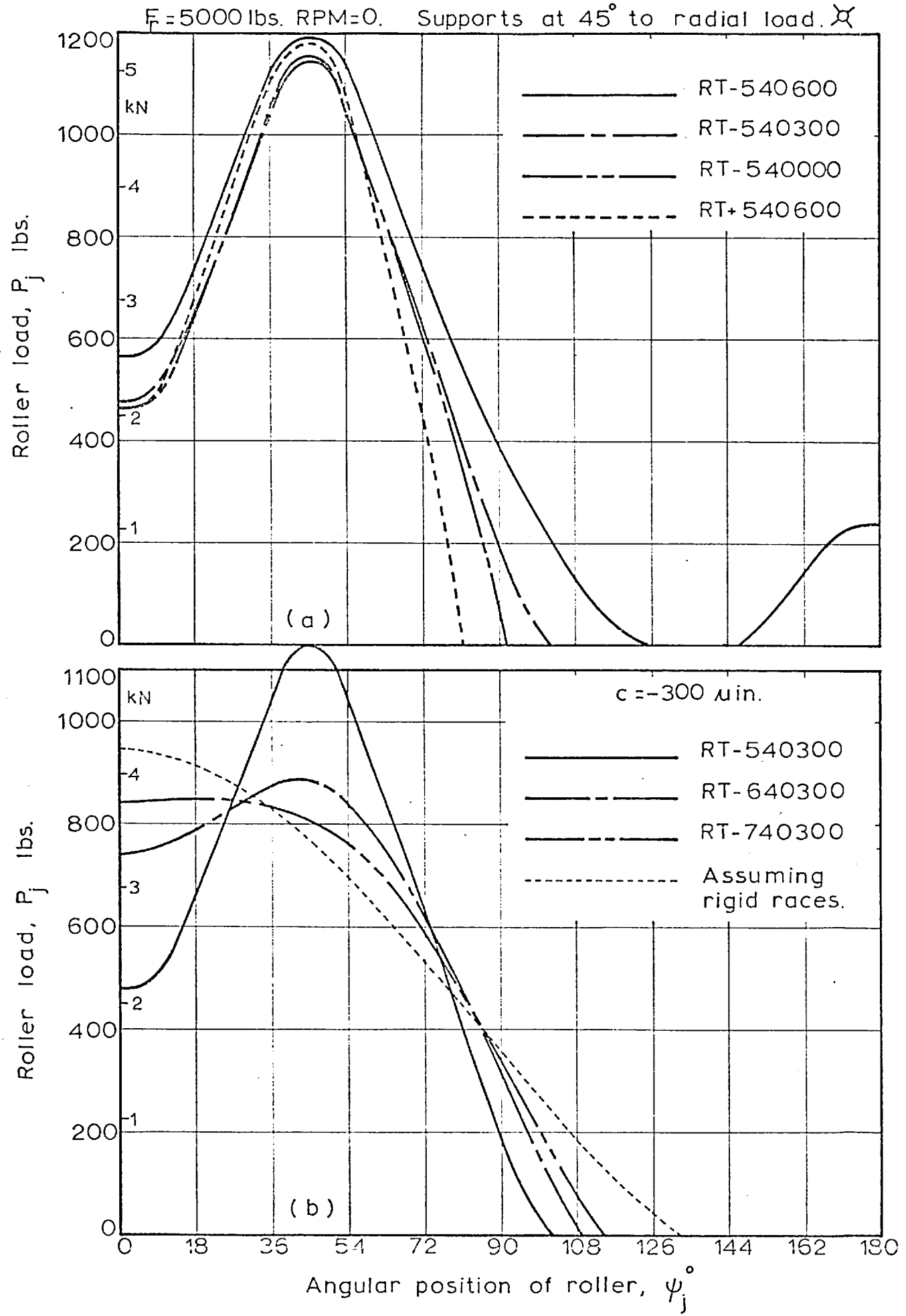


Fig. 7.72 Effect of shaft speed on
(a) radial deflection, δ_r
(b) non-dimensional equivalent radial load (P_r/F_r), and
(c) excess roller load distribution at the outer race,
of a steel radial roller bearing having thin circular housing (T 2)
with upright cruciform support.

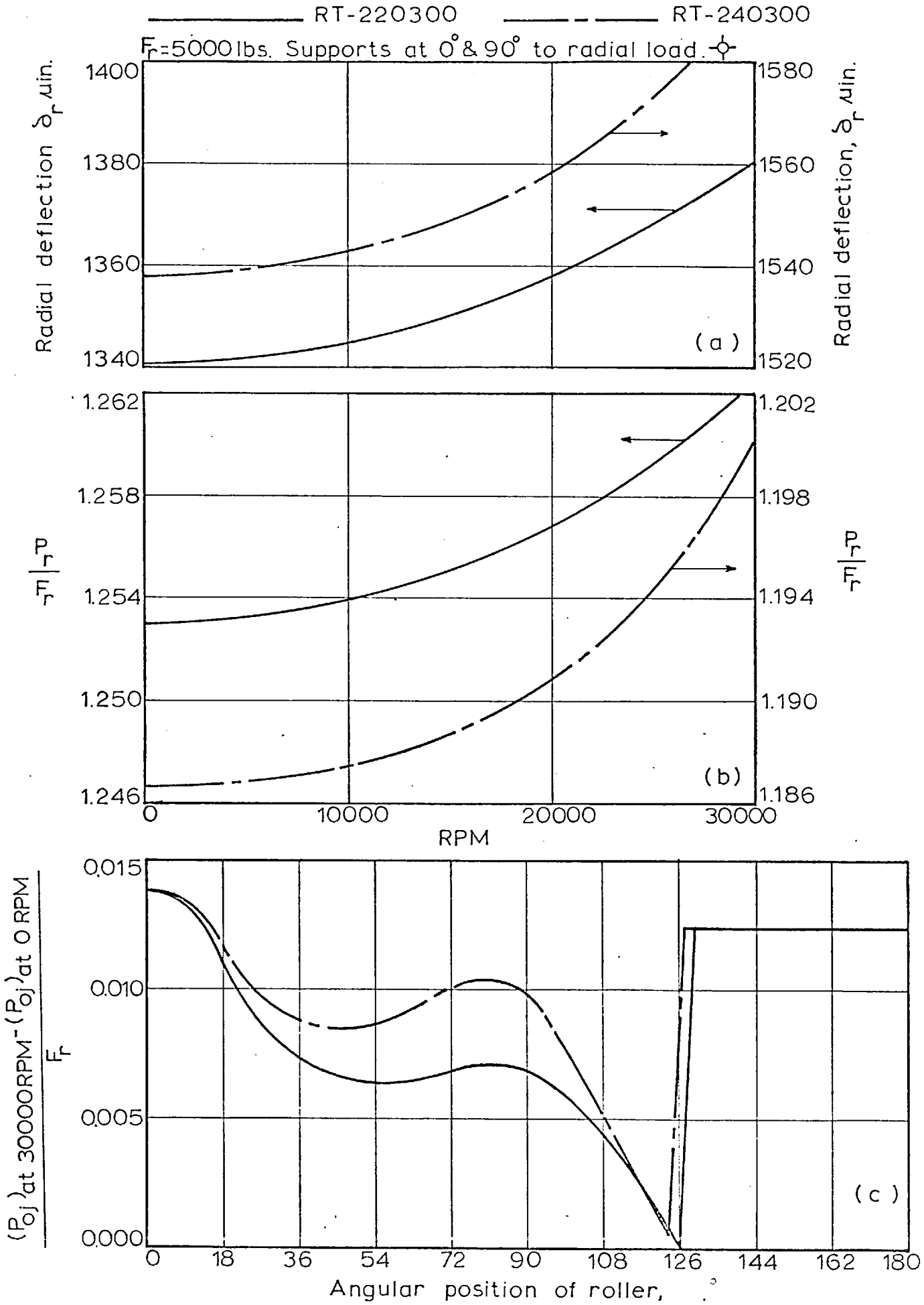


Fig. 7.73 Effect of shaft speed on
(a) radial deflection δ_r,
(b) non-dimensional equivalent radial load (P_r/F_r), and
(c) excess roller load distribution at the outer race,
of a steel radial roller bearing having thin circular housing (T 5) with diagonal cruciform support.

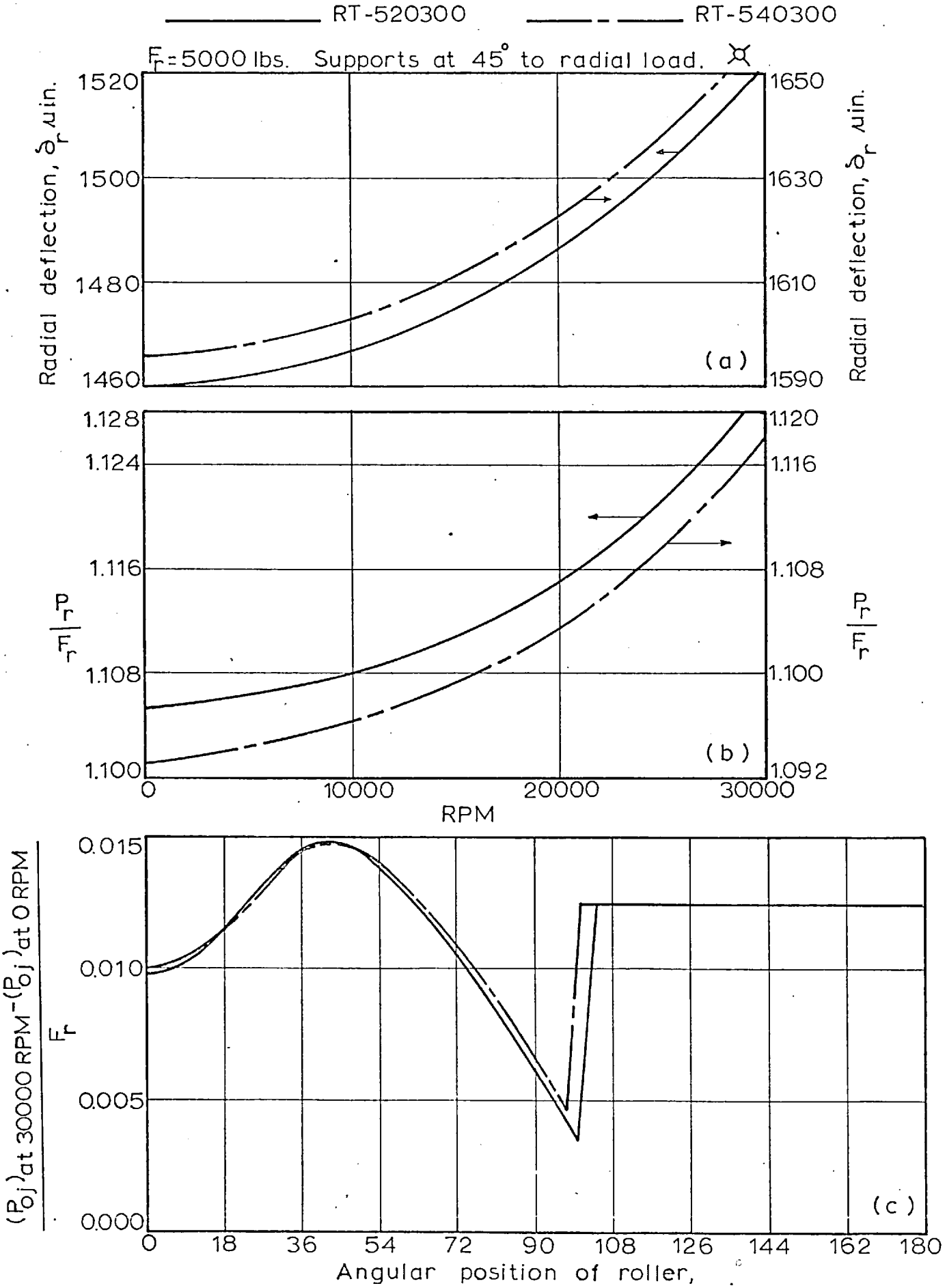


Fig. 7.74 Radial and component deflections of a steel bearing having hollow shaft (no.4) and thin circular housing with part-cruciform support.

δ_r= radial deflection, δ_b= body deflection of outer race, δ_{or}= outer race deflection, δ_{ir}= inner race deflection.

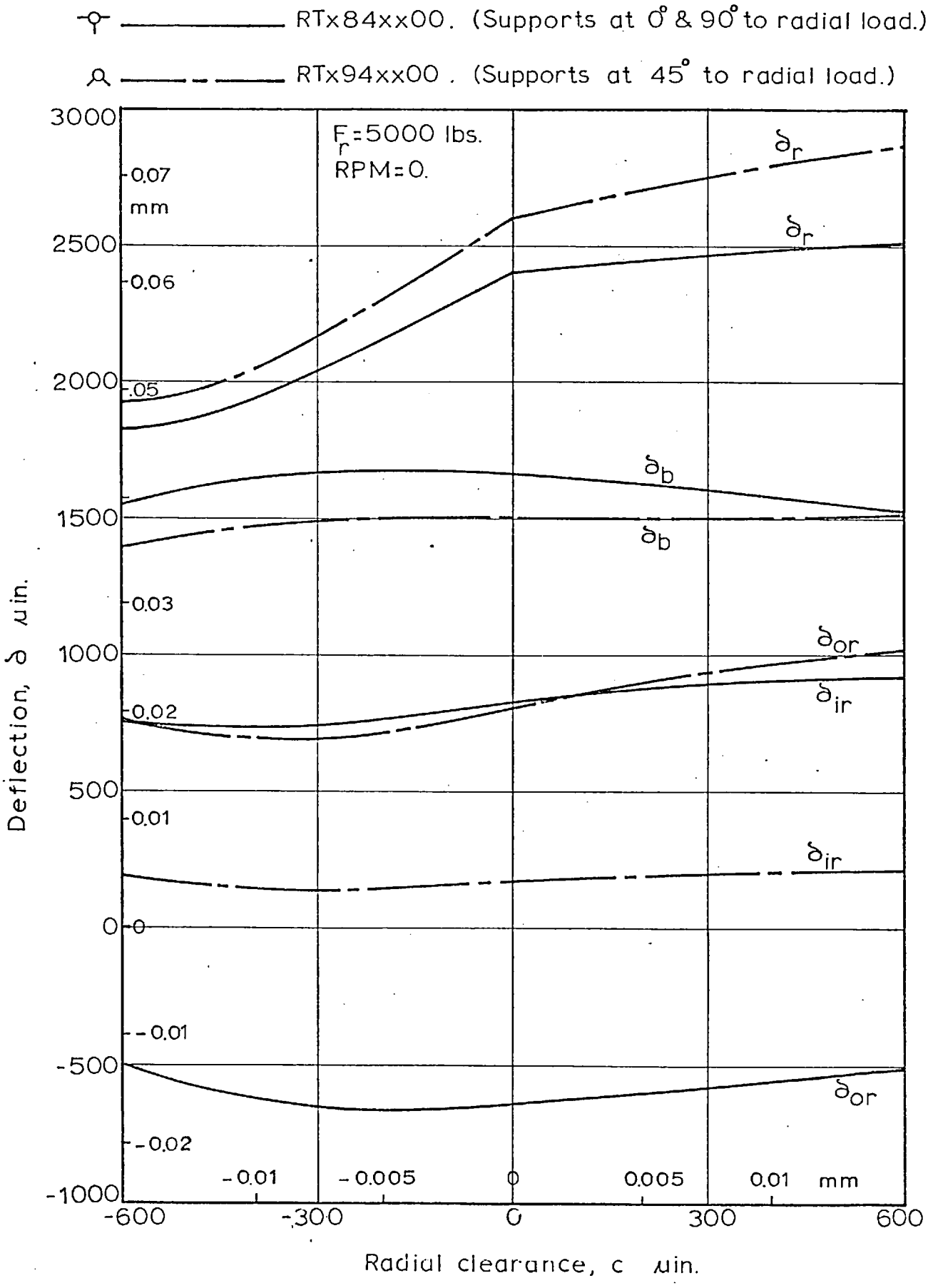


Fig. 7.75 Non-dimensional equivalent radial load (P_r/F_r) of a steel radial roller bearing having hollow shaft (no.4) and thin circular housing with part-cruciform support.

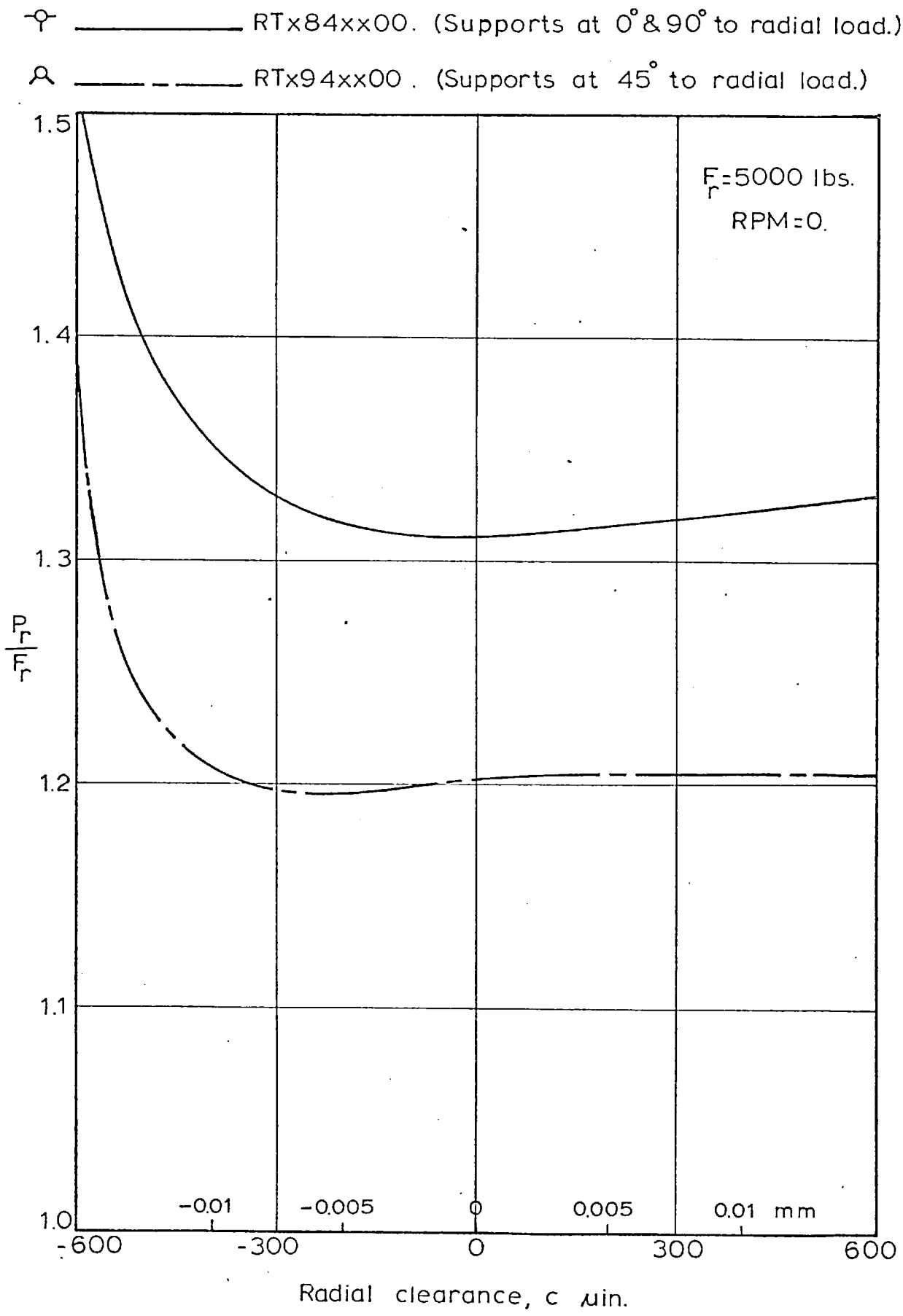


Fig. 7.76 K_t and K_b of a steel bearing having hollow shaft (no.4) and thin circular housing with part-cruciform support.

$$K_t = \frac{\delta_r \text{ for flexible races}}{\delta_r \text{ for rigid races}}, \quad K = \frac{\delta_b \text{ for flexible races}}{\delta_r \text{ for rigid races}}$$

where, δ_r = radial deflection, δ_b = body deflection of outer race.

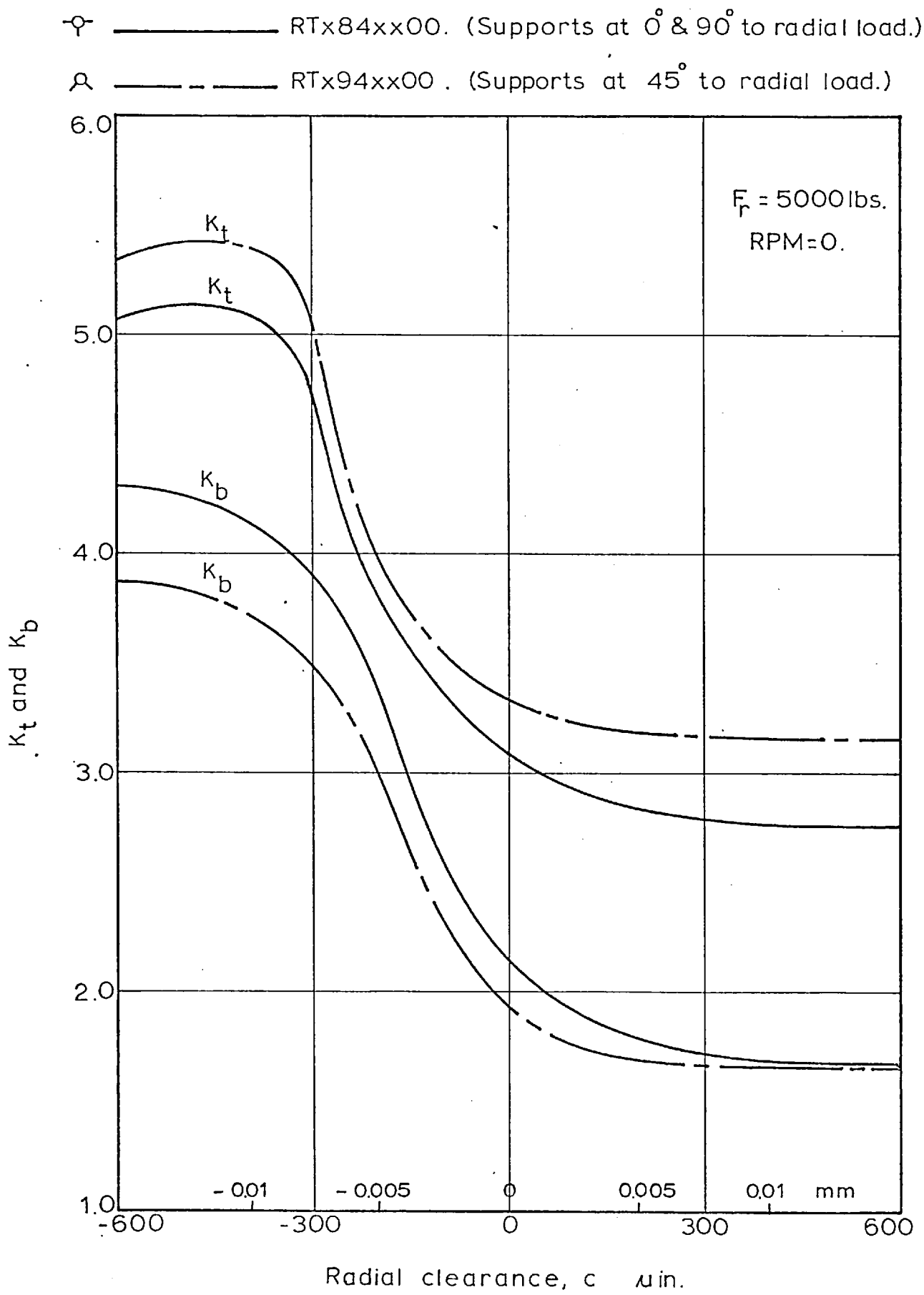


Fig. 7.77 Roller load distribution in a steel radial roller bearing with hollow shaft (no.4) and thin circular housing with part-cruciform support.

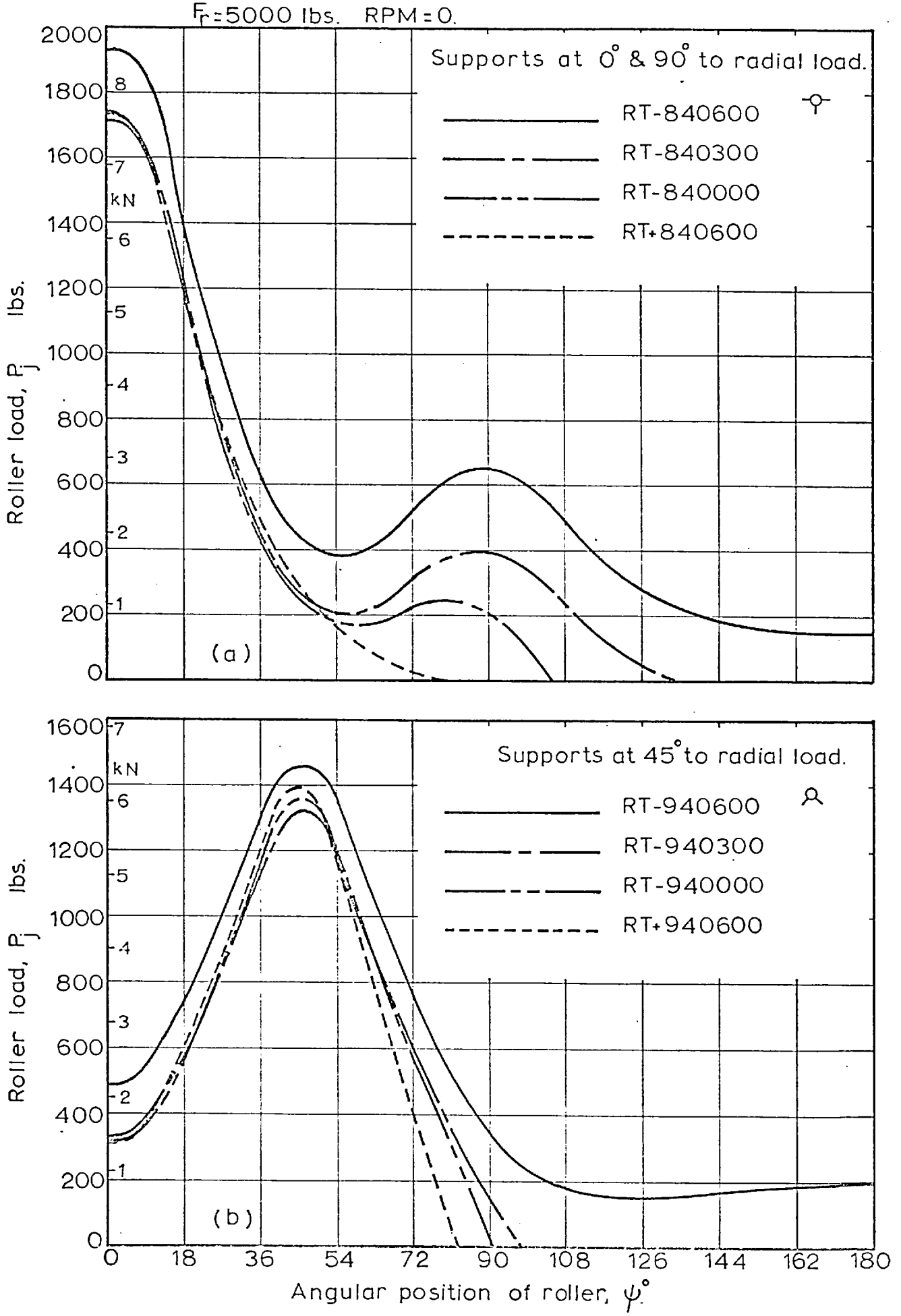
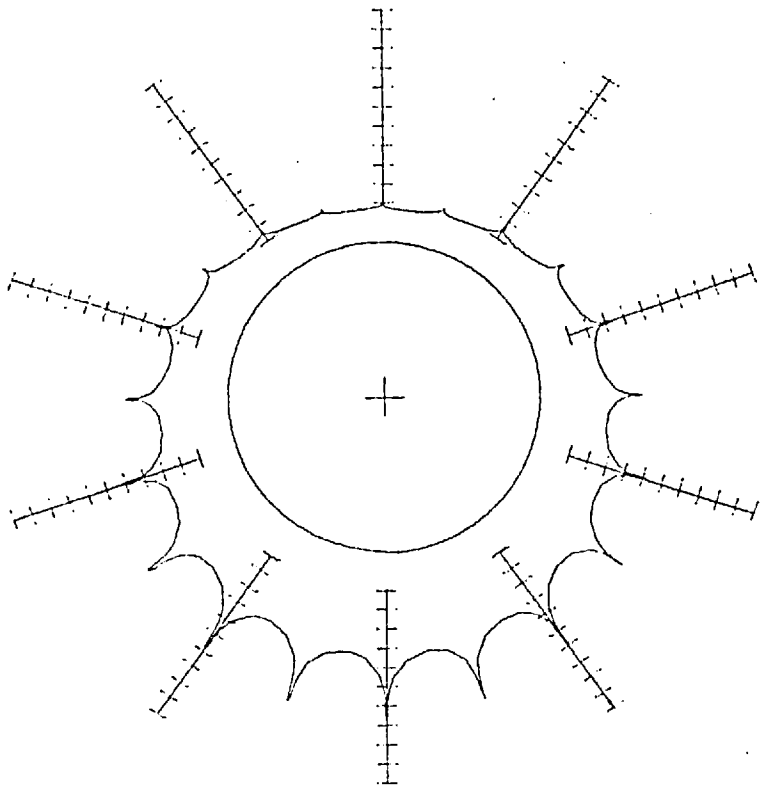


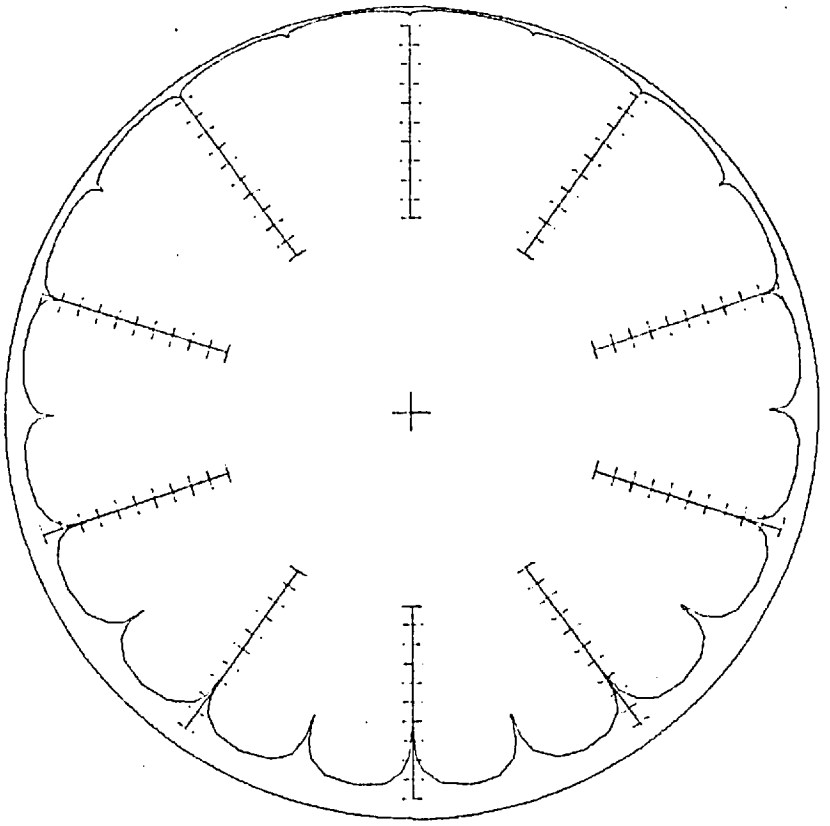
Fig. 7.78 Deflected shapes of the races of a steel radial roller bearing having solid shaft and housing in the form of a plate (S 2). Radial clearance c= −600 μin. and radial load F_r= 5000 lbs.



OUTER RACE

ONE DIV REPRESENTS 0.05 THOU

BEARING NO RS-220600 LOAD=5000 LBS RPM=0



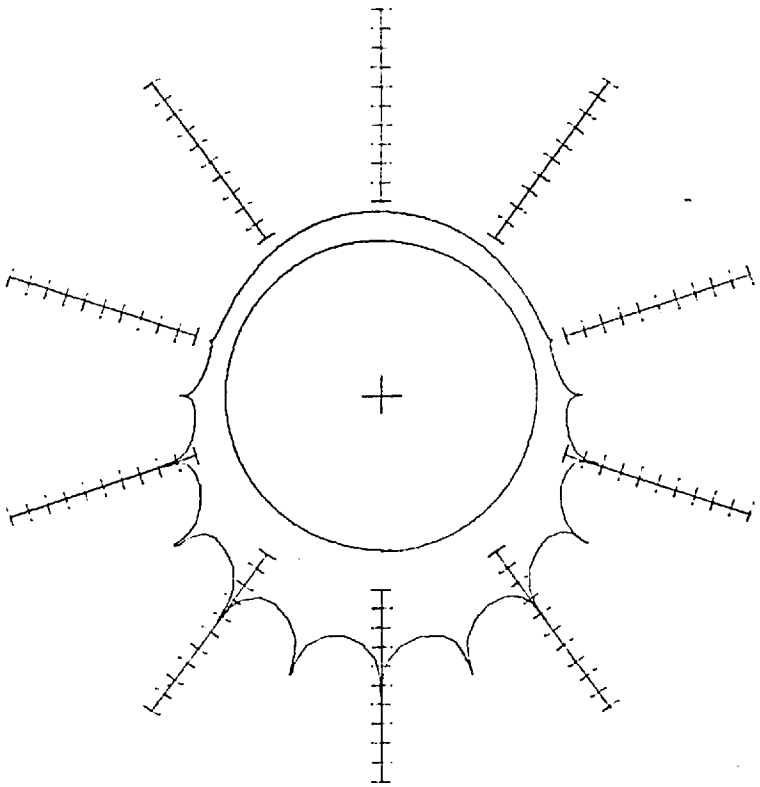
INNER RACE

ONE DIV REPRESENTS 0.05 THOU

BEARING NO RS-220600 LOAD=5000 LBS RPM=0

Fig. 7.78

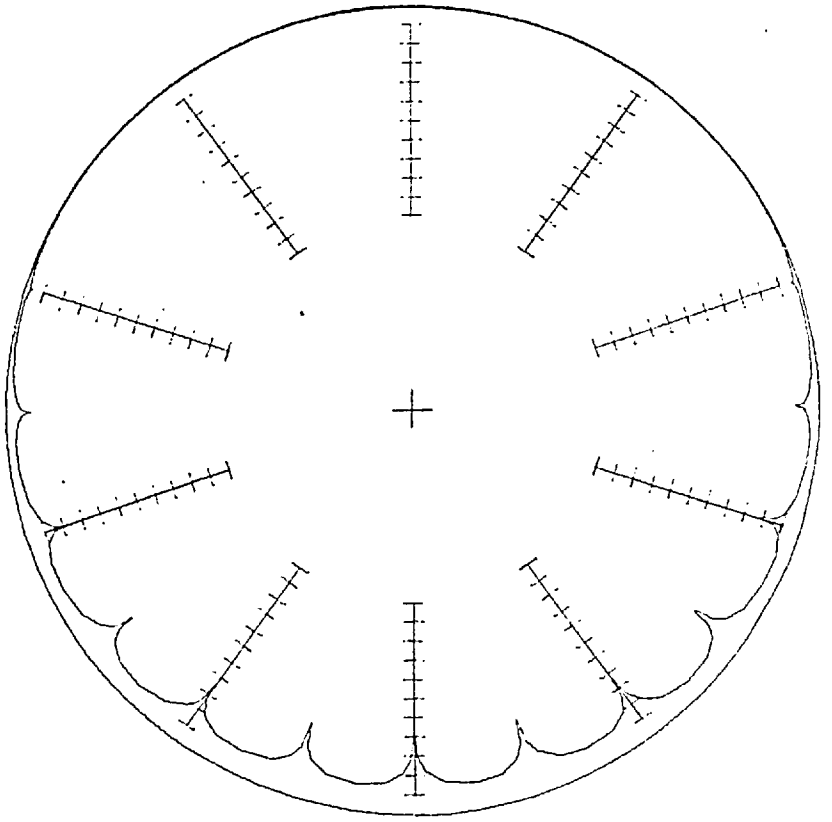
Fig. 7.79 Deflected shapes of the races of a steel radial roller bearing having solid shaft and housing in the form of a plate (S 2). Radial clearance c= −300 μin. and radial load F_r= 5000 lbs.



OUTER RACE

ONE DIV REPRESENTS 0.05 THOU

BEARING NO RS-220300 LOAD=5000 LBS RPM=0



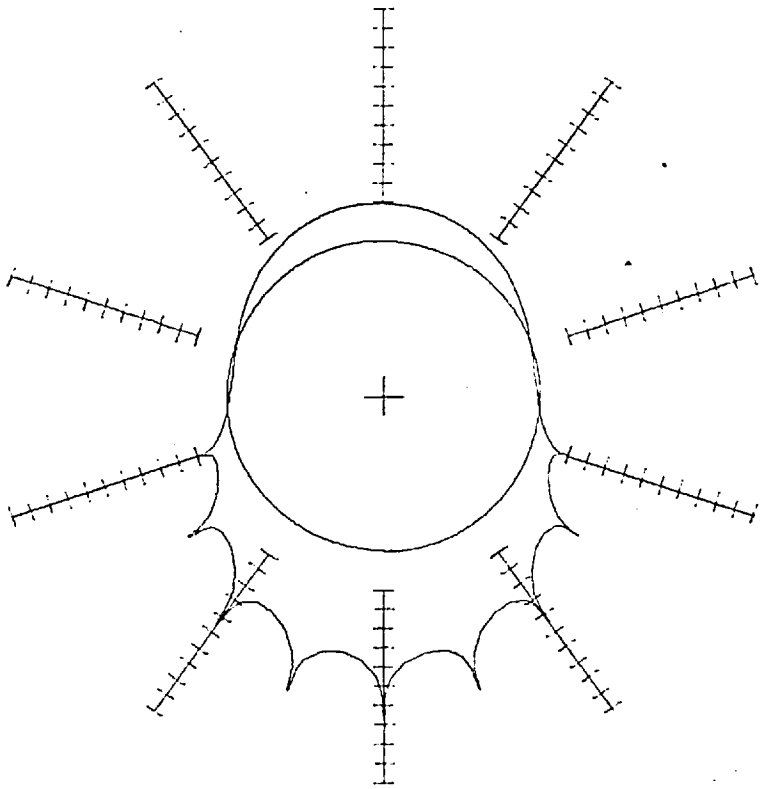
INNER RACE

ONE DIV REPRESENTS 0.05 THOU

BEARING NO RS-220300 LOAD=5000 LBS RPM=0

Fig. 7.79

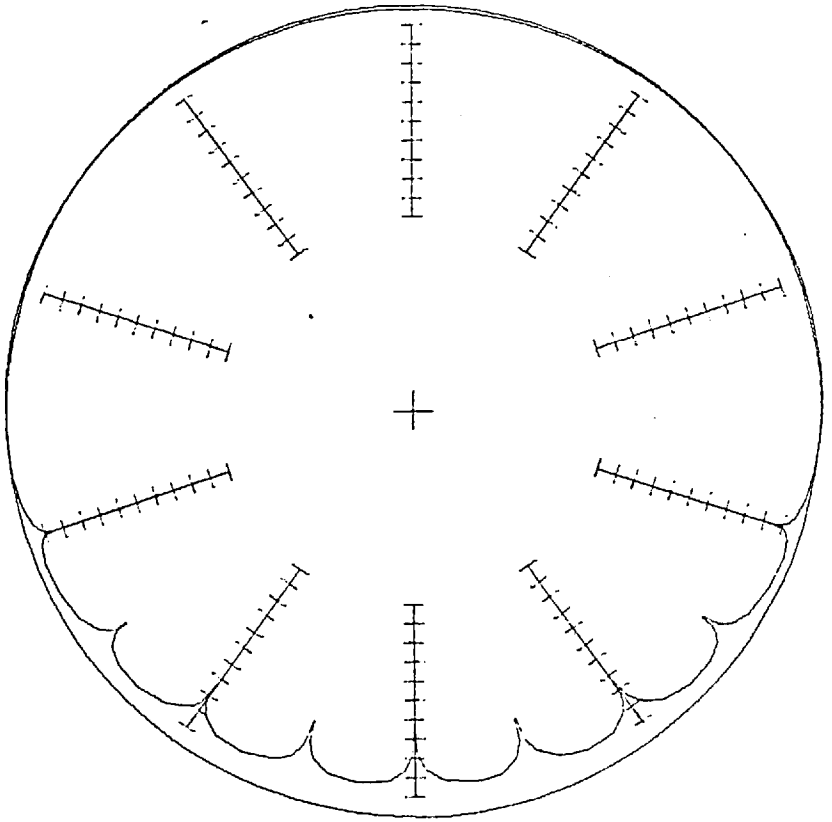
Fig. 7.80 Deflected shapes of the races of a steel radial roller bearing having solid shaft and housing in the form of a plate (S 2). Radial clearance c= 0.0 and radial load F_r= 5000 lbs.



OUTER RACE

ONE DIV REPRESENTS 0.05 THOU

BEARING NO RS-220000 LOAD=5000 LBS RPM=0



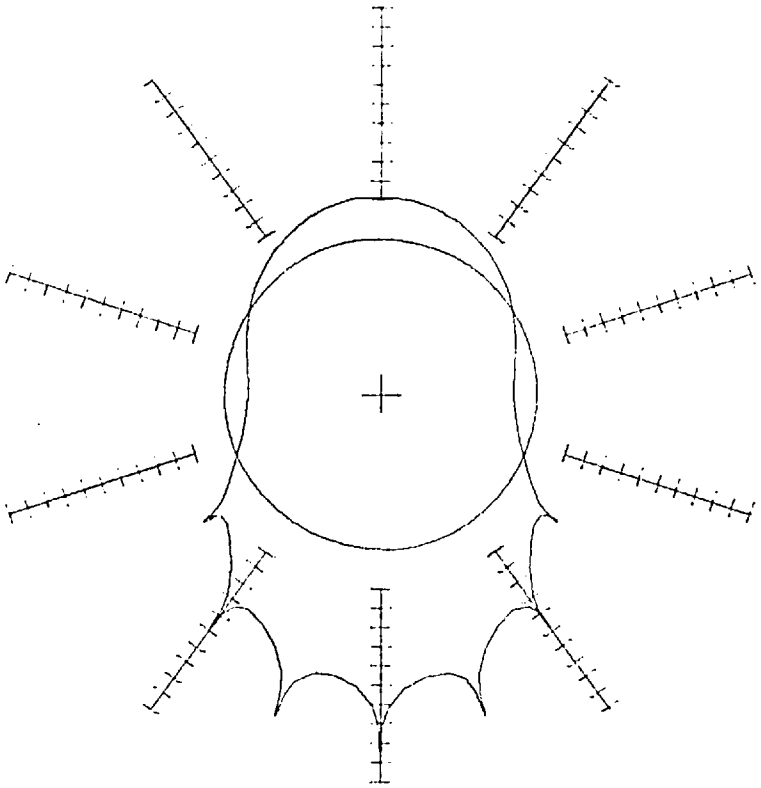
INNER RACE

ONE DIV REPRESENTS 0.05 THOU

BEARING NO RS-220000 LOAD=5000 LBS RPM=0

Fig. 7.80

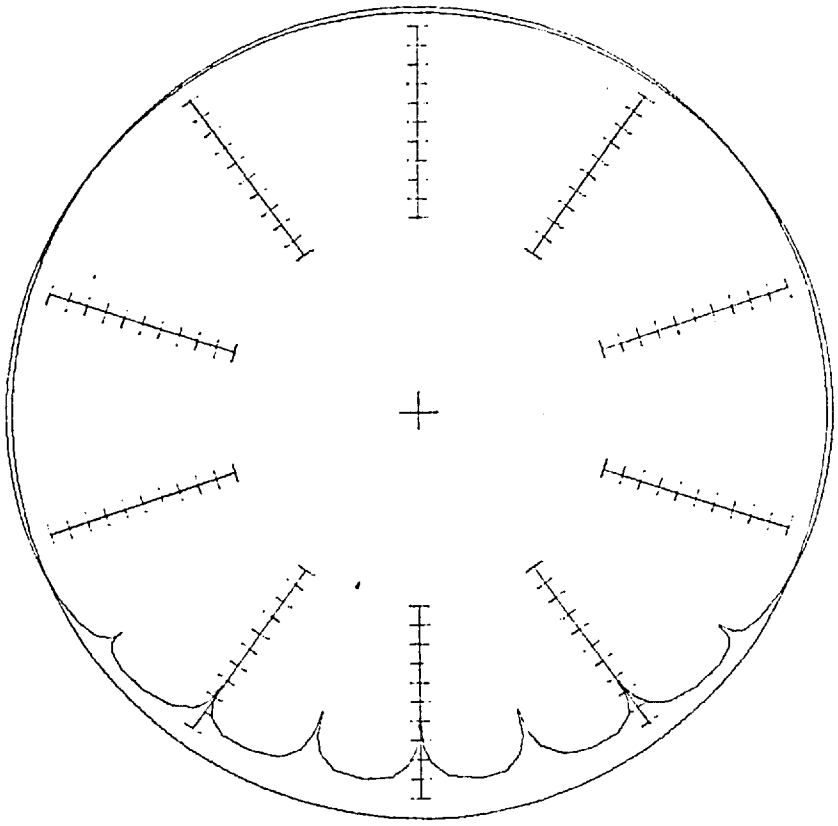
Fig. 7.81 Deflected shapes of the races of a steel radial roller bearing having solid shaft and housing in the form of a plate (S 2). Radial clearance c= +600 μin. and radial load F_r= 5000 lbs.



OUTER RACE

ONE DIV REPRESENTS 0.05 THOU

BEARING NO RS220600 LOAD=5000 LBS RPM=0



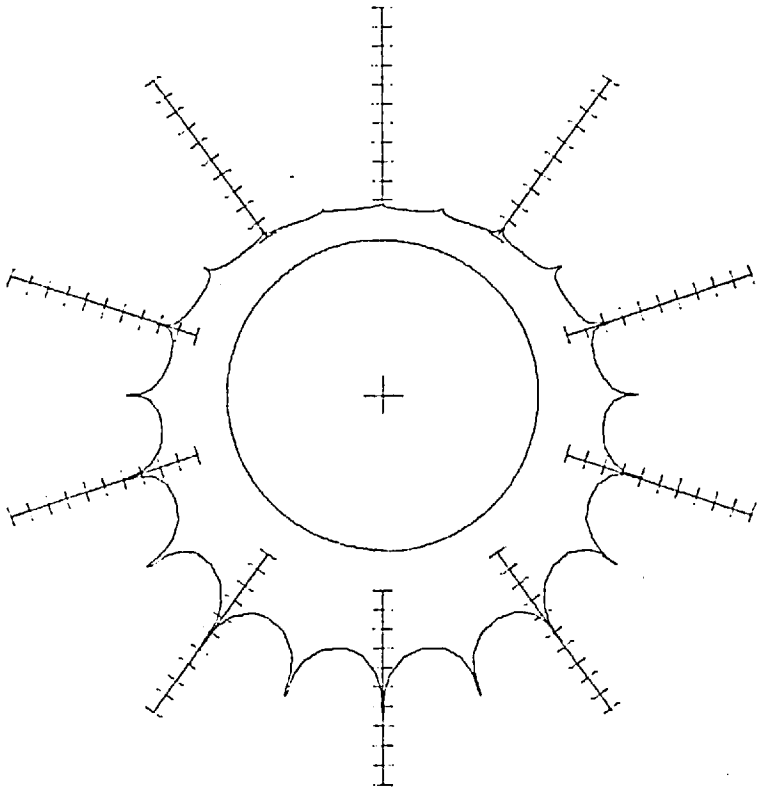
INNER RACE

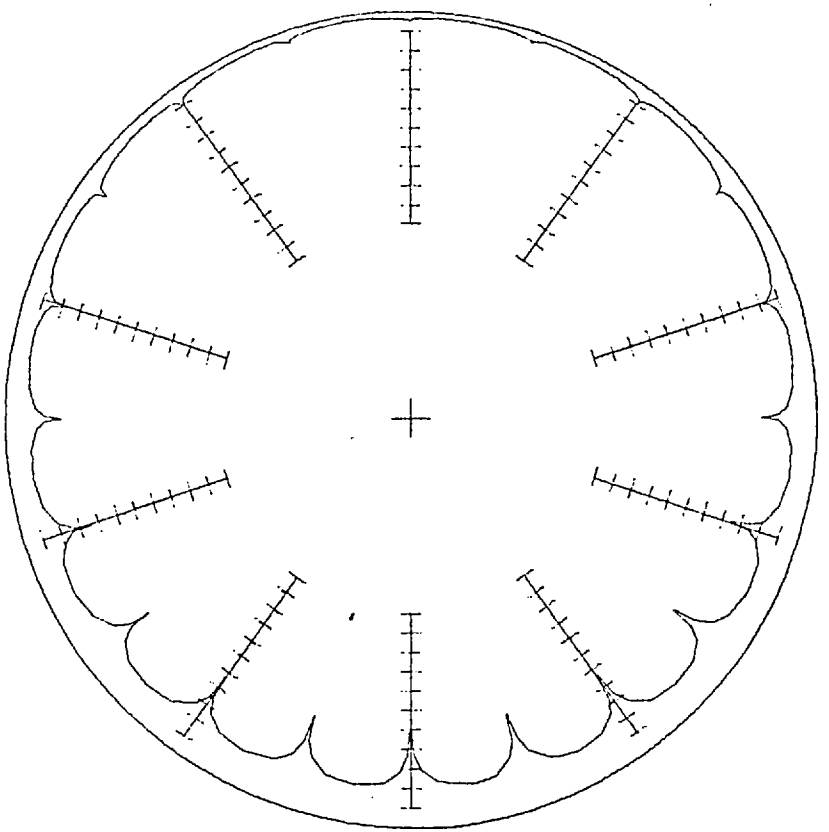
ONE DIV REPRESENTS 0.05 THOU

BEARING NO RS220600 LOAD=5000 LBS RPM=0

Fig. 7.81

Fig. 7.82 Deflected shapes of the races of a steel radial roller bearing having hollow shaft (no.3, inner to outer diameter ratio 0.372) and housing in the form of a plate. Radial clearance c= -600 μin. and radial load F_r= 5000 lbs.





OUTER RACE

INNER RACE

ONE DIV REPRESENTS 0.05 THOU BEARING NO RS-230600 LOAD=5000 LBS RPM=0

Fig. 7.82

Fig. 7.83 Deflected shapes of the races of a steel radial roller bearing having hollow shaft (no.3, inner to outer diameter ratio 0.372) and housing in the form of a plate (S 2). Radial clearance c= +600 μin. and radial load F_r= 5000 lbs.

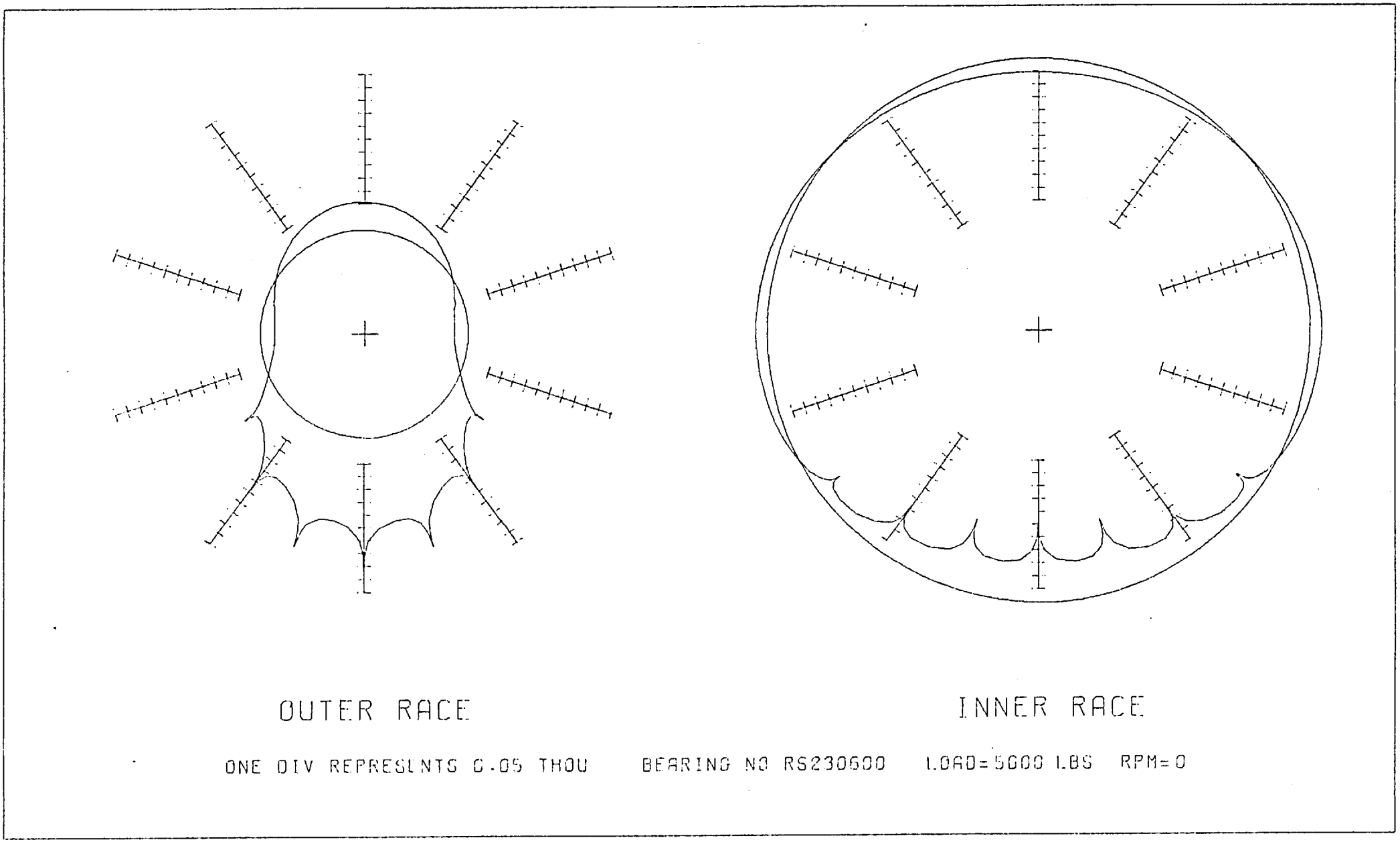
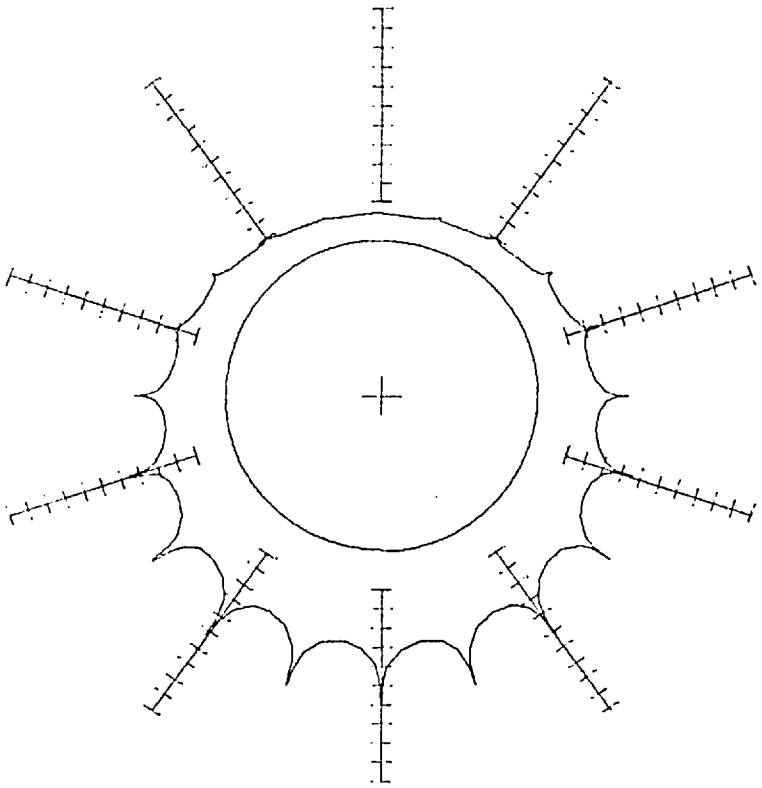


Fig. 7.83

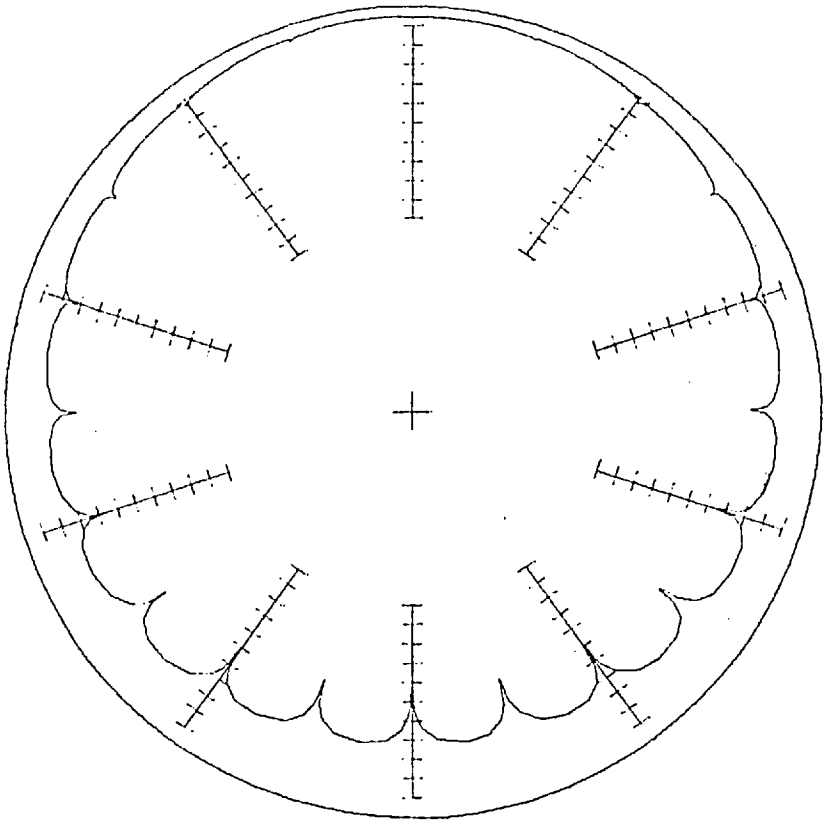
Fig. 7.84 Deflected shapes of the races of a steel radial roller bearing having hollow shaft (no.4, inner to outer diameter ratio 0.651) and housing in the form of a plate (S 2). Radial clearance c= -600 μin. and radial load F_r= 5000 lbs.



OUTER RACE

ONE DIV REPRESENTS 0.05 THOU

BEARING NO RS-240600 LOAD=5000 LBS RPM=0



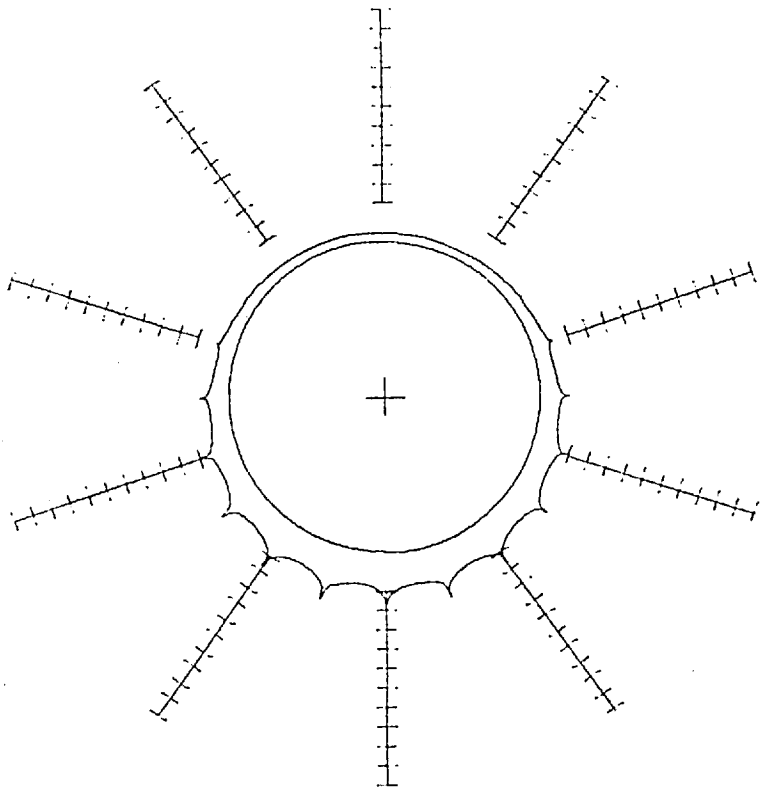
INNER RACE

ONE DIV REPRESENTS 0.05 THOU

BEARING NO RS-240600 LOAD=5000 LBS RPM=0

Fig. 7.84

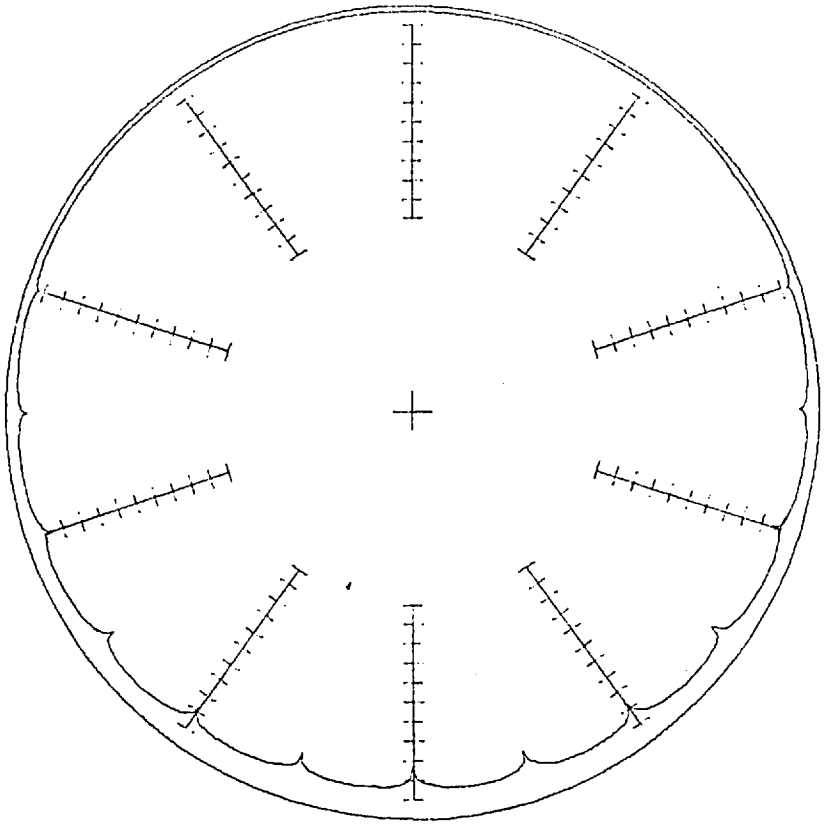
Fig. 7.85 Deflected shapes of the races of a steel radial roller bearing having hollow shaft (no.4, inner to outer diameter ratio 0.651) and housing in the form of a plate (S 2). Radial clearance c= -200 µin. and radial load F_r = 2000 lbs.



OUTER RACE

ONE DIV REPRESENTS 0.05 THOU

BEARING NO RS-240200 LOAD=2000 LBS RPM=0



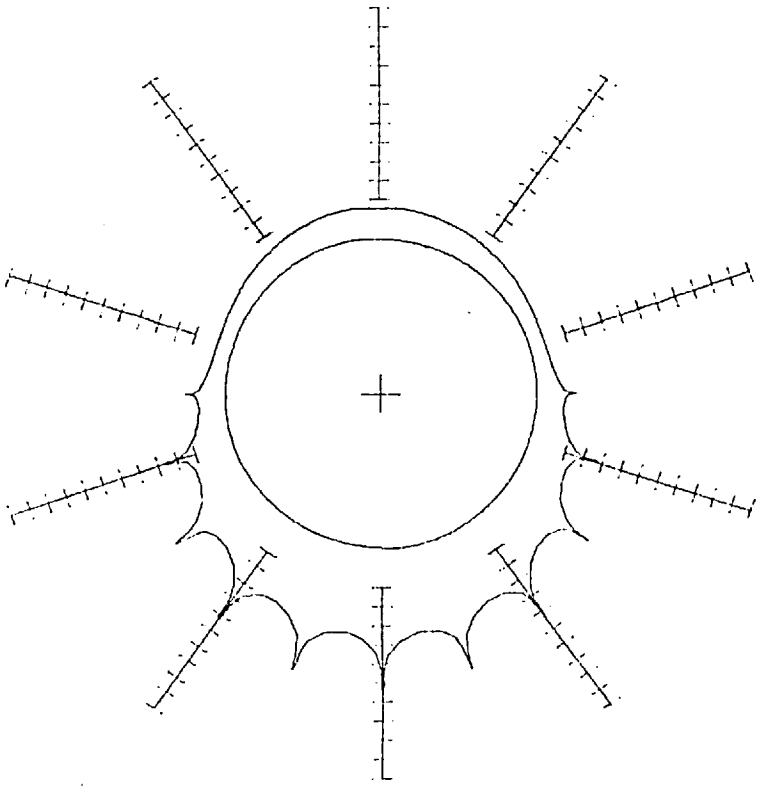
INNER RACE

ONE DIV REPRESENTS 0.05 THOU

BEARING NO RS-240200 LOAD=2000 LBS RPM=0

Fig. 7.85

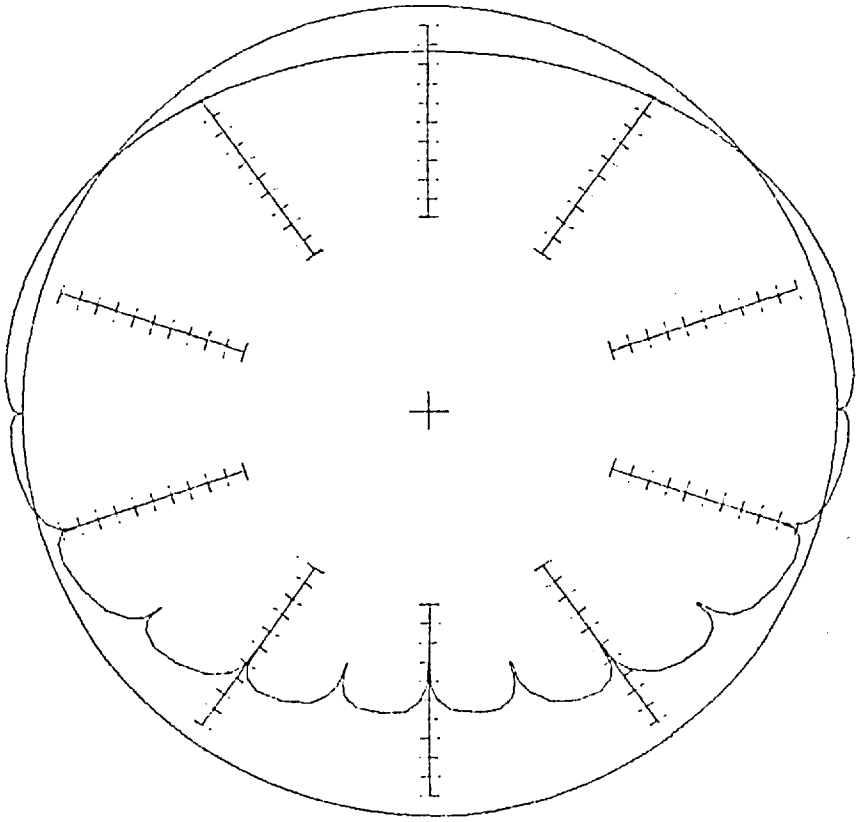
Fig. 7.86 Deflected shapes of the races of a steel radial roller bearing having hollow shaft (no.4, inner to outer diameter ratio 0.651) and housing in the form of a plate (S 2). Radial clearance c= -200 μin. and radial load F_r= 5000 lbs.



OUTER RACE

ONE DIV REPRESENTS 0.05 THOU

BEARING NO RS-240200 LOAD=5000 LBS RPM=0



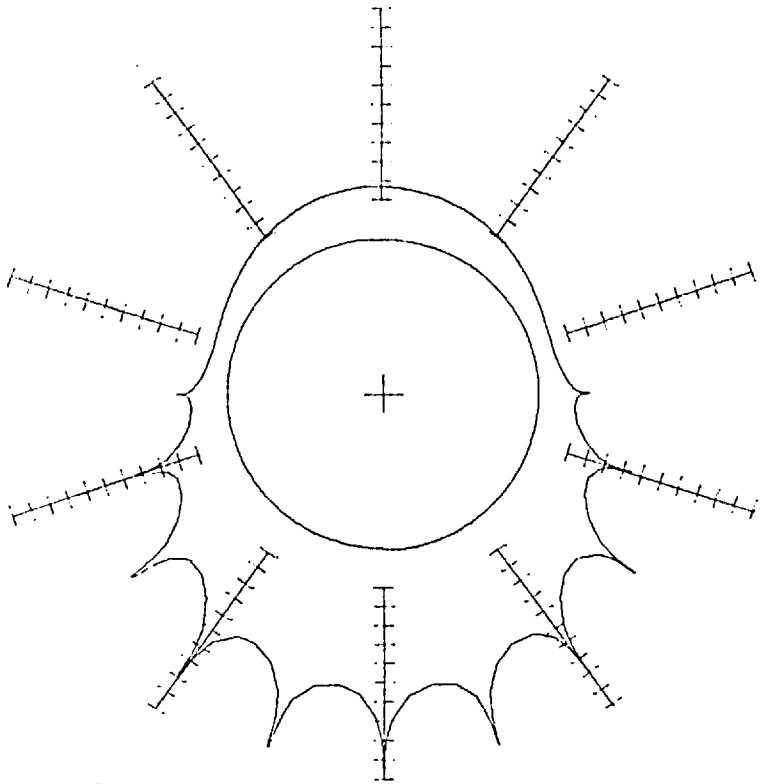
INNER RACE

ONE DIV REPRESENTS 0.05 THOU

BEARING NO RS-240200 LOAD=5000 LBS RPM=0

Fig. 7.86

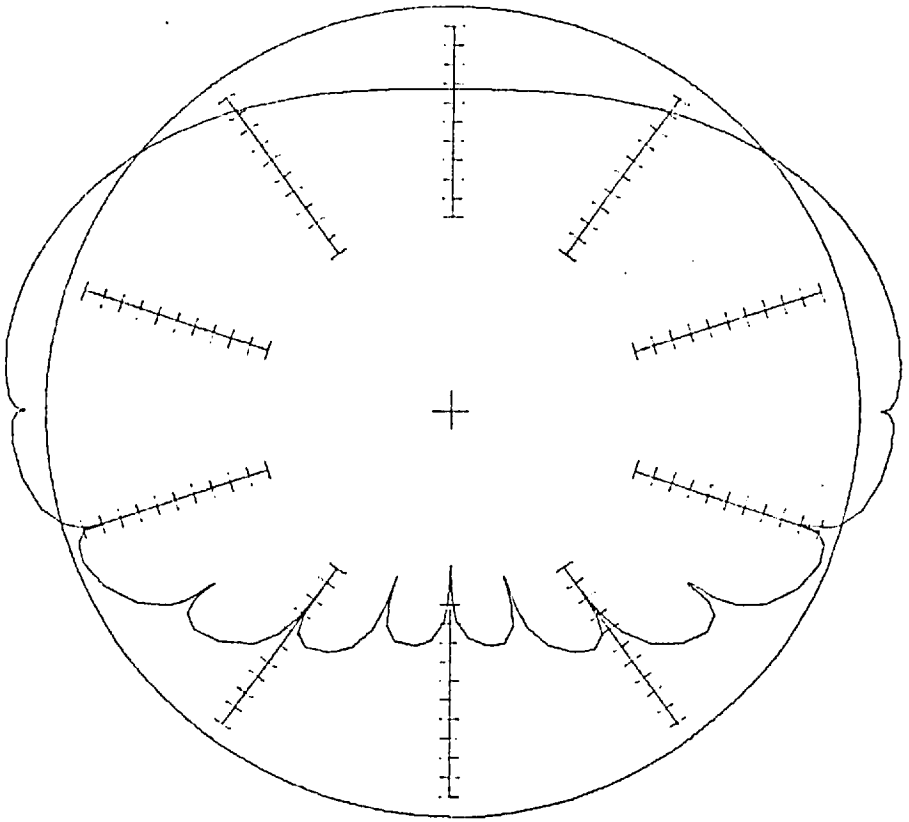
Fig. 7.87 Deflected shapes of the races of a steel radial roller bearing having hollow shaft (no.4, inner to outer diameter ratio 0.651) and housing in the form of a plate (S 2). Radial clearance c= -200 μin. and radial load F_r = 8000 lbs.



OUTER RACE

ONE DIV REPRESENTS 0.05 THOU

BEARING NO RS-240200 LOAD=8000 LBS RPM=0



INNER RACE

ONE DIV REPRESENTS 0.05 THOU

BEARING NO RS-240200 LOAD=8000 LBS RPM=0

Fig. 7.87

Fig. 7.88 Deflected shapes of the races of a steel radial roller bearing having hollow shaft (no.4, inner to outer diameter ratio 0.651) and housing in the form of a plate (S 2). Radial clearance c= +600 μin. and radial load F_r= 5000 lbs.

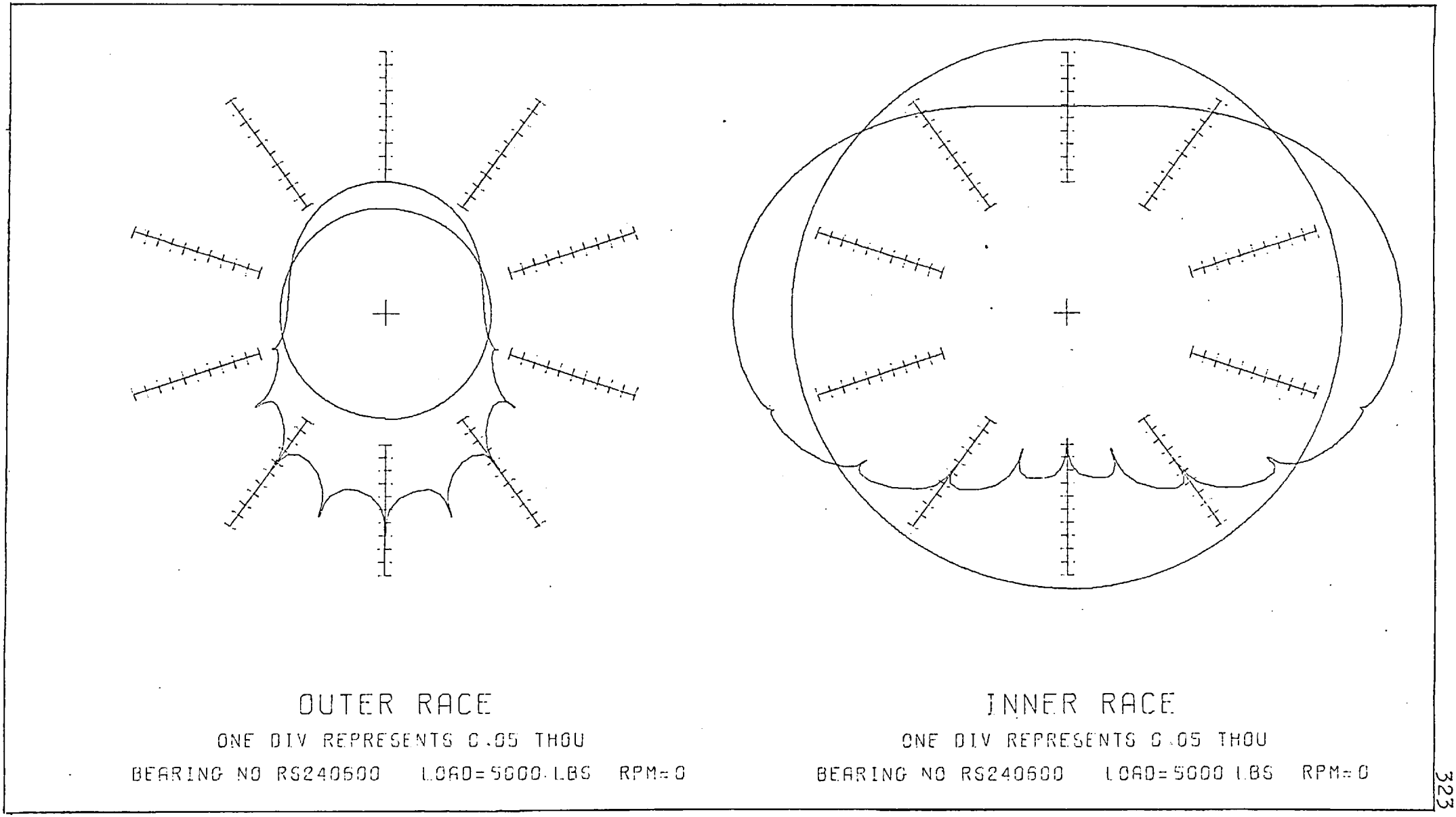
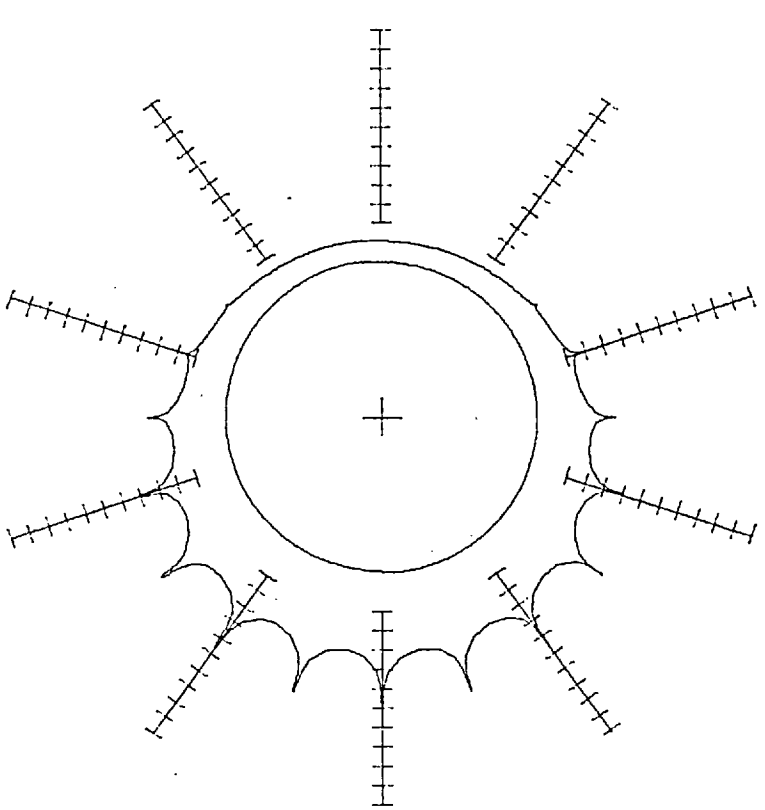
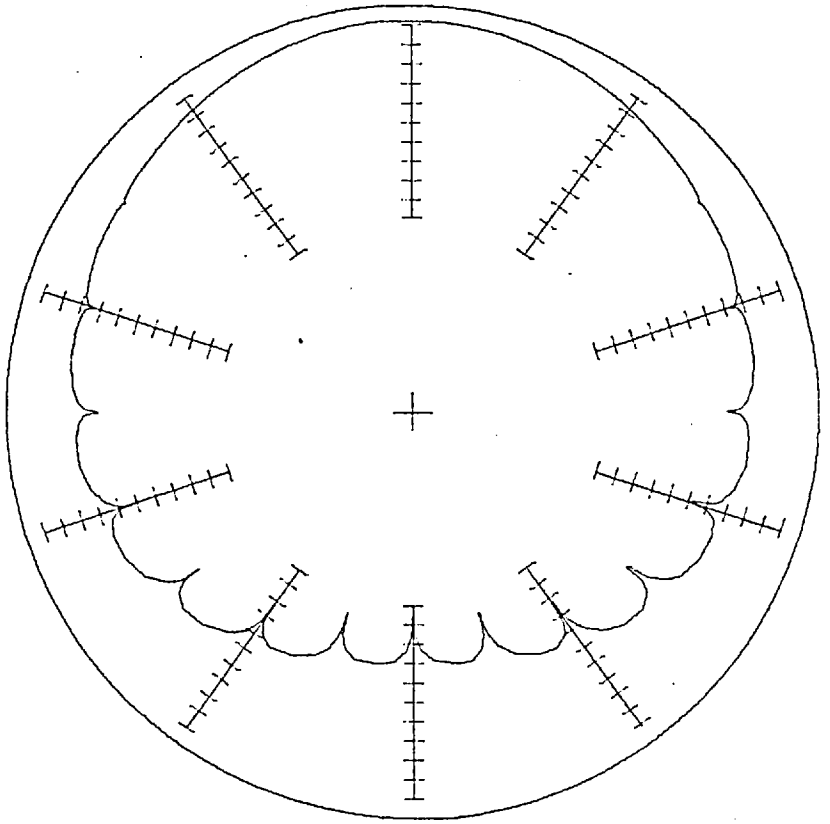


Fig. 7.88

Fig. 7.89 Deflected shapes of the races of a steel radial roller bearing having hollow shaft (no.5, inner to outer diameter ratio 0.837) and housing in the form of a plate. Radial clearance c= -600 μin. and radial load F_r= 5000 lbs.



OUTER RACE



INNER RACE

BEARING NO RS-250600 LOAD=5000 LBS RPM=0

ONE DIV REPRESENTS 0.05 THOU

Fig. 7.89

Fig. 7.90 Deflected shapes of the races of a steel radial roller bearing having hollow shaft (no.5, inner to outer diameter ratio 0.837) and housing in the form of a plate (S 2). Radial clearance c= 0.0 and radial load F_r= 5000 lbs.

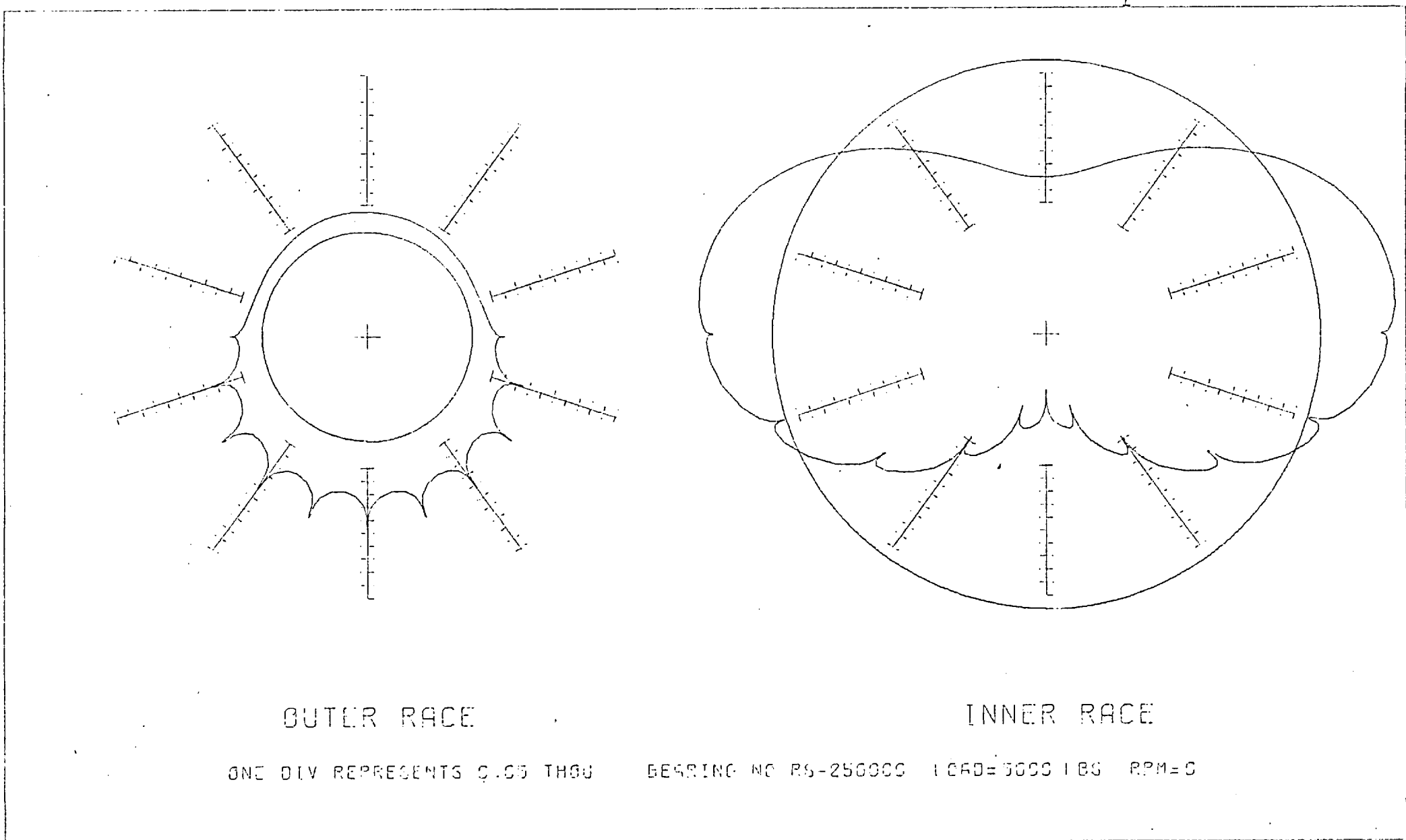


Fig. 7.90

Fig. 7.91 Deflected shapes of the races of a steel radial roller bearing having hollow shaft (no.5, inner to outer diameter ratio 0.837) and housing in the form of a plate (S 2). Radial clearance c= +600 μin. and radial load F_r = 5000 lbs.

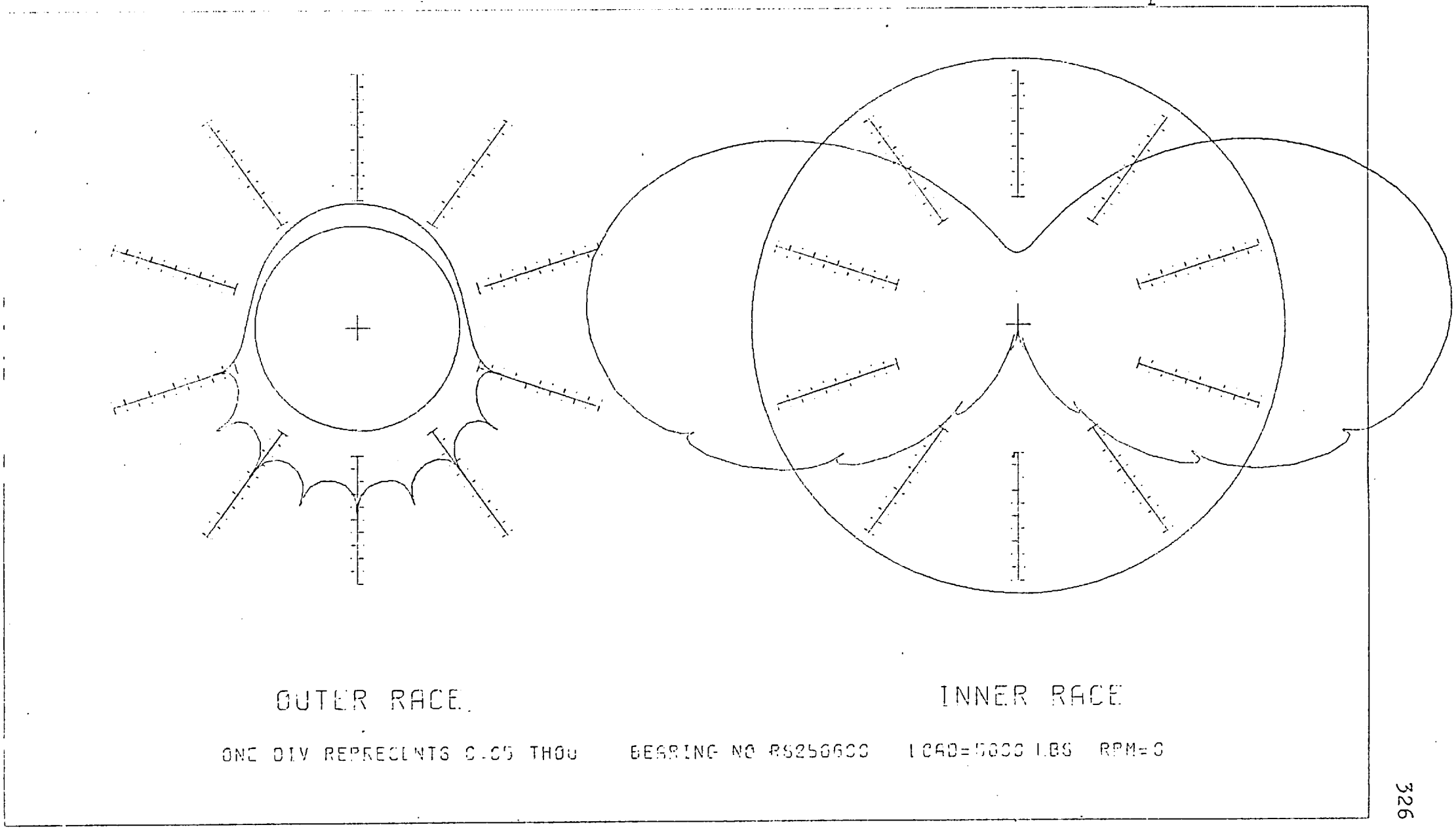
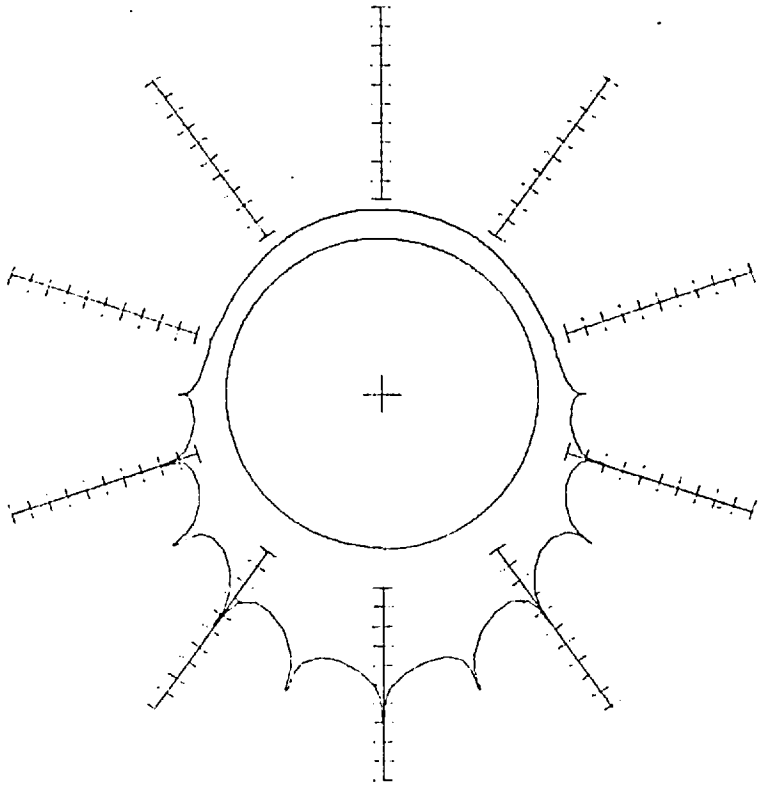
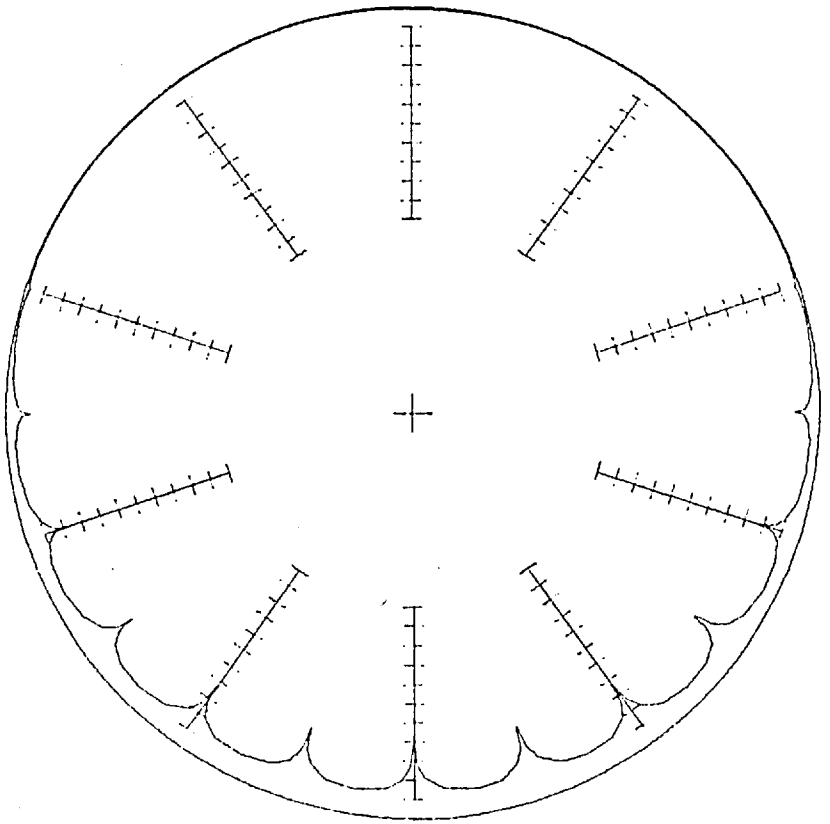


Fig. 7.91

Fig. 7.92 Deflected shapes of the races of a steel radial roller bearing having solid shaft and housing with a hole in the direction of the radial load. Radial clearance c= -300 μin. and radial load F_r= 5000 lbs.





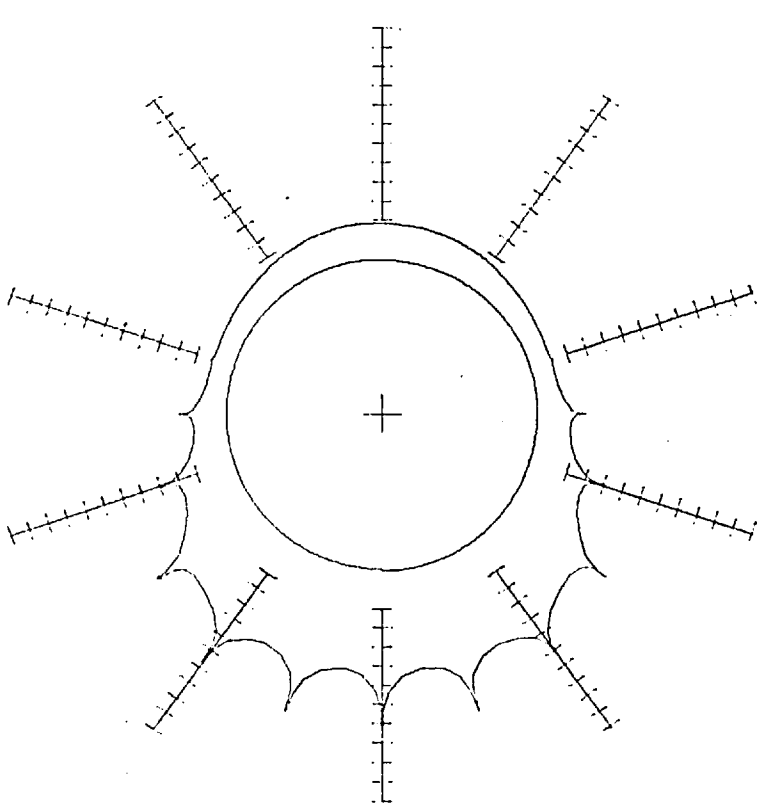
OUTER RACE

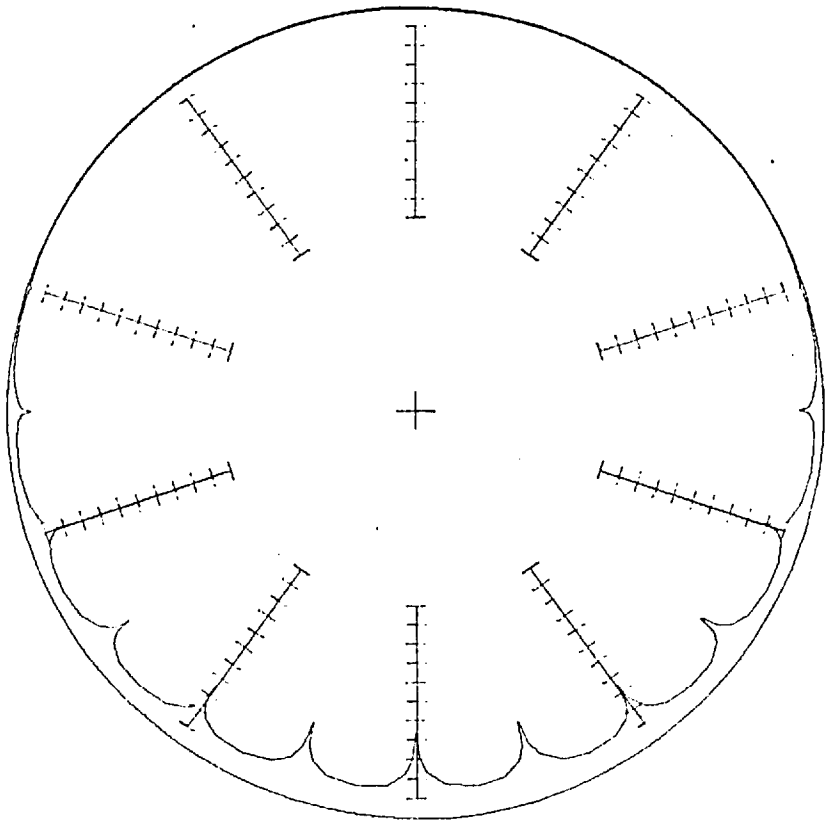
INNER RACE

ONE DIV REPRESENTS 0.05 THOU BEARING NO RS-320300 LOAD=5000 LBS RPM=0

Fig. 7.92

Fig. 7.93 Deflected shapes of the races of a steel radial roller bearing having solid shaft and housing with holes at 45° to the radial load on each side. Radial clearance c= -300 μin. and radial load F_r= 5000 lbs.





OUTER RACE

INNER RACE

ONE DIV REPRESENTS 0.05 THOU BEARING NO RS-420300 LOAD=5000 LBS RPM=0

Fig. 7.93

Fig. 7.94 Deflected shapes of the races of a steel radial roller bearing having solid shaft and housing with holes at 90° to the radial load on each side. Radial clearance c= -600 μin. and radial load F_r= 5000 lbs.

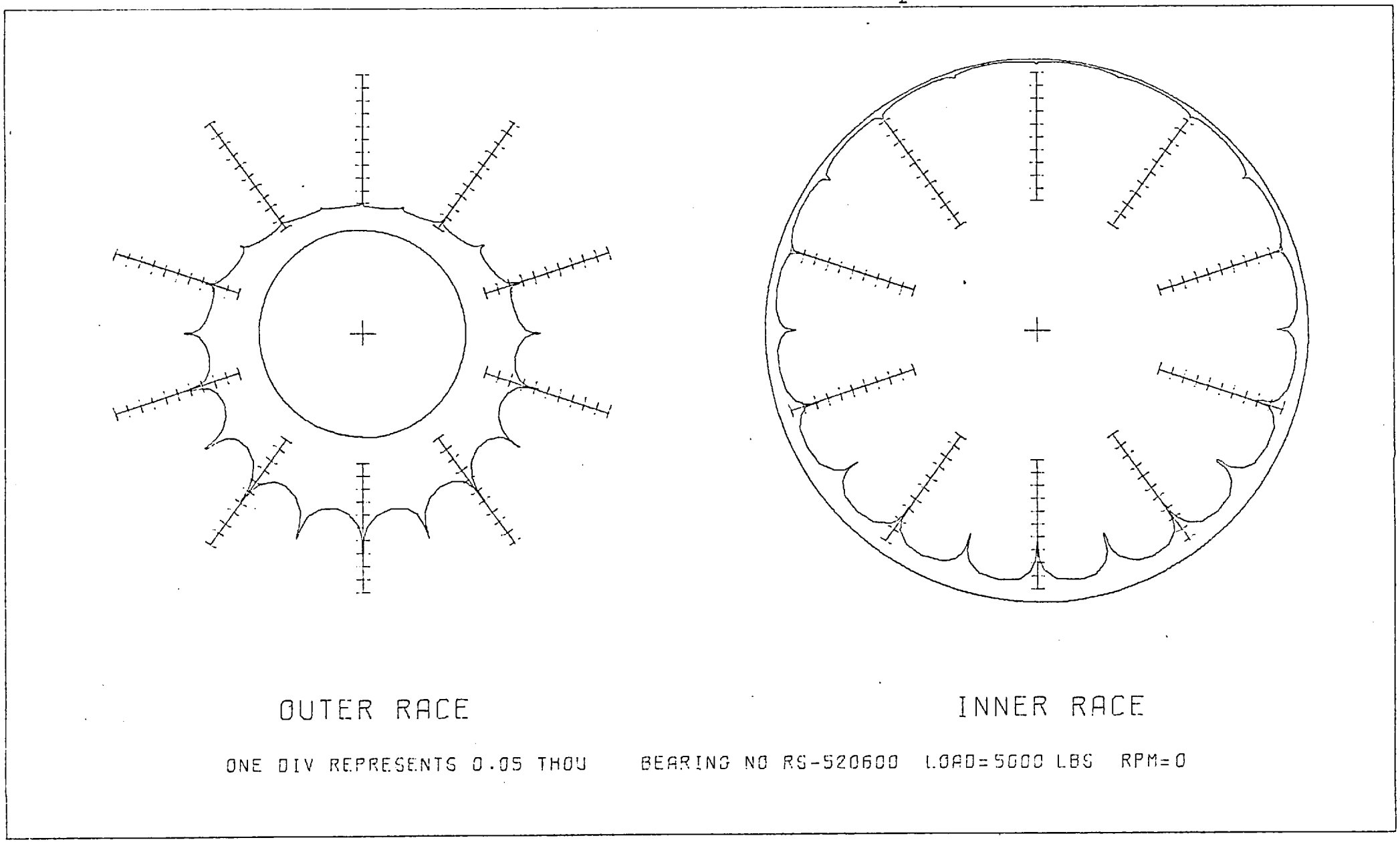
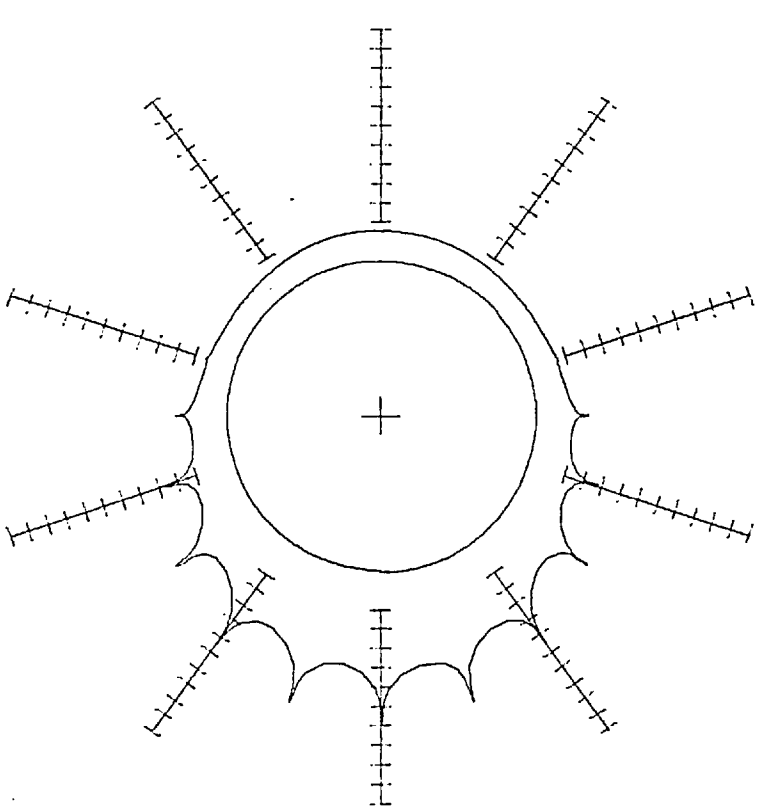
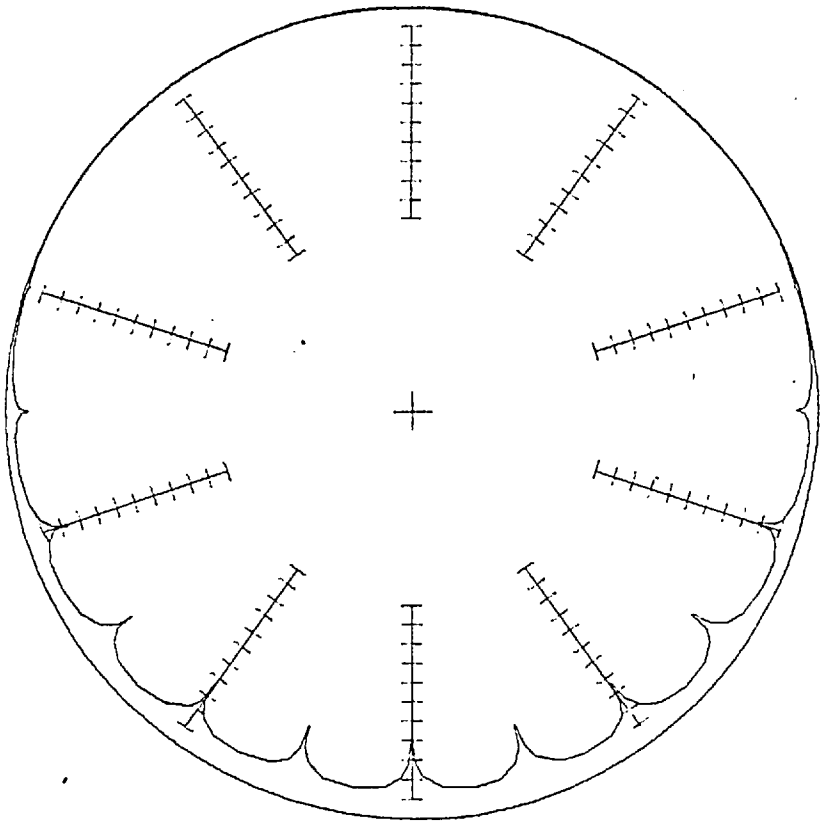


Fig. 7.94

Fig. 7.95 Deflected shapes of the races of a steel radial roller bearing having solid shaft and housing with holes at 90° to the radial load on each side. Radial clearance c= -300 μin. and radial load F_r= 5000 lbs.





OUTER RACE

INNER RACE

ONE DIV REPRESENTS 0.05 THOU BEARING NO RS-520300 LOAD=5000 LBS RPM=0

Fig. 7.95

Fig. 7.96 Deflected shapes of the races of a steel radial roller bearing having hollow shaft (no.4, inner to outer diameter ratio 0.651) and housing with a hole in the direction of the radial load. Radial clearance c= -300 μin. and radial load F_r= 5000 lbs.

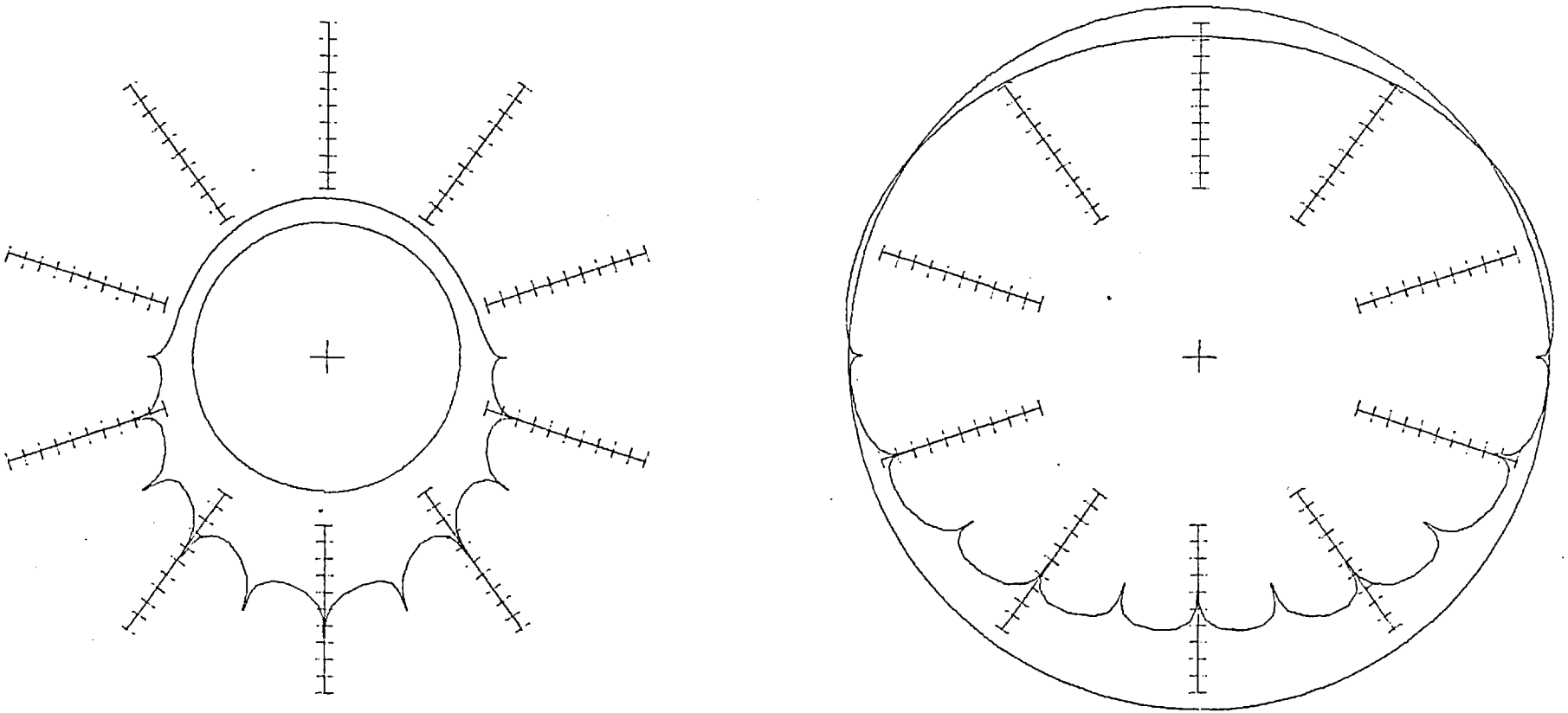


Fig. 7.96

Fig. 7.97 Deflected shapes of the races of a steel radial roller bearing having hollow shaft (no.4, inner to outer diameter ratio 0.651) and housing having holes at 45° to the radial load on each side. Radial clearance c= -300 μin. and radial load F_r= 5000 lbs.

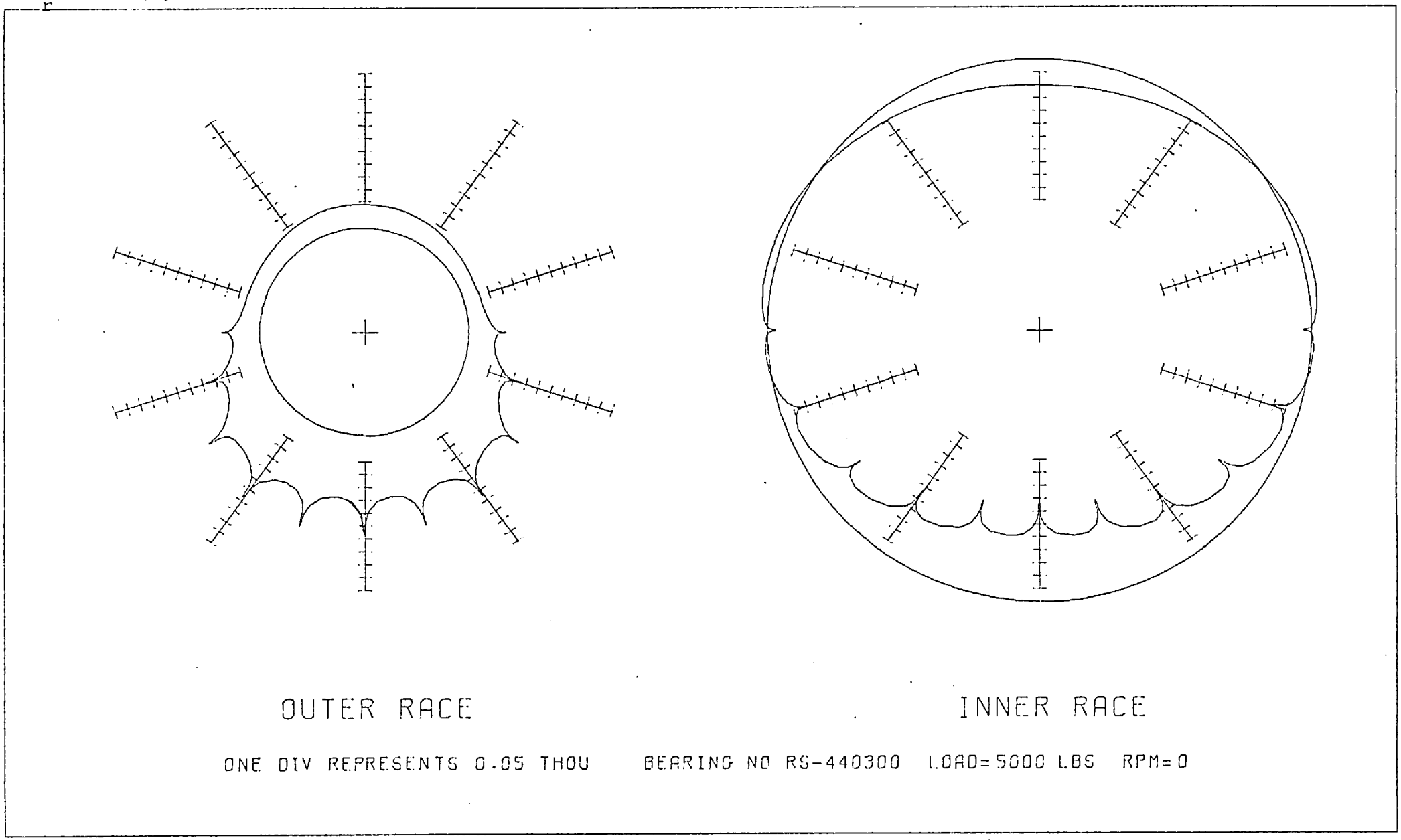


Fig. 7.97

Fig. 7.98 Deflected shapes of the races of a steel radial roller bearing having hollow shaft (no.4, inner to outer diameter ratio 0.651) and housing with boss (outer to inner diameter ratio 1.145). Radial clearance c= -600 μin. and radial load F_r= 5000 lbs.

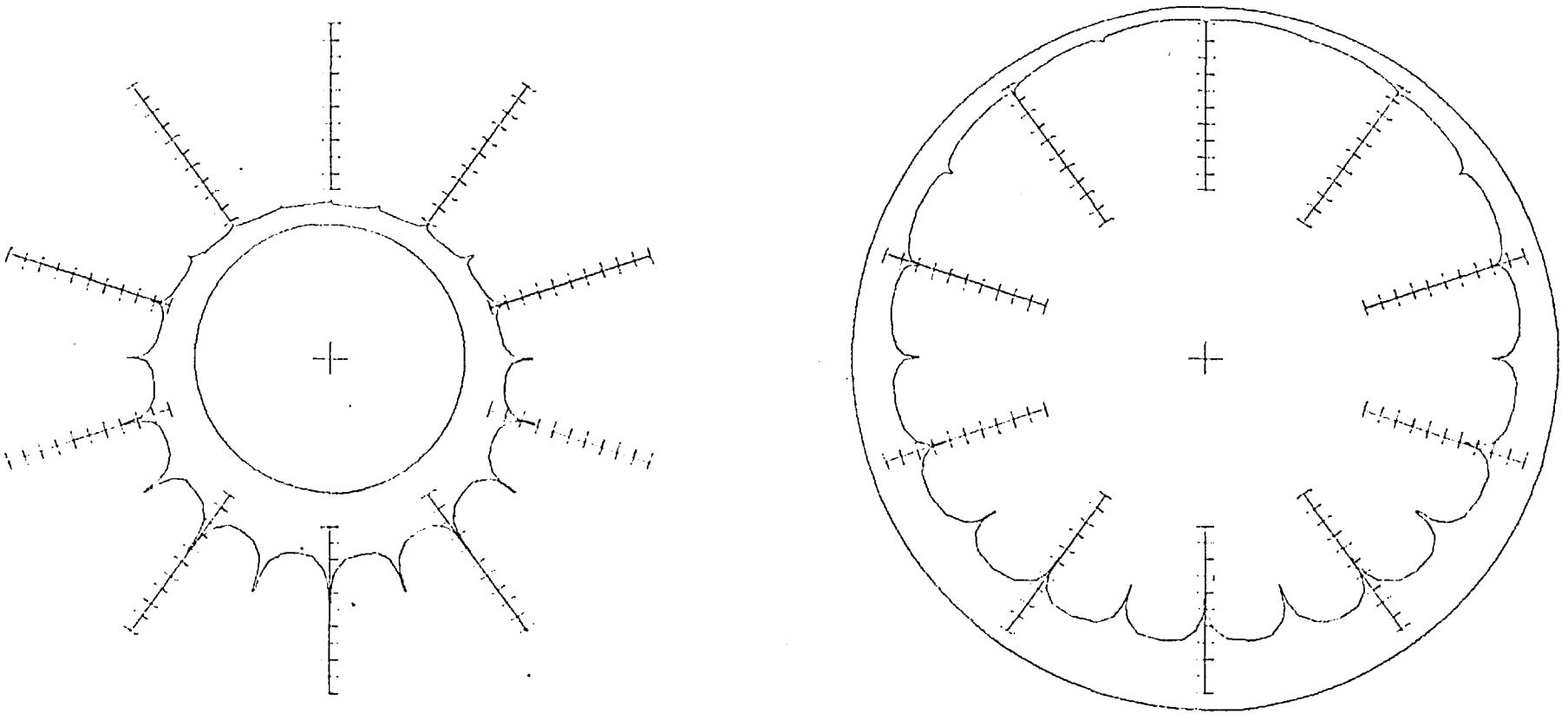


Fig. 7.98

Fig. 7.99 Deflected shapes of the races of a steel radial roller bearing having hollow shaft (no.4, inner to outer diameter ratio 0.651) and housing with boss (outer to inner diameter ratio 1.145). Radial clearance c= -300 μin. and radial load F_r= 5000 lbs.

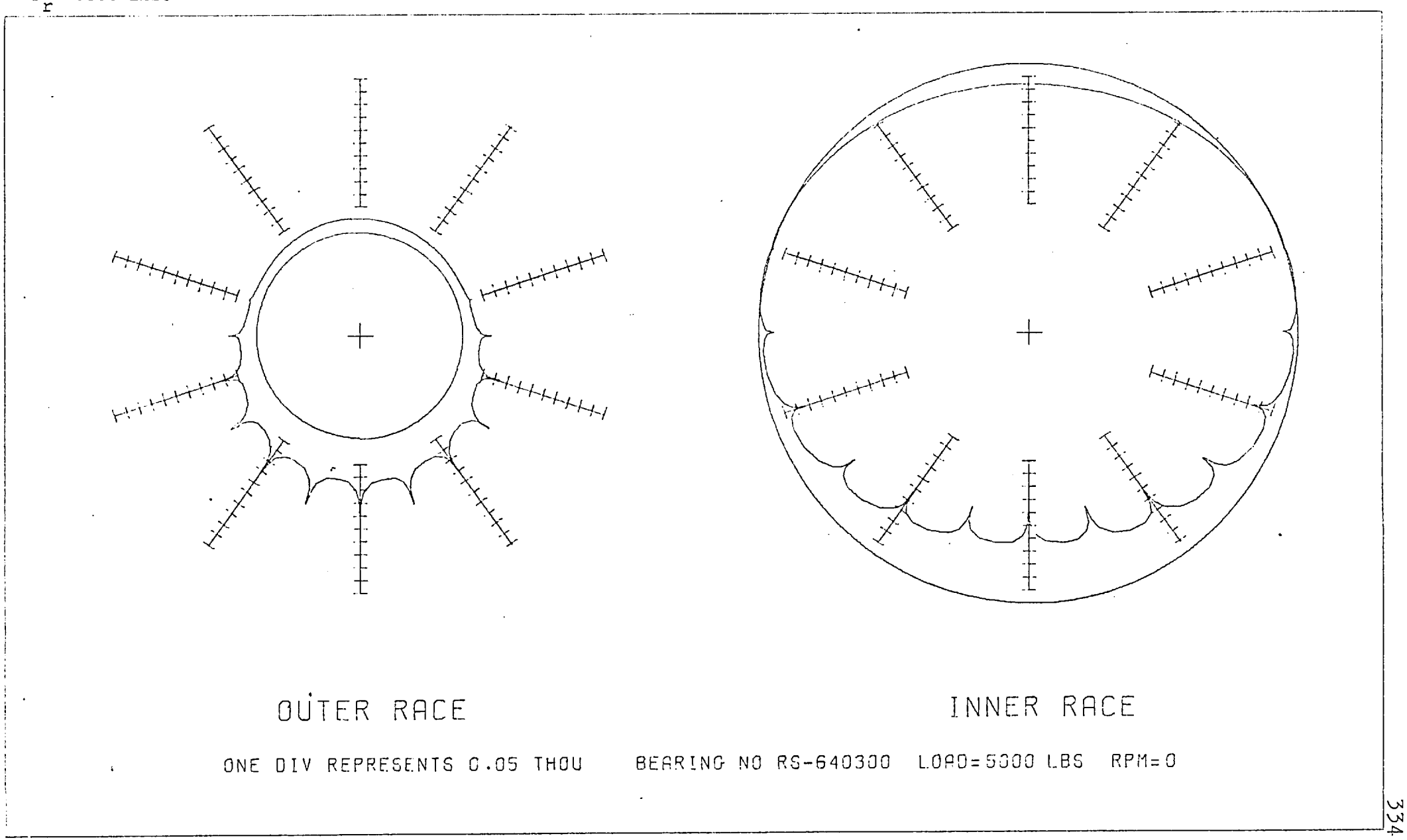


Fig. 7.99

Fig. 7.100 Deflected shapes of the races of a steel radial roller bearing having hollow shaft (no.4, inner to outer diameter ratio 0.651) and housing with boss (outer to inner diameter ratio 1.385). Radial clearance c= -300 μin. and radial load F_r= 5000 lbs.

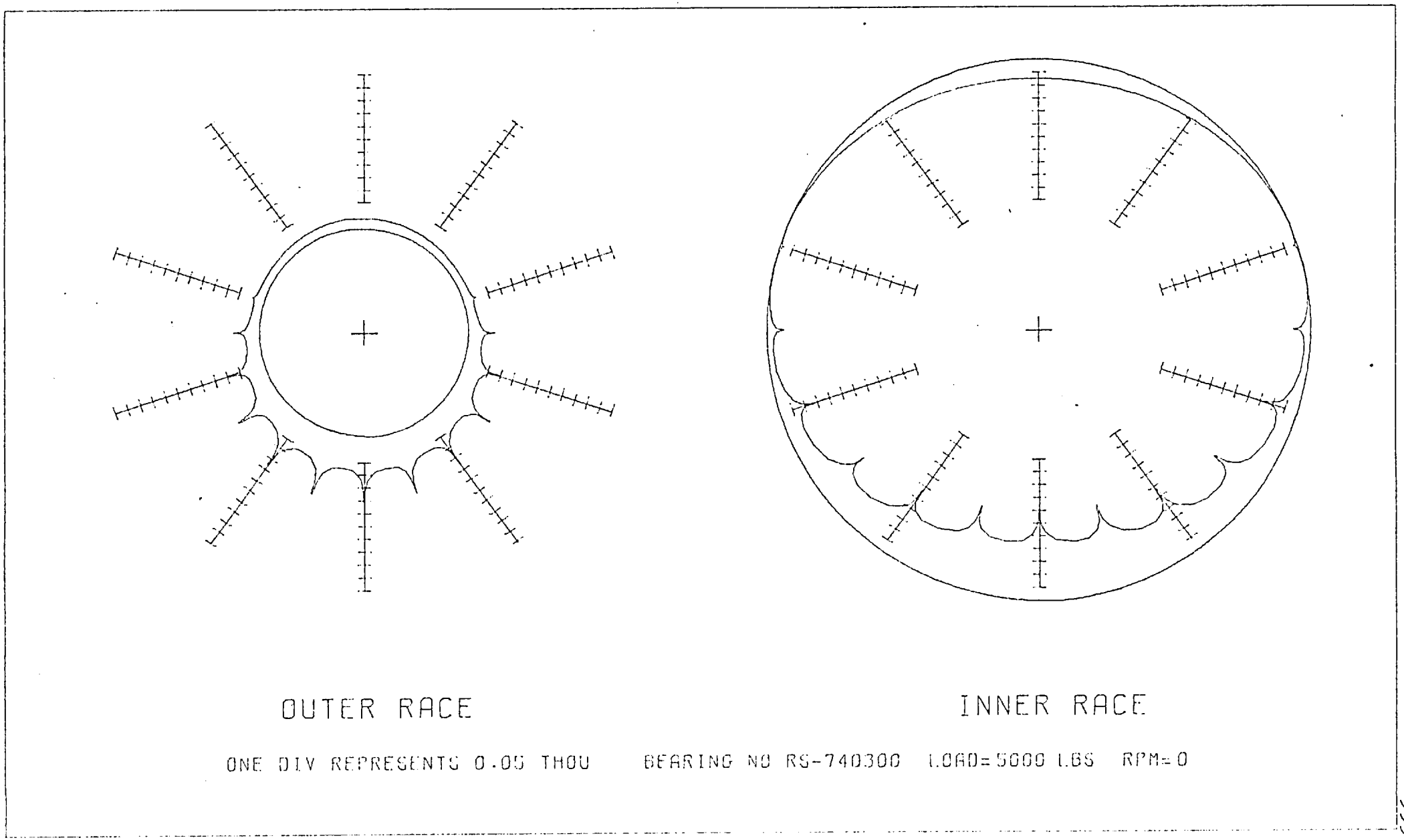


Fig. 7.100

Fig. 7.101 Deflected shapes of the races of a steel radial roller bearing having solid shaft and housing with boss (outer to inner diameter ratio 1.847). Radial clearance c= -300 μin. and radial load F_r = 5000 lbs.

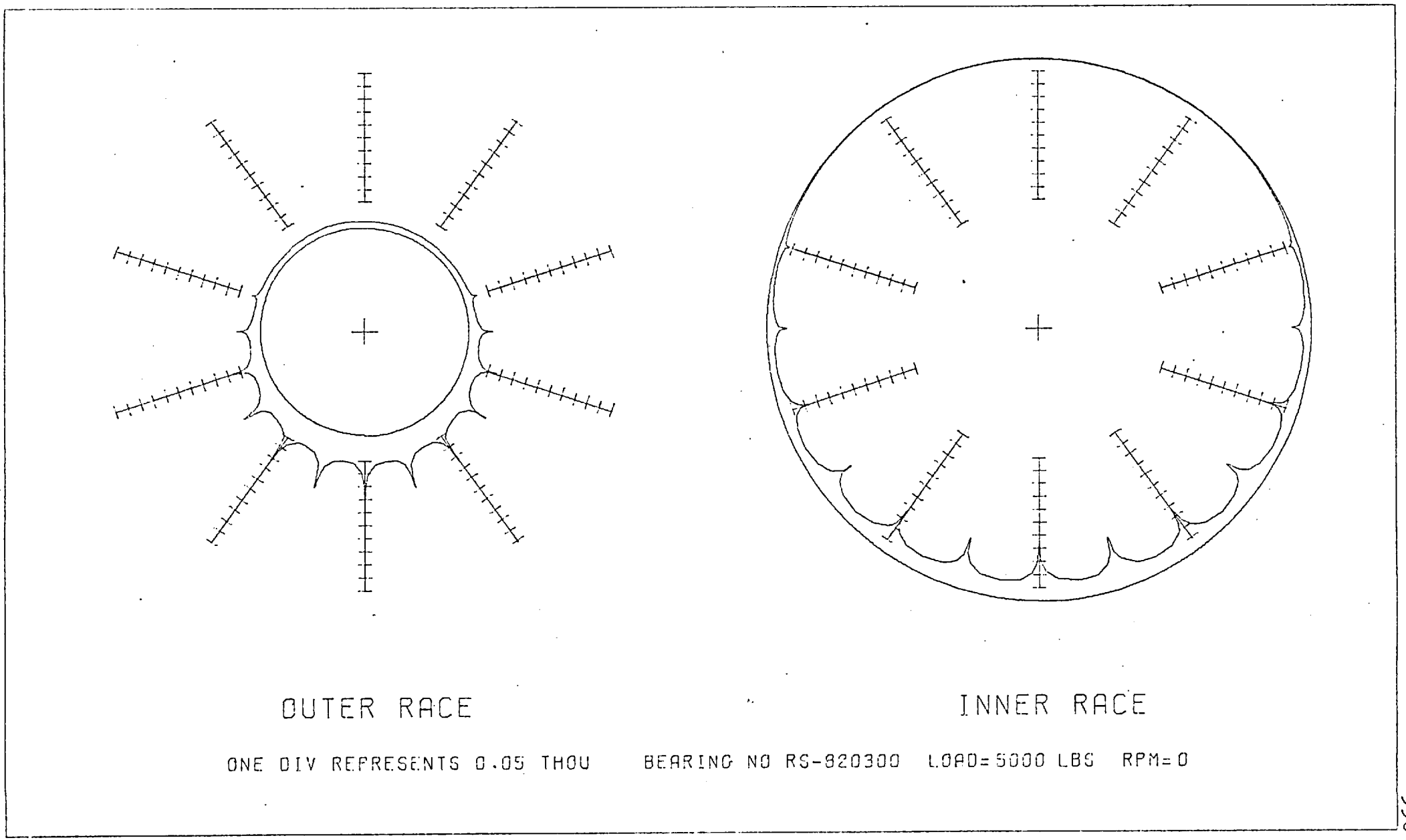


Fig. 7.101

Fig. 7.102 Deflected shapes of the races of a steel radial roller bearing having hollow shaft (no.4, inner to outer diameter ratio 0.651) and housing with boss (outer to inner diameter ratio 1.847). Radial clearance c= -600 μin. and radial load F_r= 5000 lbs.

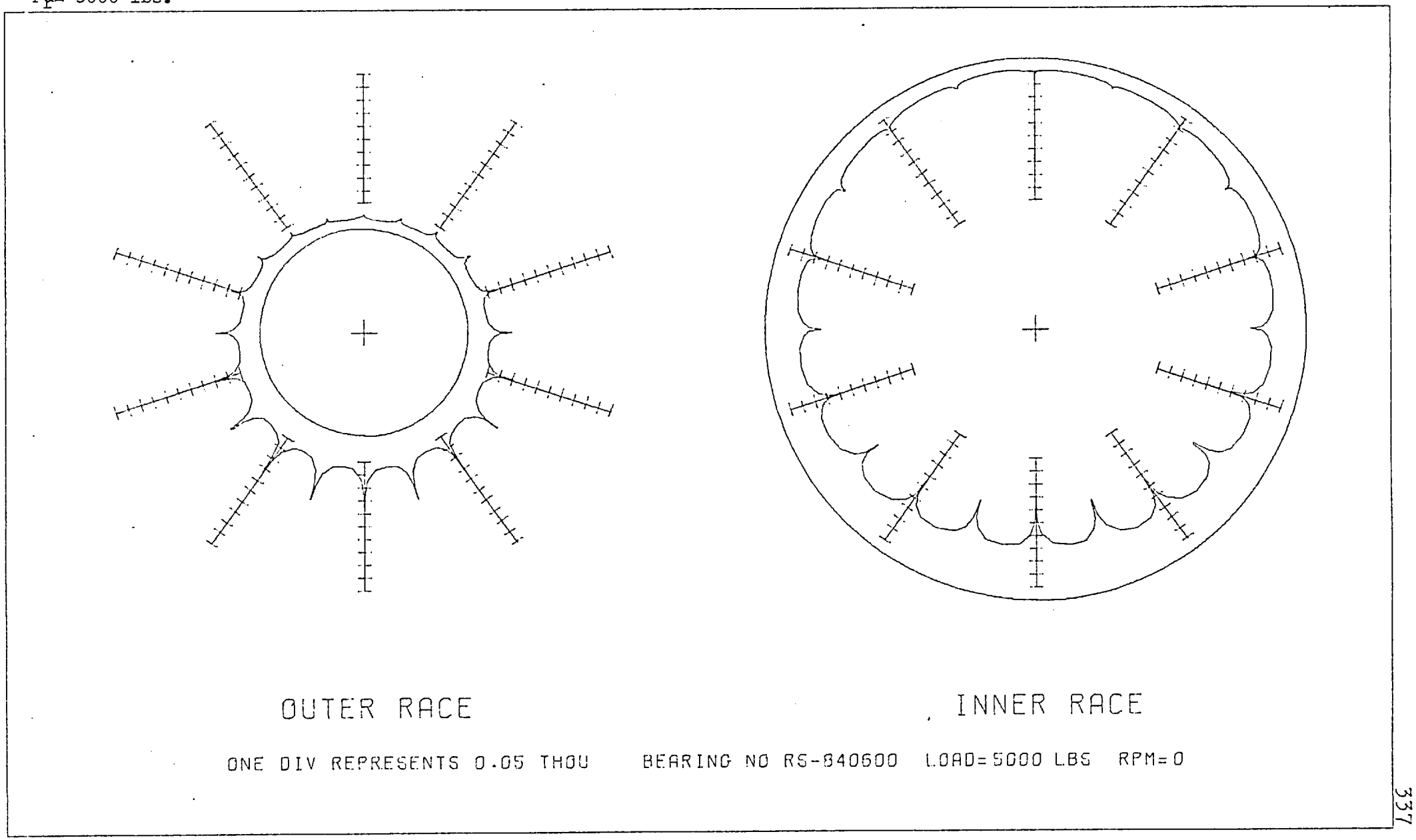


Fig. 7.102

Fig. 7.103 Deflected shapes of the races of a steel radial roller bearing having hollow shaft (no.4, inner to outer diameter ratio 0.651) and housing with boss (outer to inner diameter ratio 1.847). Radial clearance c= -300 μin. and radial load F_r= 5000 lbs.

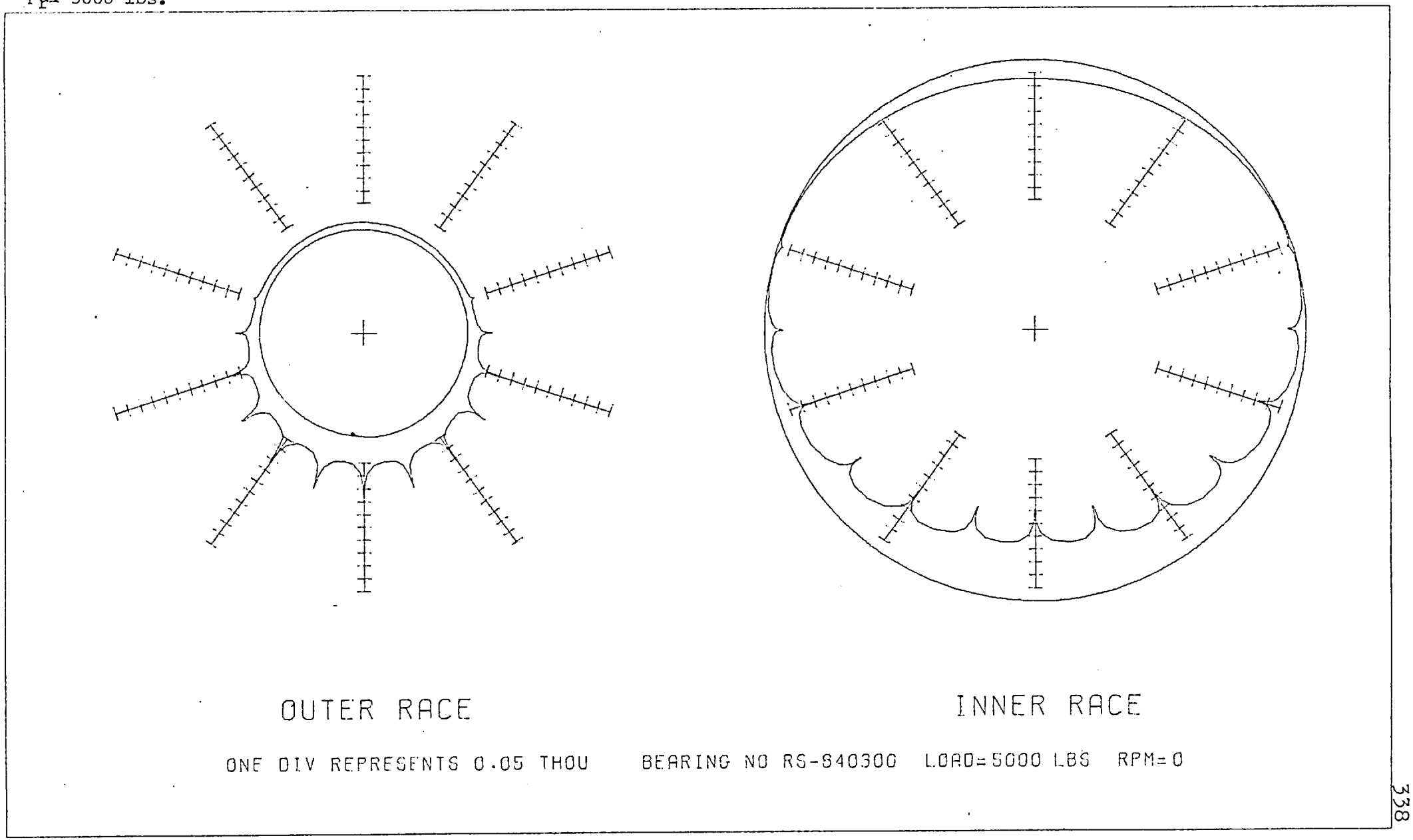


Fig. 7.103

Fig. 7.104 Deflected shapes of the races of a steel radial roller bearing having hollow shaft (no.4, inner to outer diameter ratio 0.651) and housing with upright cruciform ribs (boss outer to inner diameter ratio 1.145). Radial clearance c= -300 μin.

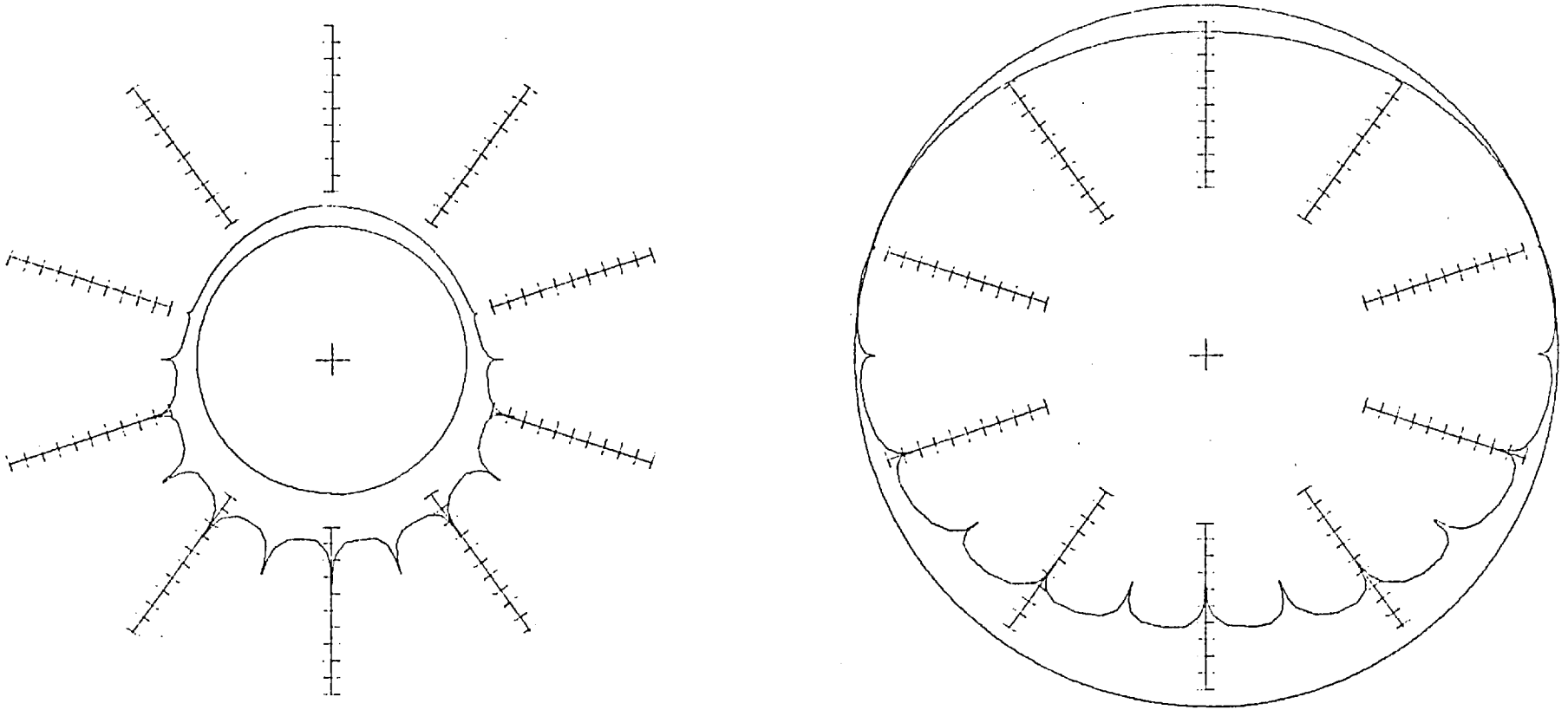


Fig. 7.104

Fig. 7.105 Deflected shapes of the races of a steel radial roller bearing having hollow shaft (no.4, inner to outer diameter ratio 0.651) and housing with diagonal cruciform ribs (boss outer to inner diameter ratio 1.145). Radial clearance c= -300 μin. and radial load F_r= 5000 lbs.

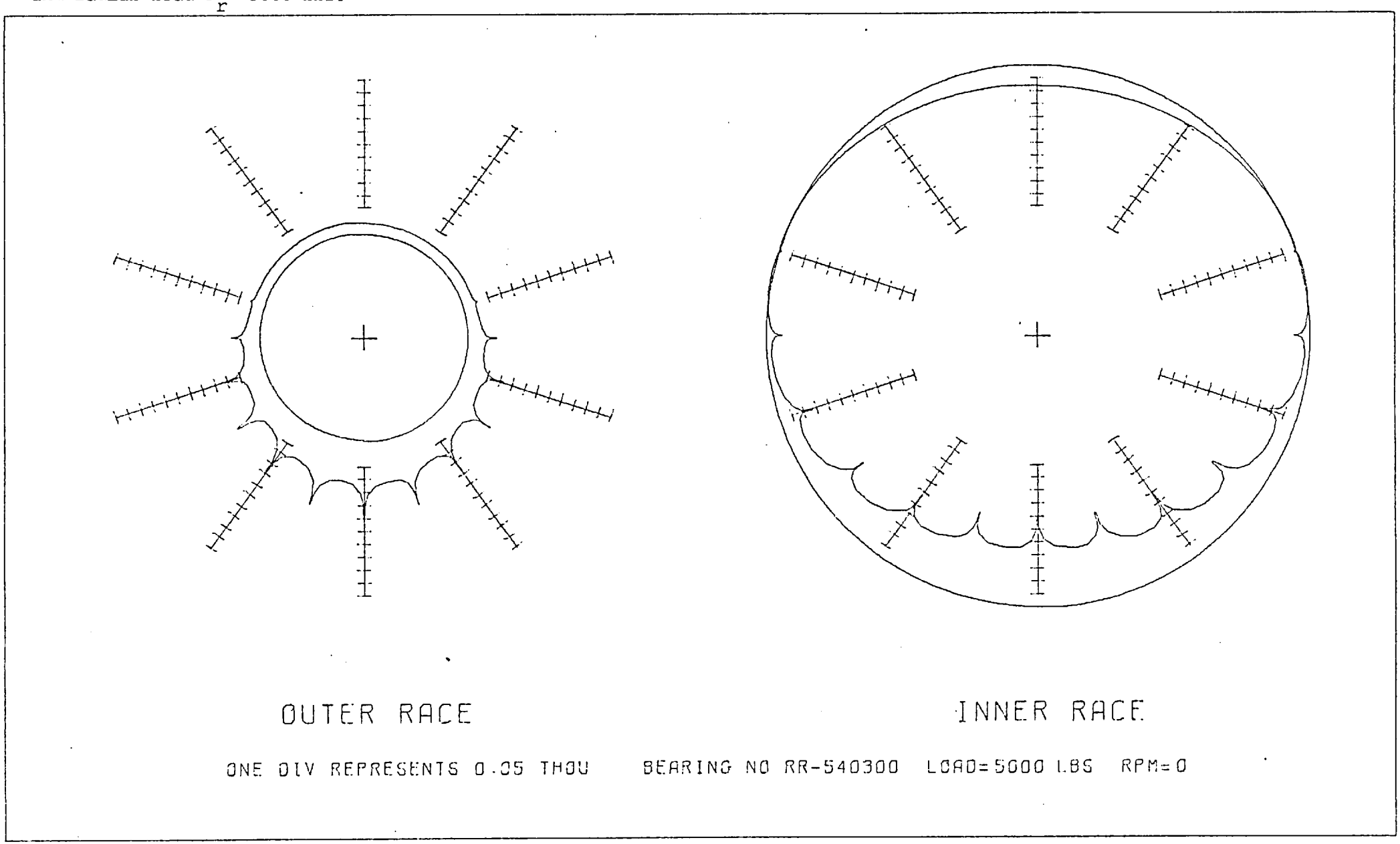


Fig. 7.105

Fig. 7.106 Deflected shapes of the races of a steel radial roller bearing having solid shaft and circular housing (outer to inner diameter ratio 1.145) with upright cruciform support. Radial clearance c= -300 μin. and radial load F_r= 5000 lbs.

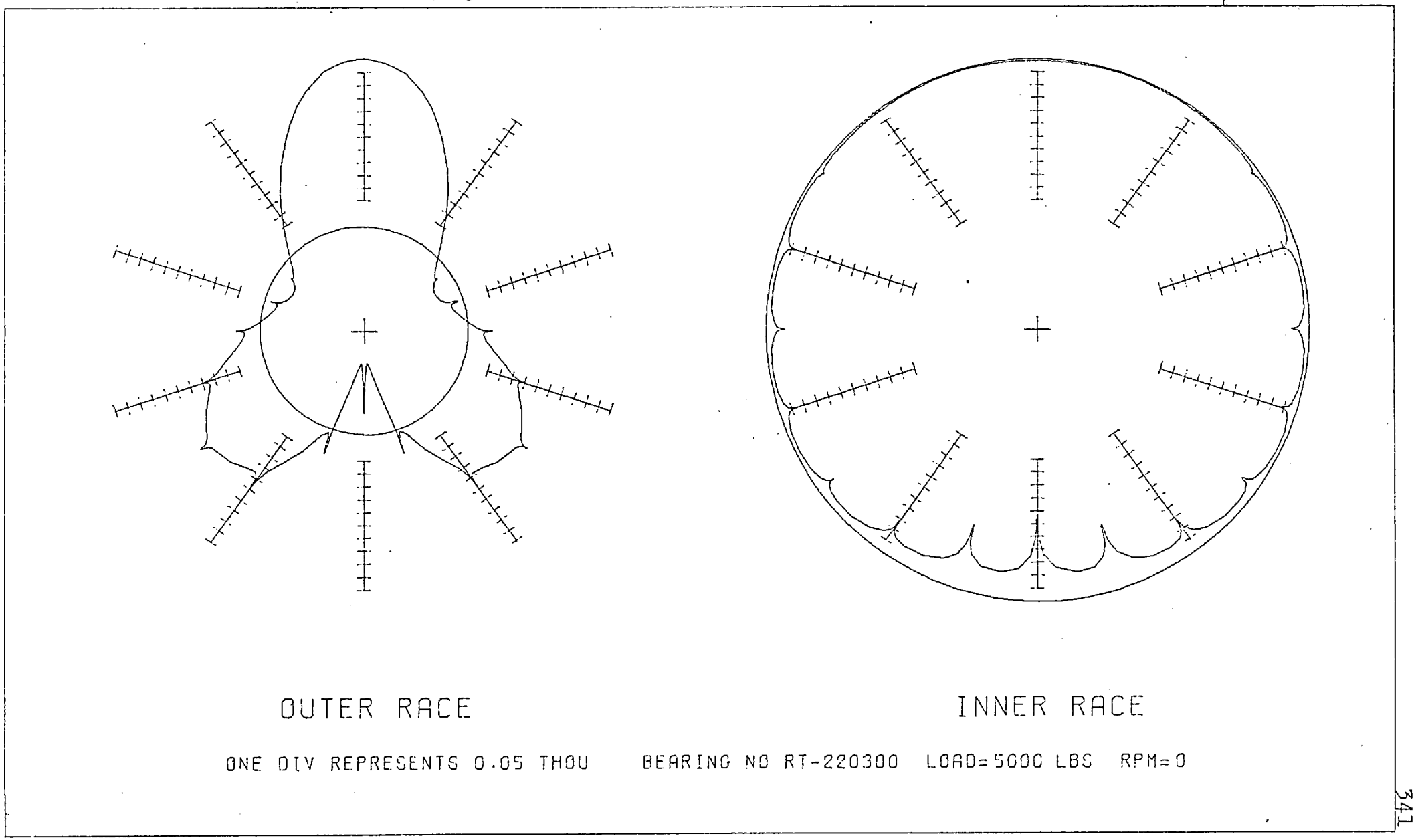


Fig. 7.106

Fig. 7.107 Deflected shapes of the races of a steel radial roller bearing having hollow shaft (no.4, inner to outer diameter ratio 0.651) and circular housing (outer to inner diameter ratio 1.145) with upright cruciform support. Radial clearance c= -600 μin. and radial load F_r= 5000 lbs.

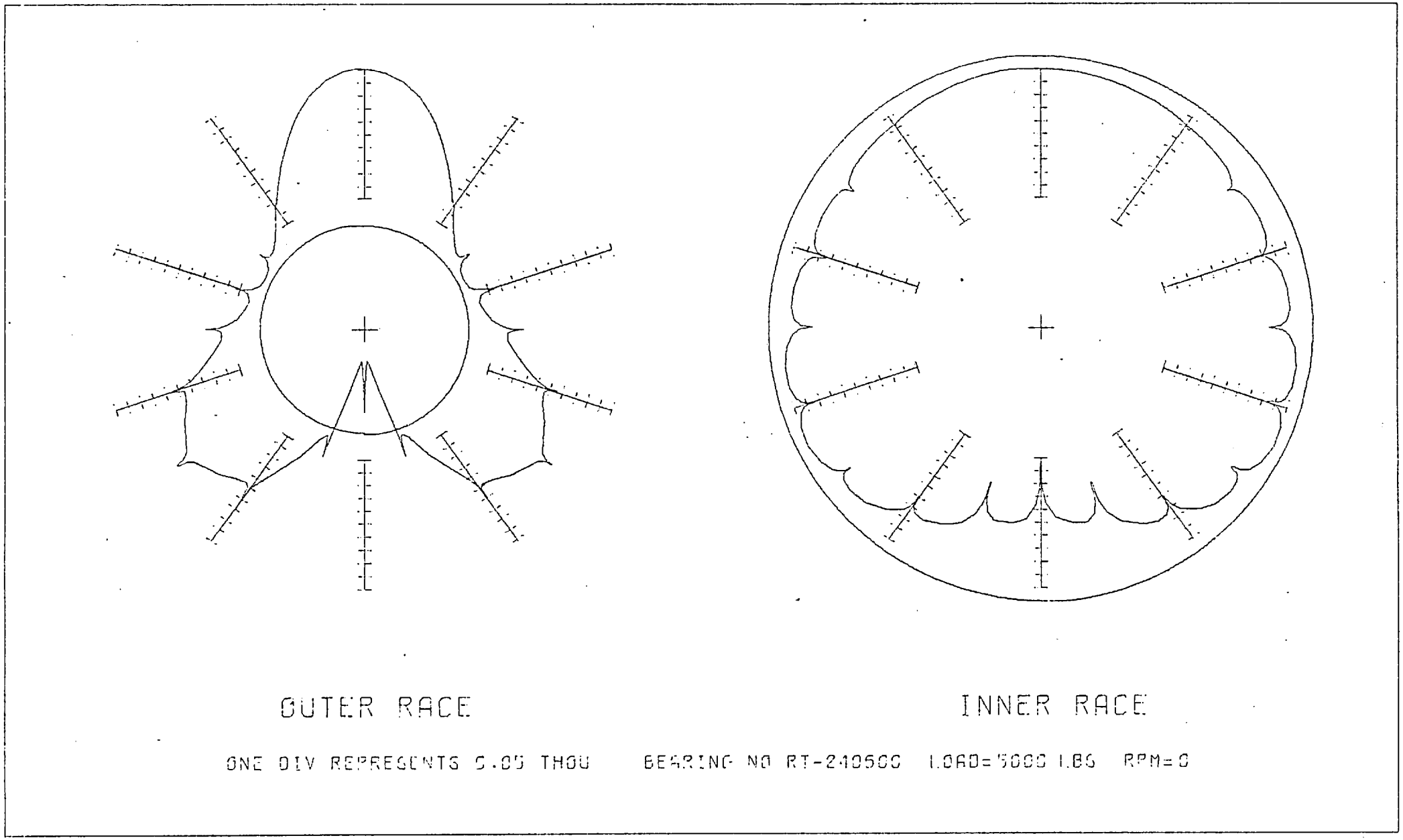


Fig. 7.107

Fig. 7.108 Deflected shapes of the races of a steel radial roller bearing having hollow shaft (no.4, inner to outer diameter ratio 0.651) and circular housing (outer to inner diameter ratio 1.145) with upright cruciform support. Radial clearance c= -300 μin. and radial load F_r= 5000 lbs.

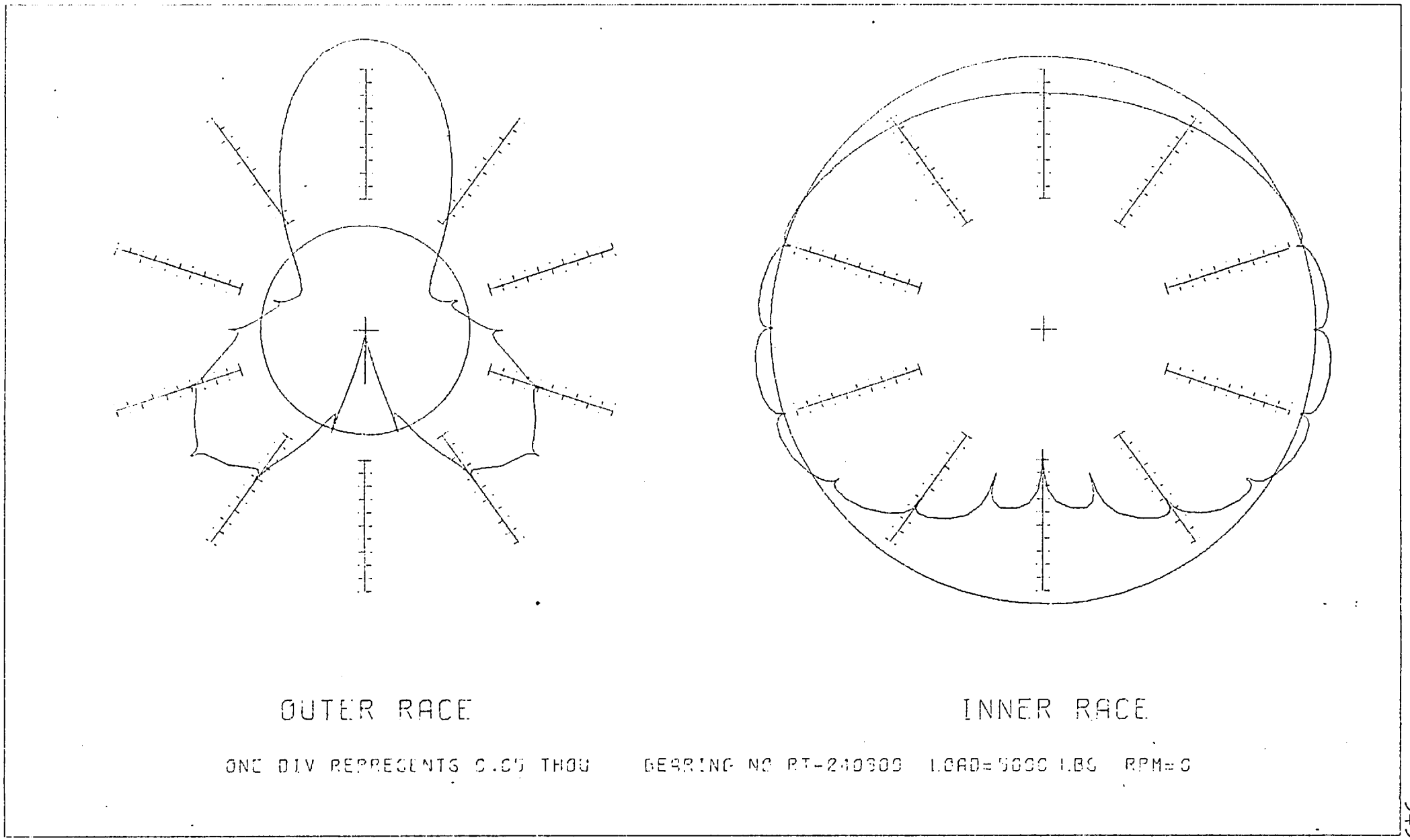


Fig. 7.108

Fig. 7.109 Deflected shapes of the races of a steel radial roller bearing having hollow shaft (no.4, inner to outer diameter ratio 0.651) and circular housing (outer to inner diameter ratio 1.145) with upright cruciform support. Radial clearance c= 0.0 and radial load F_r= 5000 lbs.

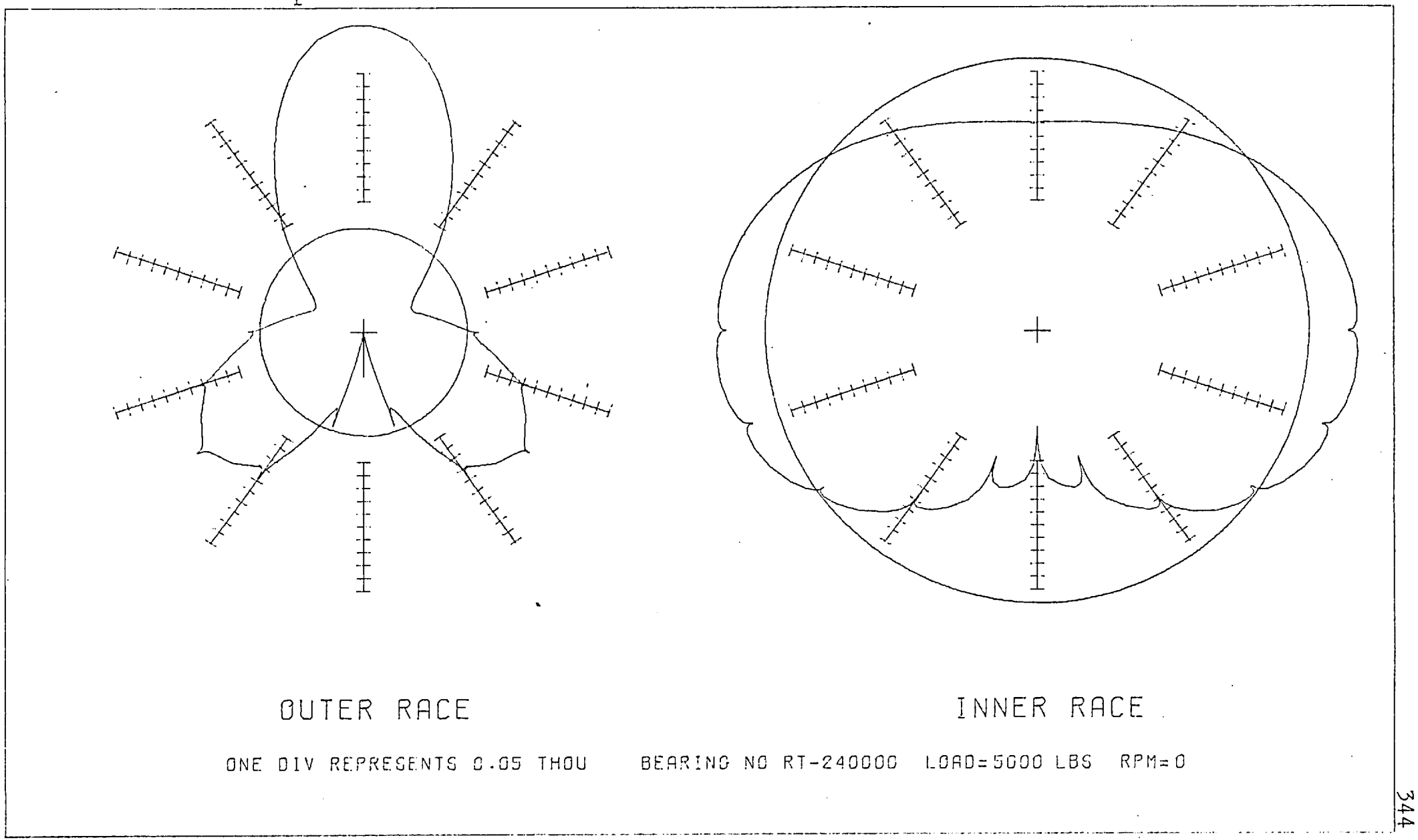


Fig. 7.109

Fig. 7.110 Deflected shapes of the races of a steel radial roller bearing having hollow shaft (no.4, inner to outer diameter ratio 0.651) and circular housing (outer to inner diameter ratio 1.145) with upright cruciform support. Radial clearance c= +600 μin. and radial load F_r= 5000 lbs.

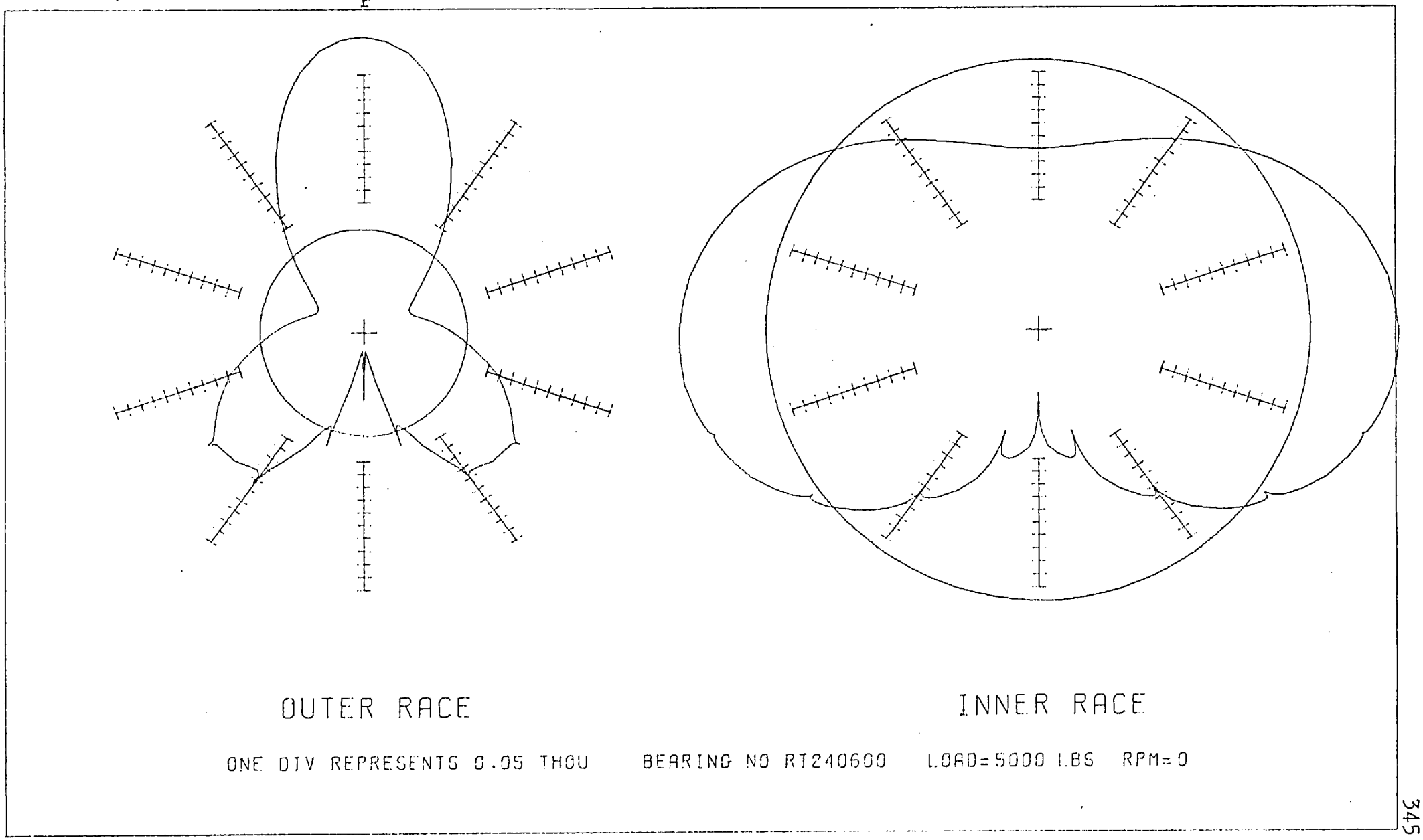


Fig. 7.110

Fig. 7.111 Deflected shapes of the races of a steel radial roller bearing having hollow shaft (no.4, inner to outer diameter ratio 0.651) and circular housing (outer to inner diameter ratio 1.385) with upright cruciform support. Radial clearance c= -300 μin. and radial load F_r= 5000 lbs.

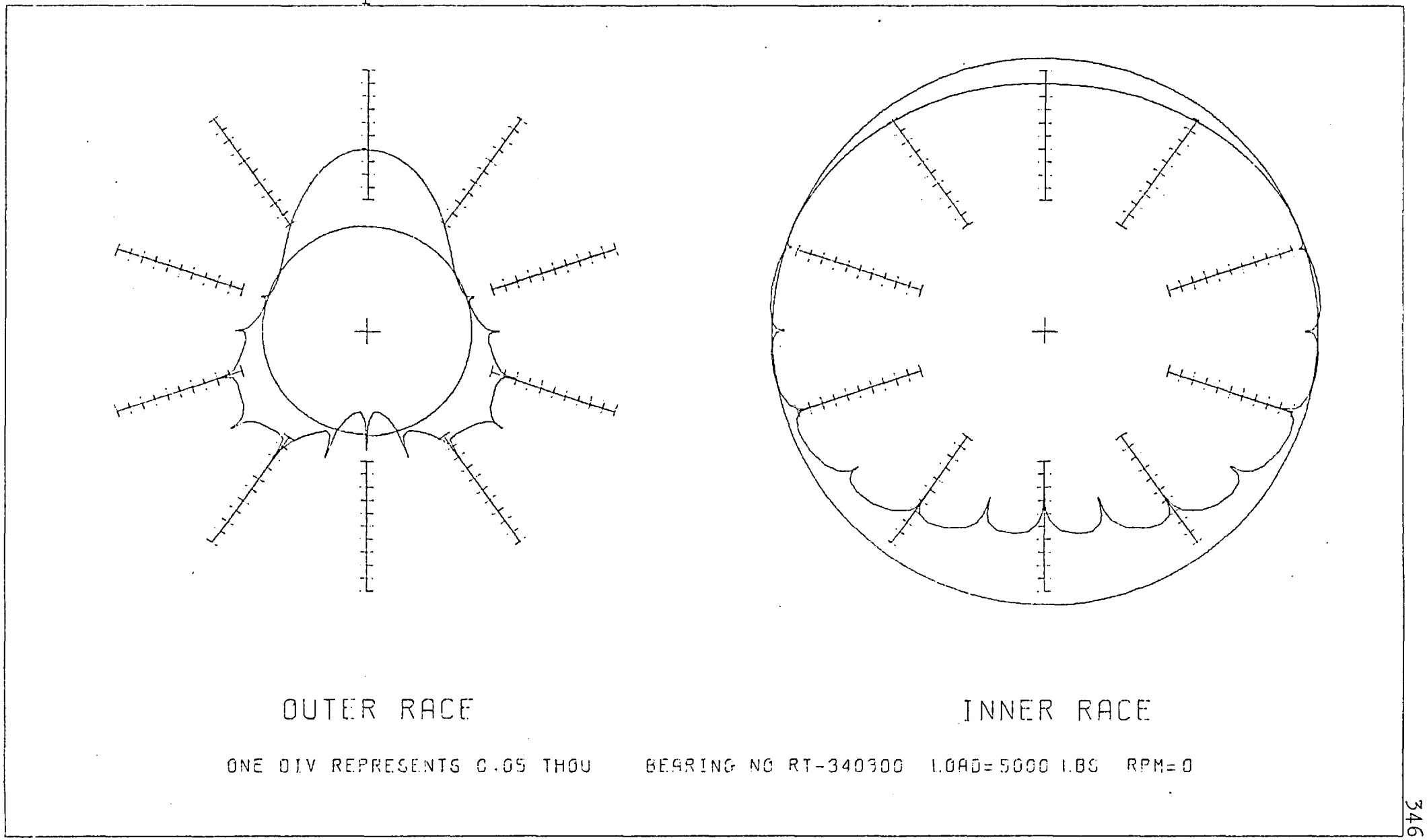


Fig. 7.111

Fig. 7.112 Deflected shapes of the races of a steel radial roller bearing having hollow shaft (no.4, inner to outer diameter ratio 0.651) and circular housing (outer to inner diameter ratio 1.847) with upright cruciform support. Radial clearance c= -300 μin. and radial load F_r= 5000 lbs.

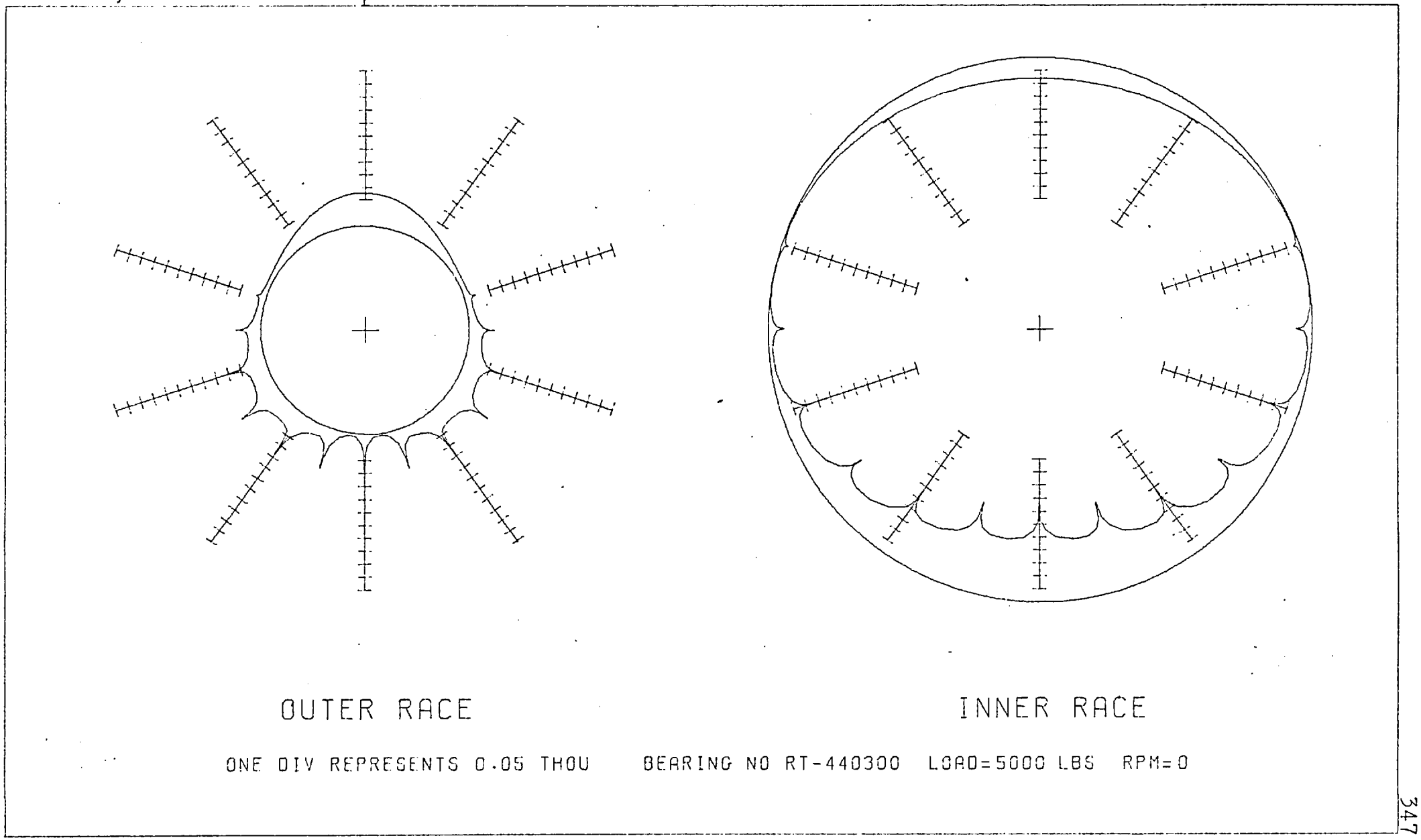


Fig. 7.112

Fig. 7.113 Deflected shapes of the races of a steel radial roller bearing having hollow shaft (no.4, inner to outer diameter ratio 0.651) and circular housing (outer to inner diameter ratio 1.145) with diagonal cruciform support. Radial clearance c= -600 μin. and radial load F_r= 5000 lbs.

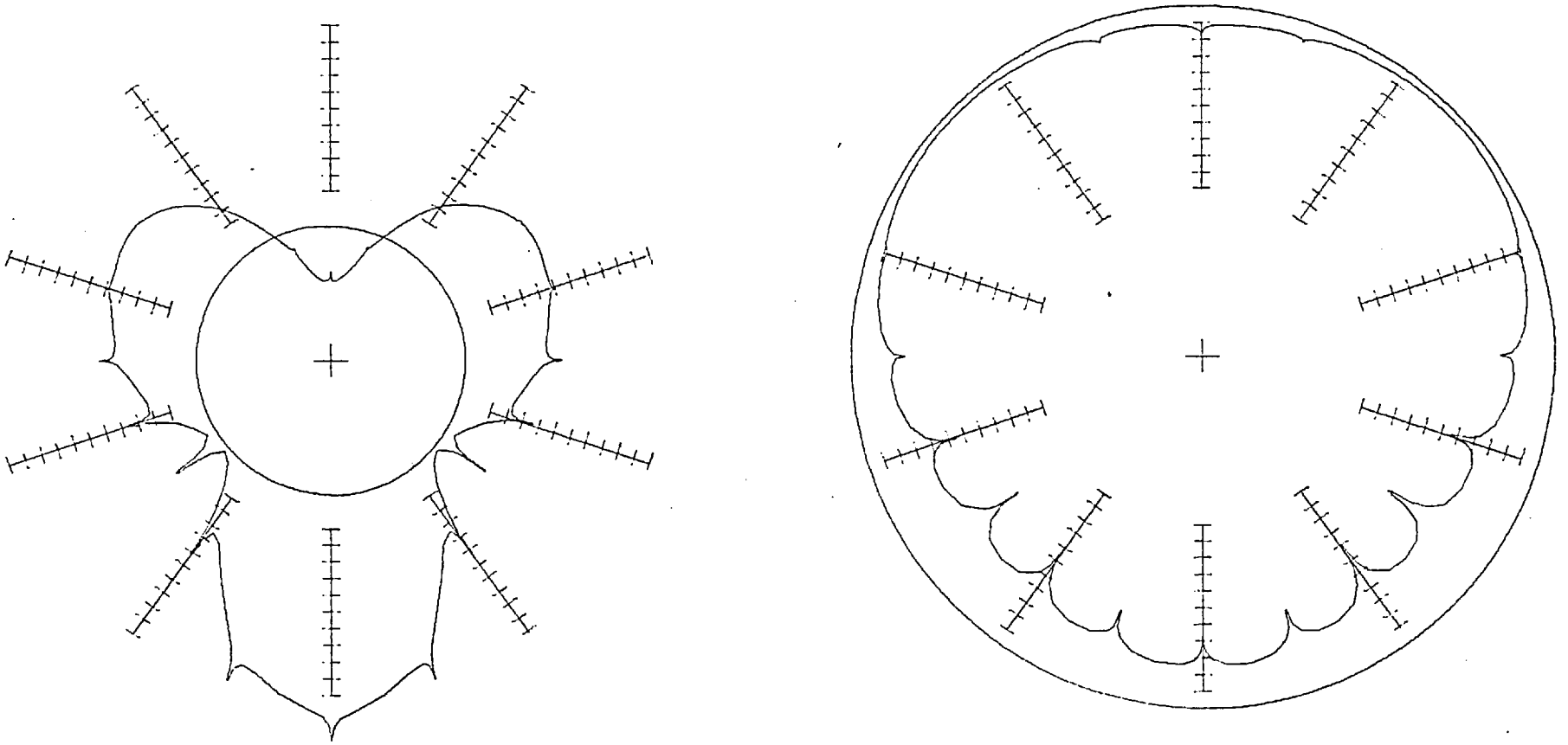


Fig. 7.113

Fig. 7.114 Deflected shapes of the races of a steel radial roller bearing having hollow shaft (no.4, inner to outer diameter ratio 0.651) and circular housing (outer to inner diameter ratio 1.145) with diagonal cruciform support. Radial clearance c= -300 μin. and radial load F_r= 5000 lbs.

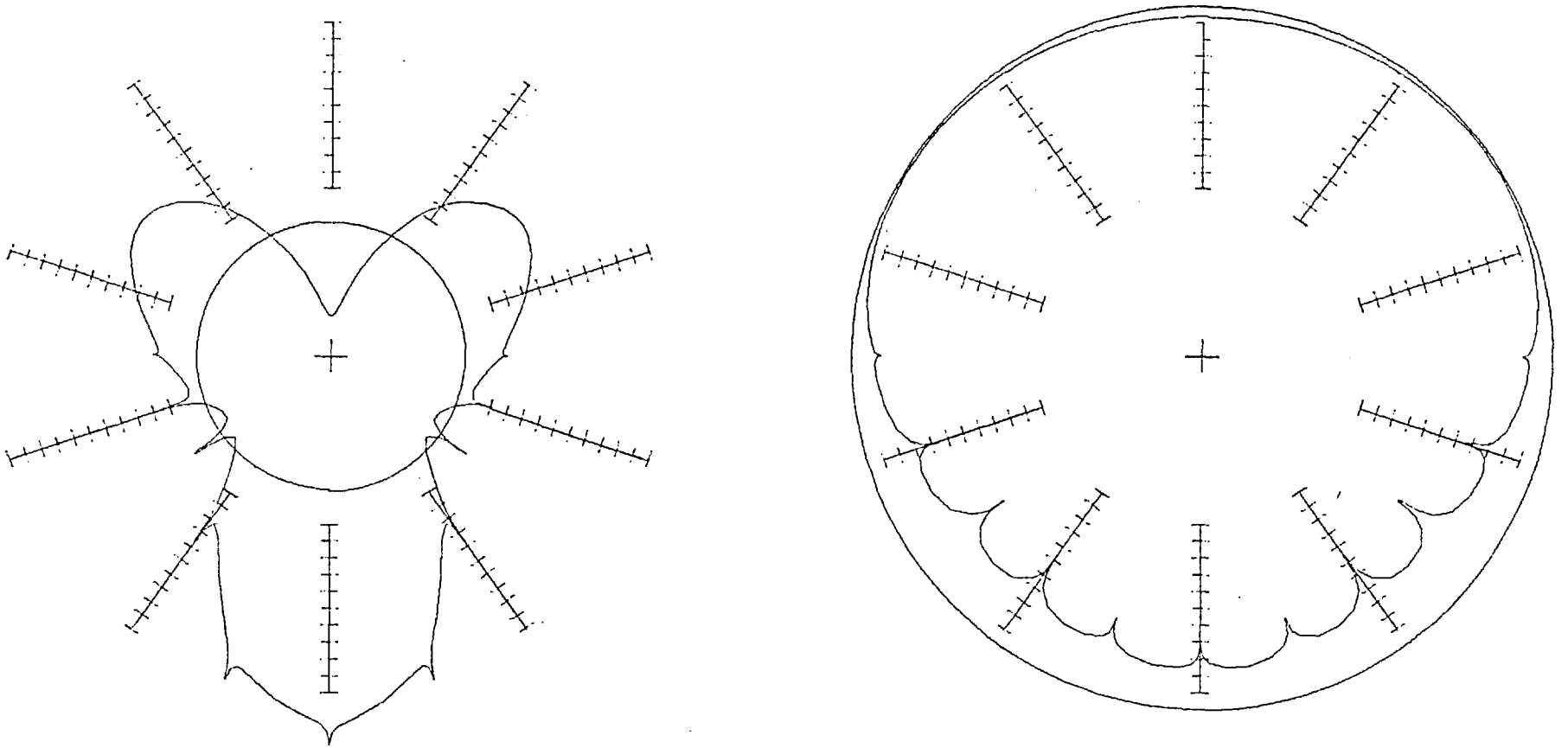


Fig. 7.114

Fig. 7.115 Deflected shapes of the races of a steel radial roller bearing having hollow shaft (no.4, inner to outer diameter ratio 0.651) and circular housing (outer to inner diameter ratio 1.145) with diagonal cruciform support. Radial clearance c= 0.0 and radial load F_r= 5000 lbs.

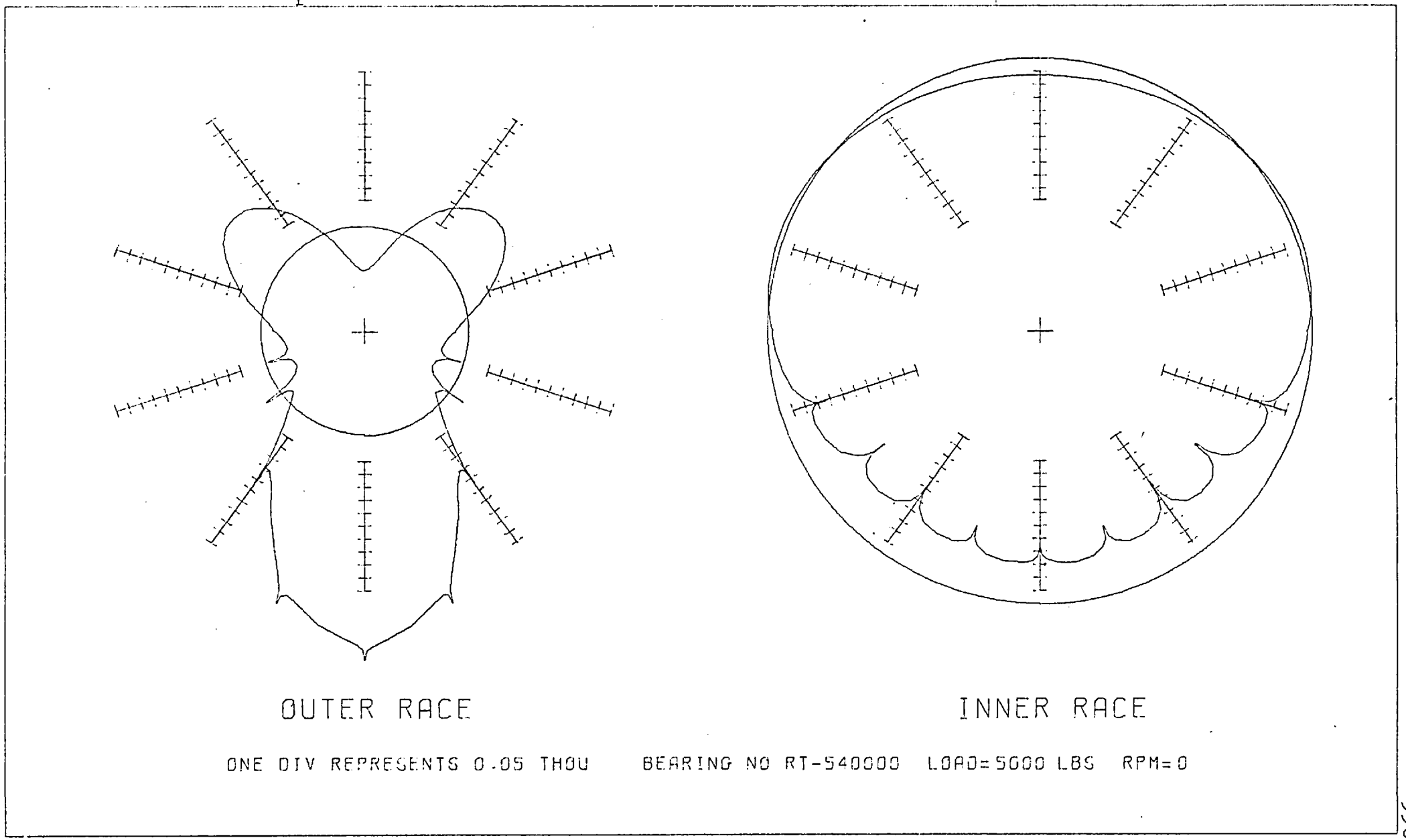


Fig. 7.115

Fig. 7.116 Deflected shapes of the races of a steel radial roller bearing having hollow shaft (no.4, inner to outer diameter ratio 0.651) and circular housing (outer to inner diameter ratio 1.145) with diagonal cruciform support. Radial clearance c= +600 μin. and radial load F_r= 5000 lbs.

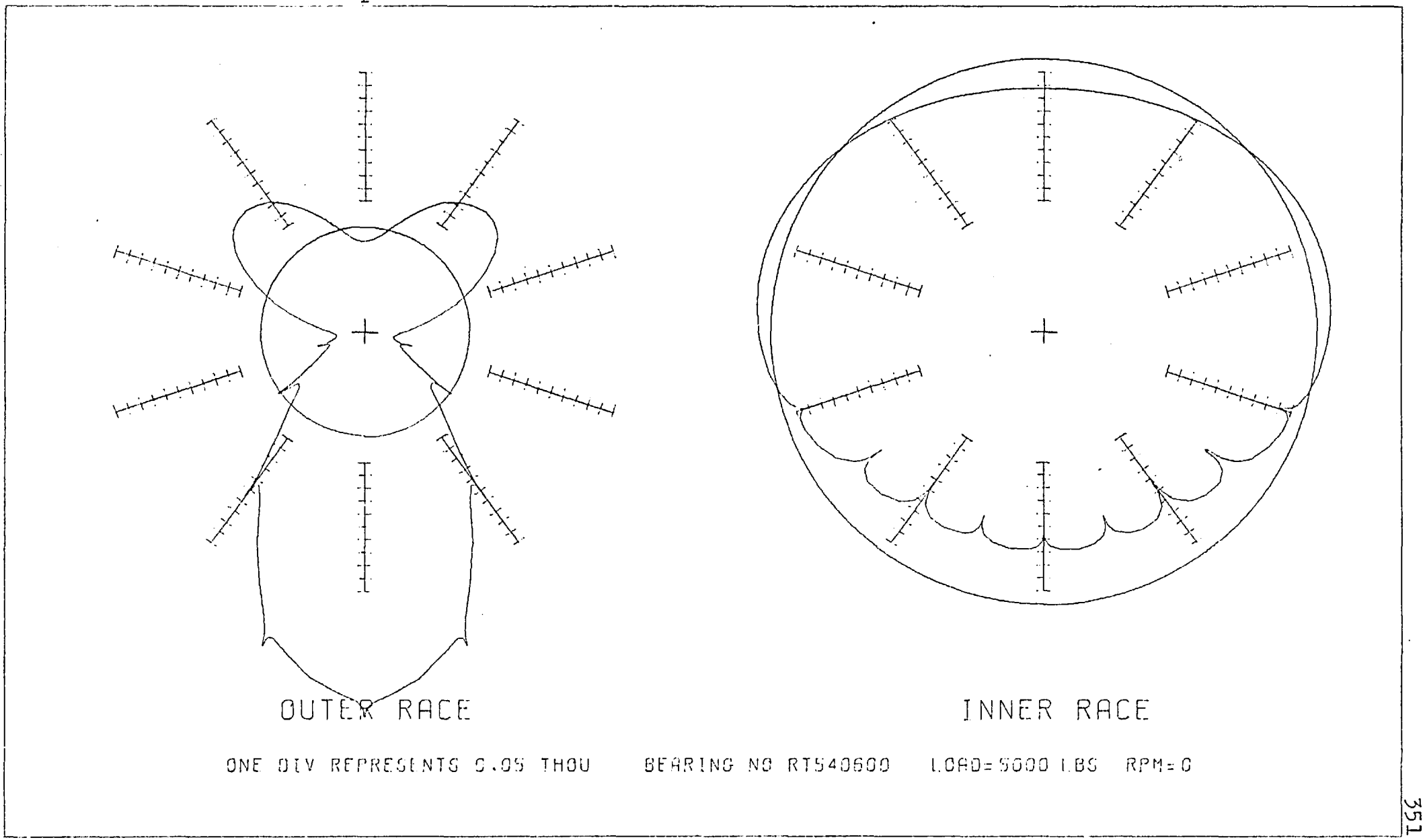


Fig. 7.116

Fig. 7.117 Deflected shapes of the races of a steel radial roller bearing having hollow shaft (no.4, inner to outer diameter ratio 0.651) and circular housing (outer to inner diameter ratio 1.145) with diagonal cruciform support. Radial clearance c= -300 μin. and radial load F_r= 5000 lbs. Shaft speed is 30,000 R.P.M.

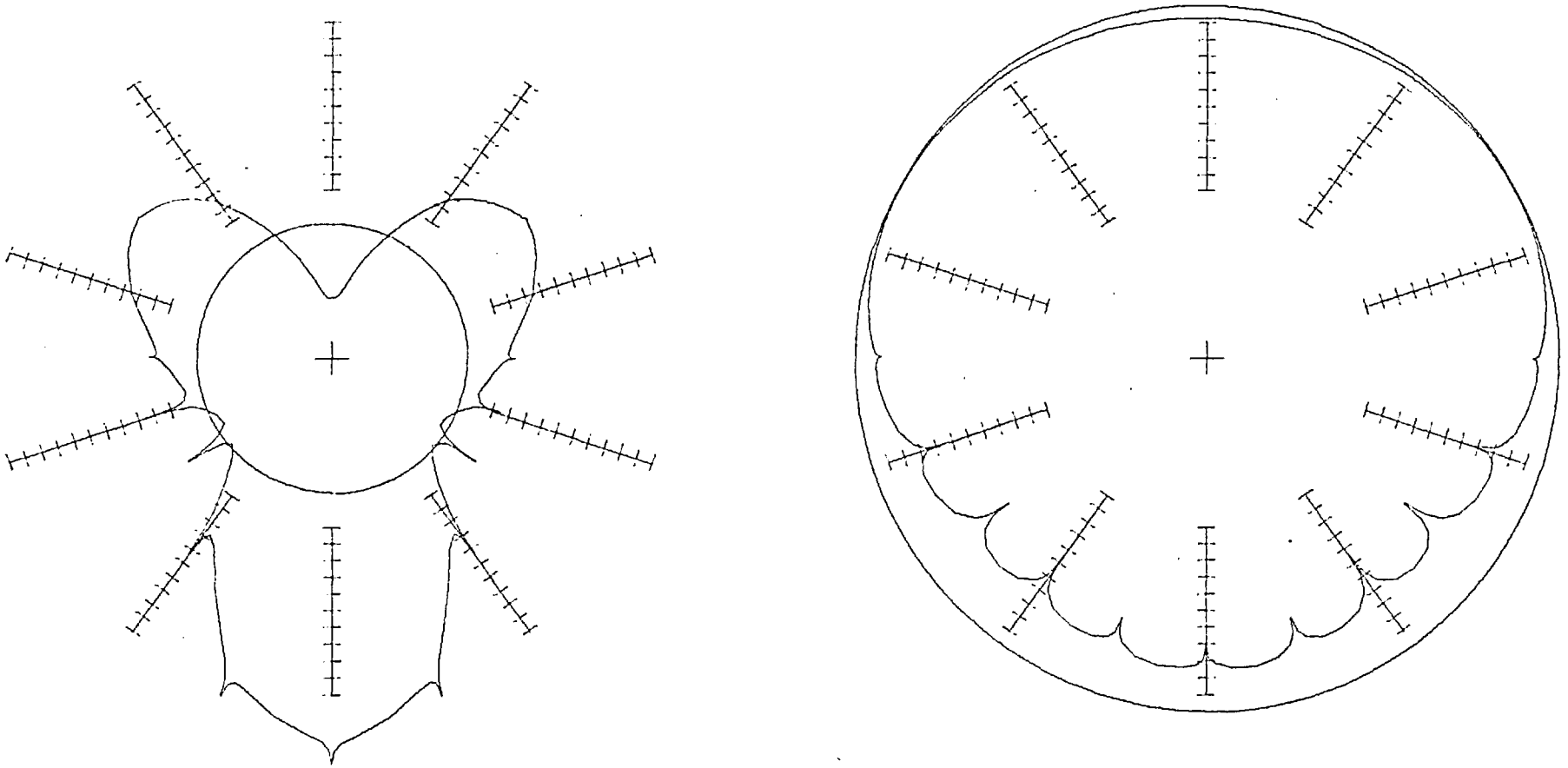


Fig. 7.117

Fig. 7.118 Deflected shapes of the races of a steel radial roller bearing having hollow shaft (no.4, inner to outer diameter ratio 0.651) and circular housing (outer to inner diameter ratio 1.385) with diagonal cruciform support. Radial clearance c= -300 μin. and radial load F_r = 5000 lbs.

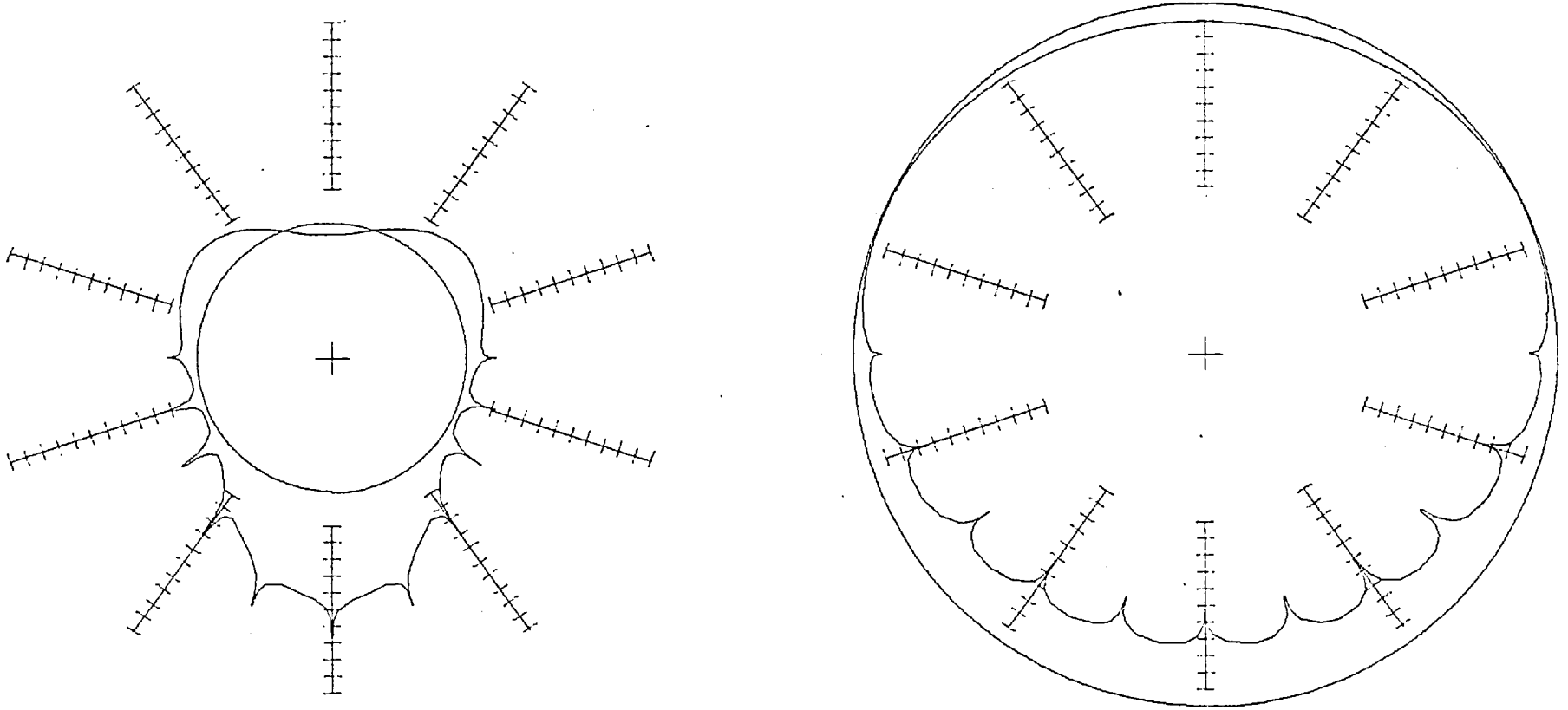


Fig. 7.118

Fig. 7.119 Deflected shapes of the races of a steel radial roller bearing having hollow shaft (no.4, inner to outer diameter ratio 0.651) and circular housing (outer to inner diameter ratio 1.847) with diagonal cruciform support. Radial clearance c= -300 μin. and radial load F_r= 5000 lbs.

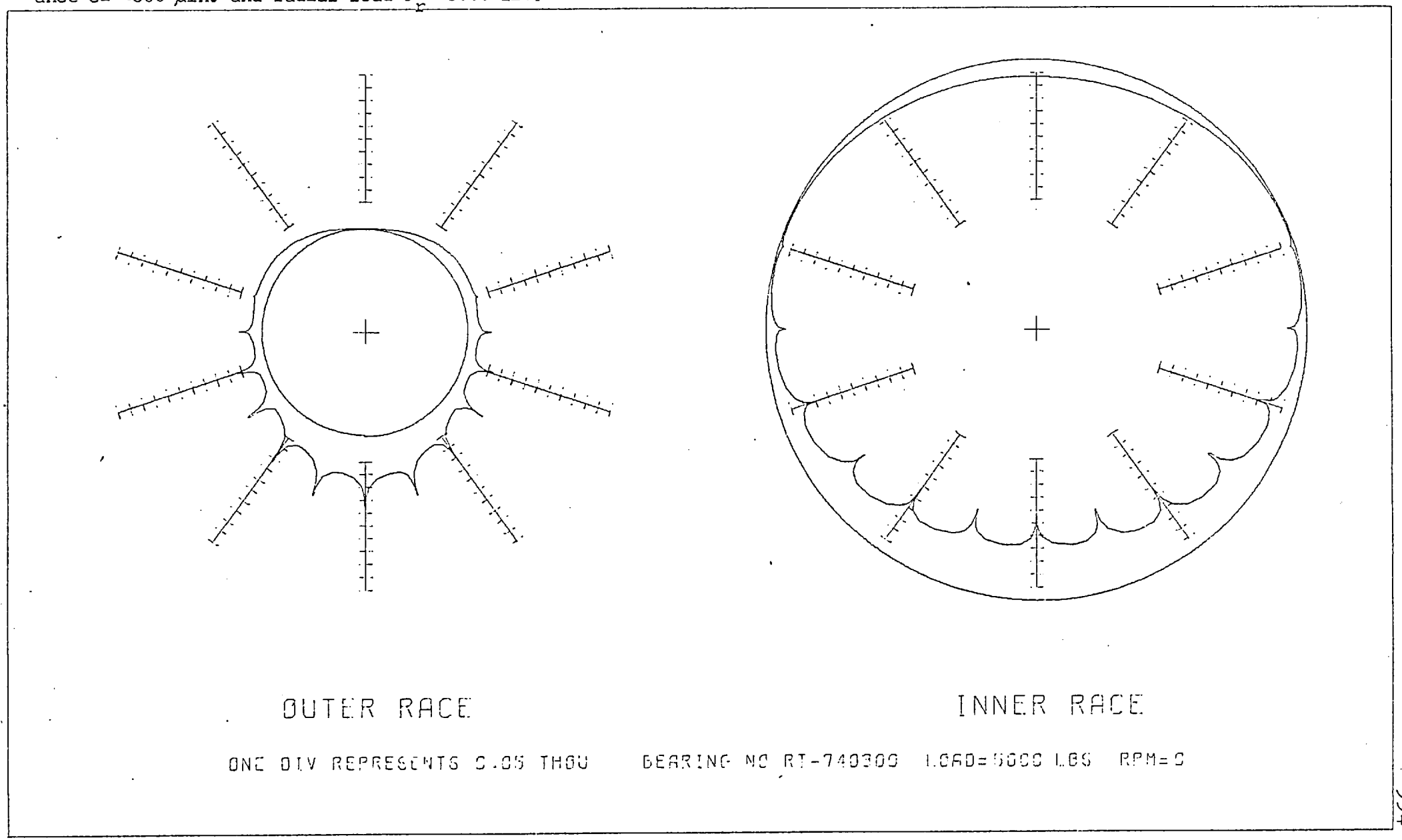


Fig. 7.119

Fig. 7.120 Deflected shapes of the races of a steel radial roller bearing having hollow shaft (no.4, inner to outer diameter ratio 0.651) and circular housing (outer to inner diameter ratio 1.145) with upright part-cruciform support. Radial clearance c= -300 μin. and radial load F_r= 5000 lbs.

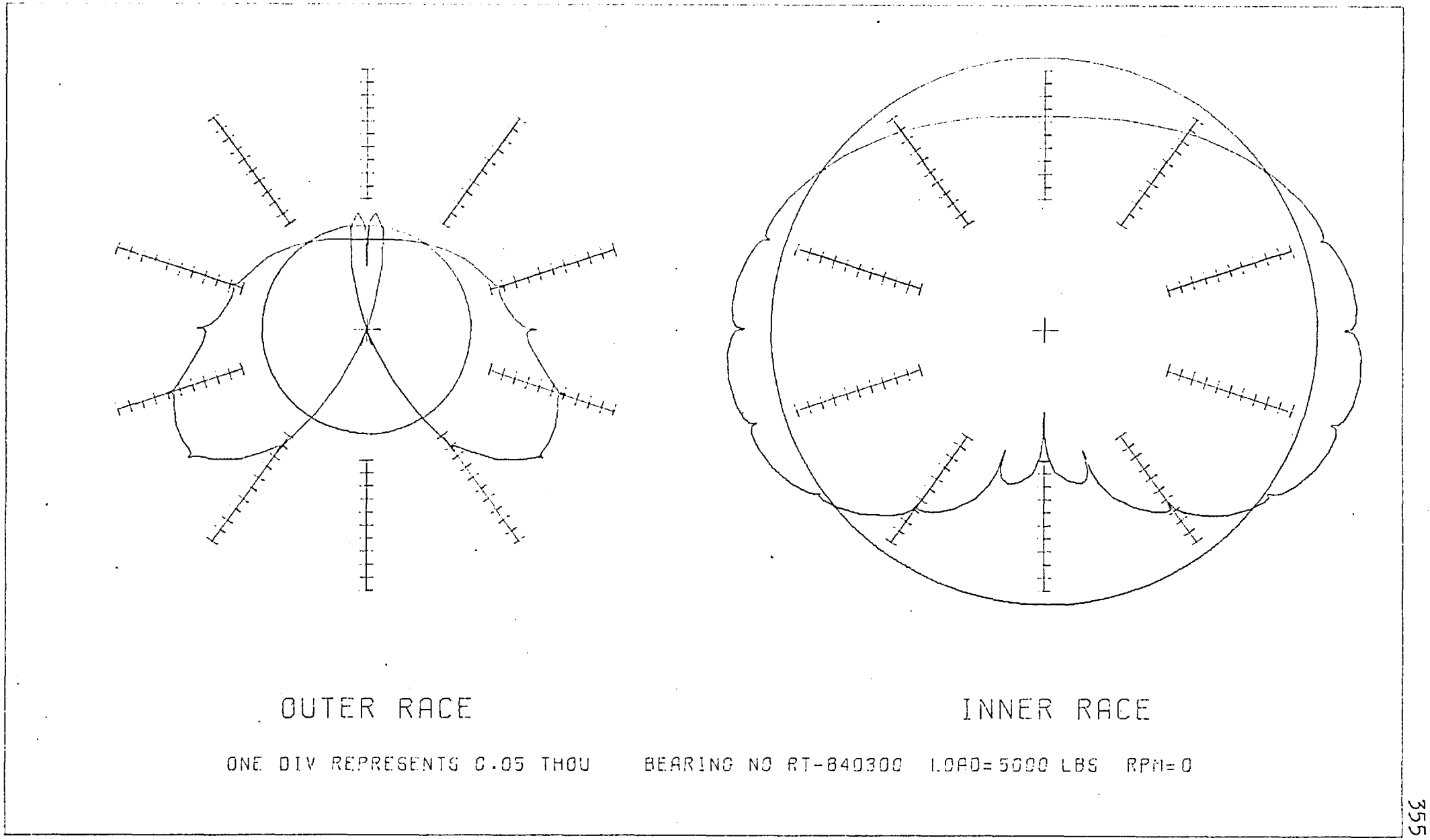


Fig. 7.120

Fig. 7.121 Deflected shapes of the races of a steel radial roller bearing having hollow shaft (no.4, inner to outer diameter ratio 0.651) and circular housing (outer to inner diameter ratio 1.145) with diagonal part-cruciform support. Radial clearance c= -300 μin. and radial load F_r= 5000 lbs.

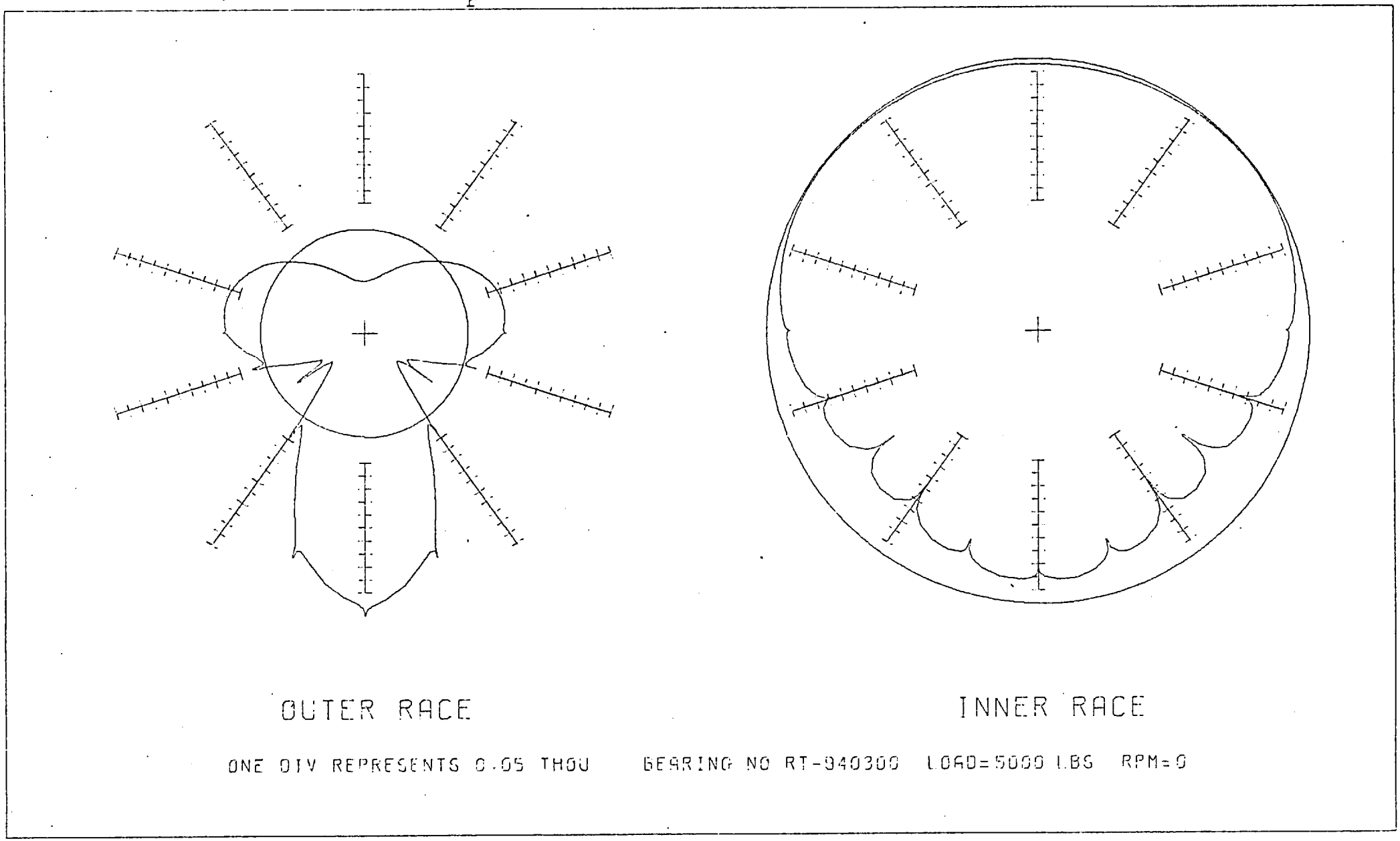


Fig. 7.121

Table 1.1 Values of the constant 'K' for roller and ball bearings. (From Stansfield and Bell (4))

K = Ratio of actual radial deflection of bearing to theoretical radial deflection for a geometrically perfect bearing in a rigid housing.

Conditions	Value of K	Probable Scatter
Specially-stiff bearing arrangement i.e. Lapped housing bore; Preloaded bearing; Rigid housing (depth of housing at least four times the depth of the outer race with no intermediate bushes).	$1\frac{1}{3}$	$\pm \frac{1}{3}$
Normal bearing mounting: e.g. Normal manufacture of housing bore but not lapped; Bearing not preloaded (but negligible clearance); Rigid housing (depth of housing at least four times the depth of the outer race with no intermediate bushes).	$2\frac{1}{3}$	$\pm$ 1

Note: For low loads, as in finishing cuts, the value of K can be upto 7.

Table 1.2 The percentage of element contribution for different arrangement gearboxes. (From El Tamimi (18))

Arrangement	Bearing	Shaft	Gear	Keyway	Av. stiffness lb.in./rad.
1.	57.0	16.9	16.1	-	0.9×10^5
2.	31.5	23.3	45.2	-	1.7×10^5
3.	24.8	26.0	49.2	-	1.9×10^5
4.	13.2	29.5	57.3	-	2.3×10^5
5.	12.5	28.0	54.1	5.4	2.2×10^5
6.	11.4	25.4	49.4	13.8	1.8×10^5

Arrangement;

1. Ball bearing, integrated shaft and pinion.
2. Roller bearing, integrated shaft and pinion.
3. Taper roller bearing, integrated shaft and pinion.
4. Needle bearing, integrated shaft and pinion.
5. Needle bearing, keyed shaft and pinion.
6. Needle bearing, keyed shaft and pinion (smaller length of key)

Table 2.1 Width of contact area for a roller loaded between flat platens, by Hertz's formula.

(a) For steel

Load on Roller lbs.	Width of contact area 2b, thou.
250	5.06
500	7.16
750	8.76
1000	10.10
1250	11.30
1500	12.40
1750	13.38
2000	14.30
2500	16.00
3000	17.50

(b) For Araldite

Load on Roller lbs.	Width of contact area 2b, thou.
0.5	22.0
1.0	31.0
2.0	43.8
3.0	53.7
4.0	62.0
5.0	69.3
6.0	76.0
7.0	82.0
8.0	87.6
9.0	93.0
10.0	98.0

Table 2.2 Comparison of different deflection formulae for line contact. Deflection given by the approach of two flat steel platens when a steel roller is loaded between them.

Load on Roller lbs.	Deflection according to formula given by				
	Palmgren thou.	Bochmann thou.	Föppl thou.	Hoffmann Mfg. Co. thou.	Dowson & Higginson thou.
250	0.237	0.183	0.219	0.212	0.200
500	0.442	0.367	0.408	0.397	0.370
750	0.637	0.550	0.586	0.567	0.529
1000	0.825	0.733	0.757	0.735	0.681
1250	1.009	0.917	0.922	0.905	0.828
1500	1.189	1.100	1.083	1.066	0.970
1750	1.366	1.283	1.240	1.220	1.108
2000	1.540	1.467	1.395	1.382	1.244
2500	1.883	1.833	1.696	1.675	1.507
3000	2.218	2.200	1.988	1.985	1.761

Table 2.3 Comparison of different deflection formulae for line contact. Deflection given by the approach of two flat Araldite platens when an Araldite roller is loaded between them.

Load on Roller lbs.	Deflection according to formula given by			
	Palmgren thou.	Bochmann thou.	Föppl thou.	Dowson & Higginson thou.
1.0	6.0	6.6	5.0	4.5
2.0	11.2	13.3	8.9	7.8
3.0	16.1	19.9	12.4	10.8
4.0	20.9	26.6	15.7	13.5
5.0	25.6	33.2	18.7	16.0
6.0	30.1	39.9	21.6	18.4
7.0	34.6	46.5	24.4	20.6
8.0	39.0	53.1	27.0	22.7
9.0	43.3	59.8	29.6	24.8
10.0	47.6	66.4	32.0	26.7

Table 2.4 Total deflection given by the approach of two flat Araldite platens when a hollow Araldite roller is loaded between them.

Load on Roller lbs.	Deflection for Solid Roller by Föppl formula δ_{solid} thou.	Deflection of Hollow Roller as a cylinder Δd thou.	Total deflection for Hollow Roller $\delta_{hollow}=\delta_{solid}+\Delta d$ thou.
0.5	2.8	0.7	3.5
1.0	5.0	1.3	6.3
2.0	8.9	2.7	11.6
3.0	12.4	4.0	16.4
4.0	15.7	5.3	21.0
5.0	18.7	6.7	25.4
6.0	21.6	8.0	29.6
7.0	24.4	9.3	33.7
8.0	27.0	10.6	37.6
9.0	29.6	12.0	41.6
10.0	32.0	13.3	45.3

E = 2730psi. (18.82 MN/m^2)
m = 2.0
r_m = 0.1 in. (2.54 mm)
h = 0.1 in. (2.54 mm)

See fig.2.6 for notations used for the various dimensions.

Table 2.5 Value of load distribution integral $J_r(\epsilon)$ for radial rolling bearings with line contact and that with point contact.

ϵ	Line Contact	Point Contact
0	1/Z	1/Z
0.1	0.1268	0.1156
0.2	0.1737	0.1590
0.3	0.2055	0.1892
0.4	0.2286	0.2117
0.5	0.2453	0.2288
0.6	0.2568	0.2416
0.7	0.2636	0.2505
0.8	0.2658	0.2559
0.9	0.2628	0.2576
1.0	0.2523	0.2546
1.25	0.2078	0.2289
1.67	0.1589	0.1871
2.5	0.1075	0.1339
5.0	0.0544	0.0711
∞	0	0

Table 4.1 Calibration of solid rollers between Araldite platens.
(Width of platen=0.616 in. Thickness of platen=0.545 in.)

Load lbs.	Deflection of roller thou.	Deflection of platens		Total Deflect^{n}. thou.	Width of contact area in thou.	
		Upper thou.	Lower thou.		Upper platen	Lower platen
0.63	1.6	0.7	0.6	2.9	19.7	27.6
1.13	3.4	1.1	1.2	5.7	41.4	41.4
2.13	5.0	1.9	2.2	9.1	47.2	52.7
3.13	6.4	3.1	3.4	12.9	72.8	72.8
4.13	7.8	3.6	4.3	15.7	75.6	66.5
5.13	8.9	5.2	5.2	19.3	74.8	74.8
6.13	11.2	5.9	5.3	22.4	85.8	86.6
7.13	12.7	5.9	6.0	24.6	86.6	98.4
8.13	15.5	7.3	6.5	29.3	110.0	92.5
10.13	17.0	9.3	9.2	35.5	114.0	126.0

Curves of the form $\delta=AxP^{N}$ fitted by the method of least squares from the above experimental results:

Load lbs.	Deflection of roller thou.	Deflection of platens thou.	Total Deflect^{n}. thou.	Width of contact area in thou.
1.00	2.6	1.03	4.7	33.9
2.00	4.6	1.97	8.5	49.0
3.00	6.3	2.88	12.1	60.7
4.00	8.0	3.77	15.6	70.7
5.00	9.6	4.65	18.9	79.6
6.00	11.1	5.51	22.2	87.7
7.00	12.6	6.37	25.4	95.2
8.00	14.0	7.22	28.4	102.2
9.00	15.4	8.06	31.6	108.8
10.00	16.8	8.90	34.6	115.1
$\delta=AxP^{N}$	A_2=0.0026 N=0.81	A_1=0.00103 N=0.94	A_2=0.0047 N=0.87	A=0.0339 N=0.53

Values of A are given taking unit of deflection as in.

Table 4.2 Calibration of hollow rollers between Araldite platens. (Width of platen=0.616 in. Thickness of platen=0.545 in.)

Load lbs.	Deflection of roller thou.	Deflection of platens		Total Deflect^{n}. thou.	Width of contact area in thou.	
		Upper thou.	Lower thou.		Upper platen	Lower platen
0.63	1.9	0.70	0.70	3.30	26.8	26.8
1.13	3.9	1.50	1.50	6.90	39.4	39.4
2.13	7.5	2.19	2.47	12.16	54.0	46.0
3.13	9.7	3.43	3.66	16.79	63.0	62.2
4.13	14.7	3.93	4.47	23.10	70.0	71.6
5.13	17.6	5.29	5.30	28.19	85.0	84.6
6.13	18.0	6.34	5.70	30.04	83.5	86.6
7.13	20.6	5.90	6.23	32.73	82.6	87.5
8.13	26.9	6.90	6.93	40.73	105.5	103.2
10.13	29.0	9.23	8.40	46.63	105.1	112.2

Curves of the form $\delta = AxP^{N}$ fitted by the method of least squares from the above experimental results:

Load lbs.	Deflection of roller thou.	Deflection of platens thou.	Total Deflect^{n}. thou.	Width of contact area in thou.
1.00	3.3	1.2	5.7	35.1
2.00	6.4	2.2	10.9	49.5
3.00	9.6	3.1	15.9	60.5
4.00	12.7	4.0	20.8	69.8
5.00	15.8	4.9	25.6	77.9
6.00	18.9	5.7	30.4	85.3
7.00	22.0	6.5	35.1	92.1
8.00	25.0	7.3	39.7	98.4
9.00	28.1	8.1	44.3	104.3
10.00	31.2	8.9	48.9	109.9
$\delta = AxP^{N}$	A_2=0.0033 N=0.98	A_1=0.0012 N=0.87	A_2=0.00571 N=0.93	A=0.0351 N=0.50

Values of A are given taking unit of deflection as in.

Table 4.3 Calibration of solid rollers between Araldite platens. (Width of platen=0.450 in. Thickness of platen=0.545 in.)

Load lbs.	Deflection of roller thou.	Deflection of platens		Total Deflect^{n}. thou.	Width of contact area in thou.	
		Upper thou.	Lower thou.		Upper platen	Lower platen
0.62	2.1	0.62	0.94	3.7	28.0	30.3
1.13	3.1	1.03	1.70	5.8	33.1	37.0
2.12	6.0	2.26	2.88	11.1	53.5	55.5
3.13	7.4	3.75	4.11	15.3	59.5	67.0
4.13	9.9	5.00	5.12	20.0		73.3
5.13	12.1	6.03	6.21	24.3	78.8	78.8
6.12	13.3	6.69	6.90	26.9	80.7	
7.12	13.9	7.25	7.25	28.4	82.7	90.6
8.13	18.0	8.54	8.70	35.2	98.5	102.3
10.13	20.0	11.41	11.25	42.7	94.5	105.8

Curves of the form $\delta = AxP^{N}$ fitted by the method of least squares from the above experimental results:

Load lbs.	Deflection of roller thou.	Deflection of platens thou.	Total Deflect^{n}. thou.	Width of contact area in thou.
1.00	3.0	1.2	5.5	36.
2.00	5.3	2.4	10.2	50.
3.00	7.4	3.5	14.5	60.
4.00	9.4	4.6	18.7	69.
5.00	11.3	5.7	22.8	76.
6.00	13.2	6.8	26.7	83.
7.00	15.0	7.8	30.6	89.
8.00	16.7	8.9	34.4	95.
9.00	18.4	10.0	38.2	100.
10.00	20.1	11.0	41.9	105.
$\delta = AxP^{N}$	$\hat{A}$=0.0030 $\hat{N}$=0.82	$\hat{A}_1$=0.00123. $\hat{N}$=0.953	$\hat{A}$=0.00553 $\hat{N}$=0.88	A=0.036 N=0.47

Values of A are given taking unit of deflection as in.

Table 4.4 Calibration of hollow rollers between Araldite platens. (Width of platen=0.450 in. Thickness of platen=0.545 in.)

Load lbs.	Deflection of roller thou.	Deflection of platens		Total Deflectn thou.	Width of contact area in thou.	
		Upper thou.	Lower thou.		Upper platen	Lower platen
0.63	2.92	1.01	1.02	4.95	24.8	24.4
1.13	4.10	1.60	1.75	7.45	34.3	37.4
2.13	8.57	2.37	2.91	13.85	48.0	48.0
3.13	11.65	3.83	4.12	19.60	61.8	61.8
4.13	13.83	4.53	4.96	23.32	69.0	69.0
5.13	16.85	5.54	5.83	28.22	75.6	78.8
6.13	16.45	7.30	6.36	30.11	80.7	84.3
7.13	21.82	6.91	6.92	35.65	90.6	91.0
8.13	28.07	8.09	7.60	43.76	103.2	101.2

Curves of the form $\delta = AxP^N$ fitted by the method of least squares from the above experimental results:

Load lbs.	Deflection of roller thou	Deflection of platens thou.	Total Deflectn thou.	Width of contact area in thou.
1.00	4.16	1.5	7.17	32.5
2.00	7.51	2.6	12.78	47.0
3.00	10.62	3.6	17.92	58.3
4.00	13.57	4.6	22.78	68.0
5.00	16.41	5.5	27.44	76.6
6.00	19.18	6.35	31.95	84.4
7.00	21.87	7.2	36.33	91.6
8.00	24.51	8.0	40.61	98.4
9.00	27.10	8.8	44.80	104.8
10.00	29.65	9.6	48.91	110.8
$\delta = AxP^N$	$A_2=0.00416$ $N=0.853$	$A_1=0.0015$ $N=0.805$	$A_2=0.0072$ $N=0.834$	$A=0.0325$ $N=0.533$

Values of A are given taking unit of deflection as in.

Table 4.5 Calibration of solid Araldite rollers between Aluminium platens.

(a) Experimental results.

Load lbs.	Deflection of roller thou.
0.61	2.0
1.11	3.0
2.11	5.5
3.11	7.7
4.11	9.4
5.11	12.7
6.11	13.4
7.11	15.0
8.11	18.9
10.11	20.1

(b) Curve of the form, $\delta=A_2xP^N$ fitted by the method of least squares from the experimental results.

Load lbs.	Deflection of roller thou.
1.0	2.9
2.0	5.3
3.0	7.5
4.0	9.5
5.0	11.5
6.0	13.5
7.0	15.4
8.0	17.2
9.0	19.0
10.0	20.8
$\delta=A_2xP^N$	$A_2=0.0029$ $N=0.85$

Value of A_2 is given taking unit of deflection as in.

Table 4.6 Calibration of hollow Araldite rollers between Aluminium platens.

(a) Experimental results.

Load lbs.	Deflection of roller thou.
0.61	3.0
1.11	5.2
2.11	8.7
3.11	12.2
4.11	14.4
5.11	18.3
6.11	19.8
7.11	22.7
8.11	29.0
10.11	32.4

(b) Curve of the form, $\delta=A_2 x P^N$ fitted by the method of least squares from the experimental results.

Load lbs.	Deflection of roller thou.
1.0	4.6
2.0	8.3
3.0	11.6
4.0	14.8
5.0	17.8
6.0	20.7
7.0	23.5
8.0	26.3
9.0	29.0
10.0	31.7
$\delta=A_2 x P^N$	$A_2=0.00463$ $N=0.836$

Value of A_2 is given taking unit of deflection as in.

Table 4.7 Components of total radial deflection of the Araldite radial roller bearing with 0.010 in. (0.254mm) interference fit and a radial load of 9.5 lbs. (42.26 N.) acting on it.

	Considering rigid races (thou.)	Experimental results (thou.)	By finite element method (thou.)
Deflection of outer race($=\Delta R_A$)	4.35	7.13	7.08
Deflection of inner race($=\Delta R_F$)	4.35	3.46	3.44
Body deflection of outer race($=\Delta DE$)	0.00	2.46	3.01
Peak roller deflection	6.34	5.63	5.70
Total bearing deflection	5.04	8.68	9.23

Table 4.8 Roller load distribution in the Araldite radial roller bearing with 0.010 in. (0.254mm) interference fit and a radial load of 9.5 lbs. (42.26 N) acting on it.

Angular position of roller ψ_j degrees	Considering rigid races lbs.	Experimental According to deflection, of races lbs.	Experimental According to deflection, of roller lbs.	Experimental According to deflection, total lbs.	By finite element analysis lbs.
0	2.624	2.329	2.284	2.302	2.281
18	2.574	2.238	2.147	2.187	2.184
36	2.430	2.035	1.962	1.994	1.924
54	2.208	1.662	1.483	1.566	1.604
72	1.934	1.264	1.288	1.275	1.222
90	1.635	1.018	0.865	0.935	0.911
108	1.344	0.726	0.542	0.625	0.677
126	1.089	0.582	0.481	0.527	0.512
144	0.892	0.459	0.429	0.444	0.407
162	0.768	0.440	0.319	0.373	0.353
180	0.727	0.402	0.368	0.385	0.337
-18	2.574	2.238	2.205	2.217	2.184
-36	2.430	2.035	1.814	1.918	1.924
-54	2.208	1.662	1.497	1.573	1.604
-72	1.934	1.264	1.160	1.207	1.222
-90	1.635	1.018	0.738	0.866	0.911
-108	1.344	0.726	0.654	0.687	0.677
-126	1.089	0.582	0.485	0.529	0.512
-144	0.892	0.459	0.336	0.391	0.407
-162	0.768	0.440	0.271	0.344	0.353

Table 6.1 Total deflection given by the approach of two flat Araldite platens when an Araldite roller is loaded between them, and also roller and platen deflections as obtained by finite-element method.

Width of platen= length of roller= 0.45in.

Load P lbs.	Roller Deflect^n $\frac{\delta_{roller}}{2}$ thou.	δ_{roller} thou.	Platen Deflection δ_C thou.	δ_A thou.	$(\delta_C-\delta_A)$ thou.	Total Deflection $\delta_{roller}+2\delta_C$ thou.	$\delta_{roller}+2(\delta_C-\delta_A)$ thou.
0.5	0.775	1.550	0.997	0.196	0.801	3.544	3.152
1.0	1.431	2.862	1.875	0.393	1.482	6.612	5.826
2.0	2.549	5.098	3.440	0.789	2.651	11.978	10.400
3.0	3.608	7.216	4.947	1.187	3.760	17.110	14.736
4.0	4.538	9.076	6.327	1.586	4.741	21.730	18.558
5.0	5.432	10.864	7.670	1.988	5.682	26.204	22.228
6.0	6.306	12.612	8.992	2.390	6.602	30.596	25.816
7.0	7.157	14.314	10.291	2.794	7.497	34.896	29.308
8.0	7.990	15.980	11.571	3.198	8.373	39.122	32.726
9.0	8.806	17.612	12.834	3.602	9.232	43.280	36.076
10.0	9.608	19.216	14.084	4.007	10.077	47.384	39.370
$\delta=AxP^N$		$A_2=0.0028291$ $N=0.8353$	$A_1=0.0018636$ $N=0.8794$			$A_2=0.0065459$ $N=0.8618$	

Values of A are given taking unit of deflection as in.

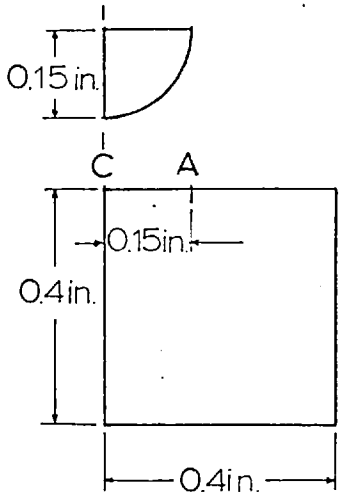


Table 6.2 Effect of platen curvature on Araldite platen deflection when an Araldite roller is loaded on it. Results obtained by using finite-element method.

Width of Platen=0.45 in. Diameter of Roller= 0.30 in.

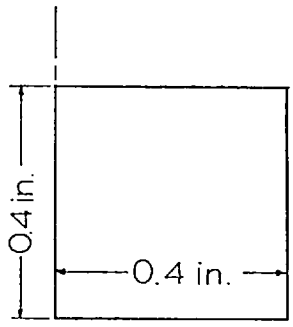
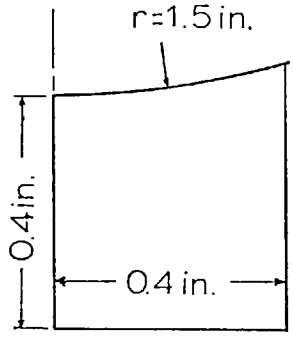
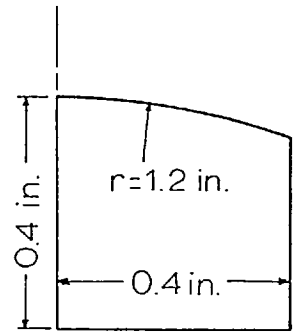
Load P lbs.	 Flat Platen $\Sigma(1/r)=6.667$ δ_c thou.	 Outer Race $\Sigma(1/r)=6.00$ δ_c thou.	 Inner Race $\Sigma(1/r)=7.50$ δ_c thou.
0.5	0.997	0.985	1.012
1.0	1.875	1.853	1.900
2.0	3.440	3.391	3.495
3.0	4.947	4.879	5.022
4.0	6.327	6.212	6.506
5.0	7.670	7.541	7.816
6.0	8.992	8.844	9.157
7.0	10.291	10.124	10.476
8.0	11.571	11.385	11.777
9.0	12.834	12.631	13.060
10.0	14.084	13.722	14.328

TABLE 6.3 SUMMARY OF RESULTS OBTAINED BY FINITE ELEMENT ANALYSIS FOR ARALDITE RADIAL ROLLER BEARINGS.

SL NO	BEARING NUMBER	RADL LOAD LBS	RPM IN 1000	LOAD DISTRIBUTION IN THE BEARING IN POUNDS ROLLER POSITION 1	2	3	4	5	6	7	8	9	10	11	TOTAL DFLNS IN THOU OF O.R.	I.R.	BRG.	AV STENS LB/IN	BODY DFLN O.R.	EPSLN ϵ	LOAD SHRG FCTR	EQV. LOAD LBS	RACES
1	RE-111000	10.0	0.00	2.68	2.63	2.47	2.24	1.95	1.63	1.33	1.06	.85	.73	.68	4.43	4.43	5.30	1.887		1.44	5.36	15.00	RIGID
*				2.23	2.14	1.88	1.57	1.16	.86	.60	.41	.28	.22	.20	6.62	5.01	11.16	.896	3.39		4.46	11.43	FLXBL
2	RE-111000	9.5	0.00	2.62	2.57	2.43	2.21	1.93	1.63	1.34	1.09	.89	.77	.73	4.35	4.35	5.04	1.885		1.49	5.52	14.77	RIGID
*				2.20	2.11	1.86	1.54	1.16	.85	.61	.44	.34	.28	.27	6.28	4.94	10.59	.897	3.78		4.64	11.28	FLXBL
3	RE-111000	9.5	0.00	2.62	2.57	2.43	2.21	1.93	1.63	1.34	1.09	.89	.77	.73	4.35	4.35	5.04	1.885		1.49	5.52	14.77	RIGID
*				2.28	2.18	1.91	1.58	1.19	.88	.65	.49	.40	.35	.34	6.66	4.04	10.08	.942	3.68		4.80	11.64	FLXBL
4	RE-111000	9.5	0.00	2.62	2.57	2.43	2.21	1.93	1.63	1.34	1.09	.89	.77	.73	4.35	4.35	5.04	1.885		1.49	5.52	14.77	RIGID
*				2.31	2.20	1.93	1.60	1.20	.89	.66	.51	.42	.37	.36	6.77	3.74	9.92	.956	3.65		4.85	11.76	FLXBL
5	RE-111000	9.5	0.00	2.62	2.57	2.43	2.21	1.93	1.63	1.34	1.09	.89	.77	.73	4.35	4.35	5.04	1.885		1.49	5.52	14.77	RIGID
*				2.33	2.22	1.95	1.61	1.21	.90	.67	.52	.43	.39	.38	6.86	3.51	9.79	.970	3.63		4.90	11.85	FLXBL
6	RE-111000	9.5	0.00	2.62	2.57	2.43	2.21	1.93	1.63	1.34	1.09	.89	.77	.73	4.35	4.35	5.04	1.885		1.49	5.52	14.77	RIGID
*				2.35	2.25	1.97	1.62	1.22	.91	.69	.54	.45	.41	.40	6.99	3.18	9.61	.989	3.59		4.96	11.99	FLXBL
7	RE-111000	9.5	0.00	2.62	2.57	2.43	2.21	1.93	1.63	1.34	1.09	.89	.77	.73	4.35	4.35	5.04	1.885		1.49	5.52	14.77	RIGID
*				2.28	2.18	1.92	1.66	1.22	.91	.68	.51	.41	.35	.34	7.08	3.44	9.23	1.029	3.01		4.80	11.70	FLXBL
8	RE-110800	9.5	0.00	2.26	2.21	2.07	1.84	1.56	1.26	.97	.72	.53	.41	.37	3.82	3.82	5.24	1.813		1.26	4.76	12.43	RIGID
				2.07	1.98	1.72	1.40	1.02	.71	.47	.30	.20	.15	.13	5.91	3.13	9.55	.995	3.31		4.36	10.48	FLXBL
9	RE-110600	9.5	0.00	1.93	1.88	1.73	1.49	1.21	.90	.61	.37	.18	.08	.05	3.32	3.32	5.54	1.715		1.04	4.06	10.32	RIGID
				1.89	1.80	1.53	1.26	.82	.50	.24	.05	0.00	0.00	0.00	5.22	2.97	10.55	.900	3.48		3.99	9.41	FLXBL
10	RE-110300	9.5	0.00	1.82	1.75	1.53	1.26	.81	.40	.05	0.00	0.00	0.00	0.00	3.16	3.16	7.97	1.192		.69	3.83	9.22	RIGID
				1.93	1.82	1.51	1.09	.61	.17	0.00	0.00	0.00	0.00	0.00	5.19	3.03	13.50	.704	3.45		4.07	9.41	FLXBL
11	RE-110000	9.5	0.00	1.96	1.85	1.53	1.06	.50	0.00	0.00	0.00	0.00	0.00	0.00	3.36	3.36	11.68	.813		.50	4.12	9.50	RIGID
				2.02	1.89	1.52	1.01	.41	0.00	0.00	0.00	0.00	0.00	0.00	5.56	3.26	17.00	.569	3.28		4.25	9.63	FLXBL
12	RE-110300	9.5	0.00	2.10	1.95	1.53	.91	.22	0.00	0.00	0.00	0.00	0.00	0.00	3.58	3.58	12.40	.766		.40	4.42	9.89	RIGID
				2.10	1.95	1.53	.93	.20	0.00	0.00	0.00	0.00	0.00	0.00	6.21	3.50	18.02	.527	3.06		4.41	9.88	FLXBL

1* WITHOUT BODY FORCE IN OUTER RACE
2* INNER RACE CORE THICKNESS= 0.450 INS. WITH BODY FORCE IN OUTER RACE
3* INNER RACE CORE THICKNESS= 0.675 INS. WITH BODY FORCE IN OUTER RACE
4* INNER RACE CORE THICKNESS= 0.7875INS. WITH BODY FORCE IN OUTER RACE
5* INNER RACE CORE THICKNESS= 0.900 INS. WITH BODY FORCE IN OUTER RACE
6* INNER RACE CORE THICKNESS= 1.125 INS. WITH BODY FORCE IN OUTER RACE
7* I.R.CORE THICKNESS=0.0IN.NO BODY FORCE IN O.R. IN THIS AND SUBSEQUENT CASES

CONTINUED

TABLE 4.7 SUMMARY OF RESULTS OBTAINED BY FINITE ELEMENT ANALYSIS FOR ARALDITE RADIAL ROLLER BEARINGS.

SL NO	BEARING NUMBER	RADL LOAD LBS	RPM IN 1000	LOAD DISTRIBUTION IN THE BEARING IN POUNDS — ROLLER POSITION 1	2	3	4	5	6	7	8	9	10	11	TOTAL DFLNS IN THOU OF O.R.	I.R.	BRG.	AV STFNS LB/IN	BODY DFLN O.R.	EPSLN ∈	LOAD SHRG FCTR	EQV. LOAD LBS	RACES
13	RH-110600	9.5	0.00	2.23	2.05	1.53	.77	0.00	0.00	0.00	0.00	0.00	0.00	0.00	3.77	3.77	13.07	.727		.34	4.70	10.29	RIGID
				2.18	2.02	1.54	.83	.00	0.00	0.00	0.00	0.00	0.00	0.00	6.70	3.72	18.77	.566	2.89		4.60	10.16	FLXBL
14	RH-110600	4.0	0.00	1.32	1.30	1.24	1.14	1.03	.90	.78	.67	.59	.54	.52	2.37	2.37	2.30	1.739		1.00	6.58	7.63	RIGID
				1.11	1.06	.95	.83	.67	.54	.44	.37	.32	.29	.29	3.89	1.64	3.94	1.017	1.09		5.53	5.62	FLXBL
15	RH-110600	8.0	0.00	1.76	1.71	1.59	1.40	1.16	.90	.66	.45	.29	.19	.16	3.06	3.06	4.64	1.724		1.15	4.39	9.51	RIGID
				1.65	1.57	1.35	1.07	.76	.50	.30	.16	.07	.03	.02	4.69	2.60	8.50	.942	2.88		4.12	8.26	FLXBL
16	RH-110600	12.0	0.00	2.29	2.22	2.01	1.70	1.31	.90	.52	.21	.00	0.00	0.00	3.86	3.86	7.37	1.628		.91	3.81	12.02	RIGID
				2.38	2.25	1.91	1.47	.94	.49	.11	0.00	0.00	0.00	0.00	6.35	3.65	14.27	.841	4.42		3.97	11.76	FLXBL
17	RH-110000	4.0	0.00	.82	.78	.64	.45	.21	0.00	0.00	0.00	0.00	0.00	0.00	1.57	1.57	5.54	.722		.50	4.12	4.00	RIGID
				.84	.79	.64	.43	.18	0.00	0.00	0.00	0.00	0.00	0.00	2.49	1.50	7.77	.515	1.38		4.22	4.04	FLXBL
18	RH-110000	8.0	0.00	1.65	1.55	1.29	.89	.42	0.00	0.00	0.00	0.00	0.00	0.00	2.89	2.89	10.07	.794		.50	4.12	8.00	RIGID
				1.69	1.58	1.28	.86	.36	0.00	0.00	0.00	0.00	0.00	0.00	4.84	2.80	14.72	.543	2.73		4.23	8.09	FLXBL
19	RH-110000	12.0	0.00	2.47	2.33	1.93	1.34	.63	0.00	0.00	0.00	0.00	0.00	0.00	4.13	4.13	14.28	.840		.50	4.12	12.00	RIGID
				2.54	2.37	1.92	1.29	.53	0.00	0.00	0.00	0.00	0.00	0.00	7.09	4.02	21.30	.563	4.10		4.23	12.13	FLXBL
20	RH-110300	4.0	0.00	.94	.86	.64	.32	0.00	0.00	0.00	0.00	0.00	0.00	0.00	1.77	1.77	6.23	.642		.34	4.72	4.35	RIGID
				.92	.85	.65	.36	0.00	0.00	0.00	0.00	0.00	0.00	0.00	3.05	1.76	8.70	.460	1.20		4.60	4.28	FLXBL
21	RH-110300	8.0	0.00	1.79	1.66	1.29	.75	.15	0.00	0.00	0.00	0.00	0.00	0.00	3.10	3.10	10.79	.741		.39	4.47	8.36	RIGID
				1.78	1.65	1.29	.77	.14	0.00	0.00	0.00	0.00	0.00	0.00	5.37	3.04	15.54	.515	2.55		4.44	8.35	FLXBL
22	RH-110300	12.0	0.00	2.62	2.44	1.94	1.19	.34	0.00	0.00	0.00	0.00	0.00	0.00	4.35	4.35	15.01	.799		.42	4.36	12.39	RIGID
				2.63	2.45	1.94	1.19	.29	0.00	0.00	0.00	0.00	0.00	0.00	7.60	4.25	22.07	.544	3.91		4.38	12.41	FLXBL
23	RH-111000	9.5	1.73	2.64	2.59	2.45	2.22	1.95	1.65	1.36	1.11	.91	.79	.74	4.38	4.33	5.03	1.889		1.49	5.56	14.71	RGD OR
				2.61	2.56	2.41	2.19	1.92	1.62	1.33	1.07	.88	.75	.71							5.49		RGD IR
				2.30	2.20	1.95	1.63	1.24	.93	.70	.53	.43	.37	.36	7.04	3.39	9.10	1.044	3.02		4.84	11.67	FLX OR
				2.27	2.17	1.91	1.59	1.21	.90	.67	.51	.39	.34	.32							4.77		FLX IR
24	RH-111000	9.5	3.46	2.69	2.64	2.50	2.28	2.00	1.70	1.41	1.16	.96	.84	.80	4.45	4.25	5.03	1.889		1.49	5.67	14.54	RGD OR
				2.56	2.51	2.36	2.14	1.87	1.57	1.28	1.02	.82	.70	.66							5.38		RGD IR
				2.33	2.23	1.98	1.66	1.27	.96	.73	.56	.46	.40	.39	7.19	3.30	9.08	1.046	2.98		4.91	11.40	FLX OR
				2.19	2.10	1.84	1.52	1.14	.83	.59	.43	.32	.27	.25							4.62		FLX IR
25	RH-111000	9.5	5.19	2.78	2.73	2.58	2.36	2.09	1.79	1.50	1.24	1.05	.92	.88	4.58	4.13	5.03	1.889		1.49	5.85	14.31	RGD OR
				2.47	2.42	2.28	2.06	1.78	1.48	1.19	.96	.74	.62	.57							5.20		RGD IR
				2.39	2.29	2.03	1.71	1.33	1.02	.78	.62	.51	.46	.44	7.42	3.14	9.02	1.053	2.92		5.03	11.03	FLX OR
				2.68	1.98	1.72	1.40	1.02	.71	.46	.31	.21	.15	.14							4.38		FLX IR

CONTINUED

TABLE 6.3 SUMMARY OF RESULTS OBTAINED BY FINITE ELEMENT ANALYSIS FOR ARALDITE RADIAL ROLLER BEARINGS.

SL NO	BEARING NUMBER	RADL LOAD LBS	RPM IN 1000	LOAD DISTRIBUTION IN THE BEARING IN POUNDS ROLLER POSITION 1	2	3	4	5	6	7	8	9	10	11	TOTAL DFLNS IN THOU OF O.R.	I.R.	BRG.	AV STRSS LB/TH	BODY DFLN O.R.	EPSLN ϵ	LOAD SHRG FCTR	EQV. LOAD LBS	RACES
26	RN-111000	9.5	6.92	2.90	2.85	2.71	2.48	2.21	1.91	1.62	1.37	1.17	1.05	1.00	4.75	3.96	5.04	1.885		1.49	6.11	14.12	RGO OR
				2.36	2.31	2.16	1.94	1.66	1.37	1.07	.82	.62	.50	.46							4.96		RGO IR
				2.47	2.37	2.11	1.79	1.41	1.10	.86	.68	.57	.55	.55	7.79	3.00	9.14	1.040	2.81		5.19	10.67	FLX OR
				1.92	1.82	1.56	1.24	.86	.55	.31	.14	.03	0.00	0.00							4.04		FLX IR
27	RN-110600	4.0	6.92	1.59	1.57	1.51	1.42	1.30	1.18	1.05	.95	.86	.81	.79	2.80	1.96	2.31	1.732		1.86	7.94	7.32	RGO OR
				1.06	1.04	.98	.88	.77	.64	.52	.41	.33	.28	.26							5.28		RGO IR
				1.32	1.28	1.17	1.03	.86	.72	.60	.53	.53	.53	.53	4.96	1.41	4.19	.954	.81		6.62	5.38	FLX OR
				.79	.75	.64	.50	.33	.19	.07	0.00	0.00	0.00	0.00							3.95		FLX IR
28	RN-110000	9.5	1.73	1.99	1.88	1.56	1.06	.52	.03	.03	.03	.03	.03	.03	3.42	3.37	11.79	.806		.50	4.20	9.55	RGO OR
				1.96	1.85	1.53	1.05	.49	0.00	0.00	0.00	0.00	0.00	0.00							4.13		RGO IR
				2.04	1.91	1.55	1.05	.44	.03	.03	.03	.03	.03	.03	5.91	3.30	17.48	.543	3.10		4.30	9.66	FLX OR
				2.01	1.88	1.52	1.02	.41	0.00	0.00	0.00	0.00	0.00	0.00							4.24		FLX IR
29	RN-110000	9.5	3.46	2.11	1.99	1.66	1.17	.59	.13	.13	.13	.13	.13	.13	3.59	3.39	12.11	.764		.50	4.43	9.73	RGO OR
				1.98	1.86	1.53	1.04	.46	0.00	0.00	0.00	0.00	0.00	0.00							4.16		RGO IR
				2.16	2.03	1.65	1.13	.48	.13	.13	.13	.13	.13	.13	6.47	3.34	18.07	.526	3.03		4.55	9.86	FLX OR
				2.03	1.90	1.52	1.00	.35	0.00	0.00	0.00	0.00	0.00	0.00							4.28		FLX IR
30	RN-110000	9.5	5.19	2.29	2.17	1.82	1.30	.70	.29	.29	.29	.29	.29	.29	3.86	3.43	12.63	.752		.50	4.82	10.07	RGO OR
				2.00	1.88	1.53	1.01	.41	0.00	0.00	0.00	0.00	0.00	0.00							4.21		RGO IR
				2.36	2.21	1.82	1.26	.55	.29	.29	.29	.29	.29	.29	7.41	3.41	19.06	.498	2.77		4.96	10.23	FLX OR
				2.07	1.92	1.53	.97	.26	0.00	0.00	0.00	0.00	0.00	0.00							4.35		FLX IR
31	RN-110000	9.5	6.92	2.55	2.42	2.05	1.49	.85	.51	.51	.51	.51	.51	.51	4.24	3.48	13.36	.711		.50	5.36	10.63	RGO OR
				2.03	1.90	1.53	.98	.34	0.00	0.00	0.00	0.00	0.00	0.00							4.28		RGO IR
				2.63	2.47	2.05	1.44	.66	.51	.51	.51	.51	.51	.51	8.73	3.52	20.46	.464	2.40		5.53	10.82	FLX OR
				2.11	1.96	1.53	.93	.14	0.00	0.00	0.00	0.00	0.00	0.00							4.45		FLX IR
32	RN-110606	9.5	0.00	1.71	1.67	1.55	1.37	1.15	.90	.37	0.00	0.00	0.00	0.00	2.99	2.99	10.41	.913		.79	3.61	9.27	RIGID
*				1.85	1.76	1.50	1.18	.02	.54	.04	0.00	0.00	0.00	0.00	4.86	2.87	16.06	.592	3.60		3.89	9.24	FLXBL
33	RN-110400	4.0	0.00	.98	.96	.90	.81	.69	.57	.44	.34	.25	.20	.19	1.84	1.84	2.46	1.026		1.31	4.92	5.44	RIGID
				.89	.85	.74	.60	.44	.31	.21	.14	.10	.08	.07	2.94	1.55	4.47	.805	1.33		4.44	4.50	FLXBL
34	RN-110440	8.0	0.00	1.52	1.47	1.33	1.11	.85	.57	.30	.09	0.00	0.00	0.00	2.69	2.69	5.39	1.404		.87	3.80	7.93	RIGID
				1.60	1.51	1.27	.95	.59	.28	.03	0.00	0.00	0.00	0.00	4.33	2.53	9.97	.802	2.96		4.01	7.86	FLXBL
35	RN-110400	9.5	0.00	1.80	1.73	1.55	1.27	.92	.57	.24	0.00	0.00	0.00	0.00	3.12	3.12	6.83	1.391		.79	3.78	9.23	RIGID
				1.90	1.79	1.51	1.13	.69	.29	0.00	0.00	0.00	0.00	0.00	5.15	3.00	12.46	.762	3.47		3.99	9.32	FLXBL

32* LOWER HALF OF OUTER RACE RELIEF IS OF THE FORM, REL(THETA)=AMPL*COS(THETA)

CONTINUED

TABLE 6.3 SUMMARY OF RESULTS OBTAINED BY FINITE ELEMENT ANALYSIS FOR ARALDITE RADIAL ROLLER BEARINGS.

SL NO	BEARING NUMBER	RADL LOAD LBS	RPM IN 1000	LOAD DISTRIBUTION IN THE BEARING IN POUNDS — ROLLER POSITION 1	2	3	4	5	6	7	8	9	10	11	TOTAL DFLNS IN THOU OF O.R.	I.R.	BRG.	AV STRSS LB/IN	BODY DFLN O.R.	EPSLN ϵ	LOAD SHRG FCTR	EQV. LOAD LBS	RACES
36	RH-110400	12.0	0.00	2.29	2.20	1.94	1.54	1.06	.57	.13	0.00	0.00	0.00	0.00	3.86	3.86	9.37	1.281		.71	3.82	11.64	RIGID
				2.42	2.28	1.91	1.41	.81	.26	0.00	0.00	0.00	0.00	0.00	6.53	3.76	16.53	.736	4.33		4.03	11.83	FLXBL
37	RH-111001	9.5	0.00	2.43	2.43	2.38	2.21	1.92	1.55	1.18	.91	.78	.73	.72	4.07	4.07	5.07	1.074		1.49	5.12	14.20	RIGID
*				2.14	2.09	1.98	1.62	1.23	.86	.57	.39	.34	.34	.35	6.52	3.23	9.32	1.019	3.16		4.51	11.32	FLXBL
38	RH-111003	9.5	0.00	2.05	2.15	2.27	2.21	1.89	1.38	.86	.58	.57	.66	.70	3.51	3.51	5.16	1.041		1.47	4.32	13.21	RIGID
				1.87	1.90	1.85	1.66	1.24	.77	.36	.17	.21	.31	.36	5.43	2.82	9.52	.997	3.45		3.94	10.65	FLXBL
39	RH-111005	9.5	0.00	1.69	1.88	2.17	2.22	1.87	1.22	.56	.26	.36	.58	.68	2.95	2.95	5.28	1.799		1.46	3.56	12.46	RIGID
				1.61	1.72	1.81	1.69	1.25	.66	.14	0.00	.07	.27	.37	4.43	2.44	9.84	.966	3.71		3.39	10.15	FLXBL
40	RH-111003	4.0	0.00	1.48	1.60	1.80	1.87	1.72	1.38	1.03	.87	.98	1.16	1.23	2.63	2.63	2.16	1.852		2.81	7.39	11.09	RIGID
				1.14	1.22	1.32	1.31	1.11	.82	.55	.44	.55	.69	.76	4.43	1.83	3.44	1.161	.97		5.72	7.73	FLXBL
41	RH-111003	8.0	0.00	1.89	2.00	2.14	2.12	1.84	1.38	.91	.66	.68	.79	.84	3.26	3.26	4.34	1.843		1.65	4.73	12.56	RIGID
				1.67	1.71	1.70	1.56	1.20	.78	.41	.24	.30	.41	.46	5.15	2.55	7.85	1.018	2.78		4.18	9.79	FLXBL
42	RH-111003	12.0	0.00	2.33	2.41	2.49	2.37	1.98	1.38	.79	.45	.39	.44	.48	3.91	3.91	6.55	1.832		1.26	3.87	14.40	RIGID
				2.22	2.22	2.11	1.83	1.31	.75	.28	.06	.07	.15	.19	5.87	3.28	12.25	.930	4.58		3.70	12.21	FLXBL
43	RH-111005	4.0	0.00	1.12	1.33	1.69	1.86	1.69	1.22	.72	.54	.77	1.08	1.22	2.06	2.06	2.21	1.810		2.76	5.59	10.37	RIGID
				.89	1.04	1.26	1.34	1.12	.73	.34	.22	.41	.66	.78	3.36	1.39	3.59	1.115	1.26		4.42	7.35	FLXBL
44	RH-111005	8.0	0.00	1.53	1.72	2.03	2.12	1.82	1.22	.61	.34	.47	.71	.83	2.71	2.71	4.43	1.866		1.63	3.82	11.81	RIGID
				1.41	1.53	1.66	1.66	1.21	.68	.20	.04	.16	.38	.48	4.09	2.15	8.09	.989	3.06		3.51	9.29	FLXBL
45	RH-110601	9.5	0.00	1.76	1.75	1.68	1.50	1.20	.83	.46	.21	.09	.05	.04	3.06	3.06	5.63	1.687		1.03	3.69	9.82	RIGID
				1.80	1.74	1.54	1.24	.83	.45	.12	0.00	0.00	0.00	0.00	4.84	2.81	10.88	.873	3.58		3.78	9.21	FLXBL
46	RH-110602	9.5	0.00	1.59	1.63	1.64	1.51	1.19	.75	.32	.07	.01	.02	.02	2.80	2.80	5.75	1.652		1.02	3.34	9.40	RIGID
				1.71	1.70	1.56	1.29	.85	.39	.01	0.00	0.00	0.00	0.00	4.50	2.67	11.27	.843	3.66		3.61	9.12	FLXBL
47	RH-110603	9.5	0.00	1.46	1.55	1.64	1.54	1.20	.67	.18	0.00	0.00	0.00	0.00	2.60	2.60	6.09	1.580		.99	3.08	9.22	RIGID
				1.64	1.66	1.59	1.34	.86	.32	0.00	0.00	0.00	0.00	0.00	4.23	2.55	11.76	.868	3.71		3.46	9.09	FLXBL
48	RH-110604	9.5	0.00	1.37	1.50	1.66	1.60	1.21	.60	.04	0.00	0.00	0.00	0.00	2.46	2.46	6.59	1.442		.96	2.89	9.24	RIGID
				1.58	1.64	1.62	1.40	.88	.26	0.00	0.00	0.00	0.00	0.00	4.01	2.44	12.30	.772	3.76		3.32	9.08	FLXBL
49	RH-110602	4.0	0.00	.97	1.04	1.14	1.14	1.00	.75	.49	.36	.39	.47	.51	1.81	1.81	2.36	1.695		1.77	4.83	6.69	RIGID
				.84	.87	.89	.83	.65	.42	.21	.12	.17	.25	.28	2.96	1.43	4.28	.935	1.34		4.19	5.07	FLXBL

37* FROM CASE NO.37 TO 55 BEARING OUTER RACE RELIEF IS TRI-LOBED.

CONTINUED

TABLE 6.3 SUMMARY OF RESULTS OBTAINED BY FINITE ELEMENT ANALYSIS FOR ARALDITE RADIAL ROLLER BEARINGS.

SL NO	BEARING NUMBER	RADL LOAD LBS	RPM IN 1000	LOAD DISTRIBUTION IN THE BEARING IN POUNDS ROLLER POSITION 1	2	3	4	5	6	7	8	9	10	11	TOTAL DFLNS IN THOU OF O.R.	I.R.	BRG.	AV STRSS LB/SQ IN	BODY DFLN O.R.	EPSLN ϵ	LOAD SHRG FCTR	EQV. LOAD LBS	RACES
50	RU-110602	8.0	0.00	1.41	1.46	1.50	1.40	1.14	.75	.37	.15	.10	.13	.14	2.51	2.51	4.78	1.674		1.13	3.51	8.57	RIGID
				1.41	1.41	1.33	1.13	.78	.40	.08	0.00	0.00	0.00	0.00	3.81	2.26	8.99	.890	3.10		3.53	7.68	FLXBL
51	RU-110602	12.0	0.00	2.04	2.06	2.01	1.77	1.33	.75	.21	0.00	0.00	0.00	0.00	3.49	3.49	8.12	1.478		.87	3.41	11.53	RIGID
				2.23	2.18	1.96	1.57	.97	.36	0.00	0.00	0.00	0.00	0.00	5.83	3.41	15.29	.785	4.53		3.72	11.58	FLXBL
52	RU-110002	4.0	0.00	.69	.72	.71	.55	.24	0.00	0.00	0.00	0.00	0.00	0.00	1.34	1.34	6.75	.593		.56	3.45	3.87	RIGID
				.73	.75	.70	.52	.18	0.00	0.00	0.00	0.00	0.00	0.00	2.06	1.26	8.85	.452	1.47		3.67	3.92	FLXBL
53	RU-110002	8.0	0.00	1.50	1.49	1.36	1.01	.46	0.00	0.00	0.00	0.00	0.00	0.00	2.66	2.66	11.28	.769		.50	3.75	7.82	RIGID
				1.58	1.54	1.34	.94	.35	0.00	0.00	0.00	0.00	0.00	0.00	4.28	2.52	15.62	.512	2.86		3.95	7.95	FLXBL
54	RU-110002	9.5	0.00	1.81	1.78	1.60	1.18	.54	0.00	0.00	0.00	0.00	0.00	0.00	3.13	3.13	12.89	.737		.50	3.80	9.31	RIGID
				1.88	1.83	1.59	1.12	.43	0.00	0.00	0.00	0.00	0.00	0.00	5.29	3.05	18.38	.517	3.32		3.96	9.43	FLXBL
55	RU-110002	12.0	0.00	2.32	2.26	2.01	1.46	.67	0.00	0.00	0.00	0.00	0.00	0.00	3.90	3.90	15.50	.774		.50	3.86	11.79	RIGID
				2.41	2.32	1.99	1.39	.53	0.00	0.00	0.00	0.00	0.00	0.00	6.68	3.81	22.47	.534	4.18		4.01	11.95	FLXBL
56	RU-111001	9.5	0.00	2.44	2.41	2.31	2.15	1.92	1.63	1.32	1.02	.77	.61	.55	4.08	4.08	5.10	1.863		1.48	5.13	14.07	RIGID
*				2.17	2.09	1.85	1.57	1.21	.91	.66	.47	.34	.26	.24	6.56	3.26	9.45	1.006	3.16		4.57	11.24	FLXBL
57	RU-111003	9.5	0.00	2.07	2.08	2.06	2.03	1.89	1.63	1.28	.88	.53	.29	.21	3.54	3.54	5.27	1.803		1.45	4.36	12.82	RIGID
				1.96	1.90	1.72	1.50	1.19	.89	.62	.38	.19	.08	.05	5.52	2.90	9.90	.960	3.46		4.13	10.37	FLXBL
58	RU-111005	9.5	0.00	1.75	1.78	1.87	1.93	1.87	1.63	1.23	.73	.29	.02	0.00	3.04	3.04	5.58	1.763		1.40	3.68	11.80	RIGID
				1.79	1.75	1.63	1.46	1.19	.89	.57	.26	.02	0.00	0.00	4.68	2.60	10.62	.895	3.70		3.77	9.75	FLXBL
59	RU-111007	9.5	0.00	1.54	1.60	1.76	1.90	1.89	1.63	1.14	.53	.02	0.00	0.00	2.72	2.72	6.49	1.464		1.27	3.24	11.44	RIGID
				1.69	1.67	1.59	1.47	1.22	.90	.51	.09	0.00	0.00	0.00	4.18	2.42	11.66	.881	3.85		3.56	9.46	FLXBL
60	RU-110601	9.5	0.00	1.80	1.76	1.69	1.47	1.21	.90	.58	.28	.06	0.00	0.00	3.12	3.12	5.86	1.621		1.01	3.79	9.83	RIGID
				1.85	1.77	1.53	1.21	.84	.50	.20	0.00	0.00	0.00	0.00	4.99	2.88	11.19	.849	3.55		3.90	9.28	FLXBL
61	RU-110603	9.5	0.00	1.66	1.65	1.60	1.48	1.25	.90	.48	.08	0.00	0.00	0.00	2.91	2.91	7.14	1.331		.92	3.50	9.44	RIGID
				1.80	1.73	1.53	1.25	.88	.50	.11	0.00	0.00	0.00	0.00	4.69	2.76	12.71	.747	3.64		3.79	9.19	FLXBL
62	RU-110602	4.0	0.00	.98	.99	1.02	1.03	1.00	.90	.74	.55	.36	.24	.19	1.82	1.82	2.41	1.660		1.74	4.88	6.48	RIGID
				.89	.87	.81	.73	.61	.49	.37	.26	.17	.11	.09	2.98	1.47	4.48	.893	1.35		4.47	4.89	FLXBL
63	RU-110602	8.0	0.00	1.47	1.46	1.42	1.32	1.15	.90	.60	.30	.05	0.00	0.00	2.62	2.62	5.13	1.559		1.08	3.68	8.48	RIGID
				1.53	1.47	1.30	1.07	.78	.50	.24	.02	0.00	0.00	0.00	4.09	2.39	9.58	.835	3.05		3.83	7.82	FLXBL

56* FROM CASE NO.56 TO 72 BEARING OUTER RACE RELIEF IS BI-LONED.

CONTINUED

TABLE 6.3 SUMMARY OF RESULTS OBTAINED BY FINITE ELEMENT ANALYSIS FOR ARALDITE RADIAL ROLLER BEARINGS.

SL. NO	BEARING NUMBER	RADL LOAD LBS	RPM IN 1000	LOAD DISTRIBUTION IN THE BEARING IN POUNDS — ROLLER POSITION 1	2	3	4	5	6	7	8	9	10	11	TOTAL DFLNS IN THOU OF O.R.	I.R.	BRG.	AV STRNS LB/TH	BODY DFLN O.R.	EPSLN ϵ	LOAD SHRG FCTR	EQV. LOAD LBS	RACES
64	RH-110602	9.5	0.00	1.72	1.70	1.62	1.47	1.23	.90	.54	.18	0.00	0.00	0.00	3.00	3.00	6.45	1.473		.97	3.62	9.60	RIGID
				1.83	1.75	1.53	1.23	.86	.50	.15	0.00	0.00	0.00	0.00	4.83	2.62	11.94	.796	3.60		3.85	9.23	FLXBL
65	RH-110602	12.0	0.00	2.17	2.12	1.98	1.72	1.36	.90	.42	.01	0.00	0.00	0.00	3.68	3.68	8.77	1.358		.84	3.62	11.66	RIGID
				2.33	2.22	1.91	1.50	.98	.48	.03	0.00	0.00	0.00	0.00	6.11	3.55	15.89	.755	4.50		3.88	11.66	FLXBL
66	RH-111003	4.0	0.00	1.48	1.52	1.60	1.68	1.71	1.63	1.45	1.20	.95	.77	.70	2.64	2.64	2.20	1.818		2.77	7.42	10.91	RIGID
				1.23	1.21	1.18	1.15	1.06	.95	.82	.67	.54	.45	.42	4.51	1.93	3.79	1.055	.97		6.13	7.42	FLXBL
67	RH-111003	8.0	0.00	1.91	1.92	1.95	1.94	1.84	1.63	1.33	.97	.64	.42	.34	3.29	3.29	4.42	1.810		1.63	4.77	12.20	RIGID
				1.76	1.71	1.57	1.40	1.15	.91	.67	.46	.29	.18	.15	5.23	2.61	8.21	.974	2.78		4.39	9.49	FLXBL
68	RH-111003	12.0	0.00	2.36	2.35	2.31	2.20	1.98	1.63	1.20	.73	.34	.10	.03	3.96	3.96	6.71	1.708		1.25	3.93	13.97	RIGID
				2.33	2.25	2.00	1.66	1.27	.88	.52	.22	.01	0.00	0.00	6.21	3.43	12.98	.924	4.52		3.89	12.08	FLXBL
69	RH-110001	4.0	0.00	.80	.76	.65	.47	.24	0.00	0.00	0.00	0.00	0.00	0.00	1.53	1.53	6.40	.625		.50	3.99	3.95	RIGID
				.83	.78	.64	.45	.19	0.00	0.00	0.00	0.00	0.00	0.00	2.39	1.45	8.54	.466	1.41		4.13	4.01	FLXBL
70	RH-110001	8.0	0.00	1.62	1.54	1.30	.92	.45	0.00	0.00	0.00	0.00	0.00	0.00	2.85	2.85	10.93	.732		.50	4.05	7.94	RIGID
				1.68	1.58	1.26	.87	.36	0.00	0.00	0.00	0.00	0.00	0.00	4.63	2.70	15.36	.521	2.80		4.20	8.07	FLXBL
71	RH-110001	9.5	0.00	1.93	1.83	1.54	1.09	.53	0.00	0.00	0.00	0.00	0.00	0.00	3.32	3.32	12.53	.758		.50	4.06	9.44	RIGID
				2.00	1.88	1.52	1.03	.43	0.00	0.00	0.00	0.00	0.00	0.00	5.46	3.15	17.82	.503	3.31		4.21	9.59	FLXBL
72	RH-110001	12.0	0.00	2.44	2.31	1.94	1.36	.66	0.00	0.00	0.00	0.00	0.00	0.00	4.09	4.09	15.14	.793		.50	4.07	11.94	RIGID
				2.52	2.36	1.93	1.31	.55	0.00	0.00	0.00	0.00	0.00	0.00	7.00	3.98	22.15	.542	4.12		4.19	12.09	FLXBL
73	RH-111000	9.5	0.00	2.62	2.57	2.43	2.21	1.93	1.63	1.34	1.09	.89	.77	.73	4.35	4.35	5.03	1.889		1.49	5.52	14.77	RIGID
*				2.27	2.18	1.93	1.61	1.23	.91	.67	.50	.40	.36	.35	7.05	3.56	9.32	1.020	3.02		4.78	11.69	FLXBL

73* WITH PARABOLIC SHEAR STRESS DISTRIBUTION IN INNER RACE.

Table 7.1 Total deflection given by the approach of two flat steel platens when a steel roller is loaded between them, and also roller and platen deflections as obtained by the finite-element method.

Width of platen= length of roller= 0.45 in.

Load on Roller P lbs.	Half of Roller deflection thou.	Roller deflection thou.	Platen deflection (each) thou.	Total deflection thou.
250	0.0485	0.0970	0.0589	0.2148
500	0.0919	0.1838	0.1128	0.4094
750	0.1327	0.2654	0.1640	0.5934
1000	0.1716	0.3432	0.2133	0.7698
1250	0.2099	0.4198	0.2620	0.9438
1500	0.2475	0.4950	0.3101	1.1152
1750	0.2847	0.5694	0.3577	1.2848
2000	0.3215	0.6430	0.4049	1.4528
2500	0.3900	0.7800	0.4942	1.7684
3000	0.4570	0.9140	0.5821	2.0782
$\delta = AxP^N$		$A_2=0.6688x10^{-6}$ N=0.9031	$A_1=0.3650x10^{-6}$ N=0.9220	$A_2=0.1396x10^{-5}$ N=0.9136

Values of A are given taking unit of deflection as in.

TABLE 7.2 SUMMARY OF RESULTS OBTAINED BY FINITE ELEMENT ANALYSIS FOR STEEL RADIAL ROLLER BEARINGS.

SL NO	BEARING NUMBER	RADL LOAD LBS	RPM IN 1000	LOAD DISTRIBUTION IN THE BEARING IN POUNDS ROLLER POSITION 1	2	3	4	5	6	7	8	9	10	11	TOTAL DFLNS IN μ IN OF O.R.	I.R.	BRG.	AV STFNS LB/μ IN	BODY DFLN O.R.	EPSLN ϵ	LOAD SHRG FCTR	EQV. LOAD LBS	RACES
1	RS-220600	5000	0	1277	1251	1177	1062	919	763	609	473	368	301	279	267	267	361	13.850		1.33	5.11	7159	RIGID
*				1053	1038	979	875	728	557	393	255	159	106	89	447	234	685	7.299	245		4.21	5858	FLXBL
2	RS-220600	5000	0	1277	1251	1177	1062	919	763	609	473	368	301	279	267	267	361	13.850		1.33	5.11	7159	RIGID
*				1056	1041	981	876	730	559	396	257	161	108	90	443	235	666	7.508	229		4.22	5870	FLXBL
3	RS-220600	5000	0	1277	1251	1177	1062	919	763	609	473	368	301	279	267	267	361	13.850		1.33	5.11	7159	RIGID
*				1059	1043	982	877	731	561	398	260	163	109	92	439	235	652	7.669	217		4.24	5882	FLXBL
4	RS-220600	5000	0	1277	1251	1177	1062	919	763	609	473	368	301	279	267	267	361	13.850		1.33	5.11	7159	RIGID
*				1060	1045	984	878	732	562	400	262	165	111	93	437	236	641	7.800	208		4.24	5894	FLXBL
5	RS-220600	5000	0	1277	1251	1177	1062	919	763	609	473	368	301	279	267	267	361	13.850		1.33	5.11	7159	RIGID
*				1065	1049	987	882	736	566	404	266	168	114	96	431	236	619	8.078	190		4.26	5914	FLXBL
6	RS-220600	5000	0	1277	1251	1177	1062	919	763	609	473	368	301	279	267	267	361	13.850		1.33	5.11	7159	RIGID
*				1062	1046	985	879	733	564	402	263	166	112	94	434	236	633	7.899	201		4.25	5901	FLXBL
7	RS-220400	5000	0	1014	988	911	794	648	489	335	201	100	39	20	216	216	378	13.228		1.03	4.06	5475	RIGID
				915	898	832	719	562	378	194	36	0	0	0	375	208	702	7.123	204		3.66	4941	FLXBL
8	RS-220300	5000	0	944	914	829	697	533	357	189	48	0	0	0	202	202	429	11.655		.85	3.78	4969	RIGID
				909	889	815	687	508	292	69	0	0	0	0	381	209	810	6.173	206		3.64	4839	FLXBL
9	RS-220200	2000	0	437	427	397	350	292	229	168	114	72	47	38	99	99	161	12.422		1.12	4.37	2389	RIGID
				379	372	346	303	245	176	110	54	14	0	0	159	91	273	7.326	81		3.79	2066	FLXBL
10	RS-220200	3000	0	569	552	502	426	331	229	131	48	0	0	0	127	127	259	11.583		.89	3.79	3017	RIGID
				545	534	491	416	312	187	59	0	0	0	0	232	130	484	6.198	123		3.63	2910	FLXBL
11	RS-220200	5000	0	950	913	807	643	442	229	34	0	0	0	0	203	203	533	9.381		.69	3.80	4868	RIGID
				920	896	812	664	456	199	0	0	0	0	0	395	213	932	5.365	206		3.68	4829	FLXBL
12	RS-220200	8000	0	1554	1485	1287	985	616	229	0	0	0	0	0	320	320	949	8.430		.61	3.88	7834	RIGID
				1491	1450	1303	1044	669	207	0	0	0	0	0	639	335	1593	5.022	327		3.73	7756	FLXBL

1* THICKNESS OF OUTER RACE SHEAR AREA =0.450 INCHES
2* THICKNESS OF OUTER RACE SHEAR AREA =0.675 INCHES
3* THICKNESS OF OUTER RACE SHEAR AREA =0.900 INCHES
4* THICKNESS OF OUTER RACE SHEAR AREA =1.125 INCHES
5* THICKNESS OF OUTER RACE SHEAR AREA =1.800 INCHES
6* THICKNESS OF O.R. SHEAR AREA OF THIS AND SUBSEQUENT CASES=1.35 IN.

CONTINUED

TABLE 7.2 SUMMARY OF RESULTS OBTAINED BY FINITE ELEMENT ANALYSIS FOR STEEL RADIAL ROLLER BEARINGS.

SL NO	BEARING NUMBER	RADL LOAD LBS	RPM IN 1000	LOAD DISTRIBUTION IN THE BEARING IN POUNDS ROLLER POSITION 1	2	3	4	5	6	7	8	9	10	11	TOTAL DFLNS IN μ IN OF O.R.	I.R.	BRG.	AV STFNS LB/μ IN	BODY DFLN O.R.	EPSLN ϵ	LOAD SHRG FCTR	EQV. LOAD LBS	RACES
13	RS-220000	5000	0	1018	964	807	569	282	0	0	0	0	0	0	216	216	781	6.402		.50	4.07	5000	RIGID
				961	929	818	623	347	11	0	0	0	0	0	431	225	1188	4.209	202		3.84	4900	FLXBL
14	RS-220600	5000	0	1209	1102	797	344	0	0	0	0	0	0	0	254	254	914	5.470		.30	4.84	5575	RIGID
				1110	1046	834	469	0	0	0	0	0	0	0	524	260	1347	3.712	187		4.44	5302	FLXBL
15	RS-240600	5000	0	1277	1251	1177	1062	919	763	609	473	368	301	279	267	267	361	13.850		1.33	5.11	7159	RIGID
				986	974	920	821	674	496	326	186	96	50	37	400	337	677	7.386	202		3.94	5478	FLXBL
16	RS-240400	5000	0	1014	988	911	794	648	489	335	201	100	39	20	216	216	378	13.228		1.03	4.06	5475	RIGID
				884	874	825	728	574	371	150	0	0	0	0	361	343	817	6.120	207		3.54	4862	FLXBL
17	RS-240200	2000	0	437	427	397	350	292	229	168	114	72	47	38	99	99	161	12.422		1.12	4.37	2389	RIGID
				362	357	336	297	238	164	89	23	0	0	0	152	137	308	6.494	82		3.62	1994	FLXBL
18	RS-240200	5000	0	950	913	807	643	442	229	34	0	0	0	0	203	203	533	9.381		.69	3.80	4868	RIGID
				872	864	818	712	525	248	0	0	0	0	0	367	398	1078	4.638	209		3.49	4795	FLXBL
19	RS-240200	8000	0	1554	1485	1287	985	616	229	0	0	0	0	0	320	320	949	8.430		.61	3.88	7834	RIGID
				1399	1387	1313	1138	809	312	0	0	0	0	0	585	651	1834	4.362	334		3.50	7674	FLXBL
20	RS-240000	5000	0	1018	964	807	569	282	0	0	0	0	0	0	216	216	781	6.402		.50	4.07	5000	RIGID
				885	877	826	701	464	99	0	0	0	0	0	386	450	1350	3.704	207		3.54	4807	FLXBL
21	RS-240600	5000	0	1209	1102	797	344	0	0	0	0	0	0	0	254	254	914	5.470		.30	4.84	5575	RIGID
				962	946	856	627	191	0	0	0	0	0	0	448	572	1548	3.230	197		3.85	4962	FLXBL
22	RS-250600	5000	0	1277	1251	1177	1062	919	763	609	473	368	301	279	267	267	361	13.850		1.33	5.11	7159	RIGID
				869	872	853	780	632	429	225	66	0	0	0	349	532	789	6.337	206		3.48	5005	FLXBL
23	RS-250400	5000	0	1014	988	911	794	648	489	335	201	100	39	20	216	216	378	13.228		1.03	4.06	5475	RIGID
				834	839	828	760	628	400	97	0	0	0	0	335	630	1067	4.696	211		3.34	4854	FLXBL
24	RS-250200	2000	0	437	427	397	350	292	229	168	114	72	47	38	99	99	161	12.422		1.12	4.37	2389	RIGID
				338	339	333	307	250	164	62	0	0	0	0	141	242	396	5.051	84		3.38	1951	FLXBL
25	RS-250200	5000	0	950	913	807	643	442	229	34	0	0	0	0	203	203	533	9.381		.69	3.80	4868	RIGID
				813	821	821	773	630	351	0	0	0	0	0	328	734	1361	3.674	214		3.25	4814	FLXBL
26	RS-250200	8000	0	1554	1485	1287	985	616	229	0	0	0	0	0	320	320	949	8.430		.61	3.88	7834	RIGID
				1293	1309	1315	1246	1010	510	0	0	0	0	0	515	1209	2299	3.480	343		3.23	7701	FLXBL
27	RS-250000	5000	0	1018	964	807	569	282	0	0	0	0	0	0	216	216	781	6.402		.50	4.07	5000	RIGID
				803	816	826	785	624	263	0	0	0	0	0	330	834	1660	3.012	214		3.21	4811	FLXBL

CONTINUED

TABLE 7.2 SUMMARY OF RESULTS OBTAINED BY FINITE ELEMENT ANALYSIS FOR STEEL RADIAL ROLLER BEARINGS.

SL NO	BEARING NUMBER	RADL LOAD LBS	RPM IN 1000	LOAD DISTRIBUTION IN THE BEARING IN POUNDS ROLLER POSITION 1	2	3	4	5	6	7	8	9	10	11	TOTAL DFLNS IN μ IN OF O.R.	I.R.	BRG.	AV STFNS LB/μ IN	BODY DFLN O.R.	EPSLN ε	LOAD SHRG FCTR	EQV. LOAD LBS	RACES
28	RS-250600	5000	0	1209	1102	797	344	0	0	0	0	0	0	0	254	254	914	5.470		.30	4.84	5575	RIGID
				777	802	842	823	598	11	0	0	0	0	0	335	1130	1952	2.561	215		3.11	4836	FLXBL
29	RS-250200	2000	5	438	428	397	351	293	230	168	115	73	48	39	99	99	161	12.422		1.12	4.38	2387	RGD OR
				436	426	396	349	291	228	167	113	72	46	38							4.36		RGD IR
				340	341	335	308	252	166	63	2	2	2	2	142	243	398	5.025	84		3.40	1954	FLX OR
				338	339	333	307	250	164	61	0	0	0	0							3.38		FLX IR
30	RS-250200	2000	10	441	430	400	363	296	233	171	117	76	50	42	100	99	161	12.422		1.12	4.41	2378	RGD OR
				434	423	393	347	289	226	164	110	69	44	35							4.34		RGD IR
				345	346	340	314	257	171	66	7	7	7	7	144	245	403	4.963	84		3.45	1959	FLX OR
				338	339	333	307	250	164	59	0	0	0	0							3.38		FLX IR
31	RS-250200	2000	20	451	440	410	364	306	243	181	127	86	61	52	102	97	161	12.422		1.12	4.51	2348	RGD OR
				424	413	383	336	279	215	154	100	59	33	25							4.24		RGD IR
				363	365	359	334	278	189	76	27	27	27	27	153	252	422	4.739	84		3.63	1986	FLX OR
				336	337	332	307	251	162	49	0	0	0	0							3.36		FLX IR
32	RS-230600	5000	0	1277	1251	1177	1062	919	763	609	473	368	301	279	267	267	361	13.850		1.33	5.11	7159	RIGID
				1045	1030	969	864	718	547	385	246	150	96	79	427	258	642	7.788	201		4.18	5798	FLXBL
33	RS-230300	5000	0	944	914	829	697	533	357	189	48	0	0	0	202	202	429	11.655		.85	3.78	4969	RIGID
				903	885	816	692	513	292	60	0	0	0	0	379	239	838	5.967	206		3.61	4832	FLXBL
34	RS-230000	5000	0	1018	964	807	569	282	0	0	0	0	0	0	216	216	781	6.402		.50	4.07	5000	RIGID
				948	921	820	636	365	22	0	0	0	0	0	424	265	1219	4.102	202		3.79	4880	FLXBL
35	RS-230600	5000	0	1209	1102	797	344	0	0	0	0	0	0	0	254	254	914	5.470		.30	4.84	5575	RIGID
				1088	1032	840	496	7	0	0	0	0	0	0	515	312	1385	3.610	188		4.35	5247	FLXBL
36	RS-320600	5000	0	1277	1251	1177	1062	919	763	609	473	368	301	279	267	267	361	13.850		1.33	5.11	7159	RIGID
				974	1014	996	888	728	549	382	242	146	93	75	502	219	672	7.440	216		3.90	5782	FLXBL
37	RS-320300	5000	0	944	914	829	697	533	357	189	48	0	0	0	202	202	429	11.655		.85	3.78	4969	RIGID
				849	877	842	709	514	283	49	0	0	0	0	450	198	862	5.800	218		3.40	4823	FLXBL
38	RS-320000	5000	0	1018	964	807	569	282	0	0	0	0	0	0	216	216	781	6.402		.50	4.07	5000	RIGID
				898	919	849	649	354	4	0	0	0	0	0	505	213	1243	4.023	213		3.59	4872	FLXBL
39	RS-320600	5000	0	1209	1102	797	344	0	0	0	0	0	0	0	254	254	914	5.470		.30	4.84	5575	RIGID
				1037	1034	871	499	0	0	0	0	0	0	0	608	247	1407	3.554	198		4.15	5231	FLXBL
40	RS-340600	5000	0	1277	1251	1177	1062	919	763	609	473	368	301	279	267	267	361	13.850		1.33	5.11	7159	RIGID
				914	951	933	826	665	480	308	169	81	37	24	469	313	714	7.003	216		3.66	5390	FLXBL

CONTINUED

TABLE 7.2 SUMMARY OF RESULTS OBTAINED BY FINITE ELEMENT ANALYSIS FOR STEEL RADIAL ROLLER BEARINGS.

SL NO	BEARING NUMBER	RADL LOAD LBS	RPM IN 1000	LOAD DISTRIBUTION IN THE BEARING IN POUNDS ROLLER POSITION 1	2	3	4	5	6	7	8	9	10	11	TOTAL DFLNS IN μ IN OF O.R.	I.R.	BRG.	AV STFNS LB/μ IN	BODY DFLN O.R.	EPSLN ∈	LOAD SHRG FCTR	EQV. LOAD LBS	RACES
41	RS-340300	5000	0	944	914	829	697	533	357	189	48	0	0	0	202	202	429	11.655		.85	3.78	4969	RIGID
				819	856	842	735	553	306	26	0	0	0	0	431	357	995	5.025	221		3.28	4810	FLXBL
42	RS-340000	5000	0	1018	964	807	569	282	0	0	0	0	0	0	216	216	781	6.402		.50	4.07	5000	RIGID
				832	870	853	719	465	87	0	0	0	0	0	458	434	1401	3.569	218		3.33	4807	FLXBL
43	RS+340600	5000	0	1209	1102	797	344	0	0	0	0	0	0	0	254	254	914	5.470		.30	4.84	5575	RIGID
				904	939	885	647	190	0	0	0	0	0	0	527	553	1601	3.123	208		3.62	4945	FLXBL
44	RS-420600	5000	0	1277	1251	1177	1062	919	763	609	473	368	301	279	267	267	361	13.850		1.33	5.11	7159	RIGID
				1087	1045	906	791	705	549	378	230	129	73	55	449	240	710	7.042	251		4.35	5707	FLXBL
45	RS-420300	5000	0	944	914	829	697	533	357	189	48	0	0	0	202	202	429	11.655		.85	3.78	4969	RIGID
				959	915	775	645	508	289	42	0	0	0	0	417	219	911	5.488	245		3.84	4866	FLXBL
46	RS-420000	5000	0	1018	964	807	569	282	0	0	0	0	0	0	216	216	781	6.402		.50	4.07	5000	RIGID
				1007	951	779	597	360	12	0	0	0	0	0	480	234	1288	3.882	230		4.03	4943	FLXBL
47	RS+420600	5000	0	1209	1102	797	344	0	0	0	0	0	0	0	254	254	914	5.470		.30	4.84	5575	RIGID
				1145	1057	797	469	5	0	0	0	0	0	0	592	266	1447	3.455	201		4.58	5332	FLXBL
48	RS-440600	5000	0	1277	1251	1177	1062	919	763	609	473	368	301	279	267	267	361	13.850		1.33	5.11	7159	RIGID
				1006	973	852	747	656	489	308	158	64	18	5	412	344	751	6.658	251		4.02	5317	FLXBL
49	RS-440300	5000	0	944	914	829	697	533	357	189	48	0	0	0	202	202	429	11.655		.85	3.78	4969	RIGID
				917	888	780	680	558	320	22	0	0	0	0	389	392	1050	4.762	251		3.67	4823	FLXBL
50	RS-440000	5000	0	1018	964	807	569	282	0	0	0	0	0	0	216	216	781	6.402		.50	4.07	5000	RIGID
				930	901	789	669	475	100	0	0	0	0	0	424	467	1454	3.439	243		3.72	4826	FLXBL
51	RS+440600	5000	0	1209	1102	797	344	0	0	0	0	0	0	0	254	254	914	5.470		.30	4.84	5575	RIGID
				1002	962	817	609	211	0	0	0	0	0	0	500	583	1649	3.032	222		4.01	4985	FLXBL
52	RS-520600	5000	0	1277	1251	1177	1062	919	763	609	473	368	301	279	267	267	361	13.850		1.33	5.11	7159	RIGID
				1033	1023	976	884	726	516	362	247	156	103	85	451	231	648	7.716	212		4.13	5807	FLXBL
53	RS-520300	5000	0	944	914	829	697	533	357	189	48	0	0	0	202	202	429	11.655		.85	3.78	4969	RIGID
				896	879	816	698	514	269	42	0	0	0	0	398	206	831	6.017	217		3.58	4820	FLXBL
54	RS-520000	5000	0	1018	964	807	569	282	0	0	0	0	0	0	216	216	781	6.402		.50	4.07	5000	RIGID
				950	921	820	637	362	4	0	0	0	0	0	451	222	1212	4.125	212		3.80	4881	FLXBL
55	RS+520600	5000	0	1209	1102	797	344	0	0	0	0	0	0	0	254	254	914	5.470		.30	4.84	5575	RIGID
				1097	1037	838	489	0	0	0	0	0	0	0	550	257	1377	3.631	198		4.39	5265	FLXBL

CONTINUED

TABLE 7.2 SUMMARY OF RESULTS OBTAINED BY FINITE ELEMENT ANALYSIS FOR STEEL RADIAL ROLLER BEARINGS.

SL NO	BEARING NUMBER	RADL LOAD LBS	RPM IN 1000	LOAD DISTRIBUTION IN THE BEARING IN POUNDS ROLLER POSITION 1	2	3	4	5	6	7	8	9	10	11	TOTAL DFLNS IN μ IN OF O.R.	I.R.	BRG.	AV STFNS LB/μ IN	BODY DFLN O.R.	EPSLN ε	LOAD SHRG FCTR	EQV. LOAD LBS	RACES
56	RS-540600	5000	0	1277	1251	1177	1062	919	763	609	473	368	301	279	267	267	361	13.850		1.33	5.11	7159	RIGID
				961	954	905	829	674	460	296	174	87	40	26	416	334	693	7.215	213		3.84	5397	FLXBL
57	RS-540300	5000	0	944	914	829	697	533	357	189	48	0	0	0	202	202	429	11.655		.85	3.78	4969	RIGID
				863	858	812	731	558	295	21	0	0	0	0	378	371	968	5.165	219		3.45	4802	FLXBL
58	RS-540000	5000	0	1018	964	807	569	282	0	0	0	0	0	0	216	216	781	6.402		.50	4.07	5000	RIGID
				879	874	821	713	473	84	0	0	0	0	0	406	447	1374	3.639	217		3.52	4802	FLXBL
59	RS-540600	5000	0	1209	1102	797	344	0	0	0	0	0	0	0	254	254	914	5.470		.30	4.84	5575	RIGID
				956	942	849	639	204	0	0	0	0	0	0	471	565	1573	3.179	207		3.82	4946	FLXBL
60	RS-620600	5000	0	1277	1251	1177	1062	919	763	609	473	368	301	279	267	267	361	13.850		1.33	5.11	7159	RIGID
				1120	1103	1041	935	789	620	459	321	223	167	149	375	248	604	8.278	202		4.48	6254	FLXBL
61	RS-620300	5000	0	944	914	829	697	533	357	189	48	0	0	0	202	202	429	11.655		.85	3.78	4969	RIGID
				912	891	818	693	522	318	109	0	0	0	0	313	209	742	6.739	205		3.65	4854	FLXBL
62	RS-620000	5000	0	1018	964	807	569	282	0	0	0	0	0	0	216	216	781	6.402		.50	4.07	5000	RIGID
				962	929	817	623	351	22	0	0	0	0	0	361	225	1119	4.448	202		3.85	4899	FLXBL
63	RS-620600	5000	0	1209	1102	797	344	0	0	0	0	0	0	0	254	254	914	5.470		.30	4.84	5575	RIGID
				1118	1051	832	457	0	0	0	0	0	0	0	447	262	1277	3.915	189		4.47	5325	FLXBL
64	RS-640600	5000	0	1277	1251	1177	1062	919	763	609	473	368	301	279	267	267	361	13.850		1.33	5.11	7159	RIGID
				1028	1016	962	863	717	540	370	230	138	92	78	343	352	649	7.704	202		4.11	5743	FLXBL
65	RS-640300	5000	0	944	914	829	697	533	357	189	48	0	0	0	202	202	429	11.655		.85	3.78	4969	RIGID
				877	867	820	721	558	333	75	0	0	0	0	298	363	873	5.727	208		3.51	4828	FLXBL
66	RS-640000	5000	0	1018	964	807	569	282	0	0	0	0	0	0	216	216	781	6.402		.50	4.07	5000	RIGID
				884	875	825	702	470	112	0	0	0	0	0	320	445	1279	3.909	207		3.54	4805	FLXBL
67	RS-640600	5000	0	1209	1102	797	344	0	0	0	0	0	0	0	254	254	914	5.470		.30	4.84	5575	RIGID
				962	946	856	627	189	0	0	0	0	0	0	377	573	1479	3.381	198		3.85	4963	FLXBL
68	RS-720600	5000	0	1277	1251	1177	1062	919	763	609	473	368	301	279	267	267	361	13.850		1.33	5.11	7159	RIGID
				1160	1142	1078	972	827	660	498	361	262	204	186	339	256	578	8.651	191		4.64	6497	FLXBL
69	RS-720300	5000	0	944	914	829	697	533	357	189	48	0	0	0	202	202	429	11.655		.85	3.78	4969	RIGID
				915	892	820	696	528	332	134	0	0	0	0	274	209	693	7.215	194		3.66	4865	FLXBL
70	RS-720000	5000	0	1018	964	807	569	282	0	0	0	0	0	0	216	216	781	6.402		.50	4.07	5000	RIGID
				967	932	816	618	345	23	0	0	0	0	0	318	226	1068	4.682	192		3.87	4907	FLXBL

CONTINUED

TABLE 7.2 SUMMARY OF RESULTS OBTAINED BY FINITE ELEMENT ANALYSIS FOR STEEL RADIAL ROLLER BEARINGS.

SL NO	BEARING NUMBER	RADL LOAD LBS	RPM IN 1000	LOAD DISTRIBUTION IN THE BEARING IN POUNDS ROLLER POSITION 1	2	3	4	5	6	7	8	9	10	11	TOTAL DFLNS IN μ IN OF O.R.	I.R.	BRG.	AV STFNS LB/μ IN	BODY DFLN O.R.	EPSLN ∈	LOAD SHRG FCTR	EQV. LOAD LBS	RACES
71	RS+720600	5000	0	1209	1102	797	344	0	0	0	0	0	0	0	254	254	914	5.470		.30	4.84	5575	RIGID
				1132	1059	828	437	0	0	0	0	0	0	0	393	265	1222	4.092	181		4.53	5364	FLXBL
72	RS-740600	5000	0	1277	1251	1177	1062	919	763	609	473	368	301	279	267	267	361	13.850		1.33	5.11	7159	RIGID
				1058	1045	990	891	744	568	399	259	167	120	106	308	362	623	8.026	192		4.23	5921	FLXBL
73	RS-740300	5000	0	944	914	829	697	533	357	189	48	0	0	0	202	202	429	11.655		.85	3.78	4969	RIGID
				881	869	821	722	561	342	94	0	0	0	0	262	359	822	6.083	196		3.52	4837	FLXBL
74	RS-740000	5000	0	1018	964	807	569	282	0	0	0	0	0	0	216	216	781	6.402		.50	4.07	5000	RIGID
				886	875	825	701	470	117	0	0	0	0	0	280	444	1227	4.075	196		3.54	4805	FLXBL
75	RS+740600	5000	0	1209	1102	797	344	0	0	0	0	0	0	0	254	254	914	5.470		.30	4.84	5575	RIGID
				967	948	857	622	181	0	0	0	0	0	0	331	577	1429	3.499	189		3.87	4971	FLXBL
76	RS-820600	5000	0	1277	1251	1177	1062	919	763	609	473	368	301	279	267	267	361	13.850		1.33	5.11	7159	RIGID
				1194	1174	1096	1000	855	688	528	390	290	231	211	312	263	541	9.242	164		4.78	6672	FLXBL
77	RS-820300	5000	0	944	914	829	697	533	357	189	48	0	0	0	202	202	429	11.655		.85	3.78	4969	RIGID
				921	898	813	697	531	340	150	0	0	0	0	246	210	640	7.813	166		3.68	4873	FLXBL
78	RS-820000	5000	0	1018	964	807	569	282	0	0	0	0	0	0	216	216	781	6.402		.50	4.07	5000	RIGID
				986	941	808	610	333	16	0	0	0	0	0	282	229	1012	4.941	164		3.92	4925	FLXBL
79	RS+820600	5000	0	1209	1102	797	344	0	0	0	0	0	0	0	254	254	914	5.470		.30	4.84	5575	RIGID
				1155	1074	814	413	0	0	0	0	0	0	0	343	269	1160	4.310	157		4.62	5422	FLXBL
80	RS-840600	5000	0	1277	1251	1177	1062	919	763	609	473	368	301	279	267	267	361	13.850		1.33	5.11	7159	RIGID
				1083	1069	1002	912	764	588	420	280	187	140	125	283	369	586	8.532	165		4.33	6047	FLXBL
81	RS-840300	5000	0	944	914	829	697	533	357	189	48	0	0	0	202	202	429	11.655		.85	3.78	4969	RIGID
				886	874	815	724	563	347	107	0	0	0	0	236	358	769	6.502	168		3.54	4843	FLXBL
82	RS-840000	5000	0	1018	964	807	569	282	0	0	0	0	0	0	216	216	781	6.402		.50	4.07	5000	RIGID
				890	880	818	701	467	118	0	0	0	0	0	250	447	1173	4.263	167		3.56	4807	FLXBL
83	RS+840600	5000	0	1209	1102	797	344	0	0	0	0	0	0	0	254	254	914	5.470		.30	4.84	5575	RIGID
				977	957	849	615	169	0	0	0	0	0	0	290	585	1373	3.642	162		3.91	4987	FLXBL
84	RR-220600	5000	0	1277	1251	1177	1062	919	763	609	473	368	301	279	267	267	361	13.850		1.33	5.11	7159	RIGID
*				1160	1115	1038	930	790	644	476	331	230	173	157	347	255	590	8.475	196		4.64	6316	FLXBL

84* BEARING OUTER RACES FOR CASE NOS.84 TO 131 HAVE RIBS.

CONTINUED

TABLE 7.2 SUMMARY OF RESULTS OBTAINED BY FINITE ELEMENT ANALYSIS FOR STEEL RADIAL ROLLER BEARINGS.

SL NO	BEARING NUMBER	RADL LOAD LBS	RPM IN 1000	LOAD DISTRIBUTION IN THE BEARING IN POUNDS ROLLER POSITION 1	2	3	4	5	6	7	8	9	10	11	TOTAL DFLNS IN μ IN OF O.R.	I.R.	BRG.	AV STFNS LB/μ IN	BODY DFLN O.R.	EPSLN ∈	LOAD SHRG FCTR	EQV. LOAD LBS	RACES
85	RR-220300	5000	0	944	914	829	697	533	357	189	48	0	0	0	202	202	429	11.655		.85	3.78	4969	RIGID
				938	895	810	684	517	329	121	0	0	0	0	288	213	724	6.906	200		3.75	4868	FLXBL
86	RR-220000	5000	0	1018	964	807	569	282	0	0	0	0	0	0	216	216	781	6.402		.50	4.07	5000	RIGID
				989	932	807	612	342	24	0	0	0	0	0	333	230	1099	4.550	197		3.96	4918	FLXBL
87	RR+220600	5000	0	1209	1102	797	344	0	0	0	0	0	0	0	254	254	914	5.470		.30	4.84	5575	RIGID
				1150	1055	819	441	0	0	0	0	0	0	0	413	268	1253	3.990	184		4.60	5365	FLXBL
88	RR-240600	5000	0	1277	1251	1177	1062	919	763	609	473	368	301	279	267	267	361	13.850		1.33	5.11	7159	RIGID
				1062	1025	959	859	717	558	383	237	144	97	83	316	360	635	7.874	197		4.25	5788	FLXBL
89	RR-240300	5000	0	944	914	829	697	533	357	189	48	0	0	0	202	202	429	11.655		.85	3.78	4969	RIGID
				901	870	813	713	554	343	86	0	0	0	0	273	368	855	5.848	202		3.60	4837	FLXBL
90	RR-240000	5000	0	1018	964	807	569	282	0	0	0	0	0	0	216	216	781	6.402		.50	4.07	5000	RIGID
				906	877	817	694	465	119	0	0	0	0	0	293	451	1260	3.968	202		3.62	4809	FLXBL
91	RR+240600	5000	0	1209	1102	797	344	0	0	0	0	0	0	0	254	254	914	5.470		.30	4.84	5575	RIGID
				987	947	848	619	183	0	0	0	0	0	0	347	582	1460	3.425	193		3.95	4976	FLXBL
92	RR-320600	5000	0	1277	1251	1177	1062	919	763	609	473	368	301	279	267	267	361	13.850		1.33	5.11	7159	RIGID
				1177	1149	1077	967	826	668	508	367	265	206	187	326	259	568	8.803	186		4.71	6524	FLXBL
93	RR-320300	5000	0	944	914	829	697	533	357	189	48	0	0	0	202	202	429	11.655		.85	3.78	4969	RIGID
				926	897	816	690	524	336	141	0	0	0	0	262	211	602	7.331	189		3.70	4872	FLXBL
94	RR-320000	5000	0	1018	964	807	569	282	0	0	0	0	0	0	216	216	781	6.402		.50	4.07	5000	RIGID
				979	935	812	611	339	23	0	0	0	0	0	304	228	1056	4.735	187		3.92	4918	FLXBL
95	RR+320600	5000	0	1209	1102	797	344	0	0	0	0	0	0	0	254	254	914	5.470		.30	4.84	5575	RIGID
				1146	1063	822	427	0	0	0	0	0	0	0	376	267	1207	4.143	176		4.58	5388	FLXBL
96	RR-340600	5000	0	1277	1251	1177	1062	919	763	609	473	368	301	279	267	267	361	13.850		1.33	5.11	7159	RIGID
				1072	1051	989	887	742	574	407	264	169	121	106	296	365	613	8.157	187		4.29	5939	FLXBL
97	RR-340300	5000	0	944	914	829	697	533	357	189	48	0	0	0	202	202	429	11.655		.85	3.78	4969	RIGID
				890	873	818	717	558	346	101	0	0	0	0	250	361	812	6.158	192		3.56	4842	FLXBL
98	RR-340000	5000	0	1018	964	807	569	282	0	0	0	0	0	0	216	216	781	6.402		.50	4.07	5000	RIGID
				894	878	822	697	466	120	0	0	0	0	0	267	448	1216	4.112	191		3.58	4808	FLXBL
99	RR+340600	5000	0	1209	1102	797	344	0	0	0	0	0	0	0	254	254	914	5.470		.30	4.84	5575	RIGID
				976	951	853	616	177	0	0	0	0	0	0	316	581	1417	3.529	184		3.90	4980	FLXBL

CONTINUED

TABLE 7.2 SUMMARY OF RESULTS OBTAINED BY FINITE ELEMENT ANALYSIS FOR STEEL RADIAL ROLLER BEARINGS.

SL NO	BEARING NUMBER	RADL LOAD LBS	RPM IN 1000	LOAD DISTRIBUTION IN THE BEARING IN POUNDS ROLLER POSITION											TOTAL DFLNS IN μ IN OF			AV STFNS LB/μ IN	BODY DFLN O.R.	EPSLN ∈	LOAD SHRG FCTR	EQV. LOAD LBS	RACES
				1	2	3	4	5	6	7	8	9	10	11	O.R.	I.R.	BRG.						
100	RR-420600	5000	0	1277	1251	1177	1062	919	763	609	473	368	301	279	267	267	361	13.850		1.33	5.11	7159	RIGID
				1199	1177	1096	998	854	690	531	393	291	231	211	308	264	535	9.346	160		4.80	6679	FLXBL
101	RR-420300	5000	0	944	914	829	697	533	357	189	48	0	0	0	202	202	429	11.655		.85	3.78	4969	RIGID
				924	900	812	695	529	341	153	0	0	0	0	242	210	634	7.886	162		3.70	4876	FLXBL
102	RR-420000	5000	0	1018	964	807	569	282	0	0	0	0	0	0	216	216	781	6.402		.50	4.07	5000	RIGID
				983	943	807	607	330	17	0	0	0	0	0	277	230	1005	4.975	160		3.93	4930	FLXBL
103	RR-420600	5000	0	1209	1102	797	344	0	0	0	0	0	0	0	254	254	914	5.470		.30	4.84	5575	RIGID
				1159	1076	812	409	0	0	0	0	0	0	0	338	270	1152	4.340	152		4.64	5431	FLXBL
104	RR-440600	5000	0	1277	1251	1177	1062	919	763	609	473	368	301	279	267	267	361	13.850		1.33	5.11	7159	RIGID
				1087	1071	1001	911	763	590	423	282	188	139	124	279	371	580	8.621	160		4.35	6049	FLXBL
105	RR-440300	5000	0	944	914	829	697	533	357	189	48	0	0	0	202	202	429	11.655		.85	3.78	4969	RIGID
				889	876	814	722	561	349	110	0	0	0	0	232	359	762	6.562	163		3.56	4845	FLXBL
106	RR-440000	5000	0	1018	964	807	569	282	0	0	0	0	0	0	216	216	781	6.402		.50	4.07	5000	RIGID
				893	881	817	699	465	119	0	0	0	0	0	245	448	1166	4.268	163		3.57	4808	FLXBL
107	RR-440600	5000	0	1209	1102	797	344	0	0	0	0	0	0	0	254	254	914	5.470		.30	4.84	5575	RIGID
				980	958	848	613	168	0	0	0	0	0	0	285	586	1366	3.660	158		3.92	4990	FLXBL
108	RR-520600	5000	0	1277	1251	1177	1062	919	763	609	473	368	301	279	267	267	361	13.850		1.33	5.11	7159	RIGID
				1110	1101	1069	968	799	623	463	330	237	181	164	374	246	576	8.681	179		4.44	6328	FLXBL
109	RR-520300	5000	0	944	914	829	697	533	357	189	48	0	0	0	202	202	429	11.655		.85	3.78	4969	RIGID
				893	879	832	710	521	316	110	0	0	0	0	308	205	705	7.092	182		3.57	4848	FLXBL
110	RR-520000	5000	0	1018	964	807	569	282	0	0	0	0	0	0	216	216	781	6.402		.50	4.07	5000	RIGID
				946	920	832	633	345	17	0	0	0	0	0	354	222	1081	4.625	179		3.78	4888	FLXBL
111	RR-520600	5000	0	1209	1102	797	344	0	0	0	0	0	0	0	254	254	914	5.470		.30	4.84	5575	RIGID
				1105	1045	848	455	0	0	0	0	0	0	0	434	259	1239	4.036	169		4.42	5316	FLXBL
112	RR-540600	5000	0	1277	1251	1177	1062	919	763	609	473	368	301	279	267	267	361	13.850		1.33	5.11	7159	RIGID
				1019	1013	986	891	722	541	373	235	148	103	90	343	350	621	8.052	180		4.08	5797	FLXBL
113	RR-540300	5000	0	944	914	829	697	533	357	189	48	0	0	0	202	202	429	11.655		.85	3.78	4969	RIGID
				861	857	832	735	555	329	75	0	0	0	0	295	356	835	5.988	184		3.44	4828	FLXBL
114	RR-540000	5000	0	1018	964	807	569	282	0	0	0	0	0	0	216	216	781	6.402		.50	4.07	5000	RIGID
				869	866	839	714	465	107	0	0	0	0	0	315	440	1240	4.032	183		3.48	4804	FLXBL

CONTINUED

TABLE 7.2 SUMMARY OF RESULTS OBTAINED BY FINITE ELEMENT ANALYSIS FOR STEEL RADIAL ROLLER BEARINGS.

SL NO	BEARING NUMBER	RADL LOAD LBS	RPM IN 1000	LOAD DISTRIBUTION IN THE BEARING IN POUNDS ROLLER POSITION 1	2	3	4	5	6	7	8	9	10	11	TOTAL DFLNS IN μ IN OF O.R.	I.R.	BRG.	AV STFNS LB/μ IN	BODY DFLN O.R.	EPSLN ε	LOAD SHRG FCTR	EQV. LOAD LBS	RACES
115	RR-540600	5000	0	1209	1102	797	344	0	0	0	0	0	0	0	254	254	914	5.470		.30	4.84	5575	RIGID
				949	939	872	633	180	0	0	0	0	0	0	369	569	1441	3.470	176		3.80	4959	FLXBL
116	RR-620600	5000	0	1277	1251	1177	1062	919	763	609	473	368	301	279	267	267	361	13.850		1.33	5.11	7159	RIGID
				1156	1143	1081	990	834	661	498	362	267	211	193	341	255	558	8.961	171		4.62	6523	FLXBL
117	RR-620300	5000	0	944	914	829	697	533	357	189	48	0	0	0	202	202	429	11.655		.85	3.78	4969	RIGID
				907	889	819	706	530	331	131	0	0	0	0	275	207	669	7.474	173		3.63	4859	FLXBL
118	RR-620000	5000	0	1018	964	807	569	282	0	0	0	0	0	0	216	216	781	6.402		.50	4.07	5000	RIGID
				963	931	816	624	343	18	0	0	0	0	0	316	225	1044	4.789	171		3.85	4902	FLXBL
119	RR-620600	5000	0	1209	1102	797	344	0	0	0	0	0	0	0	254	254	914	5.470		.30	4.84	5575	RIGID
				1130	1061	827	438	0	0	0	0	0	0	0	387	264	1197	4.177	163		4.52	5364	FLXBL
120	RR-640600	5000	0	1277	1251	1177	1062	919	763	609	473	368	301	279	267	267	361	13.850		1.33	5.11	7159	RIGID
				1055	1045	992	906	749	568	398	259	170	126	112	311	360	603	8.292	172		4.22	5941	FLXBL
121	RR-640300	5000	0	944	914	829	697	533	357	189	48	0	0	0	202	202	429	11.655		.85	3.78	4969	RIGID
				874	867	820	731	562	340	92	0	0	0	0	263	356	798	6.266	175		3.50	4835	FLXBL
122	RR-640000	5000	0	1018	964	807	569	282	0	0	0	0	0	0	216	216	781	6.402		.50	4.07	5000	RIGID
				880	874	824	710	469	113	0	0	0	0	0	280	442	1203	4.156	175		3.52	4804	FLXBL
123	RR-640600	5000	0	1209	1102	797	344	0	0	0	0	0	0	0	254	254	914	5.470		.30	4.84	5575	RIGID
				963	949	857	627	177	0	0	0	0	0	0	328	576	1404	3.561	169		3.85	4969	FLXBL
124	RR-720600	5000	0	1277	1251	1177	1062	919	763	609	473	368	301	279	267	267	361	13.850		1.33	5.11	7159	RIGID
				1191	1174	1100	1006	858	689	527	390	291	234	215	313	262	528	9.470	151		4.76	6681	FLXBL
125	RR-720300	5000	0	944	914	829	697	533	357	189	48	0	0	0	202	202	429	11.655		.85	3.78	4969	RIGID
				917	896	815	701	532	340	148	0	0	0	0	247	209	626	7.987	153		3.67	4870	FLXBL
126	RR-720000	5000	0	1018	964	807	569	282	0	0	0	0	0	0	216	216	781	6.402		.50	4.07	5000	RIGID
				977	940	810	612	332	15	0	0	0	0	0	281	229	997	5.015	151		3.91	4922	FLXBL
127	RR-720600	5000	0	1209	1102	797	344	0	0	0	0	0	0	0	254	254	914	5.470		.30	4.84	5575	RIGID
				1153	1074	815	413	0	0	0	0	0	0	0	342	269	1145	4.367	144		4.61	5421	FLXBL
128	RR-740600	5000	0	1277	1251	1177	1062	919	763	609	473	368	301	279	267	267	361	13.850		1.33	5.11	7159	RIGID
				1081	1068	1005	917	767	588	419	280	188	142	128	285	369	573	8.726	152		4.32	6054	FLXBL
129	RR-740300	5000	0	944	914	829	697	533	357	189	48	0	0	0	202	202	429	11.655		.85	3.78	4969	RIGID
				883	873	816	726	563	347	106	0	0	0	0	237	356	754	6.631	154		3.53	4842	FLXBL

CONTINUED

TABLE 7.2 SUMMARY OF RESULTS OBTAINED BY FINITE ELEMENT ANALYSIS FOR STEEL RADIAL ROLLER BEARINGS.

SL NO	BEARING NUMBER	RADL LOAD LBS	RPM IN 1000	LOAD DISTRIBUTION IN THE BEARING IN POUNDS ROLLER POSITION 1	2	3	4	5	6	7	8	9	10	11	TOTAL DFLNS IN μ IN OF O.R.	I.R.	BRG.	AV STFNS LB/μ IN	BODY DFLN O.R.	EPSLN ϵ	LOAD SHRG FCTR	EQV. LOAD LBS	RACES
130	RR-740000	5000	0	1018	964	807	569	282	0	0	0	0	0	0	216	216	781	6.402		.50	4.07	5000	RIGID
				888	879	820	703	467	116	0	0	0	0	0	250	446	1158	4.318	154		3.55	4806	FLXBL
131	RR+740600	5000	0	1209	1102	797	344	0	0	0	0	0	0	0	254	254	914	5.470		.30	4.84	5575	RIGID
				975	957	851	616	168	0	0	0	0	0	0	290	584	1358	3.682	149		3.90	4986	FLXBL
132	RT-220600	5000	0	1277	1251	1177	1062	919	763	609	473	368	301	279	267	267	361	13.850		1.33	5.11	7159	RIGID
*				1673	1260	699	493	566	661	572	418	176	0	0	11	349	1080	4.630	774		6.69	6834	FLXBL
133	RT-220300	5000	0	944	914	829	697	533	357	189	48	0	0	0	202	202	429	11.655		.85	3.78	4969	RIGID
				1581	1159	573	328	329	356	290	104	0	0	0	-82	336	1341	3.729	871		6.32	6265	FLXBL
134	RT-220000	5000	0	1018	964	807	569	282	0	0	0	0	0	0	216	216	781	6.402		.50	4.07	5000	RIGID
				1587	1145	527	241	158	72	0	0	0	0	0	-87	344	1678	2.980	903		6.35	6225	FLXBL
135	RT+220600	5000	0	1209	1102	797	344	0	0	0	0	0	0	0	254	254	914	5.470		.30	4.84	5575	RIGID
				1671	1206	542	134	0	0	0	0	0	0	0	42	363	1755	2.849	806		6.68	6560	FLXBL
136	RT-220300	5000	10	950	920	834	702	537	361	191	50	7	7	7	203	202	431	11.601		.85	3.80	4972	RGD OR
				943	914	827	695	531	354	184	43	0	0	0							3.77		RGD IR
				1589	1165	577	332	332	360	292	104	7	7	7	-81	336	1345	3.717	872		6.36	6270	FLX OR
				1582	1150	570	325	326	353	286	97	0	0	0							6.33		FLX IR
137	RT-220300	5000	20	969	939	851	716	550	371	199	57	27	27	27	207	201	437	11.442		.84	3.80	4973	RGD OR
				941	911	824	689	523	343	172	29	0	0	0							3.76		RGD IR
				1612	1183	589	342	344	371	300	104	27	27	27	-75	337	1358	3.682	875		6.45	6284	FLX OR
				1584	1156	562	315	316	344	272	76	0	0	0							6.34		FLX IR
138	RT-220300	5000	30	1000	969	879	742	571	388	213	69	62	62	62	213	201	447	11.186		.84	4.00	4990	RGD OR
				938	907	818	680	510	326	151	7	0	0	0							3.75		RGD IR
				1656	1214	610	360	363	390	312	104	62	62	62	-67	338	1380	3.623	881		6.60	6312	FLX OR
				1588	1152	548	299	301	329	251	42	0	0	0							6.35		FLX IR
139	RT-240600	5000	0	1277	1251	1177	1062	919	763	609	473	368	301	279	267	267	361	13.850		1.33	5.11	7159	RIGID
				1570	1189	670	486	555	622	515	346	64	0	0	-86	530	1208	4.139	848		6.28	6486	FLXBL
140	RT-240300	5000	0	944	914	829	697	533	357	189	48	0	0	0	202	202	429	11.655		.85	3.78	4969	RIGID
				1489	1106	577	378	415	440	312	29	0	0	0	-192	589	1538	3.251	952		5.96	5933	FLXBL
141	RT-240000	5000	0	1018	964	807	569	282	0	0	0	0	0	0	216	216	781	6.402		.50	4.07	5000	RIGID
				1473	1084	545	334	330	266	23	0	0	0	0	-229	681	1938	2.580	1002		5.89	5860	FLXBL

132* BEARING OUTER RACES FOR CASE NOS.132 TO 191 HAVE CRUCIFORM SUPPORTS.

CONTINUED

TABLE 7.2 SUMMARY OF RESULTS OBTAINED BY FINITE ELEMENT ANALYSIS FOR STEEL RADIAL ROLLER BEARINGS.

SL NO	BEARING NUMBER	RADL LOAD LBS	RPM IN 1000	LOAD DISTRIBUTION IN THE BEARING IN POUNDS ROLLER POSITION 1	2	3	4	5	6	7	8	9	10	11	TOTAL DFLNS IN μ IN OF O.R.	I.R.	BRG.	AV STFNS LB/μ IN.	BODY DFLN O.R.	EPSLN ∈	LOAD SHRG FCTR	EQV. LOAD LBS	RACES
142	RT-240600	5000	0	1209	1102	797	344	0	0	0	0	0	0	0	254	254	914	5.470		.30	4.84	5575	RIGID
				1514	1116	569	311	123	0	0	0	0	0	0	-137	805	2102	2.379	938		6.06	5995	FLXBL
143	RT-240300	5000	10	950	920	834	702	537	361	191	50	7	7	7	203	202	431	11.601		.85	3.80	4972	RGD OR
				943	914	827	695	531	354	184	43	0	0	0							3.77		RGD IR
				1496	1112	581	382	426	446	316	30	7	7	7	-191	591	1543	3.240	953		5.98	5939	FLX OR
				1489	1105	575	376	413	439	309	23	0	0	0							5.96		FLX IR
144	RT-240300	5000	20	969	939	851	716	550	371	199	57	27	27	27	207	201	437	11.442		.84	3.88	4973	RGD OR
				941	911	824	689	523	343	172	29	0	0	0							3.76		RGD IR
				1518	1130	595	395	435	462	327	32	27	27	27	-187	595	1558	3.209	957		6.07	5948	FLX OR
				1490	1103	567	368	408	435	300	4	0	0	0							5.96		FLX IR
145	RT-240300	5000	30	1000	969	879	742	571	388	213	69	62	62	62	213	201	447	11.186		.84	4.00	4990	RGD OR
				938	907	818	680	510	326	151	7	0	0	0							3.75		RGD IR
				1550	1164	621	421	465	489	337	62	62	62	62	-175	603	1587	3.151	959		6.23	6007	FLX OR
				1496	1102	560	360	403	428	275	0	0	0	0							5.98		FLX IR
146	RT-320600	5000	0	1277	1251	1177	1062	919	763	609	473	368	301	279	267	267	361	13.850		1.33	5.11	7159	RIGID
				1344	1203	949	791	715	664	565	427	267	112	41	161	290	811	6.165	513		5.38	6473	FLXBL
147	RT-320300	5000	0	944	914	829	697	533	357	189	48	0	0	0	202	202	429	11.655		.85	3.78	4969	RIGID
				1143	1002	740	557	440	344	214	34	0	0	0	92	253	976	5.123	545		4.57	5201	FLXBL
148	RT-320000	5000	0	1018	964	807	569	282	0	0	0	0	0	0	216	216	781	6.402		.50	4.07	5000	RIGID
				1176	1019	720	477	260	36	0	0	0	0	0	126	266	1329	3.762	541		4.70	5245	FLXBL
149	RT-320600	5000	0	1209	1102	797	344	0	0	0	0	0	0	0	254	254	914	5.470		.30	4.84	5575	RIGID
				1317	1126	728	310	0	0	0	0	0	0	0	215	299	1450	3.448	497		5.27	5744	FLXBL
150	RT-340600	5000	0	1277	1251	1177	1062	919	763	609	473	368	301	279	267	267	361	13.850		1.33	5.11	7159	RIGID
				1224	1101	880	740	656	578	461	322	174	38	0	117	408	862	5.800	526		4.90	5908	FLXBL
151	RT-340300	5000	0	944	914	829	697	533	357	189	48	0	0	0	202	202	429	11.655		.85	3.78	4969	RIGID
				1075	957	743	603	500	379	187	0	0	0	0	57	434	1118	4.472	562		4.30	5028	FLXBL
152	RT-340000	5000	0	1018	964	807	569	282	0	0	0	0	0	0	216	216	781	6.402		.50	4.07	5000	RIGID
				1068	950	735	578	416	168	0	0	0	0	0	64	523	1517	3.296	568		4.27	4977	FLXBL
153	RT-340600	5000	0	1209	1102	797	344	0	0	0	0	0	0	0	254	254	914	5.470		.30	4.84	5575	RIGID
				1137	1011	766	517	149	0	0	0	0	0	0	127	654	1703	2.936	539		4.55	5192	FLXBL
154	RT-420600	5000	0	1277	1251	1177	1062	919	763	609	473	368	301	279	267	267	361	13.850		1.33	5.11	7159	RIGID
				1264	1205	1059	936	813	692	562	427	300	199	158	226	276	676	7.396	351		5.06	6669	FLXBL

CONTINUED

TABLE 7.2 SUMMARY OF RESULTS OBTAINED BY FINITE ELEMENT ANALYSIS FOR STEEL RADIAL ROLLER BEARINGS.

SL NO	BEARING NUMBER	RADL LOAD LBS	RPM IN 1000	LOAD DISTRIBUTION IN THE BEARING IN POUNDS ROLLER POSITION 1	2	3	4	5	6	7	8	9	10	11	TOTAL DFLNS IN μ IN OF O.R.	I.R.	BRG.	AV STFNS LB/μ IN	BODY DFLN O.R.	EPSLN ∈	LOAD SHRG FCTR	EQV. LOAD LBS	RACES
155	RT-420300	5000	0	944	914	829	697	533	357	189	48	0	0	0	202	202	429	11.655		.85	3.78	4969	RIGID
				1002	941	790	645	495	342	181	20	0	0	0	159	225	786	6.361	359		4.01	4977	FLXBL
156	RT-420000	5000	0	1018	964	807	569	282	0	0	0	0	0	0	216	216	781	6.402		.50	4.07	5000	RIGID
				1055	977	777	553	292	15	0	0	0	0	0	189	244	1146	4.363	354		4.22	5038	FLXBL
157	RT+420600	5000	0	1209	1102	797	344	0	0	0	0	0	0	0	254	254	914	5.470		.30	4.84	5575	RIGID
				1225	1105	778	353	0	0	0	0	0	0	0	250	282	1279	3.909	336		4.90	5580	FLXBL
158	RT-440600	5000	0	1277	1251	1177	1062	919	763	609	473	368	301	279	267	267	361	13.850		1.33	5.11	7159	RIGID
				1143	1095	970	860	732	593	449	311	197	114	80	194	386	719	6.954	354		4.57	6044	FLXBL
159	RT-440300	5000	0	944	914	829	697	533	357	189	48	0	0	0	202	202	429	11.655		.85	3.78	4969	RIGID
				951	906	792	681	539	360	143	0	0	0	0	144	384	918	5.447	363		3.80	4885	FLXBL
160	RT-440000	5000	0	1018	964	807	569	282	0	0	0	0	0	0	216	216	781	6.402		.50	4.07	5000	RIGID
				951	907	790	655	444	133	0	0	0	0	0	152	475	1317	3.797	364		3.80	4845	FLXBL
161	RT+440600	5000	0	1209	1102	797	344	0	0	0	0	0	0	0	254	254	914	5.470		.30	4.84	5575	RIGID
				1036	982	822	573	150	0	0	0	0	0	0	193	614	1513	3.305	351		4.14	5060	FLXBL
162	RT-520600	5000	0	1277	1251	1177	1062	919	763	609	473	368	301	279	267	267	361	13.850		1.33	5.11	7159	RIGID
				589	775	1189	1222	803	443	188	22	45	211	300	718	143	1212	4.125	739		2.36	6396	FLXBL
163	RT-520300	5000	0	944	914	829	697	533	357	189	48	0	0	0	202	202	429	11.655		.85	3.78	4969	RIGID
				458	638	1040	1063	640	203	0	0	0	0	0	706	115	1460	3.425	769		1.83	5527	FLXBL
164	RT-520000	5000	0	1018	964	807	569	282	0	0	0	0	0	0	216	216	781	6.402		.50	4.07	5000	RIGID
				448	640	1062	1058	602	52	0	0	0	0	0	848	116	1900	2.632	769		1.79	5535	FLXBL
165	RT+520600	5000	0	1209	1102	797	344	0	0	0	0	0	0	0	254	254	914	5.470		.30	4.84	5575	RIGID
				456	671	1118	1025	411	0	0	0	0	0	0	1101	121	2166	2.308	774		1.82	5508	FLXBL
166	RT-520300	5000	10	950	920	834	702	537	361	191	50	7	7	7	203	202	431	11.601		.85	3.80	4972	RGD OR
				943	914	827	695	531	354	184	43	0	0	0							3.77		RGD IR
				464	645	1048	1070	646	207	7	7	7	7	7	712	115	1467	3.408	769		1.86	5540	FLX OR
				457	638	1041	1064	639	200	0	0	0	0	0							1.83		FLX IR
167	RT-520300	5000	20.	969	939	851	716	550	371	199	57	27	27	27	207	201	437	11.442		.84	3.88	4973	RGD OR
				941	911	824	689	523	343	172	29	0	0	0							3.76		RGD IR
				480	664	1072	1093	664	217	27	27	27	27	27	731	114	1486	3.365	768		1.92	5574	FLX OR
				451	637	1044	1066	636	189	0	0	0	0	0							1.81		FLX IR

CONTINUED

TABLE 7.2 SUMMARY OF RESULTS OBTAINED BY FINITE ELEMENT ANALYSIS FOR STEEL RADIAL ROLLER BEARINGS.

SL NO	BEARING NUMBER	RADL LOAD LBS	RPM IN 1000	LOAD DISTRIBUTION IN THE BEARING IN POUNDS ROLLER POSITION 1	2	3	4	5	6	7	8	9	10	11	TOTAL DFLNS IN μ IN OF O.R.	I.R.	BRG.	AV STFNS LB/μ IN	BODY DFLN O.R.	EPSLN ε	LOAD SHRG FCTR	EQV. LOAD LBS	RACES
168	RT-520300	5000	30	1000	969	879	742	571	388	213	69	62	62	62	213	201	447	11.186		.84	4.00	4990	RGD OR
				938	907	818	680	510	326	151	7	0	0	0							3.75		RGD IR
				567	696	1112	1132	693	233	62	62	62	62	62	763	113	1519	3.292	767		2.03	5649	FLX OR
				446	634	1051	1070	631	172	0	0	0	0	0							1.78		FLX IR
169	RT-540600	5000	0	1277	1251	1177	1062	919	763	609	473	368	301	279	267	267	361	13.850		1.33	5.11	7159	RIGID
				564	737	1122	1139	739	395	133	0	0	138	234	732	212	1300	3.846	751		2.26	5995	FLXBL
175	RT-540300	5000	0	944	914	829	697	533	357	189	48	0	0	0	202	202	429	11.655		.85	3.78	4969	RIGID
				474	649	1034	1044	632	193	0	0	0	0	0	754	194	1596	3.133	773		1.90	5465	FLXBL
171	RT-540000	5000	0	1018	964	807	569	282	0	0	0	0	0	0	216	216	781	6.402		.50	4.07	5000	RIGID
				462	647	1053	1046	605	55	0	0	0	0	0	866	225	2035	2.457	772		1.85	5490	FLXBL
172	RT-540600	5000	0	1209	1102	797	344	0	0	0	0	0	0	0	254	254	914	5.470		.30	4.84	5575	RIGID
				460	668	1105	1029	441	0	0	0	0	0	0	1077	279	2303	2.171	775		1.84	5497	FLXBL
173	RT-540300	5000	10	950	920	834	702	537	361	191	50	7	7	7	203	202	431	11.601		.85	3.80	4972	RGD OR
				943	914	827	695	531	354	184	43	0	0	0							3.77		RGD IR
				474	653	1045	1056	638	190	7	7	7	7	7	768	196	1617	3.092	774		1.90	5494	FLX OR
				467	646	1038	1049	632	183	0	0	0	0	0							1.87		FLX IR
174	RT-540300	5000	20	969	939	851	716	550	371	199	57	27	27	27	207	201	437	11.442		.84	3.88	4973	RGD OR
				941	911	824	689	523	343	172	29	0	0	0							3.76		RGD IR
				496	674	1066	1075	656	207	27	27	27	27	27	777	195	1622	3.083	772		1.98	5518	FLX OR
				469	647	1039	1048	629	180	0	0	0	0	0							1.88		FLX IR
175	RT-540300	5000	30	1000	969	879	742	571	388	213	69	62	62	62	213	201	447	11.186		.84	4.00	4990	RGD OR
				938	907	818	680	510	326	151	7	0	0	0							3.75		RGD IR
				524	706	1106	1114	686	226	62	62	62	62	62	806	196	1655	3.021	771		2.10	5589	FLX OR
				462	644	1044	1052	625	164	0	0	0	0	0							1.85		FLX IR
176	RT-620600	5000	0	1277	1251	1177	1062	919	763	609	473	368	301	279	267	267	361	13.850		1.33	5.11	7159	RIGID
				960	1017	1108	1085	863	602	377	224	191	230	253	476	216	1008	4.960	587		3.84	6352	FLXBL
177	RT-620300	5000	0	944	914	829	697	533	357	189	48	0	0	0	202	202	429	11.655		.85	3.78	4969	RIGID
				741	792	875	840	611	325	45	0	0	0	0	429	174	1154	4.333	589		2.96	4893	FLXBL
178	RT-620000	5000	0	1018	964	807	569	282	0	0	0	0	0	0	216	216	781	6.402		.50	4.07	5000	RIGID
				756	809	887	813	508	87	0	0	0	0	0	531	182	1568	3.189	589		3.02	4849	FLXBL
179	RT-620600	5000	0	1209	1102	797	344	0	0	0	0	0	0	0	254	254	914	5.470		.30	4.84	5575	RIGID
				845	890	922	719	200	0	0	0	0	0	0	701	205	1789	2.795	589		3.38	4912	FLXBL

CONTINUED

TABLE 7.2 SUMMARY OF RESULTS OBTAINED BY FINITE ELEMENT ANALYSIS FOR STEEL RADIAL ROLLER BEARINGS.

SL NO	BEARING NUMBER	RADL LOAD LBS	RPM IN 1000	LOAD DISTRIBUTION IN THE BEARING IN POUNDS ROLLER POSITION 1	2	3	4	5	6	7	8	9	10	11	TOTAL DFLNS IN μ IN OF O.R.	I.R.	BRG.	AV STFNS LB/μ IN	BODY DFLN O.R.	EPSLN ε	LOAD SHRG FCTR	EQV. LOAD LBS	RACES
180	RT-640600	5000	0	1277	1251	1177	1062	919	763	609	473	368	301	279	267	267	361	13.850		1.33	5.11	7159	RIGID
				891	942	1021	992	775	525	303	148	110	145	166	456	310	1063	4.704	587		3.56	5826	FLXBL
181	RT-640300	5000	0	944	914	829	697	533	357	189	48	0	0	0	202	202	429	11.655		.95	3.78	4969	RIGID
				737	787	870	839	615	319	11	0	0	0	0	430	295	1275	3.922	589		2.95	4882	FLXBL
182	RT-640000	5000	0	1018	964	807	569	282	0	0	0	0	0	0	216	216	781	6.402		.50	4.07	5000	RIGID
				737	793	884	837	551	118	0	0	0	0	0	497	355	1701	2.939	588		2.95	4870	FLXBL
183	RT+640600	5000	0	1209	1102	797	344	0	0	0	0	0	0	0	254	254	914	5.470		.30	4.84	5575	RIGID
				778	840	922	793	323	0	0	0	0	0	0	620	454	1936	2.583	588		3.11	4865	FLXBL
184	RT-720600	5000	0	1277	1251	1177	1062	919	763	609	473	368	301	279	267	267	361	13.850		1.33	5.11	7159	RIGID
				1128	1133	1108	1039	874	673	487	343	267	243	239	355	250	874	5.721	486		4.51	6608	FLXBL
185	RT-720300	5000	0	944	914	829	697	533	357	189	48	0	0	0	202	202	429	11.655		.85	3.78	4969	RIGID
				863	863	832	745	564	341	120	0	0	0	0	293	198	978	5.112	486		3.45	4846	FLXBL
186	RT-720000	5000	0	1018	964	807	569	282	0	0	0	0	0	0	216	216	781	6.402		.50	4.07	5000	RIGID
				907	898	831	677	394	41	0	0	0	0	0	349	214	1363	3.668	486		3.63	4838	FLXBL
187	RT+720600	5000	0	1209	1102	797	344	0	0	0	0	0	0	0	254	254	914	5.470		.30	4.84	5575	RIGID
				1067	1025	852	514	1	0	0	0	0	0	0	441	252	1540	3.247	484		4.27	5215	FLXBL
188	RT-740600	5000	0	1277	1251	1177	1062	919	763	609	473	368	301	279	267	267	361	13.850		1.33	5.11	7159	RIGID
				1030	1036	1013	945	779	576	387	242	169	151	149	328	353	918	5.447	486		4.12	6003	FLXBL
189	RT-740300	5000	0	944	914	829	697	533	357	189	48	0	0	0	202	202	429	11.655		.85	3.78	4969	RIGID
				839	847	831	760	583	340	78	0	0	0	0	285	337	1101	4.541	486		3.36	4832	FLXBL
195	RT-740000	5000	0	1018	964	807	569	282	0	0	0	0	0	0	216	216	781	6.402		.50	4.07	5000	RIGID
				843	853	837	743	495	117	0	0	0	0	0	313	418	1512	3.307	486		3.37	4797	FLXBL
191	RT+740600	5000	0	1209	1102	797	344	0	0	0	0	0	0	0	254	254	914	5.470		.30	4.84	5575	RIGID
				919	923	870	669	212	0	0	0	0	0	0	374	547	1723	2.962	485		3.60	4917	FLXBL
192	RT-840600	5000	0	1277	1251	1177	1062	919	763	609	473	368	301	279	267	267	361	13.850		1.33	5.11	7159	RIGID
*				1926	1379	623	379	520	652	477	271	174	149	146	-498	753	1829	2.734	1555		7.70	7578	FLXBL
193	RT-840300	5000	0	944	914	829	697	533	357	189	48	0	0	0	202	202	429	11.655		.85	3.78	4969	RIGID
				1736	1201	455	200	301	395	237	28	0	0	0	-645	740	2033	2.459	1675		6.94	6648	FLXBL

192* BEARING OUTER RACES FOR CASE NOS.192 TO 199 HAVE PART CRUCIFORM SUPPORTS.

CONTINUED

TABLE 7.2 SUMMARY OF RESULTS OBTAINED BY FINITE ELEMENT ANALYSIS FOR STEEL RADIAL ROLLER BEARINGS.

SL NO	BEARING NUMBER	RADL LOAD LBS	RPM IN 1000	LOAD DISTRIBUTION IN THE BEARING IN POUNDS ROLLER POSITION 1	2	3	4	5	6	7	8	9	10	11	TOTAL DFLNS IN μ IN OF O.R.	I.R.	BRG.	AV STFNS LB/μ IN	BODY DFLN O.R.	EPSLN ϵ	LOAD SHRG FCTR	EQV. LOAD LBS	RACES
194	RT-840000	5000	0	1018	964	807	569	282	0	0	0	0	0	0	216	216	781	6.402		.50	4.07	5000	RIGID
				1709	1178	438	174	225	213	0	0	0	0	0	-642	819	2399	2.084	1667		6.84	6557	FLXBL
195	RT+840600	5000	0	1209	1102	797	344	0	0	0	0	0	0	0	254	254	914	5.470		.30	4.84	5575	RIGID
				1733	1206	474	163	24	0	0	0	0	0	0	-504	920	2511	1.991	1532		6.93	6645	FLXBL
196	RT-940600	5000	0	1277	1251	1177	1062	919	763	609	473	368	301	279	267	267	361	13.850		1.33	5.11	7159	RIGID
				491	739	1299	1356	768	337	176	146	161	180	185	759	192	1928	2.593	1396		1.96	6931	FLXBL
197	RT-940300	5000	0	944	914	829	697	533	357	189	48	0	0	0	202	202	429	11.655		.85	3.78	4969	RIGID
				333	574	1124	1182	596	140	0	0	0	0	0	689	141	2151	2.325	1493		1.33	5978	FLXBL
198	RT-940000	5000	0	1018	964	807	569	282	0	0	0	0	0	0	216	216	781	6.402		.50	4.07	5000	RIGID
				319	571	1143	1184	574	22	0	0	0	0	0	806	167	2594	1.928	1498		1.27	6010	FLXBL
199	RT+940600	5000	0	1209	1102	797	344	0	0	0	0	0	0	0	254	254	914	5.470	.	.30	4.84	5575	RIGID
				316	591	1197	1167	409	0	0	0	0	0	0	1019	213	2871	1.742	1515		1.26	6015	FLXBL

APPENDIX 2.1 SOLUTION OF THE SIMULTANEOUS NON-LINEAR EQUATIONS, DEVELOPED IN SECTION 2.7.4, USING THE NEWTON-RAPHSON METHOD

The solution is presented for equations developed in section 2.7.4, for the deflection distribution at the different rolling element positions. This will then lead to a determination of the load distribution. The races are considered to be symmetrical on both sides of the radial load. Variation in roller diameter can be taken into account; it is normally assumed, therefore, that due to the assumption of symmetry, the diameters of rollers on one side of the line of action of the radial load are the 'mirror image' of the other side. The assumption of symmetry allows a reduction in the number of equations to just over one half, and represent the cases of bearings considered in the finite-element section. When there is no such symmetry present, the method given here can still be used. The only difference is that the number of rolling element equilibrium equations reverts to that associated with the full number of rolling elements.

Equations (2.59) and (2.57), which are to be solved, can be rewritten in the following form

$$\frac{F_r}{2K_1} - \sum_{j=1}^{Z/2+1} \tau_j \, \delta_j^t \cos\psi_j = \chi_o \qquad \text{(A2.1.1)}$$

$$(\delta_o \cos\psi_j - c_j - \delta_j)^t - \delta_j^t - \frac{F_c}{K_1} = \chi_j \qquad \text{(A2.1.2)}$$

where,

δ_o is the radial deflection of the bearing,

$\tau_j = 0.5$ when $\psi_j = 0^o$ and 180^o

$\tau_j = 1.0$ for any other value of ψ_j

The upper limit ($Z/2+1$) in equation (A2.1.1) is for an even number of rolling elements. If the number of rolling elements is odd, it will be $(\frac{Z+1}{2})$. All the other equations written here are for an even number of rollers. For an odd number of rollers, similar changes are necessary.

In this appendix, for simplicity, the subscripts 'i' are dropped from all the δ_{ij} values. Thus δ_1, δ_2, δ_3 ... represent the deflections at the inner race, and are not the total deflections at the corresponding rolling element positions. δ_r is replaced by δ_o in equation (A2.1.2).

As the rollers cannot take tension,

$$\delta_o \cos\psi_j - c_j \geqslant 0 \qquad \text{(A2.1.3)}$$

if $\delta_o \cos\psi_j - c_j \leqslant 0, \quad \delta_j = 0$

and $\delta_{oj}^{t} = (\delta_o \cos\psi_j - c_j - \delta_j)^t = \frac{F_c}{K_1}$ (A2.1.3)

which leads to $\chi_j = 0$

The equations (A2.1.1) and (A2.1.2) are solved by using the Newton-Raphson method, taking care to satisfy conditions (A2.1.3) as follows:

1. A first assumption of δ_o, δ_1, δ_2 ... is made, according to Stribeck's solution as given in section 2.7.1. From equation (2.34)

$$P_1 = \frac{S_f \times F_r}{Z}$$

where, S_f = 4.08 for line contact and 4.37 for point contact. Using the above equation, and an expression of the form (2.28) for a single contact area,

$$\delta_o = 2\delta_1 = 2\left(\frac{P_1}{K_1}\right)^{1/t} = 2 \times \left(\frac{S_f \times F_r}{Z\, K_1}\right)^{1/t} \qquad \text{(A2.1.4)}$$

hence $\delta_j = \frac{\delta_o}{2} \cos\psi_j \qquad j = 1,2,3 \ldots$

2. Using these values of deflection, the following system of simultaneous linear equations is solved for the error vector ε_j, where j=0,1,2 .. $(\frac{Z}{2}+1)$

$$\chi_o + \frac{\partial\chi_o}{\partial\delta_o}\varepsilon_o + \frac{\partial\chi_o}{\partial\delta_1}\varepsilon_1 + \frac{\partial\chi_o}{\partial\delta_2}\varepsilon_2 + .. + \frac{\partial\chi_o}{\partial\delta_{Z/2+1}}\varepsilon_{Z/2+1} = 0$$

$$\chi_1 + \frac{\partial\chi_1}{\partial\delta_o}\varepsilon_o + \frac{\partial\chi_1}{\partial\delta_1}\varepsilon_1 + \frac{\partial\chi_1}{\partial\delta_2}\varepsilon_2 + .. + \frac{\partial\chi_1}{\partial\delta_{Z/2+1}}\varepsilon_{Z/2+1} = 0$$

$$\chi_2 + \frac{\partial\chi_2}{\partial\delta_o}\varepsilon_o + \frac{\partial\chi_2}{\partial\delta_1}\varepsilon_1 + \frac{\partial\chi_2}{\partial\delta_2}\varepsilon_2 + .. + \frac{\partial\chi_2}{\partial\delta_{Z/2+1}}\varepsilon_{Z/2+1} = 0$$

- -

$$\chi_{Z/2+1} + \frac{\partial\chi_{Z/2+1}}{\partial\delta_o}\varepsilon_o + \frac{\partial\chi_{Z/2+1}}{\partial\delta_1}\varepsilon_1 + \frac{\partial\chi_{Z/2+1}}{\partial\delta_2}\varepsilon_2 + .. + \frac{\partial\chi_{Z/2+1}}{\partial\delta_{Z/2+1}}\varepsilon_{Z/2+1} = 0$$

(A2.1.5)

The above equations can be written in a more compact form as

$$\chi_k + \sum_{j=o}^{Z_{/2}+1} \frac{\partial \chi_K}{\partial \delta_j} \varepsilon_j = 0, \quad \text{where } K=0,1,2 \ldots Z_{/2}+1 \qquad \text{(A2.1.5)}$$

3. Solving these equations for the error vector ε_k, the new deflection vector can be calculated as

$$\delta_j' = \delta_j^o + \varepsilon_j \qquad \text{where, } j=0,1 \ldots Z_{/2}+1 \qquad \text{(A2.1.6)}$$

where δ_j^o is the initial deflection vector assumed, or the deflection vector in the previous iteration.

4. The above process is repeated until the root mean square error, which is given by

$$\text{rms. error} = \left[\frac{1}{Z_{/2}+2} \sum_{j=o}^{Z_{/2}+1} \varepsilon_j^2\right]^{\frac{1}{2}} \qquad \text{(A2.1.7)}$$

is sufficiently small in comparison with the deflections.

From equation (A2.1.1)

$$\frac{\partial \chi_o}{\partial \delta_j} = -t\, \tau_j\, \delta_j^{t-1} \cos\psi_j$$

$$\frac{\partial \chi_o}{\partial \delta_o} = 0 \qquad \text{(A2.1.8)}$$

From equation (A2.1.2) it follows,

$$\frac{\partial \chi_K}{\partial \delta_j} = 0 \quad \text{when } K \neq j \text{ and } j \neq 0$$

$$= -t\left[(\delta_o \cos\psi_j - c_j - \delta_j)^{t-1} + \delta_j^{t-1}\right]$$

and if, $\delta_o \cos\psi_j - c_j \leqslant 0$, $\quad \frac{\partial \chi_K}{\partial \delta_j} = 0$ (taken)

when $K = j$

$$\frac{\partial \chi_K}{\partial \delta_o} = t\,(\delta_o \cos\psi_K - c_K - \delta_K)^{t-1} \cos\psi_K$$

$$= 0, \text{if } \delta_o \cos\psi_K - c_K \leqslant 0 \qquad \text{(A2.1.9)}$$

As 'zero' cannot be used as a subscript in a computer program, '1' is added to all the subscripts in the computer subroutine DTBN.

APPENDIX 5.1 STIFFNESS MATRIX FOR A TYPICAL ELEMENT

The development of the stiffness matrix for a typical element is given briefly in this Appendix; however, a more detailed analysis for the formation of element stiffness matrices is given in refs. 38, 39.

Assuming a linear displacement field inside the element, the strains in terms of corner displacements, as shown in fig. A5.1.1, can be expressed by the following matrix equation:

$$\begin{bmatrix} \epsilon_x \\ \epsilon_y \\ \gamma_{xy} \end{bmatrix} = \frac{1}{2\Delta} \begin{bmatrix} (y_j-y_k) & 0 & (y_k-y_i) & 0 & (y_i-y_j) & 0 \\ 0 & (x_k-x_j) & 0 & (x_i-x_k) & 0 & (x_j-x_i) \\ (x_k-x_j) & (y_j-y_k) & (x_i-x_k) & (y_k-y_i) & (x_j-x_i) & (y_i-y_j) \end{bmatrix} \begin{bmatrix} u_i \\ v_i \\ u_j \\ v_j \\ u_k \\ v_k \end{bmatrix} \quad \text{(A5.1.1a)}$$

where ϵ_x and ϵ_y are the normal strains in x and y directions respectively, γ_{xy} is the shear strain, and Δ is the area of the triangular element. Dimensions and corner displacements of the element are as shown in fig. A5.1.1. Equation (A5.1.1a) can be represented in symbolic form as

$$[\epsilon] = [B]\,[\delta] \quad \text{(A5.1.1b)}$$

The stress-strain relationship can be represented as,

$$[\sigma] = \begin{bmatrix} \sigma_x \\ \sigma_y \\ \tau_{xy} \end{bmatrix} = [D]\,[\epsilon] \quad \text{(A5.1.2)}$$

where σ_x and σ_y are the normal stresses in x and y directions respectively, and τ_{xy} is the shear stress. For isotropic materials in plane stress [D] matrix is given by,

$$[D] = \frac{E}{1-\frac{1}{m^2}} \begin{bmatrix} 1 & \frac{1}{m} & 0 \\ \frac{1}{m} & 1 & 0 \\ 0 & 0 & (1-\frac{1}{m})/2 \end{bmatrix} \quad \text{(A5.1.3)}$$

and in plane strain [D] matrix is given by,

$$[D] = \frac{E}{(1+1/m)(1-2/m)} \begin{bmatrix} (1-1/m) & (1/m) & 0 \\ (1/m) & (1-1/m) & 0 \\ 0 & 0 & (1-2/m)/2 \end{bmatrix} \quad \text{(A5.1.4)}$$

where, E and (1/m) are the Young's modulus and Poisson's ratio respectively.

The next step in the development of the stiffness of a typical element is to replace the uniform stresses acting on the edges of the element with stress resultants acting at the corners of the element. The corner forces can be expressed in terms of the three components of stresses as,

$$\begin{bmatrix} U_i \\ V_i \\ U_j \\ V_j \\ U_k \\ V_k \end{bmatrix} = \frac{t}{2} \begin{bmatrix} (y_j-y_k) & 0 & (x_k-x_j) \\ 0 & (x_k-x_j) & (y_j-y_k) \\ (y_k-y_i) & 0 & (x_i-x_k) \\ 0 & (x_i-x_k) & (y_k-y_i) \\ (y_i-y_j) & 0 & (x_j-x_i) \\ 0 & (x_j-x_i) & (y_i-y_j) \end{bmatrix} \begin{bmatrix} \sigma_x \\ \sigma_y \\ \tau_{xy} \end{bmatrix} \qquad \text{(A5.1.5a)}$$

where t is the thickness of the element. The element corner forces are as shown in fig. A5.1.1 . Comparing with equations (A5.1.1a) and (A5.1.1b), equation (A5.1.5a) can be rewritten in symbolic form as,

$$[F] = t\Delta\, [B]^T [\sigma] \qquad \text{(A5.1.5b)}$$

where $[B]^T$ is the transpose of matrix $[B]$ and $[F]$ is the element corner force matrix. Substituting equation (A5.1.1b) into equation (A5.1.2)

$$[\sigma] = [D]\,[B]\,[\delta] \qquad \text{(A5.1.6)}$$

The substitution of equation (A5.1.6) into equation (A5.1.5b) yields,

$$[F] = t\Delta\, [B]^T [D]\,[B]\,[\delta] \qquad \text{(A5.1.7)}$$

Equation (A5.1.7), which is an expression for corner forces in terms of corner displacements, can be rewritten in the following symbolic form,

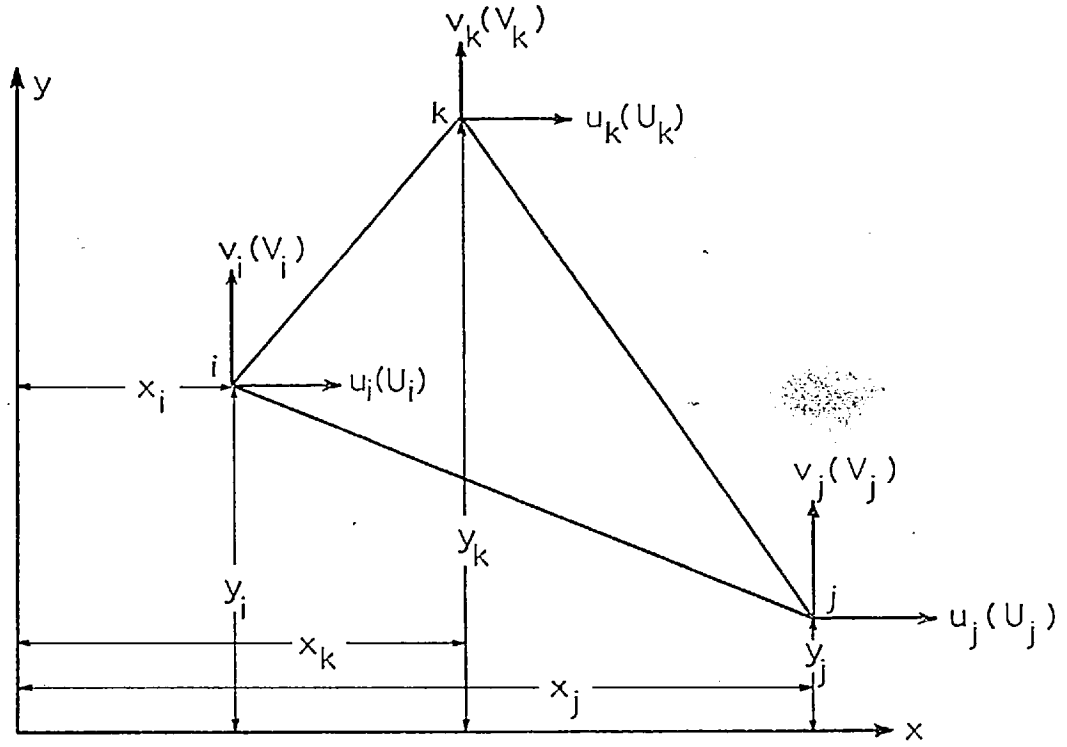
$$[F] = [k]\,[\delta] \qquad \text{(A5.1.8)}$$

where $[k]$ is the 6 x 6 stiffness matrix for the element and is given by

$$[k] = [B]^T [D]\,[B]\, t.\, \Delta \qquad \text{(A5.1.9)}$$

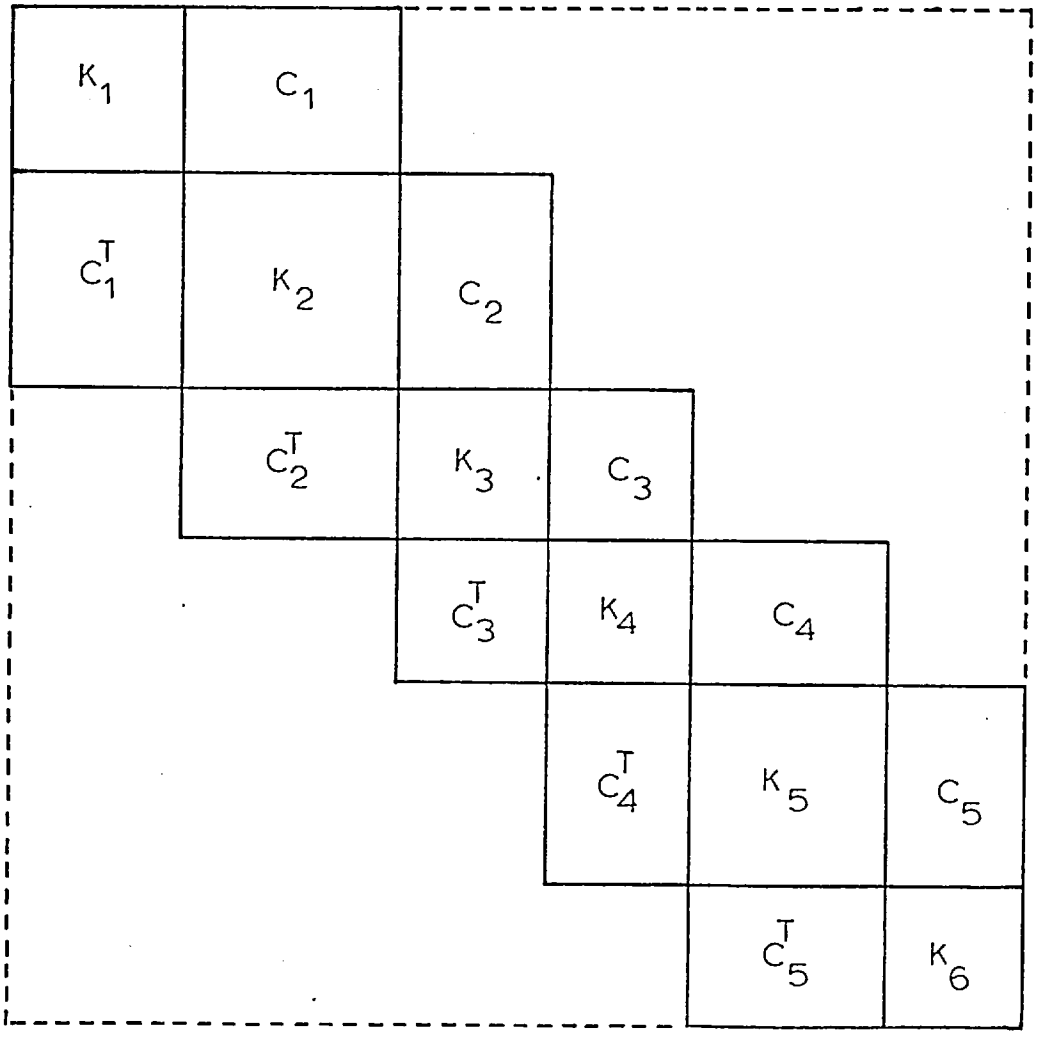
The element stress matrix and stiffness matrix given by equations (A5.1.6) and (A5.1.9) respectively are calculated by the subroutine FEM which is taken from ref. 38. In this subroutine the origin of coordinates is shifted to the centroid of the elements.

Fig.A5.1.1 A typical element.



u and v are element corner displacements.
U and V are element corner forces.

Fig.A5.2.1 Tridiagonalised partitions of the overall stiffness matrix.



APPENDIX 5.2 SOLUTION OF THE SYSTEM OF SIMULTANEOUS LINEAR EQUATIONS (5.1)

The partitioned form of the overall stiffness matrix, which corresponds to the physical division of the actual structure, can be seen in fig. A5.2.1. Every matrix, except for the matrices in the first and last portion, is connected to only two other matrices (both in rows and columns). This partitioning is known as 'tridiagonal'. Physically, this corresponds to the fact that the partitions are connected in series and the sub matrices $[C_i]$ and $[C_i]^T$ represent the coupling effects between the two adjacent parts of the structure.

Equation (5.1), with the overall stiffness matrix subdivided in a tridiagonalised manner and the deflection and load matrices sub-divided accordinly can be re-written as,

$$\begin{bmatrix} K_1 & C_1 & 0 & - & - & 0 & 0 & - & - & 0 \\ C_1^T & K_2 & C_2 & - & - & 0 & 0 & - & - & 0 \\ 0 & C_2^T & K_3 & - & - & 0 & 0 & - & - & 0 \\ - & - & - & - & - & - & - & - & - & - \\ - & - & - & - & - & - & - & - & - & - \\ 0 & 0 & 0 & - & - & K_i & C_i & - & - & 0 \\ 0 & 0 & 0 & - & - & C_i^T & K_{i+1} & - & - & 0 \\ - & - & - & - & - & - & - & - & - & - \\ - & - & - & - & - & - & - & - & - & - \\ 0 & 0 & - & - & 0 & 0 & 0 & - & - & K_N \end{bmatrix} \begin{bmatrix} \delta_1 \\ \delta_2 \\ \delta_3 \\ - \\ - \\ \delta_i \\ \delta_{i+1} \\ - \\ - \\ \delta_N \end{bmatrix} = \begin{bmatrix} F_1 \\ F_2 \\ F_3 \\ - \\ - \\ F_i \\ F_{i+1} \\ - \\ - \\ F_N \end{bmatrix} \qquad \text{(A5.2.1)}$$

Equation (A5.2.1) may be solved for the displacements $[\delta]$ produced by any given set of loads $[F]$ by a recursion relationship as given in references 42, 38. To develop this, the first two matrix equations can be written as follows:

$$F_1 = K_1 \delta_1 + C_1 \delta_2 \qquad \text{(A5.2.2)}$$

$$F_2 = C_1^T \delta_1 + K_2 \delta_2 + C_2 \delta_3 \qquad \text{(A5.2.3)}$$

In these and following equations the matrix notations [ ] have been dropped for simplicity. The first equation gives

$$\delta_1 = K_1^{-1} F_1 - K_1^{-1} C_1 \delta_2 \qquad \text{(A5.2.4)}$$

and substituting this into the second yields:

$$F_2 = C_1^T K_1^{-1} F_1 - C_1^T K_1^{-1} C_1 \delta_2 + K_2 \delta_2 + C_2 \delta_3 \qquad (A5.2.5)$$

This equation may be rearranged in the form

$$F_2 - C_1^T K_1^{-1} F_1 = [K_2 - C_1^T K_1^{-1} C_1] \delta_2 + C_2 \delta_3 \qquad (A5.2.6)$$

Finally, by defining the new symbols

$$\bar{F}_2 = F_2 - C_1^T K_1^{-1} F_1 \qquad (A5.2.7)$$

$$\bar{K}_2 = K_2 - C_1^T K_1^{-1} C_1 \qquad (A5.2.8)$$

Equation (A5.2.6) may be rewritten as

$$\bar{F}_2 = \bar{K}_2 \delta_2 + C_2 \delta_3 \qquad (A5.2.9)$$

This equation is of the form of equation (A5.2.2). So, the displacements, δ_1 of the first partition have been eliminated. The third matrix equation of equation (A5.2.1) can be written as

$$F_3 = C_2^T \delta_2 + K_3 \delta_3 + C_3 \delta_4 \qquad (A5.2.10)$$

In the same way, δ_2 can be eliminated from equations (A5.2.9) and (A5.2.10), leading to an equation equivalent to equation (A5.2.9):

$$\bar{F}_3 = \bar{K}_3 \delta_3 + C_3 \delta_4 \qquad (A5.2.11)$$

in which

$$\bar{F}_3 = F_3 - C_2^T \bar{K}_2^{-1} F_2 \qquad (A5.2.12)$$

$$\bar{K}_3 = K_3 - C_2^T \bar{K}_2^{-1} C_2 \qquad (A5.2.13)$$

The general recursion equation thus is

$$\bar{F}_i = \bar{K}_i \delta_i + C_i \delta_{(i+1)} \qquad (A5.2.14)$$

in which

$$\bar{F}_i = F_i - C_{(i-1)}^T \bar{K}_{(i-1)}^{-1} F_{(i-1)} \qquad (A5.2.15)$$

$$\bar{K}_i = K_i - C_{(i-1)}^T \bar{K}_{(i-1)}^{-1} C_{(i-1)} \qquad (A5.2.16)$$

Continuing this process of substitution and elimination leads to an equation containing displacements of the last partition 'N',

$$\bar{F}_N = \bar{K}_N \delta_N$$

that may be solved for δ_N by direct inversion. Displacements of the other partitions can then be found in the reverse sequence by back-substitution of the known values of deflection into equation of the form (A5.2.4). In the subroutine MSM, which forms the modified stiffness matrices $\bar{K}_i$, the following intermediate matrices are stored for use in other subroutines:

(a) The matrices $C_i^T \times \bar{K}_i^{-1}$, which are the product of two individual matrices C_i^T and $\bar{K}_i^{-1}$ of each partition, are stored on tape no. 2 in order of partition number. They are used later in subroutine MFM, which forms the modified force matrices $\bar{F}_i$ from equation (A5.2.15).

(b) The matrices $\bar{K}_i^{-1}$ and C_i are stored on tape no. 2 in the reverse order of partition number, so that they can be used readily in subroutine SOLVE, which is used for the back-substitution process, described earlier, to obtain the deflections.

(c) The matrices K_i and C_i are stored in tape no. 3 in order of partition number. They are used in subroutine FORCE, which is used to calculate the nodal point forces from the solved displacements.

As the outer and inner races are solved as separate problems in the finite-element part of the program, the intermediate matrices for both of them are stored in the tapes in the proper order. All the intermediate matrices stated in (a), (b) and (c) are also stored on magnetic tape no. 8 so that they can be used by the smaller version of the program to solve bearing problems having the same outer and inner races.

A physical explanation of the recursion equation solution described in this appendix is given in reference 42.

APPENDIX 5.3 EQUIVALENT RADIAL LOAD OF A RADIAL ROLLING BEARING FOR AN ARBITRARY ROLLING ELEMENT LOAD DISTRIBUTION

When the load distribution in the bearing has been found by any method described in this thesis, or some other method, the equivalent radial load acting on the bearing can be found by the following method. It is assumed that the inner ring rotates with respect to the radial load and that the outer ring is fixed. A more generalised derivation may be found in references 26, 27, 44, 12.

Fig. 5.2a shows any arbitrary rolling element load distribution of a radial rolling bearing. The equilibrium equation in the direction of radial load is

$$F_r = \sum P_j \cos\psi \simeq \int_{-\psi_{\ell 1}}^{+\psi_{\ell 2}} \frac{P_j}{\frac{\pi D_o}{Z} \times \ell} \times \ell \times \frac{D_o}{2} \cos\psi \, d\psi$$

$$= \frac{Z}{2\pi} \int_{-\psi_{\ell 2}}^{+\psi_{\ell 2}} P(\psi) \cos\psi d\psi = \frac{Z P_{ref}}{2\pi} \int_{-\psi_{\ell 1}}^{+\psi_{\ell 2}} q(\psi) \cos\psi d\psi$$

$$= Z \, P_{ref} \times M_r \qquad \text{(A5.3.1)}$$

where

P_j = load on the rolling element at position j.

$P(\psi) \simeq P_j$ as a function of ψ.

P_{ref} = any suitable reference load (P_1 of the outer race is taken as the reference load in the computer program EQLOD).

$q(\psi) = P(\psi)/P_{ref}$

$$M_r = \frac{1}{2\pi} \int_{-\psi_{\ell 1}}^{+\psi_{\ell 2}} q(\psi) \cos\psi d\psi \qquad \text{(A5.3.2)}$$

$\psi_{\ell 1}$ and $\psi_{\ell 2}$ are the extent of loaded zone on the two sides of F_r as shown in fig. 5.2a.

M_r is the same for inner or outer race if P_{ref} is the same. According to Lundberg and Palmgren (27) the equivalent rolling element load for the inner race is,

$$P_{ci} = \left[\frac{1}{2\pi} \int_{-\psi_{\ell 1}}^{+\psi_{\ell 2}} P^p(\psi) \, d\psi\right]^{1/p} \qquad \text{(A5.3.3)}$$

With line contact against both races p = 4. With point contact against both races p = 3. The above equation can be written as,

$$P_{ci} = P_{ref} \times M_1 \tag{A5.3.4}$$

where

$$M_1 = \left[\frac{1}{2\pi}\int_{-\psi_{\ell 1}}^{+\psi_{\ell 2}} q^p(\psi)\, d\psi\right]^{1/p} \tag{A5.3.5}$$

Taking $P_{ref} = P_1 = P_{max}$, for rigid races the following equations may be derived in the same way as is done in chapter 2 (equation 2.49).

$$M_r = J_r(\epsilon) = \frac{1}{2\pi}\int_{-\psi_\ell}^{+\psi_\ell} \left[1-\frac{1}{2\epsilon}(1-\cos\psi)\right]^t \cos\psi\, d\psi \tag{A5.3.6}$$

$$M_1 = J_1(\epsilon) = \left[\frac{1}{2\pi}\int_{-\psi_\ell}^{+\psi_\ell} \left\{1-\frac{1}{2\epsilon}(1-\cos\psi)\right\}^{pt} d\psi\right]^{1/p} \tag{A5.3.7}$$

where, t = 1.5 for point contact and $\simeq$ 1.1 for line contact.

The equivalent rolling element load for the outer race according to Lundberg and Palmgren (27) is

$$P_{co} = \left[\frac{1}{2\pi}\int_{-\psi_{\ell 1}}^{+\psi_{\ell 2}} P^w(\psi)\, d\psi\right]^{1/w} \tag{A5.3.8}$$

again introducing $q(\psi)$,

$$P_{co} = P_{ref} \times M_2 \tag{A5.3.9}$$

where

$$M_2 = \left[\frac{1}{2\pi}\int_{-\psi_{\ell 1}}^{+\psi_{\ell 2}} q^w(\psi)\, d\psi\right]^{1/w} \tag{A5.3.10}$$

With line contact against both the races, w = 9/2. With point contact against both races w = 10/3.

For rigid races

$$M_2 = J_2(\epsilon) = \left[\frac{1}{2\pi}\int_{-\psi_\ell}^{+\psi_\ell} \left\{1-\frac{1}{2\epsilon}(1-\cos\psi)\right\}^{wt} d\psi\right]^{1/w} \tag{A5.3.11}$$

From equations (A5.3.1), (A5.3.4) and (A5.3.9) the equivalent rolling element loads for inner and outer races are,

$$P_{ci} = P_{ref}\, M_1 = \frac{F_r}{Z} \times \frac{M_1}{M_r} \qquad \text{(A5.3.12)}$$

$$P_{co} = P_{ref}\, M_2 = \frac{F_r}{Z} \times \frac{M_2}{M_r} \qquad \text{(A5.3.13)}$$

If P_{ri} and P_{ro} are the radial loads for the respective races when $\epsilon = 0.5$, giving the same equivalent rolling element load as F_r, then

$$P_{ci} = \frac{P_{ri}}{Z} \times \frac{J_1(0.5)}{J_r(0.5)} \qquad \text{(A5.3.14)}$$

$$P_{co} = \frac{P_{ro}}{Z} \times \frac{J_2(0.5)}{J_r(0.5)} \qquad \text{(A5.3.15)}$$

From equations (A5.3.12) to (A5.3.15)

$$\frac{P_{ri}}{F_r} = \frac{J_r(0.5)}{J_1(0.5)} \times \frac{M_1}{M_r} \qquad \text{(A5.3.16)}$$

$$\frac{P_{ro}}{F_r} = \frac{J_r(0.5)}{J_2(0.5)} \times \frac{M_2}{M_r} \qquad \text{(A5.3.17)}$$

According to Lundberg and Palmgren (26) the probability S, that a race will endure for L mr (million revolutions) for a load F is given by

$$\log \frac{1}{S} = k\, F^w\, L^e \qquad \text{(A5.3.18)}$$

where k is a proportionality factor and e = w/p.

If C_i is the basic dynamic capacity for the inner race (i.e. for $L_i = 1$ and $S_i = 0.9$) and C_o is the basic dynamic capacity of the outer race (i.e. for $L_o = 1$ and $S_o = 0.9$) then equation (A5.3.18) may be used to derive the following equations to find the lives of the respective races,

$$\log \frac{1}{S_i} = \left(\frac{P_{ri}}{C_i}\right)^w L_i^e \log \frac{1}{0.9} \qquad \text{(A5.3.19)}$$

$$\log \frac{1}{S_o} = \left(\frac{P_{ro}}{C_o}\right)^w L_o^e \log \frac{1}{0.9} \qquad \text{(A5.3.20)}$$

If P_r and C are the equivalent radial load and basic dyanamic

capacity of the bearing, then

$$\log \frac{1}{S} = \left(\frac{P_r}{C}\right)^w L^e \log \frac{1}{0.9} \qquad \text{(A5.3.21)}$$

From equations (A5.3.19) to (A5.3.21), for $L_i = L_o = L$, and noting that the probability that the complete bearing will endure is the product of the probabilities that each race will endure (i.e. $S = S_i \times S_o$), it is found that

$$\left(\frac{P_r}{C}\right)^w = \left(\frac{P_{ri}}{C_i}\right)^w + \left(\frac{P_{ro}}{C_o}\right)^w \qquad \text{(A5.3.22)}$$

Substituting equations (A5.3.16) and (A5.3.17) into equation (A5.3.22), the ratio of equivalent radial load to radial load of the bearing is obtained;

$$\frac{P_r}{F_r} = \left[\left(\frac{C}{C_i} \times \frac{J_r(0.5)}{J_1(0.5)} \times \frac{M_1}{M_r}\right)^w + \left(\frac{C}{C_o} \times \frac{J_r(0.5)}{J_2(0.5)} \times \frac{M_2}{M_r}\right)^w\right]^{1/w} \qquad \text{(A5.3.23)}$$

Further, from equation (A5.3.18) the following relation may be found(see reference 26).

$$\frac{1}{C^w} = \frac{1}{C_i^w} + \frac{1}{C_o^w} \qquad \text{(A5.3.24)}$$

From reference 27 for radial roller bearing,

$$\frac{C_i}{C_o} = 1.04 \left[\frac{1-\gamma}{1+\gamma}\right]^{143/108}$$

where $\gamma = \frac{d}{D}$

For the bearings under investigation, $\gamma = \frac{d}{D} = \frac{0.3}{2.7} = \frac{1}{9}$, and hence

$$\frac{C_i}{C_o} = 1.04\ (0.8)^{143/108} = 0.774$$

The values of $J_r(0.5)$, $J_1(0.5)$ and $J_2(0.5)$ are 0.2453, 0.6495 and 0.6744 respectively, according to references 27, 12.

The computer program for calculating the equivalent radial load for radial roller bearing is given in subroutine EQLOD. This subroutine considers the symmetrical roller load distribution on both sides of the line of action of the radial load, as in the cases considered by the finite element analysis, but could be easily modified to consider unsymmetrical roller load distribution. The subroutine used for numerical integration, using Simpson's

Rule (see, for example reference 45), in the above program is called SIMRUL.

The values of $J_r(0.5)$, $J_1(0.5)$ and $J_2(0.5)$ taken in subroutine EQLOD are 0.24568, 0.65161 and 0.67543 respectively for steel bearing cases and 0.2427, 0.6473 and 0.6714 respectively for Araldite bearing cases considered. It may be noted that these are the mean values for the rigid race cases having $\in = 0.5$. These values are slightly different from the values mentioned in the previous paragraphs. This is mainly on account of the fact that the values for the constants A and N, in the equation $\delta = AP^N$ for a single roller and platen, taken in references 27, 12 are slightly different from those in the present investigation. This may also be in a small measure due to the slight rounding off of the roller load distribution data supplied to the program TABLE (of which EQLOD is a subroutine). The error due to the rounding-off of roller load distribution can be avoided by using the subroutine EQLOD in the program FINELM directly.

APPENDIX 6.1 CALCULATION OF THE SHAPE OF OUTER RACE RELIEF

If a ring is subjected to loads of equal magnitude Q and equally spaced at an angle $\Delta\Psi$ as shown in the figure at the bottom of table A6.1.1, the radial deflection at an angle Θ between any two loads is, according to reference (12) (page 191), given by

$$u_\theta = \frac{QR^3}{2EI}\left[\left\{\frac{\Delta\Psi\cos(\frac{1}{2}\Delta\Psi)}{4\sin^2(\frac{1}{2}\Delta\Psi)} + \frac{1}{2\sin(\frac{1}{2}\Delta\Psi)}\right\}\cos\theta + \frac{\theta\sin\theta}{2\sin(\frac{1}{2}\Delta\Psi)} - \frac{2}{\Delta\Psi}\right] \qquad (A6.1.1)$$

$$= C'_\theta \times \frac{QR^3}{EI}$$

where, I is the moment of inertia of the cross section of the ring, R is the ring radius to the neutral axis, and E is the Young's modulus of the ring material.

Depth of metal removed at an angle Θ (which is equal to the relief in the outer race at this angle) during machining the deflected outer race ring to a circular form just touching the valleys (which are at $\Theta = 0$) of it, is given by

$$\text{relief}_\theta = u_\theta - u_0 = (C'_\theta - C'_0)\frac{QR^3}{EI} \qquad (A6.1.2)$$

The relief is maximum at $\theta = \frac{\Delta\Psi}{2}$, where,

$$\text{relief}_{\frac{\Delta\Psi}{2}} = \text{amplitude of relief} = (C'_{\frac{\Delta\Psi}{2}} - C'_0)\frac{QR^3}{EI} \qquad (A6.1.3)$$

From (A6.1.2) and (A6.1.3)

$$\text{relief}_\theta = \frac{C'_\theta - C'_0}{C'_{\frac{\Delta\Psi}{2}} - C'_0} \times \text{amplitude of relief}$$

$$= C_\theta \times \text{amplitude of relief} \qquad (A6.1.4)$$

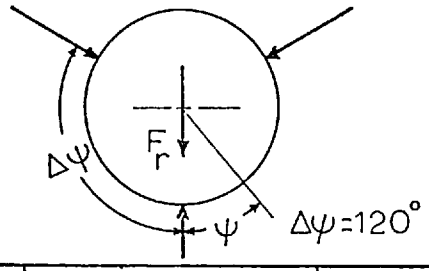
Equation (A6.1.4) suggests that it is not necessary to know the deflecting force Q. It is only necessary to deflect the ring so that the radial distance between peak to valley is equal to the desired amplitude of relief. Table A6.1.1 gives the values of the constant C_θ for relief in the outer race. It is also interesting to note that the relieved shape is independent of R, I and E.

It was found that the bi-lobed relief shape is close to the curve obtained by the equation,

$$C_\theta = \tfrac{1}{2}(1 - \cos 2\theta) \qquad (A6.1.5)$$

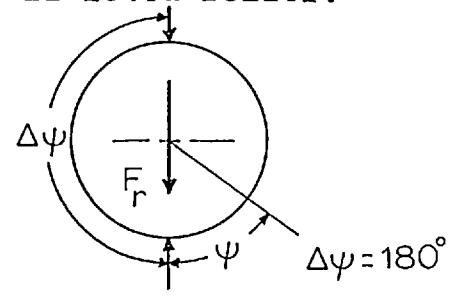
TableA6.1.1 Values of the constant C_θ for relief in the outer race. (Relief at an angle $\theta^\circ = C_\theta$ x Amplitude of relief.)

(a) Tri-lobed relief.

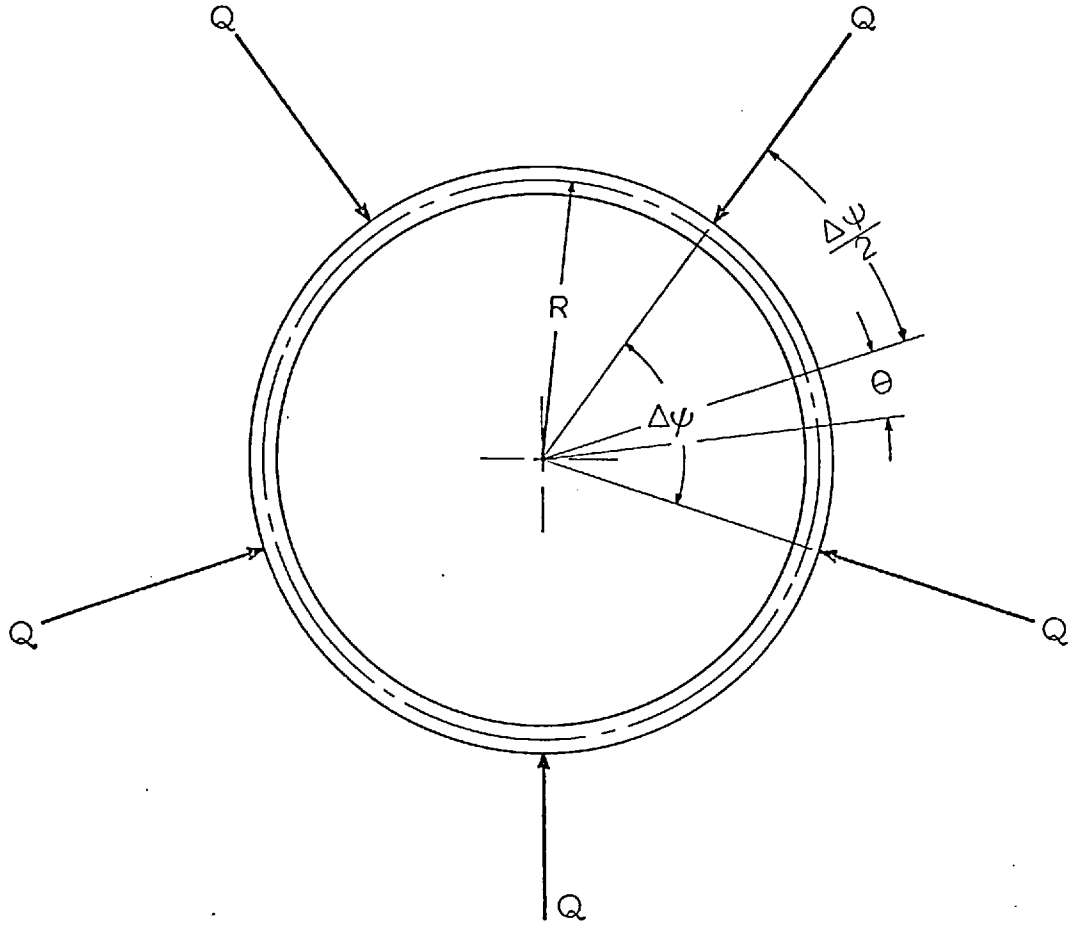


θ°	Corresponding roller position ψ_j°	C_θ
0	180	0.000
6	54	0.02064
12	72	0.0811
18	162	0.1774
24	36	0.3025
30	90	0.448
36	144	0.601
42	18	0.750
48	108	0.877
54	126	0.966
60	0	1.000

(b) Bi-lobed relief.



θ°	Corresponding roller positions ψ_j°	C_θ
0	90	0.000
18	72 & 108	0.084
36	54 & 126	0.312
54	36 & 144	0.616
72	18 & 162	0.882
90	0 & 180	1.000



APPENDIX 7.1 THICKNESS OF THE OUTER RACE SHEAR AREA - EFFECTIVE WIDTH OF THE SIDE WALLS

The housing and the outer race as a whole is termed here the 'outer race', and is connected to the side walls as shown in fig. A7.1a. Each side wall acts as the flange of a beam, and this beam may be approximated in two different ways. If the outer race track diameter (D_o) is comparatively large compared with the length of the housing (2L), the four side walls can be considered, with adjoining parts of the housing, as four beams connected together at the ends. The bending moment diagram will be approximately cosinosoidal as shown in fig. A7.1e due to the action of the radial load on the bearing and the adjoining beams, which introduce bending moments at the supports. Apart from this interaction of the bending moment diagrams the beams are considered separately as shown in fig. A7.1b, with some mean height of the web.

When the outer race track diameter (D_o) is small compared with the housing (2L), the beam may be considered as a channel with the housing as the web and the two opposite walls as the two flanges as shown in fig. A7.1a. In this case the effect of the hole is neglected on account of its size, and also because its centre is on the nautral axis of the beam.

Both models were tried and it was found that they give the same expression for the effective width of the flange. Only the procedure for the first model, which appears to be a better approximation, is given here. It may be noted that some of the symbols used here represent different variables in the main text of the thesis. The method followed here is based on the case considered in reference 46 (pages 262 - 267). It is assumed here that,

(a) the width of the flange is infinitely large and its thickness very small in comparison with the depth of the beam,

(b) the forces are transmitted to the flange in its mid-plane so that the stress distribution in the flange presents a two-dimensional problem.

The stress function in the flange is taken as a series of the form,

$$\phi = \sum_{n=1}^{\infty} f_n(y) \cos \frac{n\pi x}{L} \qquad \text{(A7.1.1)}$$

where $f_n(y)$ are functions of y. This stress function must satisfy the biharmonic equation,

$$\frac{\partial^4 \phi}{\partial x^4} + 2\frac{\partial^4 \phi}{\partial x^2 \partial y^2} + \frac{\partial^4 \phi}{\partial y^4} = 0 \qquad \text{(A7.1.2)}$$

Substituting equation (A7.1.1) in (A7.1.2) the following expression is found

$$f_n(y)=A_n e^{\frac{-n\pi y}{L}} + B_n\left(1+\frac{n\pi y}{L}\right)e^{\frac{-n\pi y}{L}} + C_n e^{\frac{n\pi y}{L}} + D_n\left(1+\frac{n\pi y}{L}\right)e^{\frac{n\pi y}{L}} \quad \text{(A7.1.3)}$$

The relations between the stresses and stress function are

$$\sigma_x = \frac{\partial^2\phi}{\partial y^2}, \quad \sigma_y = \frac{\partial^2\phi}{\partial x^2}, \tau_{xy} = -\frac{\partial^2\phi}{\partial x \partial y} \quad \text{(A7.1.4)}$$

As the flange is very wide, the stress at infinite value of y must vanish. From this condition and from equations (A7.1.3) and (A7.1.4), $C_n = D_n = 0$. Equation (A7.1.1) then becomes

$$\phi = \sum_{n=1}^{\infty} \left[A_n e^{\frac{-n\pi y}{L}} + B_n\left(1+\frac{n\pi y}{L}\right)e^{\frac{-n\pi y}{L}}\right] \cos\left(\frac{n\pi x}{L}\right) \quad \text{(A7.1.5)}$$

The true stress distribution is that which makes the strain energy of the flange, together with that of the web, a minimum. From this condition A_n and B_n are to be determined.

The strain energy of the flange is given by

$$V_1 = \frac{h}{2E}\int_0^{\infty}\int_0^{2L} \left[\sigma_x^2 + \sigma_y^2 - \frac{2}{m}\sigma_x\sigma_y + 2\left(1+\frac{1}{m}\right)\tau_{xy}^2\right] dx\, dy$$

where, $\frac{1}{m}$ is the Poisson's ratio.

Using equations (A7.1.4) and (A7.1.5) this equation becomes,

$$V_1 = h\sum_{n=1}^{\infty} \frac{n^3\pi^3}{L^2}\left(\frac{B_n^2}{E} + \frac{A_n B_n}{2G} + \frac{A_n^2}{2G}\right) \quad \text{(A7.1.6)}$$

The symmetrical bending moment distribution of the beam can be represented by the generalised series

$$M = M_o + M_1 \cos\frac{\pi x}{L} + M_2 \cos\frac{2\pi x}{L} + \ldots \quad \text{(A7.1.7)}$$

If N is the total force in the flange and e the distance from the centroid of the web to the mid-plane of the flange, and

M' = Moment taken by the web

M" = Moment taken by the flange

then,

M" = Ne

$$N = h\int_0^\infty \sigma_x\, dy = h\int_0^\infty \frac{\partial^2\phi}{\partial y^2}\, dy = h\left|\frac{\partial\phi}{\partial y}\right|_0^\infty$$

$$= -h\sum_{n=1}^{\infty} \frac{n\pi}{L} A_n \cos\frac{n\pi x}{L} = -\sum_{n=1}^{\infty} X_n \cos\frac{n\pi x}{L} \qquad \text{(A7.1.8)}$$

where $$X_n = h\frac{n\pi}{L} A_n \qquad \text{(A7.1.9)}$$

$$M' = M - Ne = M + e\sum_{n=1}^{\infty} X_n \cos\frac{n\pi x}{L}$$

$$= M_o + \sum_{n=1}^{\infty} (M_n + e\,X_n)\cos\frac{n\pi x}{L} \qquad \text{(A7.1.10)}$$

The strain energy of the web is,

$$V_2 = \int_0^{2L} \frac{N^2 dx}{2AE} + \int_0^{2L} \frac{M'^2 dx}{2EI} \qquad \text{(A7.1.11)}$$

where A and I are the cross-sectional area and moment of inertia about the horizontal axis through the centroid of the web.

Substituting equations (A7.1.8) and (A7.1.10) into equation (A7.1.11), the resulting expression for the strain energy of the web is,

$$V_2 = \frac{L}{2AE}\sum_{n=1}^{\infty} X_n^2 + \frac{M_o^2 L}{EI} + \frac{L}{2EI}\sum_{n=1}^{\infty} (M_n + eX_n)^2 \qquad \text{(A7.1.12)}$$

Using notation X_n from equation (A7.1.9) and Y_n as given below,

$$Y_n = h\frac{n\pi}{L} B_n \qquad \text{(A7.1.13)}$$

equation (A7.1.6) for strain energy of the flange becomes

$$V_1 = \frac{1}{h}\sum_{n=1}^{\infty} n\pi \left(\frac{Y_n^2}{E} + \frac{X_n Y_n}{2G} + \frac{X_n^2}{2G}\right) \qquad \text{(A7.1.14)}$$

The total strain energy of the beam is given by

$$V = V_1 + V_2$$

$$= \frac{\pi}{hE}\sum_{n=1}^{\infty} n\left[Y_n^2 + \left(1+\frac{1}{m}\right) X_n Y_n + \left(1+\frac{1}{m}\right)X_n^2\right] + \frac{L}{2AE}\sum_{n=1}^{\infty} X_n^2$$

$$+ \frac{M_o^2 L}{EI} + \frac{L}{2EI}\sum_{n=1}^{\infty} (M_n + eX_n)^2 \qquad \text{(A7.1.15)}$$

From the conditions of minimum strain energy given by

$$\frac{\partial V}{\partial Y_n} = \frac{\partial V}{\partial X_n} = 0$$

the expression for X_n can be found from equation (A7.1.15) as

$$X_n = -\frac{M_n}{e} \frac{1}{1+\frac{I}{Ae^2} + \frac{2n\pi I}{hLe^2} \cdot \frac{3m^2+2m-1}{4m^2}} \qquad \text{(A7.1.16)}$$

Considering the particular bending moment diagram in fig. A7.1e which is given by

$$M = M_1 \cos \frac{\pi x}{L}$$

the effective width can be found as follows:
Moment carried by the flange,

$$M'' = eN = -e\, X_1 \cos \frac{\pi x}{L} \qquad \text{(from equation (A7.1.8))}$$

$$= \frac{M}{1+\frac{I}{Ae^2} + \frac{2\pi I}{he^2 L} \cdot \frac{3m^2+2m-1}{4m^2}} \qquad \text{(A7.1.17)}$$

The effective width of the flange, λ, is that width such that the uniform stress distribution (given by elementary theory of bending) over the flange cross-section shown by the shaded area in fig. A7.1b gives the same bending moment M" given by equation (A7.1.17). If σ_c is the stress at the centroid of the web and σ_e the stress at the mid-plane of the flange, then from elementary theory of bending,

$$\sigma_e = \sigma_c + \frac{M'e}{I}$$

From equilibrium,

$$\lambda h \sigma_e + \sigma_c A = 0$$

$$\lambda h \sigma_e\, e = M''$$

Thus, $$M' = \frac{I}{e}(\sigma_e - \sigma_c) = \frac{I}{e}\left(1+\frac{\lambda h}{A}\right)\sigma_e$$

and $$\frac{M''}{M'+M''} = \frac{M''}{M} = \frac{\lambda h e \sigma_e}{\lambda h e \sigma_e + \frac{I}{e}\left(1+\frac{\lambda h}{A}\right)\sigma_e}$$

$$= \frac{1}{1+\frac{I}{Ae^2} + \frac{I}{\lambda he^2}} \qquad \text{(A7.1.18)}$$

From equations (A7.1.17) and (A7.1.18)

$$\frac{1}{1+\frac{I}{Ae^2}+\frac{2\pi I}{he^2 L}\,\frac{3m^2+2m-1}{4m^2}} = \frac{1}{1+\frac{I}{Ae^2}+\frac{I}{\lambda he^2}}$$

From which,

$$\lambda = \frac{2Lm^2}{\pi(3m^2+2m-1)} \qquad \text{(A7.1.19)}$$

This relation is the same for the case given in reference 46 and also found to be the same for the case of fig. A7.1a. For steel, $m = \frac{10}{3}$, and equation (A7.1.19) becomes

$$\lambda = 0.181\ L$$

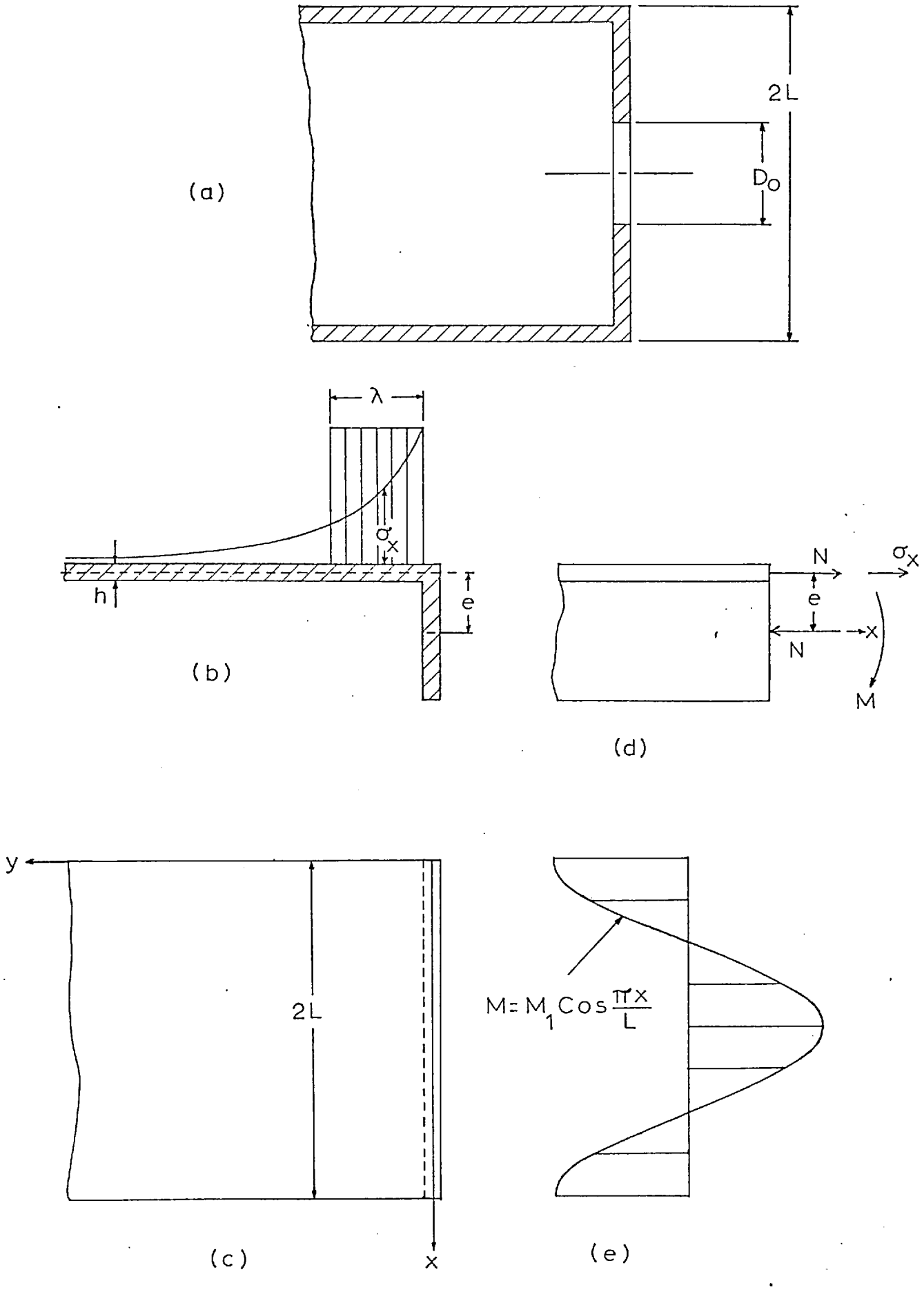
In the present case ths span of the beam is 10 in. (i.e. L = 5 in.), which makes,

$$\lambda = 0.9 \text{ in.}$$

Hence the thickness of the elements in the outer race shear area,

$$= \lambda + \text{thickness of bearing plate}$$
$$= 0.9 + 0.45$$
$$= 1.35$$

Fig. A7.1 Effective width of the side walls.



LISTING OF COMPUTER PROGRAMS

```
      PROGRAM RRBC(INPUT,OUTPUT,TAPE5=INPUT,TAPE6=OUTPUT)
C * * * * * * * * * * * * * * * * * * * * * * * * * * * * * * * * * * * * *
C     LOAD DISTRIBUTION IN A RADIAL ROLLER BEARING ASSUMING RIGID RACES.
C     FOR BALL BEARING THE SAME PROGRAM CAN BE USED WITH A LITTLE
C     MODIFICATION IN THE LOAD-DEFLECTION RELATIONSHIP OF A SINGLE
C     ROLLING ELEMENT LOADED BETWEEN TWO PLATENS.
C * * * * * * * * * * * * * * * * * * * * * * * * * * * * * * * * * * * * *
      DIMENSION COMPR(50,25),P(50,25),DELTA(50,25),CLA(25),ALOAD(50),
     1BLOAD(50),CLOAD(50),STIF(50),ASTF(50),ACOMP(25),AP(25)
   10 FORMAT(4F8.5,I3)
   11 FORMAT(1H1,38H LOAD DISTRIBUTION OF A ROLLER BEARING,10X,
     122HUSING PALMGREN FORMULA)
   12 FORMAT(///1X,16HOUTER RACE DIA.=,F7.4,7H INCHES,30X,15HINNER RACE
     1DIA=,F7.4,7H INCHES/1X,12HROLLER DIA.=,F7.4,7H INCHES,34X,17HLENGT
     2H OF ROLLER=,F7.4,7H INCHES/1X,14HNO OF ROLLERS=,I3/1X,37HMODULUS
     3OF ELASTICITY OF ROLLER MAT.=,F10.1,4H PSI,9X,35HMODULUS OF ELASTI
     4CITY OF RACE MAT.=,F10.1,4H PSI/1X,29HPOISSON RATIO OF ROLLER MAT.
     5=,F5.2,26X,27HPOISSON RATIO OF RACE MAT.=,F5.2)
   26 FORMAT(//1X,19HNEGATIVE CLEARANCE=,F8.5,7H INCHES,10X,24HDLS. NEGA
     1TIVE CLEARANCE=,F8.5)
   55 FORMAT(//1X,12HNO CLEARANCE,F8.5,7H INCHES,10X,14HDLS CLEARANCE=,
     1 F8.5)
   76 FORMAT(//1X,19HPOSITIVE CLEARANCE=,F8.5,7H INCHES,10X,24HDLS. POSI
     1TIVE CLEARANCE=,F8.5)
  141 FORMAT(/1X,10HEXT. LOAD=,F6.0,3H LB,5X,14HAV. STIFFNESS=,F6.0,
     18H LB/THOU,3X,16HINST. STIFFNESS=,F6.0,8H LB/THOU,1X,22HDEFLECTION
     2 OF BEARING=,F4.2,5H THOU)
  142 FORMAT(1X,10HDLS. LOAD=,F8.5,6X,16HDLS PK RLR LOAD=,F8.5,
     17X,14HDLS BRG STFNS=,F6.3,11X,20HDLS DFLN OF BEARING=,F7.5)
  143 FORMAT(1X,18HRDL LD SHRNG FCTR=,F5.2,1X,18HDLS PK RLR RDL LD=,
     1F8.5,5X,8HEPSILON=,F5.2,18X,13HBEARING LIFE=,F9.2,3H MR)
  144 FORMAT(1X,21HCOMPR. OF EACH ROLLER,2X,(13(F7.2)))
  145 FORMAT(1X,19HLOAD ON EACH ROLLER,4X,(13(F7.0)))
  161 FORMAT(1X,21HLOAD SHEARING FACTOR=,F5.2,29X,8HEPSILON=,F5.2,18X,
     113HBEARING LIFE=,F9.2,3H MR)
C     DLS. LOAD= EXT. LOAD /(L**2*E),     L= DIA OF ROLLER
C     DLS.CLEARANCE= RAD. CLEARANCE / L,    DLS. DEFLECTN.= DEFLECTN/L
C     DLS. PEAK RLR. LOAD= P(1) / LOAD,  DLS STIFFNESS=STIFFNESS/(E*L)
C     RDL LD. SHRNG FCTR= RDL COMP. OF LOAD ON PEAK RLR/LOAD*NO OF RLR
  100 READ(5,10)DB,DI,D,AL,N
C     DB=OUTER RACE DIAMETER, DI=INNER RACE DIAMETER, D=ROLLER DIAMETER,
C     AL=LENGTH OF ROLLER, N=NUMBER OF ROLLING ELEMENTS.
      E1=30000000.0
      E2=30000000.0
      AM1=10./3.
      AM2=10./3.
      WRITE(6,11)
      WRITE(6,12)DB,DI,D,AL,N,E1,E2,AM1,AM2
      A=2.*3.14159/FLOAT(N)
C     PALMGREN FORMULA
      CONST=2.*0.00031/(2.205**0.9*AL**0.8*25.4**1.8)
C     DELTA=CONST*P**0.9
      N1=N/2
      PLAY=(DB-DI)/2.-D
      RL=D
      APLA=PLAY/RL
      IF(N.NE.2*N1)GO TO 53
      N2=N/4
      IF(N.EQ.N2*4)GO TO 51
      J=(N+2)/4
      GO TO 101
```

```
   51 J=N/4+1
      GO TO 101
   53 N3=(N+1)/4
      IF(N.NE.4*N3)GO TO 54
      J=(N+1)/4
      GO TO 101
   54 J=(N+3)/4
  101 IDB=DB*10.**5
      IDI=DI*10.**5
      ID=D*10.**5
      IF((IDB-IDI)/2-ID)20,50,70
C     NEGATIVE CLEARANCE
   20 WRITE(6,26)PLAY,APLA
      DELO=D-(DB-DI)/2.
      IF(N.NE.2*N1)GO TO 103
      NO=N/2+1
      GO TO 102
  103 NO=(N+1)/2
  102 DO 45 I=1,40,1
      DEL=FLOAT(I*5)/100000.
      PI=0.0
      DO 40 M=1,NO,1
      K=M-1
      IF(DELO+DEL*COS(FLOAT(K)*A))41,41,42
   41 COMPR(I,M)=0.0
      GO TO 43
   42 COMPR(I,M)=DELO+DEL*COS(FLOAT(K)*A)
   43 P(I,M)=(COMPR(I,M)/CONST)**(1./0.9)
      PI=PI+2.*P(I,M)*COS(FLOAT(K)*A)
   40 CONTINUE
      IF(N.NE.2*N1)GO TO 56
      ALOAD(I)=PI-(P(I,1)+P(I,NO)*COS(FLOAT(NO-1)*A))
      GO TO 57
   56 ALOAD(I)=PI-P(I,1)
   57 STIF(I)=ALOAD(I)/(DEL*1000.)
      IF(I.GE.3)GO TO 58
      IF(I.EQ.2)GO TO 71
      GO TO 45
   71 ASTF(I-1)=ALOAD(I)*10.
      GO TO 45
   58 ASTF(I-1)=(ALOAD(I)-ALOAD(I-2))*10.
   45 CONTINUE
      EXLD=500.
      IF(ALOAD(1).LT.EXLD)GO TO 130
      EXLD=1000.
      IF(ALOAD(1).LT.EXLD)GO TO 130
      EXLD=2000.
  130 DO 150 I=1,39,1
      IF(ALOAD(I).LT.EXLD)GO TO 150
      IF(ALOAD(I-1).GT.EXLD) GO TO 150
      CO=(EXLD-ALOAD(I-1))/(ALOAD(I)-ALOAD(I-1))
      DO 140 M=1,NO,1
      ACOMP(M)=(COMPR(I-1,M)+CO*(COMPR(I,M)-COMPR(I-1,M)))*1000.
      AP(M)=P(I-1,M)+CO*(P(I,M)-P(I-1,M))
  140 CONTINUE
      AVSTF=STIF(I-1)+CO*(STIF(I)-STIF(I-1))
      STF=ASTF(I-1)+CO*(ASTF(I)-ASTF(I-1))
      DEFL=ACOMP(1)-DELO*1000.
      DLD=EXLD/(RL**2*E1)
      DPRLD=AP(1)/EXLD
      DBSTF=STF/(E1*RL)*1000.
      DBDFL=DEFL/(RL*1000.)
      PLD=(-PLAY/CONST)**(1./0.9)
      RLSF=(AP(1)-PLD)/EXLD*FLOAT(N)
      DPRL=(AP(1)-PLD)/EXLD
```

```
      DPLD=PLD/EXLD
      DELR=DEFL/1000.
      CALL BLIFE (PLAY,DELR,DI,D,AL,EXLD,ALIFE,EPS,N)
      WRITE(6,141)EXLD,AVSTF,STF,DEFL
      WRITE(6,142)DLD,DPRLD,DBSTF,DBDFL
      WRITE(6,143)RLSF,DPRL,EPS,ALIFE
      WRITE(6,144)(ACOMP(M),M=1,NO,1)
      WRITE(6,145)(AP(M),M=1,NO,1)
  150 CONTINUE
      IF(EXLD.LT.1000.)GO TO 151
      IF(EXLD.LT.4000.) GO TO 152
      EXLD=EXLD+2000.
      IF(EXLD.LE.10000.) GO TO 130
      GO TO 95
  151 EXLD=1000.
      GO TO 130
  152 EXLD=EXLD+1000.
      GO TO 130
C     NO CLEARANCE
   50 WRITE(6,55)PLAY,APLA
      DO 65 I=1,40,1
      DELTA(I,1)=FLOAT(I*5)/100000.
      P(I,1)=(DELTA(I,1)/CONST)**(1./0.9)
      BLOAD(I)=P(I,1)
      DO 60 M=2,J,1
      DELTA(I,M)=DELTA(I,1)*COS(FLOAT(M-1)*A)
      P(I,M)=(DELTA(I,M)/CONST)**(1./0.9)
      B=M-1
      BLOAD(I)=BLOAD(I)+2.*P(I,M)*COS(B*A)
   60 CONTINUE
      STIF(I)=BLOAD(I)/(DELTA(I,1)*1000.)
      IF(I.GE.3)GO TO 67
      IF(I.EQ.2) GO TO 66
      GO TO 65
   66 ASTF(I-1)=BLOAD(I)*10.
      GO TO 65
   67 ASTF(I-1)=(BLOAD(I)-BLOAD(I-2))*10.
   65 CONTINUE
      EXLD=500.
      IF(BLOAD(1).LT.EXLD)GO TO 160
      EXLD=1000.
      IF(BLOAD(1).LT.EXLD)GO TO 160
      EXLD=2000.
  160 DO 170 I=1,39,1
      IF(BLOAD(I).LT.EXLD)GO TO 170
      IF(BLOAD(I-1).GT.EXLD)GO TO 170
      CO=(EXLD-BLOAD(I-1))/(BLOAD(I)-BLOAD(I-1))
      DO 165 M=1,J,1
      ACOMP(M)=(DELTA(I-1,M)+CO*(DELTA(I,M)-DELTA(I-1,M)))*1000.
      AP(M)=P(I-1,M)+CO*(P(I,M)-P(I-1,M))
  165 CONTINUE
      AVSTF=STIF(I-1)+CO*(STIF(I)-STIF(I-1))
      STF=ASTF(I-1)+CO*(ASTF(I)-ASTF(I-1))
      DEFL=ACOMP(1)
      DLD=EXLD/(RL**2*E1)
      DPRLD=AP(1)/EXLD
      DBSTF=STF/(E1*RL)*1000.
      DBDFL=DEFL/(RL*1000.)
      RLSF=AP(1)/EXLD*FLOAT(N)
      DELR=DEFL/1000.
      CALL BLIFE (PLAY,DELR,DI,D,AL,EXLD,ALIFE,EPS,N)
      WRITE(6,141)EXLD,AVSTF,STF,DEFL
      WRITE(6,142)DLD,DPRLD,DBSTF,DBDFL
      WRITE(6,161)RLSF,EPS,ALIFE
      WRITE(6,144)(ACOMP(M),M=1,J,1)
```

```
      WRITE(6,145)(AP(M),M=1,J,1)
  170 CONTINUE
      IF(EXLD.LT.1000.) GO TO 183
      IF(EXLD.LT.4000.) GO TO 182
      EXLD=EXLD+2000.
      IF(EXLD.LE.10000.) GO TO 160
      GO TO 95
  183 EXLD=1000.
      GO TO 160
  182 EXLD=EXLD+1000.
      GO TO 160
C     POSITIVE CLEARANCE
   70 WRITE(6,76)PLAY,APLA
      DO 90 I=1,40,1
      DELTA(I,1)=FLOAT(I*5)/100000.
      P(I,1)=(DELTA(I,1)/CONST)**(1./0.9)
      CLOAD(I)=P(I,1)
      DO 80 M=2,J,1
      CLA(M)=((DB-DI)/2.-D)*(1.-COS(FLOAT(M-1)*A))
      C=M-1
      IF(CLA(M)-DELTA(I,1)*COS(C*A))73,74,74
   73 DELTA(I,M)=DELTA(I,1)*COS(FLOAT(M-1)*A)-CLA(M)
      GO TO 75
   74 DELTA(I,M)=0.0
   75 P(I,M)=(DELTA(I,M)/CONST)**(1./0.9)
      CLOAD(I)=CLOAD(I)+2.*P(I,M)*COS(C*A)
   80 CONTINUE
      STIF(I)=CLOAD(I)/(DELTA(I,1)*1000.)
      IF(I.GE.3)GO TO 84
      IF(I.EQ.2)GO TO 83
      GO TO 90
   83 ASTF(I-1)=CLOAD(I)*10.
      GO TO 90
   84 ASTF(I-1)=(CLOAD(I)-CLOAD(I-2))*10.
   90 CONTINUE
      EXLD=500.
      IF(CLOAD(1).LT.EXLD)GO TO 171
      EXLD=1000.
      IF(CLOAD(1).LT.EXLD) GO TO 171
      EXLD=2000.
  171 DO 180 I=1,39,1
      IF(CLOAD(I).LT.EXLD)GO TO 180
      IF(CLOAD(I-1).GT.EXLD)GO TO 180
      CO=(EXLD-CLOAD(I-1))/(CLOAD(I)-CLOAD(I-1))
      DO 175 M=1,J,1
      ACOMP(M)=(DELTA(I-1,M)+CO*(DELTA(I,M)-DELTA(I-1,M)))*1000.
      AP(M)=P(I-1,M)+CO*(P(I,M)-P(I-1,M))
  175 CONTINUE
      AVSTF=STIF(I-1)+CO*(STIF(I)-STIF(I-1))
      STF=ASTF(I-1)+CO*(ASTF(I)-ASTF(I-1))
      DEFL=ACOMP(1)
      DLD=EXLD/(RL**2*E1)
      DPRLD=AP(1)/EXLD
      DBSTF=STF/(E1*RL)*1000.
      DBDFL=DEFL/(RL*1000.)
      RLSF=AP(1)/EXLD*FLOAT(N)
      DELR=DEFL/1000.+PLAY
      CALL BLIFE (PLAY,DELR,DI,D,AL,EXLD,ALIFE,EPS,N)
      WRITE(6,141)EXLD,AVSTF,STF,DEFL
      WRITE(6,142)DLD,DPRLD,DBSTF,DBDFL
      WRITE(6,161)RLSF,EPS,ALIFE
      WRITE(6,144)(ACOMP(M),M=1,J,1)
      WRITE(6,145)(AP(M),M=1,J,1)
  180 CONTINUE
```

```
      IF(EXLD.LT.1000.) GO TO 191
      IF(EXLD.LT.4000.) GO TO 192
      EXLD=EXLD+2000.
      IF(EXLD.LE.10000.) GO TO 171
      GO TO 95
  191 EXLD=1000.
      GO TO 171
  192 EXLD=EXLD+1000.
      GO TO 171
   95 GO TO 100
      END

      SUBROUTINE BLIFE(PLAY,DELR,DI,D,AL,EXLD,ALIFE,EPS,N)
C * * * * * * * * * * * * * * * * * * * * * * * * * * * * * * * * * * * * * *
C     SUBROUTINE TO CALCULATE BEARING LIFE ACCORDING TO THE METHOD GIVEN
C     BY J. H. RUMBARGER, (1961). REF.11.
C * * * * * * * * * * * * * * * * * * * * * * * * * * * * * * * * * * * * * *
      DIMENSION EPSL(14),R(10),FC(14,10),AFC(14)
      DATA(EPSL(I),I=1,14)/0.1,0.2,0.3,0.4,0.5,0.6,0.7,0.8,0.9,1.0,1.25,
     11.67,2.5,5.0/,(R(J),J=1,10)/0.01,0.03,0.06,0.09,0.10,0.15,0.18,
     20.20,0.26,0.30/,F/49500./,((FC(I,J),I=1,14),J=1,10)/0.059,0.077,
     30.084,0.091,0.095,0.097,0.097,0.097,0.094,0.090,0.071,0.052,0.033,
     40.015,0.076,0.097,0.107,0.115,0.120,0.123,0.124,0.123,0.120,0.114,
     50.091,0.066,0.042,0.019,0.088,0.111,0.124,0.133,0.139,0.143,0.144,
     60.142,0.139,0.132,0.104,0.076,0.049,0.023,0.095,0.120,0.134,0.144,
     70.150,0.154,0.155,0.153,0.149,0.142,0.112,0.082,0.053,0.024,0.096,
     80.122,0.136,0.146,0.152,0.156,0.157,0.156,0.152,0.144,0.115,0.084,
     90.053,0.025,0.101,0.128,0.142,0.153,0.159,0.163,0.164,0.162,0.158,
     10.150,0.119,0.087,0.056,0.026,0.101,0.129,0.144,0.155,0.161,0.164,
     20.165,0.164,0.160,0.151,0.120,0.088,0.056,0.026,0.102,0.129,0.144,
     30.155,0.161,0.164,0.165,0.163,0.159,0.151,0.120,0.088,0.056,0.026,
     40.099,0.126,0.140,0.150,0.156,0.160,0.161,0.159,0.155,0.147,0.117,
     50.085,0.054,0.025,0.096,0.122,0.136,0.146,0.152,0.155,0.155,0.155,
     60.151,0.144,0.114,0.083,0.053,0.024/
      ALMDA=1.0
C     ACCURATELY GUIDED ROLLERS. MODIFIED LINE CONTACT)
      V=1.0
C     INNER RACE ROTATING
      ER=D/(DI+D)
C     ER LIES BETWEEN 0.01 AND 0.30
      DO 210 J=1,10
      IF(R(J).GT.ER) GO TO 210
      M=J
  210 CONTINUE
      IF(M.EQ.10) GO TO 211
      DK=(ER-R(M))/(R(M+1)-R(M))
      GO TO 212
  211 DK=0.0
  212 DO 220 I=1,14
      AFC(I)=FC(I,M)+DK*(FC(I,M+1)-FC(I,M))
  220 CONTINUE
      EPS=0.5*(1.-PLAY/DELR)
      IF(EPS.GT.EPSL(1).AND.EPS.LT.EPSL(14)) GO TO 200
      AAFC=0.0
      GO TO 234
  200 DO 230 I=1,14
      IF(EPSL(I).GT.EPS) GO TO 230
      L=I
  230 CONTINUE
      IF(L.EQ.14) GO TO 232
      CK=(EPS-EPSL(L))/(EPSL(L+1)-EPSL(L))
      GO TO 233
  232 CK=0.0
  233 AAFC=AFC(L)+CK*(AFC(L+1)-AFC(L))
```

```
  234 ALDRAT=ALMDA*AAFC*F*AL**(7./9.)*FLOAT(N)**(3./4.)*D**(29./27.)
      ALIFE=(ALDRAT/(V*EXLD))**(10./3.)
C     LIFE IN MILLION REVOLUTIONS
      RETURN
      END
```

```
      PROGRAM ELSTCT(INPUT,OUTPUT,TAPE5=INPUT,TAPE6=OUTPUT)
C * * * * * * * * * * * * * * * * * * * * * * * * * * * * * * * * * * * *
C     PROGRAM TO FIND THE VALUE OF YOUNG'S MODULUS OF TENSILE TEST PIECE
C     FROM THE READINGS OF UNIVERSAL MEASURING MACHINE, USING METHOD OF
C     LEAST SQUARES
C * * * * * * * * * * * * * * * * * * * * * * * * * * * * * * * * * * * *
C     INFORMATION
      DIMENSION A1(6),B1(6),A2(6),B2(6),G(18),DEL(18),Y(18),DIF(18)
   10 FORMAT(6F10.5/6F10.5/6F10.5/6F10.5/3F10.5)
   11 FORMAT(1H1,43HMODULUS OF ELASTICITY OF TENSILE TEST PIECE)
   12 FORMAT(////1X,6F10.5/1X,6F10.5/1X,6F10.5/1X,6F10.5/1X,5HAREA=,
     1F7.4,1HX,F7.4,4X,5HLOAD=,F5.2)
   13 FORMAT(1H1,22HEQU. OF THE FORM Y=M*X/1X,12HMEAN STRAIN=,F8.5/1X,
     112HMEAN STRESS=,F7.2,4H PSI/1X,22HMODULUS OF ELASTICITY=,F7.1,
     24H PSI)
   14 FORMAT(1H1,24HEQU. OF THE FORM Y=M*X+C/1X,12HMEAN STRAIN=,F7.4/1X,
     112HMEAN STRESS=,F7.2,4H PSI/1X,22HMODULUS OF ELASTICITY=,F7.1,
     24H PSI/1X,20HINITIAL DEFORMATION=,F8.5,3H IN)
   32 FORMAT(//1X,16HMEAN DIFFERENCE=,F8.5,3H IN)
   33 FORMAT(1X,13HGAUGE NUMBER=,I2,4X,13HGAUGE LENGTH=,F8.5,3H IN,
     14X,11HDIFFERENCE=,F8.5,3H IN)
   52 FORMAT(//,1X,12HGAUGE NUMBER,4X,12HGAUGE LENGTH,4X,10HELONGATION)
   51 FORMAT(4X,I2,11X,F8.5,3H IN,5X,F8.5,3H IN)
  100 READ(5,10)((A1(I),I=1,6,1),(B1(J),J=1,6,1),(A2(K),K=1,6,1),
     1(B2(L),L=1,6,1),WTH,TH,ALOAD)
      WRITE(6,11)
      WRITE(6,12)((A1(I),I=1,6,1),(B1(J),J=1,6,1),(A2(K),K=1,6,1),
     1(B2(L),L=1,6,1),WTH,TH,ALOAD)
C     A1 AND B1 ARE THE READINGS OF THE UNIVERSAL MEASURING MACHINE FOR
C     THE MARKED LINES ON THE OPPOSITE SIDES OF THE TENSILE TEST PIECE
C     BEFORE STRESS FREEZING, AND A2 AND B2 ARE THE CORRESPONDING
C     READINGS AFTER STRESS FREEZING. WTH AND TH ARE THE WIDTH AND
C     THICKNESS OF THE TENSILE TEST PIECE. ALOAD IS THE LOAD ON IT.
C     GAUGE LENGTHS
      G(1)=A1(4)-A1(3)
      G(2)=A1(4)-A1(2)
      G(3)=A1(4)-A1(1)
      G(4)=A1(5)-A1(3)
      G(5)=A1(5)-A1(2)
      G(6)=A1(5)-A1(1)
      G(7)=A1(6)-A1(3)
      G(8)=A1(6)-A1(2)
      G(9)=A1(6)-A1(1)
      G(10)=B1(4)-B1(3)
      G(11)=B1(4)-B1(2)
      G(12)=B1(4)-B1(1)
      G(13)=B1(5)-B1(3)
      G(14)=B1(5)-B1(2)
      G(15)=B1(5)-B1(1)
      G(16)=B1(6)-B1(3)
      G(17)=B1(6)-B1(2)
      G(18)=B1(6)-B1(1)
C     ELONGATION
      DEL(1)=A2(4)-A2(3)-G(1)
      DEL(2)=A2(4)-A2(2)-G(2)
      DEL(3)=A2(4)-A2(1)-G(3)
      DEL(4)=A2(5)-A2(3)-G(4)
      DEL(5)=A2(5)-A2(2)-G(5)
```

```
      DEL(6)=A2(5)-A2(1)-G(6)
      DEL(7)=A2(6)-A2(3)-G(7)
      DEL(8)=A2(6)-A2(2)-G(8)
      DEL(9)=A2(6)-A2(1)-G(9)
      DEL(10)=B2(4)-B2(3)-G(10)
      DEL(11)=B2(4)-B2(2)-G(11)
      DEL(12)=B2(4)-B2(1)-G(12)
      DEL(13)=B2(5)-B2(3)-G(13)
      DEL(14)=B2(5)-B2(2)-G(14)
      DEL(15)=B2(5)-B2(1)-G(15)
      DEL(16)=B2(6)-B2(3)-G(16)
      DEL(17)=B2(6)-B2(2)-G(17)
      DEL(18)=B2(6)-B2(1)-G(18)
      WRITE(6,52)
      DO 50 L=1,18,1
      WRITE(6,51)L,G(L),DEL(L)
   50 CONTINUE
      A=0.0
      DO 20 I=1,18,1
      A=A+G(I)
   20 CONTINUE
      B=18.0
      D=0.0
      DO 21 I=1,18,1
      D=D+DEL(I)
   21 CONTINUE
      E=0.0
      DO 22 I=1,18,1
      E=E+G(I)**2
   22 CONTINUE
      F=A
      H=0.0
      DO 23 I=1,18,1
      H=H+G(I)*DEL(I)
   23 CONTINUE
C     EQUATION OF THE FORM Y=M*X
      AMS=H/E
      STR=ALOAD/(WTH*TH)
      ELA=STR/AMS
      WRITE(6,13)AMS,STR,ELA
      SUM=0.0
      DO 30 I=1,18,1
      Y(I)=AMS*G(I)
      DIF(I)=DEL(I)-Y(I)
      SUM=SUM+ABS(DIF(I))
   30 CONTINUE
      ADIF=SUM/18.0
      WRITE(6,32)ADIF
      DO 34 I=1,18,I
      IF(ABS(DIF(I)).LE.(1.5*ADIF)) GO TO 34
      WRITE(6,33)I,G(I),DIF(I)
   34 CONTINUE
C     EQUATION OF THE FORM Y=M*X+C
      AMS=(D/B-H/F)/(A/B-E/F)
      C=D/B-(A/B)*AMS
      ELA=STR/AMS
      WRITE(6,14)AMS,STR,ELA,C
      SUM=0.0
      DO 40 J=1,18,1
      Y(J)=AMS*G(J)+C
      DIF(J)=DEL(J)-Y(J)
      SUM=SUM+ABS(DIF(J))
   40 CONTINUE
      ADIF=SUM/18.0
      WRITE(6,32) ADIF
      DO 41 K=1,18,1
```

```
      IF(ABS(DIF(K)).LE.(1.5*ADIF)) GO TO 41
      WRITE(6,33) K,G(K),DIF(K)
   41 CONTINUE
      GO TO 100
      END
      PROGRAM POWER(INPUT,OUTPUT,TAPE5=INPUT,TAPE6=OUTPUT)
C * * * * * * * * * * * * * * * * * * * * * * * * * * * * * * * * * * * * * *
C     TO DETERMINE EQU OF THE FORM Y=A*X**N FOR A SET OF POINTS USING
C     METHOD OF LEAST SQUARES. USED IN DETERMINING THE LOAD-DEFLECTION
C     RELATIONHSIP OF A ROLLER LOADED BETWEEN TWO PLATENS
C * * * * * * * * * * * * * * * * * * * * * * * * * * * * * * * * * * * * * *
      DIMENSION DIF(100),DL(100),AL(100),ALOAD(100),DEFL(100)
   10 FORMAT(I4)
   11 FORMAT(1X,4HLOAD,10X,10HDEFLECTION)
   12 FORMAT(1X,F10.2,4X,F10.7)
   30 FORMAT(1X,2HA=,E16.8,4X,2HN=,F7.4)
   32 FORMAT(1X,7HLOAD LB,4X,13HDEFLECTION IN)
   36 FORMAT(1X,F10.2,3X,F10.7)
   33 FORMAT(1X,33HEQUATION OF THE FORM DELTA=A*P**N)
   41 FORMAT(///1X,16HMEAN DIFFERENCE=,F10.7,3H IN)
   43 FORMAT(1X,5HLOAD=,F10.2,3H LB,4X,11HDIFFERENCE=,F10.7,3H IN///)
   50 FORMAT(1H1,27HEQUATION FOR DEFORMATION OF/
     11X,30HUSING METHOD OF LEAST SQUARES.///)
   51 FORMAT(5F10.2)
   52 FORMAT(5F10.7)
      READ(5,10) NCASE
      DO 1000 NCA=1,NCASE
      READ(5,10) N
      READ(5,51) (ALOAD(I),I=1,N,1)
      READ(5,52) (DEFL(J),J=1,N,1)
C     N IS THE TOTAL NUMBER OF POINTS GIVEN. ALOAD AND DEFL ARE THE
C     LOAD AND DEFLECTIONS RESPECTIVELY.
      WRITE(6,50)
      WRITE(6,11)
      DO 15 I=1,N,1
      WRITE(6,12)ALOAD(I),DEFL(I)
   15 CONTINUE
      DO 20 I=1,N,1
      AL(I)=ALOG(ALOAD(I))
      DL(I)=ALOG(DEFL(I))
   20 CONTINUE
      B=0.0
      C=0.0
      D=N
      F=0.0
      G=0.0
      DO 25 J=1,N,1
      B=B+AL(J)
      C=C+DL(J)
      F=F+AL(J)**2
      G=G+AL(J)*DL(J)
   25 CONTINUE
      AN=(C/D-G/B)/(B/D-F/B)
      A1=C/D-AN*(B/D)
      A=EXP(A1)
      WRITE(6,33)
      WRITE(6,30)A,AN
      SUM=0.0
      DO 40 I=1,N,1
      DIF(I)=DEFL(I)-A*ALOAD(I)**AN
      SUM=SUM+ABS(DIF(I))
   40 CONTINUE
      ADIF=SUM/D
      WRITE(6,41)ADIF
      DO 42 M=1,N,1
      IF(ABS(DIF(M)).LE.(1.5*ADIF)) GO TO 42
```

```
      WRITE(6,43)ALOAD(M),DIF(M)
   42 CONTINUE
C     DELTA=A*P**N
      WRITE(6,32)
      DO 35 K=1,11,1
      P=FLOAT(K)*250.
      DELTA=A*P**AN
      WRITE(6,36)P,DELTA
   35 CONTINUE
 1000 CONTINUE
      STOP
      END
```

Notations of some variables read from the data cards of program FINELM

FR -Radial load on the bearing.
AMPL -Amplitude of relief in the outer race.
D -Diameter of roller.
AL -Length of roller.
RHO -Specific weight of roller material.
RPM -Speed of shaft.
CON1,CON2,AAN1,AAN2 -Constants for load-deflection relationship of roller and platen of the form $\delta = CON \times P^{AAN}$. More details are given in subroutine RWST.
LA -LA=1, Outer race, LA=2, Inner race.
DR(LA) -Diameter of race-track of race LA.
Z -Number of rolling elements (the program is developed for Z=20, but can be changed easily for other numbers).
NPROB -Number of problems to be solved in one execution of program for bearings having a given combination of races.
NPART(LA) -Total number of partitions in race LA.
NPOIN(LA) -Total number of nodal points in race LA.
NELEM(LA) -Total number of elements in race LA.
NBOUN(LA) -Total number of nodal points with prescribed displacements in race LA.
NCONC(LA) -Number of points with concentrated load in race LA (=number of points in the race track of LA).
NP -NP=0, Plane strain case, any other value of NP is for plane stress case.
NYM -Total number of regions having constant elastic properties, constant body force per unit volume and constant thickness, into which the races are sub-divided.
E(I) -Young's modulus of region I.
PR(I) -Poisson's ratio of region I.
EARTH(I) -Force per unit volume in X-direction of region I.
DENSIT(I) -Force per unit volume in Y-direction of region I.
THICK(I) -Thickness of elements in region I.
NOF(I,LA) -Nodal point number of the point whose serial number is I, on race track of LA.
NOF(NCONC(LA)+1,1) -Nodal point number of the point on the outer race with respect to which bearing body deflection is measured.
NUR(J,LA) -Serial number of the point at the centre of contact area of rolling element number J on race track of LA.
NRACE(LA) -Type of race LA.
NF(I,LA) -I th nodal point number of race LA with prescribed displacement.
NB -NB(I,1,LA)=0, Displacement in X-direction is prescribed,
NB(I,2,LA)=0, Displacement in Y-direction is prescribed,
NB(I,1,LA)=1, Displacement in X-direction is not prescribed,
NB(I,2,LA)=1, Displacement in Y-direction is not prescribed.
BV -BV(I,1,LA)= Prescribed value of displacement in X-direction,
BV(I,2,LA)= Prescribed value of displacement in Y-direction.
NSTART(I,LA) -First element number of partition I in race LA.
NEND(I,LA) -Last element number of partition I in race LA.
NFIRST(I,LA) -First nodal point number of partition I in race LA.
NLAST(I,LA) -Last nodal point number of partition I in race LA.
X(J,1,LA) -X co-ordinate of nodal point J of race LA.
X(J,2,LA) -Y co-ordinate of nodal point J of race LA.
NODE(I,J) -I=1,3 Three nodal point numbers of a triangular element J counting anticlockwise.
NEPE(J) -Elastic property number relevant to element J.

```
      OVERLAY(XX,0,0)
      PROGRAM FINELM(INPUT,OUTPUT,TAPE5=INPUT,TAPE6=OUTPUT,
     1TAPE1,TAPE2,TAPE3,TAPE4,TAPE8,TAPE25,TAPE27)
      COMMON C(6,6),DBA(3,6),DB(3,6),A(6,6),B(3,6),ST(70,140),U(70,2),
     1NB(30,2,2),UT(30,2,2),UX(161,2,2),NF(30,2),DIS(70),
     2RS(70),NOF(162,2),NUR(11,2),DFL(162,2,2)
      COMMON/COM1/X(162,2,2),DR(2),NFIRST(21,2),NLAST(20,2),
     1NPART(2),NSTART(20,2),NEND(20,2),NBOUN(2),NFREE(2),NCONC(2),
     2VLM(2),NSR(2),CL(12),NNN(4),NRACE(2),FR,Z,CON1,CON2,AAN1,AAN2,
     3RPM,D,AL,RHO,Y,FOR(12,2),FORC(12,2),ITN,ERR,AMPL,NSF,NPRO,NPR,
     4RBF(2),REF(2),UF(2),DC(11),BDFL,FOR1(11,2,20)
      COMMON/COM2/FCTR,FCTR1,GRMS,NTYP
      READ(5,1000) FCTR,FCTR1,GRMS,NTYP
      WRITE(6,1000)FCTR,FCTR1,GRMS,NTYP
 1000 FORMAT(1X,F4.2,2F5.2,I5)
      CALL OVERLAY(2HXX,1,0,0)
C * * * * * * * * * * * * * * * * * * * * * * * * * * * * * * * * * * * * * *
C     FORMATION OF MODIFIED STIFFNESS MATRICES
C * * * * * * * * * * * * * * * * * * * * * * * * * * * * * * * * * * * * * *
      CALL OVERLAY(2HXX,2,0,0)
      READ(5,10) NPROB
   10 FORMAT(I4)
      DO 20 NPR=1,NPROB
      READ(5,15) FR,AMPL,D,AL,RHO,RPM,NSF
   15 FORMAT(F10.1,4F10.5,F10.1,I4)
C     IF NSF=1, STRESSES WILL BE CALCULATED AND PRINTED, DEFLECTION AND
C     FORCES  AT EACH NODAL POINT WILL BE PRINTED. ANY OTHER VALUE OF
C     NSF WILL OMMIT THESE.
      REWIND 3
      REWIND 4
      DO 30 LA=1,2
      RBF(LA)=0.
      IF(VLM(LA).GT.0.) GO TO 25
      DEN=0.
      GO TO 26
   25 DEN=FR/(2.*VLM(LA))
   26 NPA=NPART(LA)
      DO 30 II=1,NPA
      READ(3) M,(U(I,LA),I=1,M)
      IF(1-NSR(LA)) 29,27,29
   27 DO 28 MN=1,M
      U(MN,LA)=U(MN,LA)*DEN
   28 RBF(LA)=RBF(LA)+U(MN,LA)
   29 WRITE(4)M,(U(I,LA),I=1,M)
   30 CONTINUE
      CALL OVERLAY(2HXX,3,0,0)
      NPRO=NPROB-NPR
      AMGN=2000.
C     AMGN IS THE MAGNIFICATION TO WHICH THE DEFLECTED SHAPES OF THE
C     RACES ARE PLOTTED.
      CALL DRAW(AMGN)
   20 CONTINUE
      REWIND 8
      STOP
      END


      SUBROUTINE DRAW(AMGN)
C * * * * * * * * * * * * * * * * * * * * * * * * * * * * * * * * * * * * * *
C     SUBROUTINE TO DRAW THE DEFLECTED SHAPE OF RACES
C * * * * * * * * * * * * * * * * * * * * * * * * * * * * * * * * * * * * * *
      DIMENSION W(1260),Z(840),SINE(420)
      COMMON C(6,6),DBA(3,6),DB(3,6),A(6,6),B(3,6),ST(70,140),U(70,2),
     1NB(30,2,2),UT(30,2,2),UX(161,2,2),NF(30,2),DIS(70),
     2RS(70),NOF(162,2),NUR(11,2),DFL(162,2,2)
```

```
      COMMON/COM1/X(162,2,2),DR(2),NFIRST(21,2),NLAST(20,2),
     1NPART(2),NSTART(20,2),NEND(20,2),NBOUN(2),NFREE(2),NCONC(2),
     2VLM(2),NSR(2),CL(12),NNN(4),NRACE(2),FR,Q,CON1,CON2,AAN1,AAN2,
     3RPM,D,AL,RHO,Y,FOR(12,2),FORC(12,2),ITN,ERR,AMPL,NSF,NPRO,NPR,
     4RBF(2),REF(2),UF(2),DC(11),BDFL,FOR1(11,2,20)
      COMMON/COM2/FCTR,FCTR1,GRMS,NTYP
      EQUIVALENCE (ST(1,123),W(1)),(ST(1,129),Z(1)),(ST(1,135),SINE(1))
      IF(NPR.GT.1) GO TO 10
      CALL START
   10 NCON=NCONC(1)
      B=5.0
      AX=2.75
      BY=3.875
C     AMGN IS THE MAGNIFICATION
C     B IS THE Y CO-ORDINATE OF CENTRE OF RACES
C     AX IS X CO-ORDINATE OF POLE
C     BY IS Y CO-ORDINATE OF POLE
      CLN=(DR(1)-DR(2))/2.-D
      BN=CLN/ABS(CLN)*(FLOAT(NRACE(1))*10.**5+FLOAT(NRACE(2))*10.**4+
     1ABS(CLN)*10.**6+AMPL*10.**4)
      WRITE(6,50) BN
   50 FORMAT(///1X,3H***,2X,11HBEARING NO.,F8.0,2X,3H***///)
      DO 20 LA=1,2
      IF(LA-1) 12,11,12
   11 R=0.80
      CALL PLOT(2.0,0.75,-3)
      CALL SYMBOL(2.12,0.9,0.15,10HOUTER RACE,0.0,10)
      GO TO 13
   12 R=2.10
      CALL PLOT(5.2,0.0,-3)
      CALL SYMBOL(2.12,0.9,0.15,10HINNER RACE,0.0,10)
   13 CALL POLE(AX,BY,LA)
      NCON=NCONC(LA)
      AMP=0.2
      H=6.2831854/Q
      THE=0.
      NO=0
      DO 30 I=1,NCON
      SINE(I)=(X(I,2,LA)-B)/SQRT((X(I,2,LA)-B)**2+X(I,1,LA)**2)
      CS=SQRT(1.-SINE(I)**2)
      W(I)=AX+R*CS
      Z(I)=BY+R*SINE(I)
      IF((LA.EQ.2).OR.(AMPL.LT.0.1E-10)) GO TO 18
      TN=SINE(I)/CS
      IF(CS.GT.0.) GO TO 21
      ANG=3.1415927/2.+(SINE(I)/ABS(SINE(I)))*3.1415927/2.
      GO TO 22
   21 ANG=3.1415927/2.+ATAN(TN)
   22 IF(I.EQ.1) GO TO 14
      IF(ANG.LT.THE) GO TO 15
   14 THE=THE+H
      NO=NO+1
      C(1,1)=DC(NO)
      C(2,1)=DC(NO+1)
      INZ=INT(Q/2.+1.)-1
      IF(NO-INZ) 17,16,17
   16 C(3,1)=DC(NO)
      GO TO 19
   17 C(3,1)=DC(NO+2)
   19 X1=THE-H
      C3=(C(1,1)-2.*C(2,1)+C(3,1))/(2.*H**2)
      C2=(C(2,1)-C(1,1))/H-C3*(2.*X1+H)
      C1=C(1,1)-C2*X1-C3*X1**2
   15 AMP1=(C1+C2*ANG+C3*ANG**2)*0.2
      W(I)=W(I)+AMP1*CS
```

```
      Z(I)=Z(I)+AMP1*SINE(I)
   18 III=2*NCON-I
      W(III)=2.*AX-W(I)
      Z(III)=Z(I)
   30 CONTINUE
      I2=2*NCON-1
      W(I2+1)=0.
      Z(I2+1)=0.
      W(I2+2)=1.
      Z(I2+2)=1.
      CALL LINE(W,Z,I2,1,0,1)
      DO 35 I=1,NCON
      CS=SQRT(1.-SINE(I)**2)
      DELR=DFL(I,1,LA)*CS+DFL(I,2,LA)*SINE(I)
      W(I)=W(I)+DELR*AMGN*CS
      Z(I)=Z(I)+DELR*AMGN*SINE(I)
      III=2*NCON-I
      W(III)=2.*AX-W(I)
      Z(III)=Z(I)
   35 CONTINUE
      CALL LINE(W,Z,I2,1,0,1)
      IF(LA.EQ.2) GO TO 20
      FPN=100./AMGN
      CALL SYMBOL(1.70,0.5,0.1,28HONE DIV REPRESENTS       THOU,0.0,28)
      CALL NUMBER(3.6,0.5,0.1,FPN,0.0,2)
      IF(NTYP-2)1001,1002,1003
 1001 CALL SYMBOL(4.9,0.50,0.1,41HBEARING NO RS          LOAD=      LBS  R
     1PM=,0.0,41)
      GO TO 1004
 1002 CALL SYMBOL(4.9,0.50,0.1,41HBEARING NO RR          LOAD=      LBS  R
     1PM=,0.0,41)
      GO TO 1004
 1003 CALL SYMBOL(4.9,0.50,0.1,41HBEARING NO RT          LOAD=      LBS  R
     1PM=,0.0,41)
 1004 CONTINUE
      CALL NUMBER(6.20,0.50,0.1,BN,0.0,-1)
      CALL NUMBER(7.62,0.50,0.1,FR,0.0,-1)
      CALL NUMBER(9.02,0.50,0.1,RPM,0.0,-1)
   20 CONTINUE
      IF(NPRO) 40,45,40
   40 NPR3=NPR/3
      IF(3*NPR3-NPR)58,60,58
   58 CALL PLOT(-7.2,8.0,-3)
      GO TO 55
   60 CALL PLOT(7.0,-18.25,-3)
      GO TO 55
   45 CALL ENPLOT(8.0)
   55 CONTINUE
      RETURN
      END

      SUBROUTINE POLE(AX,BY,LA)
C * * * * * * * * * * * * * * * * * * * * * * * * * * * * * * * * * * * * * * *
C     SUBROUTINE TO DRAW THE POLAR SCALES
C * * * * * * * * * * * * * * * * * * * * * * * * * * * * * * * * * * * * * * *
      DIMENSION X(7),Y(7)
      X(3)=0.
      Y(3)=0.
      X(4)=1.
      Y(4)=1.
      DO 10 II=1,10
      THETA=(3.1415927/5.)*(FLOAT(II)-0.5)
      X(1)=AX+COS(THETA)
      X(2)=AX+2.*COS(THETA)
```

```
      Y(1)=BY+SIN(THETA)
      Y(2)=BY+2.*SIN(THETA)
      CALL LINE(X,Y,2,1,0,1)
      AXX=X(1)
      AYY=Y(1)
      DO 20 LL=1,11
      X(1)=AXX-SIN(THETA)/20.
      Y(1)=AYY+COS(THETA)/20.
      X(2)=AXX+SIN(THETA)/20.
      Y(2)=AYY-COS(THETA)/20.
      CALL LINE(X,Y,2,1,0,1)
      AXX=AXX+COS(THETA)/10.
      AYY=AYY+SIN(THETA)/10.
   20 CONTINUE
   10 CONTINUE
      X(1)=AX+0.1
      X(2)=AX-0.1
      Y(1)=BY
      Y(2)=BY
      CALL LINE(X,Y,2,1,0,1)
      X(1)=AX
      X(2)=AX
      Y(1)=BY+0.1
      Y(2)=BY-0.1
      CALL LINE(X,Y,2,1,0,1)
      IF(LA.EQ.2) GO TO 30
      X(1)=0.0
      Y(1)=0.0
      X(2)=10.7
      Y(2)=Y(1)
      X(3)=X(2)
      Y(3)=6.375
      X(4)=X(1)
      Y(4)=Y(3)
      X(5)=X(1)
      Y(5)=Y(1)
      X(6)=0.
      Y(6)=0.
      X(7)=1.0
      Y(7)=1.0
      CALL LINE(X,Y,5,1,0,1)
   30 CONTINUE
      RETURN
      END

      OVERLAY(XX,1,0)
      PROGRAM ONE
      CALL RWST
      RETURN
      END

      SUBROUTINE RWST
      DIMENSION XE(3,2),BV(30,2,2),NOD(3),NODE(3,4),NPOIN(2),NELEM(2),
     1NCOLN(2),DENSIT(60),EARTH(60),THICK(60),E(60),PR(60),LKK(4),
     2NEPE(4),IPD(2)
      COMMON C(6,6),DBA(3,6),DB(3,6),A(6,6),B(3,6),ST(70,140),U(70,2),
     1NB(30,2,2),UT(30,2,2),UX(161,2,2),NF(30,2),DIS(70),
     2RS(70),NOF(162,2),NUR(11,2),DFL(162,2,2)
      COMMON/COM1/X(162,2,2),DR(2),NFIRST(21,2),NLAST(20,2),
     1NPART(2),NSTART(20,2),NEND(20,2),NBOUN(2),NFREE(2),NCONC(2),
     2VLM(2),NSR(2),CL(12),NNN(4),NRACE(2),FR,Z,CON1,CON2,AAN1,AAN2,
     3RPM,D,AL,RHO,Y,FOR(12,2),FORC(12,2),ITN,ERR,AMPL,NSF,NPRO,NPR,
     4RBF(2),REF(2),UF(2),DC(11),BDFL,FOR1(11,2,20)
      READ(5,35) NYM
```

```
      DO 64 I=1,NYM
      READ(5,12) NY,E(I),PR(I),DENSIT(I),EARTH(I),THICK(I)
      IF(I-NY) 36,64,36
   36 STOP
   64 WRITE(6,12)NY,E(I),PR(I),DENSIT(I),EARTH(I),THICK(I)
   12 FORMAT(I4,E12.2,4F14.6)
      READ(5,10) (NNN(I),I=1,4)
      WRITE(6,10)(NNN(I),I=1,4)
C     NUR(I-1,LA)=NNN(1)*I-NNN(2)
C     NNN(3) GIVES THE SERIAL NO. OF THE 90 DEGREE NOD. POINT ON RACES
C     NNN(4) GIVES THE MATERIAL PROPERTY (ELASTICITY) NO. OF ELEMENTS
C     NEAR THE RACES
      READ(5,73) Z,CON1,CON2,AAN1,AAN2,DR(1),DR(2)
      WRITE(6,73)Z,CON1,CON2,AAN1,AAN2,DR(1),DR(2)
C     CON1,AAN1 FOR APPROACH OF TWO PLATENS BETWEEN WHICH A ROLLER IS
C     LOADED AND CON2,AAN2 FOR LOCAL DEFLECTION OF A PLATEN ONLY.
   73 FORMAT(F6.2,2E12.4,4F10.5)
      REWIND 1
      REWIND 2
      REWIND 3
      REWIND 4
      REWIND 8
      N3=NNN(4)
      Y=E(N3)
      WRITE(8)Z,CON1,CON2,AAN1,AAN2,(DR(I),I=1,2),NYM,Y,(NNN(I),I=1,4)
      DO 20 LA=1,2
      NFREE(LA)=2
C * * * * * * * * * * * * * * * * * * * * * * * * * * * * * * * * * * * * * * *
C     READING AND PRINTING DATA
C * * * * * * * * * * * * * * * * * * * * * * * * * * * * * * * * * * * * * * *
      READ(5,10) LLA,NRACE(LA)
      IF(LA-LLA) 3,4,3
    3 STOP
    4 IF(LA-1) 6,7,6
    6 WRITE(6,11) NRACE(LA)
   11 FORMAT(1H1,15HINNER RACE NO. ,I2//)
      GO TO 8
    7 WRITE(6,13) NRACE(LA)
   13 FORMAT(1H1,15HOUTER RACE NO. ,I2//)
    8 READ(5,10) NPART(LA),NPOIN(LA),NELEM(LA),NBOUN(LA),
     1NCONC(LA),NP,NSR(LA),IPD(LA)
      WRITE(6,10) NPART(LA),NPOIN(LA),NELEM(LA),NBOUN(LA),
     1NCONC(LA),NP,NSR(LA),IPD(LA)
   10 FORMAT(8I4)
C     IF NSR(LA)=1 EXTERNAL LOAD WILL BE DISTRIBUTED AS SHEAR STRESSES
C     ON AREAS WHOSE DENSIT IS GIVEN A VALUE (SIGN*1.), WHERE SIGN
C     REPRESENTS DIRECTION OF SHEAR STRESS. IF IPD(LA)=1 SHEAR STRESS
C     DISTRIBUTION WILL BE PARABOLIC. ANY OTHER VALUE OF IT WILL MAKE
C     THE DISTRIBUTION UNIFORM.
      VLM(LA)=0.
      NCON=NCONC(LA)+1
      NCO=NCON/18
       IF(NCO*18-NCON) 72,71,72
    72 NCO=NCO+1
    71 DO 69 J=1,NCO
       I=18*(J-1)
       READ(5,33) NOF(I+1,LA),NOF(I+2,LA),NOF(I+3,LA),NOF(I+4,LA),
     1NOF(I+5,LA),NOF(I+6,LA),NOF(I+7,LA),NOF(I+8,LA),NOF(I+9,LA),
     2NOF(I+10,LA),NOF(I+11,LA),NOF(I+12,LA),NOF(I+13,LA),NOF(I+14,LA),
     3NOF(I+15,LA),NOF(I+16,LA),NOF(I+17,LA),NOF(I+18,LA)
    69 WRITE(6,33)NOF(I+1,LA),NOF(I+2,LA),NOF(I+3,LA),NOF(I+4,LA),
     1NOF(I+5,LA),NOF(I+6,LA),NOF(I+7,LA),NOF(I+8,LA),NOF(I+9,LA),
     2NOF(I+10,LA),NOF(I+11,LA),NOF(I+12,LA),NOF(I+13,LA),NOF(I+14,LA),
     3NOF(I+15,LA),NOF(I+16,LA),NOF(I+17,LA),NOF(I+18,LA)
    33 FORMAT(18I4)
       NBO=NBOUN(LA)
```

```
      DO 50 I=1,NBO
      READ(5,46) NF(I,LA),NB(I,1,LA),NB(I,2,LA),BV(I,1,LA),BV(I,2,LA)
   50 WRITE(6,46) NF(I,LA),NB(I,1,LA),NB(I,2,LA),BV(I,1,LA),BV(I,2,LA)
   46 FORMAT(3I4,2F16.8)
      NPA=NPART(LA)
      DO 60 I=1,NPA
      READ(5,10) NPAR,NSTART(I,LA),NEND(I,LA),NFIRST(I,LA),NLAST(I,LA)
   60 WRITE(6,10)NPAR,NSTART(I,LA),NEND(I,LA),NFIRST(I,LA),NLAST(I,LA)
      WRITE(8)NPART(LA),NELEM(LA),NBOUN(LA),NSR(LA),NCONC(LA),NPA,
     1(NSTART(I,LA),I=1,NPA),(NEND(I,LA),I=1,NPA),(NFIRST(I,LA),I=1,NPA)
     2,(NLAST(I,LA),I=1,NPA),NCON,(NOF(I,LA),I=1,NCON),NBO,(NF(I,LA),
     3I=1,NBO),((NB(I,J,LA),I=1,NBO),J=1,2),NFREE(LA),((UT(I,J,LA),I=1,
     4NBO),J=1,2),NRACE(LA)
      NFIRST(NPA+1,LA)=NLAST(NPA,LA)+1
      DO 75 I=1,70
      DO 75 J=1,140
      U(I,LA)=0.
   75 ST(I,J)=0.
      DO 70 II=1,NPA
      NST=NSTART(II,LA)
      NEN=NEND(II,LA)
      K=NFIRST(II,LA)
      L=NLAST(II,LA)
      MINUS=K-1
      KL=L-K+1
      KL3=KL/3
      IF(3*KL3-KL) 31,32,31
   31 KL3=KL3+1
   32 DO 30 I=1,KL3
      READ(5,35) NOD(1),X(3*I-2,1,LA),X(3*I-2,2,LA),NOD(2),X(3*I-1,1,LA)
     1,X(3*I-1,2,LA),NOD(3),X(3*I,1,LA),X(3*I,2,LA)
   35 FORMAT(3(I4,2F10.6))
      WRITE(6,37)NOD(1),X(3*I-2,1,LA),X(3*I-2,2,LA),NOD(2),X(3*I-1,1,LA)
     1,X(3*I-1,2,LA),NOD(3),X(3*I,1,LA),X(3*I,2,LA)
   37 FORMAT(3(I4,2(4X,F10.6),4X))
   30 CONTINUE
      DO 171 NX=1,NCON
      NNOD=NOF(NX,LA)
      MMM=NNOD-K
      IF(MMM) 171,172,172
  172 MM1=NNOD-L
      IF(MM1) 173,173,171
  173 MMM1=MMM+1
      DFL(NX,1,LA)=X(MMM1,1,LA)
      DFL(NX,2,LA)=X(MMM1,2,LA)
  171 CONTINUE
      JJJ=4
      DO 80 LK=NST,NEN
      IF(JJJ.LT.4) GO TO 110
      READ(5,45) (LKK(J),(NODE(I,J),I=1,3),NEPE(J),J=1,4)
      WRITE(6,47)(LKK(J),(NODE(I,J),I=1,3),NEPE(J),J=1,4)
   45 FORMAT(4(I5,3I4,I3))
   47 FORMAT(4(4I5,I3,4X))
      JJJ=0
  110 JJJ=JJJ+1
      IF(LKK(JJJ)-LK) 120,121,120
  120 STOP
  121 CONTINUE
      DO 111 I=1,3
  111 NOD(I)=NODE(I,JJJ)
      NEP=NEPE(JJJ)
      DO 85 I=1,3
      JJ=NOD(I)-K+1
      XE(I,1)=X(JJ,1,LA)
   85 XE(I,2)=X(JJ,2,LA)
```

```
      YM=E(NEP)
      P=PR(NEP)
      TH=THICK(NEP)
      ORY=(XE(1,2)+XE(2,2)+XE(3,2))/3.
C * * * * * * * * * * * * * * * * * * * * * * * * * * * * * * * * * * * * * * *
C     CALCULATION OF ELEMENT STIFFNESS AND STRESS MATRICES
C * * * * * * * * * * * * * * * * * * * * * * * * * * * * * * * * * * * * * * *
      CALL FEM(XE,YM,P,NP,TH,NOD)
C * * * * * * * * * * * * * * * * * * * * * * * * * * * * * * * * * * * * * * *
C     C IS ELEMENT STIFFNESS MATRIX
C * * * * * * * * * * * * * * * * * * * * * * * * * * * * * * * * * * * * * * *
C     CALCULATOIN OF LOADS DUE TO BODY FORCES
C * * * * * * * * * * * * * * * * * * * * * * * * * * * * * * * * * * * * * * *
      DEN=DENSIT(NEP)
      EAR=EARTH(NEP)
      CALL LOAD(XE,NOD,LA,TH,DEN,EAR,K,VLM,ORY,NSR,IPD)
      DO 80 LL=1,3
      DO 80 KK=1,3
C * * * * * * * * * * * * * * * * * * * * * * * * * * * * * * * * * * * * * * *
C      NEXT TWO CARDS ARE FOR CHECKING
C * * * * * * * * * * * * * * * * * * * * * * * * * * * * * * * * * * * * * * *
      IF(NOD(KK)-K)80,131,131
  131 IF(NOD(KK)-L)132,132,80
  132 NFRE=NFREE(LA)
      M=NFRE*(NOD(KK)-K)
      N=NFRE*(NOD(LL)-K)
C * * * * * * * * * * * * * * * * * * * * * * * * * * * * * * * * * * * * * * *
C     M AND N GIVE LOCATION OF NODAL POINTS OF THE ELEMENT UNDER
C     CONSIDERATION IN THE TOTAL STIFFNESS MATRIX
C * * * * * * * * * * * * * * * * * * * * * * * * * * * * * * * * * * * * * * *
      I=NFRE*(KK-1)
      J=NFRE*(LL-1)
C * * * * * * * * * * * * * * * * * * * * * * * * * * * * * * * * * * * * * * *
C     I AND J GIVE LOCATION OF THE NODAL POINTS OF THE ELEMENTS UNDER
C     CONSIDERATION IN THE ELEMENT STIFFNESS MATRIX
C * * * * * * * * * * * * * * * * * * * * * * * * * * * * * * * * * * * * * * *
      IF(N)80,900,900
C * * * * * * * * * * * * * * * * * * * * * * * * * * * * * * * * * * * * * * *
C     PUTTING THE ELEMENT STIFFNESS MATRIX UNDER CONSIDERATION IN THE
C     PROPER PLACE IN TOTAL STIFFNESS MATRIX
C * * * * * * * * * * * * * * * * * * * * * * * * * * * * * * * * * * * * * * *
  900 DO 5 NJ=1,NFRE
      DO 5 MI=1,NFRE
      MMI=M+MI
      NNJ=N+NJ
      IMI=I+MI
      JNJ=J+NJ
    5 ST(MMI,NNJ)=ST(MMI,NNJ)+C(IMI,JNJ)
   80 CONTINUE
C * * * * * * * * * * * * * * * * * * * * * * * * * * * * * * * * * * * * * * *
C     INTRODUCTION OF PRESCRIBED DISPLACEMENTS
C * * * * * * * * * * * * * * * * * * * * * * * * * * * * * * * * * * * * * * *
      DO 290 I=1,NBO
C * * * * * * * * * * * * * * * * * * * * * * * * * * * * * * * * * * * * * * *
C     TO TEST WHETHER NF(I,LA) IS IN THE PARTITION UNDER STUDY OR NOT
C * * * * * * * * * * * * * * * * * * * * * * * * * * * * * * * * * * * * * * *
      L1=NFIRST(II+1,LA)-1
      M=NF(I,LA)-K
      IF(M) 290,242,242
  242 M1=NF(I,LA)-L1
      IF(M1)243,243,290
  243 DO 230 J=1,NFRE
      IF(NB(I,J,LA)) 230,245,230
  245 NMI=NFRE*M+J
```

```
C * * * * * * * * * * * * * * * * * * * * * * * * * * * * * * * * * * * * * *
C       NMI GIVES LOCATION OF THE NODE WHOSE DISPLACEMENT IS GIVEN IN THE
C       CONCERNED PARTITIONED MATRIX
C       THE DIAGONAL TERM IS MULTIPLIED BY A LARGE NUMBER
C * * * * * * * * * * * * * * * * * * * * * * * * * * * * * * * * * * * * * *
        ST(NMI,NMI)=ST(NMI,NMI)*0.1E+12
        UT(I,J,LA)=ST(NMI,NMI)*BV(I,J,LA)
  230 CONTINUE
  290 CONTINUE
        M=NFRE*((NFIRST(II+1,LA)-1)-(NFIRST(II,LA)-1))
        WRITE(4) M,((ST(I,J),J=1,M),I=1,M)
        WRITE(2)M,(U(I,LA),I=1,M)
        LR=2*KL
        MM=M+1
        LRMM=LR-M
        LRMM1=LRMM+1
        IF(NPA-II) 881,883,881
  881 DO 880 I=1,LRMM
        JI=M+I
  880 U(I,LA)=U(JI,LA)
        DO 882 I=LRMM1,70
        U(I,LA)=0.
  882 CONTINUE
  883 CONTINUE
        IF(NPA-II) 988,70,988
  988 NN=NFRE*((NFIRST(II+2,LA)-1)-(NFIRST(II,LA)-1))
        N=NN-MM+1
        WRITE(4)M,N,((ST(I,J),J=MM,NN),I=1,M)
        JXR=MM
        JIR=1
  702 JXC=MM
        JIC=1
  700 ST(JIR,JIC)=ST(JXR,JXC)
        JXC=JXC+1
        JIC=JIC+1
        IF(JXC-LR) 700,700,701
  701 JXR=JXR+1
        JIR=JIR+1
        IF(JXR-LR) 702,702,703
  703 CONTINUE
        DO 798 I=1,LRMM
        DO 798 J=LRMM1,70
  798 ST(I,J)=0.
        DO 797 I=LRMM1,70
        DO 797 J=1,70
  797 ST(I,J)=0.
   70 CONTINUE
        DO 170 IJ=1,NCON
        X(IJ,1,LA)=DFL(IJ,1,LA)
  170 X(IJ,2,LA)=DFL(IJ,2,LA)
        WRITE(8)NCON,((X(I,J,LA),I=1,NCON),J=1,2),VLM(LA)
   20 CONTINUE
        REWIND 2
        REWIND 3
        DO 806 LA=1,2
        NPA=NPART(LA)
        DO 806 II=1,NPA
        READ(2) M,(U(I,LA),I=1,M)
        WRITE(3)M,(U(I,LA),I=1,M)
        WRITE(8)M,(U(I,LA),I=1,M)
  806 CONTINUE
        REWIND 2
        REWIND 4
        WRITE(6,6000) (VLM(LA),LA=1,2)
 6000 FORMAT(//1X,11HVOLUMES ARE,F10.5,5X,F10.5)
        RETURN
        END
```

```
      SUBROUTINE LOAD(XE,NOD,LA,TH,DEN,EAR,K,VLM,ORY,NSR,IPD)
C * * * * * * * * * * * * * * * * * * * * * * * * * * * * * * * * * * * *
C     SUBROUTINE TO CALCULATE NODAL POINT FORCES DUE TO BODY FORCES
C * * * * * * * * * * * * * * * * * * * * * * * * * * * * * * * * * * * *
      DIMENSION XE(3,2),NOD(3),VLM(2),NSR(2),IPD(2)
      COMMON C(6,6),DBA(3,6),DB(3,6),A(6,6),B(3,6),ST(70,140),U(70,2),
     1NB(30,2,2),UT(30,2,2),UX(161,2,2),NF(30,2),DIS(70),
     2RS(70),NOF(162,2),NUR(11,2),DFL(162,2,2)
      IF(DEN) 10,30,10
   30 IF(EAR) 10,20,10
   10 VOL=0.166667*TH*(XE(2,1)*(XE(3,2)-XE(1,2))+XE(1,1)*(XE(2,2)-
     1XE(3,2))+XE(3,1)*(XE(1,2)-XE(2,2)))
      IF(NSR(LA).NE.1) GO TO 16
      IF(IPD(LA).NE.1) GO TO 16
      CENTRE=5.0
      ORY=ABS(ORY-CENTRE)
      HT=1.2
      IF(LA.EQ.1) HT=CENTRE
      VOL=VOL*(1.-(ORY/HT)**2)
   16 VLM(LA)=VLM(LA)+3.*VOL
      VT=VOL*DEN
      UT=VOL*EAR
      DO 86 I=1,3
      JJ=NOD(I)
      JJK1=2*(JJ-K)+1
      U(JJK1,LA)=U(JJK1,LA)+UT
      JJK2=2*(JJ-K)+2
   86 U(JJK2,LA)=U(JJK2,LA)+VT
   20 CONTINUE
      RETURN
      END

      SUBROUTINE FEM(XE,YM,P,NP,TH,NOD)
C * * * * * * * * * * * * * * * * * * * * * * * * * * * * * * * * * * * *
C     SUBROUTINE FOR FORMATION OF ELEMENT STIFFNESS AND STRESS MATRICES
C * * * * * * * * * * * * * * * * * * * * * * * * * * * * * * * * * * * *
      DIMENSION D(3,3),BTDBA(6,6),XE(3,2),ZX(3),ZY(3),NOD(3)
      COMMON C(6,6),DBA(3,6),DB(3,6),A(6,6),B(3,6),ST(70,140),U(70,2),
     1NB(30,2,2),UT(30,2,2),UX(161,2,2),NF(30,2),DIS(70),
     2RS(70),NOF(162,2),NUR(11,2),DFL(162,2,2)
C * * * * * * * * * * * * * * * * * * * * * * * * * * * * * * * * * * * *
C     FORMATION OF STIFFNESS MATRIX
C * * * * * * * * * * * * * * * * * * * * * * * * * * * * * * * * * * * *
      DO 20 J=1,6
      DO 21 I=1,3
      B(I,J)=0.
      DB(I,J)=0.
C     SPACE FOR B DB MATRIX READY, B MATRIX IS EQUAL TO B*A HERE
   21 DBA(I,J)=0.
C     DBA IS STRESS MATRIX
      DO 20 I=1,6
      A(I,J)=0.
      BTDBA(I,J)=0.
   20 C(I,J)=0.
      DO 22 J=1,3
      DO 22 I=1,3
   22 D(I,J)=0.
C     CALCULATION OF CENTROID OF THE ELEMENT
      ORX=(XE(1,1)+XE(2,1)+XE(3,1))*.333333
      ORY=(XE(1,2)+XE(2,2)+XE(3,2))*.333333
C * * * * * * * * * * * * * * * * * * * * * * * * * * * * * * * * * * * *
C     CHANGING ORIGIN TO CENTROID OF THE ELEMENT
C * * * * * * * * * * * * * * * * * * * * * * * * * * * * * * * * * * * *
      DO 5 I=1,3
      XE(I,1)=XE(I,1)-ORX
    5 XE(I,2)=XE(I,2)-ORY
```

```
C       CALCULATION OF SMALL BI CI AND AI
        ZX(1)=XE(2,2)-XE(3,2)
        ZX(2)=XE(3,2)-XE(1,2)
        ZX(3)=XE(1,2)-XE(2,2)
        ZY(1)=XE(3,1)-XE(2,1)
        ZY(2)=XE(1,1)-XE(3,1)
        ZY(3)=XE(2,1)-XE(1,1)
        ZK=XE(2,1)*XE(3,2)-XE(3,1)*XE(2,2)
        Z=3.*ZK
        IF(Z.LT.0.) WRITE(6,10)
   10 FORMAT(//1X,19H*** AREA IS -VE ***//)
C       A IS CONNECTION MATRIX AS IN THE PROBLEM
C       AND B MATRIX AS IN THEORY
        A(1,1)=ZK/Z
        A(2,1)=ZX(1)/Z
        A(3,1)=ZY(1)/Z
        A(4,2)=A(1,1)
        A(5,2)=A(2,1)
        A(6,2)=A(3,1)
        A(1,3)=ZK/Z
        A(2,3)=ZX(2)/Z
        A(3,3)=ZY(2)/Z
        A(4,4)=A(1,3)
        A(5,4)=A(2,3)
        A(6,4)=A(3,3)
        A(1,5)=ZK/Z
        A(2,5)=ZX(3)/Z
        A(3,5)=ZY(3)/Z
        A(4,6)=A(1,5)
        A(5,6)=A(2,5)
        A(6,6)=A(3,5)
        B(1,2)=1.0
        B(3,3)=1.0
        B(3,5)=1.0
        B(2,6)=1.0
        IF(NP)75,81,75
C * * * * * * * * * * * * * * * * * * * * * * * * * * * * * * * * * * * * * *
C       ELASTICITY MATRIX FOR PLANE STRAIN CASE
C * * * * * * * * * * * * * * * * * * * * * * * * * * * * * * * * * * * * * *
   81 DEN=YM*(1.-P)/((1.+P)*(1.-2.*P))
        D(1,1)=DEN
        D(1,2)=DEN*(P/(1.-P))
        D(2,1)=D(1,2)
        D(2,2)=DEN
        D(3,3)=0.5*DEN*((1.-2.*P)/(1.-P))
        GO TO 73
C * * * * * * * * * * * * * * * * * * * * * * * * * * * * * * * * * * * * * *
C       ELASTICITY MATRIX FOR PLANE STRESS CASE
C * * * * * * * * * * * * * * * * * * * * * * * * * * * * * * * * * * * * * *
   75 DEN=YM/(1.-P**2)
        D(1,1)=DEN
        D(2,2)=DEN
        D(2,1)=P*DEN
        D(1,2)=D(2,1)
        D(3,3)=DEN*.5*(1.-P)
C * * * * * * * * * * * * * * * * * * * * * * * * * * * * * * * * * * * * * *
C       FORMATION OF ELEMENT STIFFNESS MATRIX
C * * * * * * * * * * * * * * * * * * * * * * * * * * * * * * * * * * * * * *
   73 DO 30 J=1,6
        DO 30 I=1,3
        DO 30 K=1,3
   30 DB(I,J)=DB(I,J)+D(I,K)*B(K,J)
        DO 40 J=1,6
        DO 40 I=1,3
        DO 40 K=1,6
   40 DBA(I,J)=DBA(I,J)+DB(I,K)*A(K,J)
```

```
C * * * * * * * * * * * * * * * * * * * * * * * * * * * * * * * * * * * * * * *
C       STRESS MATRIX IS FORMED
C * * * * * * * * * * * * * * * * * * * * * * * * * * * * * * * * * * * * * * *
        WRITE(1) ((DBA(I,J),I=1,3),J=1,6),(NOD(I),I=1,3),ORX,ORY
        WRITE(8)((DBA(I,J),I=1,3),J=1,6),(NOD(I),I=1,3),ORX,ORY
        VOL=0.5*TH*Z
        DO 50 J=1,6
        DO 50 I=1,6
        DO 50 K=1,3
   50   BTDBA(I,J)=BTDBA(I,J)+B(K,I)*DBA(K,J)*VOL
        DO 60 J=1,6
        DO 60 I=1,6
        DO 60 K=1,6
   60   C(I,J)=C(I,J)+A(K,I)*BTDBA(K,J)
C * * * * * * * * * * * * * * * * * * * * * * * * * * * * * * * * * * * * * * *
C       STIFFNESS MATRIX IS FORMED
C * * * * * * * * * * * * * * * * * * * * * * * * * * * * * * * * * * * * * * *
        RETURN
        END

        OVERLAY(XX,2,0)
        PROGRAM TWO
        CALL MSM
        RETURN
        END

        SUBROUTINE MSM
C * * * * * * * * * * * * * * * * * * * * * * * * * * * * * * * * * * * * * * *
C       SUBROUTINE TO FORM MODIFIED STIFFNESS MATRICES
C * * * * * * * * * * * * * * * * * * * * * * * * * * * * * * * * * * * * * * *
        DIMENSION YM(70,70),AM(70,140),BM(70,70)
        COMMON C(6,6),DBA(3,6),DB(3,6),A(6,6),B(3,6),ST(70,140),U(70,2),
       1NB(30,2,2),UT(30,2,2),UX(161,2,2),NF(30,2),DIS(70),
       2RS(70),NOF(162,2),NUR(11,2),DFL(162,2,2)
        COMMON/COM1/X(162,2,2),DR(2),NFIRST(21,2),NLAST(20,2),
       1NPART(2),NSTART(20,2),NEND(20,2),NBOUN(2),NFREE(2),NCONC(2),
       2VLM(2),NSR(2),CL(12),NNN(4),NRACE(2),FR,Z,CON1,CON2,AAN1,AAN2,
       3RPM,D,AL,RHO,Y,FOR(12,2),FORC(12,2),ITN,ERR,AMPL,NSF,NPRO,NPR,
       4RBF(2),REF(2),UF(2),DC(11),BDFL,FOR1(11,2,20)
        EQUIVALENCE(AM(1,1),ST(1,1)),(BM(1,1),AM(1,71))
        DO 20 LA=1,2
        DO 140 I=1,70
        DO 140 J=1,70
  140   YM(I,J)=0.
        NPA=NPART(LA)
        DO 144 LL=1,NPA
C * * * * * * * * * * * * * * * * * * * * * * * * * * * * * * * * * * * * * * *
C       READING AM MATRIX OF EACH PARTITION
C * * * * * * * * * * * * * * * * * * * * * * * * * * * * * * * * * * * * * * *
        READ(4) M,((AM(I,J),J=1,M),I=1,M)
        DO 424 I=1,M
        DO 424 J=1,M
  424   AM(I,J)=AM(I,J)-YM(I,J)
C * * * * * * * * * * * * * * * * * * * * * * * * * * * * * * * * * * * * * * *
C       SPNIST INVERTS THE MATRIX USING AM(70,140) SPACE AND WRITES THE
C       INVERSE IN AM(70,70) SPACE.
C       AM(70,71-140) IS AFTERWARDS USED FOR STORING BM MATRIX.
C * * * * * * * * * * * * * * * * * * * * * * * * * * * * * * * * * * * * * * *
        CALL SPNIST(AM,M,70,ISIG)
        IF(NPA-LL)666,666,555
  555   READ(4) M,N,((BM(I,J),J=1,N),I=1,M)
  667   WRITE(1) M,N,((AM(I,J),I=1,M),J=1,M),((BM(I,J),I=1,M),J=1,N)
C * * * * * * * * * * * * * * * * * * * * * * * * * * * * * * * * * * * * * * *
C       MATRIX BM, INVERTED MATRIX AM OF EACH PARTITION ARE RECORDED ON
C       TAPE 1 AND LATER TRANSFERRED IN REVERSE ORDER ON TAPE 2.
C * * * * * * * * * * * * * * * * * * * * * * * * * * * * * * * * * * * * * * *
```

```
      GO TO 787
  666 WRITE(1) M,((AM(I,J),I=1,M),J=1,M)
      IF(NPA-LL) 144,144,787
  787 DO 110 J=1,M
      DO 110 I=1,N
      YM(I,J)=0.
      DO 110 K=1,M
  110 YM(I,J)=YM(I,J)+BM(K,I)*AM(K,J)
      WRITE(2) M,N,((YM(I,J),I=1,N),J=1,M)
      WRITE(8) M,N,((YM(I,J),I=1,N),J=1,M)
      DO 111 J=1,N
      DO 111 I=1,N
      AM(I,J)=0.
      DO 111 K=1,M
  111 AM(I,J)=AM(I,J)+YM(I,K)*BM(K,J)
      DO 112 I=1,N
      DO 112 J=1,N
  112 YM(I,J)=AM(I,J)
  144 CONTINUE
   20 CONTINUE
      REWIND 4
      DO 40 LA=1,2
      NPA=NPART(LA)
      DO 40 LL=1,NPA
      READ(4) M,((AM(I,J),J=1,M),I=1,M)
      WRITE(3)M,((AM(I,J),J=1,M),I=1,M)
      WRITE(8) M,((AM(I,J),J=1,M),I=1,M)
      IF(NPA-LL) 40,40,39
   39 READ(4) M,N,((BM(I,J),J=1,N),I=1,M)
      WRITE(3)M,N,((BM(I,J),J=1,N),I=1,M)
      WRITE(8)M,N,((BM(I,J),J=1,N),I=1,M)
   40 CONTINUE
      DO 60 LA=1,2
      IF(LA.EQ.1) GO TO 51
      NPA=NPART(1)
      GO TO 52
   51 NPA=NPART(2)
   52 DO 59 LL=1,NPA
      IF(LL-1) 56,56,55
   56 BACKSPACE 1
      READ(1) M,((AM(I,J),I=1,M),J=1,M)
      WRITE(2)M,((AM(I,J),I=1,M),J=1,M)
      WRITE(8)M,((AM(I,J),I=1,M),J=1,M)
      GO TO 59
   55 BACKSPACE 1
      BACKSPACE 1
      READ(1) M,N,((AM(I,J),I=1,M),J=1,M),((BM(I,J),I=1,M),J=1,N)
      WRITE(2)M,N,((AM(I,J),I=1,M),J=1,M),((BM(I,J),I=1,M),J=1,N)
      WRITE(8)M,N,((AM(I,J),I=1,M),J=1,M),((BM(I,J),I=1,M),J=1,N)
   59 CONTINUE
      BACKSPACE 1
   60 CONTINUE
      RETURN
      END

      SUBROUTINE  SPNIST(A,M,KK,ISIG)
      DIMENSION A(1)
      ISIG = 0
      N = M
      NN = KK
      N2 = N + N
      DO 10 J=1,N
      NJCOL = (N + J - 1) * NN
```

```
      DO 10 I=1,N
      KINJ = NJCOL + I
      IF(I-J)4,6,4
    4 A(KINJ) = 0.
      GO TO 10
    6 A(KINJ) = 1.
   10 CONTINUE
C  DETERMINE MAXIMUM ABS OF VARIABLE BEING ELIMINATED.  THIS BECOMES PIV
C     OTAL ROW
      L = 0
   12 L = L + 1
      LCOL = NN*L-NN
      KLL = LCOL + L
      IF(L - N)13,30,1000
C  FIND THE LARGEST ELEMENT IN THE LTH COLUMN.
   13 J1 = L
      C=ABS(A(KLL))
      L1 = L + 1
      DO 20 I = L1,N
      KIL = LCOL + I
      X=ABS(A(KIL))
      IF(C - X)14,20,20
C  RECORD THE NUMBER OF THE ROW HAVING THE GREATER ELEMENT.
   14 J1 = I
C  C BECOMES THE GREATER.
      C  = X
   20 CONTINUE
C  INTERCHANGE ROW J1 WITH ROW L. J1 IS THE ROW WITH THE LARGEST ELEMENT
C  TEST TO SEE IF INTERCHANGING IS NECESSARY.
      IF(J1 - L)22,30,22
   22 DO 24 J = L,N2
      JCOL = NN*J-NN
      KJIJ = JCOL + J1
      HOLD = A(KJIJ)
      KLJ = JCOL + L
      A(KJIJ) = A(KLJ)
      A(KLJ) = HOLD
   24 CONTINUE
C  IF  THE LARGEST ABSOLUTE ELEMENT IN A COLUMN IS ZERO WE HAVE A SINGUL
C    AR  MATRIX
   30 IF (ABS(A(KLL)) - .00000001)33,33,32
   33 WRITE(6,100)
      ISIG = 4
      GO TO 1000
C   ZERO ALL THE ELEMENTS IN THE LTH COLUMN BUT THE PIVOTAL ELEMENT.
   32 L1 = 1
      L2 = L - 1
      IF(L2)321,321,323
  321 IF(L-N)322,46,322
  322 L1 = L + 1
      L2 = N
  323 DO 324 I = L1,L2
      KIL = LCOL + I
      Z = -A(KIL)/A(KLL)
      DO 324 J = L,N2
      JCOL = NN*J - NN
      KIJ = JCOL + I
      KLJ = JCOL + L
  324 A(KIJ) = A(KIJ) + Z*A(KLJ)
      IF(N - L2)12,12,321
C  DIVIDE BY DIAGONAL ELEMENTS.
   46 DO 48 I = 1,N
      KKK = NN*I - NN + I
      ZZ = A(KKK)
      DO 48 J = 1,N2
      KKI = NN*J - NN + I
```

```
   48 A(KKI) = A(KKI)/ZZ
C    RETURN AFTER PUTTING A INVERSE INTO B
   49 DO 50 J = 1,N
      JCOL = NN*J - NN
      NJCOL = NN * N + JCOL
      DO 50 I = 1,N
      KIJ = JCOL + I
      KINJ = NJCOL + I
   50 A(KIJ) = A(KINJ)
  100 FORMAT(//20X,42H MATRIX IS SINGULAR, NO INVERSE OBTAINABLE///)
 1000 RETURN
      END
```

```
      OVERLAY(XX,3,0)
      PROGRAM THREE
      CALL SOLN
      RETURN
      END

      SUBROUTINE SOLN
      DIMENSION GAP(12),DFLN(2),CC(11),CLRN(11,20),DFLI(20),DFLO(20),
     1DFLT(20),DFLB(20),RMSER(20),RGDT(20)
      COMMON C(6,6),DBA(3,6),DB(3,6),A(6,6),B(3,6),ST(70,140),U(70,2),
     1NB(30,2,2),UT(30,2,2),UX(161,2,2),NF(30,2),DIS(70),
     2RS(70),NOF(162,2),NUR(11,2),DFL(162,2,2)
      COMMON/COM1/X(162,2,2),DR(2),NFIRST(21,2),NLAST(20,2),
     1NPART(2),NSTART(20,2),NEND(20,2),NBOUN(2),NFREE(2),NCONC(2),
     2VLM(2),NSR(2),CL(12),NNN(4),NRACE(2),FR,Z,CON1,CON2,AAN1,AAN2,
     3RPM,D,AL,RHO,Y,FOR(12,2),FORC(12,2),ITN,ERR,AMPL,NSF,NPRO,NPR,
     4RBF(2),REF(2),UF(2),DC(11),BDFL,FOR1(11,2,20)
      COMMON/COM2/FCTR,FCTR1,GRMS,NTYP
      DATA (CC(I),I=1,11)/1.00,0.750,0.3025,0.02064,0.0811,0.448,0.877,
     10.966,0.601,0.1774,0.000/
C     CC GIVES THE SHAPE OF RELIEF IN THE OUTER RACE
      DO 74 I=2,12
      DC(I-1)=CC(I-1)
      CL(I)=(DR(1)-DR(2))/2.-D+DC(I-1)*AMPL
      CLRN(I-1,1)=CL(I)*10.**6
      DO 74 LA=1,2
      NUR(I-1,LA)=NNN(1)*I-NNN(2)
   74 CONTINUE
      CLN=CL(2)
      IF(CLN.GT.0.) CLN=0.
      ITN=0
      CALL LMAT
      DFLT(1)=BDFL*10.**3
      RGDT(1)=FR/DFLT(1)
C * * * * * * * * * * * * * * * * * * * * * * * * * * * * * * * * * *
C     FORMATION OF MODIFIED FORCE MATRICES
C * * * * * * * * * * * * * * * * * * * * * * * * * * * * * * * * * *
 1000 CONTINUE
      REWIND 2
      REWIND 4
      CALL MFM
C * * * * * * * * * * * * * * * * * * * * * * * * * * * * * * * * * *
C     SOLUTION FOR DEFLECTION BY BACK SUBSTITUTION
C * * * * * * * * * * * * * * * * * * * * * * * * * * * * * * * * * *
      CALL SOLVE
      DO 180 LA=1,2
      NCON=NCONC(LA)+1
      N3=NNN(3)
      DFLN(LA)=DFL(N3,2,LA)
      WRITE(6,100) NOF(N3,LA),LA,DFLN(LA)
  100 FORMAT(//,1X,30HY-DEFLECTION OF NOD. POINT NO.,I5,12H OF RACE NO.,
     1I4,3H IS,E12.4,3H IN)
```

```
      DO 181 J=1,NCON
  181 DFL(J,2,LA)=DFL(J,2,LA)-DFLN(LA)
      DO 180 I=2,12
  180 FORC(I,LA)=FOR(I,LA)
      NCON=NCONC(1)+1
      DFLB(ITN+1)=DFL(NCON,2,1)*10.**6
      DFLO(ITN+1)=-DFL(1,2,1)*10.**6
      DFLI(ITN+1)=DFL(1,2,2)*10.**6
      DO 182 IR=2,12
      GAP(IR)=(DR(1)-DR(2))/2.
      THETA=(2.*3.1415927/Z)*FLOAT(IR-2)
      CS=COS(THETA)
      SN=SIN(THETA)
      NUR1=NUR(IR-1,1)
      NUR2=NUR(IR-1,2)
      GAP(IR)=GAP(IR)+DFL(NUR1,1,1)*SN-DFL(NUR1,2,1)*CS-DFL(NUR2,1,2)*SN
     1+DFL(NUR2,2,2)*CS
      CL(IR)=GAP(IR)-CON2*(FORC(IR,1)**AAN2+FORC(IR,2)**AAN2)-D
     1+DC(IR-1)*AMPL
  182 CLRN(IR-1,ITN+1)=CL(IR)*10.**6
      BDFL=(DFL(1,2,2)+(CON1*(FORC(2,1)**AAN1+FORC(2,2)**AAN1)/2.
     1-CON2*(FORC(2,1)**AAN2+FORC(2,2)**AAN2))-DFL(1,2,1)+DFL(NCON,2,1)
     2+CLN)*10.**6
      STFN=FR/BDFL
      DFLT(ITN+1)=BDFL
      RGDT(ITN+1)=FR/BDFL
      WRITE(6,444) BDFL,STFN
  444 FORMAT(//1X,19HBEARING DEFLECTION=,E12.4,5H U IN/
     11X,22HAV. BEARING STIFFNESS=,E12.4,9H LBS/U IN//)
      WRITE(6,400) (CL(I),I=2,12)
  400 FORMAT(//1X,17HRADIAL CLEARANCES,/11(1X,F10.6)//)
      CALL LMAT
      RMS=SQRT(ERR/(2.*(Z/2.+1.)))
      RMSER(ITN)=RMS
      WRITE(6,190) RMS
  190 FORMAT(//1X,31HRMS ERROR IN LOAD DISTRIBUTION=,F10.5)
      IF(ITN.GE.20) GO TO 184
      IF(RMS.LT.GRMS) GO TO 184
      GO TO 1000
  184 CONTINUE
C     WRITING RESULTS UPTO STATEMENT NO. 392
      WRITE(6,16) FR,AMPL,D,AL,RHO,RPM
   16 FORMAT(1H1,//13H RADIAL LOAD=,F7.0,4H LBS/35H AMPLITUDE OF RELIEF
     1ON OUTER RACE=,F8.5,7H INCHES/17H ROLLER DIAMETER=,F8.5,7H INCHES/
     215H ROLLER LENGTH=,F8.5,7H INCHES/36H SPECIFIC WEIGHT OF ROLLER MA
     3TERIAL=,F8.5,12H LBS/(IN**3)/19H SPEED OF ROTATION=,F10.1,4H RPM/)
      WRITE(6,17)
   17 FORMAT(///4H ITN,17X,46HRADIAL CLEARANCES AT ROLLER POSITIONS IN U
     1 INS/1X,3HNO.,5X,1H1,6X,1H2,6X,1H3,6X,1H4,6X,1H5,6X,1H6,6X,1H7,6X,
     21H8,6X,1H9,5X,2H10,5X,2H11/)
      DO 18 I=1,ITN
   18 WRITE(6,20) I,(CLRN(J,I),J=1,11)
   20 FORMAT(1X,I3,1X,11F7.0)
      WRITE(6,10)
   10 FORMAT(///1X,3HITN,21X,38HLOAD DISTRIBUTION AMONG ROLLERS IN LBS/
     11X,3HNO.,5X,1H1,6X,1H2,6X,1H3,6X,1H4,6X,1H5,6X,1H6,6X,1H7,6X,1H8,
     26X,1H9,5X,2H10,5X,2H11/)
      DO 15 I=1,ITN
      WRITE(6,11) I,(FOR1(J,1,I),J=1,11)
   11 FORMAT(1X,I3,1X,11F7.0)
      IF(RPM.LT.0.001) GO TO 15
      WRITE(6,12) (FOR1(J,2,I),J=1,11)
   12 FORMAT(5X,11F7.0,3X,4HI.R.)
   15 CONTINUE
```

```
      WRITE(6,21)
   21 FORMAT(///1X,3HITN,5X,46HDEFLECTION OF     BODY DFLN   STFNS      RM
     1S ERR/1X,3HNO.,3X,4HO.R.,3X,4HI.R.,3X,4HBRG.,2X,7HOF O.R.,3X,20HLB
     2/U IN    IN LD DTBN/)
      DO 25 I=1,ITN
      IF(I.EQ.1) GO TO 28
      WRITE(6,24) I,DFLO(I),DFLI(I),DFLT(I),DFLB(I),RGDT(I),RMSER(I)
   24 FORMAT(1X,I3,3F7.0,F8.0,3X,F8.3,4X,F8.2)
      GO TO 25
   28 WRITE(6,23) I,DFLT(I),RGDT(I)
   23 FORMAT(1X,I3,14X,F7.0,11X,F8.3)
   25 CONTINUE
      WRITE(6,26)
   26 FORMAT(/7X,29HALL DEFLECTIONS ARE IN U INS.)
      CLN=(DR(1)-DR(2))/2.-D
      BN=CLN/ABS(CLN)*(FLOAT(NRACE(1))*10.**5+FLOAT(NRACE(2))*10.**4+
     1ABS(CLN)*10.**6+AMPL*10.**4)
      IF(NTYP-2) 2001,2002,2003
 2001 WRITE(6,2005) BN
      GO TO 2004
 2002 WRITE(6,2006) BN
      GO TO 2004
 2003 WRITE(6,2007) BN
 2004 CONTINUE
 2005 FORMAT(///1X,3H***,2X,15HBEARING NO.  RS,F7.0,2X,3H***///)
 2006 FORMAT(///1X,3H***,2X,15HBEARING NO.  RR,F7.0,2X,3H***///)
 2007 FORMAT(///1X,3H***,2X,15HBEARING NO.  RT,F7.0,2X,3H***///)
      WRITE(6,391)
  391 FORMAT(1H1,38H DEFLECTION OF POINTS ON RACES IN INS ///9X,
     110HOUTER RACE,31X,10HINNER RACE//)
      NCON1=NCONC(1)+1
      NCON2=NCONC(2)+1
      NCON=NCON1
      IF(NCON2.GT.NCON1) NCON=NCON2
      DO 390 I=1,NCON
      III1=NOF(I,1)
      III2=NOF(I,2)
  390 WRITE(6,392) III1,DFL(I,1,1),DFL(I,2,1),III2,DFL(I,1,2),DFL(I,2,2)
  392 FORMAT(1X,I4,2E14.4,9X,I4,2E14.4)
      IF(NSF-1) 300,200,300
C * * * * * * * * * * * * * * * * * * * * * * * * * * * * * * * * * * *
C     CALCULATION OF NODAL POINT FORCES
C * * * * * * * * * * * * * * * * * * * * * * * * * * * * * * * * * * *
  200 CALL FORCE
      REWIND 1
      DO 989 LA=1,2
      NPA=NPART(LA)
      DO 989 II=1,NPA
  989 READ(4) M,(U(I,LA),I=1,M)
C * * * * * * * * * * * * * * * * * * * * * * * * * * * * * * * * * * *
C     CALCULATION OF STRESSES
C * * * * * * * * * * * * * * * * * * * * * * * * * * * * * * * * * * *
      CALL STRESS
  300 CONTINUE
      RETURN
      END

      SUBROUTINE MFM
C * * * * * * * * * * * * * * * * * * * * * * * * * * * * * * * * * * *
C     SUBROUTINE TO FORM MODIFIED FORCE MATRICES
C * * * * * * * * * * * * * * * * * * * * * * * * * * * * * * * * * * *
      COMMON C(6,6),DBA(3,6),DB(3,6),A(6,6),B(3,6),ST(70,140),U(70,2),
     1NB(30,2,2),UT(30,2,2),UX(161,2,2),NF(30,2),DIS(70),
     2RS(70),NOF(162,2),NUR(11,2),DFL(162,2,2)
```

```
      COMMON/COM1/X(162,2,2),DR(2),NFIRST(21,2),NLAST(20,2),
     1NPART(2),NSTART(20,2),NEND(20,2),NBOUN(2),NFREE(2),NCONC(2),
     2VLM(2),NSR(2),CL(12),NNN(4),NRACE(2),FR,Z,CON1,CON2,AAN1,AAN2,
     3RPM,D,AL,RHO,Y,FOR(12,2),FORC(12,2),ITN,ERR,AMPL,NSF,NPRO,NPR,
     4RBF(2),REF(2),UF(2),DC(11),BDFL,FOR1(11,2,20)
      DO 20 LA=1,2
      DO 5 LL=1,2
      DO 5 I=1,70
    5 U(I,LL)=0.
      LF=1
      IF(LA.EQ.1) LF=2
      NFRE=NFREE(LA)
      NPA=NPART(LA)
C * * * * * * * * * * * * * * * * * * * * * * * * * * * * * * * * * * * *
C     READING BODY FORCE MATRIX FROM TAPE NO. 4
C * * * * * * * * * * * * * * * * * * * * * * * * * * * * * * * * * * * *
      DO 10 II=1,NPA
      READ(4) M,(U(I,LA),I=1,M)
      M2=NFRE*((NFIRST(II+1,LA)-1)-(NFIRST(II,LA)-1))
      IF(M-M2) 40,41,40
   40 STOP
   41 CONTINUE
C * * * * * * * * * * * * * * * * * * * * * * * * * * * * * * * * * * * *
C     ADDING EXTERNAL LOAD TO BODY FORCE MATRIX TO FORM TOTAL FORCE
C     MATRIX
C * * * * * * * * * * * * * * * * * * * * * * * * * * * * * * * * * * * *
      K=NFIRST(II,LA)
      L1=NFIRST(II+1,LA)-1
      NCON=NCONC(LA)
      DO 30 J=1,NCON
C * * * * * * * * * * * * * * * * * * * * * * * * * * * * * * * * * * * *
C     TO TEST WHETHER NOF(J,LA) IS IN THE PARTITION UNDER STUDY OR NOT
C * * * * * * * * * * * * * * * * * * * * * * * * * * * * * * * * * * * *
      MM=NOF(J,LA)-K
      IF(MM)30,31,31
   31 M1=NOF(J,LA)-L1
      IF(M1) 32,32,30
   32 DO 33 I=1,NFRE
      NMI=NFRE*MM+I
      U(NMI,LA)=U(NMI,LA)+UX(J,I,LA)
   33 CONTINUE
   30 CONTINUE
C * * * * * * * * * * * * * * * * * * * * * * * * * * * * * * * * * * * *
C     INTRODUCING PRESCRIBED DISPLACEMENT
C * * * * * * * * * * * * * * * * * * * * * * * * * * * * * * * * * * * *
      NBO=NBOUN(LA)
      DO 34 I=1,NBO
C * * * * * * * * * * * * * * * * * * * * * * * * * * * * * * * * * * * *
C     TO TEST WHETHER NF(I,LA) IS IN THE PARTITION UNDER STUDY OR NOT
C * * * * * * * * * * * * * * * * * * * * * * * * * * * * * * * * * * * *
      MM=NF(I,LA)-K
      IF(MM) 34,35,35
   35 M1=NF(I,LA)-L1
      IF(M1) 36,36,34
   36 DO 37 J=1,NFRE
      IF(NB(I,J,LA)) 37,38,37
   38 NMI=NFRE*MM+J
      U(NMI,LA)=UT(I,J,LA)
   37 CONTINUE
   34 CONTINUE
      DO 54 I=1,M
   54 U(I,LA)=U(I,LA)-U(I,LF)
      WRITE(1) M,(U(I,LA),I=1,M)
      IF(NPA-II) 55,10,55
   55 READ(2) M,N,((ST(I,J),I=1,N),J=1,M)
```

```
      DO 56 L=1,N
      U(L,LF)=0.
      DO 56 I=1,M
   56 U(L,LF)=U(L,LF)+ST(L,I)*U(I,LA)
   10 CONTINUE
   20 CONTINUE
      RETURN
      END

      SUBROUTINE SOLVE
C * * * * * * * * * * * * * * * * * * * * * * * * * * * * * * * * * * * * * * *
C     SUBROUTINE TO SOLVE FOR DISPLACEMENTS BY BACK-SUBSTITUTION
C * * * * * * * * * * * * * * * * * * * * * * * * * * * * * * * * * * * * * * *
      DIMENSION AM(70,140),BM(70,70)
      COMMON C(6,6),DBA(3,6),DB(3,6),A(6,6),B(3,6),ST(70,140),U(70,2),
     1NB(30,2,2),UT(30,2,2),UX(161,2,2),NF(30,2),DIS(70),
     2RS(70),NOF(162,2),NUR(11,2),DFL(162,2,2)
      COMMON/COM1/X(162,2,2),DR(2),NFIRST(21,2),NLAST(20,2),
     1NPART(2),NSTART(20,2),NEND(20,2),NBOUN(2),NFREE(2),NCONC(2),
     2VLM(2),NSR(2),CL(12),NNN(4),NRACE(2),FR,Z,CON1,CON2,AAN1,AAN2,
     3RPM,D,AL,RHO,Y,FOR(12,2),FORC(12,2),ITN,ERR,AMPL,NSF,NPRO,NPR,
     4RBF(2),REF(2),UF(2),DC(11),BDFL,FOR1(11,2,20)
      EQUIVALENCE(AM(1,1),ST(1,1)),(BM(1,1),AM(1,71))
      DO 20 LA=1,2
      LF=1
      IF(LA.EQ.1) LF=2
      NCON=NCONC(LF)+1
      NFRE=NFREE(LF)
      NPA=NPART(LF)
      DO 144 LL=1,NPA
      BACKSPACE 1
      READ(1) M,(U(I,LA),I=1,M)
      IF(LL-1) 30,38,30
   38 READ(2) M,((AM(I,J),I=1,M),J=1,M)
      DO 31 I=1,M
      DIS(I)=0.
      DO 31 K=1,M
   31 DIS(I)=DIS(I)+AM(I,K)*U(K,LA)
      WRITE(4) M,(DIS(I),I=1,M)
C     TO FIND DEFLECTION OF POINTS ON RACES
      DO 50 J=1,NCON
      MM=NOF(J,LF)-NFIRST(NPA,LF)
      IF(MM) 50,51,51
   51 M1=NOF(J,LF)-NFIRST(NPA+1,LF)+1
      IF(M1) 52,52,50
   52 DO 53 I=1,NFRE
      NMI=NFRE*MM+I
      DFL(J,I,LF)=DIS(NMI)
   53 CONTINUE
   50 CONTINUE
C     WRITE(6,32) NPA
C  32 FORMAT(//7H DELTA ,I2//)
C     WRITE(6,33) M,(DIS(I),I=1,M)
C  33 FORMAT(//3H M=I4/(1H 6E16.8))
C * * * * * * * * * * * * * * * * * * * * * * * * * * * * * * * * * * * * * * *
C     DELTA(N) IS STORED ON TAPE NO. 4 NOW
C * * * * * * * * * * * * * * * * * * * * * * * * * * * * * * * * * * * * * * *
      GO TO 40
   30 READ(2) M,N,((AM(I,J),I=1,M),J=1,M),((BM(I,J),I=1,M),J=1,N)
      DO 35 I=1,M
      U(I,LF)=0.
      DO 35 J=1,N
   35 U(I,LF)=U(I,LF)+BM(I,J)*DIS(J)
      DO 36 I=1,M
   36 U(I,LA)=U(I,LA)-U(I,LF)
```

```
      DO 37 I=1,M
      DIS(I)=0.
      DO 37 J=1,M
   37 DIS(I)=DIS(I)+AM(I,J)*U(J,LA)
      LLLL=NPA-LL+1
C     WRITE(6,32) LLLL
C     WRITE(6,33) M,(DIS(I),I=1,M)
C     TO FIND DEFLECTION OF POINTS ON RACES
      DO 60 J=1,NCON
      MM=NOF(J,LF)-NFIRST(LLLL,LF)
      IF(MM) 60,61,61
   61 M1=NOF(J,LF)-NFIRST(LLLL+1,LF)+1
      IF(M1) 62,62,60
   62 DO 63 I=1,NFRE
      NMI=NFRE*MM+I
      DFL(J,I,LF)=DIS(NMI)
   63 CONTINUE
   60 CONTINUE
      WRITE(4) M,(DIS(I),I=1,M)
   40 BACKSPACE 1
  144 CONTINUE
   20 CONTINUE
      RETURN
      END

      SUBROUTINE LMAT
C * * * * * * * * * * * * * * * * * * * * * * * * * * * * * * * * * * * *
C     SUBROUTINE TO FORM LOAD MATRIX
C * * * * * * * * * * * * * * * * * * * * * * * * * * * * * * * * * * * *
      DIMENSION P(6)
      COMMON C(6,6),DBA(3,6),DB(3,6),A(6,6),B(3,6),ST(70,140),U(70,2),
     1NB(30,2,2),UT(30,2,2),UX(161,2,2),NF(30,2),DIS(70),
     2RS(70),NOF(162,2),NUR(11,2),DFL(162,2,2)
      COMMON/COM1/X(162,2,2),DR(2),NFIRST(21,2),NLAST(20,2),
     1NPART(2),NSTART(20,2),NEND(20,2),NBOUN(2),NFREE(2),NCONC(2),
     2VLM(2),NSR(2),CL(12),NNN(4),NRACE(2),FR,Z,CON1,CON2,AAN1,AAN2,
     3RPM,D,AL,RHO,Y,FOR(12,2),FORC(12,2),ITN,ERR,AMPL,NSF,NPRO,NPR,
     4RBF(2),REF(2),UF(2),DC(11),BDFL,FOR1(11,2,20)
      COMMON/COM2/FCTR,FCTR1,GRMS,NTYP
      ITN=ITN+1
      ERR=0.
      DO 1 I=1,2
      NCON=NCONC(I)
      NFRE=NFREE(I)
      DO 1 J=1,NCON
      DO 1 K=1,NFRE
    1 UX(J,K,I)=0.
      DI=DR(2)
      CALL DTBN(FR,Z,CON1,AAN1,RPM,D,AL,DI,RHO,CL,FOR,ITN,BDFL)
      IF(ITN.EQ.1) GO TO 45
C     UPTO STATEMENT NO.10 A CONSTANT FORCE IS ALGEBRICALLY SUBTRACTED
C     FROM ALL THE ROLLERS FOR RAPID CONVERGENCE, TAKING CARE THAT NO
C     ROLLER IS UNDER TENSION.
      DFOR=FCTR1*(FORC(12,2)-FOR(12,2))
      DO 8 I=2,12
    8 IF(FORC(I,2).LT.DFOR) DFOR=FORC(I,2)
      DO 10 LA=1,2
      DO 10 I=2,12
      ERR=ERR+(FOR(I,LA)-FORC(I,LA))**2
      FORC(I,LA)=FORC(I,LA)-DFOR
   10 CONTINUE
   45 CONTINUE
      DO 20 LA=1,2
      IF(LA-1) 11,12,11
   11 DIA=DR(LA)
```

```
      SIGN=+1.
      GO TO 13
   12 DIA=-DR(LA)
      SIGN=-1.
   13 DO 21 II=1,11
      MM=NUR(II,LA)
      FOR1(II,LA,ITN)=FOR(II+1,LA)
      IF(ITN-1) 4,5,4
    4 FOR(II+1,LA)=(FORC(II+1,LA)+FCTR*FOR(II+1,LA))/(1.+FCTR)
    5 ALOD=FOR(II+1,LA)
      CALL NPF(ALOD,Y,AL,P,M,D,DIA)
      THETA=(2.*3.1415927/Z)*FLOAT(II-1)
      CS=COS(THETA)
      SN=SIN(THETA)
      IF(II-11) 14,15,14
   14 DO 16 I=1,M
      MMI=MM+(I-1)
      UX(MMI,1,LA)=UX(MMI,1,LA)-P(I)*SN*SIGN
      UX(MMI,2,LA)=UX(MMI,2,LA)+P(I)*CS*SIGN
   16 CONTINUE
   15 IF(II-1) 17,19,17
   17 DO 18 I=1,M
      MMI=MM-(I-1)
      UX(MMI,1,LA)=UX(MMI,1,LA)-P(I)*SN*SIGN
      UX(MMI,2,LA)=UX(MMI,2,LA)+P(I)*CS*SIGN
   18 CONTINUE
   19 CONTINUE
   21 CONTINUE
   20 CONTINUE
      WRITE(6,50)(FOR(I,2),I=2,12)
   50 FORMAT(1X,38HLD DTBN AT I.R. BEFORE NEXT ITERATION,/1X,11F11.4)
C     SECTION BELOW BALANCE THE VERY SMALL UNBALANCED FORCE THAT MAY BE
C     PRESENT BETWEEN BODY FORCE AND EXTERNAL FORCE WHEN THERE IS NO
C     CONSTRAINT OF THE RACE IN Y-DIRECTION. THE UNBALANCED FORCE IS
C     ALWAYS SO SMALL THAT ITS EFFECT IS INSIGNIFICANF AS REGARDS TO
C     STRESS DISTRIBUTION, BUT, IF NOT CONSIDERED WILL INTRODUCE LARGE
C     BODY DEFLECTION OF THE RACE IN Y-DIRECTION.
      DO 30 LA=1,2
      REF(LA)=0.
      NCON=NCONC(LA)
      IF(1-NSR(LA)) 30,25,30
   25 DO 26 I=1,NCON
   26 REF(LA)=REF(LA)+UX(I,2,LA)
      UF(LA)=RBF(LA)+REF(LA)
      WRITE(6,27) RBF(LA),REF(LA),UF(LA)
   27 FORMAT(1X,21HRESULTANT BODY FORCE=,E16.8/1X,21HRESULTANT EXTL FORC
     1E=,E16.8/1X,17HUNBALANCED FORCE=,E16.8)
      UF(LA)=UF(LA)/FLOAT(NCON)
      DO 28 I=1,NCON
   28 UX(I,2,LA)=UX(I,2,LA)-UF(LA)
   30 CONTINUE
      RETURN
      END

      SUBROUTINE DTBN(FR,Z,CON,AAN,RPM,D,AL,DI,RHO,C,FOR,ITN,BDFL)
C * * * * * * * * * * * * * * * * * * * * * * * * * * * * * * * * * * *
C     SUBROUTINE TO FIND LOAD DISTRIBUTION IN A ROLLER BEARING
C     USING NEWTON RAPHSON METHOD
C * * * * * * * * * * * * * * * * * * * * * * * * * * * * * * * * * * *
      DIMENSION PD1(12),PD2(12),PD3(12),DEL(12),C(12),ERR(12),FI(12),
     1FO(12),THETA(12),EQ(12),FOR(12,2)
      WRITE(6,600)
  600 FORMAT(//1H ,37HCALCULATION OF LOAD DISTRIBUTION IN A/
     1 1X,35HBEARING USING NEWTON RAPHSON METHOD//)
```

```
      AN=1./AAN
      AK=(2./CON)**AN
      WRITE(6,150)AK,AN
  150 FORMAT(1X,3HAK=,E14.7,5X,3HAN=,F10.4)
      DO 18 J=2,12
   18 THETA(J)=2.*3.14159*(FLOAT(J-2))/Z
C     INNER RACE ROTATION. CALCULATION OF CENTRIFUGAL FORCE
      ARPM=(RPM*DI/(2.*(D+DI)))*(3.1415927/30.)
C     RHO IS SPECIFIC WEIGHT IN LBS/(IN**3)
      FC=RHO*3.1415927*(D**2)*AL*((DI+D)/2.)*(ARPM**2)/1545.6
C     C(J)=G(J)-D
C     CALCULATION OF APPROXIMATE DEFLECTION.  THIS IS DONE BY
C     CONSIDERING A BEARING AT STATIC CONDITION WITH NO CLEARANCE.
      DEL(1)=(4.08*FR/(0.5**1.11*Z*AK))**(1./AN)
      DO 12 J=2,7
   12 DEL(J)=DEL(1)*COS(THETA(J))/2.
      DO 80 J=8,12
   80 DEL(J)=0.0
      IF(DEL(1).LT.C(2)) GO TO 97
   31 S=0.
      IF(DEL(1).LT.0.) GO TO 96
      GO TO 98
   96 IF(DEL(2).GE.0.) GO TO 97
      DEL(1)=0.
      GO TO 98
   97 DEL(1)=2.*DEL(2)+C(2)
      IF(DEL(1).GE.0.) GO TO 98
      DEL(1)=0.
   98 CONTINUE
      DO 95 J=2,12
      IF((DEL(1)*COS(THETA(J))-C(J)).LE.0.) GO TO 94
      IF(DEL(J).LT.(DEL(1)*COS(THETA(J))-C(J))) GO TO 95
      DEL(J)=(DEL(1)*COS(THETA(J))-C(J))/2.
      GO TO 95
   94 DEL(J)=0.
   95 CONTINUE
C     FORMATION OF MATRIX EQ
      DO 22 J=2,12
      IF((THETA(J).GT.0.1E-20).AND.(THETA(J).LT.3.1)) GO TO 21
      TAO=0.5
      GO TO 22
   21 TAO=1.0
   22 S=S+TAO*DEL(J)**AN*COS(THETA(J))
      EQ(1)=FR/(2.*AK)-S
      DO 24 J=2,12
      IF((DEL(1)*COS(THETA(J))-C(J)).GT.0.1E-20) GO TO 23
      EQ(J)=0.0
      GO TO 24
   23 EQ(J)=(DEL(1)*COS(THETA(J))-C(J)-DEL(J))**AN-DEL(J)**AN-FC/AK
   24 CONTINUE
C     FORMATION OF PARTIAL DIFFERENTIAL MATRIX PD
      DO 30 I=1,12
      PD1(I)=0.
      PD2(I)=0.
   30 PD3(I)=0.
      DO 33 I=2,12
      IF((DEL(1)*COS(THETA(I))-C(I)).GT.0.1E-20) GO TO 32
      GO TO 33
   32 PD3(I)=AN*(DEL(1)*COS(THETA(I))-C(I)-DEL(I))**(AN-1.)
     1*COS(THETA(I))
   33 CONTINUE
      DO 35 J=2,12
      IF((THETA(J).GT.0.1E-20).AND.(THETA(J).LT.3.1)) GO TO 34
      TAO=0.5
      GO TO 35
```

```
   34 TAO=1.0
   35 PD1(J)=-AN*TAO*(DEL(J)**(AN-1.))*COS(THETA(J))
      DO 37 I=2,12
      IF((DEL(1)*COS(THETA(I))-C(I)).GT.0.1E-20) GO TO 36
      GO TO 37
   36 PD2(I)=-AN*((DEL(1)*COS(THETA(I))-C(I)-DEL(I))**(AN-1.)+DEL(I)**
     1(AN-1.))
   37 CONTINUE
      SUM1=0.
      SUM2=0.
      DO 86 I=2,12
      IF(ABS(PD2(I)).GT.0.) GO TO 85
      GO TO 86
   85 SUM1=SUM1+PD1(I)*EQ(I)/PD2(I)
      SUM2=SUM2+PD1(I)*PD3(I)/PD2(I)
   86 CONTINUE
      ERR(1)=(EQ(1)-SUM1)/SUM2
      DO 90 I=2,12
      IF(ABS(PD2(I)).GT.0.) GO TO 87
      ERR(I)=0.
      GO TO 90
   87 ERR(I)=-((EQ(I)/PD2(I))+(PD3(I)*ERR(1)/PD2(I)))
   90 CONTINUE
      DO 45 I=1,12
      IF(I.LE.1) GO TO 44
      IF((DEL(1)*COS(THETA(I))-C(I)).GT.0.1E-20) GO TO 44
      DEL(I)=0.
      GO TO 45
   44 DEL(I)=DEL(I)+ERR(I)
   45 CONTINUE
      DO 25 J=2,12
      IF(DEL(J).GE.0.)GO TO 25
      DEL(J)=0.
      ERR(J)=0.
   25 CONTINUE
      ERR1=0.
      DO 47 J=1,12
   47 ERR1=ERR1+ERR(J)**2
      RMS=(ERR1/(Z/2.+2.))**0.5
      IF(RMS.GT.0.1E-5) GO TO 31
      IF(ITN-1) 62,60,62
   60 CC1=C(2)
      IF(C(2).LE.0.) CC1=0.
      BDFL=(DEL(1)-CC1)*10.**3
      WRITE(6,61) BDFL
   61 FORMAT(///,44H BEARING DEFLECTION CONSIDERING STIFF RACES=,F6.2,
     15H THOU,///)
   62 IF(RPM.GT.0.1E-20) GO TO 55
C     NO ROTATION OR STATIC LOAD DISTRIBUTION
      DO 50 I=2,12
      FI(I)=AK*DEL(I)**AN
   50 FO(I)=FI(I)
      WRITE(6,54)(FI(I),I=2,12)
   54 FORMAT(//1X,24HSTATIC LOAD DISTRIBUTION/1X,11(1X,F10.4))
      AFI=0.
      DO 175 I=2,12
      IF((THETA(I).GT.0.1E-20).AND.(THETA(I).LT.3.1)) GO TO 174
      TAO=1.0
      GO TO 175
  174 TAO=2.0
  175 AFI=AFI+TAO*FI(I)*COS(THETA(I))
      WRITE(6,176) AFI
  176 FORMAT(//1X,24HRESULTANT EXTERNAL LOAD=,F7.0,4H LBS)
```

```
C       DYNAMIC LOAD DISTRIBUTION
        IF(RPM.LT.0.1E-20) GO TO 200
   55   DO 56 I=2,12
        FI(I)=AK*DEL(I)**AN
   56   FO(I)=FI(I)+FC
        WRITE(6,58)(FI(I),I=2,12),(FO(I),I=2,12)
        AFI=0.
        AFO=0.
        DO 186 I=2,12
        IF((THETA(I).GT.0.1E-20).AND.(THETA(I).LT.3.1)) GO TO 184
        TAO=1.0
        GO TO 185
  184   TAO=2.0
  185   AFI=AFI+TAO*FI(I)*COS(THETA(I))
        AFO=AFO+TAO*FO(I)*COS(THETA(I))
  186   CONTINUE
        WRITE(6,187) AFI,AFO
  187   FORMAT(//1X,43HRESULTANT LOAD ON INNER AND OUTER RACES ARE,F7.0,
       15H AND ,F7.0,17H LBS RESPECTIVELY)
   58   FORMAT(//1X,25HDYNAMIC LOAD DISTRIBUTION/1X,18HLOAD AT INNER RACE/
       11X,11(1X,F10.4)/1X,18HLOAD AT OUTER RACE/1X,11(1X,F10.4))
  200   DO 70 J=2,12
        FOR(J,1)=FO(J)
   70   FOR(J,2)=FI(J)
        RETURN
        END


        SUBROUTINE NPF(ALOD,Y,AL,P,M,D,DIA)
C * * * * * * * * * * * * * * * * * * * * * * * * * * * * * * * * * * * * * *
C       TO DISTRIBUTE INDIVIDUAL ROLLER LOADS ON THE NODAL POINTS IN THE
C       CONTACT AREA, TAKING SEMI-ELLIPTIC STRESS DISTRIBUTION.
C * * * * * * * * * * * * * * * * * * * * * * * * * * * * * * * * * * * * * *
        DIMENSION P(6),DS(6),S(6)
        SR=(2./D)+(2./DIA)
C       SR IS THE SUMMATION OF PRINCIPAL CURVATURES
        B=SQRT((7.28*ALOD)/(3.1415927*Y*SR*AL))
C       IN THE ABOVE EQUATION FOR B, FACTOR 7.28 IS OBTAINED TAKING
C       POISSON'S RATIO FOR STEEL TO BE 0.3
        DS(1)=0.0
        DS(2)=0.00025
        DS(3)=0.00100
        DS(4)=0.00225
        DS(5)=0.00425
        DS(6)=0.00775
        DO 20 I=1,6
   20   P(I)=0.
        IF(B.GT.DS(2)) GO TO 3
        M=1
        GO TO 8
    3   IF(B.GT.DS(3)) GO TO 4
        M=2
        GO TO 8
    4   IF(B.GT.DS(4)) GO TO 5
        M=3
        GO TO 8
    5   IF(B.GT.DS(5)) GO TO 6
        M=4
        GO TO 8
    6   IF(B.GT.DS(6)) GO TO 7
        M=5
        GO TO 8
```

```
      7 M=6
      8 IF(M-1)10,9,10
      9 P(1)=ALOD/2.
        GO TO 100
     10 DO 12 I=1,M
     12 S(I)=((2.*ALOD)/(3.14159*B*AL))*SQRT(1.-(DS(I)/B)**2)
        DO 13 J=2,M
     13 P(J-1)=((S(J-1)+S(J))/2.)*(DS(J)-DS(J-1))*AL
        P(M)=(S(M)*(B-DS(M))/2.)*AL
        P1=0.
        DO 14 I=1,M
     14 P1=P1+P(I)
        DO 15 J=2,M
     15 P(J-1)=P(J-1)+((ALOD/2.-P1)/B)*(DS(J)-DS(J-1))
        P(M)=P(M)+((ALOD/2.-P1)/B)*(B-DS(M))
    100 CONTINUE
        RETURN
        END

        SUBROUTINE FORCE
C * * * * * * * * * * * * * * * * * * * * * * * * * * * * * * * * * * * * * * * *
C       SUBROUTINE FOR CALCULATING NODAL POINT FORCES
C * * * * * * * * * * * * * * * * * * * * * * * * * * * * * * * * * * * * * * * *
        DIMENSION AM(70,140),BM(70,70)
        COMMON C(6,6),DBA(3,6),DB(3,6),A(6,6),B(3,6),ST(70,140),U(70,2),
       1NB(30,2,2),UT(30,2,2),UX(161,2,2),NF(30,2),DIS(70),
       2RS(70),NOF(162,2),NUR(11,2),DFL(162,2,2)
        COMMON/COM1/X(162,2,2),DR(2),NFIRST(21,2),NLAST(20,2),
       1NPART(2),NSTART(20,2),NEND(20,2),NBOUN(2),NFREE(2),NCONC(2),
       2VLM(2),NSR(2),CL(12),NNN(4),NRACE(2),FR,Z,CON1,CON2,AAN1,AAN2,
       3RPM,D,AL,RHO,Y,FOR(12,2),FORC(12,2),ITN,ERR,AMPL,NSF,NPRO,NPR,
       4RBF(2),REF(2),UF(2),DC(11),BDFL,FOR1(11,2,20)
        EQUIVALENCE(AM(1,1),ST(1,1)),(BM(1,1),AM(1,71))
        WRITE(6,10)
     10 FORMAT(1H1,19H NODAL POINT FORCES//)
        DO 20 LA=1,2
        LF=1
        IF(LA.EQ.1) LF=2
        DO 18 I=1,70
     18 RS(I)=0.
        NFRE=NFREE(LA)
        NBO=NBOUN(LA)
        NPA=NPART(LA)
        DO 144 LL=1,NPA
        READ(3) M,((AM(I,J),J=1,M),I=1,M)
        IF(NPA-LL) 25,26,25
     25 READ(3) M,N,((BM(I,J),J=1,N),I=1,M)
     26 BACKSPACE 4
        READ(4) M,(DIS(I),I=1,M)
        DO 29 I=1,NBO
        K=NFIRST(LL,LA)
        L=NFIRST(LL+1,LA)-1
        M5=NF(I,LA)-K
        IF(M5) 29,24,24
     24 M1=NF(I,LA)-L
        IF(M1) 27,27,29
     27 DO 30 J=1,NFRE
        IF(NB(I,J,LA)) 30,31,30
     31 NMI=NFRE*M5+J
        AM(NMI,NMI)=AM(NMI,NMI)*.1E-10
     30 CONTINUE
     29 CONTINUE
        IF(NPA-LL) 35,34,35
     35 BACKSPACE 4
        BACKSPACE 4
```

```
      READ(4) N,(U(I,LF),I=1,N)
   34 DO 40 I=1,M
      U(I,LA)=RS(I)
      DO 42 K=1,M
   42 U(I,LA)=U(I,LA)+AM(I,K)*DIS(K)
      IF(NPA-LL) 43,40,43
   43 DO 44 L=1,N
   44 U(I,LA)=U(I,LA)+BM(I,L)*U(L,LF)
   40 CONTINUE
      IF(NPA-LL) 47,144,47
   47 DO 49 I=1,N
      RS(I)=0.
      DO 49 K=1,M
   49 RS(I)=RS(I)+BM(K,I)*DIS(K)
  144 WRITE(6,53) (U(I,LA),I=1,M)
   53 FORMAT(1H 6E13.4)
      BACKSPACE 4
   20 CONTINUE
      RETURN
      END

      SUBROUTINE STRESS
C * * * * * * * * * * * * * * * * * * * * * * * * * * * * * * * * * * * * * * *
C     SUBROUTINE FOR CALCULATION OF STRESSES
C * * * * * * * * * * * * * * * * * * * * * * * * * * * * * * * * * * * * * * *
      DIMENSION NOD(3)
      COMMON C(6,6),DBA(3,6),DB(3,6),A(6,6),B(3,6),ST(70,140),U(70,2),
     1NB(30,2,2),UT(30,2,2),UX(161,2,2),NF(30,2),DIS(70),
     2RS(70),NOF(162,2),NUR(11,2),DFL(162,2,2)
      COMMON/COM1/X(162,2,2),DR(2),NFIRST(21,2),NLAST(20,2),
     1NPART(2),NSTART(20,2),NEND(20,2),NBOUN(2),NFREE(2),NCONC(2),
     2VLM(2),NSR(2),CL(12),NNN(4),NRACE(2),FR,Z,CON1,CON2,AAN1,AAN2,
     3RPM,D,AL,RHO,Y,FOR(12,2),FORC(12,2),ITN,ERR,AMPL,NSF,NPRO,NPR,
     4RBF(2),REF(2),UF(2),DC(11),BDFL,FOR1(11,2,20)
      DO 20 LA=1,2
      NPA=NPART(LA)
      DO 144 LL=1,NPA
      IF(LA-1) 24,25,24
   24 WRITE(6,26)
      GO TO 28
   25 WRITE(6,27)
   26 FORMAT(1H1,10HINNER RACE)
   27 FORMAT(1H1,10HOUTER RACE)
   28 WRITE(6,45) LL
   45 FORMAT(1H ,13HPARTITION NO.,I2)
      WRITE(6,30)
   30 FORMAT(//5H NODE,16H X-DISPLACEMENTS,16H Y-DISPLACEMENTS)
      K=NFIRST(LL,LA)
      L=NLAST(LL,LA)
      NST=NSTART(LL,LA)
      NEN=NEND(LL,LA)
      LK=NFIRST(LL+1,LA)
      MM=LK-K
      BACKSPACE 4
      READ(4) M,(DIS(I),I=1,M)
      IF(NPA-LL) 22,23,22
   22 BACKSPACE 4
      BACKSPACE 4
      READ(4) N,(RS(I),I=1,N)
   23 CONTINUE
      IF(2*MM-M) 31,32,31
   31 STOP
   32 CONTINUE
      DO 50 I=1,MM
      NN=K+I-1
```

```
      WRITE(6,33) NN,DIS(2*I-1),DIS(2*I)
   33 FORMAT(1H ,I4,E14.4,2X,E14.4)
   50 CONTINUE
      WRITE(6,34)
   34 FORMAT(//2X,3HELM,5X,3HNOD,7X,21HX AND Y  CO-ORDINATES,5X,
     18HX-STRESS,5X,8HY-STRESS,4X,9HXY-STRESS/2X,3HNO.,3X,7HNUMBERS,
     210X,11HOF CENTROID/)
      NELM=NEN-NST+1
      DO 40 II=1,NELM
      NEL=NST+II-1
      READ(1) ((DBA(I,J),I=1,3),J=1,6),(NOD(I),I=1,3),ORX,ORY
      DO 35 I=1,3
      JJ=NOD(I)-K+1
      IF(2*JJ.GT.M) GO TO 37
      C(2*I-1,1)=DIS(2*JJ-1)
      C(2*I,1)=DIS(2*JJ)
      GO TO 38
   37 JJ=NOD(I)-LK+1
      C(2*I-1,1)=RS(2*JJ-1)
      C(2*I,1)=RS(2*JJ)
   38 CONTINUE
   35 CONTINUE
      DO 41 I=1,3
      DB(I,1)=0.
      DO 41 J=1,6
   41 DB(I,1)=DB(I,1)+DBA(I,J)*C(J,1)
      WRITE(6,42) NEL,(NOD(I),I=1,3),ORX,ORY,(DB(I,1),I=1,3)
   42 FORMAT(1H ,4I4,2X,F9.6,4X,F9.6,1X,3E13.4)
   40 CONTINUE
      INTER=NEN
  144 CONTINUE
      BACKSPACE 4
   20 CONTINUE
      RETURN
      END
```

The following program 'CHOTTO' can be used for a bearing with a given combination of races when their stiffness and intermediate matrices have been developed and stored (in tape no.8) by the program 'FINELM'. This saves a considerable amount of computer time.

```
      OVERLAY(XX,0,0)
      PROGRAM CHOTTO(INPUT,OUTPUT,TAPE5=INPUT,TAPE6=OUTPUT,
     1TAPE1,TAPE2,TAPE3,TAPE4,TAPE8,TAPE25,TAPE27)
C * * * * * * * * * * * * * * * * * * * * * * * * * * * * * * * * * * * *
C     THIS PROGRAM IS USED TO SOLVE THE PROBLEMS OF BEARINGS HAVING A
C     GIVEN COMBINATION OF RACES WHOSE STIFFNESS AND THE INTERMEDIATE
C     MATRICES HAVE BEEN CALCULATED AND STORED (ON TAPE8) BY THE
C     PROGRAM FINELM
C * * * * * * * * * * * * * * * * * * * * * * * * * * * * * * * * * * * *
      COMMON C(6,6),DBA(3,6),DB(3,6),A(6,6),B(3,6),ST(70,140),U(70,2),
     1NB(30,2,2),UT(30,2,2),UX(161,2,2),NF(30,2),DIS(70),
     2RS(70),NOF(162,2),NUR(11,2),DFL(162,2,2)
      COMMON/COM1/X(162,2,2),DR(2),NFIRST(21,2),NLAST(20,2),
     1NPART(2),NSTART(20,2),NEND(20,2),NBOUN(2),NFREE(2),NCONC(2),
     2VLM(2),NSR(2),CL(12),NNN(4),NRACE(2),FR,Z,CON1,CON2,AAN1,AAN2,
     3RPM,D,AL,RHO,Y,FOR(12,2),FORC(12,2),ITN,ERR,AMPL,NSF,NPRO,NPR,
     4RBF(2),REF(2),UF(2),DC(11),BDFL,FOR1(11,2,20)
```

```
      COMMON/COM2/FCTR,FCTR1,GRMS,NTYP
      READ(5,1000) FCTR,FCTR1,GRMS,NTYP
      WRITE(6,1000)FCTR,FCTR1,GRMS,NTYP
 1000 FORMAT(1X,F4.2,2F5.2,I5)
      CALL OVERLAY(2HXX,1,0,0)
      READ(5,10) NPROB
   10 FORMAT(I4)
      DO 40 NPR=1,NPROB
      READ(5,20) FR,AMPL,D,AL,RHO,RPM,NSF
   20 FORMAT(F10.1,4F10.5,F10.1,I4)
C     IF NSF=1, STRESSES WILL BE CALCULATED AND PRINTED. DEFLECTION
C     AND FORCES AT EACH NODAL POINT WILL BE PRINTED.
C     ANY OTHER VALUE OF NSF WILL OMMIT THESE.
      REWIND 3
      REWIND 4
      DO 30 LA=1,2
      RBF(LA)=0.
      IF(VLM(LA).GT.0.) GO TO 25
      DEN=0.
      GO TO 26
   25 DEN=FR/(2.*VLM(LA))
   26 NPA=NPART(LA)
      DO 30 II=1,NPA
      READ(3) M,(U(I,LA),I=1,M)
      IF(1-NSR(LA)) 29,27,29
   27 DO 28 MN=1,M
      U(MN,LA)=U(MN,LA)*DEN
   28 RBF(LA)=RBF(LA)+U(MN,LA)
   29 WRITE(4)M,(U(I,LA),I=1,M)
   30 CONTINUE
      CALL OVERLAY(2HXX,2,0,0)
      NPRO=NPROB-NPR
      AMGN=2000.
C     AMGN IS THE MAGNIFICATION TO WHICH THE DEFLECTED SHAPES OF THE
C     RACES ARE PLOTTED.
      CALL DRAW(AMGN)
   40 CONTINUE
      STOP
      END


      OVERLAY(XX,1,0)
      PROGRAM ONE
      CALL RWTN
      RETURN
      END



      SUBROUTINE RWTN
C * * * * * * * * * * * * * * * * * * * * * * * * * * * * * * * * * * * * * * *
C     SUBROUTINE TO READ THE DATA STORED IN TAPE8 BY PROGRAM FINELM
C * * * * * * * * * * * * * * * * * * * * * * * * * * * * * * * * * * * * * * *
      DIMENSION NOD(3),NELEM(2),AM(70,140),BM(70,70)
      COMMON C(6,6),DBA(3,6),DB(3,6),A(6,6),B(3,6),ST(70,140),U(70,2),
     1NB(30,2,2),UT(30,2,2),UX(161,2,2),NF(30,2),DIS(70),
     2RS(70),NOF(162,2),NUR(11,2),DFL(162,2,2)
      COMMON/COM1/X(162,2,2),DR(2),NFIRST(21,2),NLAST(20,2),
     1NPART(2),NSTART(20,2),NEND(20,2),NBOUN(2),NFREE(2),NCONC(2),
     2VLM(2),NSR(2),CL(12),NNN(4),NRACE(2),FR,Z,CON1,CON2,AAN1,AAN2,
     3RPM,D,AL,RHO,Y,FOR(12,2),FORC(12,2),ITN,ERR,AMPL,NSF,NPRO,NPR,
     4RBF(2),REF(2),UF(2),DC(11),BDFL,FOR1(11,2,20)
      EQUIVALENCE(AM(1,1),ST(1,1)),(BM(1,1),AM(1,71))
      REWIND 1
      REWIND 2
      REWIND 3
      REWIND 8
```

```
      READ(8) Z,CON1,CON2,AAN1,AAN2,(DR(I),I=1,2),NYM,Y,(NNN(I),I=1,4)
      DO 20 LA=1,2
      READ(8) NPART(LA),NELEM(LA),NBOUN(LA),NSR(LA),NCONC(LA),NPA,
     1(NSTART(I,LA),I=1,NPA),(NEND(I,LA),I=1,NPA),(NFIRST(I,LA),I=1,NPA)
     2,(NLAST(I,LA),I=1,NPA),NCON,(NOF(I,LA),I=1,NCON),NBO,(NF(I,LA),
     3I=1,NBO),((NB(I,J,LA),I=1,NBO),J=1,2),NFREE(LA),((UT(I,J,LA),I=1,
     4NBO),J=1,2),NRACE(LA)
      NFIRST(NPA+1,LA)=NLAST(NPA,LA)+1
      NELM=NELEM(LA)
      DO 10 NE=1,NELM
      READ(8) ((DBA(I,J),I=1,3),J=1,6),(NOD(I),I=1,3),ORX,ORY
      WRITE(1)((DBA(I,J),I=1,3),J=1,6),(NOD(I),I=1,3),ORX,ORY
   10 CONTINUE
      READ(8) NCON,((X(I,J,LA),I=1,NCON),J=1,2),VLM(LA)
   20 CONTINUE
      DO 30 LA=1,2
      NPA=NPART(LA)
      DO 30 II=1,NPA
      READ(8) M,(U(I,LA),I=1,M)
      WRITE(3)M,(U(I,LA),I=1,M)
   30 CONTINUE
      DO 40 LA=1,2
      NPA=NPART(LA)
      DO 40 LL=1,NPA
      IF(NPA-LL) 40,40,35
   35 READ(8) M,N,((AM(I,J),I=1,N),J=1,M)
      WRITE(2)M,N,((AM(I,J),I=1,N),J=1,M)
   40 CONTINUE
      DO 50 LA=1,2
      NPA=NPART(LA)
      DO 50 LL=1,NPA
      READ(8)  M,((AM(I,J),J=1,M),I=1,M)
      WRITE(3)M,((AM(I,J),J=1,M),I=1,M)
      IF(NPA-LL) 50,50,45
   45 READ(8) M,N,((BM(I,J),J=1,N),I=1,M)
      WRITE(3)M,N,((BM(I,J),J=1,N),I=1,M)
   50 CONTINUE
      DO 60 LA=1,2
      IF(LA.EQ.1) GO TO 52
      NPA=NPART(1)
      GO TO 53
   52 NPA=NPART(2)
   53 DO 59 LL=1,NPA
      IF(LL-1) 56,56,55
   56 READ(8) M,((AM(I,J),I=1,M),J=1,M)
      WRITE(2)M,((AM(I,J),I=1,M),J=1,M)
      GO TO 59
   55 READ(8) M,N,((AM(I,J),I=1,M),J=1,M),((BM(I,J),I=1,M),J=1,N)
      WRITE(2)M,N,((AM(I,J),I=1,M),J=1,M),((BM(I,J),I=1,M),J=1,N)
   59 CONTINUE
   60 CONTINUE
      REWIND 8
      RETURN
      END

      OVERLAY(XX,2,0)
      PROGRAM TWO
      CALL SOLN
      RETURN
      END
```

Subroutine "SOLN" and other subroutines required in the program "CHOTTO" are same as those used in program "FINELM".

RADIAL LOAD= 5000 LBS
AMPLITUDE OF RELIEF ON OUTER RACE= 0.00000 INCHES
ROLLER DIAMETER= .30060 INCHES
ROLLER LENGTH= .45000 INCHES
SPECIFIC WEIGHT OF ROLLER MATERIAL= 0.00000 LBS/(IN**3)
SPEED OF ROTATION= 0.0 RPM

ITN	RADIAL CLEARANCES AT ROLLER POSITIONS IN μ INS										
NO.	1	2	3	4	5	6	7	8	9	10	11
1	-600	-600	-600	-600	-600	-600	-600	-600	-600	-600	-600
2	-526	-529	-526	-541	-544	-542	-541	-542	-546	-552	-555
3	-531	-534	-531	-546	-548	-547	-546	-547	-551	-557	-559
4	-532	-535	-532	-547	-549	-548	-547	-548	-552	-558	-560
5	-532	-536	-532	-547	-549	-548	-547	-548	-552	-558	-560

ITN	LOAD DISTRIBUTION AMONG ROLLERS IN LBS										
NO.	1	2	3	4	5	6	7	8	9	10	11
1	1277	1251	1177	1062	919	763	609	473	368	301	279
2	1190	1169	1088	990	847	683	523	385	283	223	203
3	1197	1176	1094	997	853	689	530	392	290	230	210
4	1198	1177	1095	998	853	690	531	393	291	231	211
5	1199	1177	1096	998	854	690	531	393	291	231	211

ITN	DEFLECTION OF		BODY DFLN	STFNS	RMS ERR
NO.	O.R.	I.R.	BRG. OF O.R.	LB/μ IN	IN LD DTRN
1			361	13.853	
2	328	279	594 159	8.411	81.53
3	311	266	545 160	9.177	13.82
4	308	264	536 160	9.323	2.36
5	308	264	535 160	9.348	.41

ALL DEFLECTIONS ARE IN μ INS.

*** BEARING NO. RR-420600 ***

Portion of a typical output of programs 'FINELM' or 'CHOTTO'.

```
      PROGRAM MESH(INPUT,OUTPUT,TAPE5=INPUT,TAPE6=OUTPUT,TAPE25,TAPE27)
C * * * * * * * * * * * * * * * * * * * * * * * * * * * * * * * * * * * * *
C     PROGRAM TO PLOT THE FINITE ELEMENT MESH OF THE RACES FROM THE DATA
C     CARDS OF PROGRAM FINELM
C * * * * * * * * * * * * * * * * * * * * * * * * * * * * * * * * * * * * *
      COMMON/COM2/NUMEL(750),NUMND(1250),NDE(750,3),XX(1250),YY(1250),
     1NEL,NND
      READ(5,85) XORIG,YORIG,AMAG
      CALL START
      CALL PLOT(XORIG,YORIG,-3)
      DO 10 LA=1,2
      CALL INPUT
      CALL DRAW(AMAG)
   10 CONTINUE
      READ(5,85) PEND
      CALL ENPLOT(PEND)
   85 FORMAT(3F10.5)
      STOP
      END

      SUBROUTINE INPUT
      DIMENSION NSTART(20),NEND(20),NFIRST(20),NLAST(20)
      COMMON/COM2/NUMEL(750),NUMND(1250),NDE(750,3),XX(1250),YY(1250),
     1NEL,NND
      READ(5,10) NEL,NND,NPART
      DO 20 I=1,NPART
      READ(5,10) NPAR,NSTART(I),NEND(I),NFIRST(I),NLAST(I)
   20 CONTINUE
   10 FORMAT(5I4)
      DO 60 II=1,NPART
      K=NFIRST(II)
      L=NLAST(II)
      NST=NSTART(II)
      NEN=NEND(II)
      KL=L-K+1
      KL3=KL/3
      IF(3*KL3-KL) 31,32,31
   31 KL3=KL3+1
   32 DO 30 I=1,KL3
      K3=3*I-3+K
      K2=3*I-2+K
      K1=3*I-1+K
      READ(5,35) NUMND(K3),XX(K3),YY(K3),NUMND(K2),XX(K2),YY(K2),
     1NUMND(K1),XX(K1),YY(K1)
      WRITE(6,35) NUMND(K3),XX(K3),YY(K3),NUMND(K2),XX(K2),YY(K2),
     1NUMND(K1),XX(K1),YY(K1)
   30 CONTINUE
      NENST=NEN-NST+1
      NENST4=NENST/4
      IF(4*NENST4-NENST) 41,42,41
   41 NENST4=NENST4+1
   42 DO 40 I=1,NENST4
      N4=4*I-4+NST
      N3=4*I-3+NST
      N2=4*I-2+NST
      N1=4*I-1+NST
      READ(5,45) NUMEL(N4),(NDE(N4,J),J=1,3),NEP,NUMEL(N3),
     1(NDE(N3,J),J=1,3),NEP,NUMEL(N2),(NDE(N2,J),J=1,3),NEP,
     2NUMEL(N1),(NDE(N1,J),J=1,3),NEP
   40 CONTINUE
   45 FORMAT(4(I5,3I4,I3))
   35 FORMAT(3(I4,2F10.6))
   60 CONTINUE
      RETURN
      END
```

```
      SUBROUTINE DRAW(AMAG)
      DIMENSION W(6),Z(6)
      COMMON/COM2/NUMEL(750),NUMND(1250),NDE(750,3),XX(1250),YY(1250),
     1NEL,NND
      W(5)=0.
      Z(5)=0.
      W(6)=1.
      Z(6)=1.
      WRITE(6,100) AMAG
  100 FORMAT(1X,5HAMAG=,F10.5)
      DO 1 I=1,NND
      IF(NUMND(I)-I) 2,1,2
    2 WRITE(6,10)
   10 FORMAT(1X,14HNOT COINCIDING)
    1 CONTINUE
      DO 3 I=1,NEL
      DO 4 J=1,3
      K=NDE(I,J)
      W(J)=XX(K)*AMAG
      Z(J)=YY(K)*AMAG
    4 CONTINUE
      AREA=0.5*(W(2)*(Z(3)-Z(1))+W(1)*(Z(2)-Z(3))+W(3)*(Z(1)-Z(2)))
      WRITE(6,15) I,(NDE(I,J),J=1,3),(W(J),Z(J),J=1,3),AREA
   15 FORMAT(1X,I4,3(2X,I4),3X,6(2X,F10.6),3X,E16.8)
      W(4)=W(1)
      Z(4)=Z(1)
      CALL LINE (W,Z,4,1,0,1)
    3 CONTINUE
      RETURN
      END
```

```
      PROGRAM TABLE(INPUT,OUTPUT,TAPE5=INPUT,TAPE6=OUTPUT)
C * * * * * * * * * * * * * * * * * * * * * * * * * * * * * * * * * * * *
C     PROGRAM TO ANALYSE AND TABULATE RESULTS OBTAINED BY PROGRAM FINELM
C * * * * * * * * * * * * * * * * * * * * * * * * * * * * * * * * * * * *
      DIMENSION NBRG(2),DFL(5),COM(10,10),P(11,4),NUM(10),ALSF(4),NO(4),
     1N(4)
      Z=20.
      NCA=0
      READ(5,18) NCASE
   18 FORMAT(I4)
   10 LINE=0
      KK=0
      KKK=0
      WRITE(6,12)
   12 FORMAT(1H1,///////1X,99HTABLE 7.2  SUMMARY OF RESULTS OBTAINED BY
     1FINITE ELEMENT ANALYSIS FOR STEEL RADIAL ROLLER BEARINGS.//)
   14 WRITE(6,15)
   15 FORMAT(3H SL,3X,7HBEARING,2X,4HRADL,1X,3HRPM,8X,42HLOAD DISTRIBUTI
     1ON IN THE BEARING IN POUNDS,9X,14HTOTAL DFLNS IN,5X,2HAV,4X,
     229HBODY EPSLN LOAD EQV.  RACES  /3H NO,3X,6HNUMBER,3X,4HLOAD,2X,
     332HIN,21X,15HROLLER POSITION,27X,7HU IN OF,7X,11HSTFNS  DFLN,7X,
     449HSHRG LOAD/15X,3HLBS,2X,4H1000,3X,1H1,4X,1H2,4X,1H3,4X,1H4,4X,
     551H5,4X,1H6,4X,1H7,4X,1H8,4X,1H9,3X,2H10,3X,2H11,3X,4HO.R.,2X,
     664HI.R.,2X,4HBRG.,2X,7HLB/U IN,1X,4HO.R.,7X,4HFCTR,2X,3HLBS/)
C******************** READING DATA CARDS ********************************
      AAK=0.3650E-06
      AAN=0.9220
   20 NCA=NCA+1
      READ(5,21) NO(1),(NBRG(I),I=1,2),FR,RPM,C,AMPL,RMS,ITN,NCOM1
   21 FORMAT(I4,7X,A8,A1,4F8.0,F8.2,2I5)
      IF(NCA.NE.NO(1)) STOP
      READ(5,22) NO(1),(DFL(I),I=1,5)
```

```
   22 FORMAT(I4,5F5.0)
      IF(NCA.NE.NO(1)) STOP
      IF(RPM.GT.0.001) GO TO 27
      READ(5,25)(NO(J),(P(I,J),I=1,11),N(J),J=1,2)
C     FIRST CARD IS FOR STIFF RACES AND SECOND ONE FOR FLEXIBLE RACES
   25 FORMAT(I4,11F5.0,I2)
      DO 26 I=1,2
      IF(NCA.NE.NO(I)) STOP
      IF(I.NE.N(I)) STOP
   26 CONTINUE
      GO TO 30
   27 READ(5,25)(NO(J),(P(I,J),I=1,11),N(J),J=1,4)
C     FIRST TWO CARDS FOR STIFF RACES ANB SECOND TWO FOR FLEXIBLE RACES
C     OF EACH OF THE TWO CARDS 1ST ONE FOR O.R. AND 2ND ONE FOR I.R.
      DO 29 I=1,4
      IF(NCA.NE.NO(I)) STOP
      IF(I.NE.N(I)) STOP
   29 CONTINUE
   30 IF(NCOM1-1) 33,31,33
   31 KK=KK+1
      NUM(KK)=NCA
      READ(5,32) NO(1),(COM(I,KK),I=1,10)
   32 FORMAT(I4,1X,9A8,A3)
C     ********** CALCULATION **********
      IF(NCA.NE.NO(1)) STOP
   33 CALL EQLOD(FR,RPM,P,PR1,PR2)
      AVSTF1=FR/DFL(1)
      AVSTF2=FR/DFL(4)
      DFL1=AAK*P(1,1)**AAN*10.**6
      DFL2=DFL1
      DEL=DFL(1)
      IF(C.GT.0.) DEL=DEL+C
      EPSLN=0.5*(1.-C/DEL)
      ARPM=RPM/1000.
      IF(RPM.GT.0.001) GO TO 38
      DO 35 I=1,2
   35 ALSF(I)=P(1,I)*Z/FR
       GO TO 70
   38 DO 39 I=1,4
   39 ALSF(I)=P(1,I)*Z/FR
      DFL2=AAK*P(1,2)**AAN*10.**6
C     ********** WRITING DATA **********
   70 IF(RPM.GT.0.001) GO TO 48
      LINE=LINE+3
      WRITE(6,40) NCA,(NBRG(I),I=1,2),FR,ARPM,(P(I,1),I=1,11),DFL1,DFL2,
     1DFL(1),AVSTF1,EPSLN,ALSF(1),PR1
   40 FORMAT(1X,I3,1X,A8,A1,F5.0,F4.0,11F5.0,1X,3F6.0,2X,F6.3,6X,
     1F5.2,F6.2,F6.0,1X,5HRIGID)
      IF(NCOM1-1) 43,41,43
   41 KKK=KKK+1
      LINE=LINE+1
      IF(KKK.EQ.1) LINE=LINE+2
      WRITE(6,42) (P(I,2),I=1,11),(DFL(I),I=2,4),AVSTF2,DFL(5),ALSF(2),
     1PR2
   42 FORMAT(3X,1H*,19X,11F5.0,1X,3F6.0,2X,F6.3,F6.0,5X,F6.2,F6.0,1X,
     15HFLXBL/)
      GO TO 60
   43 WRITE(6,44) (P(I,2),I=1,11),(DFL(I),I=2,4),AVSTF2,DFL(5),ALSF(2),
     1PR2
   44 FORMAT(23X,11F5.0,1X,3F6.0,2X,F6.3,F6.0,5X,F6.2,F6.0,1X,5HFLXBL/)
      GO TO 60
   48 LINE=LINE+5
      WRITE(6,50) NCA,(NBRG(I),I=1,2),FR,ARPM,(P(I,1),I=1,11),DFL1,DFL2,
     1DFL(1),AVSTF1,EPSLN,ALSF(1),PR1
```

```
   50 FORMAT(1X,I3,1X,A8,A1,F5.0,F4.0,11F5.0,1X,3F6.0,2X,F6.3,6X,
     1F5.2,F6.2,F6.0,1X,6HRGD OR)
      IF(NCOM1-1) 53,51,53
   51 KKK=KKK+1
      LINE=LINE+1
      IF(KKK.EQ.1) LINE=LINE+2
      WRITE(6,52) (P(I,2),I=1,11),ALSF(2)
   52 FORMAT(2X,1H*,20X,11F5.0,38X,F6.2,7X,6HRGD IR)
      GO TO 54
   53 WRITE(6,58) (P(I,2),I=1,11),ALSF(2)
   58 FORMAT(23X,11F5.0,38X,F6.2,7X,6HRGD IR)
   54 WRITE(6,55) (P(I,3),I=1,11),(DFL(I),I=2,4),AVSTF2,DFL(5),ALSF(3),
     1PR2
   55 FORMAT(23X,11F5.0,1X,3F6.0,2X,F6.3,F6.0,5X,F6.2,F6.0,1X,6HFLX OR)
      WRITE(6,56) (P(I,4),I=1,11),ALSF(4)
   56 FORMAT(23X,11F5.0,38X,F6.2,7X,6HFLX IR/)
   60 IF((NCA.EQ.NCASE).OR.(LINE.GT.42)) GO TO 65
      GO TO 20
   65 CONTINUE
      IF(KK.EQ.0) GO TO 80
      DO 68 I=1,KK
      WRITE(6,67) NUM(I),(COM(J,I),J=1,10)
   67 FORMAT(1X,I3,1H*,3X,9A8,A3)
   68 CONTINUE
   80 IF(NCA.EQ.NCASE) STOP
      WRITE(6,85)
   85 FORMAT(125X,9HCONTINUED)
      GO TO 10
      END

      SUBROUTINE EQLOD(FR,RPM,P,PR1,PR2)
C * * * * * * * * * * * * * * * * * * * * * * * * * * * * * * * * * * *
C     SUBROUTINE TO CALCULATE EQUIVALENT RADIAL LOAD OF A RADIAL ROLLER
C     BEARING FROM THE ROLLER LOAD DISTRIBUTION
C * * * * * * * * * * * * * * * * * * * * * * * * * * * * * * * * * * *
      DIMENSION P(11,4),F(11),F2(11)
      DATA Z,W,P1,CRATIO,AJR,AJ1,AJ2/20.0,4.5,4.0,0.774,0.24568,0.65161,
     10.67543/
      NZ=INT(Z/2.)+1
      W1=1./W
      CR1=1./(1.+CRATIO**W)
      CR2=1./(1.+1./CRATIO**W)
      N=0
      DO 50 KK=1,2
      N=N+1
      NR=N
      DO 15 J=1,NZ
      PHI=FLOAT(J-1)*2.*3.1415927/Z
      F(J)=P(J,N)/P(1,NR)
   15 F2(J)=F(J)*COS(PHI)
      CALL SIMRUL(F,Z,W,W,AM2)
      CALL SIMRUL(F2,Z,1.0,1.0,AMR)
      IF(RPM.GT.0.001) GO TO 20
      CALL SIMRUL(F,Z,P1,P1,AM1)
      GO TO 25
   20 N=N+1
      DO 21 J=1,NZ
   21 F(J)=P(J,N)/P(1,NR)
      CALL SIMRUL(F,Z,P1,P1,AM1)
   25 PRC=CR1*((AJR*AM1)/(AJ1*AMR))**W+CR2*((AJR*AM2)/(AJ2*AMR))**W
      PRCN=PRC**W1
      ALR=(1./((PRCN)**P1)-1.0)*100.
C     WRITE(6,100) PRCN,ALR
```

```
      IF(KK.EQ.2) GO TO 27
      PR1=FR*PRCN
      GO TO 50
   27 PR2=FR*PRCN
   50 CONTINUE
      RETURN
      END

      SUBROUTINE SIMRUL(F2,Z,W1,W2,S)
C * * * * * * * * * * * * * * * * * * * * * * * * * * * * * * * * * * * * * * *
C     SUBROUTINE FOR NUMERICAL INTEGRATION USING SIMPSON'S RULE
C * * * * * * * * * * * * * * * * * * * * * * * * * * * * * * * * * * * * * * *
      DIMENSION F(11),F2(11)
      N2=INT(Z/2.)
      IF(N2*2.NE.INT(Z)) STOP
      N=N2/2
      IF(N*2.NE.N2) N=(N2-1)/2
      N1=N2+1
      IF(INT(W1).EQ.1) GO TO 11
      DO 10 I=1,N1
   10 F(I)=F2(I)**W1
      GO TO 13
   11 DO 12 I=1,N1
   12 F(I)=F2(I)
   13 H=3.1415927/FLOAT(N2)
      S=F(1)+4.*F(2)
      N1=N-1
      DO 20 I=1,N1
   20 S=S+2.*F(2*I+1)+4.*F(2*I+2)
      IF(N*2.NE.N2) GO TO 30
      S=(H*(F(2*N+1)+S)/9.4247781)**(1./W2)
      RETURN
   30 S=(H*(F(2*N+1)+S+3.*(F(2*N+1)+F(2*N+2))/2.)/9.4247781)**(1./W2)
C 100 FORMAT(1X,22HEQUIVALENT LOAD RATIO=, F8.5,5X,61HPERCENTAGE INCREAS
C     1E IN LIFE AS COMPARED TO ZERO PLAY BEARING=,F6.2)
      RETURN
      END
```